THESE
PRESENTEE PAR

Régis MÉLIN

POUR OBTENIR LE TITRE DE DOCTEUR
DE L'UNIVERSITE JOSEPH FOURIER - GRENOBLE 1
(ARRETES MINISTERIELS DU 5 JUILLET 1994 ET
DU 30 MARS 1992)

(SPECIALITE PHYSIQUE)

- SYSTÈMES DE FERMIONS FORTEMENT CORRÉLÉS
- DYNAMIQUE DE SYSTÈMES VITREUX

DATE DE SOUTENANCE: 29 SEPTEMBRE 1995

COMPOSITION DU JURY:

Président du jury	:	J. Bellissard
Directeur de thèse	:	B. Douçot
Rapporteur	:	P. Holdsworth
Rapporteur	:	D. Poilblanc
Examinateur	:	P. Degiovanni
Examinateur	:	L. Lévy

THESE PREPAREE AU SEIN DU CENTRE DE RECHERCHE SUR LES TRES BASSES TEMPERATURES, CNRS, GRENOBLE

A mes parents

- Remerciements -

J'ai effectué cette thèse au CRTBT, laboratoire dirigé par P. Monceau que je remercie pour m'y avoir accueilli.

Je remercie Mr J. Bellissard de bien avoir voulu présider le jury. Je remercie également Mrs D. Poilblanc et P. Holdsworth d'avoir accepté d'être rapporteurs de cette thèse, ainsi que Mrs P. Degiovanni et L. Lévy pour leur participation au jury.

Je remercie mon directeur de thèse B. Douçot d' avoir encadré ce travail pendatn trois ans et de m'avoir suggéré de nombreuses idées.

Je remercie les personnes avec lesquelles j'ai collaboré pour certaines parties de ma thèse. Le chapitre 3 n'aurait pas vu le jour sans les idées de P. Degiovanni. Je remercie également J.C. Anglès d'Auriac qui m'a prêté un bon nombre d'algorithmes et pour sa contribution au chapitre 16. Je remercie aussi P. Chandra de sa contribution au chapitre 16, et également de m'avoir accueilli pendant quelques mois au laboratoire N.E.C. à Princeton. P. Butaud a également contribué au chapitre 4.

Je remercie les personnes avec lesquelles j'ai pu discuter de mon travail. Je pense en particulier à L. Lévy qui a suggéré l'expérience d'effet Hall quantique qui fait l'objet du chapitre 11. Je pense également à T. Dombre, J. Souletie, B. Barbara, K. Hasselbach et W. Wernsdorfer.

Enfin, je remercie les étudiants du groupe de travail. L'exposé de L. Gallot sur le champ bosonique libre est directement relié au liquide de Luttinger (voir le chapitre 3). L'exposé de J.Y. Fortin sur B.P.Z. m'a également été très profitable. J'ai également bénéficié des exposés de M. Magro, R. Taillet et S. Roche.

Finalement, je remercie les étudiants du laboratoire pour leur sympathie: F. Vistulo de Abreu, J.L. Gilson, H. Meyer, J.M. Robin. J'ai également bénéficié de discussions avec D. Carpentier lors de son stage au laboratoire. Je remercie plus particulièrement H. Meyer pour m'avoir aidé avec Latex.

Chapitre 1

Introduction

Le but de cette introduction est de résumer l'ensemble des travaux contenus dans cette thèse. Deux types de chapitres sont présents. Les chapitres écrits en anglais sont des articles déjà publiés ou en vue de publication. La plupart des chapitres écrits en français sont destinés à introduire les notions utilisées dans les articles. Cette thèse est divisée en deux parties: une première partie traite de certains aspects des systèmes d'électrons fortement corrélés. Une seconde partie traite de certains systèmes de spins vitreux. Bien que ces deux parties soient largement indépendantes, j'ai essayé dans les deux cas d'utiliser les techniques issues du chaos quantique pour étudier le spectre de Hamiltoniens d'électrons fortement corrélés dans la première partie, et le spectre des matrices de Glauber dans la seconde partie. Nous décrivons maintenant successivement les deux parties.

1.1 Systèmes d'électrons fortement corrélés

Une des questions auxquelles tentent de répondre les théories d'électrons fortement corrélés est de savoir si un système donné est ou n'est pas un liquide de Fermi. Cette problématique liquide de Fermi-non liquide de Fermi est abordée sous plusieurs angles dans cette thèse: aspects unidimensionnels, analyse des statistiques spectrales à une dimension puis à deux dimensions, théories de jauge et finalement effet Hall quantique à demi remplissage. S'il existe des classes de comportements bien comprises, plusieurs modèles restent actuellement mal compris. Le modèle de Hubbard pour la supraconductivité à haute température critique et le liquide de Hall à demi remplissage sont deux exemples abordés dans cette thèse pour lesquels la question de savoir si le système est ou n'est pas un liquide de Fermi est controversée.

Dans les chapitres 2 à 8, nous étudions des systèmes pour lesquels la nature liquide de Fermi ou non liquide de Fermi est clairement établie. Pour ces systèmes, nous analysons les propriétés des statistiques entre écarts de niveaux, en relation avec le comportement liquide de Fermi ou non liquide de Fermi. Les chapitres 2 à 4 sont consacrés aux systèmes unidimensionnels intégrables, et les chapitres 5 à 8 traitent des systèmes d'électrons bidimensionnels.

Le chapitre 2 contient une introduction à la théorie du liquide de Luttinger. La rédaction de ce chapitre est inspirée de l'article de Haldane[1], où la bosonisation est présentée comme une solution rigoureuse du modèle du liquide de Luttinger, au sens où il s'agit d'une identification

[1] F.D.M. Haldane, "*Luttinger liquid theory" of one dimensional quantum fluids: Properties of the Luttinger model and their extension to general 1D interacting spinless Fermi gas*, J. Phys. C, 14, 2585-2609 (1981)

précise des espaces de Hilbert. Au cours du chapitre 2, quelques compléments sont introduits par rapport à l'article original de Haldane: algèbre de Virasoro du gaz de Luttinger, séparation du spin et de la charge, et quelques liens et analogies simples avec les théories de chaînes de spin.

Le but du chapitre 3 est de montrer qu'il existe une correspondance entre le liquide de Luttinger à basse énergie et la théorie du champ bosonique compatifié. Ce chapitre est une partie d'un travail non encore publié dans le développement duquel P. Degiovanni a pris une part importante. Par rapport au chapitre 2, le cadre est plus large puisque l'on envisage simultanément tous les secteurs de la théorie de Dirac alors que, par le choix du vecteur de Fermi en position intermédiaire entre deux niveaux, les fermions sont spatialement antipériodiques au chapitre 2. Le jeu des transformations modulaires permet de passer d'un secteur à l'autre. L'identification s'effectue à plusieurs niveaux. La somme des fonctions de partition sur les quatres secteurs de la théorie de Dirac libre s'identifie à la fonction de partition du boson compactifié au point $gR^2 = 1$. Plus finement, on peut relier la fonction de partition dans chaque secteur de la théorie de Dirac à une combinaison des fonctions de partition du champ bosonique libre compactifié avec des conditions de monodromie de type demi entier (le champ revient à sa valeur initiale après deux périodes spatiales). Cette identification se généralise au cas de la théorie de Dirac en interaction (ou de Luttinger à la limite infrarouge). Dans ce cas, le produit gR^2 est relié aux paramètres physiques du liquide de Luttinger (vitesse de charge et de courant).

L'approche du chapitre 3 suppose que l'on s'est placé à la limite infrarouge où la symétrie conforme est préservée même en présence d'interactions (celles-ci sont alors locales). Dans le chapitre 4, nous traitons le cas d'interactions de portée finie pour un système de taille finie. Nous nous posons la question de déterminer le cross-over liquide de Fermi-non liquide de Fermi en fonction de la taille du système, de l'échelle d'impulsion et de la force des interactions. Nous cherchons également à comprendre quelle information contient le spectre. Les quasiparticules sont générées par branchement adiabatique à partir de l'état libre. Deux modes de destruction du liquide de Fermi sont possibles: une extinction de la quasiparticule de type 'catastrophe d'orthogonalité' et une destruction dynamique par interférences destructives entre les différentes composantes du paquet d'onde. L'effet 'catastrophe d'orthogonalité' est statique. Il a été identifié pour la première fois par Dzyaloshinskii et Larkin[2]. Au niveau du spectre, les niveaux d'énergie subissent une transformation d'échelle qui respecte l'existence de niveaux dégénérés. L'effet 'interférences' est quant à lui dynamique (il agit au bout d'un certain temps qui doit être comparé à L/v_F), et agit sur le spectre par une brisure des dégénérescences. Deux régimes sont possibles: à une faible levée de dégéneresccence correspond un régime liquide de Fermi et à un fort mélange de niveaux correspond un non liquide de Fermi. En terme de symétries, l'effet 'catastrophe d'orthogonalité' respecte la symétrie conforme et l'effet 'interférences destructives' brise la symétrie conforme.

Si à une dimension la théorie générique est celle du liquide de Lutttinger, la théorie générique à deux dimensions est la théorie de Landau (1957), au moins pour un système sans spin. Le chapitre 5 est une présentation de la théorie de Landau du liquide de Fermi, dont l'idée essentielle est l'existence de quasiparticules. A partir de cette hypothèse, on peut déduire le comportement macroscopique du liquide avec un petit nombre de paramètres phénoménologiques, accessibles expérimentalement. On déduit également une équation de transport, avec deux types de so-

[2]I.E. Dzyaloshinskii and A.I. Larkin, *Correlation functions for a one dimensional Fermi system with long-range interactions (Tomonaga model)*, Sov. Phys. JETP 38, 202 (1974).

lutions: un continuum des quasiparticules localisées et des modes collectifs. Une telle théorie doit être justifiée a posteriori à partir du Hamiltonien microscopique. C'est le but du chapitre 6 où nous présentons la bosonisation du liquide de Fermi, sous une formulation récente[3,4]. Cette technique permet de calculer sous forme approximative la fonction de corrélation à deux points et de montrer que, même en couplage fort, la renormalisation de la fonction de corrélation est finie (à une dimension, le résidu est nul: c'est l'effet 'catastrophe d'orthogonalité' mentionné plus haut).

Le but des chapitres 7 et 8 est de déterminer quelle information contient le spectre du liquide de Fermi. Dans un premier temps (chapitre 7), nous analysons le modèle de Landau avec des quasiparticules de durée de vie infinie. Les statistiques de niveaux sont poissoniennes à deux dimensions. Au chapitre 8, nous analysons les statistiques de niveaux du problème bidimensionnel. Pour celà, nous devons restreindre l'espace de Hilbert et introduire une coupure autour de la surface de Fermi, et le système devient alors non intégrable. Cependant, les statistiques de niveaux sont celles d'un système intégrable générique, même avec peu de fermions et peu d'orbitales. Ce résultat suggère que le liquide de Fermi est bien décrit par une théorie intégrable, par exemple la bosonisation de la surface de Fermi.

Le chapitre 9 traite de certains aspects des théories de jauge de la supraconductivité à haute température critique. A partir d'une approche de type 'théorie de jauge' pour le modèle t-J, il est possible de dériver un modèle de physique statistique pour un plasma de monopôles magnétiques[5]. Ces monopôles magnétiques décrivent des configurations non triviales du champ de jauge. Si les monopôles magnétiques sont dans une phase dipolaire, les spinons et les anti-holons sont déconfinés et le liquide quantique est un non liquide de Fermi. Il est donc important de tenir compte des effets collectifs dans le plasma de monopôles magnétiques. C'est ce que nous faisons en utilisant le groupe de renormalisation. Le résultat principal de cette étude est le diagramme de phase dans le plan nombre de couleurs fermioniques-dopage (figure 9.3). A dopage fixé, le non liquide de Fermi est favorisé si l'on augmente le nombre de couleurs fermioniques. Pour un nombre de couleurs fermioniques donné (par exemple 2 dans le cas de fermions portant un spin 1/2), le liquide de Fermi apparaît à faible dopage, alors que des dopages élevés favorisent le non liquide de Fermi.

Les chapitres 10,11 et 12 sont consacrés à une étude sur le liquide de Hall à demi remplissage. Le but de ces chapitres est d'analyser une expérience suggérée par L. Lévy, qui consiste à placer une charge électrique variable au centre d'un anneau mésoscopique de fluide de Hall à demi remplissage. Dans un premier temps, nous utilisons la théorie de champ moyen[6] pour décrire cette expérience. L'idée de la théorie de champ moyen est d'effectuer une transformation de jauge qui transforme le problème original de fermions sous champ magnétique en un problème de fermions portant deux tubes de flux sous champ magnétique. La théorie de champ moyen néglige les variations spatiales du champ de jauge et transforme donc le problème initial en un problème de fermions sans champ magnétique. L'effet de la charge électrique est d'induire une variation de densité des fermions composites, et donc une variation du flux traversant l'anneau entraînant l'apparition de courants permanents, fonctions de la charge électrique centrale. Nous

[3]F.D.M. Haldane, séminaire *A new look at the Fermi surface* donné à l'Université de Brown en novembre 1991.

[4]A.H. Castro Neto and E.H. Fradkin *Bosonization of Fermi liquids*, Phys. Rev. B 49, 10877-10892 (1994); *Exact solution of the Landau fixed point via bosonization*, Phys. Rev. B 51, 4084-4104 (1995).

[5]L.B. Ioffe and A.I. Larkin *Gapless fermions and gauge fields in dielectrics*, Phys. Rev. B 39, 8988 (1989).

[6]B.I. Halperin, P.A. Lee and N. Read, *Theory of the half-filled Landau level*, Phys. Rev. B 47, 7312 (1993).

Chapitre 2

Bosonisation du liquide de Luttinger

Ce chapitre est fortement inspiré de l'article de Haldane[1]. Le lecteur trouvera cependant quelques compléments, concernant la mise en évidence de l'algèbre de Virasoro de charge centrale $c = 1$ du liquide de Luttinger. Nous exposons également la séparation du spin et de la charge dans un liquide de Luttinger à spin.

2.1 Dérivation heuristique de la structure de l'espace de Hilbert de basse énergie du gaz de fermions unidimensionnel

On considère un gaz de fermions sans interactions sur un anneau de circonférence L avec des conditions aux limites périodiques. L'état fondamental à température nulle est une mer de Fermi notée $|0\rangle$. On suppose de plus que l'état fondamental est unique. En effet, selon le nombre de particules, le fondamental est soit unique, soit doublement dégénéré. Dans l'état fondamental, les fermions occupent les états indexés par les vecteurs d'onde

$$k = -N\frac{2\pi}{L}, ..., N\frac{2\pi}{L}, \tag{2.1}$$

où l'on a supposé un nombre impair de fermions, ce qui produit bien un fondamental non dégénéré. On choisit par convention le vecteur de Fermi k_F entre deux niveaux:

$$k_F = (N + \frac{1}{2})\frac{2\pi}{L}. \tag{2.2}$$

En seconde quantification, on écrit

$$|0\rangle = c^+_{-2\pi N/L}...c^+_{2\pi N/L}|\emptyset\rangle, \tag{2.3}$$

où $|\emptyset\rangle$ désigne le vide de matière. La relation de dispersion est celle des fermions libres de masse m:

$$\epsilon(k) = \frac{k^2}{2m}. \tag{2.4}$$

La mer de Fermi est représentée en figure 2.1. On note R et L les deux points de la surface

[1] F.D.M. Haldane, "*Luttinger liquid theory" of one dimensional quantum fluids: Properties of the Luttinger model and their extension to general 1D interacting spinless Fermi gas*, J. Phys. C, 14, 2585-2609 (1981)

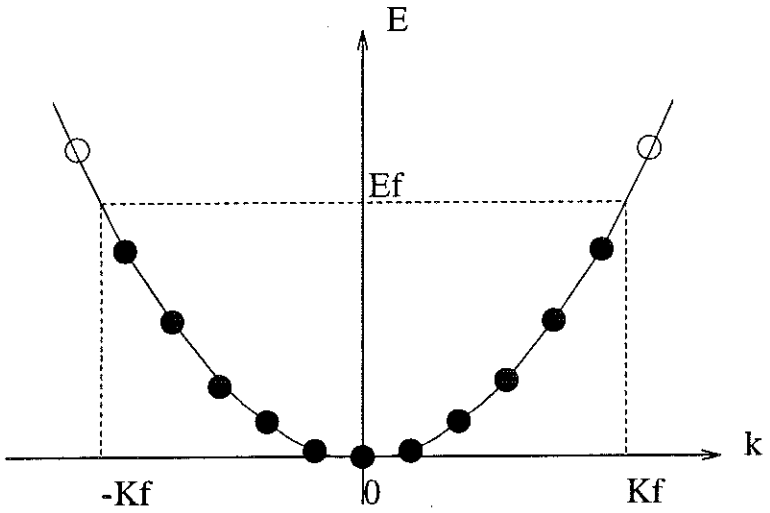

Figure 2.1: Mer de Fermi unidimensionnelle.

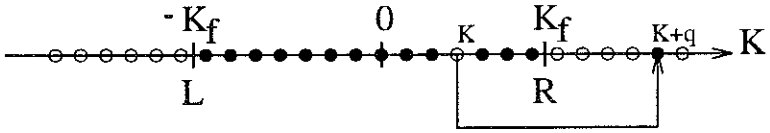

Figure 2.2: Excitation particule-trou de la mer de Fermi unidimensionnelle.

de Fermi. La limite thermodynamique est définie pour $k_F = \mu$, où μ est le potentiel chimique, maintenu constant alors que $L \to +\infty$. Dans cette limite, le nombre de modes sous la surface de Fermi augmente indéfiniment. On appelle *particule* un état à une particule occupé au-dessus de la surface de Fermi. On appelle *trou* un état à une particule vide en-dessous de la surface de Fermi. Par exemple, $c_k^+|0\rangle$ avec $k > k_F$ contient une particule de vecteur d'onde k et $c_k|0\rangle$, avec $k < k_F$ contient un trou de vecteur d'onde k. Comme, pour l'instant, on travaille dans un secteur de l'espace de Hilbert où le nombre de fermions est fixé, les états excités de la mer de Fermi sont des excitations particule-trou. La figure 2.2 représente un paire particule-trou. On note k l'impulsion du trou et $k+q$ l'impulsion de la particule. L'énergie de la paire particule-trou est

$$\omega_{k,q} = \frac{(k+q)^2}{2m} - \frac{k^2}{2m} = \frac{q^2}{2m} + \frac{pq}{m}. \tag{2.5}$$

Pour un transfert d'impulsion fixé, on regarde dans quel intervalle d'énergie se situe $\omega_{k,q}$. Si $0 \leq q \leq 2k_F$,

$$\frac{q^2}{2m} + \frac{q}{m}(k_F - q) \leq \omega_{k,q} \leq \frac{q^2}{2m} + \frac{k_F q}{m}. \tag{2.6}$$

Et si $q \leq 2k_F$, on a l'inégalité

$$\frac{q^2}{2m} - \frac{k_F q}{m} \leq \omega_{k,q} \leq \frac{q^2}{2m} + \frac{k_F q}{m}. \tag{2.7}$$

Le spectre d'énergie des paires particule-trou est représenté en figure 2.3. On remarque l'existence d'un gap qui est un effet purement unidimensionnel. En effet, à deux dimensions, il existe des

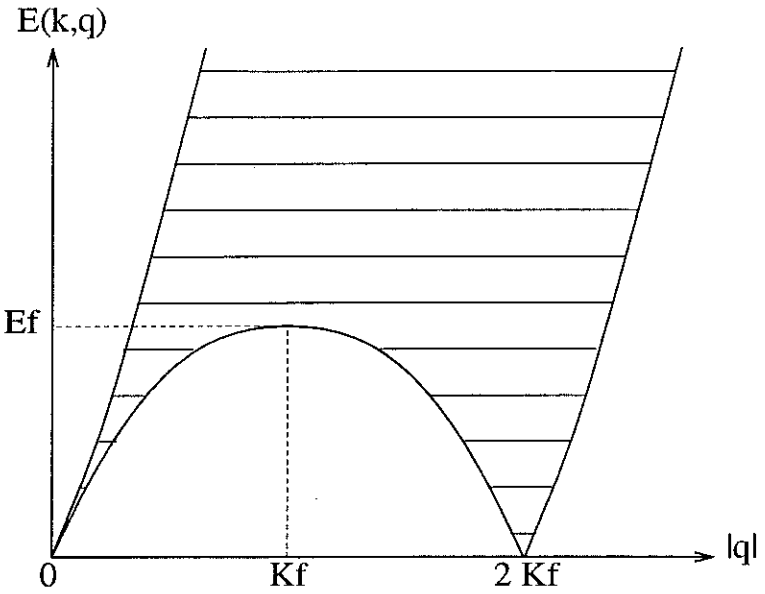

Figure 2.3: Spectre d'énergie des paires particule-trou, c'est-à-dire le lieu des $\omega_{k,q}$ dans le diagramme $(|q|, \omega_{k,q})$.

paires particule-trou d'énergie nulle quelle que soit leur impulsion. Une telle paire est représentée sur la figure 2.4. On remarque également sur le spectre des excitations particule-trou l'existence d'une branche linéaire pour $q \to 0$ et à basse énergie ($\omega_{k,q} \ll k_F^2/2m$). La relation de dispersion de cette branche linéaire s'écrit, dans la limite $q \ll k_F$:

$$\omega_{k,q} \simeq \frac{k_F}{m} q. \tag{2.8}$$

Dans cette limite, toutes les paires particule-trou de vecteur d'onde k sont dégénérées car on a négligé la courbure de la relation de dispersion au voisinage de la surface de Fermi. On reconnaît la vitesse de Fermi dans l'expression (2.8):

$$v_F = \frac{d\epsilon(k_F)}{dk} = \frac{k_F}{m}, \tag{2.9}$$

et l'énergie linéarisée d'une particule au voisinage de la surface de Fermi s'écrit

$$\epsilon(k) = \epsilon(k_F) + v_F(k - k_F) + ... \tag{2.10}$$

Si l'on regarde plus finement ce qui se passe au voisinage de $|q| = 2k_F$, on voit que ω ne s'y annule pas exactement. En effet, on doit tenir compte du processus représenté sur la figure 2.5 et qui a une énergie

$$\epsilon(k_F + \pi/L) - \epsilon(-k_F + \pi/L) = 2\pi v_F/L. \tag{2.11}$$

Pour obtenir le spectre à n particules-n trous, il suffit de superposer les diagrammes de la figure 2.3 en faisant attention au principe de Pauli pour des transferts d'impulsion $|q| = 2nk_F$ où n est un entier strictement positif. Le processus d'énergie minimale et de transfert d'impulsion $k = 2nk_F$ fixé crée n trous en

$$k = -\frac{2\pi}{L}N, ..., -\frac{2\pi}{L}(N - n + 1), \tag{2.12}$$

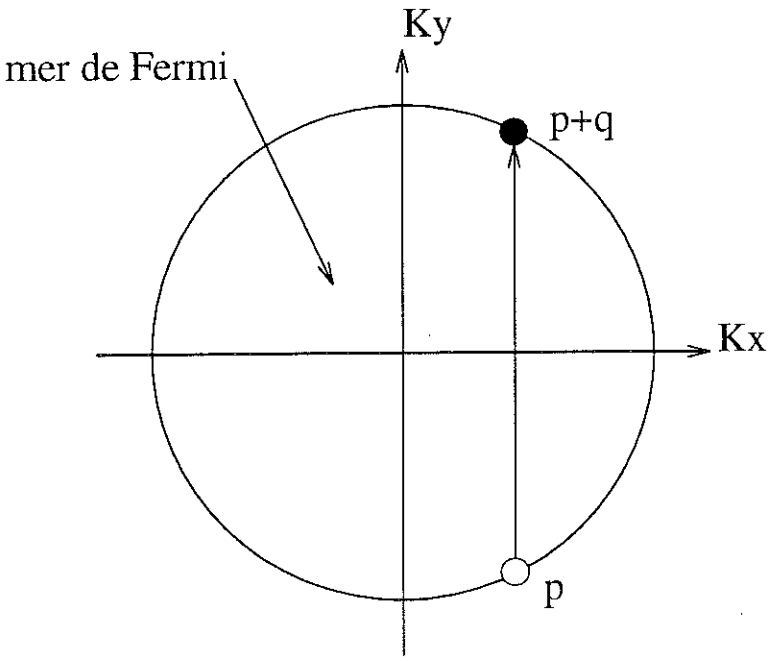

Figure 2.4: Avec une surface de Fermi connexe: une paire particule-trou d'énergie nulle pour une impulsion q fixée quelconque. Il n'y a pas de gap dans le spectre à une paire particule-trou.

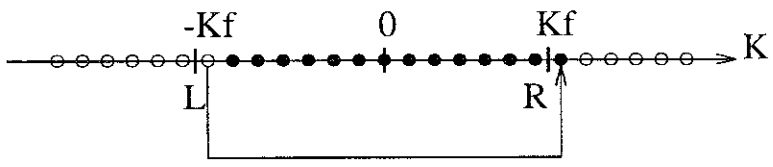

Figure 2.5: Excitation particule-trou d'énergie minimale autour de $q = 2k_F$.

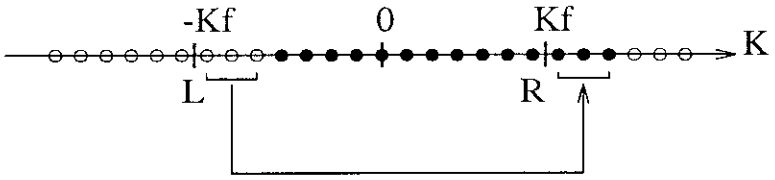

Figure 2.6: Excitation particule-trou d'énergie minimale autour de $q = 2nk_F$, avec $n = 3$ sur la figure.

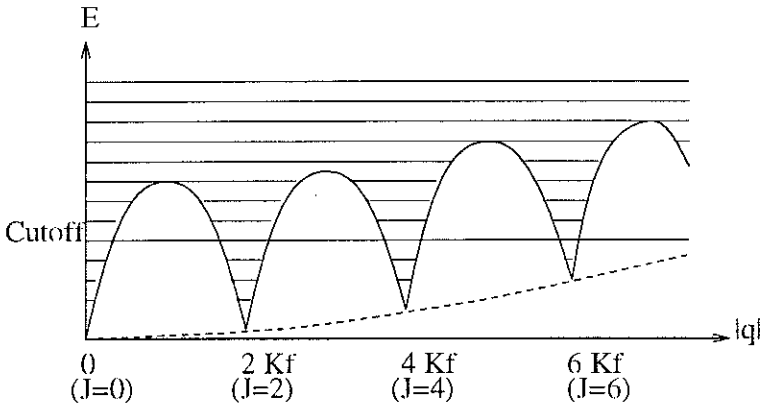

Figure 2.7: Spectre d'énergie des excitations particule-trou multiples. On a exagéré l'énergie en $q = 2nk_F$. Pour $\omega < \Lambda$, le spectre se découpe en secteurs labellés par J.

et n particules en

$$k = \frac{2\pi}{L}(N+1), ..., \frac{2\pi}{L}(N+n). \tag{2.13}$$

Cette excitation est représentée sur la figure 2.6 pour $n = 3$. L'énergie d'une telle excitation de la mer de Fermi vaut

$$\sum_{n=0}^{N-1} \frac{1}{2m}(k_F + \frac{\pi}{L} + \frac{2\pi}{L}n)^2 - \sum_{n=0}^{N} \frac{1}{2m}(-k_F + \frac{\pi}{L} + \frac{2\pi}{L}n)^2 \tag{2.14}$$

$$= \sum_{n=0}^{N-1} \frac{2k_F}{m}(\frac{\pi}{L} + \frac{2\pi}{L}n) = \frac{2\pi}{L}v_F N^2. \tag{2.15}$$

On retrouve bien le résultat établit pour $N = 1$. On en déduit le spectre d'excitations particules-trous représenté sur la figure 2.7. L'étude du spectre d'excitations de paires particules-trou multiples permet de donner de façon heuristique les caractéristiques du spectre de basse énergie. Au voisinage de $|q| \sim 0$, les objets de type $c^+_{k+q}c_k$ doivent obéir à une relation de dispersion linéaire. Ces objets sont de nature bosonique (2 fermions). Pour $|q| \sim Jk_F$, où J est multiple de 2, le spectre de basse énergie est constitué d'excitations bosoniques au-dessus d'un état d'énergie $v_F\pi J^2/2L$. On doit également tenir compte de la possibilité de faire varier le nombre de fermions sur chaque branche. Si l'on place N fermions supplémentaires au-dessus de la mer de Fermi, on peut écrire:

$$N = N_R + N_L \tag{2.16}$$

$$J = N_R - N_L, \tag{2.17}$$

où N_R et N_L désignent respectivement le nombre de fermions ajoutés au-dessus du fondamental sur la surface de Fermi droite (notée R pour Right) et gauche (notée L pour Left). L'énergie minimale des excitations à N et J fixé s'écrit

$$\frac{\pi}{2L} v_F N^2 + \frac{\pi}{2L} v_F J^2. \tag{2.18}$$

On peut résumer la structure de l'espace de Hilbert telle qu'on vient de la dériver par ces considérations heuristiques. Tout d'abord, il existe des secteur indexés par les entiers N et J, qui possèdent une énergie en l'absence de toute excitation particule-trou donnée par la relation (2.18). Au-dessus de chaque fondamental (N, J), il existe une tour d'états excités à n particules-n trous. On voit que l'objet fondamental pour décrire ces excitations est $c^+_{k+q} c_k$ car son action répétée sur le fondamental génère tous les états excités d'un secteur (N, J). On va prouver dans la suite que les excitations du type $c^+_{k+q} c_k$ sont bien bosoniques, avec la relation de dispersion linéaire que l'on a dérivée heuristiquement. On se propose maintenant de dériver rigoureusement la structure de l'espace de Hilbert de basse énergie.

2.2 Définition du liquide de Luttinger sans spin

2.2.1 Gaz de Luttinger

Nous partons du gaz de Fermi unidimensionnel et nous cherchons à en décrire le comportement infrarouge. Dans l'approximation où les excitations du système sont de basse énergie, on linéarise la relation de dispersion parabolique $\epsilon(k) = k^2/2m$ selon $\epsilon_{lin}(k) = v_F(\alpha k - k_F)$, où α désigne $+1$ ou -1 selon qu'il s'agit de la branche droite (R) ou gauche (L), et où la vitesse de Fermi v_F est définie par (2.9). Cette linéarisation n'est valable qu'au voisinage de la surface de Fermi, où l'on peut négliger les effets de la courbure de la relation de dispersion. On introduit une coupure Λ dans le spectre d'énergie à une particule et l'on se restreint aux modes contenus dans l'intervalle $[\epsilon_F - \Lambda, \epsilon_F + \Lambda]$. Dans une seconde étape, on prolonge les deux branches droite et gauche à toute énergie. Ce prolongement est légitime car il ne modifie pas la relation de dispersion à basse énergie. Les deux branches obtenues définissent la relation de dispersion du *gaz de Luttinger*, qui est représentée sur la figure 2.8. Pour que le système possède une surface de Fermi, l'état fondamental doit contenir une infinité de fermions. On remplace donc la mer de Fermi par une mer de Dirac. Cette analogie avec la théorie de Dirac est en fait complète, et le dictionnaire entre le liquide de Luttinger et les théories des champs correspondantes sera donné au chapitre 3. Les nombres d'occupation dans l'état fondamental sont

$$n^0_{k,\alpha} = \theta(k_F - \alpha k) = \langle 0 | n_{k,\alpha} | 0 \rangle. \tag{2.19}$$

On a donc transformé le modèle initial (gaz de Fermi) en un modèle équivalent (gaz de Luttinger) en ce qui concerne la physique de basse énergie. Le Hamiltonien du gaz de Luttinger est

$$H^0 = v_F \sum_{\alpha,k} (\alpha k - k_F)(n_{k,\alpha} - n^0_{k,\alpha}) \tag{2.20}$$

La soustraction de l'énergie du vide (infinie) revient à prescrire un ordre normal. Pour les fermions de la branche droite, : $c^+_k c_k := c^+_k c_k$ si $k > k_F$ et $c^+_k c_k = -c_k c^+_k$ si $k < k_f$. On vérifie que l'on a bien : $c^+_k c_k := n_k - n^0_k$. Le Hamiltonien (2.20) s'écrit donc également

$$H^0 = v_F \sum_{\alpha,k} (\alpha k - k_F) : c^+_{k,\alpha} c_{k,\alpha} : . \tag{2.21}$$

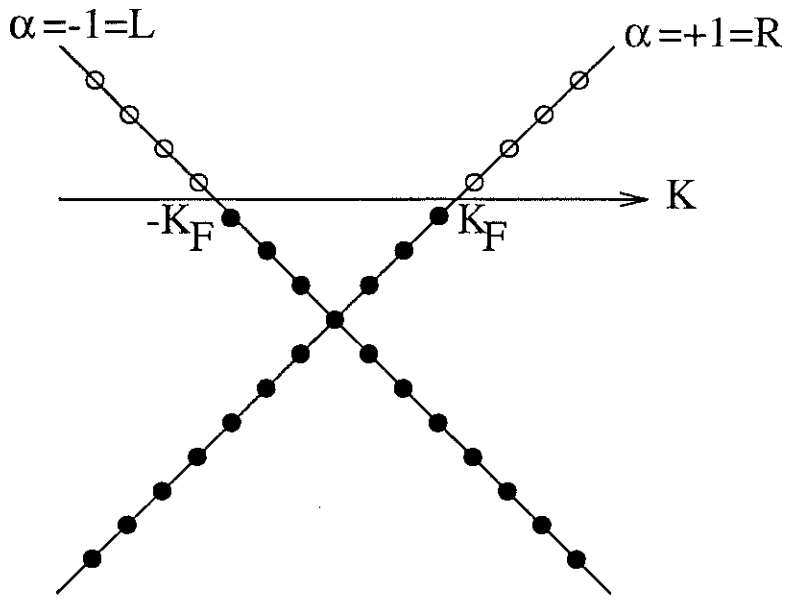

Figure 2.8: Relation de dispersion du gaz de Luttinger et mer de Dirac.

La prescription d'ordre normal est arbitraire en ce sens où deux Hamiltoniens différents d'une quantité finie sont équivalents. Un autre schéma de renormalisation, qui est utilisé en théorie des champs, et dont nous ferons usage au chapitre suivant, est la renormalisation ζ. Le Hamiltonien en renormalisation ζ diffère de $-1/12$ du Hamiltonien que nous avons avons écrit: $H^0_\zeta = H^0 - 1/12$. Par contre, l'opérateur d'impulsion est indépendant du schéma de renormalisation car le terme de renormalisation se simplifie entre la branche droite et la branche gauche. L'opérateur d'impulsion s'écrit

$$P = \sum_k k \left(: c^+_{k,R} c_{k,R} : - : c^+_{k,L} c_{k,L} : \right). \tag{2.22}$$

Les champs fermioniques sont obtenus en faisant une transformée de Fourier de $c^+_{k,\alpha}$. On définit

$$\psi^+_\alpha(x) = L^{-1/2} \sum_k e^{-ikx} c^+_{k,\alpha}. \tag{2.23}$$

Le signe dans la tranformée de Fourier (2.23) n'est pas arbitraire. Il est choisi de telle sorte que les fermions de la branche droite se déplacent vers la droite et que ceux de la branche gauche se déplacent vers la gauche. Les équations de propagation d'un paquet d'onde s'écrivent

$$U^0 \psi^+_R(x)|0\rangle = \psi^+_R(x + v_F t)|0\rangle \tag{2.24}$$
$$U^0 \psi^+_L(x)|0\rangle = \psi^+_L(x - v_F t)|0\rangle, \tag{2.25}$$

de sorte que les fermions R se déplacent vers la droite et que les fermions L se déplacent vers la gauche. Dans (2.24) et (2.25), U^0 est l'opérateur d'évolution. On vérifie aisément à partir de $\{c^+_{k,\alpha}, c_{k,\alpha'}\} = \delta_{k,k'}\delta_{\alpha,\alpha'}$, que l'on a bien

$$\{\psi^+_\alpha(x), \psi_\alpha(x')\} = \delta_{\alpha,\alpha'} \delta_{S_1}(x - x'), \tag{2.26}$$

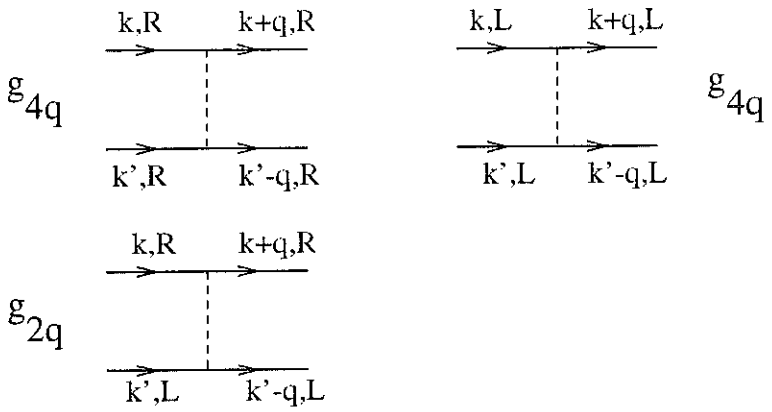

Figure 2.9: Interactions du liquide de Luttinger.

où la fonction de Dirac sur le cercle vaut

$$\delta_{S_1}(x) = \sum_{n=-\infty}^{+\infty} \delta(x - nL). \tag{2.27}$$

En terme d'opérateurs de champs fermioniques, le Hamiltonien devient

$$H^0 = v_F \sum_{\alpha} \int_{-L/2}^{L/2} dx : \psi_\alpha^+(x)(i\alpha\partial_x - k_F)\psi_\alpha(x) : . \tag{2.28}$$

2.2.2 Liquide de Luttinger

Les interactions du liquide de Luttinger sont représentées sur la figure 2.9. La diffusion de deux fermions de la branche droite vers deux fermions de la branche droite avec un transfert d'impulsion q se note g_{4q}. Par symétrie droite-gauche, le même processus sur la branche gauche possède la même force d'interaction. La diffusion d'un fermion de la branche droite et un fermion de la branche gauche pour donner un fermion de la branche droite et un fermion gauche se note g_{2q}. Ces notations sont conventionelles (g-ologie), et il n'existe pas d'autres interactions pour un liquide de Luttinger sans spin. En présence de spin, il existe d'autres types de vertex, de même que la présence d'un réseau introduirait d'autres interactions (processus Umklapp). Le Hamiltonien d'interaction du liquide de Luttinger sans spin est donc

$$H^1 = \frac{\pi}{L} \sum_{\alpha,\alpha'} \sum_{k,k'} \left(g_{4q}\delta_{\alpha,\alpha'} + g_{2q}\delta_{\alpha,-\alpha'}\right) c^+_{k+q,\alpha} c_{k,\alpha} c^+_{k'-q,\alpha'} c_{k',\alpha'}. \tag{2.29}$$

Nous allons montrer dans la suite que le modèle du liquide de Luttinger sans spin est intégrable, à l'aide de la procédure de *bosonisation*.

2.3 Bosonisation du liquide de Luttinger sans spin

2.3.1 Algèbre U(1)

On définit l'opérateur de densité comme

$$\rho_{q,\alpha} = \sum_k : c^+_{k+q,\alpha} c_{k,\alpha} : . \tag{2.30}$$

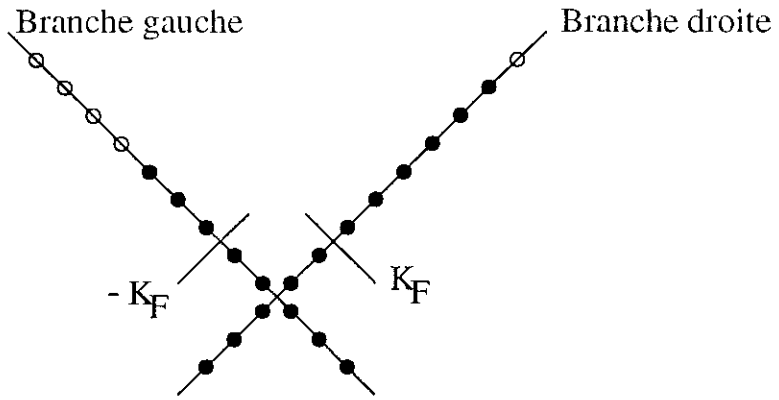

Figure 2.10: Un état du vide $|\{N_\alpha\}\rangle$ pour $N_R = 6$ et $N_L = 3$

Ces objets jouent un rôle central dans ce qui va suivre. Le produit normal signifie que, si $q \neq 0$,

$$\rho_{q,\alpha} = \sum_k c^+_{k+q,\alpha} c_{k,\alpha}, \tag{2.31}$$

et si $q = 0$,

$$\rho_{0,\alpha} = \sum_k \left(c^+_{k,\alpha} c_{k,\alpha} - \langle 0 | c^+_{k,\alpha} c_{k,\alpha} | 0 \rangle \right) = N_\alpha, \tag{2.32}$$

où N_α représente le nombre de fermions supplémentaires par rapport au fondamental sur la branche α. N_α est relié aux nombres de charge et de courant par les relations (2.16) et (2.17). Le commutateur des opérateurs de densité vaut

$$\left[\rho_{q,\alpha}, \rho^+_{q',\alpha'}\right] = \delta_{\alpha,\alpha'} \sum_{k,k'} \left[c^+_{k+q,\alpha} c_{k,\alpha}, c_{k'-q',\alpha} c_{k',\alpha} \right] \tag{2.33}$$

$$= \delta_{\alpha,\alpha'} \sum_{k,k'} \left(\delta_{k,k'-q'} c^+_{k+q,\alpha} c_{k',\alpha} - \delta_{k',k+q} c^+_{k'-q',\alpha} c_{k,\alpha} \right). \tag{2.34}$$

Cet opérateur à un corps n'est pas normal-ordonné. Afin d'effectuer les sommes sur k et k' dans (2.34), nous devons impérativement écrire les opérateurs sous leur forme normal-ordonnée. Avec la prescription d'ordre normal, la partie 'opérateur' possède des éléments de matrice finis entre tous les états de l'espace de Hilbert. On peut donc manipuler sans danger des opérateurs normal-ordonnés, et en particulier les simplifier. L'égalité (2.34) s'écrit

$$\left[\rho_{q,\alpha}, \rho^+_{q',\alpha'}\right] = \delta_{\alpha,\alpha'} \sum_{k,k'} \quad \Big(\delta_{k,k'-q'} : c^+_{k+q,\alpha} c_{k',\alpha} : + \delta_{k,k'-q'} \langle \{N_\alpha\} \rangle c^+_{k+q,\alpha} c_{k',\alpha} | \{N_\alpha\} \rangle \tag{2.35}$$

$$- \delta_{k',k+q} : c^+_{k'-q',\alpha} c_{k,\alpha} : - \delta_{k',k+q} \langle \{N_\alpha\} | c^+_{k'-q',\alpha} c_{k,\alpha} | \{N_\alpha\} \rangle \Big).$$

L'état $|\{N_\alpha\}\rangle$ désigne l'état obtenu à partir de la mer de Dirac $|0\rangle$ par ajout de N_α fermions au-dessus de la branche α. Si N_α est négatif, on retire des fermions. La figure 2.10 représente un état $|\{N_\alpha\}\rangle$. On peut maintenant effectuer la sommation en utilisant les règles habituelles, pour obtenir

$$\left[\rho_{q,\alpha}, \rho^+_{q',\alpha'}\right] = \delta_{\alpha,\alpha'} \sum_k \left(\delta_{k,k'-q'} \langle \{N_\alpha\} | c^+_{k+q,\alpha} c_{k+q',\alpha} | \{N_\alpha\} \rangle - \langle \{N_\alpha\} | c^+_{k+q-q',\alpha} c_{k,\alpha} | \{N_\alpha\} \rangle \right). \tag{2.36}$$

On ne peut clairement sommer séparément les deux termes, sinon des quantités infinies apparaissent. La somme (2.36) est finie et vaut

$$\left[\rho_{q,\alpha}, \rho^+_{q',\alpha'}\right] = -\frac{1}{2\pi}\alpha q L \delta_{\alpha,\alpha'}\delta_{q,q'}. \tag{2.37}$$

C'est la relation centrale de la procédure de bosonisation. La relation (2.37) montre que les opérateurs de densité forment une algèbre U(1). Dans l'espace réel, les opérateurs de densité valent

$$\rho_\alpha(x) = \psi^+_\alpha(x)\psi_\alpha(x) = \frac{1}{L}\sum_{k,k'} e^{-i(k-k')x} c^+_{k,\alpha} c_{k',\alpha} = \frac{1}{L}\sum_q e^{-iqx}\rho_{q,\alpha}, \tag{2.38}$$

et la représentation de l'algèbre U(1) dans l'espace réel s'écrit

$$\left[\rho_\alpha(x), \rho^+_{\alpha'}(x')\right] = -\frac{1}{2\pi} i\alpha\delta_{\alpha,\alpha'}\delta'(x-x'). \tag{2.39}$$

2.3.2 Base bosonique

On peut former des bosons à partir des opérateurs $\rho_{q,\alpha}$ de la façon suivante:

$$a^+_q = \left(\frac{2\pi}{Lq}\right)^{1/2} \rho_{q,R} \tag{2.40}$$

$$a^+_{-q} = \left(\frac{2\pi}{Lq}\right)^{1/2} \rho_{-q,L}, \tag{2.41}$$

où q est positif. On peut vérifier que $\left[a_q, a^+_{q'}\right] = \delta_{q,q'}$. On note

$$|\{n_q\},\{N_\alpha\}\rangle = \prod_{q\neq 0} \frac{1}{(n_q!)^{1/2}} (a^+_q)^{n_q} |\{N_\alpha\}\rangle. \tag{2.42}$$

Les états $|\{n_q\},\{N_\alpha\}\rangle$ sont des états propres du Hamiltonien. Pour le montrer, on calcule le commutateur $[H^0, \rho_{q,\alpha}] = v_F \alpha q \rho_{q,\alpha}$, ce qui conduit à $\left[H_0, a^+_q\right] = v_F|q|a^+_q$ pour $q \neq 0$, donc $\left[H_0, (a^+_q)^{n_q}\right] = v_F|q|(a^+_q)^{n_q}$, ce qui donne

$$H^0|\{n_q\},\{N_\alpha\}\rangle = \left(v_F\frac{\pi}{L}(N^2_R + N^2_L) + \sum_{q\neq 0}|q|a^+_q a_q\right)|\{n_q\},\{N_\alpha\}\rangle. \tag{2.43}$$

On veut maintenant vérifier que $\{|\{n_q\},\{N_\alpha\}\rangle\}$ forme une base de l'espace de Hilbert. La manière la plus convaincante d'établir ce résultat consisterait à mettre en évidence l'isomorphisme entre l'espace de Hilbert fermionique et bosonique. Nous nous contenterons ici d'identifier les fonctions de partition à température finie sur la base des fermions et sur la base des bosons. En effet, la fonction de partition est la fonction génératrice des dégénérescences. On note $x = \exp(-\beta\hbar\omega)$, où $\hbar\omega = 2\pi v_F/L$ est l'écart d'énergie entre deux niveaux consécutifs. Comme l'énergie est un multiple de $\hbar\omega$, la fonction de partition s'écrit

$$Z(x) = \sum_n g_n x^n, \tag{2.44}$$

donc

$$g_n = \frac{1}{n!}\frac{\partial^n Z}{\partial x^n}(0), \tag{2.45}$$

de telle sorte que pour montrer la complétude de la famille $|\{n_q\},\{N_\alpha\}\rangle$, il suffit de montrer que la fonction de partition calculée sur la base des fermions et sur la famille $|\{n_q\},\{N_\alpha\}\rangle$ sont égales. Sur la base des fermions, la fonction de partition vaut

$$Z_F = \left(\prod_{n=1}^{+\infty}(1+e^{-\beta(n-\frac{1}{2})\hbar\omega})\right)^4. \tag{2.46}$$

La puissance 4 provient de la symétrie particule-trou (le niveau de Fermi est entre deux niveaux quantiques) et de la symétrie droite-gauche. Pour la famille de bosons, la fonction de partition s'écrit

$$Z_B = \left(\prod_{q=1}^{\infty}\left(\sum_{n_q=0}^{+\infty}e^{-\beta\hbar\omega q}\right)\right)^2\left(\sum_{n=-\infty}^{+\infty}e^{-\beta E_n}\right)^2. \tag{2.47}$$

La puissance 2 provient de la symétrie droite-gauche, et E_n désigne l'énergie de n fermions empilés au-dessus du vide:

$$E_n = \sum_{i=1}^{n}(i-\frac{1}{2})\hbar\omega = \frac{1}{2}n^2\hbar\omega, \tag{2.48}$$

de sorte que la fonction de partition sur la famille bosonique vaut

$$Z_B = \left(\prod_{q=1}^{\infty}\left(\sum_{n_q=0}^{+\infty}e^{-\beta\hbar\omega q}\right)\right)^2\left(\sum_{n=-\infty}^{+\infty}e^{-\beta\frac{\hbar\omega}{2}n^2}\right)^2. \tag{2.49}$$

Afin d'identifier les deux expressions de la fonction de partition, on utilise l'identité de triple produit de Jacobi[2]

$$\sum_{n=-\infty}^{+\infty}y^n q^{n^2/2} = \prod_{n=1}^{+\infty}(1-q^n)\prod_{n=0}^{+\infty}(1+yq^{n+1/2})(1+y^{-1}q^{n+1/2}). \tag{2.50}$$

Avec $y=1$, on obtient l'identité

$$\sum_{n=-\infty}^{+\infty}x^{n^2} = \prod_{n=1}^{+\infty}(1+x^{2n-1})^2(1-x^{2n}), \tag{2.51}$$

qui permet d'identifier les deux fonctions de partition: $Z_F = Z_B$. La famille $|\{n_q\},\{N_\alpha\}\rangle$ forme donc une base de l'espace de Hilbert. Le Hamiltonien sur cette base vaut

$$H^0 = v_F\frac{\pi}{L}(N_R^2+N_L^2)+\sum_{q\neq 0}v_F|q|a_q^+a_q, \tag{2.52}$$

et l'opérateur d'impulsion vaut

$$P = \sum_\alpha \alpha\left(k_F+\frac{\pi}{L}N_\alpha\right)N_\alpha + \sum_{q\neq 0}qa_q^+a_q. \tag{2.53}$$

[2]Nous ne donnons pas ici de démonstration de cette formule, prouvée pour la première fois par Jacobi en 1829. Nous renvoyons le lecteur au chapitre XXI du livre de E.T. Whittaker et G.N. Watson *A course of modern analysis*, Cambridge University Press (1927).

2.3.3 Algèbre de Virasoro

Nous allons maintenant mettre en évidence une algèbre de Virasoro, ce qui permettra de calculer la charge centrale. Dans le chapitre suivant, nous identifierons la théorie du liquide de Luttinger avec un certain secteur de la théorie du boson compactifié, qui possède sa propre algèbre de Virasoro. L'identification précise des espaces de Hilbert du liquide de Luttinger et du boson compactifié fera l'objet du chapitre 3. On définit le tenseur énergie-impulsion du problème de Luttinger comme étant[3]

$$T_{n,\alpha} = \frac{1}{2}\sum_{k=-\infty}^{+\infty} \rho^+_{k,\alpha}\rho^+_{n-k,\alpha} \tag{2.54}$$

$$T_{0R} = \frac{1}{2}N_R^2 + \sum_{k>0} k a_k^+ a_k \tag{2.55}$$

$$T_{0L} = \frac{1}{2}N_L^2 + \sum_{k>0} a_{-k}^+ a_{-k} \tag{2.56}$$

La raison pour laquelle cet objet est appelé *tenseur énergie impulsion* est la suivante: si l'on considère la théorie du champ bosonique compactifié ou non compactifié, on constate que l'objet défini par (2.54) (2.55) et (2.56) est l'analogue du quantifié canonique du tenseur énergie impulsion classique[4]. Nous désirons calculer le commutateur des tenseurs énergie impulsion. Comme pour le calcul de l'algèbre U(1), il faut traiter avec précaution les termes du vide. Nous commençons par oublier l'existence de tel termes, que nous traiterons ensuite. En utilisant les relations de commutation (2.37), nous obtenons après quelques lignes de calcul

$$[T_{q,\alpha}, T_{q',\alpha'}] = \frac{\alpha}{2}\delta_{\alpha,\alpha'}(q-q')T_{q+q',\alpha}. \tag{2.57}$$

Les termes du vide vont générer une extension centrale de l'algèbre (2.57):

$$[T_{q,\alpha}, T_{q',\alpha'}] = \frac{\alpha}{2}\delta_{\alpha,\alpha'}(q-q')T_{q+q',\alpha} + \delta_{\alpha,\alpha'}A_\alpha(q,q'). \tag{2.58}$$

Nous montrons dans un premier temps que $A_\alpha(p,q) = \beta_\alpha(p)\delta_{p+q}$[5], et que l'on peut choisir $\beta_\alpha(q) = a_\alpha q + b_\alpha q^3$.

En posant $T'_{0,\alpha} = T_{0,\alpha}$ et $T'_{q,\alpha} = T_{q,\alpha} - A_\alpha(0,q)/q$ pour $q \neq 0$, on obtient

$$[T'_{0,\alpha}, T_{q,\alpha}] = [T_{0,\alpha}, T_{q,\alpha}] = -qT_{q,\alpha} + A_\alpha(0,q) = -qT'_{q,\alpha}. \tag{2.59}$$

Un changement de base permet donc de se ramener à $[T_{0,\alpha}, T_{0,q}] = -qT_{q,\alpha}$. On peut donc prendre $A_\alpha(0,q) = 0$ sans restreindre la généralité du problème. On applique maintenant l'identité de Jacobi entre $T_{0,\alpha}$,$T_{p,\alpha}$ et $T_{q,\alpha}$:

$$[T_{0,\alpha},[T_{p,\alpha},T_{q,\alpha}]] + [T_{p,\alpha},[T_{q,\alpha},T_{0,\alpha}]] + [T_{q,\alpha},[T_{0,\alpha},T_{p,\alpha}]] = 0, \tag{2.60}$$

[3]Dans toute cette partie, nous notons n au lieu de $q = 2\pi n/L$ afin d'alléger les notations.

[4]Pour une introduction pédagogique sur la théorie bosonique libre de masse nulle, se reporter à l'exposé de L. Gallot au Groupe de Travail. Les notes seront disponibles sur le serveur W_3 de l'ENSLAPP.

[5]La démonstration se trouve dans le rapport de stage d'E. Billey intitulé *Introduction aux algèbres de dimension infinie et théories conformes*, effectué sous la direction de P. Sorba à l'ENSLAPP (1992).

ce qui entraîne $(p+q)A_\alpha(p,q) = 0$ et donc $A_\alpha(p,q) = \beta_\alpha(q)\delta_{p+q}$. Et comme $A_\alpha(p,q) = -A_\alpha(q,p)$, on a $\beta_\alpha(q) = -\beta_\alpha(-q)$. En appliquant une nouvelle fois l'identité de Jacobi entre $T_{p,\alpha}$, $T_{q,\alpha}$ et $T_{r,\alpha}$, on obtient

$$(q-r)\delta_{p,-q-r}\beta_\alpha(p) + (r-p)\delta_{q,-r-p}\beta_\alpha(q) + (p-r)\delta_{r,-p-q}\beta_\alpha(r) = 0. \tag{2.61}$$

En spécialisant au cas $p+q+r=0$, et avec $r=1$, on obtient

$$(q-1)\beta_\alpha(q+1) = (q+2)\beta_\alpha(q) - (2q+1)\beta_\alpha(1). \tag{2.62}$$

Comme $\beta_\alpha(q) = -\beta_\alpha(-q)$, il suffit de calculer $\beta_\alpha(q)$ pour q positif. L'espace des solutions est de dimension 2. Comme $\beta_\alpha(q) = q$ et $\beta_\alpha(q) = q^3$ sont solutions, $\beta_\alpha(q)$ a la forme générale $\beta_\alpha(q) = a_\alpha q + b_\alpha q^3$, ce qui est bien le résultat anonncé précédemment.

Les coefficients a_α et b_α sont calculés en évaluant de deux façons différentes $\langle 0|\,[T_{1,\alpha}, T_{-1,\alpha}]\,|0\rangle$ et $\langle 0|\,[T_{2,\alpha}, T_{-2,\alpha}]\,|0\rangle$. Pour celà, on remarque que

$$T_{1,R} = \frac{1}{2}\sum_{k>0}\rho^+_{k,\alpha}\rho^+_{1-k,\alpha} = \frac{\sqrt{2}}{2}a_1^+ a_2 + \sum_{k>1}\sqrt{k}\sqrt{k+1}a_k^+ a_{k+1}. \tag{2.63}$$

On en déduit que

$$\langle 0|\,[T_{1,\alpha}, T_{-1,\alpha}]\,|0\rangle = 0 = 2\langle 0|T_{0,R}|0\rangle + a_\alpha + b_\alpha = a_\alpha + b_\alpha, \tag{2.64}$$

donc $a_\alpha + b_\alpha = 0$. On remarque également que

$$T_{2,R} = \sum_{k>0}\sqrt{k}\sqrt{k+2}a_k^+ a_{k+2} + \sqrt{2}N_R a_2 + \frac{1}{2}a_1^2 \tag{2.65}$$

$$T_{-2,R} = \sum_{k>0}\sqrt{k}\sqrt{k+2}a_{k+2}^+ a_k + \sqrt{2}N_R a_2^+ + \frac{1}{2}(a_1^+)^2, \tag{2.66}$$

et donc

$$\langle 0|\,[T_{2,R}, T_{-2,R}]\,|0\rangle = \frac{1}{4}\langle 0|(a_1)^2(a_1^+)^2|0\rangle = \frac{1}{2} \tag{2.67}$$

$$= 4\langle 0|T_{0,R}|0\rangle + \beta_R(2) = \beta_R(2). \tag{2.68}$$

Nous obtenons donc $\beta_R(2) = 1/2$. Par le même procédé, on montre que $\beta_L(2) = -1/2$. On peut donc obtenir les valeurs de a et b: $a_R = -1/12$, $a_L = 1/12$, $b_R = 1/12$ et $b_L = -1/12$. Le commutateur des tenseurs énergie impulsion vaut donc

$$[T_{q,\alpha}, T_{q',\alpha}] = \alpha\left((q-q')T_{q+q',\alpha} + \frac{1}{12}q(q^2-1)\delta_{q+q'}\right). \tag{2.69}$$

En posant $L_q = T_{q,R}$ et $\bar{L}_q = T_{-q,L}$, on obtient l'algèbre de Virasoro de charge centrale $c=1$:

$$\left[L_q, L'_q\right] = (q-q')L_{q+q'} + \frac{1}{12}q(q^2-1)\delta_{q+q'} \tag{2.70}$$

$$\left[\overline{L}_q, \overline{L}_{q'}\right] = (q-q')\overline{L}_{q+q'} + \frac{1}{12}q(q^2-1)\delta_{q+q'}. \tag{2.71}$$

Le Hamiltonien (2.52) et l'opérateur d'impulsion (2.53) s'expriment de façon très simple sur cette algèbre:

$$H = L_0 + \overline{L}_0 \tag{2.72}$$

$$P = L_0 - \overline{L}_0. \tag{2.73}$$

2.4 Opérateur d'échelle dans le secteur $q = 0$, champs de Bose

On cherche à construire un opérateur d'échelle U_α agissant dans le secteur $q = 0$ et avec les propriétés suivantes:

- U_α est unitaire.
- $\{U_R, U_L\} = 0$.
- U_α est un opérateur d'échelle, c'est-à-dire $U_R|N_R, N_L\rangle = |N_R + 1, N_L\rangle$ et $U_L|N_R, N_L\rangle = |N_R, N_L + 1\rangle$.
- $\forall\alpha, \forall q \neq 0, \left[U_\alpha, a_q^+\right] = 0$ et $[U_\alpha, a_q] = 0$.

En particulier, $c_{k,\alpha}^+$ se décompose à l'aide de U_α et d'opérateurs de bosons. Nous cherchons à écrire une telle décomposition. Les champs de bose apparaîtrons alors naturellement. La forme la plus simple à laquelle on peut penser est

$$U_\alpha^0 = \sum_k c_{k,\alpha}^+ \delta\left(k - \alpha(k_F + (2N_\alpha + 1)\frac{\pi}{L})\right), \tag{2.74}$$

ce qui revient à ajouter un fermion au-dessus de la branche droite ou gauche selon le signe de α. Pour cet opérateur, $\left[U_\alpha, a_q^+\right] \neq 0$. En effet, en utilisant la propriété $\left[\rho_{q,\alpha}, c_{k,\beta}^+\right] = \delta_{\alpha,\beta} c_{k+q,\alpha}^+$, nous voyons aisément que $[U_\alpha^0, \rho_{q,\alpha}] \neq 0$. Afin de trouver un opérateur U_α tel que $\left[U_\alpha, a_q^+\right] = 0$, nous écrivons U_α^0 sous la forme

$$U_\alpha^0 = L^{-1/2} \int_{-L/2}^{L/2} dx e^{-i\alpha k_F x} e^{-i(\phi_\alpha^0(x))^+} \psi_\alpha^+(x) e^{-i\phi_\alpha^0(x)}, \tag{2.75}$$

où l'on a utilisé (2.23) et où l'on pose

$$\phi_\alpha^0(x) = \frac{\alpha\pi x}{L} N_\alpha. \tag{2.76}$$

Nous cherchons l'opérateur U_α sous la forme (2.75), mais avec une expression modifiée pour ϕ_α, de telle sorte que $\left[U_\alpha, a_q^+\right] = 0$. On suppose de plus que le commutateur $\left[\psi_\alpha(x), a_q^+\right]$ est un c-nombre, c'est à dire que $\psi_\alpha(x)$ est une combinaison linéaire des modes bosoniques a_q^+ et a_q. Sous cette hypothèse, $\left[U_\alpha, a_q^+\right] = 0$ équivaut à

$$\left[\phi_\alpha(x) + (\phi_\alpha(x))^+, a_q^+\right] \psi_\alpha^+(x) = i\left[\psi_\alpha^+(x), a_q^+\right]. \tag{2.77}$$

Ce dernier commutateur s'évalue simplement et l'on obtient

$$\left[\phi_R(x) + \phi_R^+(x), a_q^+\right] \psi_R^+(x) = -i\left(\frac{2\pi}{Lq}\right)^{1/2} e^{iqx} \psi_R^+(x) \text{ si } q > 0 \tag{2.78}$$

$$= 0 \text{ si } q < 0 \tag{2.79}$$

$$\left[\phi_L(x) + \phi_L^+(x), a_q^+\right] \psi_L^+(x) = 0 \text{ si } q > 0 \tag{2.80}$$

$$= -i\left(\frac{2\pi}{Lq}\right)^{1/2} e^{iqx} \psi_L^+(x) \text{ si } q < 0. \tag{2.81}$$

Ces conditions sont bien satisfaites si l'on prend

$$\phi_R(x) = \frac{\pi x}{L} N_R - i \sum_{q>0} \left(\frac{2\pi}{Lq}\right)^{1/2} e^{iqx} a_q \tag{2.82}$$

$$\phi_L(x) = -\frac{\pi x}{L} N_L - i \sum_{q>0} \left(\frac{2\pi}{Lq}\right)^{1/2} e^{-iqx} a_{-q}. \tag{2.83}$$

Notons qu'il est possible d'inverser (2.75) et d'exprimer $c^+_{k,\alpha}$ en fonction de ψ_α, ψ^+_α et U_α. C'est le point de départ du calcul du chapitre 4 (relation (4.23)).

2.4.1 Formulation Hamiltonienne en termes de champs de Bose

Le but de cette section est de poursuivre le parallèle avec la théorie du champ bosonique libre, et d'écrire une formulation Hamiltonienne pour le gaz de Luttinger. Nous introduisons tout d'abord les variables de phase $\overline{\theta}_\alpha$, telles que

$$U_\alpha = (-1)^{\frac{1}{2}\alpha N_{-\alpha}} e^{i\overline{\theta}_\alpha}. \tag{2.84}$$

Les signes sont choisis de telle sorte que $\{U_R, U_L\} = 0$ avec $\left[\overline{\theta}_R, \overline{\theta}_L\right] = 0$. Les champs de phase sont définis par

$$\theta_\alpha(x) = \overline{\theta}_\alpha + \phi_\alpha(x) + \phi^+_\alpha(x). \tag{2.85}$$

En exprimant $\partial_x \theta_\alpha(x)$ en terme d'opérateur de densité, on montre que

$$\partial_x \theta_\alpha(x) = \frac{2\pi}{L} \alpha \rho_\alpha(x). \tag{2.86}$$

D'autre part, on montre également que $\rho_\alpha(x)$ et $\theta_\alpha(x)$ sont canoniquement conjugués:

$$[\theta_{\alpha'}(x), \rho_\alpha(x')] = i\delta_{\alpha,\alpha'} \delta_{S_1}(x - x'). \tag{2.87}$$

En utilisant les modes bosoniques (2.40) et (2.41), on montre que

$$\int_0^L : (\rho_\alpha(x))^2 : dx = \frac{1}{\pi} \sum_{q \neq 0} |q| a^+_q a_q + \frac{1}{L} N^2_\alpha. \tag{2.88}$$

Le produit normal des modes bosoniques est défini par : $a^+_q a_{q'} := a^+_q a_{q'}$ et : $a_q a^+_{q'} := a^+_{q'} a_q$. En comparant (2.88) avec la forme (2.52) du Hamiltonien, on obtient

$$H^0 = \frac{v_F}{4\pi} \sum_\alpha \int_0^L dx : (\partial_x \theta_\alpha(x))^2 : . \tag{2.89}$$

A partir de cette formulation, il est possible d'introduire un champ de Bose et son moment conjugué

$$\varphi(x) = \frac{1}{2}(\theta_R(x) + \theta_L(x)) \tag{2.90}$$

$$\Pi(x) = \rho_R(x) + \rho_L(x) \tag{2.91}$$

On vérifie que φ et Π sont bien canoniquement conjugués: $[\varphi(x), \Pi(x')] = i\delta(x - x')$, et que le Hamiltonien s'exprime sous la forme

$$H^0 = \frac{v_F}{2\pi} \int_{-L/2}^{L/2} dx \left(: (\partial_x \varphi)^2 : + \pi^2 : \Pi^2 : \right). \tag{2.92}$$

Cette forme du Hamiltonien est identique au Hamiltonien du champ bosonique libre (avec $v_F = 1$).

2.4.2 Fonctions de corrélations à température nulle de la théorie libre

La fonction de corrélation à deux points sur la branche droite est définie par

$$iG_R(x,t|x',t') = iG_{R>}(x,t|x',t') + iG_{R<}(x,t|x',t'), \tag{2.93}$$

avec

$$iG_{R>}(x,t|x',t') = \langle \{N_\alpha\}| e^{iH(t'-t)} \psi_R(x'-x) e^{-iH(t'-t)} \psi_R^+(0) |\{N_\alpha\}\rangle \theta(t'-t) \tag{2.94}$$

$$iG_{R<}(x,t|x',t') = -\left(x \leftrightarrow x'; t \leftrightarrow t'\right). \tag{2.95}$$

Comme le système est invariant par translation spatiale et temporelle, les fonctions de corrélation ne dépendent que des différences $x'-x$ et $t'-t$. Nous notons $G_{R>}(x'-x,t'-t) = G_{R>}(x,t|x',t')$. On se propose de calculer la fonction de corrélation directement en termes de fermions, puis à l'aide des bosons. Pour mener le calcul sur la base des fermions, il suffit d'utiliser la définition (2.23) du champ de fermions. On obtient alors

$$G^0_{R>}(x,t) = \frac{1}{2L} \frac{e^{i\frac{\pi}{L}(2N_R+1)(x-v_F t)} e^{ik_F x}}{\sin \frac{\pi}{L}(x - v_F t)}. \tag{2.96}$$

A la limite thermodynamique, $|x - v_F t| \ll L$, et l'on obtient

$$G^0_{R>}(x,t) = \frac{e^{ik_F x}}{2\pi (x - v_F t)}. \tag{2.97}$$

On peut également effectuer le calcul en passant par la base bosonisée. Le résultat en lui-même n'est pas très interessant dans le cas libre, mais la technique pour calculer la fonction de corrélation à deux points sera identique en présence d'interactions, et ce sera la seule méthode utilisable. On utilise les relations (2.75), (2.82) et (2.83) que l'on inverse selon

$$\psi_\alpha^+(x) = L^{-1/2} e^{-i\alpha k_F x} e^{-i\phi_\alpha^+(x)} U_\alpha e^{-i\phi_\alpha(x)}. \tag{2.98}$$

La fonction de corrélation s'écrit alors

$$iG^0_{R>}(x,t) = \frac{1}{L} e^{i\frac{\pi}{L}(2N_R+1)(x-v_F t)} e^{ik_F x} \tag{2.99}$$
$$\langle \{N_\alpha\}| e^{\sum_{q>0} \left(\frac{2\pi}{Lq}\right)^{1/2} e^{iqx} a_q} e^{-iv_F \sum_{q\neq 0} v_F |q| a_q^+ a_q t} e^{\sum_{q>0} \left(\frac{2\pi}{Lq}\right)^{1/2} a_q^+} |\{N_\alpha\}\rangle.$$

On utilise le fait que

$$e^{\lambda a^+ a} e^{\mu a^+} |\{N_\alpha\}\rangle = e^{\mu e^\lambda a^+} |\{N_\alpha\}\rangle \tag{2.100}$$

pour obtenir

$$iG^0_{R>}(x,t) = \frac{1}{L}e^{i\frac{\pi}{L}(2N_R+1)(x-v_Ft)}e^{ik_Fx} \langle\{N_\alpha\}| \exp\left(\sum_{q>0}\left(\frac{2\pi}{Lq}\right)^{1/2} e^{iqx}a_q\right) \exp -\left(\sum_{q>0}\left(\frac{2\pi}{Lq}\right)^{1/2} e^{iv_Fqt}a_q^+\right)|\{N_\alpha\}\rangle. \tag{2.101}$$

En utilisant le fait que $e^Ae^B = e^{[A,B]}e^Be^A$ si $[A,B]$ est scalaire, on obtient

$$iG^0_{R>}(x,t) = \frac{1}{L}e^{i\frac{\pi}{L}(2N_R+1)(x-v_Ft)}e^{ik_Fx}\exp\left(\sum_{q>0}\frac{2\pi}{Lq}e^{iq(x-v_Ft)}\right). \tag{2.102}$$

On utilise maintenant la relation

$$\sum_{n=1}^{+\infty}\frac{\lambda^n}{n} = -\ln(1-\lambda), \tag{2.103}$$

pour finalement retrouver l'expression (2.96).

2.5 Solution du liquide de Luttinger sans spin en interaction

Le terme d'interaction (2.29) s'exprime sous forme quadratique en terme des opérateurs de densité

$$H^1 = \frac{\pi}{L}\sum_q\left(g_{4q}\sum_\alpha \rho_{q,\alpha}\rho^+_{q,\alpha} + g_{2q}\sum_\alpha \rho_{q,\alpha}\rho^+_{q,-\alpha}\right). \tag{2.104}$$

L'énergie de $H^0 + H^1$ dans le secteur $q = 0$ vaut

$$\frac{\pi}{2L}\left(v_NN^2 + v_JJ^2\right), \tag{2.105}$$

où $v_N = v_F + g_{40} + g_{20}$ et $v_J = v_F + g_{40} - g_{20}$. N et J sont les nombres de charge et de courant donnés par (2.16) et (2.17). Dans les secteur $q \neq 0$, le Hamiltonien vaut

$$\frac{1}{2}\sum_{q\neq0}|q|\left(g_{4q}(a_q^+a_q + a_qa_q^+) + g_{2q}(a_q^+a_{-q}^+ + a_qa_{-q})\right). \tag{2.106}$$

On utilise une transformation de Bogoliubov pour diagonaliser (2.106):

$$b_q^+ = \cosh\varphi_q a_q^+ - \sinh\varphi_q a_{-q}. \tag{2.107}$$

On vérifie aisément que $\left[b_q, b_{q'}^+\right] = \delta_{q,q'}$. Le principe de la transformation de Bogoliubov consiste à inverser (2.107), et à exprimer le Hamiltonien en terme des bosons b, puis à choisir φ_q de telle sorte que le Hamiltonien soit diagonal en terme des bosons b. Cette condition s'écrit

$$\tanh 2\varphi_q = -\frac{g_{2q}}{v_F + g_{4q}}. \tag{2.108}$$

Le Hamiltonien du liquide de Luttinger devient alors

$$H = H^0 + H^1 = \frac{1}{2}\sum_{q\neq 0}(\omega_q - v_F|q|) + \sum_{q\neq 0}\omega_q b_q^+ b_q + \frac{\pi}{2L}\left(v_N N^2 + v_J J^2\right), \tag{2.109}$$

où

$$\omega_q = \sqrt{v_F^2 - g_{2q}^2}|q|. \tag{2.110}$$

L'énergie de point zéro peut être éventuellement infinie, ce qui n'est pas source de problèmes car on peut soustraire le terme divergent. Le nouvel état du vide est cherché sous la forme

$$|\{N_\alpha\}\rangle_b = A\exp\{\sum_{q>0}\lambda_q a_q^+ a_{-q}^+\}|\{N_\alpha\}\rangle. \tag{2.111}$$

L'état $|\{N_\alpha\}\rangle_b$ est le vide de bosons b: $\forall q \neq 0$, $b_q|\{N_\alpha\}\rangle_b = 0$. Cette condition fixe λ_q: $\lambda_q = \tanh 2\varphi_q$. D'autre part, le préfacteur A est déterminé par la condition ${}_b\langle\{N_\alpha\}|\{N_\alpha\}\rangle_b = 1$. On obtient alors

$$|\{N_\alpha\}\rangle_b = \exp\left(-\sum_{q>0}\ln\cosh\varphi_q\right)\exp\left(\sum_{q>0}\tanh\varphi_q a_q^+ a_{-q}^+\right)|\{N_\alpha\}\rangle. \tag{2.112}$$

Le préfacteur doit être non nul, sinon le nouvel espace de Hilbert est réduit à $\{0\}$, donc le traitement exposé ici concerne des interactions telles que $\sum_{q>0}\varphi_q$ soit convergente lorsque $q \to +\infty$. Afin que la limite thermodynamique soit bien définie, on impose que $\lim_{q\to 0}\varphi_q = \varphi_0 < +\infty$. L'opérateur d'impulsion (2.53) est également diagonal en terme de bosons b:

$$P = \left(k_F + \frac{\pi}{L}N\right)J + \sum_{q\neq 0} q b_q^+ b_q. \tag{2.113}$$

On peut modifier l'expression (2.53) de telle sorte que (2.98) soit encore valable, mais avec des champs de fermions normal ordonnés en terme de bosons b. Pour celà, on part de (2.82) et (2.83) et (2.98) exprimés en termes de bosons b, puis on effectue les commutations nécessaires. Après ces opérations, on obtient

$$\psi_\alpha^+(x) = L^{-1/2}e^{i\alpha k_F x}e^{-\sum_{q>0}\left(\frac{2\pi}{Lq}\right)\sinh^2\varphi_q}e^{i\phi_\alpha^+(x)}U_\alpha e^{i\phi_\alpha(x)} \tag{2.114}$$

avec l'expression modifiée de $\phi_\alpha(x)$:

$$\phi_\alpha(x) = \alpha\frac{\pi x}{L}N_\alpha + i\sum_{q\neq 0}\left(\frac{2\pi}{L|q|}\right)^{1/2}e^{-iqx}\beta_q b_q, \tag{2.115}$$

où $\beta_q = \theta(\alpha q)\cosh\varphi_q - \theta(-\alpha q)\sinh\varphi_q$.

2.5.1 Fonctions de corrélations à température nulle de la théorie en interaction

Le principe du calcul des fonctions de corrélation a déjà été exposé lors du calcul des fonctions de corrélation de la théorie libre. Nous nous contentons de donner le résultat:

$$iG_{R>}(x,t) = L^{-1}e^{i\left(k_F + \frac{\pi}{L}(2N_R+1)\right)x}e^{-i\frac{\pi}{2L}(v_N(2N+1)+V_J(2J+1))} \tag{2.116}$$

$$\exp\left(-2\sum_{q>0}\left(\frac{2\pi}{Lq}\right)\sinh^2\varphi_q\right)\exp\left(\sum_{q>0}\left(\frac{2\pi}{Lq}\right)e^{i(qx-\omega_q t)}\cosh^2\varphi_q\right)$$
$$\exp\left(\sum_{q>0}\left(\frac{2\pi}{Lq}\right)e^{-i(qx+\omega_q t)}\sinh^2\varphi_q\right).$$

Nous utilisons cette relation dans le chapitre 4 pour déterminer à quelle condition le liquide de Luttinger de taille finie peut être considéré comme un liquide de Fermi.

2.5.2 Fonctions de corrélation à température finie de la théorie en interaction

Le principe du calcul des fonctions de corrélation à température finie est le même que pour les fonctions de corrélation à température nulle, sauf qu'il faut effectuer des moyennes sur une distribution de bosons à température finie. Pour cela, on utilise la relation

$$\langle e^{\alpha b^+}e^{\alpha' b}\rangle = e^{\alpha\alpha'\langle b^+ b\rangle}. \tag{2.117}$$

Afin de montrer cette égalité, nous notons $q=\exp(-\hbar\omega)$, et le Hamiltonien vaut $h=\omega b^+ b$. La fonction de partition est donnée par $Z=(1-q)^{-1}$ et l'on peut écrire

$$\langle e^{\alpha b}e^{\alpha' b}\rangle = \frac{1}{Z}\sum_{n=0}^{+\infty}q^n\langle n|e^{\alpha b^+}e^{\alpha' b}|n\rangle \tag{2.118}$$
$$= (1-q)\sum_{n=0}^{+\infty}\sum_{k=0}^{n}q^n(\alpha\alpha')^k\frac{n!}{(k!)^2}(n-k)!. \tag{2.119}$$

En permutant les sommes sur k et n, on obtient

$$\langle e^{\alpha b}e^{\alpha' b}\rangle = (1-q)\sum_{k=0}^{+\infty}\frac{q^k(\alpha\alpha')^k}{(k!)^2}S_k, \tag{2.120}$$

où

$$S_k=\sum_{m=0}^{+\infty}\frac{(m+k)!}{m!}q^m. \tag{2.121}$$

On montre par récurrence que

$$S_k=\frac{k!}{(1-q)^{k+1}}. \tag{2.122}$$

On déduit alors aisément la relation (2.117). En utilisant la relation (2.117) dans le calcul des fonctions de corrélation, on obtient la fonction de Green à température finie sous la forme

$$iG^T_{R>}(x,t)=iG_{R>}(x,t)e^{-A(x,t)}, \tag{2.123}$$

où

$$A(x,t)=\sum_{q>0}\left(\frac{2\pi}{Lq}\right)\frac{1}{e^{\beta\omega_q}-1}e^{-i\omega_q t}\left(\cosh^2\varphi_q e^{iqx}+\sinh^2\varphi_q e^{-iqx}\right). \tag{2.124}$$

2.6 Liquide de Luttinger à la limite infrarouge

On suppose que les interactions ont une portée R dans l'espace réel, et l'on se place dans la limite où $L \gg R$. Dans cette limite, il existe une théorie de basse énergie qui diffère de la théorie libre par une renormalisation des paramètres. Cette démarche est identique à celle de Landau pour la théorie du liquide de Fermi. Dans le cas du liquide de Fermi, la théorie de basse énergie est obtenue par renormalisation[6]. Par analogie au *liquide de Fermi*, on appelle *liquide de Luttinger* la théorie effective. Notons que dans les deux cas, la théorie effective possède les mêmes symétries que la théorie libre. Pour le liquide de Fermi, la théorie de Landau est intégrable. Pour le liquide de Luttinger, la théorie effective est invariante conforme. La différence essentielle entre les deux théories effectives est que la théorie de Landau possède des quasiparticules, alors que le liquide de Luttinger est un non liquide de Fermi. Nous cherchons donc le Hamiltonien de basse énergie sous la forme

$$H = \frac{1}{2\pi}\int_{-L/2}^{L/2} dx \left(v_\varphi : (\partial_x \varphi)^2 : + v_\pi \pi^2 : \Pi^2 : \right), \tag{2.125}$$

où v_φ et v_π sont à déterminer. Dans le cas libre, $v_\varphi = v_\pi = v_F$. Afin d'identifier v_φ et v_π, nous exprimons (2.125) en terme des modes bosoniques a_q^+ et a_q. A l'aide de (2.86), nous obtenons

$$(\partial_x \varphi)^2 = \pi^2 (\rho_R - \rho_L)^2 \tag{2.126}$$

$$\Pi^2 = (\rho_R + \rho_L)^2. \tag{2.127}$$

D'autre part, on montre que

$$\int dx : (\rho_R \pm \rho_L)^2 := \frac{1}{L}\left(\pm 2 \sum_{q>0} \frac{L|q|}{2\pi} \left(a_q^+ a_{-q}^+ + a_q a_{-q} \right) + \sum_{q\neq 0} \frac{L|q|}{2\pi} a_q^+ a_q + (N_R \pm N_L)^2 \right). \tag{2.128}$$

Le Hamiltonien de basse énergie s'exprime de la façon suivante, en utilisant (2.128):

$$H = \frac{1}{4}(v_\pi - v_\varphi) \sum_{q\neq 0} |q| a_q^+ a_{-q}^+ + \frac{1}{4}(v_\pi - v_\varphi) \sum_{q\neq 0} |q| a_q a_{-q} + \frac{1}{2}(v_\varphi + v_\pi) \sum_{q\neq 0} |q| a_q^+ a_q + \frac{\pi}{2L}(v_\varphi J^2 + v_\pi N^2). \tag{2.129}$$

En identifiant (2.106) et (2.105) avec (2.129), on obtient $v_\pi = v_N$ et $v_\varphi = v_J$, ce qui conduit au Hamiltonien de basse énergie

$$H = \frac{1}{2\pi}\int_{-L/2}^{L/2} dx \left(v_J : (\partial_x \varphi)^2 : + v_N : \Pi^2 : \right). \tag{2.130}$$

On peut également calculer les fonctions de corrélation dans la limite infrarouge. Pour cela, on suppose que les interactions sont de la forme $\varphi_q = \varphi\theta(1/R - |q|)$. Outre les facteurs de phase, la fonction de corrélation (2.116) contient trois facteurs:

- un terme lié à la *catastrophe d'orthogonalité* [7]

$$\exp\left(-2 \sum_{q>0} \frac{2\pi}{Lq} \sinh^2 \varphi_q \right) \simeq \exp\left(-2 \int_{1/L}^{1/R} \frac{dq}{q} \sinh^2 \varphi \right) = \left(\frac{L}{R} \right)^{-2\sinh^2 \varphi}. \tag{2.131}$$

[6] La renormalisation du liquide de fermions est exposée dans l'article de revue de R. Shankar *Renormalization group approach to interacting fermions*, Rev. Mod. Phys. 66, 129-192 (1994).

[7] Ce terme est dû à P.W. Anderson, voir Phys. Rev. Lett. 18, 1049 (1967).

Ce préfacteur est nul à la limite thermodynamique, c'est-à-dire que la fonction de corrélation est nulle à la limite thermodynamique.

- Un terme lié au produit normal des bosons sur la branche droite:

$$\exp\left(\sum_{q>0}\frac{2\pi}{Lq}e^{-i(\omega_q t-qx)}\cosh^2\varphi_q\right)\simeq\left(-\frac{L}{2i\pi}\right)^{\cosh^2\varphi}\left(\frac{1}{x-v_S t+i\epsilon}\right)^{\cosh^2\varphi}, \quad (2.132)$$

où $v_S=\sqrt{v_N v_J}$. La prescription $\epsilon>0$ assure la convergence des séries géométriques.

- Un terme lié au produit normal des bosons sur la branche gauche:

$$\exp\left(\sum_{q>0}\frac{2\pi}{Lq}e^{-i(\omega_q t+qx)}\sinh^2\varphi_q\right)\simeq\left(\frac{L}{2i\pi}\right)^{\sinh^2\varphi}\left(\frac{1}{x+v_S t-i\epsilon}\right)^{\sinh^2\varphi}. \quad (2.133)$$

Au total, la fonction de Green dans la limite infrarouge devient

$$G_{R>}(x,t)=\frac{1}{2\pi}e^{ik_F x}\left(\frac{R}{2\pi}\right)^{2\sinh^2\varphi}\frac{1}{x-v_S t+i\epsilon}\left(\frac{1}{(x-v_S t+i\epsilon)(x+v_S t-i\epsilon)}\right)^{\sinh^2\varphi}. \quad (2.134)$$

Si $\varphi\neq 0$, la fonction de corrélation (2.134) reste critique. A l'aide de (2.134), on peut obtenir le comportement de $n(k)$ à la traversée de la surface de Fermi. En effet,

$$n_R(k)=-\frac{i}{2\pi}\int_{-\infty}^{+\infty}dx e^{i(k_F-k)x}\left(\frac{R}{2\pi}\right)^{2\sinh^2\varphi}\frac{1}{x+i\delta}\left(\frac{1}{x^2+\delta^2}\right)^{\sinh^2\varphi}, \quad (2.135)$$

où $\delta=-R/2\pi$. Ce choix de δ assure que $n(k_F)=1/2$. En utilisant la partie principale, on obtient

$$n_R(k)=\frac{1}{2}-\left(\frac{1}{2\pi}\right)^{\cosh 2\varphi}\int_{-\infty}^{+\infty}\frac{\sin(k-k_F)x}{x}\left(\frac{R}{x}\right)^{2\sinh^2\varphi}dx. \quad (2.136)$$

Pour la théorie libre, on retrouve bien $n_R(k)=\theta(k_F-k)$. Pour la théorie en interaction, on pose $u=x(k-k_F)$, et l'on obtient qu'au voisinage de la surface de Fermi,

$$n_R(k)-\frac{1}{2}\propto(k-k_F)^{2\sinh^2\varphi}. \quad (2.137)$$

En comparant (2.131) et (2.137), on voit que les mêmes échelles d'énergie d'interaction interviennent dans la catastrophe d'orthogonalité et dans l'absence de surface de Fermi. Nous avons donc mis en évidence un mécanisme qui brise le caractère *liquide de Fermi* à une dimension: la catastrophe d'orthogonalité. Nous verrons dans le chapitre 4 un second mécanisme qui intervient en taille finie et au niveau dynamique: la destruction de la quasiparticule par interférences destructives.

2.7 Séparation du spin et de la charge

2.7.1 Le modèle

En présence de spin 1/2, il apparaît une interaction supplémentaire: l'interaction g_1, qui correspond à une diffusion en arrière, avec un transfert d'impulsion de l'ordre de $2k_F$. Le vertex

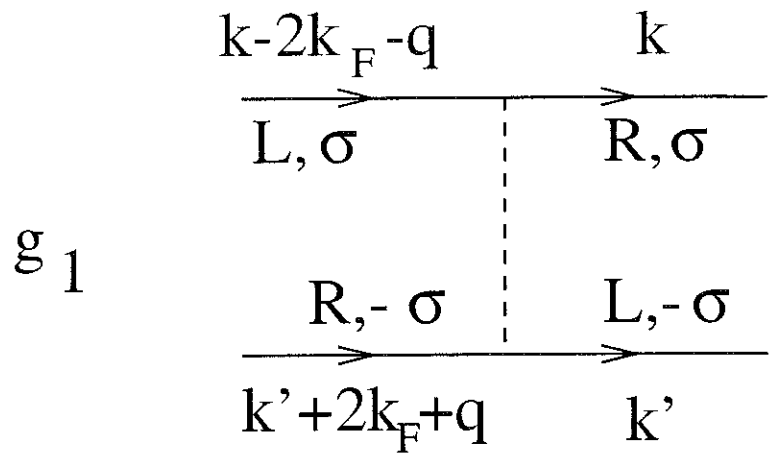

Figure 2.11: Vertex de l'interaction g_1.

correspondant est dessiné sur la figure 2.11. Cette interaction ne s'écrit pas sous forme d'une interaction densité-densité et n'est donc pas intégrable. Cependant, il est possible de la traiter à l'aide du *poor man scaling*[8], et de montrer qu'il existe un domaine dans lequel g_1 est irrelevant. Nous nous plaçons dans ce cas, et nous pouvons donc oublier le terme g_1 et le modèle devient intégrable. De plus, on ne traite que la branche droite avec des interactions g_4. Pour un modèle à une branche, on peut également utiliser la transformation de bosonisation. Comme dans le cas à deux branches, on peut montrer la complétude de la base bosonisée. On note $\rho_{q,\sigma}$ les opérateurs de densité pour un spin σ. Alors, le terme d'interaction H^4 s'écrit

$$H^4 = \frac{\pi g_4}{L} \sum_{q>0,\sigma} \rho_{q,\sigma}\rho_{q,-\sigma}. \tag{2.138}$$

On a pris une interaction locale. Afin de diagonaliser $H^0 + H^4$, on passe aux combinaisons de charge et spin:

$$\rho_q^+ = \left(\frac{\pi}{Lq}\right)^{1/2} (\rho_{q\uparrow} + \rho_{q\downarrow}) \tag{2.139}$$

$$\sigma_q^+ = \left(\frac{\pi}{Lq}\right)^{1/2} (\rho_{q\uparrow} - \rho_{q\downarrow}). \tag{2.140}$$

Les combinaisons de charge et spin vérifient $\left[\rho_q, \rho_{q'}^+\right] = \left[\sigma_q, \sigma_{q'}^+\right] = \delta_{q,q'}$. Le Hamiltonien devient

$$H = v_\rho \sum_{q>0} q\rho_q^+\rho_q + v_\sigma \sum_{q>0} q\sigma_q^+\sigma_q + \frac{\pi}{2L}(v_\rho N^2 + v_\sigma J^2). \tag{2.141}$$

où les vitesses de charge et de spin sont données par $v_\rho = v_F + g_4$ et $v_\sigma = v_F - g_4$ et $N = N_\uparrow + N_\downarrow$, $J = N_\uparrow - N_\downarrow$. Le Hamiltonien est donc diagonal en terme des variables de spin et de charge, avec des vitesses de propagation différentes pour les deux types d'excitations. De cette propriété découle l'existence d'une *séparation du spin et de la charge*. Nous allons illustrer cette propriété

[8] L'application de cette technique au modèles de fermions unidimensionnels est exposée dans l'article de revue de J. Solyom: *The Fermi gas model of one-dimensional conductors*, Adv. in Physics, 28,201-303 (1979)

de deux façons différentes: tout d'abord en calculant la fonction de corrélation à deux points, puis en étudiant la propagation d'un paquet d'ondes gaussien[9].

2.7.2 Fonction de corrélation à deux points

Nous ne reproduisons pas les détails du calcul de la fonction de corrélation puisque nous avons déjà exposé les techniques de calcul. Le résultat est:

$$\begin{aligned} G_{\uparrow>}(x,t) &= -i\langle 0,0|e^{iHt}\psi_\uparrow(x)e^{-iHt}\psi_\uparrow^+(0)|0,0\rangle \\ &= \frac{1}{2L}e^{ik_F x}\frac{1}{\sqrt{\sin\left(\frac{\pi}{L}(x-v_\rho t)\right)}}\frac{1}{\sqrt{\sin\left(\frac{\pi}{L}(x-v_\sigma t)\right)}}. \end{aligned} \tag{2.142}$$

A la limite thermodynamique, $x \ll L$ et $v_\rho t, v_\sigma t \ll L$, de sorte que la fonction de corrélation à la limite thermodynamique vaut

$$G_{\uparrow>}(x,t) = \frac{1}{2\pi}e^{ik_F x}\frac{1}{\sqrt{x-v_\rho t}}\frac{1}{\sqrt{x-v_\sigma t}}. \tag{2.143}$$

Ces relations appellent plusieurs remarques. La fonction de corrélation (2.143) possède deux singularités: une pour la charge et une pour le spin. Il s'agit bien là d'une brisure du caractère *liquide de Fermi*, qui se manifeste au niveau dynamique, pour des temps suffisamment longs comparés à x/g_4. Il convient également de noter qu'il n'apparaît pas de catastrophe d'orthogonalité dans ce système à une branche, puisqu'il n'y a pas de rotation de Bogoliubov. Nous avons donc un troisième mécanisme de brisure du liquide de Fermi, qui, tout comme la catastrophe d'orthogonalité ou la destruction du paquet d'ondes par interférences destructives, respecte l'intégrabilité.

2.7.3 Propagation d'un paquet d'ondes gaussien

Nous allons maintenant propager un paquet d'ondes gaussien soumis à la séparation du spin et de la charge. On choisit $k_F = 0$ dans la suite pour simplifier. Dans un premier temps, nous propageons le paquet d'ondes sans interactions. Ensuite, nous propagerons le paquet d'ondes en présence d'interactions. A l'instant initial, le paquet d'ondes est constitué de spins $\uparrow$, possède une largeur Δ dans l'espace de Fourier, telle que $\Delta \gg 2\pi v_F/L$. Le paquet d'ondes est centré autour de k_0, que l'on suppose très grand devant $2\pi v_F/L$, ce qui permet de supposer que le paquet d'ondes est formé uniquement d'états de type 'particule'. L'état quantique du paquet d'ondes à l'instant initial est donc

$$|\psi_0\rangle = \left(\frac{2}{L\Delta}\right)^{1/2}\pi^{1/4}\sum_{k>0}\exp\left(-\frac{(k-k_0)^2}{2\Delta^2}\right)c_{k\uparrow}^+|0,0\rangle. \tag{2.144}$$

Cet état est normé. Pour propager (2.144), on utilise la représentation de Heisenberg de l'opérateur c_k^+ et, comme la relation de dispersion est linéaire, le paquet d'ondes ne s'étale pas:

$$\psi_\uparrow(x,t) = \psi_\uparrow^0(x-v_F t). \tag{2.145}$$

[9]Pour une étude plus détaillée de la séparation du spin et de la charge, nous renvoyons le lecteur à l'article de J. Voit *Charge-spin separation and the spectral properties of Luttinger liquids*, Phys. Rev. B 47, 6740-6743 (1993)

Nous allons maintenant analyser la propagation du paquet d'ondes dans le milieu en interaction. En utilisant la représentation du champ fermionique $\psi_\uparrow^+(x)$ en terme des modes de charge et de spin, puis en utilisant la représentation de Heisenberg, nous obtenons

$$|\psi_{0\uparrow}(t)\rangle = \left(\frac{2}{L\Delta}\right)^{1/2} \pi^{1/4} \int_{-L/2}^{L/2} \frac{dy}{L} \sum_{k>0} e^{-\frac{(k-k_0)^2}{2\Delta^2}} e^{-iky} e^{-i\frac{\pi y}{L}} \tag{2.146}$$
$$\exp\left(\frac{1}{\sqrt{2}} \sum_{q>0} \left(\frac{2\pi}{Lq}\right)^{1/2} e^{-iq(y-v_\rho t)} \rho_q^+\right) \exp\left(\frac{1}{\sqrt{2}} \sum_{q>0} \left(\frac{2\pi}{Lq}\right)^{1/2} e^{-iq(y-v_\sigma t)} \sigma_q^+\right) U_\uparrow |0,0\rangle.$$

On désire calculer le recouvrement $\langle x\uparrow|\psi_\uparrow(t)\rangle$. Pour cela, nous écrivons $|x\uparrow\rangle = \psi_\uparrow^+(x)|0,0\rangle$ et nous développons $\psi_\uparrow^+(x)$ en fonction des modes de charge et de spin. Le recouvrement s'écrit finalement

$$\begin{aligned}\langle x\uparrow|\psi_\uparrow(t)\rangle &= \left(\frac{2}{\Delta}\right)^{1/2} \frac{\pi^{1/4}}{L} \int_{-L/2}^{L/2} \frac{dy}{L} \sum_{k>0} e^{-iky} e^{-\frac{(k-k_0)^2}{2\Delta^2}} e^{-i\pi\frac{y-x}{L}} \\ &\exp\left(\sum_{q>0} \left(\frac{\pi}{Lq}\right) e^{-iq(y-x-v_\rho t)}\right) \exp\left(\sum_{q>0} \left(\frac{\pi}{Lq}\right) e^{-iq(y-x-v_\sigma t)}\right).\end{aligned} \tag{2.147}$$

Les sommations sur q peuvent s'effectuer explicitement pour obtenir

$$\begin{aligned}\psi_\uparrow(x,t) &= \frac{i\Delta^{1/2}}{2\pi^{1/4}} e^{-2i\pi\frac{x}{L}} \int_{-L/2}^{L/2} \frac{dy}{L} e^{-i\left(k_0-\frac{\pi}{L}\right)y} e^{i\frac{2\pi}{L}v_F t} e^{-\frac{\Delta^2 y^2}{2}} \\ &\frac{1}{\left(\sin\frac{\pi}{L}(y-x-v_\rho t)\right)^{1/2}} \frac{1}{\left(\sin\frac{\pi}{L}(y-x-v_\sigma t)\right)^{1/2}}.\end{aligned} \tag{2.148}$$

L'expression (2.148) est une convolution du paquet d'ondes gaussien par la fonction de Green (2.142). Comme la fonction de Green présente deux singularités intégrables, le paquet d'ondes se scinde en deux composantes approximativement gaussiennes localisées en $x + v_\rho t$ et $x + v_\sigma t$.

2.8 Liens avec les théories de chaînes de spin

Nous présentons deux points communs entre la théorie du liquide de Luttinger et les théories et chaînes de spin[10]. Nous montrons tout d'abord que le mécanisme qui déstabilise l'ordre de Néel à une dimension est analogue au phénomène de catastrophe d'orthogonalité dans le liquide de Luttinger sans spin en interaction. D'autre part, nous montrons comment la théorie de la chaîne de spins 1/2 s'exprime en terme de liquide de Luttinger. L'analogie entre les théories de chaînes de spin et la théorie du liquide de Luttinger est que dans le deux cas, les théories effectives à basse énergie sont critiques bidimensionnelles pour certaines valeurs du spin. Pour certaines valeurs du spin, les théories de chaînes de spin admettent donc une théorie conforme à la limite infrarouge, mais dont la charge centrale est différente de celle du liquide de Luttinger (qui vaut 1)[11].

[10] Pour une revue sur les chaînes de spin, voir I. Affleck, *Quantum spin chains and the Haldane gap*, J. Phys. 1, 3047-3072 (1989). On peut aussi se reporter au chapitre 4 du livre de E. Fradkin *Field theories of condensed matter*, Frontiers in Physics, Addison-Wesley Publishing Compagny (1991).

[11] Pour une étude de la chaîne de spins 1/2 en termes de bosonisation non abélienne, se reporter à I. Affleck, *Critical behaviour of two dimensional systems with continuous symmetries*, Phys. Rev. Lett. 55, 1355-1358

2.8.1 Ondes de spin

On part d'un Hamiltonien de Heisenberg pour des spins quantiques antiferromagnétiques localisés sur un réseau euclidien en dimension d:

$$H = J \sum_{\langle i,j \rangle} \mathbf{S}_i . \mathbf{S}_j = J \sum_{\langle i,j \rangle} \left(\frac{1}{2}(S_i^+ S_j^- + S_i^- S_j^+) + S_i^z S_j^z \right), \tag{2.149}$$

où les spins obéissent à l'algèbre de spin usuelle $\left[\mathbf{S}^a, \mathbf{S}^b\right] = i\epsilon^{abc}\mathbf{S}^c$, avec $\mathbf{S}^2 = s(s+1)$. Dans la limite semi classique, le spin s est supposé grand et on utilise la représentation en terme de bosons de Holstein et Primakov. Sur le sous réseau A,

$$S^- = \sqrt{2s} a^+ \left(1 - \frac{a^+ a}{2s}\right)^{1/2} \tag{2.150}$$

$$S^+ = \sqrt{2s} \left(1 - \frac{a^+ a}{2s}\right)^{1/2} a \tag{2.151}$$

$$S^z = s - a^+ a, \tag{2.152}$$

où $[a, a^+] = 1$ On peut vérifier qu'il s'agit bien d'une algèbre de spins. Sur le sous réseau B, on utilise la représentation

$$S^- = \sqrt{2s} \left(1 - \frac{b^+ b}{2s}\right)^{1/2} b \tag{2.153}$$

$$S^+ = \sqrt{2s} b^+ \left(1 - \frac{b^+ b}{2s}\right)^{1/2} \tag{2.154}$$

$$S^z = -s + b^+ b, \tag{2.155}$$

où $[b, b^+] = 1$ Dans la limite où s est grand, on utilise les approximations suivantes: sur le sous réseau A, $S^- \simeq \sqrt{2s} a^+$, $S^+ \simeq \sqrt{2s} a$ et sur le sous réseau B, $S^- \simeq \sqrt{2s} b$ et $S^+ \simeq \sqrt{2s} b^+$. Le Hamiltonien à l'ordre s devient

$$H = J \sum_{\langle \mathbf{x},\mathbf{y} \rangle} -s^2 + s \left(a_\mathbf{x} b_\mathbf{y} + a_\mathbf{x}^+ b_\mathbf{y}^+ + a_\mathbf{x}^+ a_\mathbf{y} + b_\mathbf{y}^+ b_\mathbf{y} \right). \tag{2.156}$$

En utilisant les modes de Fourier

$$a_\mathbf{x}^+ = \sqrt{\frac{2}{N}} \sum_\mathbf{k} e^{i\mathbf{k}.\mathbf{x}} a_\mathbf{k}^+, \tag{2.157}$$

le Hamiltonien prend la forme

$$H = 2Jsd \sum_\mathbf{k} \left(\gamma_\mathbf{k} \left(a_\mathbf{k} b_{-\mathbf{k}} + a_\mathbf{k}^+ b_{-\mathbf{k}}^+ \right) + \left(a_\mathbf{k}^+ a_\mathbf{k} + b_\mathbf{k}^+ b_\mathbf{k} \right) \right), \tag{2.158}$$

(1985). Pour une généralisation à des spins quelconques, voir I. Affleck and F.D.M. Haldane, *Critical theory of quantum spin chains*, Phys. Rev. B 36, 5291-5300 (1987).

où

$$\gamma_{\mathbf{k}} = \frac{1}{2d}\sum_{\delta} e^{i\mathbf{k}.\delta}. \tag{2.159}$$

Cette forme de Hamiltonien est similaire à (2.106) et se diagonalise par la même technique. On pose

$$c_{\mathbf{k}} = \cosh\varphi_{\mathbf{k}} a_{\mathbf{k}} - \sinh\varphi_{\mathbf{k}} b^{+}_{-\mathbf{k}} \tag{2.160}$$

$$d_{\mathbf{k}} = \cosh\varphi_{\mathbf{k}} b_{\mathbf{k}} - \sinh\varphi_{\mathbf{k}} a^{+}_{-\mathbf{k}}. \tag{2.161}$$

Le Hamiltonien est diagonal en terme de bosons c et d à condition que $\gamma_{\mathbf{k}} = -\tanh(2\varphi_{\mathbf{k}})$. On a alors

$$H = \sum_{\mathbf{k}} \omega_{\mathbf{k}} \left(c^{+}_{\mathbf{k}} c_{\mathbf{k}} + d^{+}_{\mathbf{k}} d_{\mathbf{k}} \right), \tag{2.162}$$

où la relation de dispersion vaut $\omega_{\mathbf{k}} = 2Jd(1-\gamma_{\mathbf{k}})^{1/2}$. La dispersion est relativiste à la limite infrarouge: $\omega_{\mathbf{k}} \sim 2d^{1/2}Js|\mathrm{k}|$ si $\mathrm{k} \to 0$. Il n'existe pas de gap à cause de la présence des modes de Goldstone c et d. Le fondamental est donné par une expression analogue à (2.112):

$$|GS\rangle = \prod_{\mathbf{k}} \left(\frac{1}{\cosh\varphi_{\mathbf{k}}} \right) \exp\left(\sum_{\mathbf{k}} \tanh\varphi_{\mathbf{k}} a^{+}_{\mathbf{k}} b^{+}_{-\mathbf{k}} \right) |0\rangle. \tag{2.163}$$

Nous sommes maintenant en mesure de calculer la correction à l'aimantation d'un site du sous réseau A

$$\langle \Delta S^z \rangle = -\frac{2}{N}\sum_{\mathbf{k}} \langle a^{+}_{\mathbf{k}} a_{\mathbf{k}} \rangle. \tag{2.164}$$

Pour cela, on établit d'abord que

$$\langle a^{+}_{\mathbf{k}} a_{\mathbf{k}} \rangle = \tanh^2\varphi_{\mathbf{k}} \left(\langle b^{+}_{\mathbf{k}} b_{\mathbf{k}} \rangle + 1 \right). \tag{2.165}$$

A cause de l'invariance par échange des réseaux A et B (on suppose un nombre pair de sites), $\langle a^{+}_{\mathbf{k}} a_{\mathbf{k}} \rangle = \langle b^{+}_{\mathbf{k}} b_{\mathbf{k}} \rangle$, et donc

$$\langle \Delta S^z \rangle = -\frac{1}{2}\int \frac{d\mathrm{k}}{(2\pi)^d} \left((1-\gamma^2_{\mathbf{k}})^{-1/2} - 1 \right). \tag{2.166}$$

A une dimension, la correction $\langle \Delta S^z \rangle$ diverge logarithmiquement dans l'infrarouge. A une dimension, l'état de Néel est instable vis-à-vis des fluctuations quantiques. Cette instabilité est dûe au fait que l'état fondamental (2.163) contient une infinité de bosons de type a et b. C'est également la raison pour laquelle la fonction de Green du liquide de Luttinger est nulle à la limite thermodynamique.

2.8.2 Chaîne de spin 1/2

Dans le cas de la chaîne de spins 1/2, il est possible d'effectuer une transformation de Jordan-Wigner qui fermionise la chaîne de spins. On appelle *kink* l'opérateur

$$K_n = \exp\left(i\pi \sum_{i=1}^{n-1} S^{+}_i S^{-}_i \right). \tag{2.167}$$

On définit alors $c_n = K_n S_n^-$, qui vérifie $(c_n^+)^2 = (c_n)^2 = 0$, $\{c_n^+, c_m\} = \delta_{m,n}$ et $\{c_n, c_m\} = \{c_n^+, c_m^+\} = 0$. Les opérateurs c sont donc de nature fermionique. Le Hamiltonien de Heisenberg est généralisé au cas d'une anisotropie γ

$$H = J \sum_{i=1}^{n} \left(\frac{1}{2}(S_i^+ S_{i+1}^- + S_i^- S_{i+1}^+) + \gamma S_i^z S_{i+1}^z \right). \tag{2.168}$$

En terme des fermions, le Hamiltonien s'écrit

$$H = J \sum_{i=1}^{n} (c_i^+ c_{i+1} + c_{i+1}^+ c_i) + \gamma J \sum_{i=1}^{n} (n_i - \frac{1}{2})(n_{i+1} - \frac{1}{2}), \tag{2.169}$$

où $n_i = c_i^+ c_i$. Le terme XY peut être diagonalisé par transformation de Fourier:

$$H_{XY} = \int \frac{dk}{2\pi} \omega_k c_k^+ c_k, \tag{2.170}$$

où $\omega_k = J \cos k$. Le terme d'Ising est alors une interaction pour le gaz de fermions de Jordan-Wigner. La différence avec le cas du liquide de Luttinger que l'on vient de traiter est l'existence d'un réseau et donc l'apparition de processus umklapp. Après bosonisation, les interactions contiennent une interaction courant-courant ainsi qu'un terme de sine-Gordon. On peut montrer par renormalisation que pour $\gamma < 1$, l'interaction de sine-Gordon est non relevante et la chaîne de spins est dans le régime XY. Le domaine $\gamma \leq 1$ est une ligne de points critiques, avec une décroissance algébrique des fonctions de corrélation. Si $\gamma > 1$, il se développe un gap et la chaîne se trouve dans le régime d'Ising.

Chapitre 3

Liquide de Luttinger et boson compactifié

Le but de ce chapitre est d'établir la correspondance entre la théorie du liquide de Luttinger à la limite infrarouge et la théorie du champ bosonique compactifié. Dans un premier temps, nous revenons sur la théorie du gaz de fermions libres avec une relation de dispersion linéaire, qui n'est autre que la théorie de Dirac bidimensionnelle. Nous analysons dans la section 3.1 les symétries classiques et la section 3.2 est dédiée au calcul des fonctions de partition dans les différents secteurs. Nous calculons ensuite les fonctions de partition du boson compactifié (section 3.3) puis nous identifions la théorie de Dirac et le boson compactifié à la section 3.4. L'identification se fait au niveau d'égalités entre fonctions de partition.

3.1 Théorie de Dirac bidimensionnelle classique

3.1.1 Action et formalisme Hamiltonien

Nous décrivons la théorie de Dirac sur un cylindre muni de la métrique $ds^2 = v_F^2 dt^2 - dx^2$, où x est périodique modulo $L = 2\pi$. Nous avons introduit une vitesse de Fermi v_F pour les besoins d'une future identification de la théorie de Dirac à la théorie du gaz de Luttinger. Les matrices γ sont définies par

$$\gamma^0 = \begin{pmatrix} 0 & 1 \\ 1 & 0 \end{pmatrix} = \sigma_1 \ , \gamma^1 = \begin{pmatrix} 0 & -1 \\ 1 & 0 \end{pmatrix} = i\sigma_2, \tag{3.1}$$

qui vérifient $\{\gamma^\mu, \gamma^\nu\} = 2\eta^{\mu\nu}$ avec

$$\eta^{\mu\nu} = \begin{pmatrix} 1 & 0 \\ 0 & -1 \end{pmatrix} = \sigma_3. \tag{3.2}$$

De même que pour la théorie de Dirac en dimension 4, l'action vaut

$$S[\psi] = i \int dx dt \left(\overline{\psi} \gamma^0 \partial_0 \psi + v_F \overline{\psi} \gamma^1 \partial_1 \psi \right), \tag{3.3}$$

où le spineur ψ vaut

$$\psi = \begin{pmatrix} \psi_L \\ \psi_R \end{pmatrix}, \tag{3.4}$$

et $\overline{\psi} = \psi^+\gamma^0 = (\psi_R^+, \psi_L^+)$. Comme pour le liquide de Luttinger, l'indice R désigne la droite et L la gauche. En introduisant les coordonées du cône de lumière $x^\pm = t \pm x/v_F$ et $\partial_\pm = (\partial_0 \pm v_F\partial_1)/2$, l'action prend la forme

$$S[\psi] = iv_F \int dx^+ dx^- \left(\psi_R^+ \partial_- \psi_R + \psi_L^+ \partial_+ \psi_L\right). \tag{3.5}$$

Les équations du mouvement s'écrivent $\partial_-\psi_R = 0$ et $\partial_+\psi_L = 0$. Le champ ψ_R dépend uniquement de x_+ et ψ_L dépend uniquement de x_-, ce qui justifie les notations ψ_R et ψ_L. Afin d'écrire une formulation hamiltonienne, nous remarquons que les moments conjugués sont $\Pi_R(x) = i\psi_R^+(x)$ et $\Pi_L(x) = i\psi_L^+(x)$, soit en notation spinorielle $\Pi(x) = i\overline{\psi}(x)\gamma^0$. Le Hamiltonien vaut alors

$$H = iv_F \int dx \left(\psi_R^+(x)\partial_x\psi_R(x) - \psi_L^+(x)\partial_x\psi_L(x)\right). \tag{3.6}$$

Ce n'est autre que le Hamiltonien (2.28) du gaz de Luttinger avec $k_F = 0$.

3.1.2 Symétries

Symétrie globale U(1)

Soient O et O' deux observateurs qui décrivent le champ de deux façons différentes, reliées par

$$\psi_{O'}(x_{O'}) = e^{i\theta}\psi_O(x_O) \tag{3.7}$$

avec $x_{O'} = x_O$ et θ une constante. Les équations du mouvement sont invariantes lors de cette transformation. Le courant de Noether associé à cette symétrie U(1) vaut $J^\mu = \overline{\psi}\gamma^\mu\psi$, et vérifie $\partial_\mu J^\mu = 0$. En coordonnées du cône de lumière, l'équation de conservation s'écrit $\partial_+ J^- + \partial_- J^+ = 0$, avec $J^+ = \psi_L^+\psi_L$ et $J^- = \psi_R^+\psi_R$. Le courant conservé associé à la symétrie globale U(1) correspond donc aux opérateurs de densité (2.38) du liquide de Luttinger (à une constante multiplicative près).

Invariance conforme Minkowskienne

Tout comme le boson libre de masse nulle, le fermion libre de masse nulle possède l'invariance conforme. Soit deux observateurs O et O' qui se déduisent l'un de l'autre par une transformation conforme Minkowskienne: $x_{O'}^+ = f_+(x_O^+)$ et $x_{O'}^- = f_-(x_O^-)$. Les fonctions f_+ et f_- sont C^∞ bijectives. Comme les champs portent un spin non nul, la transformation conforme des coordonnées s'accompagne d'une transformation des champs

$$\psi_O^R(x_O) = \psi_{O'}^R(x_{O'})\left(f_+'(x_O^+)\right)^{1/2} \tag{3.8}$$

$$\psi_O^L(x_O) = \psi_{O'}^L(x_{O'})\left(f_-'(x_O^-)\right)^{1/2}. \tag{3.9}$$

On peut aisément vérifier que les équations du mouvement sont invariantes. L'invariance conforme implique l'existence d'une infinité de quantités conservées. Une transformation conforme Minkowskienne infinitésimale s'exprime comme $x'_\pm = x_\pm + \epsilon\varphi_\pm(x_\pm)$, et les courant conservés s'écrivent

$$J[\varphi_+]_\pm = T_{\pm+}(x_+, x_-)\varphi_+(x_+) \tag{3.10}$$

$$J[\varphi_-]_\pm = T_{\pm-}(x_+, x_-)\varphi_-(x_-), \tag{3.11}$$

où les composantes du tenseur énergie impulsion sont

$$T_{\mu\nu} = \frac{\partial L}{\partial(\partial_\mu \psi)}\partial_\nu \psi - \eta_{\mu\nu} L = i\overline{\psi}\gamma_\mu \partial_\nu \psi - \eta_{\mu\nu} i\overline{\psi}\gamma^\rho \partial_\rho \psi. \tag{3.12}$$

A des coefficients multiplicatifs près, on obtient, en coordonées du cône de lumière:

$$T_{++} = i\psi_R^+ \partial_+ \psi_R \tag{3.13}$$
$$T_{--} = i\psi_L^+ \partial_- \psi_L \tag{3.14}$$
$$T_{+-} = T_{-+} = 0. \tag{3.15}$$

Comme $T_{00} = T_{++} + T_{+-} + T_{-+} + T_{--} = T_{++} + T_{--}$, nous avons

$$T_{00} = i\left(\psi_R^+ \partial_+ \psi_R + \psi_L^+ \partial_- \psi_L\right), \tag{3.16}$$

et on retrouve donc $H = \int T_{00} dx$.

3.1.3 Conditions au bord pour les fermions

Pour prendre une trace sur l'espace des états fermioniques, avec des conditions aux limites périodiques ou antipériodiques, on est amené à prendre des conditions aux limites antipériodiques dans la direction temporelle. Or, dès que l'on prend des conditions aux limites différentes de PP (périodiques dans les deux directions), on est forcé de considérer tous les jeux de conditions aux limites possibles par transformation modulaire. Nous montrerons que la théorie du boson libre compactifié a la même fonction de partition sur le tore que la théorie fermionique, mais à condition de sommer sur les quatres secteurs de la théorie fermionique.

Pour les conditions aux limites périodiques, $\psi_\alpha(x + 2\pi) = \psi_\alpha(x)$, et la décomposition en modes s'écrit

$$\psi_\alpha(x) = \frac{1}{\sqrt{2\pi}} \sum_{n=-\infty}^{+\infty} e^{inx} c_{n,\alpha}. \tag{3.17}$$

L'indice α désigne la branche, avec la convention $\alpha = 1 = R$ et $\alpha = -1 = L$. Avec des conditions aux limites antipériodiques, $\psi_\alpha(x + 2\pi) = -\psi_\alpha(x)$ et la décomposition en modes s'écrit

$$\psi_\alpha(x) = \frac{1}{\sqrt{2\pi}} \sum_{n=-\infty}^{+\infty} e^{i(n+\frac{1}{2})x} c_{n+1/2,\alpha}. \tag{3.18}$$

Les modes $c_{n,\alpha}$ sont les coordonnées du champ au niveau classique. Au niveau quantique, ce sont les opérateurs de destruction de fermions dans le mode n, analogues des opérateurs introduits au chapitre 2.

3.2 Quantification canonique de la théorie de Dirac bidimensionelle

3.2.1 Algèbre fermionique, Hamiltonien et opérateur impulsion

Au niveau classique, le coordonnées du champ sont les $\psi_\alpha(x)$ et les moments conjugués sont $i\psi_\alpha^+(x)$. Les règles de quantification canonique pour les fermions donnent donc les anticommutations fermioniques usuelles

$$\{\hat{\psi}_\alpha(x), \hat{\psi}_{\alpha'}(x')\} = 0 \tag{3.19}$$

$$\{\hat{\psi}^+_\alpha(x), \hat{\psi}^+_{\alpha'}(x')\} = 0 \tag{3.20}$$
$$\{\hat{\psi}^+_\alpha(x), \hat{\psi}_{\alpha'}(x')\} = \delta_{\alpha,\alpha'}\delta(x-x'). \tag{3.21}$$

Les modes sont définis par

$$\hat{\psi}_\alpha(x) = \frac{1}{\sqrt{2\pi}} \sum_n e^{inx} \hat{c}_{n,\alpha}, \tag{3.22}$$

où n est entier pour des conditions aux limites périodiques et demi entier pour des conditions aux limites antipériodiques. Cette définition des opérateurs de champ est identique à (2.23). En terme de modes, les relations de commutation canoniques s'écrivent

$$\{\hat{c}_{n,\alpha}, \hat{c}_{m,\alpha'}\} = \{\hat{c}^+_{n,\alpha}, \hat{c}^+_{m,\alpha'}\} = 0 \tag{3.23}$$
$$\{\hat{c}^+_{n,\alpha}, \hat{c}_{m,\alpha'}\} = \delta_{\alpha,\alpha'}\delta_{n,m}. \tag{3.24}$$

Le vide est choisi comme dans le chapitre 2: les états sous la surface de Fermi sont remplis et les états au-dessus de la surface de Fermi sont inoccupés. Cette définition conduisait à un vide unique car seul le secteur antipériodique était considéré. Cependant, il subsiste une ambiguité dans le secteur périodique. En effet, dans ce secteur, le vide est quatre fois dégénéré. Sur chaque branche, on peut choisir de placer électron sur la surface de Fermi ($k_F = 0$) ou choisir de placer un trou sur la surface de Fermi. Ces 4 vides possibles possèdent la même énergie et la même impulsion. Nous devons donc tenir compte de l'existence d'un vide quatre fois dégénéré dans le secteur périodique.

Afin de symétriser les deux branches, nous notons $\hat{b}^+_{n,R} = \hat{c}^+_{n,R}$ et $\hat{b}^+_{n,L} = \hat{c}^+_{-n,L}$, de telle sorte que le Hamiltonien vaut

$$\hat{H} = \sum_n n \left(:\hat{b}^+_{n,R}\hat{b}_{n,R}: + :\hat{b}^+_{n,L}\hat{b}_{n,L}: \right). \tag{3.25}$$

La prescription d'ordre normal est la même que celle du chapitre 2. Nous notons également $\hat{N}_{n,\alpha} = \hat{b}^+_{n,\alpha}\hat{b}_{n,\alpha}$ pour $n > 0$ et $\hat{N}_{n,\alpha} = \hat{b}_{n,\alpha}\hat{b}^+_{n,\alpha}$ pour $n < 0$. Avec ces notations, le Hamiltonien devient

$$\hat{H} = v_F \sum_n |n|(N_{n,R} + N_{n,L}) - 2v_F \sum_{n>0} n. \tag{3.26}$$

Le facteur 2 provient de l'existence de deux branches droite et gauche. Afin de donner un sens à la somme

$$\sum_{n>0} n, \tag{3.27}$$

nous utilisons la renormalisation ζ[1], qui permet d'attribuer des valeurs finies à des sommes a priori divergentes:

$$\zeta_0 = \sum_{n>0} n = -\frac{1}{12} \tag{3.28}$$
$$\zeta_{1/2} = \sum_{n>0}(n + \frac{1}{2}) = \frac{1}{24}. \tag{3.29}$$

[1]Pour une introduction à la renormalisation ζ, se référer au cours de P. Cartier dans *From number theory to physics*, M. Waldschmidt, P. Moussa, J.M. Luck, C. Itzykson Ed., Springer-Verlag (1989).

Le Hamiltonien est maintenant entièrement déterminé dans chaque secteur:

$$\hat{H}_P = v_F \left(\sum_n |n|(N_{n,R} + N_{n,L}) + \frac{1}{6} \right) \tag{3.30}$$

$$\hat{H}_A = v_F \left(\sum_n |n|(N_{n,R} + N_{n,L}) - \frac{1}{12} \right). \tag{3.31}$$

L'opérateur impulsion ne dépend pas du choix du schéma de renormalisation et nous retrouvons l'expression (2.22)

$$\hat{P} = \sum_n |n|(N_{n,R} - N_{n,L}). \tag{3.32}$$

Dans la suite, nous utiliserons les notations

$$\hat{L}_0^R = \sum_n |n| \hat{N}_{n,R} + h \tag{3.33}$$

$$\hat{L}_0^L = \sum_n |n| \hat{N}_n^L + h, \tag{3.34}$$

où $h = 0$ dans le secteur périodique et $h = 1/8$ dans le secteur antipériodique, de sorte que

$$\hat{H} = v_F \left(\hat{L}_0^R + \hat{L}_0^L - \frac{1}{12} \right) \tag{3.35}$$

$$\hat{P} = \hat{L}_0^R - \hat{L}_0^L. \tag{3.36}$$

3.2.2 Fonctions de partition à température finie

A partir de maintenant, les quantités auxquelles nous nous intéressons sont différentes de celles étudiées au chapitre 2. Nous cherchons à évaluer les fonctions de partition

$$Z_P = \mathrm{Tr}_P \left(e^{-\beta \hat{H}_P} e^{i\theta \hat{P}_P} \right) \tag{3.37}$$

$$Z_A = \mathrm{Tr}_A \left(e^{-\beta \hat{H}_A} e^{i\theta \hat{P}_A} \right) \tag{3.38}$$

dans les secteurs périodiques et antipériodiques respectivement. Nous notons

$$\tau = \frac{1}{2\pi} (\theta + i\beta v_F), \tag{3.39}$$

et $q = \exp(2i\pi\tau)$, $\overline{q} = \exp(-2i\pi\overline{\tau})$. Avec ces notations, ainsi que (3.33) et (3.34), les fonctions de partition s'expriment comme

$$Z = \mathrm{Tr} \left(q^{\hat{L}_0^R - \frac{1}{24}} \overline{q}^{\hat{L}_0^L - \frac{1}{24}} \right). \tag{3.40}$$

On peut effectuer explicitement le calcul des traces dans chaque secteur pour obtenir

$$Z_{AA} = (q\overline{q})^{-1/24} \left| \prod_{n=0}^{+\infty} (1 + q^{n+1/2})^2 \right|^2 \tag{3.41}$$

$$Z_{PA} = 4(q\overline{q})^{-1/24} \left| q^{1/8} \prod_{n=1}^{+\infty} (1 + q^n)^2 \right|^2, \tag{3.42}$$

où 'PA' ('AA') signifie 'conditions aux limite (anti)périodiques spatiales et antipériodiques selon l'axe du temps'. Le préfacteur 4 dans (3.42) provient du fait qu'il existe 4 vides dégénérés dans le secteur périodique. Afin de prendre des conditions aux limites périodiques dans la direction temporelle, nous notons

$$(-1)^{\hat{F}} = (-1)^{\sum_n \hat{N}_{n,R}+\hat{N}_{n,L}}. \tag{3.43}$$

Les fonctions de partition périodiques en temps s'écrivent

$$Z_{AP} = \mathrm{Tr}_A\left((-1)^{\hat{F}} e^{-\beta \hat{H}_A} e^{i\theta \hat{P}_A}\right) = (q\bar{q})^{-1/24} \left|\prod_{n=0}^{+\infty}(1-q^{n+1/2})^2\right|^2 \tag{3.44}$$

$$Z_{PP} = \mathrm{Tr}_P\left((-1)^{\hat{F}} e^{-\beta \hat{H}_P} e^{i\theta \hat{P}_P}\right) = 0. \tag{3.45}$$

L'égalité (3.45) s'explique par le fait que dans le secteur doublement périodique, à chaque état qui possède un fermion sur un des points de la surface de Fermi correspond un état qui ne possède pas ce fermion. La contribution de ces deux états s'annule lorque l'on prend la trace. Nous utilisons maintenant l'identité du triple produit de Jacobi (2.50) que nous rappelons ici:

$$\sum_{n=-\infty}^{+\infty} y^n q^{n^2/2} = \prod_{n=1}^{+\infty}(1-q^n)\prod_{n=0}^{+\infty}(1+yq^{n+1/2})(1+y^{-1}q^{n+1/2}). \tag{3.46}$$

En spécialisant (3.46) au cas $y=1$, $y=q^{1/2}$ et $y=-1$, nous obtenons respectivement

$$Z_{AA} = \frac{1}{|\eta(q)|^2}\left|\sum_{n=-\infty}^{+\infty} q^{\frac{1}{2}n^2}\right|^2 \tag{3.47}$$

$$Z_{PA} = \frac{1}{|\eta(q)|^2}\left|\sum_{n=-\infty}^{+\infty} q^{\frac{1}{2}(n+\frac{1}{2})^2}\right|^2 \tag{3.48}$$

$$Z_{AP} = \frac{1}{|\eta(q)|^2}\left|\sum_{n=-\infty}^{+\infty} (-1)^n q^{\frac{1}{2}n^2}\right|^2, \tag{3.49}$$

où $\eta(q)$ est la fonction de Dedekind

$$\eta(q) = q^{\frac{1}{24}}\prod_{n=1}^{+\infty}(1-q^n). \tag{3.50}$$

3.3 Fonctions de partition du boson compactifié

On cherche à calculer la fonction de partition de la théorie du champ bosonique compactifié. On appelle R le rayon de compactification, c'est-à-dire que φ et $\varphi + 2\pi R$ sont identifiés. Nous travaillons sur le tore $\mathbf{T}_\Gamma = \mathbf{C}/\Gamma$ où Γ est le réseau $\Gamma = \omega_1\mathbb{Z} + \omega_2\mathbb{Z}$. L'action sécrit

$$S[\varphi] = \frac{g}{2\pi}\int_{\mathbf{T}_\Gamma} |\nabla\varphi|^2. \tag{3.51}$$

Nous considérons le jeu de conditions aux limite $[\epsilon, \epsilon']$, où $\epsilon = k/N$ et $\epsilon' = k'/N$, définis par les conditions de monodromie

$$\varphi(z+\omega_1) = \varphi(z) + 2\pi R\epsilon \ (2\pi R) \tag{3.52}$$

$$\varphi(z+\omega_2) = \varphi(z) + 2\pi R\epsilon' \ (2\pi R). \tag{3.53}$$

Rappelons que la monodromie compte le nombre de fois que le champ s'enroule autour du cercle lorsque l'on décrit un côté du parallélogramme. Nous voulons calculer la fonction de partition

$$Z_{\epsilon,\epsilon'} = \int_{[\epsilon,\epsilon']} D[\varphi] e^{-S[\varphi]}. \tag{3.54}$$

3.3.1 Instantons

Nous cherchons les solutions instantons avec le choix des conditions aux limites $[\epsilon, \epsilon']$. Tout nombre complexe z s'écrit de manière unique $z = x\omega_1 + t\omega_2$, où $(x,t) \in \mathbb{R}^2$. On note τ le paramètre modulaire du tore: $\tau = \omega_2/\omega_1$. Nous avons alors

$$x = Re\left(\frac{z}{\omega_1}\right) - \frac{Re(\tau)}{Im(\tau)} Im\left(\frac{z}{\omega_1}\right) \tag{3.55}$$

$$t = \frac{Im(z/\omega_1)}{Im(z)}. \tag{3.56}$$

Les instantons sont des solutions classiques, donc des fonctions harmoniques sur le tore avec des conditions aux limites $[\epsilon, \epsilon']$, et donc de la forme

$$\varphi_I(x,t) = 2\pi R\left((n+\epsilon)x + (m+\epsilon')t\right), \tag{3.57}$$

avec $(m,n) \in \mathbb{Z}^2$. La solution (3.57) est la seule de monodromie $(n+\epsilon, m+\epsilon')$. Pour simplifier les notations, nous introduisons $v = 2\pi R(n+\epsilon)$ et $w = 2\pi R(m+\epsilon')$, de sorte que $\varphi_I(x,t) = xv+tw$. L'action d'une configuration (3.57) du champ vaut

$$S[\varphi_I] = \frac{g}{2\pi}\int_{\mathbf{T}_\Gamma} (\nabla\varphi_I)^2 = \frac{2g}{\pi}\int_{D_\Gamma} (\partial_z\varphi_I)(\partial_{\bar z}\varphi_I)\frac{d\bar z \wedge dz}{2i}. \tag{3.58}$$

où D_Γ est une cellule élémentaire du réseau Γ. On calcule immédiatement

$$\partial_z\varphi_I = \frac{1}{2i\omega_1}\left(iv + \frac{w}{Im(\tau)} - \frac{Re(\tau)}{Im(\tau)}v\right) \tag{3.59}$$

$$\partial_{\bar z}\varphi_I = \frac{1}{2i\bar\omega_1}\left(iv - \frac{w}{Im(\tau)} + \frac{Re(\tau)}{Im(\tau)}v\right), \tag{3.60}$$

de sorte que

$$(\partial_z\varphi_I)(\partial_{\bar z}\varphi_I) = \frac{1}{4|\omega_1|^2}\left(\frac{(w - Re(\tau)v)^2}{Im(\tau)^2} + v^2\right). \tag{3.61}$$

Nous pouvons maintenant obtenir l'action d'un instanton de monodromie $(n+\epsilon, m+\epsilon')$ qui vaut

$$S[\varphi_{\epsilon+n,\epsilon'+m}] = 2\pi R^2 g Im(\tau)\left((n+\epsilon)^2 + \left(\frac{m+\epsilon' - Re(\tau)(n+\epsilon)}{Im(\tau)}\right)^2\right). \tag{3.62}$$

3.3.2 Calcul des fonctions de partition

Si φ vérifie des conditions aux limites de type $[\epsilon, \epsilon']$ et si $\varphi_{\epsilon+n,\epsilon'+m}$ est une solution classique de monodromie $(\epsilon+n, \epsilon'+m)$, alors $\phi = \varphi - \varphi_{\epsilon+n,\epsilon'+m}$ n'a pas de monodromie. On en déduit que

$$S[\varphi_{\epsilon+n,\epsilon'+m} + \phi] = S[\phi] + S[\varphi_{\epsilon+n,\epsilon'+m}]. \tag{3.63}$$

On en déduit que la fonction de partition se factorise sous la forme

$$Z_{[\epsilon,\epsilon']}(g,R) = Z_f \sum_{(m,n)\in\mathbb{Z}^2} e^{-S[\varphi_{\epsilon+n,\epsilon'+m}]}. \tag{3.64}$$

Z_f contient les contributions des fluctuations sans monodromie et des modes zéro. Nous calculons maintenant séparément la contribution des instantons et la contribution des fluctuations[2]. Nous commençons par la contribution des instantons. L'idée est d'effectuer une sommation de Poisson pour arranger la contribution des instantons à la fonction de partition. Si f est une fonction L^2 sur $\mathbb{R}$, on définit sa transformée de Fourier

$$(F.f)(y) = \int_{-\infty}^{+\infty} dx e^{2i\pi xy} f(x). \tag{3.65}$$

Alors, la formule sommatoire de Poisson s'écrit

$$\sum_{n=-\infty}^{+\infty} f(n) = \sum_{n=-\infty}^{+\infty} (F.f)(n). \tag{3.66}$$

Nous utilisons (3.66) avec

$$f(x) = \exp\left(-\frac{2\pi R^2 g}{Im(\tau)}\left(x+\epsilon'-Re(\tau)(n+\epsilon)\right)^2\right). \tag{3.67}$$

On montre aisément que

$$(F.f)(y) = e^{2i\pi(\epsilon'-Re(\tau)(n+\epsilon))m}\left(\frac{Im(\tau)}{2R^2 g}\right)^{1/2}\exp\left(-\frac{\pi Im(\tau)}{2R^2 g}y^2\right). \tag{3.68}$$

A l'aide de (3.66), on déduit immédiatement une expression pour la somme sur m dans (3.64), et finalement la contribution des instantons qui vaut

$$\left(\frac{Im(\tau)}{2R^2 g}\right)^{1/2} \sum_{(m,n)\in\mathbb{Z}^2} e^{-2i\pi m\epsilon'} q^{\frac{1}{2}\left((n+\epsilon)R\sqrt{g}+\frac{m}{2R\sqrt{g}}\right)^2} \overline{q}^{\frac{1}{2}\left((n+\epsilon)R\sqrt{g}-\frac{m}{2R\sqrt{g}}\right)^2}. \tag{3.69}$$

Les fluctuations sans monodromie dans (3.64) contribuent au préfacteur seulement, et le calcul est en tout point identique à celui qui est mené dans le cas du champ bosonique libre. Nous trouvons finalement l'expression de la fonction de partition avec des conditions aux limites $[\epsilon,\epsilon']$:

$$Z_{[\epsilon,\epsilon']}(gR^2) = \frac{1}{|\eta(q)|^2} \sum_{\substack{m\in\mathbb{Z}\\ n\in\mathbb{Z}+\epsilon}} e^{-2i\pi m\epsilon'} q^{\frac{1}{2}p^2_{n+\epsilon,m}} \overline{q}^{\frac{1}{2}\overline{p}^2_{n+\epsilon,m}}, \tag{3.70}$$

où

$$p_{n,m} = nR\sqrt{g} + \frac{m}{2R\sqrt{g}} \tag{3.71}$$

$$\overline{p}_{n,m} = nR\sqrt{g} - \frac{m}{2R\sqrt{g}}. \tag{3.72}$$

[2]Ces calculs sont présentés dans les notes de L. Gallot pour des conditions aux limites périodiques, par l'intégrale de chemin et par la quantification canonique. Nous nous concentrons surtout sur la partie 'instantons' qui dépend explicitement de ϵ et ϵ'. Les fluctuations sans monodromie contribuent seulement au préfacteur qui est le même que pour le champ bosonique libre.

3.4 Théorie de Dirac et boson compactifié

3.4.1 Somme sur les quatre secteurs

La somme des fonctions de partition sur le quatre secteurs est évidemment invariante modulaire. Nous notons

$$Z_{Dirac} = \frac{1}{2}\left(Z_{AA} + Z_{AP} + Z_{PA} + Z_{PP}\right). \tag{3.73}$$

Cette somme vaut explicitement

$$Z_{Dirac} = \frac{1}{|\eta(q)|^2}\left(\sum_{\substack{(m,\overline{m})\in\mathbb{Z}^2 \\ m\equiv\overline{m}(2)}} q^{\frac{m^2}{2}}\overline{q}^{\frac{\overline{m}^2}{2}} + \frac{1}{2}\left|\sum_{m\in\mathbb{Z}} q^{\frac{1}{2}(m+\frac{1}{2})^2}\right|^2\right). \tag{3.74}$$

Cette somme s'écrit également sous la forme

$$Z_{Dirac} = \frac{1}{|\eta(q)|^2}\sum_{(m,n)\in\mathbb{Z}^2} q^{\frac{1}{8}(n+2m)^2}\overline{q}^{\frac{1}{8}(n-2m)^2}. \tag{3.75}$$

On en déduit donc que

$$Z_{Dirac} = Z_{[0,0]}(1). \tag{3.76}$$

La théorie de Dirac libre sommée sur le quatres secteurs s'identifie donc avec le boson compactifié pour un rayon de compactification $gR^2 = 1$.

3.4.2 Identification dans le secteur AA

Nous prenons maintenant $gR^2 = 1$ puisque c'est le point pour lequel la théorie du boson compactifié s'identifie à la théorie de Dirac. Les fonctions de partition bosoniques (3.70) valent

$$Z_{[0,0]} = \frac{1}{|\eta(q)|^2}\sum_{(n,m)\in\mathbb{Z}^2} q^{\frac{1}{2}(n+\frac{m}{2})^2}\overline{q}^{\frac{1}{2}(n-\frac{m}{2})^2} \tag{3.77}$$

$$Z_{[0,\frac{1}{2}]} = \frac{1}{|\eta(q)|^2}\sum_{(n,m)\in\mathbb{Z}^2} (-1)^m q^{\frac{1}{2}(n+\frac{m}{2})^2}\overline{q}^{\frac{1}{2}(n-\frac{m}{2})^2} \tag{3.78}$$

$$Z_{[\frac{1}{2},0]} = \frac{1}{|\eta(q)|^2}\sum_{(n,m)\in\mathbb{Z}^2} q^{\frac{1}{2}(n+\frac{1}{2}+\frac{m}{2})^2}\overline{q}^{\frac{1}{2}(n+\frac{1}{2}-\frac{m}{2})^2} \tag{3.79}$$

$$Z_{[\frac{1}{2},0]} = \frac{1}{|\eta(q)|^2}\sum_{(n,m)\in\mathbb{Z}^2} (-1)^m q^{\frac{1}{2}(n+\frac{1}{2}+\frac{m}{2})^2}\overline{q}^{\frac{1}{2}(n+\frac{1}{2}-\frac{m}{2})^2}. \tag{3.80}$$

D'autre part, nous séparons Z_{AA} donné par (3.47) en deux termes

$$Z_{AA} = \frac{1}{|\eta(q)|^2}\sum_{\substack{(m,\overline{m})\in\mathbb{Z}^2 \\ m\equiv\overline{m}(2)}} q^{\frac{m^2}{2}}\overline{q}^{\frac{\overline{m}^2}{2}} + \sum_{\substack{(m,\overline{m})\in\mathbb{Z}^2 \\ m\not\equiv\overline{m}(2)}} q^{\frac{m^2}{2}}\overline{q}^{\frac{\overline{m}^2}{2}}. \tag{3.81}$$

Le premier terme de la somme (3.81) se transforme en remarquant que l'application

$$\begin{aligned} g: \quad & \mathbb{Z}^2 \longrightarrow \mathbb{Z}^2 \\ & (k,l) \longmapsto (k+l, k-l) \end{aligned} \tag{3.82}$$

est une bijection de $\mathbb{Z}^2$ sur l'ensemble des couples d'entier $(m,\overline{m})$ tels que $m \equiv \overline{m}(2)$. La réciproque de g est donnée par

$$g^{-1} : (m,\overline{m}) \longmapsto \left(\frac{m+\overline{m}}{2}, \frac{m-\overline{m}}{2}\right). \tag{3.83}$$

En utilisant cette bijection, on transforme le premier terme de (3.81) selon

$$\sum_{\substack{(m,\overline{m}) \in \mathbb{Z}^2 \\ m \equiv \overline{m}(2)}} q^{\frac{m^2}{2}} \overline{q}^{\frac{\overline{m}^2}{2}} = \sum_{(m,n)\in\mathbb{Z}^2} q^{\frac{1}{2}(n+m)^2} \overline{q}^{\frac{1}{2}(n-m)^2} \tag{3.84}$$

$$= \sum_{\substack{(m,n) \in \mathbb{Z}^2 \\ m \equiv 0(2)}} q^{\frac{1}{2}(n+\frac{m}{2})^2} \overline{q}^{\frac{1}{2}(n-\frac{m}{2})^2}, \tag{3.85}$$

et donc

$$\frac{1}{|\eta(q)|^2} \sum_{\substack{(m,\overline{m}) \in \mathbb{Z}^2 \\ m \equiv \overline{m}(2)}} q^{\frac{m^2}{2}} \overline{q}^{\frac{\overline{m}^2}{2}} = \frac{1}{2}\left(Z_{[0,0]} + Z_{[0,\frac{1}{2}]}\right). \tag{3.86}$$

De la même façon, on transforme le second terme de (3.81) en utilisant la bijection

$$h: \quad \mathbb{Z}^2 \longrightarrow \mathbb{Z}^2 \tag{3.87}$$

$$(k,l) \longmapsto (k+l, k-l+1) \tag{3.88}$$

de $\mathbb{Z}^2$ sur l'ensemble des couples $(m,\overline{m})$ tels que $m \not\equiv \overline{m}(2)$, et on obtient

$$\sum_{\substack{(m,\overline{m}) \in \mathbb{Z}^2 \\ m \not\equiv \overline{m}(2)}} q^{\frac{m^2}{2}} \overline{q}^{\frac{\overline{m}^2}{2}} = \frac{1}{2}\left(Z_{[\frac{1}{2},0]} - Z_{[\frac{1}{2},\frac{1}{2}]}\right). \tag{3.89}$$

En rassemblant les équations (3.81), (3.86) et (3.89), on obtient

$$Z_{AA} = \frac{1}{2}\left(Z_{[0,0]}(1) + Z_{[0,\frac{1}{2}]}(1) + Z_{[\frac{1}{2},0]}(1) - Z_{[\frac{1}{2},\frac{1}{2}]}\right)(1) \tag{3.90}$$

3.4.3 Identification dans les secteurs AP et PA

Par transformation modulaire $\tau \to \tau+1$ et $\tau \to -1/\tau$, on transporte l'identité (3.90) aux autres secteurs:

$$Z_{AP} = \frac{1}{2}\left(Z_{[0,0]}(1) + Z_{[0,\frac{1}{2}]}(1) + Z_{[\frac{1}{2},\frac{1}{2}]} - Z_{[\frac{1}{2},0]}(1)\right) \tag{3.91}$$

$$Z_{PA} = \frac{1}{2}\left(Z_{[0,0]}(1) + Z_{[\frac{1}{2},0]}(1) + Z_{[\frac{1}{2},\frac{1}{2}]} - Z_{[0,\frac{1}{2}]}(1)\right) \tag{3.92}$$

3.5 Identification du liquide de Luttinger et du boson compactifié

Nous avons diagonalisé au chapitre 2 le Hamiltonien du liquide de Luttinger en interaction (relation (2.109)). Nous spécialisons la relation (2.109) au cas où les interactions sont locales. En d'autres termes, on se place dans la limite infrarouge et dans le cas où la taille du système est grande devant la portée des interactions. Le Hamiltonien du liquide de Luttinger vaut alors

$$\hat{H}_A^{(Lutt)} = (v_S - v_F)\left(\sum_{n\in\mathbb{N}} n\right) - 2v_F\left(\sum_{n\in\mathbb{N}+\frac{1}{2}} n\right) + v_S\sum_{n\in\mathbb{N}^*} n(\hat{M}_{n,R}+\hat{M}_{n,L}) + \frac{v_S}{4}(\alpha\hat{N}^2+\frac{1}{\alpha}\hat{J}^2). \tag{3.93}$$

Le premier terme provient de la transformation de Bogoliubov et le second terme vient du produit normal du Hamiltonien libre. Les opérateurs $\hat{M}_{n,R}$ et $\hat{M}_{n,L}$ sont les nombres d'occupation des orbitales bosoniques. En utilisant les notations du chapitre précédent, nous avons $\hat{M}_{n,R} = b_q^+ b_q$ avec $q > 0$ et $\hat{M}_{n,L} = b_{-q}^+ b_{-q}$ avec $q > 0$. Dans le dernier terme, $\alpha = \sqrt{v_N/v_J}$. En utilisant les relations (3.28) et (3.29), nous obtenons

$$\hat{H}_A^{(Lutt)} = v_S\left(\tilde{L}_0^R + \tilde{L}_0^L - \frac{1}{12}\right) + \frac{v_S}{4}\left(\alpha\hat{N}^2 + \frac{1}{\alpha}\hat{J}^2\right), \tag{3.94}$$

où

$$\tilde{L}_0^R = \sum_{n\in\mathbb{N}} n\hat{M}_{n,R} \tag{3.95}$$

$$\tilde{L}_0^L = \sum_{n\in\mathbb{N}} n\hat{M}_{n,L}. \tag{3.96}$$

L'opérateur d'impulsion du liquide de Luttinger en interaction est donné par (2.113) et vaut

$$\hat{P}_A^{(Lutt)} = \frac{1}{2}NJ + \sum_{n\in\mathbb{N}} n(\hat{M}_{n,R} - \hat{M}_{n,L}). \tag{3.97}$$

La fonction de partition du liquide de Luttinger vaut alors

$$Z_{AA}^{(Lutt)} = Tr_A\left(e^{-\beta\hat{H}_A^{(Lutt)}} e^{i\theta\hat{P}_A^{(Lutt)}}\right). \tag{3.98}$$

En notant

$$\tau = \frac{1}{2\pi}(\theta + i\beta v_S), \tag{3.99}$$

et $q = \exp(2i\pi\tau)$, nous obtenons

$$Z_{AA}^{(Lutt)} = \frac{1}{|\eta(q)|^2}\sum_{\substack{(N,J)\in\mathbb{Z}^2 \\ N\equiv J(2)}} (q\overline{q})^{\frac{1}{8}(\alpha N^2+\frac{1}{\alpha}J^2)}(q/\overline{q})^{\frac{1}{8}NJ}. \tag{3.100}$$

Nous écrivons $N = n + m$ et $J = n - m$, où $n = N_R$ et $m = N_L$ avec les notations du chapitre 2. La fonction de partition se met alors sous la forme

$$Z_{AA}^{(Lutt)} = \frac{1}{|\eta(q)|^2}\sum_{(m,n)\in\mathbb{Z}^2} q^{\left(\frac{1}{8}(\alpha+\frac{1}{\alpha})+\frac{1}{4}\right)n^2+\left(\frac{1}{8}(\alpha+\frac{1}{\alpha})-\frac{1}{4}\right)m^2+\frac{1}{4}(\alpha-\frac{1}{\alpha})nm} \tag{3.101}$$

$$\overline{q}^{\left(\frac{1}{8}(\alpha+\frac{1}{\alpha})-\frac{1}{4}\right)n^2+\left(\frac{1}{8}(\alpha+\frac{1}{\alpha})+\frac{1}{4}\right)m^2+\frac{1}{4}(\alpha-\frac{1}{\alpha})nm}. \tag{3.102}$$

Après un peu d'algèbre, on obtient

$$Z_{AA}^{(Lutt)} = \frac{1}{|\eta(q)|^2} \sum_{(m,n)\in\mathbb{Z}^2} q^{\frac{1}{2}\left(\sqrt{\alpha}\left(\frac{n+m}{2}\right)+\frac{1}{2\sqrt{\alpha}}(n-m)\right)^2} \overline{q}^{\frac{1}{2}\left(\sqrt{\alpha}\left(\frac{n+m}{2}\right)-\frac{1}{2\sqrt{\alpha}}(n-m)\right)^2}. \tag{3.103}$$

Cete fonction de partition peut s'écrire également sous la forme

$$Z_{AA}^{(Lutt)} = \frac{1}{|\eta(q)|^2} \left(\sum_{\substack{(n,m)\in\mathbb{Z}^2 \\ m\equiv 0(2)}} + \sum_{\substack{(n,m)\in(\mathbb{Z}+1/2)\times\mathbb{Z} \\ m\equiv 1(2)}} \right) q^{\frac{1}{2}\left(n\sqrt{\alpha}+\frac{m}{2\sqrt{\alpha}}\right)^2} \overline{q}^{\frac{1}{2}\left(n\sqrt{\alpha}-\frac{m}{2\sqrt{\alpha}}\right)^2} \tag{3.104}$$

$$= \frac{1}{2}\left(Z_{[0,0]}(\sqrt{\alpha}) + Z_{[0,\frac{1}{2}]}(\sqrt{\alpha}) + Z_{[\frac{1}{2},\frac{1}{2}]}(\sqrt{\alpha}) - Z_{[\frac{1}{2},0]}(\sqrt{\alpha})\right). \tag{3.105}$$

Les spins intervenant dans (3.104) sont de la forme

$$\Delta_{n,m} = \frac{1}{2}\left(n\sqrt{\alpha}+\frac{m}{2\sqrt{\alpha}}\right)^2 - \frac{1}{2}\left(n\sqrt{\alpha}-\frac{m}{2\sqrt{\alpha}}\right)^2 = nm. \tag{3.106}$$

Il n'apparaît donc pas de statistiques exotiques dans le problème en interactions.

3.6 Conclusion

Nous avons donc montré une relation précise entre la théorie du liquide de Luttinger et la théorie du boson compactifié, qui s'identifient au point

$$gR^2 = \sqrt{\alpha} = \left(\frac{v_N}{v_J}\right)^{1/4}. \tag{3.107}$$

Notons qu'une telle identification a déjà été effectuée dans un contexte de chaînes de spins[3], mais sans une identification précise des fonctions de partition.

[3]Voir par exemple le cours de Y. Affleck *Field theory methods and quantum critical phenomena* dans Les Houches, *Champs, cordes et phénomènes critiques* (1988).

Chapitre 4

Article 1

Breakdown of the Fermi Liquid picture in one dimensional fermion systems: connection with the energy level statistics[1]

R. Mélin, B. Douçot and P. Butaud

CRTBT-CNRS, 38042 Grenoble BP 166X cédex France

Using the adiabatic switching of interactions, we establish a condition for the existence of electronic quasiparticles in a Luttinger liquid. It involves a characteristic interaction strength proportional to the inverse square root of the system length. An investigation of the exact energy level separation probability distribution shows that this interaction scale also corresponds to a cross-over from the non interacting behaviour to a rather typical case for integrable systems, namely an exponential distribution. The level spacing statistics of a spin 1/2, one branch Luttinger model are also analyzed, as well as the level statistics of a two coupled chain model.

[1]J. Phys. I France 4 (1994) 737-756

The field of strongly correlated electron systems has recently stimulated interesting discussions which are sometimes challenging some more traditional ideas on the many body problem. For instance, Anderson has proposed that the low energy properties of a two dimensional Hubbard model are not properly described by a Fermi liquid theory [1]. In a recent paper [2], he emphasizes that this question requires a non perturbative treatment, and a careful consideration of boundary conditions. As a consequence of the difficulty of the problem, a lot of effort has been recently dedicated to numerical investigations either with Monte Carlo methods or exact diagonalizations [3]. However, the available sizes remain quite small, and the interpretation of these results is often delicate. A rather different approach has been proposed [4] recently with the hope to develop new tools for extracting more information from finite systems studies. These works have shown that for a large class of low dimensionnal strongly correlated systems, the energy levels exhibit statistical properties rather well described by random matrix theory. For instance, a regime of energy level repulsion is clearly seen in most investigated cases, at the exeption of integrable models such as the nearest neighbor or the $1/r^2$ interaction Heisenberg spin chain. Such a behavior has been extensively discussed in the context of quantum chaos. More precisely, it has been verified that many time reversal symmetrical classicaly chaotic systems generate a spectrum in good agreement with the Gaussian Orthogonal ensemble predictions [5]. By contrast, simple integrable systems yield in general uncorrelated energy levels and the usual exponential distribution for energy level spacings [6].

In this paper, we are investigating some possible connections between simple physical properties of an interacting Fermi system, such as the existence of long lived electronic quasiparticles and the energy level distribution. Intuitively, if the energy levels of the interacting system keep a simple one to one correspondence with those of the non interacting system, we expect on one hand Fermi Liquid Theory to be valid, and on the other hand the statistical properties of the spectrum to remain qualitatively similar as for the free electron case. The interpretation of random matrix behaviour is not straightforward. It may simply indicate that a model is non integrable. For a normal Fermi Liquid, electronic quasiparticle are expected only at low energies compared to the Fermi energy. Furthermore, already for the particle-hole phase spaces, interactions induce new collective modes, such as the zero sound, and the idea of a one to one correspondence with the non interacting gas does not hold for the whole spectrum. Clearly, it would be very interesting to see if the spectrum of a normal Fermi Liquid exhibits some features which would distinguish it from a random matrix Hamiltonian. However, this would likely require an intensive numerical effort (since best candidates would be at least two dimensionnal systems). For the sake of simplicity, and the motivation of doing analytical calculations, we have concentrated in this work on a one dimensional model, namely the Luttinger model [7], which is integrable at any coupling strength. Interestingly, this feature holds for any system length [8]. Furthermore, it provides a good example of a non-Fermi liquid, which can be viewed as a non translation invariant fixed point for many interacting systems in one dimension.

This paper is organized as follows. A first part investigates the condition for the existence of electronic quasiparticles, using the adiabatic generation of eigenstates. An existence condition is established, from the combined requirement of having a negligeable generation of non adiabatic components and absence of decay. This criterion is satisfied if the interaction strength is less than a constant divided by the square root of the system length. As expected, no quasiparticles are found for an infinite system at any finite value of the interaction parameter. This result is also rederived from a simple a nalysis of the single particle Green's function for a finite system.

The second part is devoted to the study of the level spacing distribution as the interaction is gradually increased. We show that the typical interaction scale locating the departure from the highly degenerate non interacting system towards a more generic integrable model with a Poisson distribution is the same as the previous one. So, for this simple situation, noticeable change in the energy level distribution is reflected by the disappearance of electronic quasiparticles. Then, the last two sections of this paper are dedicated to variants of this model, namely in the spin 1/2 case and forward scattering only, for both one and two coupled one dimensionnal systems. A brief conclusion summarizes our results.

4.1 Adiabatic switching on of interactions

A formal way to generate quasiparticles in an interacting Fermi liquid is to apply the Landau switching on of interaction procedure, namely to start from a free particle added above the Fermi sea, and to switch on interactions adiabatically. The corresponding time dependent hamiltonian is:

$$H = H_0 + V_0 e^{\epsilon t}, \tag{4.1}$$

where the interactions term V_0 is switched with a rate ϵ.

Provided it is successfull, this procedure establishes a one to one correspondance between the free gas excitations, and the dressed excitations of the Fermi liquid, namely, the quasiparticles. For a Fermi liquid, the validity condition of this procedure is [9]:

$$\Gamma(\epsilon_k) \ll \epsilon \ll \epsilon_k, \tag{4.2}$$

where ϵ_k is the energy of the quasiparticle, with respect to the Fermi surface, and $\Gamma(\epsilon_k)$ is the decay rate of the quasiparticle. For a normal Fermi liquid, one can show [9] that $\Gamma(\epsilon_k) \simeq \epsilon_k^2$. At small energies, $\Gamma(\epsilon_k) \ll \epsilon_k$, so that it is possible to choose a rate ϵ to perform the switching on procedure.

The aim of this section is to investigate under which conditions the switching on procedure is valid in a one dimensional Luttinger liquid. We shall henceforth exhibit an inequality similar to equation (4.2) for the rate ϵ in the case of a Luttinger liquid.

4.1.1 Introduction

We first wish to sum up some results concerning the formalism developped in [8]. This will also permit us to fix the notations, which shall be used in the rest of the paper.

The fermions are on a ring of perimeter L, with periodic boundary conditions, so that the wave vectors are quantized ($k = \frac{2\pi}{L} n$, with n an integer).

As we treat only low energy properties of a spinless, one dimensional Fermi gas, the curvature of the dispersion relation may be neglected. The two linear branches in the dispersion relation emerging from each extremity of the Fermi surface are extended to arbitrary energies. This linearized model is the Luttinger gas model, which hamiltonian is:

$$H^0 = v_F \sum_{kp} (pk - k_F) : c_{kp}^+ c_{kp} :, \tag{4.3}$$

where v_F is the Fermi velocity and $p = +1$ or -1 labels the branch (right or left). We shall also use the real space field $\psi_p^+(x)$ associated to the right (left) free fermions. Furthermore, c_{kp}^+ is the Fourier transform of $\psi_p^+(x)$:

$$c_{kp}^+ = L^{-1/2} \int_{-L/2}^{L/2} \psi_p^+(x) e^{ikx} dx. \tag{4.4}$$

Notice that the sign of the phase factor is not arbitrary, but is chosen such as right moving fermions with a positive wave vector propagate to the right.

Because of the presence of an infinite number of fermions in the ground state, the density operators

$$\rho_{qp} = \sum_k : c_{k+q,p}^+ c_{k,p} : \tag{4.5}$$

have anomalous commutation relations (Schwinger terms):

$$[\rho_{qp}, \rho_{-q'p'}] = -\frac{Lpq}{2\pi} \delta_{pp'} \delta_{qq'}. \tag{4.6}$$

They may consequently be used to build a set of boson creators a_q^+ $(q \neq 0)$. To handle the real space bosonic field, one needs to define

$$\Phi_p(x) = p \frac{\pi x}{L} N_p - i \sum_{q \neq 0} \theta(pq) \left(\frac{2\pi}{L|q|}\right)^{1/2} e^{iqx} a_q. \tag{4.7}$$

The $q = 0$ modes correspond to charge and current excitations. Their algebra involves the unitary ladder operators U_p constructed in [8]. They act only in the $q = 0$ sector, and increase by one the charge on the p branch. The complete form of the bosonic fields, including the $q = 0$ modes, is:

$$\theta_p(x) = \bar{\theta_p} + \Phi_p(x) + \Phi_p^+(x), \tag{4.8}$$

where $\bar{\theta_p}$ is the phase conjugate to N_p.

We shall also use the important relation to pass from a real space boson description to a real space fermion description:

$$\begin{aligned} \Psi_p^+(x) &= L^{-1/2} e^{-ipk_F x} : e^{-i\theta_p(x)} : \\ &= L^{-1/2} e^{-ipk_F x} e^{-i\Phi_p^+(x)} U_p e^{-i\Phi_p(x)}. \end{aligned} \tag{4.9}$$

Expressed on this new basis, the free hamiltonian becomes:

$$H^0 = v_F \sum_{q \neq 0} |q| a_q^+ a_q + v_F \frac{\pi}{L} (N_R^2 + N_L^2), \tag{4.10}$$

where N_R (N_L) denote the number of right (left) moving fermions added above the vacuum state. In terms of charge $N = N_R + N_L$ and current $J = N_R - N_L$ variables, the energy of the charge and current excitations is: $v_F \frac{\pi}{2L}(N^2 + J^2)$.

Note that the action of the boson creation operators and of the ladder operators on the ground state generates a basis of the Hilbert space. The completeness may be shown [8] by

comparing the generating functions of the degeneracies (ie the finite temperature partitions functions) for both the free electrons basis and the boson basis. The notation for the kets of the second basis is:

$$|\{N_p\},\{n_q\}\rangle = \prod_p (U_p)^{N_p} \prod_{q\neq 0} \frac{(a_q^+)^{n_q}}{(n_q!)^{1/2}}|0\rangle \tag{4.11}$$

We now briefly describe the formalism to deal with interactions. The two-particle interactions term is written as:

$$H^1 = \frac{\pi}{L}\sum_{pq} V_q \rho_{qp}\rho_{-q-p}. \tag{4.12}$$

For simplicity, our treatment does not include interactions between fermions lying on the same side of the Fermi surface. Only g_2 interactions are relevant in the physics we shall develop. One important feature of the interactions V_q is that they are cut off for impulsions greater than the inverse of a length scale R. We shall use the following expression of V_q (for $q < 1/R$):

$$V_q = V(1-(qR)^\alpha). \tag{4.13}$$

The intensity of the interactions is parametrized by V, and the shape of V_q is parametrized by α. The bosonized form of the interaction Hamiltonian H^1 is:

$$H^1 = \frac{\pi}{2L}(v_N - v_F)N^2 + \frac{\pi}{2L}(v_J - v_F)J^2 + \sum_{q>0} qV_q(a_q^+ a_{-q}^+ + a_q a_{-q}) \tag{4.14}$$

The total hamiltonian is diagonalized by the following Bogoliubov transformation:

$$b_q^+ = \cosh\varphi_q a_q^+ - \sinh\varphi_q a_{-q}, \tag{4.15}$$

where the angle φ_q is defined as:

$$\tanh 2\varphi_q = -\frac{V_q}{v_F}. \tag{4.16}$$

The total hamiltonian reads, after the Bogoliubov transformation:

$$H = E_0 + \sum_{q\neq 0}\omega_q b_q^+ b_q + \frac{\pi}{2L}(v_N N^2 + v_J J^2). \tag{4.17}$$

The effect of the interactions is to give a non zero ground state energy:

$$E_0 = \frac{1}{2}\sum_q(\omega_q - v_F q), \tag{4.18}$$

where

$$\omega_q = (v_F^2 - V_q^2)^{1/2}|q|. \tag{4.19}$$

Interactions also shift the energies of the oscillators from $v_F|q|$ to ω_q. Finally, charge and current excitations acquire different velocities $v_N = v_S e^{-2\varphi}$ and $v_J = v_S e^{2\varphi}$. In these relations, φ is the infrared limit of φ_q and the sound velocity v_S is related to the infrared limit of the dispersion relation (4.19):

$$v_S = lim_{q\to 0}(v_F^2 - V_q^2)^{1/2}. \tag{4.20}$$

In the presence of interactions, one needs to normal order the field $\psi_p^+(x)$ in terms of b_q^+ bosons, which leads to the following expression of $\Phi_p(x)$:

$$\Phi_p(x) = p\frac{\pi x}{L}N_p - i\sum_{q\neq 0}(\theta(pq)\cosh\varphi_q - \theta(-pq)sinh\varphi_q)e^{iqx}b_q. \tag{4.21}$$

The fermion field reads, in terms of bosons:

$$\psi_p^+(x) = L^{-1/2}\exp\{-\sum_{q>0}(\frac{2\pi}{Lq})(\sinh\varphi_q)^2\}e^{-ipk_Fx}e^{-i\Phi_p^+(x)}U_pe^{-i\Phi_p(x)}. \tag{4.22}$$

4.1.2 Interaction picture for $c_{kR}^+|\{N_p\}\rangle$

As $t \to -\infty$, the system is made up of a right moving fermion, with an impulsion k added above a Dirac sea $|\{N_p\}\rangle$, and interactions are vanishing. This section deals with the propagation of this state, $c_{kR}^+|\{N_p\}\rangle$, as interactions are switched on.

The first step is to decompose the state $c_{kR}^+|\{N_p\}\rangle$ into bosonic modes. The action of c_{kR}^+ on the vacuum $|\{N_p\}\rangle$ in the $q=0$ sector is simply to increase by one the number of right moving fermions, by the action of the ladder operator U_R.

To obtain the action of c_{kR}^+ in the $q\neq 0$ sectors, we first Fourier transform c_{kR}^+ into the real space field $\psi_R^+(x)$ for right-moving fermions.

We replace the expression of $\phi_p^+(x)$ in (4.9) by its expression (4.7) in terms of bosonic modes a_q^+. The developpement of the exponential $e^{-i\Phi_R(x)}$ leads then to an expression of $c_{kR}^+|\{N_p\}\rangle$ as a linear combination of bosonic states, with occupation numbers $\{n_q\}$:

$$c_{kR}^+|\{N_p\}\rangle = \sum_{\{n_q\}}\delta\left(\sum_{q>0}qn_q - (k-(k_F+\frac{\pi}{L}(2N_R+1)))\right) \tag{4.23}$$

$$\prod_{q>0}\frac{1}{\sqrt{n_q!}}\left(\frac{2\pi}{Lq}\right)^{\frac{n_q}{2}}|\{N_R+1,N_L\},\{n_q\}\rangle. \tag{4.24}$$

The delta function insures that only bosonic states with a total impulsion equal to $k-k_F-\frac{\pi}{L}(2N_R+1)$ survive in the decomposition. As no interaction couples the two branches, creating a right-moving fermion does not generate left moving bosons.

The second step is to propagate the bosonic wave packet (4.23). Instead of dealing with the rather complicated superposition (4.23) of bosonic states, we focus on the propagation of a single term $|\{N_p\},\{n_q\}\rangle$. We shall use the bosonized form of the two-body interaction hamiltonian, and look for a solution of the time dependent Schrödinger equation:

$$i\frac{d|\{N_p\},\{n_q\}\rangle_{int}(t)}{dt} = H_{int}^1|\{N_p\},\{n_q\}\rangle_{int}(t). \tag{4.25}$$

The "int" label stands for an interaction picture. The initial conditions are:

$$lim_{t\to-\infty}|\{N_p\},\{n_q\}\rangle_{int}(t) = |\{N_p\},\{n_q\}\rangle. \tag{4.26}$$

The bosonic states are propagated under the form of a coherent state:

$$|\{N_p\},\{n_q\}\rangle_{int}(t) = N(z_q(t))e^{-i\phi(\{n_q\},t)}\prod_{q>0} e^{-iz_q(t)a_q^+a_{-q}^+}|\{N_p\},\{n_q\}\rangle. \tag{4.27}$$

The prefactor $N(z)$ normalizes $|\{N_p\},\{n_q\}\rangle_{int}(t)$:

$$N(\{z_q\}) = \prod_{q>0}\left(1-|z_q|^2\right)^{\frac{n_q+1}{2}}. \tag{4.28}$$

To determine the time dependent $\phi(\{n_q\},t)$ and $\{z_q(t)\}$ functions, we first change $z_q(t)$ into $u_q(t)$, with $z_q(t) = u_q(t)e^{2iv_Fqt}$, and then identify both sides of the Schrödinger equation. We obtain first order non linear differential equations for $\{u_q(t)\}$ and $\phi(\{n_q\},t)$:

$$\frac{du_q(t)}{dt} + 2iv_Fqu_q(t) = qV_q(t)(1-u_q^2(t)) \tag{4.29}$$

$$\frac{d\phi(\{n_q\},t)}{dt} = \sum_{q>0}(n_q+1)qV_q(t)Im(u_q(t)). \tag{4.30}$$

We have discarded in equation (4.30) a term depending only on N and J, which leads only to a global phase factor. Translated in terms of ϕ and z_q variables, the initial conditions (4.26) simply mean that $\phi(t)$ and $z_q(t)$ are vanishing as $t\to-\infty$. These differential equations describe the propagation of a single component of the wave packet (4.30). The propagation of the summation is obtained as a superposition of the different components after propagation:

$$(c_{kR}^+|\{N_p\}\rangle)_{int}(t) = \sum_{\{n_q\}}\delta\left(\sum_{q>0}qn_q-(k-(k_F+\frac{\pi}{L}(2N_R+1)))\right) \tag{4.31}$$

$$\prod_{q>0}\frac{1}{\sqrt{n_q!}}\left(\frac{2\pi}{Lq}\right)^{\frac{n_q}{2}}|\{N_R+1,N_L\},\{n_q\}\rangle_{int}(t). \tag{4.32}$$

4.1.3 Adiabaticity condition

We are looking for a solution of equation (4.30) which depends only on the variable $s=\epsilon t$, in the small ϵ limit. It is possible since the external time dependance in equation (4.30) involves only ϵt. We assume then $u_q(s) = u_q^0(s)+\epsilon u_q^1(s)+O(\epsilon^2)$. Neglecting the $O(\epsilon^2)$ terms in equation (4.30) leads to:

$$2iv_Fqu_q^0(s) = qV_q(s)(1-u_q^{(0)}(s)^2) \tag{4.33}$$

$$\frac{du_q^0}{ds}(s) + 2iv_Fqu_q^{(1)}(s) = -2qV_q(s)u_q^{(0)}(s)u_q^{(1)}(s), \tag{4.34}$$

where:

$$V_q(s) = V_q^0e^s. \tag{4.35}$$

The purely adiabatic solution $u_q^{(0)}(s)$ is given by:

$$u_q^0(s) = \frac{i}{V_q(s)}(-v_F + \sqrt{v_F^2 - V_q(s)^2}) = i \tanh \varphi_q^0(s). \tag{4.36}$$

Using this solution in equation (4.34) gives the first finite ϵ correction:

$$u_q^{(1)}(s) = i\frac{v_F}{2q(v_F^2 - V_q(s)^2)} u_q^{(0)}(s). \tag{4.37}$$

The adiabatic preparation of eigenstates is achieved if $|u_q^{(1)}(s)|\epsilon \ll |u_q^{(0)}(s)|$ for $s = 0$, which leads to:

$$\frac{v_F \epsilon}{2q(v_F^2 - V_q^2)} \ll 1. \tag{4.38}$$

This condition depends explicitely on q, and is satisfied for any value of q if

$$\epsilon \ll 4\pi v_F / L. \tag{4.39}$$

Here, we assume a weak coupling, namely $|V_q| \ll v_F$. It should be noticed that this upper bound on ϵ is a much more restrictive condition than the corresponding upper bound in equation (4.2) for a Fermi liquid. We interpret this as a consequence of the fact that the quasiparticles of the Landau theory are not exact eigenstates of the interacting system. They are obtained in a situation where the thermodynamic limit is taken first, whereas the generation of exact eigenstates would require ϵ to go to zero as the typical spacing between energy levels. Our criterion (4.39) corresponds to this second situation. This choice has been motivated by the possibility to construct the exact eigenstates of a Luttinger liquid.

4.1.4 Adiabatic propagation in a Bogoliubov subspace

The aim of this section is to propagate a fermion during the switching on procedure. We suppose that the condition (4.39) is satisfied, and we now look for a minoration of ϵ. We first search an approximation for the evolution operator in the limit $\epsilon \ll \frac{2\pi}{L} v_F$. At the order ϵ^0, the evolution operator $U_\epsilon(0, -\infty)$ realizes the Bogoliubov transformations of angles $\{\varphi_q^0\}$, corresponding to the rotation of the basis of eigenstates as interactions were switched on from zero at time $t = -\infty$ to $\{\varphi_q^0\}$ at time $t = 0$. We shall note $U^0(0, -\infty)$ the corresponding part of the evolution operator. U^0 must have the property that:

$$U^0 a_q^+ (U^0)^{-1} = \cosh \varphi_q^0 a_q^+ - \sinh \varphi_q^0 a_{-q}. \tag{4.40}$$

This equality is verified if U^0 has the following form:

$$U^0 = \exp\{\sum_{q>0} \varphi_q^0 (a_q^+ a_{-q}^+ - a_q a_{-q})\}. \tag{4.41}$$

To see it, we differentiate each operator $U^0 a_q^+ (U^0)^{-1}$ and $U^0 a_{-q} (U^0)^{-1}$ with respect to φ_q^0 and solve the differential system.

However, at higher orders in ϵ, the evolution operator must take into account the phase factor $\phi(\{n_q\}, t)$, the evolution of which is given by the equation (4.30). Assuming that the propagation is adiabatic, we approximate $Imu_q(t)$ in (4.30) by $Imu_q^0(t)$:

$$Imu_q(t) \simeq \tanh \varphi_q^0(s = \epsilon t). \tag{4.42}$$

We use the expression (4.35) for $V_q(t)$, and integrate the differential equation (4.30) for the phase factor $\phi(\{n_q\},t)$. A constant (infinite) phase factor associated to the propagation of the ground state is factored out. Thus, we obtain the form of the evolution operator in the adiabatic limit (at order ϵ^0 for the operator U^0, and at order $1/\epsilon$ for the phases):

$$U_\epsilon(0,-\infty) = U^0 \exp i\{\sum_{q>0} \frac{qn_q v_F}{\epsilon}(\varphi_q^0)^2\} \tag{4.43}$$

$$= \exp\{\sum_{q>0} \varphi_q^0(a_q^+ a_{-q}^+ - a_q a_{-q})\} \exp\{i\sum_{q>0} \frac{qn_q v_F}{\epsilon}(\varphi_q^0)^2\}. \tag{4.44}$$

In the integrations, we have assumed that the interactions are weak, and the phase factors are given, at the lowest order in φ_q^0.

The rest of this section is devoted to the calculation and the interpretation of the overlap:

$$F(x-x') \sim F(x,x') = \langle\{N_p\}|\Psi_R(x')U_\epsilon^{-1}(0,-\infty)\Psi_R^+(x)U_\epsilon(0,-\infty)|\{N_p\}\rangle, \tag{4.45}$$

between the dressed fermions $\Psi_R^+(x)U_\epsilon(0,-\infty)|\{N_p\}\rangle$, and the bare ones: $\Psi_R^+(x')U_\epsilon^{-1}(0,-\infty)|\{N_p\}\rangle$. To perform it, we use the expression (4.22) of the field for right moving fermions, and the approximation (4.44) for the evolution operator. The computation is straightforward, and $F(x,x')$ is the product of three terms:

1) a phase term

$$N = \exp\{-i(k_F + \frac{\pi}{L}(2N_R+1))(x-x')\}, \tag{4.46}$$

corresponding to the propagation in the $q=0$ sector.

2) A term corresponding to the left moving bosons normal ordering in (4.45):

$$G_1 = \exp\{-\sum_{q>0} \frac{2\pi}{Lq}(\sinh\varphi_q^0)^2\} \tag{4.47}$$

3) A term coming from the right moving bosons normal ordering:

$$G_2(x,x') = \exp\{\sum_{q>0} \frac{2\pi}{Lq} e^{-iq(x-x'-\frac{v_F(\varphi_q^0)^2}{\epsilon})}\} \tag{4.48}$$

The result for the overlap is:

$$F(x,x') = \frac{1}{L} N G_1 G_2(x,x'). \tag{4.49}$$

The G_1 term contains the usual physics of the orthogonality catastrophy [10]. If φ_q^0 is assumed to be constant between $q = \frac{2\pi}{L}$ and $q = 1/R$, and zero afterwards, and if $L \gg R$, G_1 can be calculated as:

$$G_1 = (\frac{L}{R})^{-\sinh^2\varphi^0} \tag{4.50}$$

In the weak coupling limit, one can deduce the characteristic interaction scale associated to the orthogonality catastrophy:

$$V_{o.c.} = v_F(\ln\frac{L}{2\pi R})^{-1/2}. \tag{4.51}$$

To obtain the energy scale associated to the G_2 term, we use the relation (4.13) and approximate the phase as:

$$-\frac{qv_F(\varphi_q^0)^2}{\epsilon} = -\frac{q(V^0)^2}{4v_F\epsilon} + \frac{q(V^0)^2}{2v_F\epsilon}(qR)^\alpha. \tag{4.52}$$

The first term is linear in q up to the impulsion scale $1/R$. The second term is associated to smaller impulsion scales. The formers are relevant for a quasiparticle. If k is the impulsion of the quasiparticle with respect to the Fermi level, the energy scale V_{deph} associated to the dephasing is given by:

$$\frac{kV_{deph}^2}{2v_F\epsilon}(kR)^\alpha = 2\pi, \tag{4.53}$$

that is:

$$V_{deph}(k) = (\frac{4\pi v_F\epsilon}{k(kR)^\alpha})^{1/2}. \tag{4.54}$$

The switching on procedure shall henceforth be successfull provided the intensity of interactions V is much smaller than $V_{deph}(k)$, that is:

$$\frac{kV^2(kR)^\alpha}{4\pi v_F} \ll \epsilon. \tag{4.55}$$

4.1.5 Conclusions

For the switching on procedure to create a quasiparticle, the conditions (4.39) and (4.55) have to be simultaneously satisfied, that is:

$$\frac{kV^2(kR)^\alpha}{4\pi v_F} \ll \epsilon \ll \frac{4\pi}{L}v_F. \tag{4.56}$$

This inequality is satisfied if the following consistency condition is fullfilled:

$$V \ll \frac{4\pi v_F}{(kL(kR)^\alpha)^{1/2}}. \tag{4.57}$$

As we shall see, this condition has a simple interpretation on the spectrum of the Luttinger model. At this stage, we should again emphasize that the upper bound on ϵ is more restrictive than in Landau theory. If we use the more usual condition that the spread in energy is smaller than the average density of the wave packet, equation (4.56) is replaced by:

$$\frac{kV^2(kR)^\alpha}{4\pi v_F} \ll \epsilon \ll kv_F, \tag{4.58}$$

and the consistency condition is:

$$V \ll (\frac{4\pi}{(kR)^\alpha})^{1/2}v_F. \tag{4.59}$$

The absence of Landau quasiparticle in the thermodynamic limit is then atributed to orthogonality catastrophy, as indicated by equation (4.51).

4.1.6 Comparison with the Green's function

In this section, we calculate the Green's function for the finite size Luttinger model:

$$G_R(x,t;x',t') = -i\{(\{N_p\}|e^{iH(t'-t)}\psi_R(x')e^{-iH(t'-t)}\psi_R^+(x)|\{N_p\})\theta(t'-t) \quad (4.60)$$
$$-(x \leftrightarrow x';t \leftrightarrow t')\}$$

and reestablish the consistency condition (4.57). Note that in equation (4.60), $|\{N_p\}>$ denotes an eigenstate of the interacting system.

To calculate the Green's function, we use the expression (4.9) of the field $\psi_R^+(x)$ in terms of the Bose field, and normal order the expression (4.60) of the Green's function with respect to the bosonic modes b_q^+. The computation is straightforward, and the result is:

$$\begin{aligned} G_R(x,t;x',t') = {} & \frac{-i}{L}e^{i(k_F+\pi/L)(x'-x)}e^{i\frac{\pi}{L}(v_N(2N+1)+v_J(2J+1))(t'-t)} \\ & \exp\left(-2\sum_{q>0}\frac{2\pi}{Lq}(\sinh\varphi_q)^2\right) \\ & \{[\exp\left(\sum_{q>0}(\frac{2\pi}{Lq})(\cosh\varphi_q)^2e^{iq(x'-x)}e^{-i\omega_q(t'-t)}\right) \\ & \exp\left(\sum_{q>0}(\frac{2\pi}{Lq})(\sinh\varphi_q)^2e^{-iq(x'-x)}e^{-i\omega_q(t'-t)}\right)] \\ & -[x \leftrightarrow x';t \leftrightarrow t']\theta(t-t')\} \end{aligned} \quad (4.61)$$

The dispersion in the frequencies leads to decoherence after a time t_k. (k is the impulsion of the quasiparticle, with respect to the Fermi level). t_k may be estimated in the same way as we did for U_{deph}, and one finds:

$$t_k = \frac{2\pi v_F}{V^2k(kR)^\alpha}. \quad (4.62)$$

For a system of size L, the wave packet is stable, provided it can cross the ring without decoherence:

$$v_F t_k > L, \quad (4.63)$$

that is:

$$V < (\frac{2\pi}{kL(kR)^\alpha})^{1/2}v_F. \quad (4.64)$$

Up to some numerical dimensionless constants, this criterium is the same as the consistency condition (4.57) for the switching on of interactions.

4.2 Level statistics of the interacting Luttinger model

4.2.1 Introduction

We first need to find out a proper sector of the Hilbert space, in which we shall compute the level statistics. We note H_{JN} the subspace with given current J and charge N.

In the free case, the boson basis of H_{JN} can be organized as follows: consider all the sets of occupation numbers $\{n_q^0\}$ such as, for all q, $n_q^0 = 0$ or $n_{-q}^0 = 0$. The corresponding states $|\{n_q^0\}\rangle$ are annihilated by any pair destruction operator: $a_q a_{-q}|\{n_q^0\}\rangle = 0$. Starting from $|\{n_q^0\}\rangle$, and creating pairs generates a subspace $H_{pairs}(\{n_q^0\})$. A basis of $H_{pairs}(\{n_q^0\})$ is made up of all the states $|\{n_q^0 + p_{|q|}\}\rangle$ with arbitrary occupation numbers for the pairs $\{p_q\}_{q>0}$. H_{NJ} is the direct sum of all the $H_{pairs}(\{n_q^0\})$ subspaces.

The subspaces $H_{pairs}(\{n_q^0\})$ remain stable under the action of the interaction hamiltonian H^1, so that they are appropriate to the study of the levels evolution.

We choose $N = J = 0$ and drop the energy term associated to $\{n_q^0\}$, since we always handle differences between consecutives levels. The energy levels are given by:

$$E(\{n_q\}) = \sum_{q>0} 2v_F q n_q (1 - (\frac{V_q}{v_F})^2)^{1/2} \tag{4.65}$$

where we use the expression (4.13) for V_q.

4.2.2 Description of the algorithms

In this section and the next paragraph, we use reduce units for the energies and impulsions: ω is an energy divided by $\frac{2\pi}{L}v_F$ and q is an impulsion divided by $\frac{2\pi}{L}$.

The degeneracies of the Luttinger model are given by:

$$g(\omega) = \sum_{\{n_q\}} \delta(\omega - \sum_{q>0} q n_q). \tag{4.66}$$

Replacing the δ function by its integral representation leads to:

$$g(\omega) = \int_{-L/2}^{L/2} \frac{dx}{L} \prod_{q>0} \frac{1}{1 - e^{iqx}} e^{-i\omega x}. \tag{4.67}$$

Let $g^{(k)}(\omega)$ be the number of different sets of occupation numbers, having the property that:

$$\omega = \sum_{l=k}^{\omega} l n_l. \tag{4.68}$$

Of course, $g^{(1)}(\omega) = g(\omega)$. The integral representation for $g^{(k)}(\omega)$ reads:

$$g^{(k)}(\omega) = \int_{-L/2}^{L/2} \frac{dx}{L} \prod_{q\geq k} \frac{1}{1 - e^{iqx}} e^{-i\omega x}. \tag{4.69}$$

Using the integral representations for $g^{(k)}(\omega)$, we obtain the following recurences:

$$g^{(k)}(\omega) = \sum_{\nu=k}^{\omega} g^{(\nu)}(\omega - \nu), \tag{4.70}$$

which allows us to numerically compute $g(\omega)$.

With a similar recursion, we may generate all the states of the free Luttinger model: the states with an energy ω are obtained by adding a boson with an impulsion ν on the states with an energy $\omega - \nu$.

As far as the interacting Luttinger model is concerned, we need to generate all the energy levels with an energy inferior as a given cut-off ω_0. Since there are an infinite number of levels in the sector under consideration, we need to introduce such a cut-off to compute the statistics. We shall then compute the statistical properties of this set of levels. If a sufficient number of levels with an energy inferior as ω_0 has been generated, the statistical properties are independant on ω_0. To generate the levels, we remark that the frequencies of the oscillators increase with their impulsion. So that we successively fill up the individual oscillator levels, starting with the smallest frequencies.

4.2.3 Level statistics

Degeneracies of the free Luttinger model

Using the recursion relation (4.70), we computed the degeneracies of the first 800 levels of the free Luttinger model. The asymptotic form of the density of states may be derived in terms of initial fermions. The partial degeneracies for n-particles n-holes excitations in a one branch model are:

$$g^{(n)}(\omega) = \sum_{\{k_i\}_{i=1\ldots n}} \sum_{\{k'_i\}_{i=1\ldots n}} \delta(\omega - \sum_{i=1}^{n} \omega(k_i) - \sum_{i=1}^{n} \omega(k'_i)). \tag{4.71}$$

The sets $\{k_i\}$ ($\{k'_i\}$) are the impulsions of the holes (particles), and are constrained by the Pauli principle $k_i \neq k_j$ ($k'_i \neq k'_j$) for all indices $i \neq j$. This sum is approximated by assuming a constant density of states, neglecting the Pauli exclusion principle, replacing the discrete sum by an integral:

$$g^{(n)}(\omega) = \frac{1}{(n!)^2} \int_0^{\omega} d\omega_1 \int_0^{\omega-\omega_1} d\omega_2 \ldots \int_0^{\omega-(\omega_1+\ldots+\omega_{2n-1})} d\omega_{2n} \delta(\omega - (\omega_1 + \ldots + \omega_{2n})) \tag{4.72}$$

The multiple integral is readily evaluated and leads to:

$$g(\omega) = \sum_{n=1}^{+\infty} g^{(n)}(\omega) = \sum_{n=1}^{+\infty} \frac{\omega^{2n-1}}{(n!)^2(2n-1)!}. \tag{4.73}$$

For sufficiently large energies, the sum may be approximated by its saddle point value, approximately reached for the following value of n:

$$n^* = \sqrt{\frac{\omega}{2}}. \tag{4.74}$$

The degeneracy evaluated at $n = n^*$ is:

$$g^{n^*}(\omega) \sim \frac{2^{3/4}}{(2\pi)^{3/2}} \frac{1}{\omega^{5/4}} \exp \sqrt{8\omega}. \tag{4.75}$$

We computed the summation (4.73) in order to test the accuracy of the saddle point approximation, which is plotted on figure 4.1 The exact degeneracies of the Luttinger model reveal to be inferior as the saddle point asymptotic form, which is imputed to the exclusion principle (figure 4.1).

$$\frac{1}{\sqrt{8\omega}}(\log g(\omega) + \frac{5}{2}\log\sqrt{\omega} - \frac{3}{4}\log 2 + \frac{3}{2}\log 2\pi)$$

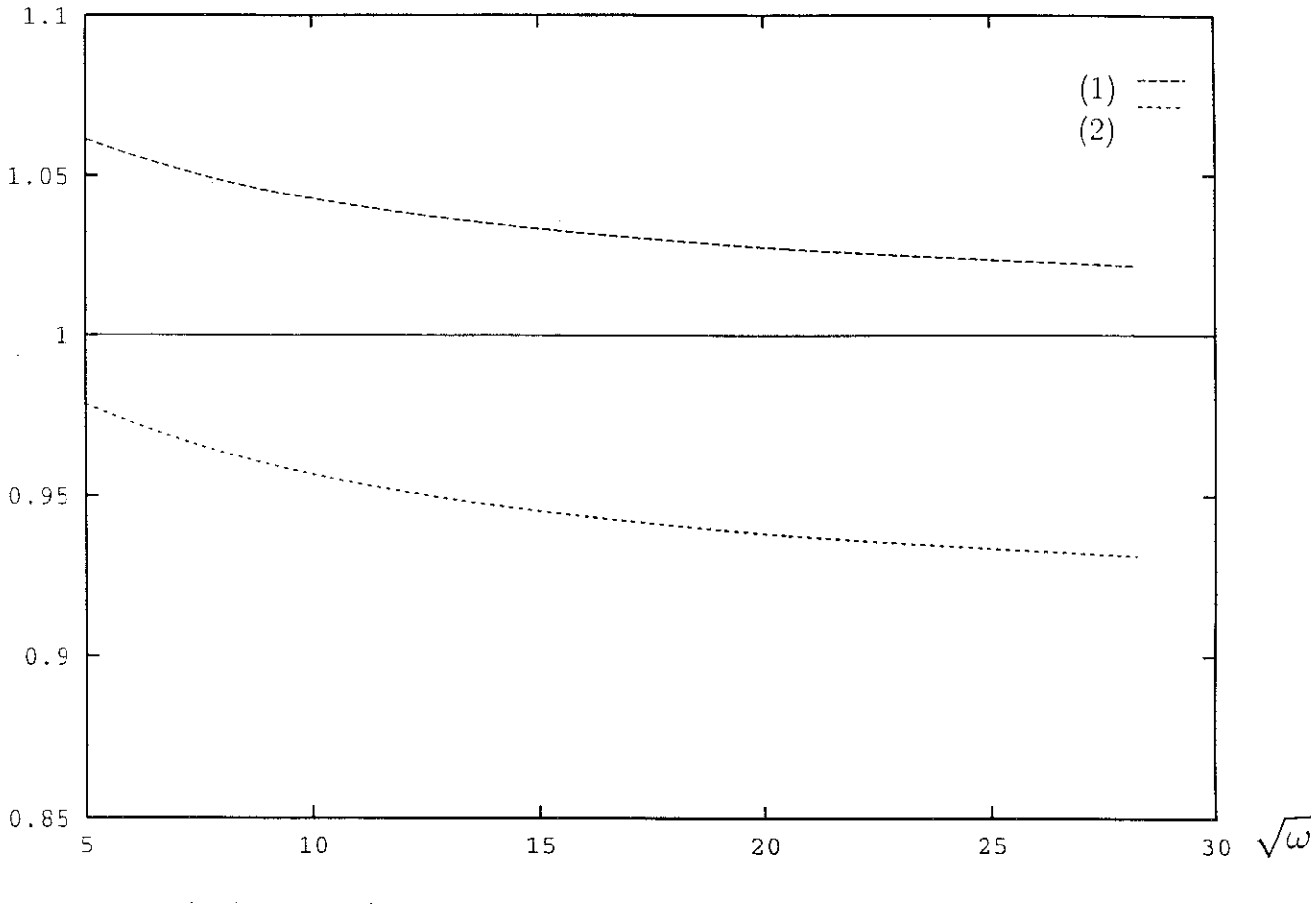

Figure 4.1: Degeneracies of the free Luttinger model, compared to the saddle point approximation.
$\{\log g(\omega) - \frac{3}{4}\log 2 + \frac{3}{2}\log 2\pi + \frac{5}{2}\log\sqrt{\omega}\}/\sqrt{8\omega}$ is plotted as a function of $\sqrt{\omega}$. This function equals 1 for the saddle point approximation. In plot (1), $g(\omega)$ is the exact degeneracies. As expected, the saddle point approximation overevaluates the degeneracies since it takes into account particle-hole excitations forbidden by the exclusion principle. In plot (2), all the terms of the summation (4.73) are taken into account. The saddle point approximation in (4.73) underevaluates the degeneracies, and becomes exact at high energies.

Qualitative structure of the spectrum

The evolution of some energy levels as a function of the interactions is plotted on figure 4.2. In this spectrum, we distinguish two regions:

1) No level crossings are present at sufficiently small energies and interactions. The free Luttinger model ($V = 0$) belongs to this part of the spectrum. In this region, the statistics are ill defined for they strongly depend on the energy cut off.

2) If E and V are large enough, level crossings occur, and level statistics are Poisson statistics. The convergence of the statistics as a function of the energy cut off e_0 is shown on figure 4.3. Here, we emphasize that these level crossings occur because the Luttinger model remains integrable at any value of the coupling constant.

To characterize the separation between these two regions of the spectrum, the location of the crossings is estimated in the following way: as the intensity of interactions V is equal to zero, the spectrum is made up of equidistant degenerate levels, separated by an amount of energy $\Delta E = \frac{2\pi}{L} v_F$. As V is turned on, the degeneracies are lifted. We focus on a single fan of levels. All the levels are degenerate if $V = 0$, and their energy is $E^0 = 2v_F k$, where k is the total impulsion of the states. For a given value of V, all the levels lie between E_{min} and E_{max}. E_{min} is obtained as all the quanta are in the smallest energy state (namely $q = \frac{2\pi}{L} v_F$), so that:

$$E_{min} = 2v_F k(1 - \frac{V^2_{q=\frac{2\pi}{L}v_F}}{v_F^2})^{1/2}. \tag{4.76}$$

E_{max} corresponds to a state with one quantum in the highest $q = k$ state:

$$E_{max} = 2v_F k(1 - \frac{V^2_{q=k}}{v_F^2})^{1/2}. \tag{4.77}$$

As the interaction parameter V increases, the levels evolve and the first crossings occur as the width of the fan $E_{max} - E_{min}$ is of order ΔE. This condition defines the interaction energy beyond which crossings exist:

$$V^* = (\frac{\pi}{kL(kR)^\alpha})^{1/2} v_F. \tag{4.78}$$

Via bosonization, the free Luttinger liquid is described as a set of harmonic oscillators with commensurable frequencies. As interactions are switched on, the oscillator frequencies vary and become incommensurable. In [6], Berry and Tabor show that a system with a finite number of generic harmonic oscillators does not exhibit level clustering. It appears that increasing the number of oscillators with incommensurable frequencies generates clustering.

Quasi particle destruction and level spacing statistics

The condition (4.78) separates two regions of the spectrum. The same energy scale controls the existence or the absence of a quasiparticle in a Luttinger liquid, in the sense of adiabatic continuation of exact eigenstates. We have thus shown that the structure of the spectrum of the finite size Luttinger liquid is related to the succes or the failure of adiabatic generation of eigenstates from the non interacting fermion system.

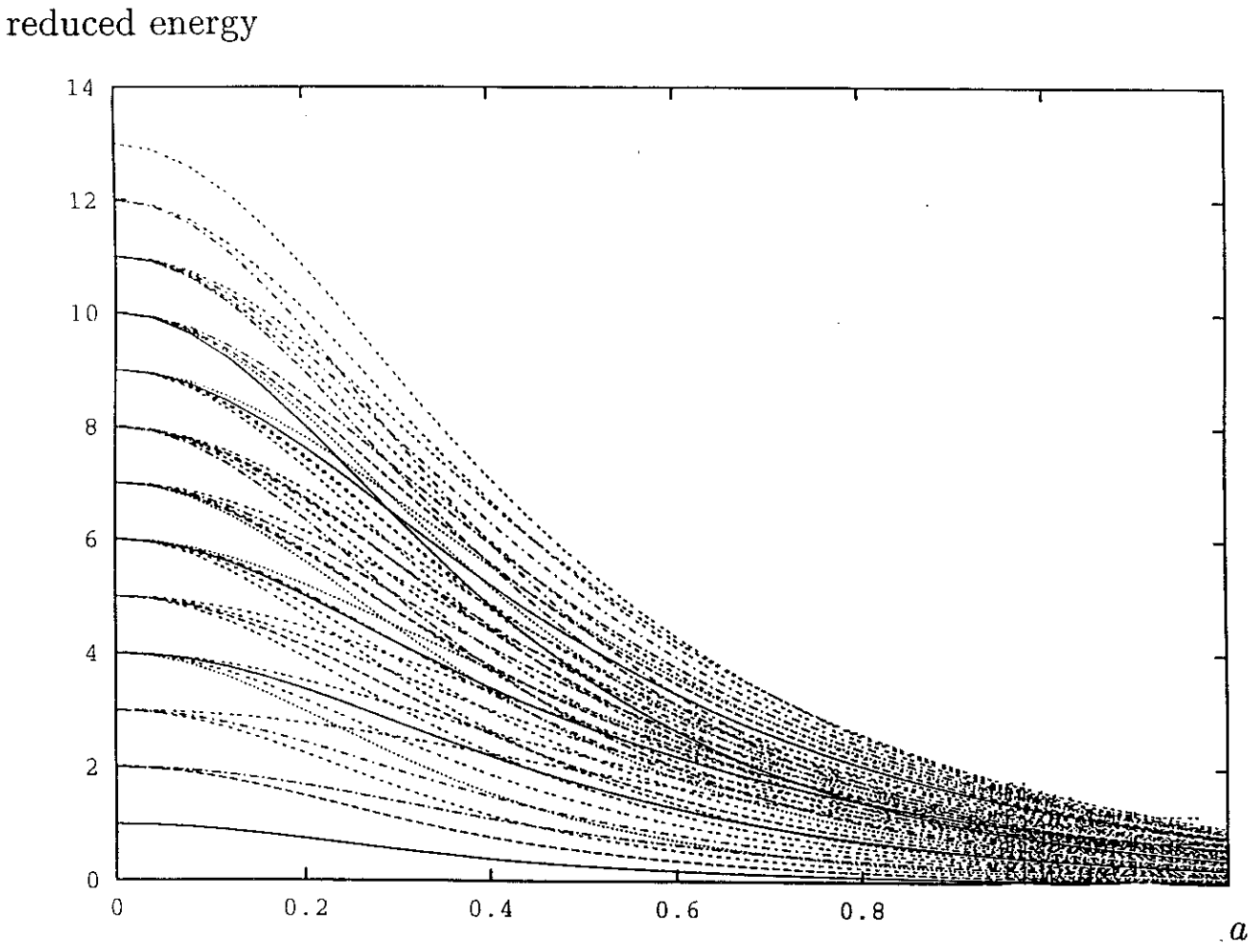

Figure 4.2: Evolution of some levels as a function of interactions. φ_q is a linear decreasing function of q, such as $\varphi_{q=0} = 2.5a$, and $\varphi_{q \geq 26L/2\pi} = 0$. a parametrizes the interaction strenght, and the energy is in units of $v_F \frac{2\pi}{L}$. For the plot to be readable, all the levels are not shown.

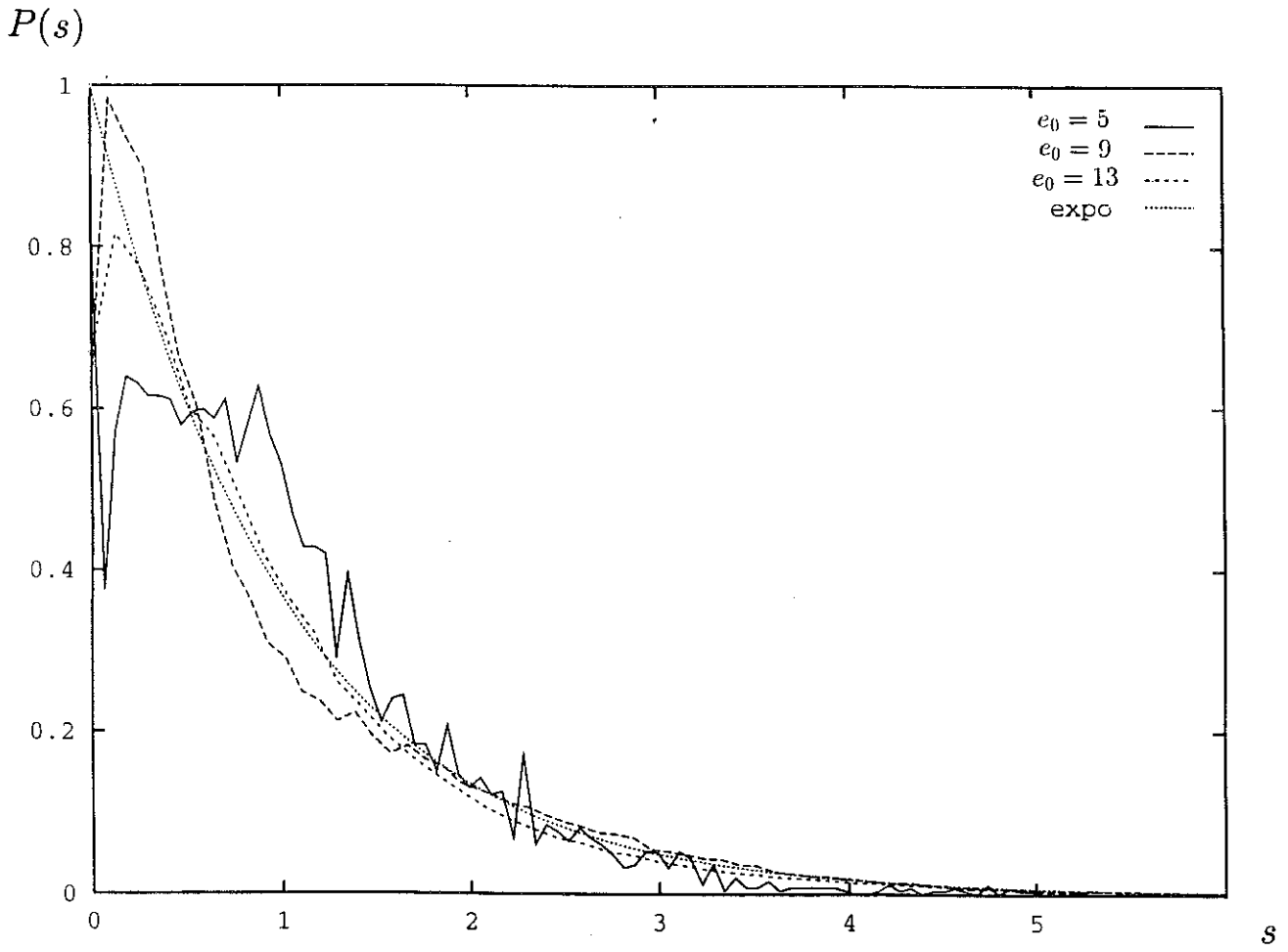

Figure 4.3: Evolution of the level spacing statistic as a function of the cut-off e_0. φ_q is a decreasing linear function, such as $\varphi_{q=0} = 0.25$ and $\varphi_{26\frac{2\pi}{L}} = 0$. The statistics converge slowly to a Poissonian distribution ("expo"). The statistics are plotted for e_0 equal to 5, 9, 13. The number of levels taken into account in the statistics is repectively: 4196, 97438, 1048214.

Limit $R = 0$

Consider the case of the two branch Luttinger liquid with $\frac{1}{R} = +\infty$, and a constant interaction, namely, for all q, $V_q = V$. In that case, all the bosonic modes keep their coherence whatever the value of ϵ. The decoherence time t_k, given in (4.62), is infinite. The condition (4.55) associated to the dephasings is always verified whatever the value of ϵ. The only remaining restriction for the switching on procedure to be successful is thus:

$$\epsilon \ll \frac{2v_F}{L}. \tag{4.79}$$

The level statistics are singular in this limit. The degeneracies of the fan of levels are never lifted, whatever the intensity of interactions V. The degenerate levels depend on V in the following way:

$$E(\{n_q\}) = \sum_{q>0} 2v_F q n_q (1 - (\frac{V}{v_F})^2)^{1/2}. \tag{4.80}$$

However, we note that the overlapp between the eigenstate thus constructed and the state obtained from the action of the bare electron operator on the interacting ground state is vanishing according to equation (4.50) since $R = 0$.

4.3 Level spacing statistics for a spin 1/2, one branch Luttinger model.

The rest of the article is devoted to the study of some models derived from the two branch, spinless Luttinger liquid model. We begin with the one branch Luttinger model, with spin 1/2, and a g_4 interaction. The kinetic energy term is:

$$H^0 = \sum_{k\sigma} v_F(k - k_F) : c^+_{k\sigma} c_{k\sigma} :, \tag{4.81}$$

where the label σ denotes the spin component along the z axis. The interaction is given by:

$$H^4 = \frac{g_4}{2L} \sum_{q\sigma} \rho_{q\sigma} \rho^+_{q-\sigma}. \tag{4.82}$$

The usual spin and charge combinations:

$$C^+_q = (\frac{\pi}{Lq})^{1/2} (\rho_{q\uparrow} + \rho_{q\downarrow}) \tag{4.83}$$

$$S^+_q = (\frac{\pi}{Lq})^{1/2} (\rho_{q\uparrow} - \rho_{q\downarrow}), \tag{4.84}$$

have bosonic commutation relations, and the total hamiltonian $H = H^0 + H^4$ is diagonal in terms of spin and charge variables:

$$H = v_C \sum_{q>0} q C^+_q C_q + v_S \sum_{q>0} q S^+_q S_q + v_F \frac{\pi}{2L} (N^2_\uparrow + N^2_\downarrow). \tag{4.85}$$

The charge and spin velocities are: $v_C = v_F + \frac{g_4}{2\pi}$ and $v_S = v_F - \frac{g_4}{2\pi}$.

The g_4 interaction is switched on adiabatically:

$$g_4(t) = g_4^0 e^{\epsilon t}. \tag{4.86}$$

The evolution operator is:

$$U_\epsilon(0, -\infty) = \exp\{-i \sum_{q>0} \frac{g_4^0}{2\pi\epsilon} q(n_{Cq} - n_{Sq})\}, \tag{4.87}$$

where $n_{Cq} = C_q^+ C_q$ and $n_{Sq} = S_q^+ S_q$. The overlap

$$F(x, x') = \langle \{N_p\} | \Psi_\uparrow(x') U_\epsilon^{-1}(0, -\infty) \Psi_\uparrow^+(x) U_\epsilon(0, -\infty) | \{N_p\} \rangle \tag{4.88}$$

is found to be equal to:

$$F(x, x') = \frac{1}{L} e^{i(\frac{\pi}{L}(2N_\uparrow + 1) + k_F)(x - x')} \frac{1}{(1 - e^{i\frac{2\pi}{L}(x - x' - \frac{g_4^0}{2\pi\epsilon})})^{1/2}} \frac{1}{(1 - e^{i\frac{2\pi}{L}(x - x' + \frac{g_4^0}{2\pi\epsilon})})^{1/2}}. \tag{4.89}$$

Spin charge separation is effective if the real space separation is of order $\frac{g_4^0}{4\pi\epsilon}$, which leads to the energy scale for spin charge decoupling:

$$g_4^* = \frac{4\pi^2\epsilon}{k}, \tag{4.90}$$

where k is the impulsion of the quasiparticle with respect to the Fermi surface. The switching on procedure is sucessful provided $g_4^0 \ll g_4^*$. Since the transformation (4.83) is independent on the interactions, there is no upper limit for the rate of switching on ϵ.

In the same way as for the Luttinger liquid, the sector of the Hilbert space has to remain stable under the action of the evolution operator (4.87). Since $U_\epsilon(0, -\infty)$ is diagonal in term of charge and spin variables, the relevant sector has a given impulsion k. This sector corresponds to a single fan of levels, with no crossings, except for $g_4 = 0$, leading to singular statistics. One may compute the statistics in the whole Hilbert space, namely to superpose the uncorrelated blocs with different impulsions. The statistics still remain singular. The degeneracies of some levels are not lifted for any value of the interaction g_4. These singularities correspond to remaining degeneracies as the impulsions of the charge and spin part are specified independently, and are reminiscent of the degeneracies of the free Luttinger model. The spectrum exhibits further singularities at non zero level spacings, due to the linear dependence of the levels in g_4: the statistics do not become poissonian even though uncorrelated sectors are superposed. Note that many degeneracies, and the singularities at non zero level spacings are expected to disappear if g_4 is not a constant as a function of q. In this more generic case, the Poisson statistics is expected.

4.4 Level spacing statistics for a model of 2 coupled chains

We now discuss the level statistics for a model of two coupled Luttinger liquids. This model is solved in [11] and we first remind some results.

The two chains kinetic energy is given by:

$$H^0 = v_F \sum_{k\alpha\sigma} (k - k_F) : c^+_{k\alpha\sigma} c_{k\alpha\sigma} :, \tag{4.91}$$

where α labels the chain and σ the spin. The interactions consist of a g_4 term:

$$H^4 = \frac{g_4}{2L} \sum_{k\sigma\alpha} \rho_{k\alpha\sigma} \rho^+_{k\alpha-\sigma}, \tag{4.92}$$

and of a hopping term between the two chains:

$$H^\perp = -t_\perp \sum_{k\sigma\alpha} c^+_{k\alpha\sigma} c_{k-\alpha\sigma}. \tag{4.93}$$

Only the case of two coupled one branch models is treated. This is sufficient since no interaction couples right and left fermions. Fabrizio and Parola [11] were able to diagonalize the hamiltonian $H = H^0 + H^4 + H^\perp$. The excitation spectrum of the model exhibits four branches:

$$\epsilon_\rho(q) = u_\rho q \tag{4.94}$$

$$\epsilon_\sigma(q) = u_\sigma q \tag{4.95}$$

$$\epsilon_+(q) = \frac{1}{2}(u_\rho + u_\sigma)q + \sqrt{(\frac{1}{2}(u_\rho - u_\sigma)q)^2 + 4t_\perp^2} \tag{4.96}$$

$$\epsilon_-(q) = \frac{1}{2}(u_\rho + u_\sigma)q - \sqrt{(\frac{1}{2}(u_\rho - u_\sigma)q)^2 + 4t_\perp^2} \tag{4.97}$$

The ground state is such as all the states with a negative energy are occupied, and all the states with a positive energy are empty. We computed the level statistics for a toy model with only the $\epsilon_-(q)$ branch, in a sector of given total impulsion q. We study the evolution of the statistics as the dimensionaless hopping constant $\tilde{t_\perp} = \frac{Lt_\perp}{\pi v_F}$ is fixed, and $\tilde{g_4} = \frac{g_4}{2\pi v_F}$ varies. The statistics exhibit a cross-over between two regimes as $\tilde{g_4}$ decreases. This cross-over is controlled by the same lenght scale $\xi = \frac{u_\rho - u_\sigma}{4t_\perp}$ as in [11]. If $q\xi \ll 1$, the statistics are singular, with a sharp peak at $s = 0$. In this regime, the dispersion relation $\epsilon_-(q)$ may be approximated as:

$$\epsilon_-(q) = \frac{1}{2}(u_\rho + u_\sigma)q - 2t_\perp. \tag{4.98}$$

The linear q dependance induces high degeneracies in the excitation spectrum, leading to a sharp peak for zero separation.

In the opposite regime ($q\xi \gg 1$), the statistics are poissonian. The corresponding spectrum is plotted on fig. 4.4. In that case, the curvature of the dispersion relation $\epsilon_-(q)$ is no longer negligeable, and individual fermion levels can no longer be considered as equidistant.

Notice that the cross-over observed here is similar to the case of the one dimensional, one branch Luttinger liquid with q-dependant interactions. In both cases, the dispersion relation is linear as the interaction parameter is set to zero (corresponding to a highly degenerate spectrum), and becomes non linear as interactions are switched on (leading to a random spectrum). This transition is independent of the bosonic or fermionic nature of the particles. In the one dimensional Luttinger liquid, we dealt with bosons, and the particles under consideration in the case of the two coupled chains are fermionic.

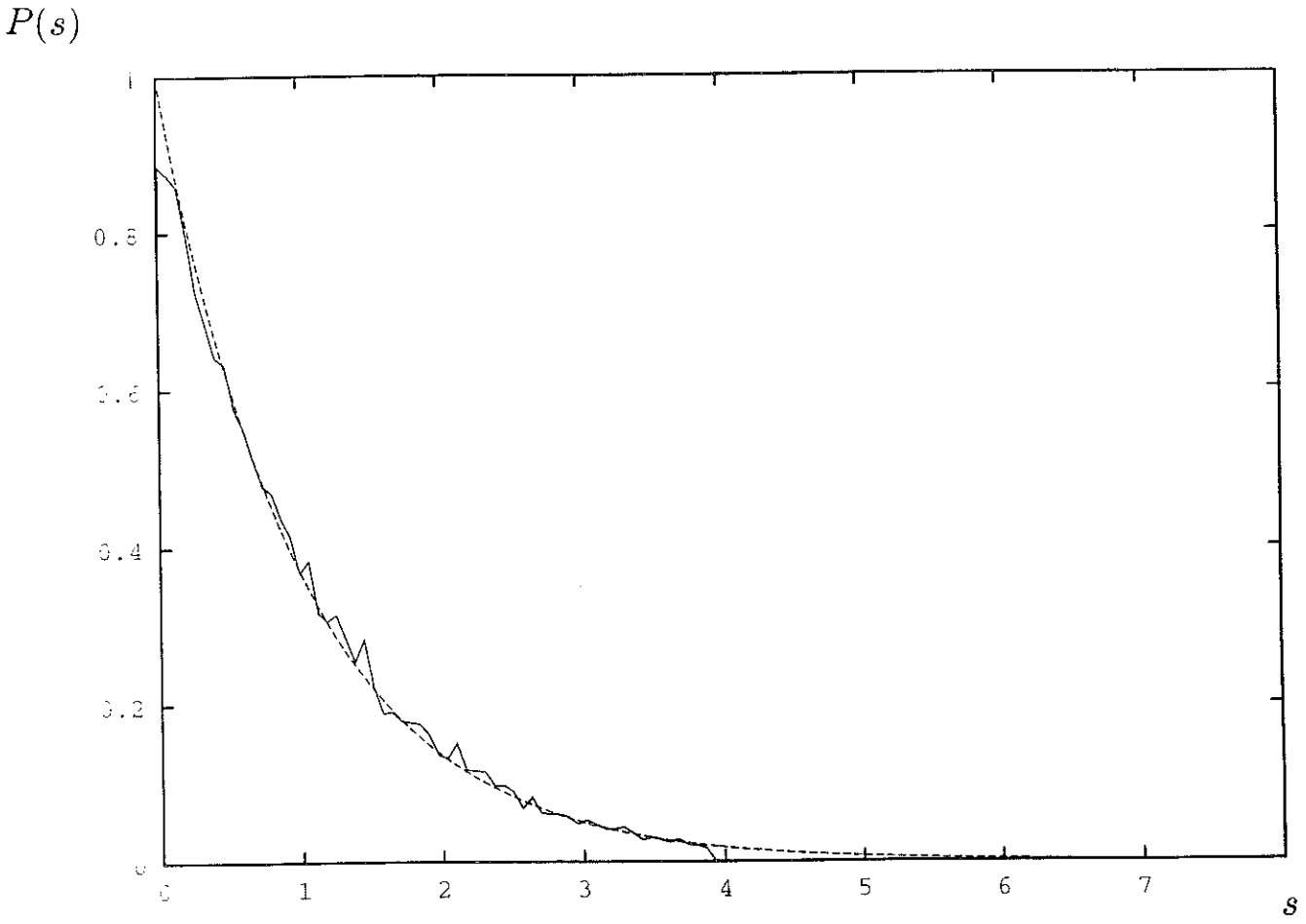

Figure 4.4: Level spacing statistics for the model of two coupled chains in the regime $q\xi \gg 1$. Only excitations of the lowest energy branch $\epsilon_-(q)$ are taken into account, and the analysis is restricted to the $1p-1h$ and $2p-2h$ excitations only, for parameters equal to: $p = 200$, $t_{per} = 20$, $g = 0.5$, with the following notations: p is the total impulsion divided by $\frac{2\pi}{L}$, $t_{per} = \frac{Lt_\perp}{\pi v_F}$ and $g = \frac{g_4}{2\pi v_F}$. 24000 states were generated. The value of the parameter $q\xi$ is 100.

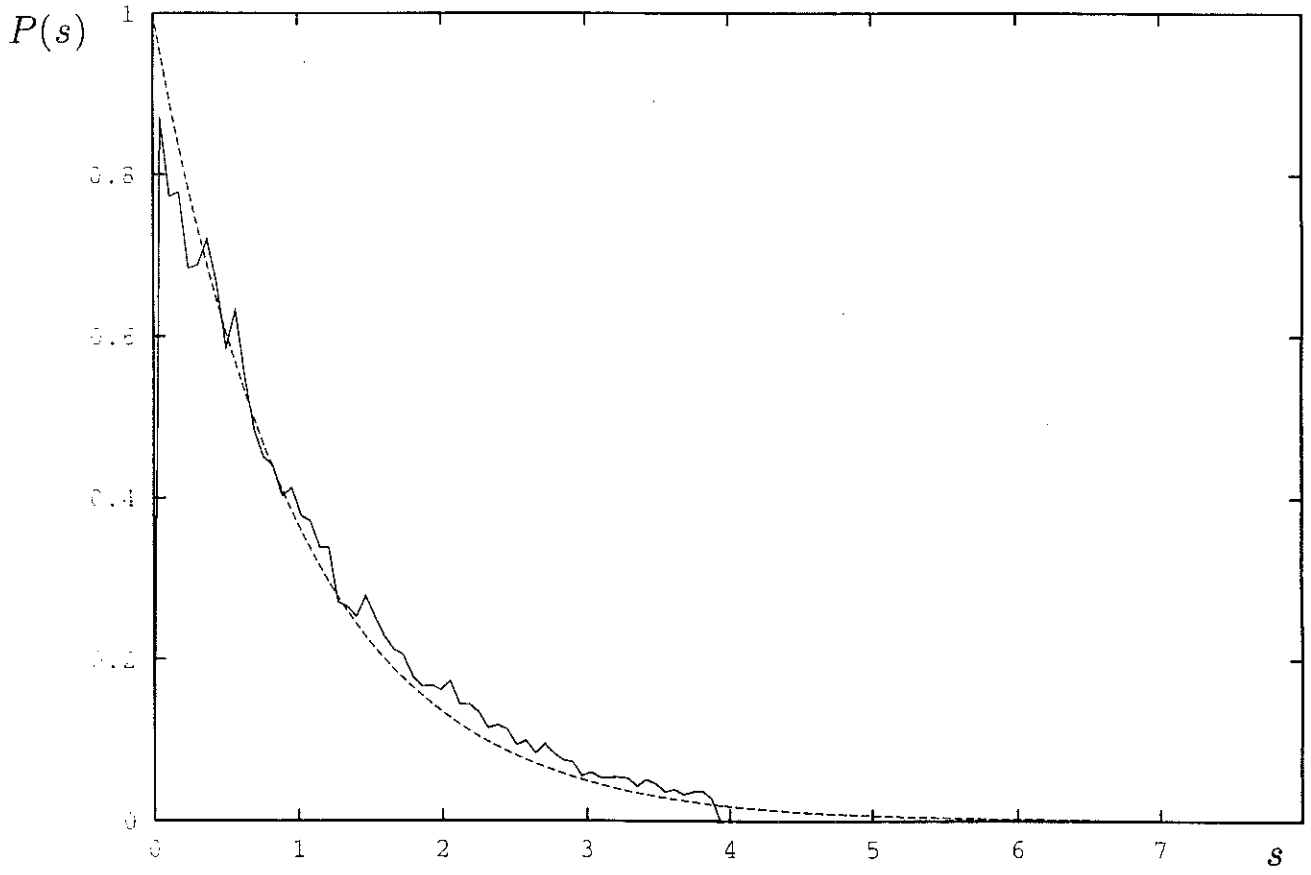

Figure 4.5: Level spacing statistics for the model of two coupled chains in the regime $q\xi \gg 1$, with the four excitation branches. Only $1p-1h$ and $2p-2h$ excitations were taken into account. The parameters are set to: $p = 100$, $t_{per} = 100$, $g = 0.5$ and $q\xi = 50$. The number of computed levels is 42692. Among them, 8293 separations are equal to zero. For visibility, the level statistics is cut off for separations inferior as 0.05, which supresses the large pic at zero separations.

What happens if we now take the four branches into account? In the regime $q\xi \gg 1$, we observe a peak for $s = 0$, coexisting with a poissonian distribution for non zero separations (see fig. 4.4, where the peak is suppressed for clarity). The peak for $s = 0$ is due to the degeneracies in the excitation spectrum, induced by the presence of the two linear branches. An exemple of such degenerate configurations, with 2 particle hole excitations is as follows: the two holes have impulsions h_1 and h_2, and belong to the ϵ_- branch. The particles with impulsions p_1 and p_2 are on the linear ϵ_ρ branch. Consider an other excitation, deduced from the previous one as follows: the holes have the same impulsions ($h_1' = h_1$ and $h_2' = h_2$). The impulsions of the particles are such as $p_1 + p_2 = p_1' + p_2'$. Since all the particles belong to the same linear branch, these configurations are degenerate.

Thus, the existence of the two regimes $q\xi \gg 1$ and $q\xi \ll 1$ in the coupled chains is reflected in the statistical properties of the spectrum. To summarize, we have studied a special class of models, since they are integrable for any value of the coupling constant. In general, a non interacting fermionic quasiparticle can be described as a linear combination of degenerate eigenstates, which undergo an energy splitting as interactions are switched on. This is responsible for the decay of such a quasiparticle state, and provides a lower bound for the switching rate ϵ, in the process of adiabatic construction of quasiparticles. The same degeneracy lifting has been found to modify the energy level spacing distribution, from a singular behaviour for a degenerate, non interacting system, to a more generic Poisson distribution already observed in many integrable systems. We should stress that both aspects are non universal features of the models. More precisely, they depends on the complete q-dependance of the interaction functions g_2 and g_4. By contrast, universal properties such as correlation function exponents depend only on the $q = 0$ limit of the couplings. We have seen that the vanishing of the quasiparticle residue, due to orthogonality catastrophy is also such an universal property, independant on the fine structure of the spectrum and its statistics.

In this paper, we couldn't address the question of strongly correlated fermion systems leading to gaussian orthogonal ensemble (G.O.E.) statistics. However, the present work indicates that one of the most interesting questions is whether the difference between G.O.E. or Poisson distribution is a universal feature of a low-energy fixed point or not. Our paper has been dedicated to fine tuning phenomenas within an integrable class of models, and the lack of universality found here is not surprising. Intuitively, the difference between Poisson and G.O.E. statistics is much more robust and might still be a way to distinguish between several physically non equivalent fixed points.

R. M. whishes to thank J.C. Anglès d'Auriac for help with programmation, P. Degiovanni for discussions about bosonisation and acknoledges the hospitality of NEC Research Institute where part of this job was performed.

References

[1] P.W. Anderson Phys. Rev. Lett. 64, 1839 (1990); Phys. Rev. Lett. 65, 2306 (1990) and Phys. Rev. Lett. 66, 3226 (1991).

[2] P.W. Anderson Phys. Rev. Lett. 71, 1220 (1993).

[3] For a recent review, see E. Dagotto, National High Magnetic Field Laboratory preprint (1993), Florida State University.

[4] G. Montambaux, D. Poilblanc, J. Belissard and C. Sire, Phys. Rev. Lett. 70, 497 (1993); T.C. Hsu and J.C. Anglès d'Auriac, Phys. Rev. B 47, 14291 (1993); D. Poilblanc, T. Ziman, J. Belissard, F. Mila and G. Montambaux, preprint (1993).

[5] A review on the connections between random matrix theory and chaos is by O. Bohigas, in "Chaos and Quantum Physics", proceeding of the Les Houches Summer School of Theoretical Physics, Les Houches, 1989, edited by M.J. Giannoni, A. Voros and J. Zinn-Justin (North Holland, Amsterdam, 1991).

[6] M.V. Berry and Tabor, Proc. R. Soc. Lond. A 356, 375 (1977).

[7] J.M. Luttinger, J. Math. Phys., 4, 1154 (1963).

[8] F.D.M. Haldane, J. Phys. C, 14, 2585 (1981).

[9] P. Nozières, "Le probleme à N corps", Dunod, Paris 1963.

[10] P.W. Anderson, Phys. Rev. Lett. 18, 1049 (1967).

[11] M. Fabrizio and A. Parola, Phys. Rev. Lett 70, 226 (1993).

Chapitre 5

Théorie de Landau du liquide de Fermi

Ce chapitre présente la théorie de Landau du liquide de Fermi. On fait l'hypothèse qu'il existe des quasiparticules et on cherche alors à en déduire les conséquences pour les grandeurs observables. Dans le chapitre 6, nous nous attacherons à retrouver le liquide de Fermi à partir d'une approche microscopique en utilisant la bosonisation de la surface de Fermi. Pour écrire ce chapitre, je me suis inspiré du livre de P.W. Anderson[1], du livre de Pines et Nozières[2], ainsi que du livre de J.W. Negele et H. Orland[3].

5.1 Notion de quasiparticule

5.1.1 Branchement adiabatique des interactions

La notion centrale de la théorie de Landau du liquide de Fermi (écrite par Landau autour de 1957) est la notion de quasiparticule. Si les interactions au sein d'un système de fermions sont suffisamment faibles, le système est dans un état liquide. Si la force des interactions augmente, il peut se produire une instabilité du liquide vers un état solide, le cross-over se produisant pour une interaction de l'ordre de la vitesse de Fermi, qui sera définie par la suite. On dira que les fermions sont dans l'état gazeux s'ils n'interagissent pas entre eux. Dans l'état gazeux et à température nulle, les fermions occupent une mer de Fermi: du fait du principe d'exclusion, les fermions s'empilent à raison d'un fermion par ensemble de nombres quantiques dans l'état d'énergie minimale. Avant de définir ce qu'est une quasiparticule, il convient de définir la notion de particule. On apelle *particule* un état à une particule occupé au-dessus de la surface de Fermi, et *trou* un état à une particule vide au-dessous de la surface de Fermi. La notion de quasiparticule s'appuie sur l'existence d'une procédure de branchement adiabatique des interactions, à partir de l'état gazeux. Durant le branchement adiabatique, les états de même symétrie sont supposés ne pas se croiser, et restent approximativement dans le même ordre. On se restreindra donc aux

[1] P.W. Anderson. *Basic notions of condensed matter physics*, Frontiers in physics, The Benjamin/Cummings publishing compagny (1984).

[2] D. Pines and P. Nozières, *The theory of quantum liquids*, vol. I *Normal Fermi liquids*, Advanced book classics, Addison-Wesley publishing compagny (1966).

[3] J. W. Negele and H. Orland *Quantum Many particule systems*, Frontiers in physics, The Benjamin/Cummings publishing compagny (1990).

systèmes dits *normaux*, c'est-à-dire tels que les interactions ne génèrent pas d'états liés, comme c'est le cas pour la théorie BCS de la supraconductivité. La théorie que nous allons décrire s'applique à ^{3}He liquide, au gaz d'électrons dans les métaux et à la matière nucléaire. D'autre part, on effectuera la simplification d'oublier le spin, qui n'apportera pas grand chose puisque l'on exclut a priori les systèmes supraconducteurs. L'utilisation d'électrons fictifs sans spin ne changera qualitativement pas la physique que nous allons décrire. Cependant, nous sommes conscients du fait que le spin joue un rôle crucial pour d'autres modèles de liquides quantiques, tels que le modèle de Hubbard, pour lequel le traitement suivant est inadapté. On prend l'exemple de la physique nucléaire afin de donner une illustration expérimentale à la notion de quasiparticule. Il existe des résonances géantes, visibles dans les sections efficaces de réactions lorsque l'on ajoute un nucléon dans une réaction. Ces résonances géantes peuvent s'interpréter comme le fait que le nucléon s'installe d'abord dans un état de quasiparticule, qui n'est pas un état propre exact du système. Au cours du temps, cet état décroît dans quelques dizaines ou quelques centaines d'états propres exacts du système. Une quasiparticule ne correspond donc pas à un état propre exact du système. Cependant, sur une échelle de temps courte par rapport à la durée de vie de la quasiparticule, on peut considérer que la quasiparticule remplit un état à une particule. Sur le plan théorique, on définit[4] une quasiparticule par une expérience de pensée qui consiste à partir du gaz au temps $t = -\infty$ et à brancher les interactions avec un temps de branchement de l'ordre de $1/\epsilon$. Les informations expérimentales que nous avons données auparavant sur les état de type 'quasiparticule' dans la matière nucléaire permettent d'imposer des conditions sur le taux du branchement des interactions ϵ. La première condition sur le taux de branchement est que la résolution en énergie permise par la procédure de branchement des interactions soit petite comparée à l'énergie des états propres. Si l'on veut propager adiabatiquement une excitation du gaz d'énergie ϵ_k, il faut que $1/\epsilon \gg 1/\epsilon_k$, soit encore $\epsilon \ll \epsilon_k$. La seconde condition que doit vérifier le taux de branchement est que le temps sur lequel les interactions sont branchées soit petit comparé à la durée de vie de la quasiparticule, sans quoi la quasiparticule s'est décomposée sur les états propres exacts du système avant même la fin du branchement des interactions. Si l'on désigne par τ la durée de vie de la quasiparticule, le taux de branchement doit être tel que $\epsilon \gg 1/\tau$. Les deux conditions énoncées ci-dessus se resument en

$$\frac{1}{\tau} \ll \epsilon \ll \epsilon_k. \tag{5.1}$$

Un liquide quantique est descriptible par la théorie de Landau à condition qu'il existe un taux de branchement satisfaisant (5.1), c'est-à-dire à condition que la condition de compatibilité

$$\frac{1}{\tau} \ll \epsilon_k \tag{5.2}$$

soit bien vérifiée.

5.1.2 Règle d'or pour le liquide de Fermi en dimension $d > 1$

On se propose de montrer à l'aide de la règle d'or de Fermi que la condition de compatibilité $1/\tau \ll \epsilon_k$ est bien satisfaite pour le liquide de Fermi en dimension $d > 1$. Pour ce faire, on doit évaluer le temps de vie de l'état constitué d'une particule d'impulsion initiale $\mathbf{k}$ habillée par les interactions. L'effet des interactions entre la particule et la mer de Fermi est de créer

[4] en suivant les idées de Landau.

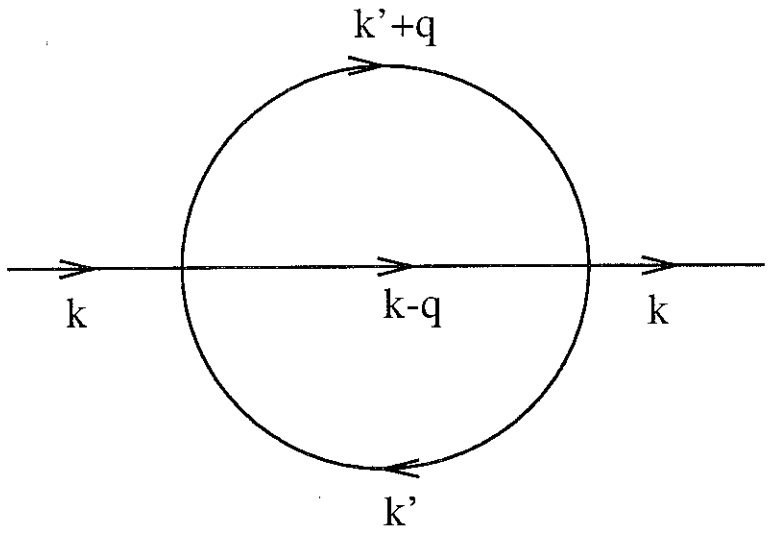

Figure 5.1: Diagramme de Feynman symbolisant l'habillage d'un fermion d'impulsion $\mathbf{k}$ par une paire particule-trou. L'état intermédiaire est constitué par deux fermions d'impulsions $\mathbf{k}-\mathbf{q}$ et $\mathbf{k}'+\mathbf{q}$, ainsi que d'un trou d'impulsion $\mathbf{k}'$.

des paires particule-trou. A l'ordre le plus bas en interaction, on considère uniquement le processus d'excitation d'une seule paire particule-trou, c'est-à-dire l'habillage du fermion initial d'impulsion $\mathbf{k}$ par une paire particule-trou. L'état habillé correspond à une quasiparticule simplifiée. L'état intermédiaire sera constitué de deux particules d'impulsions $\mathbf{k}-\mathbf{q}$ et $\mathbf{k}'+\mathbf{q}$, où $\mathbf{q}$ désigne le transfert d'impulsion. Ce processus est schématisé sur le diagramme de Feynman de la figure 5.1. Par convention, une flèche vers la droite symbolise une particule et une flèche vers la gauche un trou. La variation en énergie due à la présence de la paire particule-trou s'obtient au second ordre de la théorie des perturbations comme

$$\Delta E = \int d\mathbf{q}d\mathbf{k}' \frac{|V(\mathbf{q})|^2}{\epsilon_{\mathbf{k}-\mathbf{q}} + \epsilon_{\mathbf{k}'+\mathbf{q}} - \epsilon_{\mathbf{k}} - \epsilon_{\mathbf{k}'} - i\eta}. \tag{5.3}$$

Dans cette expression, $\mathbf{k}'$ est en-dessous du niveau de Fermi, $\mathbf{k}'+\mathbf{q}$ et $\mathbf{k}-\mathbf{q}$ sont au-dessus du niveau de Fermi. Le signe de la petite partie imaginaire au dénominateur est choisi de telle sorte que la partie imaginaire de ΔE, qui s'interprète comme l'inverse du temps de vie de l'état intermédiaire, soit positive. On déduit de (5.3) le temps de vie τ de l'état à trois corps

$$\frac{1}{\tau} = \int d\mathbf{q}d\mathbf{k}'|V(\mathbf{q})|^2 \mathrm{Im}\left(\frac{1}{\epsilon_{\mathbf{k}-\mathbf{q}} + \epsilon_{\mathbf{k}'+\mathbf{q}} - \epsilon_{\mathbf{k}} - \epsilon_{\mathbf{k}'} - i\eta}\right). \tag{5.4}$$

Comme

$$\lim_{\eta\to 0} \frac{1}{x+i\eta} = P\frac{1}{x} - i\pi\delta(x), \tag{5.5}$$

on obtient

$$\frac{1}{\tau} = \pi \int d\mathbf{q}d\mathbf{k}'\delta(\epsilon_{\mathbf{k}-\mathbf{q}} + \epsilon_{\mathbf{k}'+\mathbf{q}} - \epsilon_{\mathbf{k}} - \epsilon_{\mathbf{k}'})|V(\mathbf{q})|^2. \tag{5.6}$$

L'intégrale double correspond à l'espace des phases du diagramme de la figure 5.1, que l'on va maintenant évaluer grossièrement. La première approximation consiste à supposer que $V(\mathbf{q})$ est

une constante V indépendante de $\mathbf{q}$, ce qui revient à choisir des interactions locales. A cause de la contrainte imposée par la fonction δ de Dirac

$$\epsilon_{\mathbf{k}} - \mu = (\epsilon_{\mathbf{k}-\mathbf{q}} - \mu) + (\epsilon_{\mathbf{k}'+\mathbf{q}} - \mu) - (\epsilon_{\mathbf{k}'} - \mu), \tag{5.7}$$

et comme les énergies $\epsilon_{\mathbf{k}} - \mu$, $\epsilon_{\mathbf{k}-\mathbf{q}} - \mu$, $\epsilon_{\mathbf{k}'+\mathbf{q}} - \mu$ et $-\epsilon_{\mathbf{k}'} + \mu$, sont positives, les energies $\epsilon_{\mathbf{k}-\mathbf{q}} - \mu$, $\epsilon_{\mathbf{k}'+\mathbf{q}} - \mu$ et $-\epsilon_{\mathbf{k}'} + \mu$ sont dans l'intervalle $[0, \epsilon_{\mathbf{k}}]$, ce qui permet d'évaluer simplement l'espace de phases de l'intégrale (5.6) et d'obtenir l'approximation suivante pour l'inverse du temps de vie de la quasiparticule

$$\frac{1}{\tau} \sim (\epsilon_{\mathbf{k}} - \mu)^2 V^2. \tag{5.8}$$

Cependant, cette expression n'est pas homogène. Afin de l'homogénéiser, il faut diviser par la puissance troisième d'une énergie. On choisit de normaliser par rapport à l'énergie de Fermi ϵ_f. Finalement, on peut majorer l'interaction V par l'énergie de Fermi, qui n'est autre que la condition à laquelle le système reste liquide. On obtient donc la minoration suivante du temps de vie de l'état à trois corps qui représente une quasiparticule à l'ordre le plus bas en interaction:

$$\frac{1}{\tau} \leq \frac{(\epsilon_{\mathbf{k}} - \mu)^2}{\epsilon_f}. \tag{5.9}$$

Comme, par définition du potentiel chimique, $\epsilon_{\mathbf{k}} - \mu \to 0$ si $|\mathbf{k}| \to k_f$, la condition de compatibilité (5.2) est automatiquement vérifiée pour des quasiparticules au voisinage de la surface de Fermi en dimension supérieure a 1. En dimension 1, cette condition n'est pas vérifiée, ce qui prouve que le liquide quantique de dimension 1 n'est pas un liquide de Fermi. Dans ce cas, on obtient un *liquide de Luttinger*, que l'on se propose d'étudier dans un chapitre ultérieur. Il s'avère que dans le domaine perturbatif, le liquide de Luttinger sur un anneau de taille finie est un liquide de Fermi sous réserve qu'une condition de compatibilité analogue à (5.2) soit vérifiée. On démontrera cette relation au chapitre 4, en étudiant la propagation adiabatique des états dans le liquide de Luttinger.

5.1.3 Paramétrisation des interactions dans la théorie de Landau

Dans le reste de ce chapitre, on note $\epsilon_{\mathbf{k}}$ l'énergie des fermions libres, comptée par rapport au niveau de Fermi. L'énergie d'interaction entre les quasiparticules $\mathbf{k}$ et $\mathbf{k}'$ est notée $f_{\mathbf{k},\mathbf{k}'}$. Une configuration de quasiparticules est notée $\{\delta n_{\mathbf{k}}\}$, où $\delta n_{\mathbf{k}} = +1$ pour une quasiparticule et $\delta n_{\mathbf{k}} = -1$ pour un quasitrou, c'est-à-dire que

$$\delta n_{\mathbf{k}} = n_{\mathbf{k}} - n^0_{\mathbf{k}}, \tag{5.10}$$

où

$$n^0_{\mathbf{k}} = \theta(\mu - \epsilon_{\mathbf{k}}) \tag{5.11}$$

à température nulle, μ désignant le potentiel chimique. L'énergie d'une configuration de quasiparticules s'écrit (l'énergie du fondamental étant choisie nulle):

$$\delta E = \sum_{\mathbf{k}} \epsilon_{\mathbf{k}} \delta n_{\mathbf{k}} + \frac{1}{2V} \sum_{\mathbf{k},\mathbf{k}'} f_{\mathbf{k},\mathbf{k}'} \delta n_{\mathbf{k}} \delta n_{\mathbf{k}'}. \tag{5.12}$$

L'énergie d'une quasiparticule d'impulsion k renormalisée par la présence des autres quasiparticules est notée $\tilde{\epsilon}_{\mathbf{k}}$ et vaut

$$\tilde{\epsilon}_{\mathbf{k}} = \frac{\delta E}{\delta n_{\mathbf{k}}} = \epsilon_{\mathbf{k}} + \frac{1}{V}\sum_{\mathbf{k}'} f_{\mathbf{k},\mathbf{k}'}\delta n_{\mathbf{k}'} \tag{5.13}$$

La dérivée seconde de l'énergie donne l'interaction entre quasiparticules

$$\frac{1}{V} f_{\mathbf{k},\mathbf{k}'} = \frac{\delta^2 E}{\delta n_{\mathbf{k}} \delta n_{\mathbf{k}'}}, \tag{5.14}$$

ce qui montre que les paramètres des interactions $f_{\mathbf{k},\mathbf{k}'}$ sont symétriques: $f_{\mathbf{k},\mathbf{k}'} = f_{\mathbf{k}',\mathbf{k}}$. Comme on ne s'interesse qu'à des excitations particule-trou localisées au voisinage de la surface de Fermi, k et k′ sont localisés sur la surface de Fermi, et, pour un système invariant par translation, $f_{\mathbf{k},\mathbf{k}'}$ ne dépend que de l'angle θ entre k et k′. On peut donc développer les paramètres de Landau $f_{\mathbf{k},\mathbf{k}'}$ sur la base des polynômes de Legendre:

$$f_{\mathbf{k},\mathbf{k}'} = \sum_{l=0}^{+\infty} f_l P_l(\cos\theta). \tag{5.15}$$

En utilisant la relation d'orthogonalité des polynômes de Legendre

$$\frac{2l+1}{2}\int_{-1}^{1} P_l(\cos\theta)P_{l'}(\cos\theta)d(\cos\theta) = \delta_{l,l'}, \tag{5.16}$$

la relation (5.15) s'inverse selon

$$f_l = \frac{2l+1}{4\pi}\int d\Omega P_l(\cos\theta) f_{\mathbf{k},\mathbf{k}'}. \tag{5.17}$$

En pratique, on se contente des premiers coefficients, ce qui donne seulement un petit nombre de paramètres phénoménologiques à la théorie. Comme on le verra par la suite, on peut relier les premiers coefficients f_l à des quantités accessibles expérimentalement. Ainsi, f_1 est relié à la masse effective, et accessible via une mesure de chaleur spécifique; f_0 est relié à la compressibilité du système.

5.2 Propriétés d'équilibre du liquide de Fermi normal

Un des paramètres important de la théorie est la masse effective M^*, définie en terme de vitesse de groupe à la surface de Fermi

$$v_f = \frac{d\epsilon_{k_f}}{dk} = \frac{k_f}{M^*}, \tag{5.18}$$

et de même,

$$\mathbf{v}_{\mathbf{k}} = \nabla_{\mathbf{k}}\epsilon_{\mathbf{k}} = \frac{\mathbf{k}}{M^*} \tag{5.19}$$

Comme on va le voir, la masse effective M^* est reliée à la chaleur spécifique du liquide de Fermi.

5.2.1 Chaleur spécifique du liquide de fermi

La distribution de quasiparticules à température non nulle obéit à la statistique de Fermi-Dirac, dont la fonction de distribution est donnée par

$$n^0_{\mathbf{k}}(T) = [1 + \exp\beta(\epsilon_{\mathbf{k}} - \mu)]^{-1}. \tag{5.20}$$

β est défini par $\beta = 1/k_B T$, où k_B est la constante de Boltzmann. A température nulle, les équations (5.10), (5.11),(5.12) et (5.20) forment un système d'équations auto-cohérentes. Cependant, afin de calculer la chaleur spécifique, il n'est pas nécessaire de résoudre ce système compliqué à condition que l'on ne s'intéresse qu'au comportement dominant à basses températures. En effet, le terme proportionnel à $\delta n_{\mathbf{k}}$ dans (5.12) donne une contribution à l'énergie proportionnelle à T^2 et donc une chaleur spécifique linéaire, alors que le terme d'interactions entre quasiparticules de (5.12) contribue à des ordres supérieurs à la chaleur spécifique. La chaleur spécifique à l'ordre linéaire en T est indépendante des paramètres $f_{\mathbf{k},\mathbf{k}'}$, et le calcul se mène de la façon suivante. Tout d'abord, l'énergie s'écrit

$$\delta E = \sum_{\mathbf{k}} \epsilon_{\mathbf{k}} \delta n_{\mathbf{k}} \tag{5.21}$$

$$= \sum_{\mathbf{k},|\mathbf{k}|<k_f} v_f|\mathbf{k}|(n^0_{\mathbf{k}}(T) - 1) + \sum_{\mathbf{k},|\mathbf{k}|>k_f} v_f|\mathbf{k}|n^0_{\mathbf{k}}(T) \tag{5.22}$$

On veut maintenant transformer les sommations sur k en des intégrales sur l'énergie. Pour cela, on utilise

$$\sum_{\mathbf{k}} f(|\mathbf{k}|) = \int dE \sum_{\mathbf{k}} \delta(\epsilon_{\mathbf{k}} - E) f(E). \tag{5.23}$$

Dans cette expression, la somme

$$\sum_{\mathbf{k}} \delta(\epsilon_{\mathbf{k}} - E - \mu) \tag{5.24}$$

compte le nombre d'états d'énergie E par rapport à l'énergie de Fermi. Cette quantité est continue à la traversée de la surface de Fermi dans les systèmes qui nous interessent, et l'on fait l'approximation qu'elle est constante au voisinage de la surface de Fermi. On note $N(0)$ la densité d'états par rapport au niveau de Fermi:

$$N(0) = \frac{1}{V} \sum_{\mathbf{k}} \delta(\epsilon_{\mathbf{k}} - \mu). \tag{5.25}$$

En utilisant (5.18), la densité d'états au niveau de Fermi s'exprime selon

$$N(0) = \frac{1}{(2\pi)^3} \int 4\pi k^2 dk \delta(v_f(k - k_f)) = \frac{M^* k_f}{2\pi^2}. \tag{5.26}$$

En utilisant la densité d'états au niveau de Fermi, on peut transformer les sommations (5.22) en utilisant

$$\frac{1}{V} \sum_{\mathbf{k}} f(\mathbf{k}) = N(0) \int dE f(E), \tag{5.27}$$

ce qui donne

$$\frac{\delta E}{V} = 2N(0) \int_0^{+\infty} \frac{E}{1 + \exp\beta E} dE = 2N(0) k_B^2 T^2 \int_0^{+\infty} \frac{u}{1 + \exp u} du. \tag{5.28}$$

En utilisant le résultat

$$\int_0^{+\infty} \frac{u}{1+\exp u} = \frac{\pi^2}{12}, \tag{5.29}$$

on obtient

$$\frac{\delta E}{V} = \frac{\pi^2}{6} N(0) k_B^2 T^2. \tag{5.30}$$

La chaleur spécifique est reliée à l'énergie par la définition

$$c_V = \frac{1}{V}\left(\frac{\partial \delta E}{\partial T}\right)_V, \tag{5.31}$$

ce qui permet d'obtenir

$$c_V = \frac{\pi^2}{3} N(0) k_B^2 T = \frac{1}{6} M^* k_f k_B^2 T. \tag{5.32}$$

Une mesure de chaleur spécifique à l'ordre linéaire en T donne donc accès à la masse effective M^*. Pour ^{3}He, le rapport M^*/M vaut environ 3 à pression nulle. Pour les composés à fermions lourds, tels que Ce Cu_2 Si_2, U Pt_3, U_2 Zn_{17} et Ce Al_3, M^*/M vaut environ 10^2 à 10^3.

5.2.2 Compressibilité et vitesse du son

La compressibilité χ d'un fluide est définie par

$$\frac{1}{\chi} = -V\frac{\partial P}{\partial V} = \rho \frac{\partial P}{\partial \rho} \tag{5.33}$$

où $\rho = N/V$ est la densité. La vitesse du son c dans le fluide est reliée à la compressibilité par la relation usuelle

$$c^2 = \frac{1}{M}\frac{\partial P}{\partial \rho} = \frac{1}{M\rho\chi}. \tag{5.34}$$

On cherche maintenant à exprimer la compressibilité en fonction des paramètres de la théorie de Landau. Pour celà, on remarque que l'énergie libre est extensive, et qu'elle peut par conséquent s'exprimer sous la forme

$$F(T,V,N) = V f(T,\rho), \tag{5.35}$$

où f est l'énergie libre par unité de volume. La compressibilité se réexprime en fonction de f selon

$$\frac{1}{\chi} = \rho^2 \frac{\partial^2}{\partial \rho^2} f(T,\rho) \tag{5.36}$$

On peut aussi exprimer la compressibilité à l'aide du potentiel chimique

$$\mu = \frac{\partial F}{\partial N} = \frac{\partial}{\partial \rho} f(T,\rho). \tag{5.37}$$

La compressibilité devient alors

$$\frac{1}{\chi} = \rho^2 \frac{\partial \mu}{\partial \rho} \tag{5.38}$$

Afin de calculer $\partial\mu/\partial\rho$, on remarque que $\mu = \tilde{\epsilon}_{k_f}$, où $\tilde{\epsilon}$ est la fonctionelle (5.13) de $\delta n_{\mathbf{k}}$, et on obtient

$$\frac{\partial \mu}{\partial \rho} = \frac{\partial \epsilon_{k_f}}{\partial \rho} + \frac{1}{V}\sum_{\mathbf{k}'} f(\mathbf{k_f}, \mathbf{k}') \frac{\partial \delta n_{\mathbf{k}'}}{\partial k_k} \frac{\partial k_f}{\partial \rho} \tag{5.39}$$

En utilisant le fait que $\rho = k_f^3/6\pi^2$, on obtient $\partial k_f/\partial\rho = 2\pi^2/k_f^2$. D'autre part, $\partial\delta n_{\mathbf{k}}/\partial k_f = \delta(|\mathbf{k}| - k_f)$. En utilisant en outre (5.18), l'expression (5.39) se transforme en

$$\frac{\partial\mu}{\partial\rho} = \frac{2\pi^2}{M^* k_f} + \frac{2\pi^2}{k_f^2}\int \frac{d\mathbf{k}'}{(2\pi)^3} f(\mathbf{k_f}, \mathbf{k}')\delta(|\mathbf{k}'| - k_f) \tag{5.40}$$

$$= \frac{2\pi^2}{M^* k_f} + \frac{1}{4\pi}\int d\Omega f(\Omega). \tag{5.41}$$

La compressibilité s'exprime donc comme

$$\frac{1}{\chi} = \frac{\rho k_f^2}{3M^*}(1 + F_0), \tag{5.42}$$

où les coefficients F_l sont définis par

$$F_l = \frac{k_f M^*}{2\pi^2} f_l = N(0) f_l. \tag{5.43}$$

Connaissant la masse effective M^* par une mesure de la chaleur spécifique, on obtient F_0 par une mesure de compressibilité. La relation (5.42) indique que le liquide de Fermi est stable à condition que

$$F_0 > -1. \tag{5.44}$$

Nous verrons ultérieurement qu'il existe une condition de stabilité analogue à (5.44) pour tous les coefficients F_l.

5.3 Théorie cinétique du gaz de quasiparticules

Jusqu'à présent, la distribution $n_{\mathbf{k}}$ était indépendante de l'espace et du temps. On applique maintenant au sytème une petite perturbation dépendant de l'espace et du temps, et l'on suppose que le système répond à cette perturbation de façon linéaire. On est donc amené à introduire une fonction de distribution $n_{\mathbf{k}}(\mathbf{x}, t)$ dépendant de l'espace et du temps. Le principe d'incertitude n'est pas violé si l'on se restreint à des phénomènes macroscopiques. Ayant supposé une réponse linéaire du système, chaque mode de Fourier peut être traité séparément. Il suffit donc de considérer un mode de Fourier particulier.

$$n_{\mathbf{k}}(\mathbf{x}, t) = n^0_{\mathbf{k}} + \delta n_{\mathbf{k}}(\mathbf{q}, \omega) e^{i(\mathbf{q}.\mathbf{x} - \omega t)}. \tag{5.45}$$

Le principe d'incertitude de Heisenberg donne lieu à une incertitude en impulsion de l'ordre de $\hbar\mathbf{q}$ et une incertitude en énergie de l'ordre de $\hbar\omega$. Cette incertitude est à comparer avec l'échelle de variation de $n^0_{\mathbf{k}}$ à la température T, qui vaut $k_B T$. On déduit donc que la relation (5.45) a un sens à condition que

$$\hbar q v_f \ll k_B T \tag{5.46}$$

$$\hbar\omega \ll k_B T \tag{5.47}$$

Sous ces hypothèses, l'énergie est une fonctionelle de $\delta n_{\mathbf{k}}(\mathbf{x}, t)$. La forme la plus générale du développement à l'ordre 2 de l'énergie en fonction de $\delta n_{\mathbf{k}}(\mathbf{x}, t)$ est

$$\delta E = \sum_{\mathbf{k}} \int d\mathbf{x}\epsilon(\mathbf{k}, \mathbf{x})\delta n_{\mathbf{k}}(\mathbf{x}) + \frac{1}{2V}\sum_{\mathbf{k},\mathbf{k}'}\int\int d\mathbf{x}d\mathbf{x}' f(\mathbf{k}\mathbf{x}, \mathbf{k}'\mathbf{x}')\delta n_{\mathbf{k}}(\mathbf{x})\delta n_{\mathbf{k}'}(\mathbf{x}'). \tag{5.48}$$

On simplifie (5.48) en faisant plusieurs hypothèses. Tout d'abord, le système est invariant par translation, donc $f(\mathrm{kx}, \mathrm{k'x'})$ ne dépend que de la différence $\mathrm{x}-\mathrm{x'}$. D'autre part, on ne s'interesse qu'à des forces à courte portée, ne jouant que sur des distances de l'ordre de la taille atomique (c'est effectivement le cas pour ^{3}He). Comme la perturbation est macroscopique, $\delta n_{\mathbf{k}}(\mathrm{x})$ varie sur des échelles macroscopiques, et est donc constant à l'échelle des interactions. On peut donc remplacer dans (5.48) $\delta n_{\mathbf{k}}(\mathrm{x'})$ par $\delta n_{\mathbf{k}}(\mathrm{x})$.Ces simplifications conduisent à la forme suivante de l'énergie

$$\delta E = \int \delta E(\mathrm{x}) \tag{5.49}$$

$$\delta E(\mathrm{x}) = \sum_{\mathbf{k}} \epsilon_{\mathbf{k}} \delta n_{\mathbf{k}}(\mathrm{x}) + \frac{1}{2V} \sum_{\mathbf{k},\mathbf{k'}} f_{\mathbf{k},\mathbf{k'}} \delta n_{\mathbf{k}}(\mathrm{x}) \delta n_{\mathbf{k'}}(\mathrm{x}), \tag{5.50}$$

avec

$$f_{\mathbf{k},\mathbf{k'}} = \int d\mathrm{x'} f(\mathrm{kx}, \mathrm{k'x'}). \tag{5.51}$$

A cause des interactions à courte portée, les relations définissant les interactions sont locales. On est maintenant en mesure d'écrire l'équation de transport des quasiparticules. Selon (5.50), l'énergie d'excitation locale d'une quasiparticule est égale à

$$\tilde{\epsilon}_{\mathbf{k}}(\mathrm{x}) = \epsilon_{\mathbf{k}} + \frac{1}{V} \sum_{\mathbf{k'}} f_{\mathbf{k},\mathbf{k'}} \delta n_{\mathbf{k'}}(\mathrm{x}). \tag{5.52}$$

Landau a considéré un gaz de quasiparticules indépendantes, décrites par un Hamiltonien classique $\tilde{\epsilon}_{\mathbf{k}}(\mathrm{x})$. On va donc s'attacher à écrire une théorie cinétique du gaz de quasiparticules. L'écoulement des quasiparticules dans l'espace des phases (x, k) est soumis tout d'abord à un entraînement $\nabla_{\mathbf{k}} \tilde{\epsilon}_{\mathbf{k}}$ dû à la vitesse de la quasiparticule, et également à une force de diffusion $-\nabla_{\mathrm{x}} \tilde{\epsilon}_{\mathbf{k}}$ qui pousse les quasiparticules vers les régions d'énergie minimale. L'équation de transport, en l'absence de collisions, traduit la conservation des quasiparticules sous ces deux actions. Soit $\delta N(\mathrm{x}, \mathrm{k}, t)$ le nombre de quasiparticules autour du point de coordonnées (x, k), dans un élément de volume $(\delta \mathrm{x}, \delta \mathrm{k})$. Alors,

$$\delta N(\mathrm{x}, \mathrm{k}, t) = \delta N(\mathrm{x} + \nabla_{\mathbf{k}} \tilde{\epsilon}_{\mathbf{k}} \delta t, \mathrm{k} - \nabla_{\mathrm{x}} \tilde{\epsilon}_{\mathbf{k}} \delta t, t + \delta t) \tag{5.53}$$

à cause de la conservation du nombre de quasiparticules lors de l'écoulement dans l'espace des phases. En développant l'équation (5.53) sous la forme

$$\nabla_{\mathrm{x}} \delta N . \nabla_{\mathbf{k}} \tilde{\epsilon}_{\mathbf{k}} \delta t - \nabla_{\mathbf{k}} \delta N . \nabla_{\mathrm{x}} \tilde{\epsilon}_{\mathbf{k}} \delta t + \partial_t \delta N \delta t = 0, \tag{5.54}$$

et en utilisant

$$\delta N(\mathrm{x}, \mathrm{k}, t) = \frac{V}{(2\pi)^3} n_{\mathbf{k}}(\mathrm{x}) \delta \mathrm{x} \delta \mathrm{p}, \tag{5.55}$$

on obtient

$$\frac{\partial n_{\mathbf{k}}}{\partial t} + \nabla_{\mathrm{x}} n_{\mathbf{k}} . \nabla_{\mathbf{k}} \tilde{\epsilon}_{\mathbf{k}} - \nabla_{\mathbf{k}} n_{\mathbf{k}} . \nabla_{\mathrm{x}} \epsilon_{\mathbf{k}} = 0. \tag{5.56}$$

L'équation (5.56) contient $n_{\mathbf{k}}$ qui est la fonction de distribution totale. Il faut extraire de (5.56) une équation de transport pour les quasiparticules excitées uniquement. En utilisant (5.45), on obtient

$$\frac{\partial \delta n_{\mathbf{k}}(\mathrm{x}, t)}{\partial t} + \mathrm{v}_{\mathbf{k}} . \nabla_{\mathrm{x}} \delta n_{\mathbf{k}}(\mathrm{x}, t) - \frac{1}{V} \nabla_{\mathbf{k}} n^0_{\mathbf{k}} \sum_{\mathbf{k'}} f_{\mathbf{k},\mathbf{k'}} \nabla_{\mathrm{x}} \delta n_{\mathbf{k'}}(\mathrm{x}, t) = 0, \tag{5.57}$$

où l'on a utilisé

$$\nabla_{\mathbf{k}} n^0_{\mathbf{k}} = -\mathrm{v}_{\mathbf{k}} \delta(\epsilon_{\mathbf{k}} - \mu), \tag{5.58}$$

et où l'on ne s'interesse qu'à des excitations proches de la surface de Fermi. Les deux premiers termes de (5.57) décrivent l'écoulement dans l'espace des phases de quasiparticules totalement indépendantes. Le dernier terme est dû aux interactions et correspond à l'écoulement de quasiparticules drainées par l'inhomogénéité de la distribution d'excitations. On peut réexprimer (5.57) à l'aide de la différence $\delta\overline{n}_{\mathbf{k}}$ entre la distribution de quasiparticules et la distribution de quasiparticules à l'équilibre local

$$\overline{n}^0_{\mathbf{k}} = n^0(\tilde{\epsilon}_{\mathbf{k}} - \mu) = \theta(\mu - \tilde{\epsilon}_{\mathbf{k}}) \tag{5.59}$$

à température nulle. On a la relation suivante entre $\delta\overline{n}_{\mathbf{k}}$ et $\delta n_{\mathbf{k}}$:

$$\begin{aligned} \delta\overline{n}_{\mathbf{k}} &= n_{\mathbf{k}} - n^0(\tilde{\epsilon}_{\mathbf{k}} - \mu) && (5.60)\\ &= n_{\mathbf{k}} - n^0(\epsilon_{\mathbf{k}} - \mu) + (n^0(\epsilon_{\mathbf{k}} - \mu) - n^0(\tilde{\epsilon}_{\mathbf{k}} - \mu)) && (5.61)\\ &= \delta n_{\mathbf{k}} + \frac{\partial n^0_{\mathbf{k}}(\epsilon_{\mathbf{k}} - \mu)}{\partial \epsilon_{\mathbf{k}}}(\epsilon_{\mathbf{k}} - \tilde{\epsilon}_{\mathbf{k}}). && (5.62) \end{aligned}$$

En utilisant (5.13), on obtient

$$\delta\overline{n}_{\mathbf{k}} = \delta n_{\mathbf{k}} - \frac{1}{V}\frac{\partial n^0_{\mathbf{k}}(\epsilon_{\mathbf{k}} - \mu)}{\partial \epsilon_{\mathbf{k}}} \sum_{\mathbf{k}'} f_{\mathbf{k},\mathbf{k}'} \delta n_{\mathbf{k}'} \tag{5.63}$$

A température nulle,

$$\frac{\partial n^0_{\mathbf{k}}(\epsilon_{\mathbf{k}} - \mu)}{\partial \epsilon_{\mathbf{k}}} = -\delta(\epsilon_{\mathbf{k}} - \mu), \tag{5.64}$$

ce qui permet d'écrire la relation (5.63) sous la forme

$$\delta\overline{n}_{\mathbf{k}} = \delta n_{\mathbf{k}} + \frac{1}{V}\sum_{\mathbf{k}'} f_{\mathbf{k},\mathbf{k}'} \delta n_{\mathbf{k}'} \delta(\epsilon_{\mathbf{k}} - \mu). \tag{5.65}$$

En comparant les expressions (5.57) et (5.65), on voit que l'équation cinétique peut s'écrire sous la forme compacte

$$\frac{\partial \delta n_{\mathbf{k}}}{\partial t}(\mathrm{x}, t) + \mathrm{v}_{\mathbf{k}} . \nabla_{\mathrm{x}} \delta\overline{n}_{\mathbf{k}}(\mathrm{x}, t) = 0, \tag{5.66}$$

qui contient la dérivée temporelle de $\delta n_{\mathbf{k}}$ et la dérivée spatiale de $\delta\overline{n}_{\mathbf{k}}$. Les dérivées spatiales correspondent à une diffusion, proportionelle au gradient de l'écart de la distribution par rapport à l'équilibre local. Jusqu'à présent, on n'a pas tenu compte des collisions entre quasiparticules, similaires aux collisions de la théorie cinétique des gaz usuels. On associe à ces collisions une fréquence de collision ν. Comme les collisions sont inhibées par le principe de Pauli, ν est petit à basse température. Les collisions n'interviennent donc qu'à basse fréquence $\omega \ll \nu$ pour les phénomènes de viscosité, conduction thermique, etc. L'effet des collisions est alors pris en compte par une *intégrale de collision* $I(\delta n_{\mathbf{k}})$ qui mesure le taux de changement de $\delta n_{\mathbf{k}}$ dû aux collisions. L'équation de transport en présence de collisions s'écrit donc

$$\frac{\partial \delta n_{\mathbf{k}}}{\partial t} + \mathrm{v}_{\mathbf{k}} . \nabla_{\mathrm{x}} \delta\overline{n}_{\mathbf{k}} = I(\delta n_{\mathbf{k}}). \tag{5.67}$$

Cette équation associée à l'expression (5.65) de $\delta\overline{n}_{\mathbf{k}}$, forme un système d'équations intégrales pour $\delta n_{\mathbf{k}}$.

5.4 Expression des courants

On note $\mathbf{J}(\mathrm{x},t)$ la densité de courant de particules à l'instant t au point x. On pourrait être tenté de donner l'expression suivante pout $\mathbf{J}(\mathrm{x},t)$

$$\mathbf{J}(\mathrm{x},t)=\sum_{\mathbf{k}}\mathrm{v}_{\mathbf{k}}\delta n_{\mathbf{k}}, \tag{5.68}$$

dans laquelle chaque quasiparticule porte un courant $\mathrm{v}_{\mathbf{k}}$. Cette forme de la densité de courant de quasiparticules est *fausse* car une quasiparticule entraîne le milieu avec elle à cause des interactions. Il faut partir de l'équation de conservation de la matière

$$\nabla\mathbf{J}+\frac{\partial\rho}{\partial t}=0, \tag{5.69}$$

dans laquelle on peut écrire

$$\delta\rho(\mathrm{x},t)=\sum_{\mathbf{k}}\delta n_{\mathbf{k}}(\mathrm{x},t). \tag{5.70}$$

Afin d'écrire l'équation (5.69), on somme sur k l'équation de transport (5.67), et l'on utilise le fait que

$$\sum_{\mathbf{k}}I(\delta n_{\mathbf{k}})=0 \tag{5.71}$$

pour obtenir l'équation de conservation de la matière

$$\frac{\partial\delta\rho}{\partial t}+\nabla_{\mathrm{x}}\sum_{\mathbf{k}}\mathrm{v}_{\mathbf{k}}\delta\overline{n}_{\mathbf{k}}=0, \tag{5.72}$$

ce qui permet d'identifier la densité de courant de particules

$$\mathbf{J}(\mathrm{x},t)=\sum_{\mathbf{k}}\mathrm{v}_{\mathbf{k}}\delta\overline{n}_{\mathbf{k}}. \tag{5.73}$$

Au lieu de $\delta n_{\mathbf{k}}$, il faut donc utiliser la différence $\delta\overline{n}_{\mathbf{k}}$ entre la fonction de distribution et la fonction de distribution à l'équilibre local.

L'équation de conservation de l'impulsion s'obtient en multipliant l'équation de transport (5.67) par k_α, en sommant sur l'impulsion, et en utilisant le fait que

$$\sum_{\mathbf{k}}\mathrm{k}_\alpha I(\delta n_{\mathbf{k}})=0. \tag{5.74}$$

On obtient finalement

$$\frac{\partial}{\partial t}(\sum_{\mathbf{k}}\mathrm{k}_\alpha\delta n_{\mathbf{k}})+\sum_{\beta}\nabla_{\mathrm{x},\beta}\mathbf{\Pi}_{\alpha,\beta}=0, \tag{5.75}$$

où l'on a identifié le tenseur énergie impulsion

$$\mathbf{\Pi}_{\alpha,\beta}=\sum_{\mathbf{k}}\mathrm{k}_\alpha\mathrm{v}_{\mathbf{k},\beta}\delta\overline{n}_{\mathbf{k}}(\mathrm{x}). \tag{5.76}$$

On dérive la conservation de l'énergie en multipliant l'équation de transport (5.67) par $\epsilon_{\mathbf{k}}$, en sommant sur k et en utilisant le fait que

$$\sum_{\mathbf{k}}\epsilon_{\mathbf{k}}I(\delta n_{\mathbf{k}})=0. \tag{5.77}$$

On obtient alors

$$\frac{\partial}{\partial t}(\sum_{\mathbf{k}} \epsilon_{\mathbf{k}} \delta n_{\mathbf{k}}) + \nabla_{\mathbf{x}} \mathbf{Q} = 0, \tag{5.78}$$

où le vecteur courant d'énergie $\mathbf{Q}$ est

$$\mathbf{Q} = \sum_{\mathbf{k}} \epsilon_{\mathbf{k}} \mathbf{v}_{\mathbf{k}} \delta \overline{n}_{\mathbf{k}}. \tag{5.79}$$

Dans les expressions (5.73), (5.76) et (5.79), il apparaît un terme dû à l'écoulement des quasi-particules en interaction avec la quasiparticule que l'on considère. Ce terme peut être mis explicitement en évidence en utilisant la relation (5.65) entre $\delta \overline{n}_{\mathbf{k}}$ et $\delta n_{\mathbf{k}}$.

5.5 Relation entre la masse nue et la masse effective

Dans cette partie, on cherche à utiliser l'invariance galiléenne du liquide de Fermi. En exprimant l'énergie dans un référentiel au repos et dans un référentiel en translation rectiligne uniforme par rapport au référentiel au repos, on déduit une relation entre la masse nue et la masse effective. L'opérateur de courant est donné par

$$\mathbf{J} = \sum_i \frac{\mathbf{k}_i}{M}, \tag{5.80}$$

où $\mathbf{k}_i$ est l'impulsion de la i-ième particule et M sa masse nue. A condition que le système soit invariant par translation (ce qui exclu le cas des métaux qui possèdent un réseau de Bravais), l'impulsion totale $\mathbf{k}$ est un bon nombre quantique, et

$$\mathbf{J} = \frac{\mathbf{k}}{M}. \tag{5.81}$$

On se propose tout d'abord de redériver l'expression (5.73) du courant par une autre méthode. Pour celà, on remarque que le courant total est donné par

$$\mathbf{J} = \langle \varphi | \sum_i \frac{\mathbf{k}_i}{M} | \varphi \rangle, \tag{5.82}$$

où $|\varphi\rangle$ désigne un état excité du système. On cherche à décrire le système dans un référentiel se déplaçant à la vitesse $-\mathbf{q}/M$ par rapport au référentiel au repos. L'effet de la translation rectiligne uniforme est de déplacer la surface de Fermi, ainsi que les quasiparticules excitées d'une quantité $\mathbf{q}$. L'énergie d'interaction est la même dans le référentiel au repos et dans le référentiel en mouvement. Par contre, l'énergie cinétique varie de

$$\sum_i \frac{(\mathbf{k}_i + \mathbf{q})^2}{2M} - \frac{\mathbf{k}_i^2}{2M} = \sum_i \frac{\mathbf{q}.\mathbf{k}_i}{M} + \frac{\mathbf{q}^2}{2M}. \tag{5.83}$$

Si $\mathbf{q}$ est petit, la correction en énergie est donnée par la théorie de perturbation au premier ordre

$$\delta E = \langle \varphi | \sum_i \frac{\mathbf{q}.\mathbf{k}_i}{M} | \varphi \rangle + O(\mathbf{q}^2) \tag{5.84}$$

$$= \mathbf{q}.\mathbf{J} + O(\mathbf{q}^2). \tag{5.85}$$

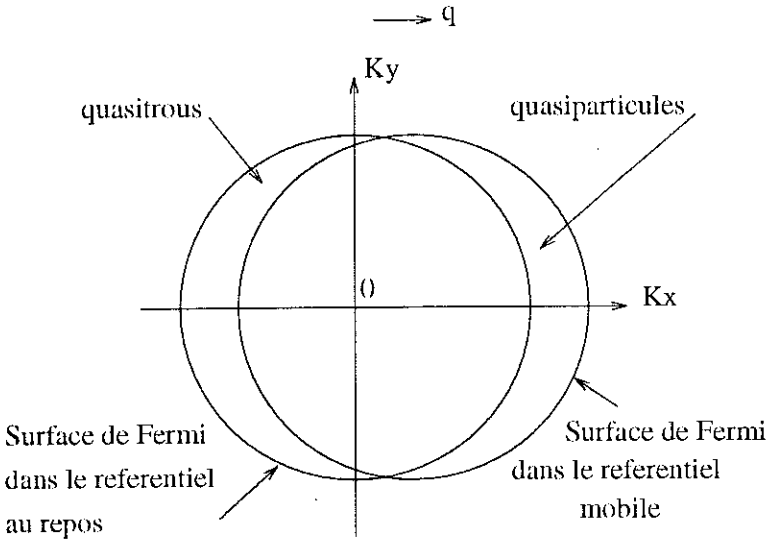

Figure 5.2: Translation de la surface de Fermi lors du changement d'observateurs.

Le courant s'obtient donc en dérivant l'énergie par rapport à $\mathbf{q}$:

$$\mathbf{J}_\alpha = \frac{dE}{dq_\alpha}. \tag{5.86}$$

Dans l'état fondamental, le courant est nul par symétrie, donc $dE_0/dq_\alpha = 0$. On va réaliser la translation de la mer de Fermi et des quasiparticules en deux étapes. Dans un premier temps, on translate les quasiparticules et ensuite on translate la mer de Fermi. On considère pour simplifier un état dans le référentiel au repos ne comportant qu'une seule quasiparticule excitée d'impulsion $\mathbf{k}$, et on translate d'abord le mode $\mathbf{k}$ seul sans modifier la surface de Fermi. L'énergie $\epsilon_\mathbf{k}$ varie d'une quantité $\mathbf{q}.\mathbf{v}_\mathbf{k}$, ce qui donne une contribution $\mathbf{v}_\mathbf{k}$ au courant, d'après (5.86). On translate maintenant la surface de Fermi, ce qui engendre une modification $\delta n_\mathbf{k}$ de la fonction de distribution. Le changement d'énergie totale s'écrit

$$\delta E = \mathbf{q}.\mathbf{j}_\mathbf{k} = \mathbf{q}.\mathbf{v}_\mathbf{k} + \frac{1}{V}\sum_{\mathbf{k}'} f_{\mathbf{k},\mathbf{k}'}\delta n_{\mathbf{k}'}, \tag{5.87}$$

où

$$\delta n_{\mathbf{k}'} = -\mathbf{q}.\nabla_{\mathbf{k}'} n^0_{\mathbf{k}'} = -\mathbf{q}.\mathbf{v}_{\mathbf{k}'}\frac{\partial n^0}{\partial \epsilon_{\mathbf{k}'}} \tag{5.88}$$

correspond à la formation de quasiparticules d'un côté de la surface de Fermi, et de quasitrous de l'autre côté lors de la translation de la surface de Fermi (voir figure 5.2). En insérant (5.88) dans l'énergie (5.87), on obtient bien l'expression (5.73) de la densité de courant de particules.

D'autre part, dans le cas d'une seule excitation de type quasiparticule, la relation (5.73) fournit l'identité

$$\mathbf{j}_\mathbf{k} = \frac{\mathbf{k}}{M} = \mathbf{v}_\mathbf{k} - \frac{1}{V}\sum_{\mathbf{k}'} f_{\mathbf{k},\mathbf{k}'}\frac{\partial n^0}{\partial \epsilon_{\mathbf{k}'}}\mathbf{v}_{\mathbf{k}'}. \tag{5.89}$$

Dans un système isotrope, comme ^{3}He, $\mathbf{j_k}$ et $\mathbf{v_k}$ sont parallèles à $\mathbf{k}$. On peut alors effectuer la sommation de l'équation (5.89) à l'aide de (5.15) et de (5.19), pour obtenir

$$\frac{1}{M} = \frac{1}{M^*} + \frac{k_f f_1}{6\pi^2}, \tag{5.90}$$

soit

$$\frac{M^*}{M} = 1 + \frac{k_f M^*}{6\pi^2} f_1 = 1 + \frac{F_1}{3}, \tag{5.91}$$

où l'on a utilisé la relation (5.43) reliant F_l à f_l. Le liquide de Fermi est stable à condition que la masse effective M^* soit positive. Dans le cas contraire, le système gagne à créer des quasiparticules et la mer de Fermi est instable. La condition de stabilité imposée par la masse effective s'écrit

$$F_1 > -3. \tag{5.92}$$

5.6 Stabilité de la mer de Fermi vis-à-vis des modes collectifs

On se propose de généraliser les relations (5.44) et (5.92) pour tous les coefficients F_l. Pour celà, on considère une distorsion quelconque de la surface de Fermi, paramétrisée par $k_f(\theta)$, et on cherche à quelle condition la mer de Fermi est stable vis-à-vis d'une telle distorsion. La fonction de distribution s'écrit $n_\mathbf{k} = \theta(k_f(\theta) - |\mathbf{k}|)$, ce qui permet d'obtenir les nombres d'occupation $\delta n_\mathbf{k}$ au second ordre en δk_f

$$\begin{aligned}
\delta n_\mathbf{k} &= \theta(k_f(\theta) - |\mathbf{k}|) - \theta(k_f - |\mathbf{k}|) && (5.93)\\
&= \delta k_f(\theta)\delta(k_f - |\mathbf{k}|) + \frac{1}{2}(\delta k_f(\theta))^2 \frac{\partial}{\partial k_f}\delta(k_f - |\mathbf{k}|) && (5.94)\\
&= \delta k_f(\theta)\delta(k_f - |\mathbf{k}|) - \frac{1}{2}(\delta k_f(\theta))^2 \frac{\partial}{\partial |\mathbf{k}|}\delta(k_f - |\mathbf{k}|). && (5.95)
\end{aligned}$$

La variation d'énergie par unité de volume induite par la distorsion de la surface de Fermi vaut

$$\delta\left(\frac{E-\mu N}{V}\right) = \frac{1}{V}\sum_\mathbf{k}(\epsilon_\mathbf{k} - \mu)\delta n_\mathbf{k} + \frac{1}{2V^2}\sum_{\mathbf{k},\mathbf{k}'} f_{\mathbf{k},\mathbf{k}'}\delta n_\mathbf{k}\delta n_{\mathbf{k}'}, \tag{5.96}$$

où $\delta n_\mathbf{k}$ est donné par la relation (5.95). Le premier ordre du développement de $\delta((E-\mu N)/V)$ en puissances de $\delta k_f(\theta)$ s'annule:

$$\delta\left(\frac{E-\mu N}{V}\right) = \frac{1}{V}\sum_\mathbf{k}(\epsilon_\mathbf{k} - \mu)\delta k_f(\theta)\delta(k_f - |\mathbf{k}|) = 0 \tag{5.97}$$

Au second ordre,

$$\begin{aligned}
\delta\left(\frac{E-\mu N}{V}\right) &= -\frac{1}{2V}\sum_\mathbf{k}(\epsilon_\mathbf{k} - \mu)(\delta k_f(\theta))^2 \frac{\partial}{\partial|\mathbf{k}|}\delta(k_f - |\mathbf{k}|)| && (5.98)\\
&\quad + \frac{1}{2V^2}\sum_{\mathbf{k},\mathbf{k}'} f_{\mathbf{k},\mathbf{k}'}\delta(|\mathbf{k}| - k_f)\delta(|\mathbf{k}'| - k_f)\delta k_f(\theta)\delta k_f(\theta') + O(\delta k_f^3).
\end{aligned}$$

En remplaçant les sommations par des intégrales, on obtient

$$\delta\left(\frac{E-\mu N}{V}\right) = \frac{v_f k_f^2}{8\pi^2}\int d(\cos\theta)(\delta k_f(\theta))^2 + \frac{1}{2}\frac{k_f^4}{(2\pi)^4}\int d(\cos\theta)d(\cos\theta')f(\theta,\theta')\delta k_f(\theta)\delta k_f(\theta') + O(\delta k_f^3). \tag{5.99}$$

En développant $\delta k_f(\theta)$ sur les polynômes de Legendre

$$\delta k_f(\theta) = \sum_l k_l P_l(\cos\theta), \tag{5.100}$$

et en utilisant (5.16), ainsi que la relation

$$\int P_l(\hat{\mathbf{n}}_1.\hat{\mathbf{n}}_2)P_l(\hat{\mathbf{n}}_2.\hat{\mathbf{n}}_3)d\Omega_2 = \delta_{l,l'}\frac{4\pi}{2l+1}P_l(\hat{\mathbf{n}}_1.\hat{\mathbf{n}}_3), \tag{5.101}$$

on obtient

$$\int d(\cos\theta)(\delta k_f(\theta))^2 = \sum_l \frac{2k_l^2}{2l+1} \tag{5.102}$$

$$\int d(\cos\theta)d(\cos\theta')f(\theta,\theta')\delta k_f(\theta)\delta k_f(\theta') = \sum_l \frac{4k_l^2 f_l}{(2l+1)^2}. \tag{5.103}$$

Il ne reste plus qu'à reporter (5.102) et (5.103) dans la relation (5.100) pour obtenir

$$\delta\left(\frac{E-\mu N}{V}\right) = \frac{v_f k_f^2}{4\pi^2}\sum_l \frac{k_l^2}{2l+1}(1+\frac{F_l}{2l+1}) + O(\delta k_f^3). \tag{5.104}$$

Le liquide de Fermi et stable à condition que la surface de Fermi ne se déforme pas spontanément, à condition que

$$F_l > -(2l+1) \tag{5.105}$$

pour tout $l \geq 0$. On retrouve bien les relations (5.44) et (5.92) que l'on avait obtenues à partir de la positivité de la masse effective et de la compressibilité.

5.7 Solutions de l'équation de transport

Les solutions de l'équation de transport (5.66) en l'absence de collisions décrivent les excitations naturelles du liquide de Fermi. Ces excitations sont de deux types, de structure très différente: les quasiparticules localisées et les modes collectifs. On considère des excitations périodiques dans l'espace et dans le temps, caractérisées par une fonction de distribution

$$\delta n_{\mathbf{k}}(\mathbf{x},t) = \delta n_{\mathbf{k}}(\mathbf{q},\omega)e^{i(\mathbf{q}.\mathbf{x}-\omega t)} + c.c. \tag{5.106}$$

La fréquence ω est grande par rapport à la fréquence de collision ν, ce qui permet de négliger l'intégrale de collision. L'équation de transport devient alors

$$-\omega\delta n_{\mathbf{k}}(\mathbf{q},\omega) + \mathbf{q}.\mathbf{v}_{\mathbf{k}}\delta\overline{n}_{\mathbf{k}}(\mathbf{q},\omega) = 0. \tag{5.107}$$

En remplaçant $\delta\overline{n}_{\mathbf{k}}$ par son expression (5.65), on obtient

$$(\mathbf{q}.\mathbf{v}_{\mathbf{k}} - \omega)\delta n_{\mathbf{k}} - \mathbf{q}.\mathbf{v}_{\mathbf{k}} \left(\frac{\partial n^0}{\partial \epsilon_{\mathbf{k}}}\right) \sum_{\mathbf{k}'} \frac{1}{V} f_{\mathbf{k},\mathbf{k}'} \delta n_{\mathbf{k}'} = 0 \tag{5.108}$$

Cette équation, qui s'applique à la fois aux quasiparticules localisées et aux modes collectifs, n'a de solution que pour certaines valeurs de ω.

5.7.1 Quasiparticules localisées

Dans le cas d'une seule particule ajoutée avec un moment $\mathbf{k}_0$, la distribution correspondante à (5.106) s'écrit

$$\delta n_{\mathbf{k}} = \delta_{\mathbf{k},\mathbf{k}_0}. \tag{5.109}$$

Il faut en plus tenir compte du fait que le milieu se polarise à cause des interactions. La quasiparticule nue (5.109) est alors habillée par un nuage de polarisation induit par les autres quasiparticules, et $\delta n_{\mathbf{k}}$ prend la forme

$$\delta n_{\mathbf{k}} = \delta_{\mathbf{k},\mathbf{k}_0} + \xi_{\mathbf{k}}, \tag{5.110}$$

où $\xi_{\mathbf{k}}$ décrit le nuage de polarisation et est de l'ordre de $1/N$. $\xi_{\mathbf{k}}$ n'est pas négligeable car il existe de l'ordre de N valeurs possibles pour $\mathbf{k}$. L'excitation représentée par (5.110) est appelée une *excitation individuelle* du système et $\mathbf{k}_0$ joue un rôle central pour cette excitation. En appliquant l'équation de transport au cas $\mathbf{k} = \mathbf{k}_0$, on obtient

$$\omega = \mathbf{q}.\mathbf{v}_{\mathbf{k}_0} \tag{5.111}$$

et les autres termes disparaissent à cause du facteur $1/V$. La relation (5.111) fixe ω pour $\mathbf{q}$ donné. En collectant les termes d'ordre $1/N$ pour $\mathbf{k} \neq \mathbf{k}_0$, on obtient d'après (5.108)

$$(\mathbf{q}.\mathbf{v}_{\mathbf{k}} - \omega)\xi_{\mathbf{k}} - \frac{1}{V}\mathbf{q}.\mathbf{v}_{\mathbf{k}}(\frac{\partial n^0}{\partial \epsilon_{\mathbf{k}}}) \sum_{\mathbf{k}'} f_{\mathbf{k},\mathbf{k}'} \xi_{\mathbf{k}'} = \frac{1}{V}\mathbf{q}.\mathbf{v}_{\mathbf{k}}(\frac{\partial n^0}{\partial \epsilon_{\mathbf{k}}}) f_{\mathbf{k},\mathbf{k}_0} \tag{5.112}$$

On remarque que le mouvement de $\xi_{\mathbf{k}}$ est forcé par le mode $\mathbf{k} = \mathbf{k}_0$, ce qui est caractéristique d'une excitation individuelle.

5.7.2 Modes collectifs

Les modes collectifs représentent un mouvement cohérent de l'ensemble des quasiparticules autour d'un état d'équilibre. Dans un tel mode, la notion de quasiparticule en tant qu'objet individuel perd sa signification. La structure des modes collectifs est contenue dans (5.108), lorsque la fonction de distribution s'étend de façon continue sur l'ensemble de la surface de Fermi. On utilise comme variable dynamique le déplacement normal $u_{\mathbf{k}}$ de la surface de Fermi au point $\mathbf{k}$. Les variables $\delta n_{\mathbf{k}}$ sont reliées aux déplacements par la relation

$$\delta n_{\mathbf{k}} = \delta(\epsilon_{\mathbf{k}} - \mu) v_f u_{\mathbf{k}} \tag{5.113}$$

et l'équation de transport s'écrit, en terme de déplacements de la surface de Fermi:

$$(\mathbf{q}.\mathbf{v}_{\mathbf{k}} - \omega)u_{\mathbf{k}} + \frac{1}{V}\mathbf{q}.\mathbf{v}_{\mathbf{k}} \sum_{\mathbf{k}'} f_{\mathbf{k},\mathbf{k}'} \delta(\epsilon_{\mathbf{k}'} - \mu) u_{\mathbf{k}'} = 0. \tag{5.114}$$

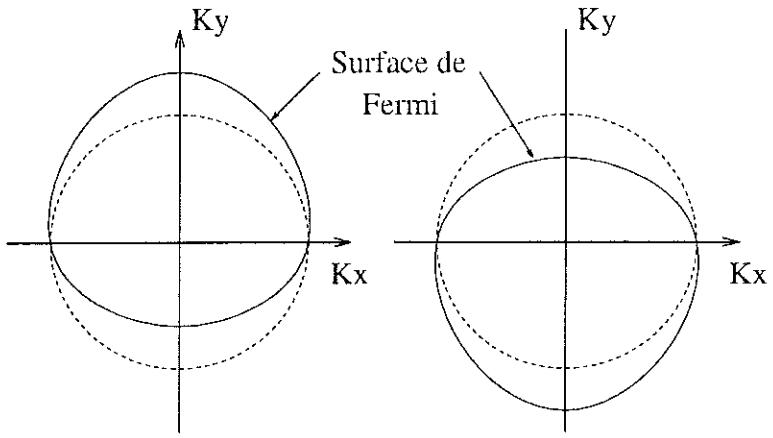

Figure 5.3: Fonction de distribution $n_{\mathbf{k}}(\mathbf{R})$ pour le son zéro. On a représenté en pointillés la surface de Fermi non déformée et en trait pleins la surface de Fermi. Les deux figures correspondent à $R = 0$ et $R = \pi/q$ respectivement.

En remplaçant la somme discrète par une intégrale et en sommant sur $\mathbf{k}'$, on obtient

$$(\cos\theta - \lambda)u(\Omega) + \frac{\cos\theta}{4\pi}\int d\Omega' u(\Omega')F(\hat{\mathrm{k}},\hat{\mathrm{k}}') = 0 \tag{5.115}$$

où la définition de λ est

$$\lambda = \frac{\omega}{qv_f}. \tag{5.116}$$

Les modes propres correspondent à des valeurs discrètes de λ. On suppose dans la suite que la fonction d'interaction F est une constante F_0 et on étudie le mode collectif corespondant, appelé *son zéro*. Sous cette hypothèse, l'équation (5.115) devient

$$(\cos\theta - \lambda)u(\Omega) + F_0\frac{\cos\theta}{4\pi}\int d\Omega' u(\Omega') = 0, \tag{5.117}$$

qui a pour solution

$$u(\Omega) = C\frac{\cos\theta}{\lambda - \cos\theta}, \tag{5.118}$$

où la constante C vaut

$$C = F_0\int \frac{d\Omega'}{4\pi}u(\Omega') \tag{5.119}$$

En reportant (5.118) dans (5.119), on obtient

$$\frac{1}{F_0} = \frac{1}{2}\int d\theta\frac{\sin\theta\cos\theta}{\lambda - \cos\theta}d\theta = -1 + \frac{\lambda}{2}\ln\frac{\lambda+1}{\lambda-1} \tag{5.120}$$

Si $F_0 > 0$ (interaction entre quasiparticules répulsive), il existe une seule solution avec $\lambda > 1$. Dans ce cas, le son zéro n'est pas amorti. Si $-1 < F_0 < 0$, la solution de (5.120) est complexe, et représente un son zéro amorti. Si $F_0 < -1$, le son zéro est instable. Les déformations de la surface de Fermi correspondant au son zéro sont représentées sur la figure 5.3

Chapitre 6

Bosonisation du liquide de Fermi

Ce chapitre est consacré à la présentation de la technique de bosonisation de la surface de Fermi en dimension 2 ou 3. Pour simplifier, nous nous placerons en dimension 2, mais les généralisations à la dimension 3 sont immédiates. L'idée est de décrire les excitations de la surface de Fermi par des champs de Bose, tout comme à une dimension. La différence essentielle avec le cas unidimensionnel est que la procédure de bosonisation de la surface de Fermi est un procédure d'intégration approchée, alors qu'à une dimension, la bosonisation est exacte. Toutefois, les approximations effectuées sont justifiées a postériori par le fait que l'on retrouve bien le liquide de Fermi. Nous donnons au chapitre 8 une autre justification: nous obtenons des statistiques de niveaux intégrables pour le liquide de Fermi (même avec un petit nombre d'électrons et un petit nombre d'orbitales), ce qui valide l'approche via une théorie intégrable.

Les premières tentatives de bosonisation de la surface de Fermi en dimension supérieure à 1 datent des travaux de A. Luther[1]. Dans des travaux non publiés, F.D.M. Haldane[2] a ouvert la voie à la formulation actuelle de cette théorie, qui a été développée ensuite par A.H. Castro Neto et E.H. Fradkin[3] et par A. Houghton et B. Marston[4].

6.1 Algèbre de Kac-Moody en dimension 2

Le principe de la bosonisation de la surface de Fermi est de paver la surface de Fermi par des sphères de rayon Λ, tel que le rayon de courbure de la surface de Fermi soit grand devant Λ, et tel que Λ soit grand devant les transferts d'impulsion lors des processus de diffusion de fermions. On suppose donc de façon ad hoc l'existence d'une physique simple à basse énergie, qui s'avèrera être celle du liquide de Fermi.

La surface de Fermi munie du pavage par les sphères est représentée sur la figure 6.1. Chaque sphère est indexée par un entier α. On définit alors les opérateurs

$$\rho_{\mathbf{q},\alpha} = \sum_{\mathbf{q}} \theta_\alpha(\mathbf{k} + \frac{\mathbf{q}}{2})\theta_\alpha(\mathbf{k} - \frac{\mathbf{q}}{2})n_{\mathbf{q}}(\mathbf{k}) \tag{6.1}$$

[1] A. Luther, *Tomonaga fermions and the Dirac equation in three dimensions*, Phys. Rev. B 19, 320-330 (1979).

[2] J'ai utilisé les photocopies des transparents du séminaire de F.D.M. Haldane *A new look at the Fermi surface* donné à l'Université de Brown en novembre 1991.

[3] A.H. Castro Neto and E.H. Fradkin *Bosonization of Fermi liquids*, Phys. Rev. B 49, 10877-10892 (1994); *Exact solution of the Landau fixed point via bosonization*, Phys. Rev. B 51, 4084-4104 (1995).

[4] A. Houghton and B. Marston, Phys. Rev. B 48, 7790 (1993).

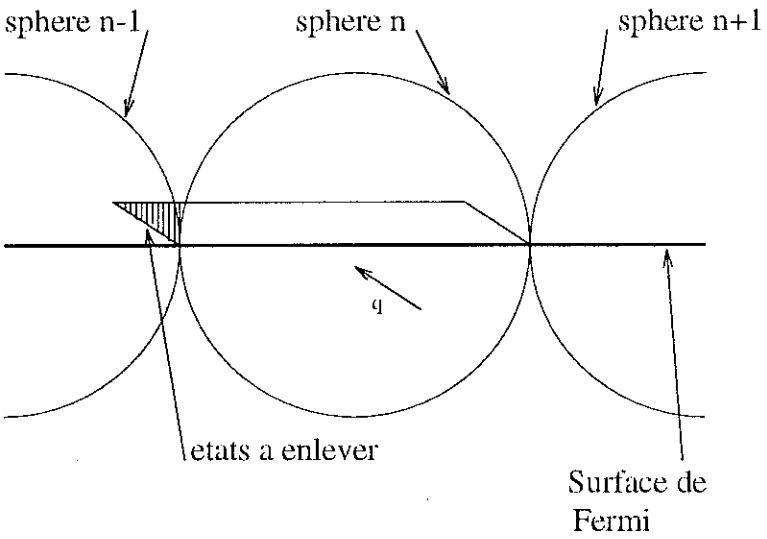

Figure 6.1: Pavage de la surface de Fermi bidimensionnelle

avec

$$n_{\mathbf{q}}(\mathrm{k}) = c^{+}_{\mathbf{k}-\mathbf{q}/2} c_{\mathbf{k}+\mathbf{q}/2}. \tag{6.2}$$

Dans l'expression (6.1), nous avons noté $\theta_\alpha(\mathrm{k})$ la fonction caractéristique de la sphère α. Tout comme à une dimension, il faut utiliser un produit normal lors de l'évaluation du commutateur $[\rho_{\mathbf{q},\alpha}, \rho_{\mathbf{q}',\alpha'}]$, et l'on obtient

$$[\rho_{\mathbf{q},\alpha}, \rho_{\mathbf{q}',\alpha'}] = \delta_{\alpha,\alpha'}\delta_{\mathbf{q}+\mathbf{q}',0} \sum_{\mathbf{k}} C_\alpha(\mathrm{k},\mathrm{q}) \left(n^0_{\mathbf{k}+\mathbf{q}/2} - n^0_{\mathbf{k}-\mathbf{q}/2} \right), \tag{6.3}$$

où la contrainte $C_\alpha(\mathbf{k},\mathbf{q})$ vaut

$$C_\alpha(\mathrm{k},\mathrm{q}) = \theta_\alpha(\mathrm{k}+\frac{\mathbf{q}}{2})\theta_\alpha(\mathrm{k}-\frac{\mathbf{q}}{2})\theta_\alpha(\mathrm{k}'+\frac{\mathbf{q}'}{2})\theta_\alpha(\mathrm{k}'-\frac{\mathbf{q}'}{2}). \tag{6.4}$$

Afin de simplifier le commutateur (6.3), nous utilisons l'hypothèse que la surface de Fermi est plate dans chaque sphère α. Nous appelons $\mathbf{n}_\alpha$ la normale à la surface de Fermi dans la sphère α. Afin de préciser la condition de non courbure de la surface de Fermi, nous imposons qu'il n'existe pas de paire particule trou avec un angle $\theta > \pi/2$, où θ désigne l'angle entre $\mathbf{k}_f$ et le transfert d'impulsion $\mathbf{q}$. L'angle maximal θ est tel que

$$\tan\left(\theta - \frac{\pi}{2}\right) \leq \frac{2\pi}{L\Lambda}, \tag{6.5}$$

ce qui impose la restriction

$$\Lambda \leq \left(\frac{4\pi|\mathrm{k}_f|}{L}\right)^{1/2}. \tag{6.6}$$

On a donc l'encadrement

$$\frac{2\pi}{L} \ll \Lambda \leq \left(\frac{4\pi|\mathrm{k}_f|}{L}\right)^{1/2}. \tag{6.7}$$

Cette condition montre que, dans la limite $L \to +\infty$, le cut-off doit également tendre vers 0 plus vite que $1/\sqrt{L}$ et moins vite que $1/L$. Cette limite n'est donc pas la véritable limite thermodynamique, dans laquelle le cut-off Λ serait constant. De même, ce n'est pas la limite dans laquelle s'effectue la renormalisation de la surface de Fermi[5]. Sous les hypothèses précédemment énoncées, le terme dominant du commutateur (6.3) devient

$$[\rho_{\mathbf{q},\alpha}, \rho_{\mathbf{q}',\alpha'}] = \delta_{\alpha,\alpha'}\delta_{\mathbf{q}+\mathbf{q}',0} V a(\mathbf{q}.\mathbf{n}_\alpha), \tag{6.8}$$

où $V = L^2$ et la longueur découpée par la sphère α sur la surface de Fermi a une mesure $(2\pi)^2 a$. Le terme de droite dans (6.8) représente le nombre d'états contenus dans le paralélogramme de la figure 6.1. Cependant, il est clair que l'on a surévalué le commutateur (6.3), en particulier lorque $\mathbf{q}$ est faiblement incliné par rapport à la surface de Fermi. En effet, il faut alors enlever à (6.8) le nombre d'états contenus dans le triangle hachuré de la figure 6.1. Les relations de commutation prennent alors la forme

$$[\rho_{\mathbf{q},\alpha}, \rho_{\mathbf{q}',\alpha'}] = \delta_{\alpha,\alpha'}\delta_{\mathbf{q}+\mathbf{q}',0} V a(\mathbf{q}.\mathbf{n}_\alpha) \left(1 + O\left(\frac{|\mathbf{q} \wedge \mathbf{n}_\alpha|}{|\mathbf{k}_f|}\right)\right). \tag{6.9}$$

Sachant que l'on travaille sous les hypothèse $|\mathbf{q}| \ll \Lambda \ll |\mathbf{k}_f|$, il est légitime de négliger les corrections au commutateur et de supposer correcte la relation (6.8). Cependant, l'algèbre définie par (6.8) n'est pas assez forte pour permettre d'intégrer le liquide de Fermi car les excitations sont moyennées sur une sphère de rayon Λ. Afin d'augmenter le nombre de générateurs de l'espace vectoriel bosonique, nous définissons

$$\rho_{\mathbf{q}}(\mathbf{k}_f) = \sum_{\mathbf{k}} \theta\left(\Lambda - \left|\mathbf{k} - \mathbf{k}_f - \frac{\mathbf{q}}{2}\right|\right) \theta\left(\Lambda - \left|\mathbf{k} - \mathbf{k}_f + \frac{\mathbf{q}}{2}\right|\right) n_{\mathbf{q}}(\mathbf{k}). \tag{6.10}$$

A l'ordre 1 en $|\mathbf{k}|/|\mathbf{k}_f|$, nous obtenons

$$\left[\rho_{\mathbf{q}}(\mathbf{k}_f), \rho_{\mathbf{q}'}(\mathbf{k}'_f)\right] = \delta_{\mathbf{q}+\mathbf{q}',0} V a(\mathbf{q}.\mathbf{n}) F\left(\frac{|\mathbf{k}_f - \mathbf{k}'_f|}{2\Lambda}\right), \tag{6.11}$$

avec $F(x) = 1 - x$ si $|x| \leq 1$ et $F(x) = 0$ si $x \geq 1$. Dans (6.11), $\mathbf{n}$ désigne la normale à la surface de Fermi. Nous définissons alors

$$\begin{array}{ll} a^+_{\mathbf{q}}(\mathbf{k}_f) = \rho_{\mathbf{q}}(\mathbf{k}_f) & \text{si } \mathbf{q}.\mathbf{v}_{\mathbf{k}_f} > 0 \\ a^+_{\mathbf{q}}(\mathbf{k}_f) = \rho_{-\mathbf{q}}(\mathbf{k}_f) & \text{si } \mathbf{q}.\mathbf{v}_{\mathbf{k}_f} < 0. \end{array} \tag{6.12}$$

Cette définission est analogue à (2.40) et (2.41) dans le cas unidimensionnel, et conduit à des relations de commutation de nature bosonique

$$\left[a_{\mathbf{q}}(\mathbf{k}_f), a^+_{\mathbf{q}'}(\mathbf{k}'_f)\right] = N_\Lambda V |\mathbf{q}.\mathbf{v}_{\mathbf{k}_f}| F\left(\frac{|\mathbf{k}_f - \mathbf{k}'_f|}{2\Lambda}\right) (\delta_{\mathbf{q},\mathbf{q}'} + \delta_{\mathbf{q},-\mathbf{q}'}), \tag{6.13}$$

où $N_\Lambda = a/v_f$ est la densité d'états locale

$$N_\Lambda = \frac{1}{V} \sum_{\mathbf{k}} \theta(\Lambda - |\mathbf{k} - \mathbf{k}_f|) \delta(\mu - \epsilon_{\mathbf{k}}). \tag{6.14}$$

[5] Voir la revue de R. Shankar *Renormalization group approach to interacting fermions*, Rev. Mod. Phys. 66, 129-192 (1994).

Les systèmes que nous considérons possèdent une surface de Fermi isotrope et n'ont pas de singularité de Van Hove. Nous pouvons donc remplacer N_Λ par sa limite lorsque $\Lambda \to 0$:

$$N_\Lambda = N(0) = \frac{1}{V}\sum_{\mathbf{k}} \delta(\mu - \epsilon_{\mathbf{k}}). \tag{6.15}$$

La densité d'états au niveau de Fermi a déjà été introduite au chapitre 5 (équation 5.25). Les opérateurs (6.13) sont définis de telle sorte que la mer de Fermi soit un état de plus haut poids:

$$a_{\mathbf{q}}(\mathrm{k}_f)|FS\rangle = 0 \tag{6.16}$$

On utilisera de préférence les opérateurs

$$b_{\mathbf{q}}(\mathrm{k}_f) = \left(N(0)V|\mathrm{q}.\mathrm{v}_{\mathrm{k}_f}|\right)^{-1/2} a_{\mathbf{q}}(\mathrm{k}_f) \tag{6.17}$$

qui vérifient l'agèbre

$$\left[b_{\mathbf{q}}(\mathrm{k}_f), b^+_{\mathbf{q}'}(\mathrm{k}'_f)\right] = (\delta_{\mathbf{q},\mathbf{q}'} + \delta_{\mathbf{q},-\mathbf{q}'})F\left(\frac{|\mathrm{k}_f - \mathrm{k}'_f|}{2\Lambda}\right). \tag{6.18}$$

L'algèbre (6.18) est non locale car les opérateurs $b_{\mathbf{q}}(\mathrm{k}_f)$ et $b^+_{\mathbf{q}'}(\mathrm{k}'_f)$ ne commutent pas nécessairement si $\mathrm{k}_f \neq \mathrm{k}'_f$. Il subsiste en effet un terme de 'contact' lorsque k_f et k'_f sont à une distance inférieure à 2Λ. Afin de simplifier, on prend d'abord la limite $\Lambda \to 0$, puis ensuite la limite thermodynamique. Il est clair que cette façon de procéder est inconsistente avec la condition (6.7) $\Lambda \gg 2\pi/L$. Cependant, nous adopterons cette façon de faire[6], qui conduit à une algèbre de commutation locale sur la surface de Fermi

$$\left[b_{\mathbf{q}}(\mathrm{k}_f), b^+_{\mathbf{q}'}(\mathrm{k}'_f)\right] = \delta_{\mathrm{k}_f,\mathrm{k}'_f}(\delta_{\mathbf{q},\mathbf{q}'} + \delta_{\mathbf{q},-\mathbf{q}'}). \tag{6.19}$$

Dans la limite simplificatrice $\Lambda \to 0$, la somme (6.11) ne contient qu'un seul terme et vaut

$$\rho_{\mathbf{q}}(\mathrm{k}_f) = n_{\mathbf{q}}(\mathrm{k}_f). \tag{6.20}$$

6.2 Etats cohérents et opérateurs de fermions

6.2.1 Etats cohérents

Nous définissons les opérateurs d'états cohérents

$$U[\phi] = \exp - \sum_{\mathrm{k}_f,\mathbf{q}} \left(\frac{1}{N(0)V\mathrm{q}.\mathrm{v}_{\mathrm{k}_f}}\right) \phi_{\mathbf{q}}(\mathrm{k}_f) n_{-\mathbf{q}}(\mathrm{k}_f), \tag{6.21}$$

et mettons en évidence certaines de leurs propriétés. L'unitarité $U^{-1} = U^+$ impose que

$$\phi_{\mathbf{q}}(\mathrm{k}_f) = \overline{\phi}_{-\mathbf{q}}(\mathrm{k}_f). \tag{6.22}$$

[6] C'est ce que font A.H. Castro Neto et E.H. Fradkin, mais sans mettre en évidence l'approximation effectuée. Le traitement complet de l'agèbre (6.18) reste une question ouverte.

En utilisant les modes $b^+_{\mathbf{q}}(\mathrm{k}_f)$, nous pouvons écrire (6.21) sous la forme

$$U[\phi] = \exp - \sum_{\mathbf{k}_f,\mathbf{q}}{}' \left(\frac{1}{N(0)V|\mathbf{q}.\mathrm{v}_{\mathbf{k}_f}|} \right)^{1/2} \left(\phi_{\mathbf{q}}(\mathrm{k}_f) b^+_{\mathbf{q}}(\mathrm{k}_f) - \overline{\phi}_{\mathbf{q}}(\mathrm{k}_f) b_{\mathbf{q}}(\mathrm{k}_f) \right). \tag{6.23}$$

Le symbole $\sum'$ signifie que la somme est prise sur les vecteurs d'onde tels que $\mathbf{q}.\mathrm{v}_{\mathbf{k}_f} > 0$. Les états cohérents résultent de l'action de $U[\phi]$ sur la mer de Fermi:

$$|[\phi]\rangle = U[\phi]|FS\rangle. \tag{6.24}$$

On vérifie que les états $|[\phi]\rangle$ sont des états propres de l'opérateur d'annihilation:

$$b_{\mathbf{q}}(\mathrm{k}_f)|[\phi]\rangle = - \left(\frac{1}{N(0)V|\mathbf{q}.\mathrm{v}_{\mathbf{k}_f}|} \right)^{1/2} \phi_{\mathbf{q}}(\mathrm{k}_f)|[\phi]\rangle \tag{6.25}$$

si $\mathbf{q}.\mathrm{v}_{\mathbf{k}f} > 0$ et

$$b_{\mathbf{q}}(-\mathrm{k}_f)|[\phi]\rangle = - \left(\frac{1}{N(0)V|\mathbf{q}.\mathrm{v}_{\mathbf{k}_f}|} \right)^{1/2} \overline{\phi}_{\mathbf{q}}(-\mathrm{k}_f)|[\phi]\rangle \tag{6.26}$$

si $\mathbf{q}.\mathrm{v}_{\mathbf{k}f} > 0$. On peut écrire l'état cohérent $|[\phi]\rangle$ sous la forme

$$|[\phi]\rangle = \exp \left(-\frac{1}{2} \sum_{\mathbf{k}_f,\mathbf{q}}{}' \left(\frac{1}{N(0)|\mathbf{q}.\mathrm{v}_{\mathbf{k}f}|} \right) |\phi_{\mathbf{q}}(\mathrm{k}_f)|^2 \right) \tag{6.27}$$

$$\exp \left(\sum_{\mathbf{k}_f,\mathbf{q}}{}' \left(\frac{1}{N(0)|\mathbf{q}.\mathrm{v}_{\mathbf{k}f}|} \right)^{1/2} b^+_{\mathbf{q}}(\mathrm{k}_f) \right) |FS\rangle \tag{6.28}$$

D'autre part, le recouvrement entre états cohérents vaut

$$\langle [\phi]|[\varphi]\rangle = \exp \left(-\frac{1}{2} \sum_{\mathbf{k}_f,\mathbf{q}}{}' \left(\frac{1}{N(0)V|\mathbf{q}.\mathrm{v}_{\mathbf{k}_f}|} \right) \left(|\phi_{\mathbf{q}}(\mathrm{k}_f)|^2 + |\varphi_{\mathbf{q}}(\mathrm{k}_f)|^2 \right) \right) \tag{6.29}$$

$$\exp \left(\sum_{\mathbf{k}_f,\mathbf{q}}{}' \left(\frac{1}{N(0)V|\mathbf{q}.\mathrm{v}_{\mathbf{k}_f}|} \right) \overline{\phi}_{\mathbf{q}}(\mathrm{k}_f) \varphi_{\mathbf{q}}(\mathrm{k}_f) \right).$$

On voit que les états cohérents sont automatiquement normés: $\langle [\phi]|[\phi]\rangle = 1$. Comme tous les états cohérents, la famille $|[\phi]\rangle$ génère l'espace de Hilbert mais n'est pas libre puisque le recouvrement entre deux états cohérents est non nul.

6.2.2 Les opérateurs de fermions

La construction des opérateurs de fermions dans le cas bidimensionnel est moins rigoureuse que dans le cas unidimensionnel puisque l'on va identifier des algèbres de commutation sans chercher à identifier les espaces de Hilbert. En suivant Luther, nous décomposons le champ de fermions

$$\psi(\mathrm{x}) = \frac{1}{\sqrt{V}} \sum_{\mathbf{k}} e^{i\mathbf{k}.\mathrm{x}} c_{\mathbf{k}} \tag{6.30}$$

sous la forme

$$\psi(\mathrm{x}) = \sum_{\mathrm{k}_f} \Psi(\mathrm{x}, \mathrm{k}_f), \tag{6.31}$$

avec

$$\Psi(\mathrm{x}, \mathrm{k}_f) = f(\mathrm{k}_f) e^{J(\mathrm{x}, \mathrm{k}_f)}. \tag{6.32}$$

Nous imposons de plus que $[n_{\mathbf{q}}(\mathrm{k}), f(\mathrm{k}_f)] = 0$ et que $[n_{\mathbf{q}}(\mathrm{k}), J(\mathrm{x}, \mathrm{k}_f)]$ soit un c-nombre. Sous ces hypothèses,

$$\left[\Psi(\mathrm{x}, \mathrm{k}_f), n_{\mathbf{q}}(\mathrm{k}'_f)\right] = \left[J(\mathrm{x}, \mathrm{k}_f), n_{\mathbf{q}}(\mathrm{k}'_f)\right] \Psi(\mathrm{x}, \mathrm{k}_f). \tag{6.33}$$

D'autre part, on utilise les relations de commutation des fermions pour obtenir

$$\left[\psi(\mathrm{x}), \sum_{\mathrm{k}} n_{\mathbf{q}}(\mathrm{k})\right] = e^{-i\mathbf{q}.\mathbf{r}} \psi(\mathrm{x}). \tag{6.34}$$

On suppose que l'on a le droit d'en déduire que

$$\left[\Psi(\mathrm{x}, \mathrm{k}_f), n_{\mathbf{q}}(\mathrm{k}'_f)\right] = \delta_{\mathrm{k}_f, \mathrm{k}'_f} e^{-i\mathbf{q}.\mathrm{x}} \Psi(\mathrm{x}, \mathrm{k}_f). \tag{6.35}$$

En identifiant (6.33) et (6.35), nous obtenons

$$\left[J(\mathrm{x}, \mathrm{k}_f), n_{\mathbf{q}}(\mathrm{k}_f)\right] = e^{-i\mathbf{q}.\mathrm{x}}. \tag{6.36}$$

Sous toutes les simplifications réalisées dans la section 6.1, nous voyons que le choix

$$J(\mathrm{x}, \mathrm{k}_f) = -\sum_{\mathbf{q}} \frac{1}{N(0) V \mathbf{q}.\mathbf{v}_{\mathrm{k}_f}} e^{-i\mathbf{q}.\mathrm{x}} n_{-\mathbf{q}}(\mathrm{k}_f) \tag{6.37}$$

assure bien la commutation (6.36). Nous voyons donc que l'opérateur $e^{J(\mathrm{x}, \mathrm{k}_f)}$ et l'opérateur (6.21) s'identifient à condition que

$$\phi_{\mathbf{q}}(\mathrm{k}'_f) = e^{-i\mathbf{q}.\mathrm{x}} \delta_{\mathrm{k}_f, \mathrm{k}'_f}. \tag{6.38}$$

Nous notons $|\mathrm{k}_f, \mathrm{x}, t\rangle$ l'état cohérent (6.24) obtenu avec le choix (6.38). Le propagateur des fermions s'exprime de façon simple à l'aide de $|\mathrm{k}_f, \mathrm{x}, t\rangle$:

$$G_{R>}(\mathrm{x}, t) = \langle FS | \psi^+(\mathrm{x}, t) \psi(0, 0) | FS \rangle = \sum_{\mathrm{k}_f, \mathrm{k}'_f} \overline{f}(\mathrm{k}_f) f(\mathrm{k}'_f) \langle \mathrm{k}_f, \mathrm{x}, t | \mathrm{k}'_f, 0, 0 \rangle. \tag{6.39}$$

Nous allons maintenant nous consacrer au calcul du recouvrement $\langle \mathrm{k}_f, \mathrm{x}, t | \mathrm{k}'_f, 0, 0 \rangle$ dans le cas libre.

6.3 Le cas libre

Le terme cinétique du Hamiltonien vaut

$$H^0 = \sum_{\mathrm{k}} : c^+_{\mathrm{k}} c_{\mathrm{k}} : . \tag{6.40}$$

En utilisant les modes fermioniques, on montre que

$$\left[H^0, n_{\mathbf{q}}(\mathrm{k}_f)\right] = -\mathbf{q}.\mathrm{v}_{\mathbf{k}_f} n_{\mathbf{q}}(\mathrm{k}_f). \tag{6.41}$$

La commutation (6.41) doit être réalisée pour k_f et $\mathbf{q}$ quelconques (pour $\mathbf{q}.\mathrm{v}_{\mathbf{k}_f} > 0$ et pour $\mathbf{q}.\mathrm{v}_{\mathbf{k}_f} < 0$). La relation de commutation (6.41) est effectivement réalisée pour le Hamiltonien

$$H^0 = \sum_{\mathbf{q},\mathrm{v}_{\mathbf{k}}}{}' \frac{1}{N(0)V} n_{-\mathbf{q}}(\mathrm{k}) n_{\mathbf{q}}(\mathrm{k}). \tag{6.42}$$

Encore une fois, il ne s'agit pas là d'une identification des espaces de Hilbert, mais d'une identification des algèbres (donc moins rigoureuse). Le Hamiltonien (6.42) peut s'exprimer sous la forme

$$H^0 = \sum_{\mathbf{q},\mathrm{v}_{\mathbf{k}_f}}{}' \mathbf{q}.\mathrm{v}_{\mathbf{k}_f} b^+_{\mathbf{q}}(\mathrm{k}_f) b_{\mathbf{q}}(\mathrm{k}_f). \tag{6.43}$$

Nous avons donc maintenant facilement accès aux fonctions de corrélation. Pour celà, il faut évaluer les éléments de matrice de l'opérateur dévolution entre deux états cohérents

$$\langle[\varphi]|U(t,0)|[\tilde{\varphi}]\rangle_0. \tag{6.44}$$

On utilise le fait que[7]

$$\exp\left(\lambda b^+ b\right) \exp\left(\mu b^+\right)|0\rangle = \exp\left(\mu e^{\lambda} b^+\right)|0\rangle, \tag{6.45}$$

pour obtenir

$$\begin{aligned} \langle[\varphi]|U(t,0)|[\tilde{\varphi}]\rangle_0 \;=\; & \exp\left(-\frac{1}{2}\sum_{\mathrm{k}_f,\mathbf{q}}{}' \left(\frac{1}{N(0)V|\mathbf{q}.\mathrm{v}_{\mathbf{k}f}|}\right)\left(|\varphi_{\mathbf{q}}(\mathrm{k}_f)|^2 + |\tilde{\varphi}_{\mathbf{q}}(\mathrm{k}_f)|^2\right)\right) \\ & \exp\left(\sum_{\mathrm{k}_f,\mathbf{q}}{}' \left(\frac{1}{N(0)V|\mathbf{q}.\mathrm{v}_{\mathbf{k}_f}|}\right)|\mathbf{q}.\mathrm{v}_{\mathbf{k}_f}|\tilde{\varphi}_{\mathbf{q}}(\mathrm{k}_f)\overline{\varphi}_{\mathbf{q}}(\mathrm{k}_f) e^{-i|\mathbf{q}.\mathrm{v}_{\mathbf{k}_f}|t}\right). \end{aligned} \tag{6.46}$$

Afin d'obtenir les fonctions de corrélation, il faut utiliser la prescription (6.38). De plus, nous ajoutons un facteur exponentiel dont le but est de régulariser les intégrales dans l'ultraviolet. Nous avons donc

$$\varphi_{\mathbf{q}}(\mathrm{p}_f) \;=\; \delta_{\mathrm{p}_f,\mathrm{k}_f} e^{-i\mathbf{q}.\mathrm{x}} \exp\left(-\frac{\epsilon|\mathbf{q}.\mathrm{v}_{\mathbf{k}_f}|}{2|\mathrm{v}_{\mathbf{k}_f}|}\right) \tag{6.47}$$

$$\tilde{\varphi}_{\mathbf{q}}(\mathrm{p}_f) \;=\; \delta_{\mathrm{p}_f,\mathrm{k}'_f} \exp\left(-\frac{\epsilon|\mathbf{q}.\mathrm{v}_{\mathrm{k}'f}|}{2|\mathrm{v}_{\mathrm{k}'f}|}\right), \tag{6.48}$$

[7] Soulignons que cette méthode est beaucoup plus simple que celle utilisée par A.H. Castro Neto et E.H. Fradkin dans leur article. La méthode préconisée par ces auteurs consiste à écrire une formalisme d'intégrale de chemin pour la surface de Fermi. Il semble bien qu'il n'y ait pas lieu de recourir à la méthode d'intégrale de chemins.

où l'on prendra la limite $\epsilon = 0^+$. En reportant les relations (6.47) et (6.48) dans la fonction de corrélation (6.46), nous obtenons

$$\begin{aligned}\langle \mathrm{k}_f, \mathrm{x}, t | \mathrm{k}'_f, 0, 0\rangle_0 \;=\; & \exp\left(-\frac{1}{2}{\sum_{\mathbf{q}}}' \frac{1}{N(0)V|\mathbf{q}.\mathbf{v}_{\mathbf{k}f}|} \exp\left(-\frac{\epsilon|\mathbf{q}.\mathbf{v}_{\mathbf{k}f}|}{|\mathbf{v}_{\mathbf{k}f}|}\right)\right) \\ & \exp\left(-\frac{1}{2}{\sum_{\mathbf{q}}}' \frac{1}{N(0)V|\mathbf{q}.\mathbf{v}_{\mathbf{k}'f}|} \exp\left(-\frac{\epsilon|\mathbf{q}.\mathbf{v}_{\mathbf{k}'f}|}{|\mathbf{v}_{\mathbf{k}'f}|}\right)\right) \\ & \exp\left(\delta_{\mathbf{k}_f,\mathbf{k}'_f} {\sum_{\mathbf{q}}}' \frac{1}{N(0)V|\mathbf{q}.\mathbf{v}_{\mathbf{k}f}|} \exp\left(i(\mathbf{q}.\mathbf{x} - |\mathbf{q}.\mathbf{v}_{\mathbf{k}f}|t)\right) \exp\left(-\frac{\epsilon|\mathbf{q}.\mathbf{v}_{\mathbf{k}f}|}{|\mathbf{v}_{\mathbf{k}f}|}\right)\right)\end{aligned} \tag{6.49}$$

A cause de la divergence logarithmique dans l'infrarouge, le recouvrement (6.49) est nul si $\mathrm{k}_f \neq \mathrm{k}'_f$. Nous obtenons donc

$$\langle \mathrm{k}_f, \mathrm{x}, t | \mathrm{k}'_f, 0, 0\rangle_0 = \delta_{\mathbf{k}_f,\mathbf{k}'_f} \exp\left(\sum_{\mathbf{q}}' \frac{1}{N(0)V|\mathbf{q}.\mathbf{v}_{\mathbf{k}f}|} \left(e^{i(\mathbf{q}.\mathbf{x}-|\mathbf{q}.\mathbf{v}_{\mathbf{k}f}|t)} - 1\right) \exp\left(-\frac{\epsilon|\mathbf{q}.\mathbf{v}_{\mathbf{k}f}|}{|\mathbf{v}_{\mathbf{k}f}|}\right)\right). \tag{6.50}$$

Il reste maintenant à évaluer la somme sur $\mathbf{q}$ dans (6.50). Nous décomposons $\mathbf{q}$ en une partie tangentielle $\mathbf{q}_{||}$ et une partie perpendiculaire $\mathbf{q}_\perp = (\mathbf{q}.\mathbf{n})\mathbf{n}$. La somme sur $\mathbf{q}_{||}$ contribue seulement à la densité d'états. En effet, la sommation est du type

$$\int dq_{||} q_{||}^{d-2} e^{iq_{||}x_{||}} = \frac{1}{i^{d-2}} \frac{\partial^{d-2}}{(\partial x_{||})^{d-2}} \delta(x_{||}), \tag{6.51}$$

et ne dépend pas de $\mathbf{x}$ à longue distance. Afin d'évaluer le préfacteur associé à la sommation sur $\mathbf{q}_{||}$, nous remarquons que la densité d'états vaut

$$N(0) = \frac{1}{(2\pi)^d} \int \frac{d\Omega}{S_d} \int d^{d-1}q_{||}(\Omega) dq_\perp(\Omega) \delta(\mu - \epsilon_{\mathbf{k}_f+\mathbf{q}}) = \frac{1}{(2\pi)^d} \frac{1}{v_f} \int \frac{d\Omega}{S_d} \int d^{d-1}q_{||}(\Omega), \tag{6.52}$$

où la sommation sur $\mathbf{q}$ s'effectue dans le repère local de l'intersection de la surface de Fermi et de l'angle solide $d\Omega$. D'autre part, nous pouvons écrire

$${\sum_{\mathbf{q}}}' = \frac{V}{(2\pi)^d} \int \frac{d\Omega}{S_d} \int d^{d-1}q_{||}(\Omega) dq_\perp(\Omega). \tag{6.53}$$

Nous déduisons de (6.52) et (6.53) que

$${\sum_{\mathbf{q}}}' = V v_F N(0) \int dq_{||}. \tag{6.54}$$

Nous déduisons de (6.54) que

$$\langle \mathrm{k}_f, \mathrm{x}, t | \mathrm{k}'_f, 0, 0\rangle_0 = \delta_{\mathbf{k}_f,\mathbf{k}'_f} \exp\left(-\int_0^{+\infty} \frac{d\mathbf{q}_{||}}{\mathbf{q}_{||}} \left(1 - e^{i\mathbf{q}_{||}(\mathbf{n}_{\mathbf{k}_f}.\mathbf{x} - |\mathbf{v}_{\mathbf{k}_f}|t)}\right) e^{-\epsilon\mathbf{q}_{||}}\right). \tag{6.55}$$

L'intégrale sur $\mathbf{q}_{||}$ s'effectue explicitement en utilisant la relation

$$\int_0^{+\infty} \frac{dx}{x}(1-e^{iax})e^{-\epsilon x} = \ln\left(1-i\frac{a}{\epsilon}\right). \tag{6.56}$$

Pour montrer (6.56), il suffit de décomposer e^{iax} en série entière. Nous avons alors

$$\langle \mathrm{k}_f, \mathrm{x}, t|\mathrm{k}'_f, 0, 0\rangle_0 = \frac{i\epsilon\delta_{\mathbf{k}_f,\mathbf{k}'_f}}{\mathbf{n}_{\mathbf{k}f}.\mathbf{x}+|\mathbf{v}_{\mathbf{k}f}|t+i\epsilon}, \tag{6.57}$$

qui correspond au résultat attendu pour la fonction de corrélation du gaz de Fermi.

6.4 Liquide de Fermi en interaction

6.4.1 Continuum et mode collectif

Le terme d'interaction du liquide de Fermi vaut

$$H^1 = \frac{1}{2V}\sum_{\mathbf{k},\mathbf{k}',\mathbf{q}} U(\mathbf{q})c^+_{\mathbf{k}+\mathbf{q}/2}c_{\mathbf{k}-\mathbf{q}/2}c^+_{\mathbf{k}'-\mathbf{q}/2}c_{\mathbf{k}'+\mathbf{q}/2}. \tag{6.58}$$

Etant donné que l'on travaille dans la limite $\Lambda \to 0$, ce terme d'interaction prend la forme

$$H^1 = \frac{1}{2V}\sum_{\mathbf{k},\mathbf{k}',\mathbf{q}} U(\mathbf{q})n_{-\mathbf{q}}(\mathbf{p})n_{\mathbf{q}}(\mathbf{p}'), \tag{6.59}$$

où les opérateurs particule-trou $n_{\mathbf{q}}(\mathbf{p})$ sont de nature bosonique. En terme des modes $b^+_{\mathbf{q}}(\mathrm{k}_f)$, le terme d'interaction prend la forme

$$\begin{aligned} H^1 = {\sum_{\mathbf{k}_f,\mathbf{k}'_f,\mathbf{q}}}' \quad & \sqrt{(\mathbf{q}.\mathbf{v}_{\mathbf{k}f})(\mathbf{q}.\mathbf{v}_{\mathbf{k}'_f})}N(0)U(\mathbf{q})\left(b^+_{\mathbf{q}}(\mathrm{k}_f)b_{\mathbf{q}}(\mathrm{k}'_f)+b^+_{\mathbf{q}}(-\mathrm{k}_f)b_{\mathbf{q}}(-\mathrm{k}'_f)\right. \\ + \quad & \left. b_{\mathbf{q}}(-\mathrm{k}_f)b_{\mathbf{q}}(-\mathrm{k}'_f)+b^+_{\mathbf{q}}(-\mathrm{k}'_f)b^+_{\mathbf{q}}(\mathrm{k}_f)\right). \end{aligned} \tag{6.60}$$

Afin d'utiliser des notations plus sympathiques, nous indexons les points de la surface de Fermi par un entier et nous notons

$$\mathbf{q}.\mathbf{v}_{\mathbf{k}j} = v_f|\mathbf{q}|s_j, \tag{6.61}$$

avec $s_j = \cos\theta_j$, et nous utilisons les notations $b_{\mathbf{q}}(\mathrm{k}_j) = b_j$ et $b_{\mathbf{q}}(-\mathrm{k}_j) = a_j$. Avec ces notations, le Hamiltonien prend la forme

$$H = \sum_{\mathbf{q}} v_f|\mathbf{q}|H(\mathbf{q}), \tag{6.62}$$

avec

$$H(\mathbf{q}) = \sum_i s_i\left(b^+_i b_i + a^+_i a_i\right) + g\sum_{i,j}\sqrt{s_i s_j}\left(b^+_i b_j + a^+_i a_j + a_i b_j + b^+_i a^+_j\right), \tag{6.63}$$

où $g = N(0)U(\mathbf{q})$. Pour simplifier les notations, nous avons oublié l'indice $\mathbf{q}$ dans (6.63). Le Hamiltonien (6.63) est quadratique en terme de bosons. Nous allons le diagonaliser par une

transformation de Bogoliubov généralisée, définie par

$$b_i = \sum_l \left(M_{i,l}\beta_l + N_{i,l}\alpha_l^+ \right) \tag{6.64}$$

$$a_i = \sum_l \left(M_{i,l}\alpha_l + N_{i,l}\beta_l^+ \right). \tag{6.65}$$

Les nouveaux opérateurs bosoniques vérifient $\left[\beta_l, \beta_k^+\right] = \left[\alpha_l, \alpha_k^+\right] = \delta_{k,l}$ et $[\beta_l, \beta_k] = [\alpha_l, \alpha_k] = 0$, ce qui impose les contraintes

$$\delta_{i,j} = \sum_l (M_{i,l}M_{j,l} - N_{i,l}N_{j,l}) \tag{6.66}$$

$$0 = \sum_l (M_{i,l}N_{j,l} - N_{i,l}M_{j,l}). \tag{6.67}$$

De plus, le Hamiltonien doit être diagonal en terme des nouveaux bosons, c'est-à-dire

$$H = \sum_l S_l \left(\beta_l^+ \beta_l + \alpha_l^+ \alpha_l \right). \tag{6.68}$$

En effectuant les relations de commutation appropriées, nous obtenons

$$(S_l - s_i)M_{i,l} = g \sum_j \sqrt{s_i s_j}(M_{j,l} + N_{j,l}) \tag{6.69}$$

$$(S_l + s_i)N_{i,l} = -g \sum_j \sqrt{s_i s_j}(M_{j,l} + N_{j,l}). \tag{6.70}$$

Les énergies sont alors définies par l'équation implicite

$$1 = g \sum_i \frac{2s_i^2}{S_l^2 - s_i^2}. \tag{6.71}$$

Le continuum particule-trou correspond aux solutions telles que $-1 < S_l < 1$. Les modes collectifs sont tels que $|S_l| > 1$. Les fréquences propres du continuum sont déplacées d'une quantité d'ordre $1/N$ (où N est le nombre de points sur la surface de Fermi) par rapport aux fréquences propres de la théorie libre, alors que le mode colllectif se détache du continuum. Nous examinons successivement les deux types de solutions.

Continuum

Etant donné que les fréquences propres S_l dans le continuum sont décalées d'une quantité $1/N$ par rapport aux fréquence propres du problème libre, on cherche à prendre la limite $S_l = s_l$. On suppose de plus que

$$\lim_{l \to i} \frac{1}{S_l - s_i} = Z_i, \tag{6.72}$$

ce qui permet d'obtenir à partir de (6.69)

$$M_{i,l} = Z_l g \sqrt{s_l} C_l \delta_{i,l} + \frac{g\sqrt{s_i} C_l}{s_l - s_i}(1 - \delta_{i,l}), \tag{6.73}$$

où

$$C_l = \sum_j \sqrt{s_j}\,(M_{j,l} + N_{j,l})\,. \tag{6.74}$$

L'expression (6.72) de Z_i dépend explicitement du nombre de points à la surface de Fermi. La relation (6.73) n'a donc de sens que si le produit $Z_l C_l$ ne dépend plus de N à la limite thermodynamique. Comme nous le verrons plus loin, c'est effectivement le cas. En utilisant (6.70), nous obtenons

$$N_{i,l} = -\frac{g\sqrt{s_i}C_l}{s_l + s_i}, \tag{6.75}$$

où nous avons pris directement la limite $S_l = s_l$ dans (6.70). En remplaçant (6.73) et (6.75) dans l'expression (6.74) de C_l, nous obtenons

$$Z_l = \frac{1}{g s_l}\left(1 - g\sum_j \frac{2s_j^2}{s_l^2 - s_j^2}\right). \tag{6.76}$$

Nous cherchons maintenant à trouver une expression pour le produit $Z_i C_i$. Pour celà, nous utilisons les relations (6.66) et (6.67) dans lesquelles nous remplaçons $M_{i,l}$ et $N_{i,l}$ par leurs expressions (6.73) et (6.75). Nous obtenons alors les identités

$$\delta_{i,j} = \delta_{i,j} Z_i^2 C_i^2 g^2 s_i + g^2\sqrt{s_i s_j}(s_i + s_j)\left(\frac{Z_i C_i^2 - Z_j C_j^2}{s_i^2 - s_j^2} + \sum_l \frac{2C_l^2 s_l}{(s_l^2 - s_j^2)(s_l^2 - s_i^2)}\right) \tag{6.77}$$

et

$$0 = \frac{Z_i C_i^2 - Z_j C_j^2}{s_i^2 - s_j^2} + \sum_l \frac{2C_l^2 s_l}{(s_l^2 - s_j^2)(s_l^2 - s_i^2)}, \tag{6.78}$$

ce qui montre que

$$C_i Z_i = \frac{1}{g\sqrt{s_i}}. \tag{6.79}$$

D'autre part, on montre que

$$\sum_j \frac{2s_j^2}{s_l^2 - s_j^2} = \frac{N}{2\pi}\left(s_l \int_0^{2\pi} \frac{d\theta}{s_l - \cos\theta} - 2\pi\right) = -N, \tag{6.80}$$

car la partie principale de l'intégrale (6.80) s'annule pour $|s_l| < 1$. Nous obtenons donc finalement

$$M_{i,l} = \delta_{i,l} + \frac{g}{1 + Ng}\frac{\sqrt{s_i s_l}}{s_l - s_i} \tag{6.81}$$

$$N_{i,l} = -\frac{g}{1 + Ng}\frac{\sqrt{s_i s_l}}{s_l + s_i}, \tag{6.82}$$

qui constitue la solution de la transformation de Bogoliubov dans le continuum.

Mode collectif

Dans le cas du mode collectif, nous obtenons l'équation

$$g\sum_j \frac{2s_j^2}{s^2-s_j^2}=1 \tag{6.83}$$

qui prend la forme

$$U(\mathbf{q})\Pi(S)=1, \tag{6.84}$$

où $\Pi(S)$ est la fonction de polarisation R.P.A.

$$\Pi\left(\frac{\omega}{qv_f}\right)=N(0)\int\frac{d\Omega}{S_d}\frac{\mathbf{q}.\mathbf{v}_f}{\omega-\mathbf{q}.\mathbf{v}_f}. \tag{6.85}$$

L'équation (6.84) est donc l'équation des modes collectifs.

6.4.2 Propagateur du liquide de Fermi

La première étape consiste à exprimer les états cohérents en terme de bosons α et β. Pour celà, on part de la définition (6.23) des états cohérents et on remplace les opérateurs $b_{\mathbf{q}}(\mathbf{k}_f)$ et $b_{\mathbf{q}}^+(\mathbf{k}_f)$ par leur expresssion (6.64):

$$\begin{aligned}|[\phi]\rangle &= \exp\left(-\sum_{i,l,\mathbf{q}}\left(\frac{1}{2N(0)V|\mathbf{q}|v_f s_i}\right)\left(|\phi(i)|^2(M_{i,l}^2+N_{i,l}^2)\right)\right)\\ &\exp\left(-\sum_{i,l,\mathbf{q}}\left(\frac{1}{N(0)V|\mathbf{q}|v_f s_i}\right)^{1/2}\phi(i)M_{i,l}\beta_l^+\right)\\ &\exp\left(\sum_{i,l,\mathbf{q}}\left(\frac{1}{N(0)V|\mathbf{q}|v_f s_i}\right)^{1/2}\overline{\phi}(i)N_{i,l}\alpha_l^+\right)|FS\rangle.\end{aligned} \tag{6.86}$$

Etant donnée la forme (6.68) du Hamiltonien, il est immédiat de calculer le propagateur (en utilisant la relation (6.45)):

$$\begin{aligned}\langle[\phi]|U(t,0)|[\phi]\rangle &= \exp\left(-\sum_{i,l,\mathbf{q}}\left(\frac{1}{2N(0)V|\mathbf{q}|v_f s_i}\right)\left((|\phi(i)|^2+|\varphi(i)|^2)(M_{i,l}^2+N_{i,l}^2)\right)\right)\\ &\exp\left(\sum_{i,j,l,\mathbf{q}}\left(\frac{1}{N(0)V|\mathbf{q}|v_f\sqrt{s_i s_j}}\right)\varphi(i)\overline{\phi}(j)M_{i,l}M_{j,l}e^{-iS_l|\mathbf{q}|v_f t}\right)\\ &\exp\left(\sum_{i,j,l,\mathbf{q}}\left(\frac{1}{N(0)V|\mathbf{q}|v_f\sqrt{s_i s_j}}\right)\overline{\varphi}(i)\phi(j)N_{i,l}N_{j,l}e^{-iS_l|\mathbf{q}|v_f t}\right).\end{aligned} \tag{6.87}$$

Pour que les états cohérents décrivent des états fermioniques, nous devons appliquer les prescriptions $\varphi(j')=\delta_{j,j'}$ et $\phi(i')=e^{-i\mathbf{q}.\mathbf{x}}\delta_{i,i'}$ qui conduisent à

$$\langle i,\mathbf{x},t|j,0,0\rangle = \exp\left(\sum_{l,\mathbf{q}}\left(\frac{1}{N(0)V|\mathbf{q}|v_f}\right)\left(\frac{M_{i,l}^2+N_{i,l}^2}{s_i}\right)\right) \tag{6.88}$$

$$\exp\left(\sum_{l,i,j,\mathbf{q}}\left(\frac{1}{N(0)V|\mathbf{q}|v_f}\right)\left(\frac{M_{i,l}M_{j,l}}{\sqrt{s_is_j}}e^{i(\mathbf{q}.\mathbf{x}-s_l|\mathbf{q}|v_ft)}+\frac{N_{i,l}N_{j,l}}{\sqrt{s_is_j}}e^{-i(\mathbf{q}.\mathbf{x}+s_l|\mathbf{q}|v_ft)}\right)\right).$$

On peut également s'interesser au propagateur entre points de la sphère de Fermi n'appartenant pas au même hémisphère. On obtient alors

$$\begin{aligned}\langle\tilde{i},\mathbf{x},t|j,0,0\rangle &= \exp\left(\sum_{l,\mathbf{q}}\left(\frac{1}{N(0)V|\mathbf{q}|v_f}\right)\left(\frac{M_{i,l}^2+N_{i,l}^2}{s_i}\right)\right) \qquad (6.89)\\ &\exp\left(\sum_{l,i,j,\mathbf{q}}\left(\frac{1}{N(0)V|\mathbf{q}|v_f}\right)\left(\frac{M_{i,l}N_{j,l}}{\sqrt{s_is_j}}\right)\left(e^{i(\mathbf{q}.\mathbf{x}-s_l|\mathbf{q}|v_ft)}+e^{-i(\mathbf{q}.\mathbf{x}+s_l|\mathbf{q}|v_ft)}\right)\right).\end{aligned}$$

Le symbole $\tilde{}$ signifie que l'on a remplacé les opérateurs b_i par les opérateurs a_i dans l'expression de $U[\phi]$. Afin d'évaluer les sommes sur l'indice l dans (6.88) et (6.89), nous utilisons les relations (6.81) et (6.82). Nous obtenons ainsi

$$\begin{aligned}\sum_l M_{i,l}N_{i,l}e^{iqv_fs_lt} &= \delta_{i,j}e^{iqv_fs_it}+\frac{g}{1+Ng}\frac{\sqrt{s_is_j}}{s_i-s_j}\left(e^{iqv_fs_it}-e^{iqv_fs_jt}\right) \qquad (6.90)\\ &+\left(\frac{g}{1+Ng}\right)^2\sqrt{s_is_j}\sum_l\frac{s_le^{iqv_fs_lt}}{(s_l-s_i)(s_l-s_j)}. \qquad (6.91)\end{aligned}$$

La double singularité s'exprime à l'aide du théorème de Poincaré

$$P\frac{1}{(s_l-s_i)(s_l-s_j)}=P\frac{1}{s_i-s_j}\left(\frac{1}{s_l-s_i}-\frac{1}{s_l-s_j}\right)+\pi^2\delta(s_l-s_i)\delta(s_l-s_j), \qquad (6.92)$$

où

$$\delta(s_l-s_i)=\frac{N}{2\pi}\frac{\delta_{i,l}}{\sqrt{1-s_i^2}}. \qquad (6.93)$$

On obtient alors

$$\sum_l M_{i,l}N_{i,l}e^{iqv_fs_lt}=\left(1+\frac{1}{4}\left(\frac{gN}{1+gN}\right)^2\frac{s_i^2}{1-s_i^2}\right)\delta_{i,j}e^{iqv_fs_it}+O\left(\frac{1}{N}\right). \qquad (6.94)$$

De même, on montre que

$$\sum_l N_{i,l}N_{j,l}e^{iqv_fs_lt}=O\left(\frac{1}{N}\right). \qquad (6.95)$$

Nous sommes maintenant en mesure d'exprimer la fonction de corrélation (6.88) sous la forme

$$\langle i,\mathbf{x},t|j,0,0\rangle=\langle i,\mathbf{x},t|j,0,0\rangle_0\exp\left(-\sum_{\mathbf{q}}\frac{1}{4N(0)v_FV}\left(\frac{N(0)U(\mathbf{q})}{1+N(0)U(\mathbf{q})}\right)^2\frac{q_\perp}{q_{||}^2}(1-e^{i(qv_fq_\perp t-\mathbf{q}.\mathbf{x})})\right). \qquad (6.96)$$

En utilisant les mêmes techniques de calcul qu'à la section 6.3, nous obtenons

$$\langle i,\mathbf{x},t|j,0,0\rangle=Z_F\langle i,\mathbf{x},t|j,0,0\rangle_0, \qquad (6.97)$$

où le résidu de la quasiparticule vaut

$$Z_F=\exp\left(-\frac{1}{4}\left(\frac{N(0)U}{1+N(0)U}\right)^2\right). \qquad (6.98)$$

Chapitre 7

Article 2

Level spacing statistics of the bidimensional Fermi liquid: I. Landau fixed point and integrability[1]

R. Mélin

CRTBT-CNRS, 38042 Grenoble BP 166X cédex France

We investigate the statistical properties of the excitation spectrum of one and two dimensional models for Landau liquids. The level spacing statistics are found to be poissonian for non-zero separations and sufficiently strong interactions. In the poissonian regime, the level spacing statistics are independent on the precise form of the interaction parameters.

[1]J. Phys. I France 5 (1995) 159-179

7.1 Introduction

The statistical distribution of energy level spacings has been recently studied in several strongly correlated fermion systems [1],[2],[3],[4]. One potentially very interesting conclusion is the presence of energy level repulsion in some parameter domain of the two dimensional t-J model [1], which is one of the most investigated models of strongly correlated fermions. This behaviour is interesting since most integrable systems exhibit by contrast an uncorrelated distribution of energy levels. This property has first been proved in the context of semi-classical quantization of classically integrable systems with a finite number of degrees of freedom [6]. It has also been found in a broad class of exactly solvable models in one dimension, such as spin 1/2 chains [2] or the Luttinger model [4]. In more than one spatial dimension, it is much more difficult to construct integrable interacting fermion models. This paper is the second one devoted to the study of level spacing statistics of integrable quantum liquids. Non integrability effects in the Fermi liquid shall be studied in a forthcoming paper. The one dimensional Luttinger liquid has already been analyzed in reference [4], in connection with the breakdown of the Fermi liquid behaviour as the g_2 interaction is switched on. In this case, the spectrum was treated in terms of the bosonic excitations, which generate the $q \neq 0$ part of the Hilbert space. We now give the main idea of the present paper.

A normal Fermi liquid in the vicinity of its ground state is described by a set of elementary excitations (the Landau quasiparticles) which are in one to one correspondence with the Fermi gas excitations. Landau has shown that the energy of a configuration is given by

$$H[\{\delta n_k\}] = \sum_k \epsilon_k \delta n_k + \frac{1}{L^D} \sum_{\langle kk' \rangle} f_{kk'} \delta n_k \delta n_{k'} + ..., \tag{7.1}$$

where only the first two terms are relevant at low temperatures. D is the spatial dimension (1 or 2). The system is in a cubic box of linear size L. Only the spinless case is studied in this paper. δn_k is the difference between the single quasiparticle occupation numbers in the given configuration, and in the ground state. $\delta n_k = 1$ for a quasiparticle, and $\delta n_k = -1$ for a quasihole. The renormalized dispersion $\epsilon(k)$ is

$$\epsilon(k) = \frac{k^2}{2m}, \tag{7.2}$$

where m denotes the effective mass. The ground state is obtained by filling all the states under the Fermi level $\epsilon_F = k_F^2/2m$. We consider the energies given by (7.1) as the exact eigenvalues of a toy model of a Fermi liquid, for which the eigenstates are labelled in the same way as for the Fermi gas. We study the statistics of level spacings for a one and two dimensional phase space. However, the one dimensional case can only be seen as a toy model since the Fermi liquid theory breaks down in one dimension. The hamiltonian (7.1) is a quadratic form of the quasiparticles and quasiholes occupation numbers, and is obviously integrable. The remaining correlations may only originate from a special form of the interaction functions $f_{k,k'}$ which generate the spectrum. The aim of this article is to check that the interaction between quasiparticles induces a crossover towards a random level spacing statistics, and to study the cross-over as a function of the strength of the interactions, the system size, the temperature and the dimensionality.

In a first step, we analyse the level spacing statistics of one dimensional toy models for Landau Fermi liquids. This gives us the possibility to compare the behaviour of a one dimensional

liquid of fermionic Landau quasiparticules and the behaviour of a Luttinger liquid [4] which has bosonic excitations.The technical difference between the present paper and the study of Luttinger liquids is that the one dimensional Fermi system is treated here directly in terms of fermions, whereas we used bosonic excitations in [4]. In the case of a Fermi surface consisting of two points, one is left with a collection of infinite size Hilbert space sectors, labelled by the total momentum. By contrast, the sectors of given momentum have a finite size for a one branch model. The momentum of the single particle states are restricted to the range $k_F - \lambda$ to $k_F + \lambda$, λ being a cut-off on the momenta. The level spacing statistics are analyzed in this regularized Hilbert space H_λ. Within this approach, we analyze the effects of a quadratic correction to the linear Luttinger liquid dispersion relation on the level spacing statistics. The statistics are found to be singular, and depend on the magnetic flux through the ring. As far as the one dimensional Landau liquid is concerned, the quasiparticle interaction function is taken as

$$f_{k,k'} = V f(\frac{R}{2\pi}|k - k'|), \tag{7.3}$$

with R the range of the interactions, V their intensity, and f a decreasing function. If the intensity is given, a cross-over is found as the range increases, to a level spacing distribution slightly different from the expected Poisson distribution. The aim of the one dimensional toy model is to specify the cross-over scales to the Poisson distribution level spacing statistics. The level spacing statistics of the integrable $1/r^2$ Haldane-Shastry spin chain are analyzed as well. The Hamiltonian has a Landau form in terms of the semionic excitations [5].

As far as two dimensional Landau liquids are concerned, the quasiparticle interaction function $f_{k,k'}$ has been assumed to be of the form

$$f_{kk'} = A(1 + B\cos\theta(k, k')), \tag{7.4}$$

where $\theta(k, k')$ denotes the angle between k and k'. The statistics are found to be poissonian for sufficiently large parameters A and B.

7.2 Level spacing statistics of fermions on a non linear dispersion relation

7.2.1 Introduction

We begin with the study of one dimensional models. As mentioned in the introduction, the study of the one dimensional Luttinger liquid fixed point has already been done in [4]. It should be interesting to compare the case of a one dimensionnal Hamiltonian of the Landau form, with interacting fermionic quasiparticules. This shall be done in the next section. As far as now, we consider only free fermions, and study the effects of a non linear dispersion relation on the level spacing statistics. The standard treatment of the excitations of a Fermi gas in the vicinity of its Fermi surface involves the linearization of the dispersion relation in the vicinity of the Fermi surface. In this case, the excitation spectrum is made up of equidistant degenerate levels and thus leads to singular level spacing statistics. We address the question of what are the level statistics if one incorporates non linear terms in the dispersion relation. In the case of the parabolic free electron dispersion relation, one obtains a second order deviation to the linearized dispersion relations, which should modify the high energy excitation spectrum. If the deviation

to the dispersion relation is a polynomial with a low degree, the energy spectrum depends only on a small number of independent parameters. For instance, in the case of a parabolic dispersion relation, the excitation spectrum depends only on two parameters, the mass and the position of the Fermi level. One must moreover add the constraint that the mean value of the level spacing is normalized to unity. Since only a few parameters enter its composition, the spectrum is correlated in a non universal way, which depends on the detailed value of the parameters. If the degree of the polynomial defining the deviation to the dispersion relation increases, one expects that the level spacing statistics should transit to a universal Poisson regime. We did not test this assertion in the present paper, but an example is provided in [4], where we studied the level spacing statistics of a model of two coupled Luttiger liquids [11]. The dispersion relation has the form

$$\epsilon_{-}(q) = \frac{1}{2}(u_\rho - u_\sigma)q - \sqrt{(\frac{1}{2}(u_\rho - u_\sigma)q)^2 + 4t_\perp^2}, \tag{7.5}$$

where u_ρ and u_σ are respectively the charge and spin velocities, $t_\perp$ is the transverse hopping. One can develop the square root of (7.5) in powers of $q\xi$, where the length scale ξ is defined by $\xi = (u_\rho - u_\sigma)/4t_\perp$, and obtain the deviation to the linear dispersion relation $(u_\rho - u_\sigma)q/2 - 2t_\perp$ as a series in powers of $q\xi$. In the regime $q\xi \gg 1$, the number of terms required to describe the dispersion relation as a series in $q\xi$ is high. By contrast to the case of a dispersion relation depending only on a small number of parameters, the transition to a universal level spacing statistics thus requires a higher number of independent parameters. If they are numerous enough, the level spacing statistics are not influenced by the detailed value of the parameters, but fall in a universal regime, described by the poissonian case of random matrix theory.

7.2.2 Regularisation of the Hilbert space

The dispersion relation is right-left symmetric $\epsilon(k) = \epsilon(-k)$. The boundary conditions are periodic. The Hamiltonian reads

$$H_1 = \sum_k v_F \alpha_k \Delta k \delta n_k + \sum_k \delta\epsilon(\Delta k)\delta n_k. \tag{7.6}$$

The first term is the Luttinger gas hamiltonian, with $v_F = d\epsilon(k_F)/dk$ the Fermi velocity. k is a multiple of $2\pi/L$, and runs over the momentum of the excitations, $\alpha_k = +1, -1 = R, L$ and $\Delta k = k - \alpha_k k_F$. The second term contains non linear deviations to the linearized dispersion branches. The spectrum of the Luttinger gas is made up of equidistant degenerate levels, with separations equal to $2\pi v_F/L$, leading to a singular level spacing statistics. We analyze the statistics as the deviation from the Luttinger model dispersion relation $\delta\epsilon(\Delta k)$ increases. The non-linear terms in the energy are expected to randomize the Luttinger gas spectrum, and the randomization is expected to increase with the energy. The dimension of a sector of the two branch model with a given momentum is infinite in the absence of a momentum cut-off, and is obtained as a sum over the infinity of direct products of the right and left sectors with momenta k_R, k_L such as $k = k_R + k_L$. The Hilbert space is regularized in the following way: only one branch is taken into account, and a momentum cut-off λ is introduced, restricting the particle momenta between $2\pi v_F/L$ and λ, and the holes momenta from $-\lambda + 2\pi v_F/L$ to 0. In the same way as for the two-branch model, sectors with different momenta are superposed, leading to a subspace H_λ containing $(2\lambda)!/(\lambda!)^2$ states. The spectrum shall be denoted Sp_λ. In the absence of a deviation $\delta\epsilon(\Delta k)$, the spectrum shall be denoted Sp_λ^0, and is in the energy range 0 to

$\lambda^2 L v_F/2\pi$. Sp^0_λ has the property that $Sp^0_\lambda \subset Sp^0_{\lambda'}$ if $\lambda < \lambda'$. Sp^0_λ is exact only for energies lower than $v_F\lambda$, but states are missing for energies greater than $v_F\lambda$. The particle-hole symmetry transforms each level E^0_α into an level $\lambda^2 L v_F/2\pi - E^0_\alpha$ which belongs to the spectrum, so that the density of states $\rho_\lambda(\epsilon)$ reaches its maximum value for the energy $\lambda^2 L v_F/4\pi$ if $\lambda L/2\pi$ is even, and

$$\frac{2\pi}{L} v_F((\frac{\lambda L}{2\pi})^2 \pm 1) \tag{7.7}$$

if $\lambda L/2\pi$ is odd. The density of states ρ^0_λ is plotted in figure (7.1), and is numerically found to be gaussian around its maximum value. The density of states $\rho(\epsilon)$ in the limit $\lambda \to +\infty$ is computed recursively from the bosonic basis [4] and is plotted on figure (7.2). The asymptotic form of the density of states is [4]

$$\rho^0(\epsilon) \sim \frac{2^{3/4}}{(2\pi)^{3/2}} \frac{1}{\epsilon^{5/4}} \exp(\sqrt{8\epsilon}), \tag{7.8}$$

so that the density of states $\rho^0(\epsilon)$ of the restricted spectrum Sp^0_λ converges non-uniformly to $\rho^0(\epsilon)$. The level spacing statistics were computed only in the low energy part of the spectrum Sp^0_λ, for the first slices of about one million levels, as shown in figure 7.2.

The cut-off λ may be seen as a temperature in the following way. The probability of thermally activated excitations is given by the Fermi distribution function. The energy scale associated to the vanishing of the Fermi distribution function in the vicinity of the Fermi surface is $k_B T$, with k_B the Boltzman constant. The cut-off λ may thus be seen as an effective temperature T through the relation $T = v_F\lambda/k_B$.

7.2.3 Random corrections to the linear dispersion relation

We first analyze the generic case of a random correction to the linear dispersion relation. One is left with only one parameter: the amplitude of the random deviations compared to the interlevel spacing of the Luttinger gas, equal to $2\pi v_F/L$. However, each level is decoupled from each other since there is no deterministic dispersion relation. The level spacing statistics are thus expected to transit to a poissonian level spacing statistics as the amplitude of the random corrections increases. The individual fermionic energy levels are chosen to be $\epsilon(\Delta k) = v_F(k - k_F) + A_0 R(\Delta k)$, where $R(\Delta k)$ is chosen randomly between 0 and 1, with a constant density, and A_0 controls the amplitude of the random deviations. The statistics are studied in the complete Sp_λ spectrum. If A_0 is non-zero, levels originating from the degeneracy k are distributed in the energy interval $[v_F k, v_F k + A_0\lambda L/2\pi]$. The level spacing statistics shall change over to a poisson distribution as the width of the interval goes to $2\pi v_F/L$, namely if $A_0 > A^*_0$, with

$$A^*_0 = \frac{v_F}{\lambda}(\frac{2\pi}{L})^2. \tag{7.9}$$

The scale A^*_0 is numerically found to control the cross-over to a poissonian level spacing distribution, as shown in figure 7.3.

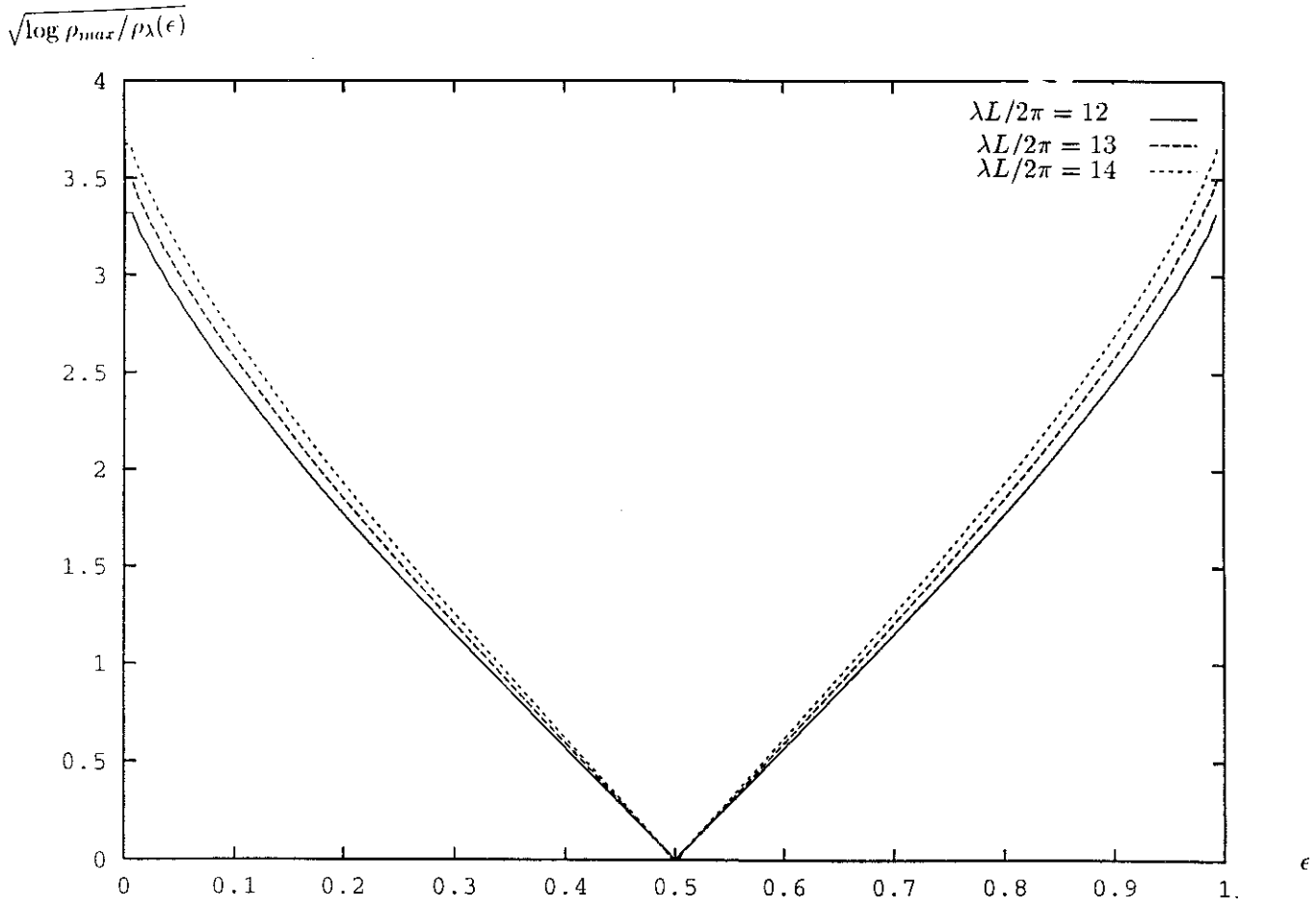

Figure 7.1: Density of states of the truncated spectrum Sp^0_λ.
The density of states $\rho_\lambda(\epsilon)$ was computed for $\lambda L/2\pi = 12, 13, 14$. $\sqrt{\log(\rho_{max}/\rho_\lambda(\epsilon))}$ is plotted as a function of $2\pi\epsilon/v_F\lambda^2 L$. The density of states has a gaussian shape around its maximum value.

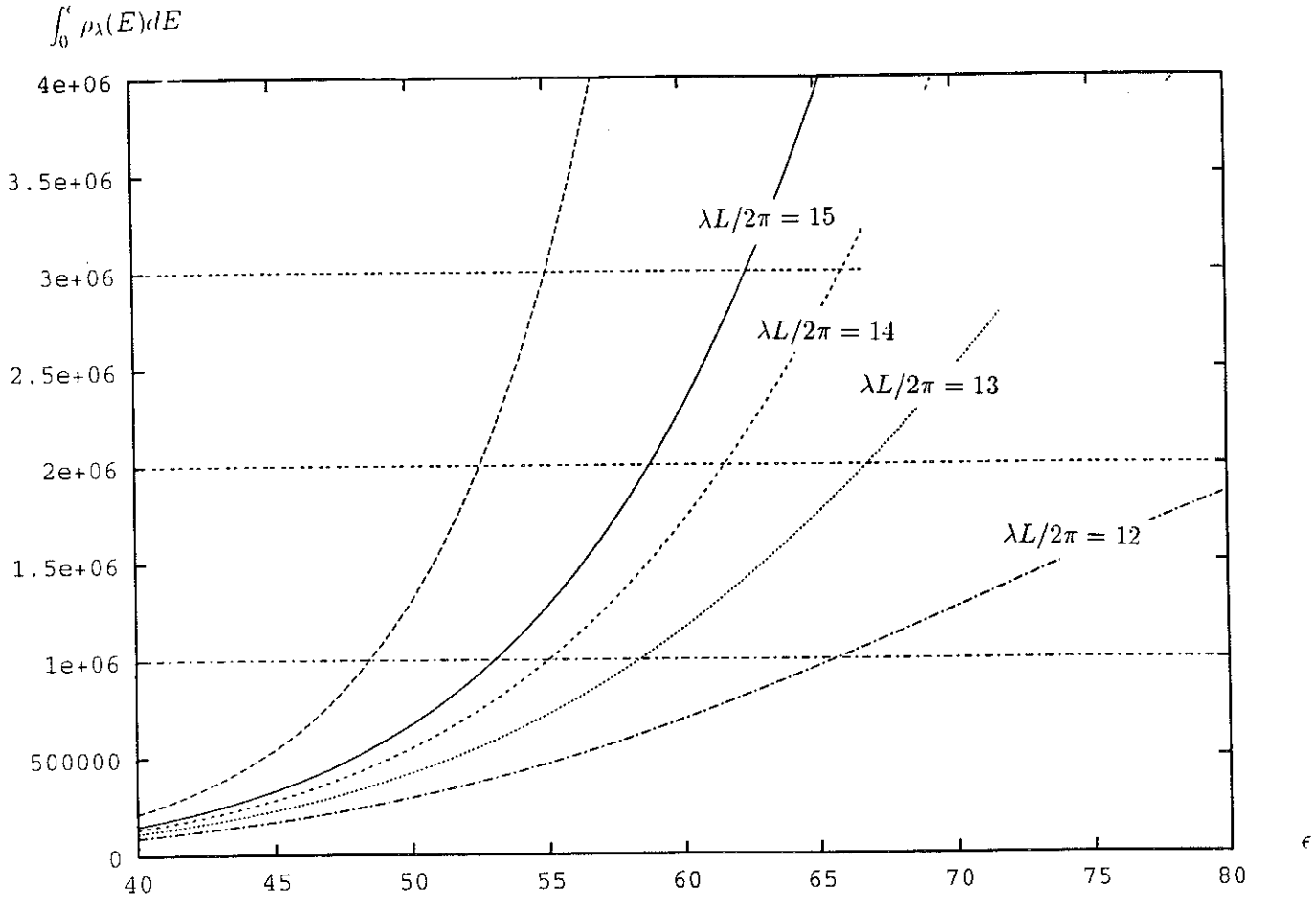

Figure 7.2: Integrated density of states of the truncated spectra compared to integrated density of states in the absence of a cut-off.
The integrated density of states corresponding to the spectra Sp^0_λ is plotted for $\lambda L/2\pi = 12, 13, 14, 15$, as well as the integrated density of states $\rho^0(\epsilon)$ calculated from the boson basis. The energy variable is $\epsilon L/2\pi v_F$.

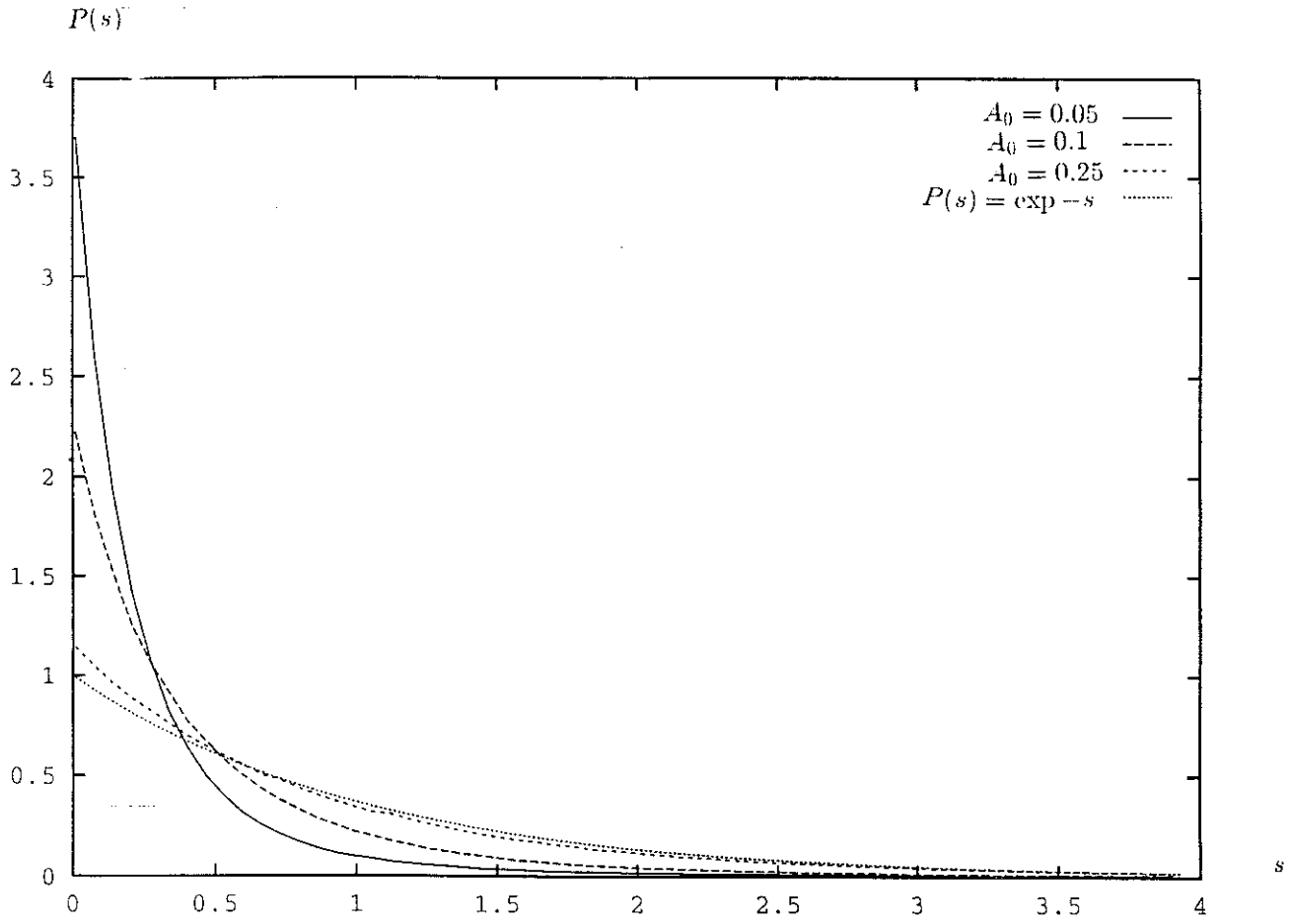

Figure 7.3: Level spacing statistics for linear random corrections to the Luttinger gas dispersion relation.
The length L of the ring is taken equal to 2π, and the Fermi velocity equals 1. The cut-off on the momentum of the fermions is chosen equal to $\lambda = 11$, which generates a Hilbert space of size 705432. The statistics are plotted for various values of the amplitude A_0 of the deviation to the linear dispersion relation, corresponding to $A_0 = 0.05, 0.1, 0.25$. As expected, the statistics converge towards a poisson distribution. The cross-over is controlled by the value $A_0^* = 0.091$

7.2.4 Parabolic dispersion relation

Cross-over scales

We now discuss the level spacing statistics corresponding to the dispersion relation (7.6), $\delta\epsilon(\Delta k)$ being a quadratic deviation to the linear dispersion relation

$$\delta\epsilon(\Delta k) = \frac{(\Delta k)^2}{2m}. \tag{7.10}$$

Non universal effects are expected to emerge. In order to build the spectrum, we use the regularisation procedure which is described in the previous section. Due to the invariance $\epsilon(k + \Delta k) = \epsilon(k) + v_F \Delta k$ of the linearized dispersion relation, the excitation spectrum is parametrized by the single parameter v_F. In the presence of quadratic corrections, one has to additionally specify the Fermi level k_F. In this section, the independant quantities which parametrize the parabolic branches are the mass m and the Fermi velocity v_F. This choice makes it possible to switch on the curvature continuously with different choices of the mass m, while keeping the Fermi velocity constant. The spectrum Sp^0_λ in the case of an infinite mass has been discussed in the previous section. Let E^0 be the energy of a given degeneracy in Sp_λ, in the absence of a quadratic term. The effect of the quadratic deviation is to split the degeneracy. The resulting level spacing statistics are however not poissonian. The quadratic energy term is expected to play a role only at high enough energies. Moreover, the lower bound on the momenta has to be positive, for the excitations to belong to the same right-moving branch. This condition reads: $k_F \geq \lambda - 2\pi/L$, which restricts the study to masses greater than $m_1^\lambda = (\lambda - 2\pi/L)/v_F$. In order to estimate the energy cross-over, we first calculate the energy scale $W(E^0)$ associated with the splitting of a given degeneracy E^0, for a finite mass. The configurations with the maximum and minimum deviations shall be respectively noted $|(+), n, \lambda\rangle$ and $|(-), n, \lambda\rangle$. The excited state $|(+), n, \lambda\rangle$ contains n holes, with wave vectors from k_F down to $k_F - 2\pi(n-1)/L$, and n particles in the highest possible excited particle states, with wave vectors from $k_F + \lambda - 2\pi(n-1)/L$ up to $k_F + \lambda$. The contribution of the quadratic order term to the energy of the excited state $|(+), n, \lambda\rangle$ reads

$$\Delta E_n^{(+)} = \frac{\lambda n}{2m}(\lambda - \frac{2\pi}{L}(n-1)). \tag{7.11}$$

The excited state $|(-), n, \lambda\rangle$ contains n holes with wave vectors from $k_F - \lambda + 2\pi/L$ up to $k_F - \lambda + 2\pi n/L$, and n particles with wave vectors from $k_F + 2\pi/L$ up to $k_F + n\pi/L$, with the following contribution of the quadratic order term to the energy

$$\Delta E_n^{(-)} = -\frac{\lambda n}{2m}(\lambda - \frac{2\pi}{L}(n+1)). \tag{7.12}$$

The levels with an energy E_n^0 in the absence of a quadratic correction are spread on an energy interval of width $W_\lambda^{(n)}$

$$W_\lambda^{(n)} = \Delta E_n^{(+)} - \Delta E_n^{(-)} = \frac{\lambda n}{m}(\lambda - \frac{2\pi}{L}n). \tag{7.13}$$

If $\lambda L/2\pi$ is even, the maximum of the width $W_\lambda^{(n)}$ equals $\lambda^3 L/8\pi m$, and is reached for a number of particle-hole excitations n equal to $n = \lambda L/4\pi$. If $\lambda L/2\pi$ is odd, the maximum width is reached for

$$n = \frac{1}{2}(\frac{\lambda L}{2\pi} \pm 1), \tag{7.14}$$

and equals

$$\frac{\lambda}{4m}\frac{2\pi}{L}((\frac{\lambda L}{2\pi})^2 - 1). \tag{7.15}$$

The maximum in the density of states $\rho^0_\lambda(\epsilon)$ is found to correspond to the maximum in the dispersion of the levels coming from a given degeneracy. The expression (7.3) is exact only for the degeneracies of the form $E^0_n = v_F\lambda n$. We use it to find an approximation of the expression for the width $W(E^0)$ for an arbitrary energy, not necessarily of the form $E^0_n = v_F\lambda n$. We get

$$W_\lambda(E^0) = \frac{E^0}{mv_F}(\lambda - \frac{2\pi}{L}\frac{E^0}{v_F\lambda}). \tag{7.16}$$

The influence of the quadratic term on the level spacing statistics shall be significant provided $W_\lambda(E^0) \geq 2\pi v_F/L$, which leads to the expression of the cross-over energy

$$E^\lambda_{c.o.} = \frac{v_F\lambda^2 L}{4\pi}(1 - \sqrt{1 - \frac{16\pi^2 m v_F}{\lambda^3 L^2}}). \tag{7.17}$$

Note that this energy is proportional to $2\pi m v_F^2/\lambda L$ if $mv_F \ll \lambda^3 L^2$.

Random quadratic corrections

As we shall see in the following section, correlations between the parabolic deviations (7.10) and the linear dispersion relation occur. We first check that, in the absence of these correlations, the level spacing is poissonian. The value of the cross-over parameters are the ones computed in the previous section. This section is just a test for the validity of the arguments we used to treat the cross-overs in the previous section. The deviations to the linear dispersion relation are taken equal to

$$\delta\epsilon(\Delta k) = \frac{k^2}{2m}R(k), \tag{7.18}$$

with $R(k)$ a random number distributed uniformly between 0 and 1. The statistics are computed in the low energy part of the spectrum, for energies in the range $[0, E_{max}]$, where E_{max} is chosen before the computation of the level statistics. If the mass decreases from $m = +\infty$, the statistics shall transit provided the energy cross-over $E^\lambda_{c.o.}$ is effectively in the energy interval $[0, E_{max}]$. The condition $E^\lambda_{c.o.} = E_{max}$, or equivalently $W_\lambda(E_{max}) = 2\pi v_F/L$, leads to the mass cross-over scale

$$m^*_2 = \frac{E_{max}}{v_F^2}(\frac{\lambda L}{2\pi} - \frac{E_{max}}{v_F\lambda}), \tag{7.19}$$

which controls the begining of the cross-over to a poisson distribution as the mass m decreases. The cross-over scale m^*_2 is well observed numerically (figure 7.4).

Level spacing statistics for fermions in a magnetic field, with a parabolic dispersion relation

We shall study the statistics as a function of the magnetic field through the ring of spinless fermions. The effect of the magnetic field is to displace the energy levels by a quantity

$$\delta k_F = \frac{2\pi}{L}\frac{\phi}{\phi_0}, \tag{7.20}$$

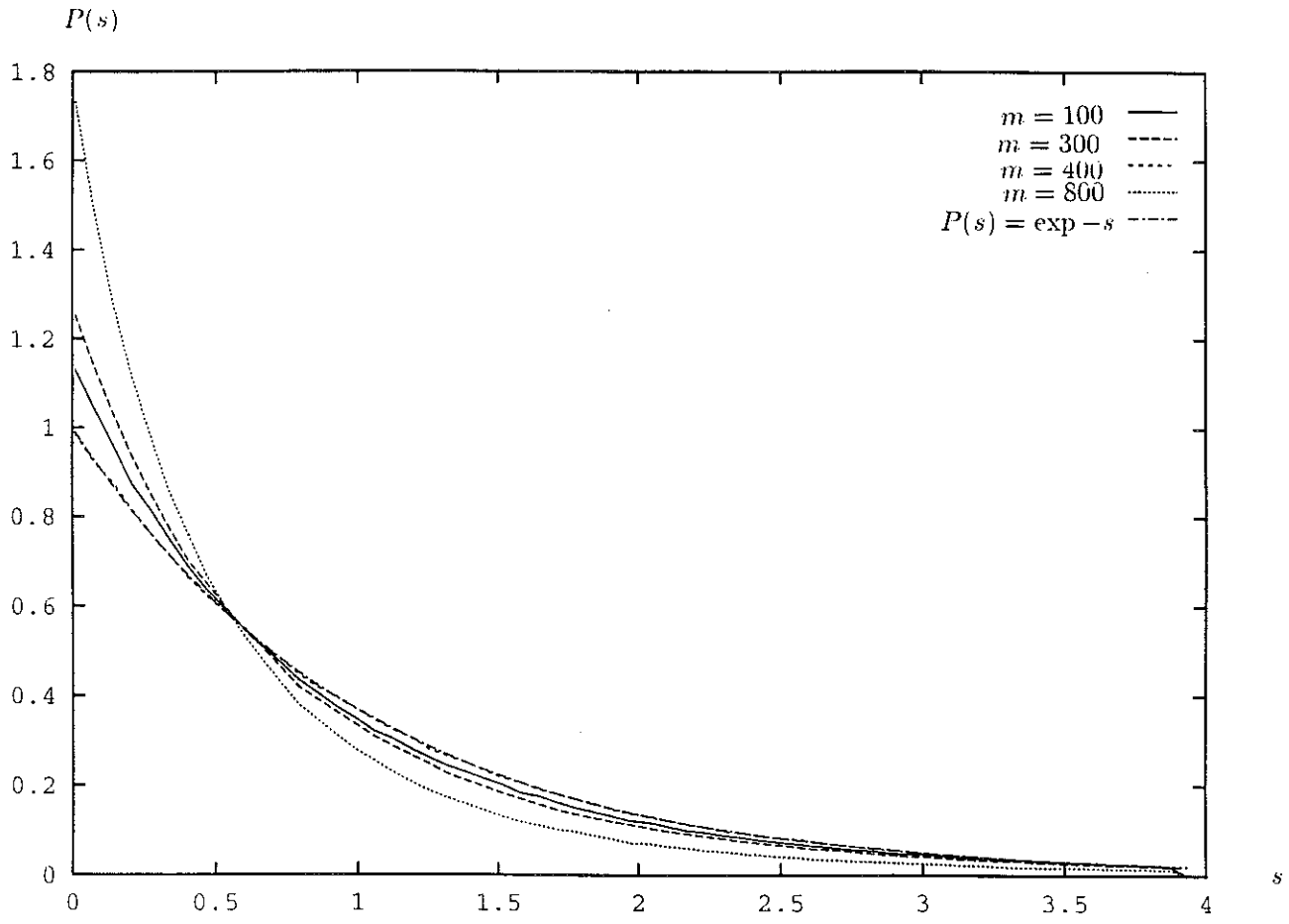

Figure 7.4: Level spacing statistics for quadratic random corrections to the Luttinger gas dispersion relation.
The length L of the ring is taken to be 2π, and the Fermi velocity to be 1. The cut-off on the momentum of the fermions is chosen equal to $\lambda = 14$. The linear order energy of the states which are generated is in the range 0 to 55, which corresponds to 997610 levels. The statistics are plotted for the following values of the masses: $m = 800, 400, 300, 100$. The cross-over mass scale is $m_2^* \simeq 554$. The plot corresponding to $m = 100$ is superposed with the poisson distribution. In the case $m = 100$, we computed the statistics of the 885225 states with a linear order energy in the range $[56, 61]$. The level spacing statistics of this set of level are poissonian, which is consistent with the fact that the spectrum is disordered at all energies greater than $E^{\lambda}_{c.o.}$.

with ϕ_0 the flux quantum. The energy in the presence of the magnetic field is given by

$$H_1(\phi) = \sum_k v_F \alpha_k \Delta k \delta n_k + \sum_k \delta\epsilon(\Delta k - \delta k_F)\delta n_k. \tag{7.21}$$

The introduction of the magnetic field is motivated by the fact that we found non universal level spacing statistics for a zero magnetic field. Maybe, this was due to special correlations between the parabolic deviation $\delta\epsilon(\Delta k)$ and the linear dispersion relation. Since the effect of the magnetic field is to translate the deviation $\delta\epsilon(\Delta k)$ by a factor $-\delta k_F$, we analyze the level spacing statistics as a function of the magnetic field. We find that the presence of a non zero magnetic field is not sufficient to decorrelate the spectrum, and the level spacing statistics remain singular, even in the presence of the magnetic field. Moreover, the statistics of level spacing depend on the precise value of the magnetic field. Unlike the case of a random quadratic correction, the level spacing does not evolve to Poisson statistics as the mass decreases, but exhibit correlations due to the special form of the dispersion relation, with an accumulation of zero separations. The structure of the statistics at non zero separations seems to depend on the ratio ϕ/ϕ_0. If it is a rational, the statistics have peaks for some discrete values. If it is not a rational, the shape of the level spacing statistics is continuous. The statistics are plotted on figure 7.5 for $\phi/\phi_0 = 1/\pi$.

However, the statistics are not stable by translations in the spectrum. In particular, there seems to be a trend for an increase of the peaks in the statistics $P(s)$ as we look at regions with higher and higher energy in the spectrum. However, one cannot conclude on whether this property is due to the regularization, or still persists in the limit $\lambda \to +\infty$.

7.3 One dimensional Landau toy-model

7.3.1 Introduction

An other way to perturb the spectrum of the one dimensional Luttinger gas is to introduce interactions. We have already studied in a previous paper [4] the effect of a g_2 interaction, in the framework of the Luttinger liquid fixed point. We now study Landau interactions. The Hamiltonian is made up of a linear dispersion relation, and an interaction term between quasiparticles

$$H_2 = \sum_k v_F \alpha_k \Delta k \delta n_k + \frac{1}{L} \sum_{<k,k'>} f_{k,k'} \delta n_k \delta n_{k'}. \tag{7.22}$$

We use this Hamiltonian as a toy-model, and study its level spacing statistics. This form of one dimensional Hamiltonian describes for instance the low energy excitations of many models which can be solved by Bethe Ansatz, as shown in reference [12]. So equation 7.22 may describe some physicaly interesting one dimensional models (such as the one dimensional Hubbard model), although they are not Fermi liquids. In this case, δn_k refers to the exact many body elementary excitations of the system, which are not simply expressed in terms of the bare fermionic operators. The Hilbert space is regularized in the same way as in the previous section, with the help of a cut-off λ on the fermionic momenta. The form of the interactions is given in equation (7.3)

$$f_{k,k'} = V f(\frac{R}{2\pi}|k - k'|). \tag{7.23}$$

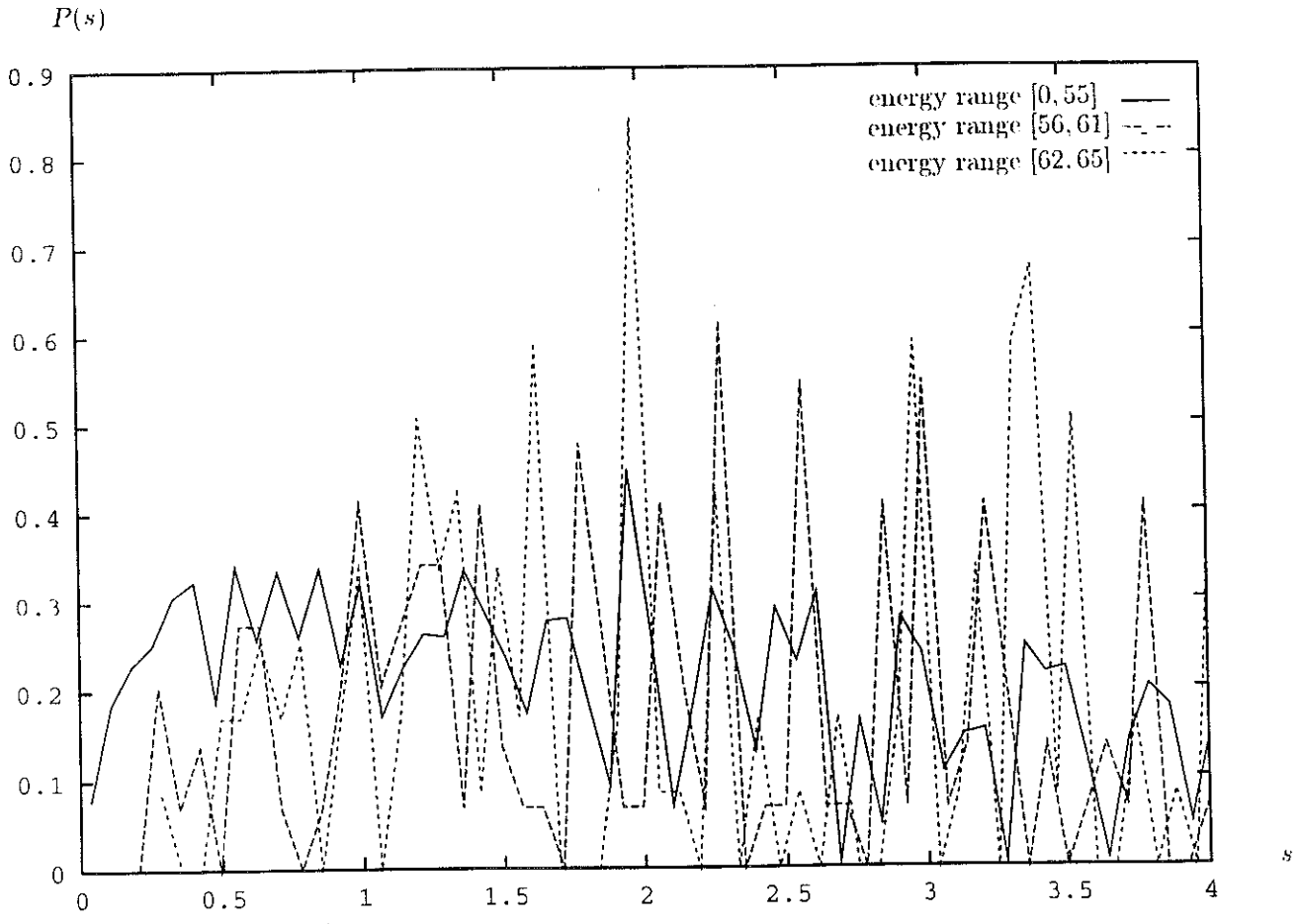

Figure 7.5: Level spacing statistics for a quadratic correction to the Luttinger gas dispersion relation. The length L of the ring is taken to be 2π, and the Fermi velocity to be 1. The mass is taken equal to 20. The momentum cut-off is $\lambda = 14$. The flux is $\phi/\phi_0 = 1/\pi$. The statistics are plotted in the energy range $[0, 55]$, $[56, 61]$,$[62, 65]$, which corresponds respectively to 997610, 885225 and 866526 levels. Among these levels, the number of degenerate separations is respectively: 984431, 882225 and 864432.

$f(x)$ is a decreasing function of the reduced momentum separation $x = R|k - k'|/2\pi$. The interaction shape $f(x)$ is of order of unity for x lower than 1, and vanishes for x greater than 1. This section is organized as follows. We first investigate the case of finite range Landau parameters and finite size. The interactions take zero values for $|k - k'| > 2\pi/R$. In that case, degeneracies are expected to remain, due to the fact that the interactions do not affect excitations with a sufficiently large momentum separation. In a second step, we analyze the statistics for still a short range interaction, but with non compact support in the k space. A discussion of the thermodynamic limit and of finite size effects follows. We shall end this section with a comparison between the Luttinger case and the Fermi liquid case. As a complement, we treat the case of the Haldane-Shastry $1/r^2$ spin chain. The Hamiltonian has the Landau liquid form, but with special interactions in terms of spin one half bosons. Due to the special form of the dispersion relation, the statistics are singular for this model.

7.3.2 Finite range Landau parameters and finite size

In order to analyze the effect of a finite cut-off on the interactions, the shape of the interactions is taken equal to

$$f(x) = (1 - |x|)\exp(-\alpha|x|)\theta(1 - |x|), \tag{7.24}$$

where α parametrizes the interactions and $x = kR/2\pi$ is the reduced momentum. The interaction cut-off $2\pi/R$ is allowed to vary, whereas the size L of the system is fixed. As far as the zero separation part of the level statistics is concerned, the number of states belonging to degenerate subspaces decreases as the interaction cut-off $2\pi/R$ increases. For the case under study, $\lambda L/2\pi = 11$, and the proportion of degenerate levels is equal to 99.7% if the interaction cut-off $2\pi/R$ is in the range $]2\pi/L, 4\pi/L[$, but falls down to 32.0% if $2\pi/R \in]9\pi/L, 10\pi/L[$. The evolution of the non-zero separation part of the statistics as a function of the interaction cut-off $2\pi/R$ is plotted on figure 7.6.

The statistics are found to converge for $L/R \sim 7$. However, the statistics are not found to converge towards a Poisson distribution: the probability of small separations is reduced compared to the Poisson distribution, and increased at large separations. These correlations may originate from the truncation of the Hilbert space. The evolution of the statistics as the interaction cut-off increases is similar to the decoherence of the spectrum of a one dimensional Luttinger liquid as the range of the g_4 interaction increases in momentum space [3]. In the later case, the spectrum is the convolution of the spectra of harmonic oscillators whose frequencies are related to the interaction strength. Starting from the non-interacting case, where the frequencies of all the oscillators are equal to $n2\pi v_F/L$ (with n an integer), an increase of the range of the interactions increases the number of non-commensurate oscillators, thus leading to lifting of degeneracies and decoherence of the spectrum. In the former case, the interactions act as a coupling between excitations on the reciprocal space lattice, with a strength $J_n = V/Lf(nR/L)$, where $k = 2\pi n/L$ (with n an integer) is the momentum separation between excitations. The sign is positive for particle-particle and hole-hole interactions, negative for particle-hole interactions. If $2\pi/R \in]2m\pi/L, 2(m+1)\pi/L[$, only $J_1, ..., J_m$ are non zero. Decoherence of the spectrum occurs as the number of non zero couplings is large enough (of order 7, which also corresponds to the magnitude of the number of oscillators with incommensurable frequencies leading to a Poisson spectrum in the case of a Luttinger liquid). In the regime where the statistics have converged, the statistics are expected to be independent of the precise values of the interactions J_n. As far as the interaction shapes (7.24) are concerned, we checked that the level spacing

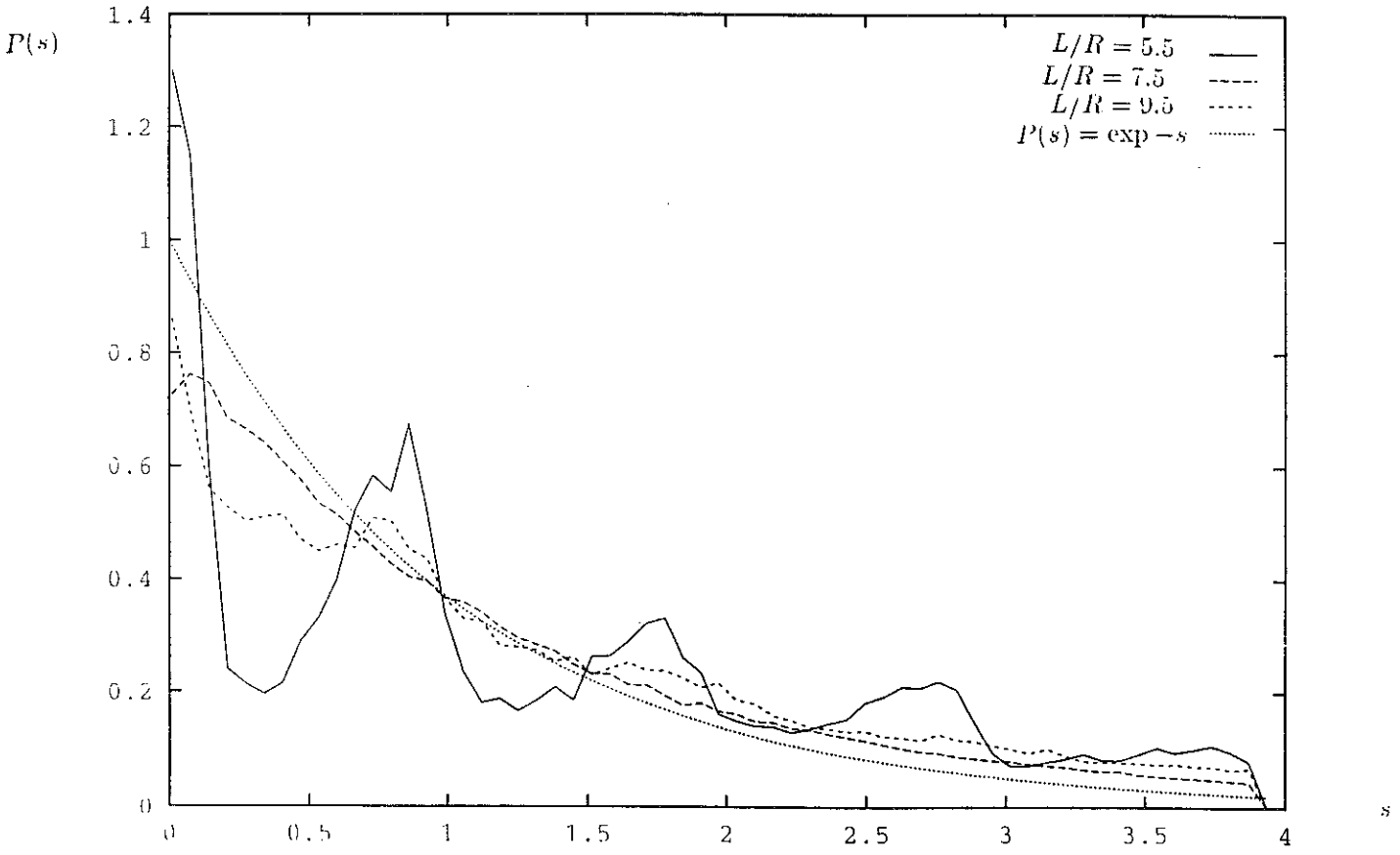

Figure 7.6: Level spacing statistics of the one dimensional Fermi liquid with short range interactions. The length L of the ring is taken to be 2π, and the Fermi velocity to be 1. The statistics are plotted for an interaction shape $f(x) = (1-|x|)\exp(-\alpha|x|)\theta(1-|x|)$. The cut-off is: $\lambda = 11$. The strength of the interaction is $V = 0.3$, and the reduced ranges are: $L/R = 5.5, 7.5, 9.5$. α is taken to be 1. The statistics exhibit a cross-over for $L/R \sim 7$, but to a distribution slightly different from a poisson distribution. The density of small separations is reduced ($P(0) \simeq 0.8$) compared to the poisson case. For $L/R = 9.5$, the statistics have converged, we checked that the level spacing statistics are identical as for $\alpha = -1$.

statistics are independent of the value of α. the effect of the parameter V shall be studied in section 3.4.

7.3.3 Non-compact support Landau parameters and finite size

The statistics corresponding to the case of short range interactions with an unrestricted tail can be seen as the limit of the case of short range interactions with compact support, but with a large support compared to $2\pi/L$ Strong degeneracies are not present with an unrestricted tail. We studied the evolution of the statistics as the range $2\pi/R$ is given, the interaction shape being taken equal to $f(x) = exp(-x)$. The interaction strength V increases from $V = 0$. A cross-over from a singular spectrum is expected to occur as the maximum interaction energy equals the interlevel spacing of the free model. The configuration for which the interaction energy is maximum contains the fermions in the highest excited states, with wave vectors from $2\pi/L$ to λ. The energy of this configuration is equal to

$$\frac{V}{L}\{(\frac{\lambda L}{\pi} - 3)f(R/L) + (\frac{\lambda L}{\pi} - 6)f(2R/L) + ...\} \tag{7.25}$$

The omitted terms contain contributions from next nearest neighbours, ... If $2\pi/R$ is of order of $2\pi/L$, the cross-over intensity is determined only by nearest neighbour interactions and equals

$$V^* = \frac{2\pi v_F}{(\lambda L/\pi - 3)f(R/L)}. \tag{7.26}$$

The cross over is well observed, and the statistics converge to the same distribution as the one in the case of finite range interactions with compact support (see figure 7.7).

7.3.4 Thermodynamic limit and finite size effects

We now assume that the range $2\pi/R$ of the Landau parameters $f_{k,k'}$ is given. $f_{k,k'}$ is zero for $|k - k'| \geq 2\pi/R$. The size L of the system is variable, and the thermodynamic limit corresponds to $L \gg R$. The cut-off λ remains unchanged, which means that the temperature scale T remains constant in the scaling $L \to +\infty$. We showed in the previous section that a way to obtain statistics close to Poisson statistics was to produce a sufficient number of non commensurable coefficients $f_{k,k'}$, which is verified if the ratio L/R is of order 7. This condition to have a statistics close to Poisson statistics is automatically verified in the thermodynamic limit. However, it is not sufficient. One has to check that the displacement of the energy levels induced by the interaction term is of order $2\pi v_F/L$. A rigorous treatment consists in evaluating the width $W(E)$ as we did for the parabolic dispersion relation. We did not compute it, but calculate the energy displacement ΔE induced by the interactions for the following state

$$\prod_{\lambda<k\leq 0} c_k \prod_{0<k\leq\lambda} c_k^+ |FS\rangle, \tag{7.27}$$

for which the interaction intensity is maximal. The length scale associated to the beginning of the cross-over as L increases shall thus be obtained as $\Delta E \sim 2\pi v_F/L$. We separate different contributions to the energy ΔE. First, the contribution due to particle-particle interactions is equal to

$$\Delta E_1 = \frac{1}{L} \sum_{0<k<k'\leq\lambda} f_{k,k'}. \tag{7.28}$$

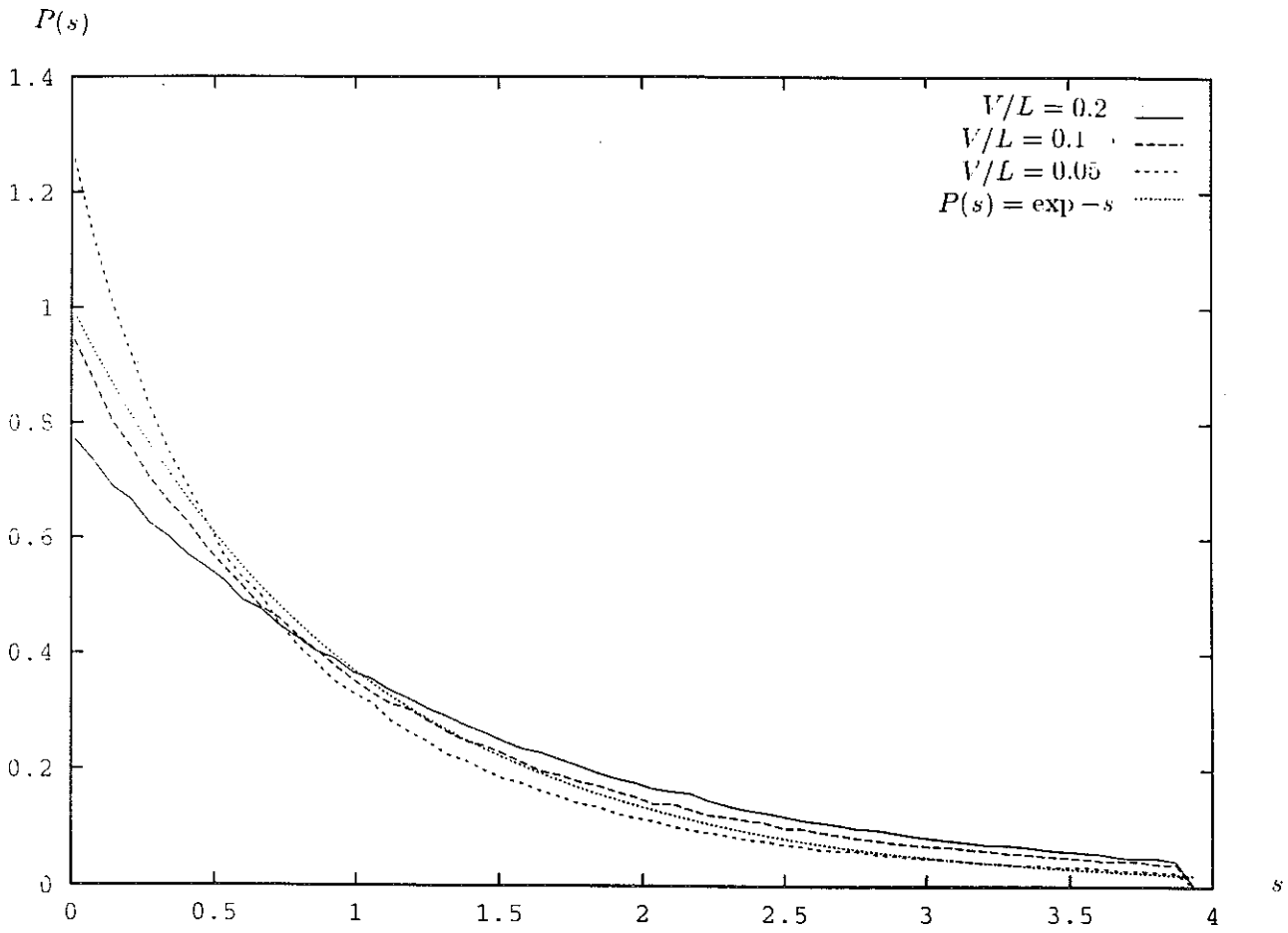

Figure 7.7: Level spacing statistics of the one dimensional Fermi liquid. The length L of the ring is taken to be 2π, and the Fermi velocity equals 1. The statistics are plotted for an interaction range $R = L = 2\pi$, and $f(x) = \exp(-x)$. The interaction cut-off λ is taken equal to 11. The statistics are plotted for the following interaction intensities: $V/L = 0.2, 0.1, 0.05$. The cross-over is expected for $V^*/2\pi = 0.108$. A cross-over is well observed, but to a distribution with a reduced density for small separations.

If the cut off λ is large compared to the range of the interactions $2\pi/R$, the summation (7.28) may be evaluated as

$$\Delta E_1 = \frac{\lambda}{2\pi}(1 + O(\frac{2\pi}{R\lambda})) \sum_{q=2\pi/L}^{2\pi/R} f_q, \tag{7.29}$$

where $q = |k - k'|$, and $f_q = f_{k,k'}$. In the thermodynamic limit, $L \gg R$ and the summation in (7.29) may be approximated by the corresponding integral

$$\Delta E_1 = \frac{\lambda L}{(2\pi)^2}(1 + O(\frac{2\pi}{R\lambda})) \int_0^{2\pi/R} f_q dq. \tag{7.30}$$

Due to the particle-hole symmetry of the state (7.27), the energy contribution ΔE_2 of the excited holes is equal to ΔE_1. The contribution ΔE_3 due to particle-hole interactions reads

$$\Delta E_3 = -\frac{1}{L} \sum_{0 \le k < 2\pi/R} \sum_{0 < l \le 2\pi/R} f_{k,l}. \tag{7.31}$$

ΔE_3 is bounded by

$$|\Delta E_3| \le \frac{1}{L} \sum_{0 \le k < 2\pi/R} \sum_{0 < l \le 2\pi/R} f_l. \tag{7.32}$$

After changing the summation into an integration ($L/R \gg 1$), we obtain

$$|\Delta E_3| \le \frac{L}{2\pi R} \int_0^{2\pi/R} f_k dk. \tag{7.33}$$

Since the length scales are such that $\lambda \gg 2\pi/R \gg 2\pi/L$, the total energy shift $\Delta E = \Delta E_1 + \Delta E_2 + \Delta E_3$ is approximated by

$$\Delta E = \frac{\lambda L}{2\pi^2}(1 + O(\frac{2\pi}{R\lambda})) \int_0^{2\pi/R} f_q dq. \tag{7.34}$$

It is now straightforward to obtain a criterium for the beginning of the transition from a singular statistics to a statistics close to Poisson statistics. The cross-over scale, such as $\Delta E \sim 2\pi v_F/L^*$, is

$$L^* = (\frac{4\pi^3 v_F}{\lambda \int_0^{2\pi/R} f_q dq})^{1/2}. \tag{7.35}$$

We thus distinguish two regimes as far as finite size effects are concerned. The strength of the interactions f_k is fixed and one compares systems of different sizes. A first regime corresponds to a mesoscopic regime, where $L \le L^*$. In this case, the strength of the interactions is not large enough to perturbe the statistics and one is left with a non universal level spacing statistics. Since it is non universal, the shape of the statistics depends on the size of the system in a complicated way. The second regime $L \gg L^*$ corresponds to the thermodynamic regime. In this case, the shape of the statistics is universal, namely close to poissonian statistics, and in particular does not depend on the size of the system. The level spacing statistics are thus a good tool to determine when the system is weakly interacting (in a mesoscopic regime) or strongly interacting(in the thermodynamic regime).

7.3.5 Comparison between the Luttinger liquid case and the Landau Fermi liquid case

We have studied two different types of interacting Fermi liquids in one dimension. The first one is the Luttinger liquid, which we studied in [4] and the second one is the Landau Fermi liquid. One may ask whether level spacing statistics are appropiate to differentiate between the two different one dimensional quantum liquids. The answer is yes. In both cases, the level spacing statistics have the following feature. The level spacing statistics are not universal if the number of interaction parameters is inferior as 7, namely if the ratio L/R is inferior as 7. Both models present a typical length scale associated to the cross-over from a mesoscopic regime to a thermodynamic regime, or in other words, a typical interaction strength V^* which controls the cross-over of the level spacing statistics from a non universal regime to a regime close to a poissonian regime. In the case of the Landau model, the poissonian regime was only approximate, since we did not find strictly Poisson level spacing statistics. In the case of the Luttinger liquid, the interaction V^* was found to be equal to [4]

$$V^*_{Lutt} = (\frac{\pi}{kL(kR)^\alpha})^{1/2} v_F, \tag{7.36}$$

where k is the momentum of the quasiparticule. The typical length scale V^* is easily obtained in the case of the Landau liquid theory, using (7.23) and (7.35)

$$V^*_{F.L.} = v_F \frac{2\pi^2}{\lambda L^2 \int_0^1 f(x)dx}. \tag{7.37}$$

In the case of the Luttinger liquid, $V^*_{Lutt} \sim L^{-1/2}$ and in the case of the Fermi liquid, $V^*_{F.L.} \sim L^{-2}$. The level spacing statistics are thus a good tool to distinguish between the one dimensional Landau Fermi liquid and the one dimensionnal Luttinger liquid. To distinguish both cases, it is sufficient to look at the scaling of the cross-over interaction as a function of the system size.

7.3.6 Complement: Haldane-Shastry $1/r^2$ spin chain

The spin 1/2 chain with periodic boundary conditions and interactions proportional to the inverse square of the chord distance has been integrated by Haldane [7] and Shastry [8]. The hamiltonian in term of spins is

$$H_3 = J \sum_{m<n} [d(n-m)]^{-2} \mathbf{S}_n . \mathbf{S}_m, \tag{7.38}$$

with $d(n) = N/\pi \sin \pi|n|/N$. The excitations of the spin chain are spin one-half bosons (spinons). We first summarize the results concerning the model [9].

The spectrum is the superposition of the different sectors labelled by the integer M, corresponding to different values of the number of spinons $N_{sp} = N - 2M$. The ground state energy in a sector of given M is

$$E_0(M) = J(\pi/N)^2 \{\frac{1}{6}N(N^2-1) + \frac{1}{3}M(M^2+2) - \frac{1}{4}MN^2\}. \tag{7.39}$$

The $M+1$ orbitals of the branch labelled by M have their momentum in the range $-k_0, ..., +k_0$ with $k_0 = \pi M/N$, and an increment $2\pi/N$. The total momentum and spins in the sector M

are

$$K = \pi MN + \sum_k kn_k (mod 2\pi) \tag{7.40}$$

$$S_z = \frac{1}{2}\sum_k (n_{k\uparrow} - n_{k\downarrow}). \tag{7.41}$$

The spinon energy term in a sector of given M is

$$J\sum_{k\sigma} \epsilon_0(k) n_{k\sigma} + \frac{J}{2N}\sum_{k\sigma,k'\sigma'} V(k-k') n_{k\sigma} n_{k'\sigma'}, \tag{7.42}$$

where $\epsilon_0(k) = 1/2(k_0^2 - k^2)$ and $V(k) = (\pi/2)(k_0 - |k|)$. The Hamiltonian in terms of spinons has thus the Landau form. However, the form of the one spinon term and of the interaction term is very unusual.

Level spacing statistics

The level spacing statistics are singular in the conformal limit, with only a peak at $s = 0$, since the spinon energy levels are equidistant in this limit

$$H_4 = \frac{\pi^2 J}{N}((\frac{N_{sp}}{2})^2) + \sum_\sigma \sum_{k=0}^{+\infty} k n_{k\sigma}. \tag{7.43}$$

What is the shape of the level spacing statistics for a finite size ring, with the Hamiltonian (7.42)? We computed the level spacing statistics of an 18 sites spin chain in a sector with a given spin S_z and a total momentum of the spinons K. The statistics are found to exhibit strong degeneracies. The level spacing statistics for non-zero separations exhibit a singular behaviour, even when sectors with different momenta are superposed. The level spacing statistics of this model were already computed in [2] with the help of exact diagonalization. The authors found a deformed Poisson level spacing statistics with an increase of the probability density for small separations. Our results suggest that the poissonian part of the level spacing statistics found by these authors is rather due to their use of open boundary conditions. The level spacing statistics of the $1/r^2$ Haldane Shastry is an exemple of model with very simple interaction functions, depending on a few parameters. The remarks we have made in the case of deviations to the linear dispersion relation remain valid for the interaction function. The spectrum depends only on a few parameters and thus falls in a non universal class. We have seen in the case of the one dimensional Landau theory, with finite range Landau parameters, that the number of independant parameters needed to obtain statistics close to Poisson statistics was of order 7. The number of independant parameters in the case of the Haldane Shatry $1/r^2$ spin chain is much fewer, and it is thus not surprising that the resulting level spacing statistics are singular.

7.4 Bidimensional Landau model

7.4.1 Approximations and level spacing statistics

The hamiltonian is given by the equation (7.1), in the bidimensional case

$$H[\{\delta n_k\}] = \sum_k \epsilon_k \delta n_k + \frac{1}{L^2}\sum_{\langle kk'\rangle} f_{kk'} \delta n_k \delta n_{k'} + ..., \tag{7.44}$$

with $f_{k,k'}$ given by the equation (7.4)

$$f_{k,k'} = A(1 + B\cos\theta(k,k')), \tag{7.45}$$

where $\theta(k,k')$ is the angle between k and k'. By contrast to our previous study in one dimension, only the angular dependence of the interaction function is considered. Furthermore, for the sake of simplicity, we assume rotation invariance and keep only the first circular harmonic. In order to evaluate the cross-overs, we shall use the same arguments as for the one dimensional toy model. However, fluctuations of the density of states are present in the two dimensional case, and do not exist in the one dimensional Luttinger gas. The following evaluation of the cross-over is a rough evaluation, so that we do not take the effect of these fluctuations into account.

One needs to generate all the excited states above the bidimensional Fermi sea, and to compute their energy in the presence of interactions. The first step is to generate the energy levels of the free model, with an energy inferior to E_C^0, in the absence of interactions. The configurations are generated by choosing the first hole with an energy inferior to E_C^0, the Fermi energy being taken equal to zero. The second excitation is chosen in the restricted phase space. The displacement of the energy of a configuration with n particles and n holes is bounded as follows

$$|\frac{1}{L^2}\sum_{<k,k'>} A(1 + B\cos\theta(k,k'))\delta n_k \delta n_{k'}| \leq \frac{1}{L^2} n(2n-1)|A|(1+|B|). \tag{7.46}$$

This inequality means that a way to generate all the energy levels in the presence of interactions, with an energy inferior to a given cut-off E_C, is to generate all the energy levels in the absence of interactions, with an energy inferior to $E_C^0 = E_C + n(2n-1)|A|(1+|B|)/L^2$. However, this procedure is not realistic since the number of levels to be eliminated is huge. Instead of generating the whole low energy spectrum, we take E_C and E_C^0 as independent variables, that is we generate all the states in the absence of interactions with an energy inferior to E_C^0, compute the displacement induced by the interactions, and retain only the energy levels with an energy inferior to E_C. As mentioned in the introduction, the spectrum is expected to be poissonian. We assume that this procedure does not induce correlations. Moreover, the spectrum is generated in a sector of given particle-hole excitations n. The Hilbert space is thus regularized by the 3 parameters n, E_C and E_C^0. The total momentum K is fixed. Some degeneracies appear, due to the fact that the momentum is constrained to a reciprocal space lattice. The energy (7.44) is invariant under the transformations in the reciprocal space which preserve the origin, the unoriented angles and the square lattice, that is the rotations of angles $\pi/2$, $3\pi/2$ and the symmetries with respect to the two axis and the two diagonals. If the total momentum K is chosen along the 4 symmetry directions of the square lattice, supplementary degeneracies are expected, and an accumulation of zero level spacings is indeed observed. To avoid it, the total momentum K is not chosen among the symmetry directions of the square lattice. If a configuration contains a subset of m particles (or holes), on a polygon, then the total energy (7.44) of the configuration is independent on the orientation of the polygon, and the total momentum is unchanged since the polygon is regular. However, the vertices of the polygon still have to belong to a square lattice, which implies that $\cot(\pi/m)$ is rational number, which allows only the possibilities $m = 2$ and $m = 4$. If the second harmonic, namely a $\cos 2\theta$ term in the hamiltonian (7.44) is taken into account, only the $m = 4$ symmetry survives, and no symmetry exists for higher harmonics. As far as the energy (7.44) is concerned, the excitations of the Fermi sea must therefore be factored by the $m = 2$ symmetry described above. We did

not perform the elimination of redundant configurations numerically, but eliminated the sharp peak at zero separations in the level spacing statistics. In the one dimensional case, we were able to produce exact expressions for the width of the fan of levels emerging from a given set of degenerate levels. We do not evaluate the exact width of the fan in the two dimensional phase space, but give an estimation of the cross-over as a function of the parameters A and B. If $B = 0$, the displacement depends only on the number of particle-hole excitations. Its value is $-An/L^2$. The energy shift induced by the first harmonic is

$$\frac{AB}{L^2} \sum_{<k,k'>} \cos\theta(k,k')\delta n_k \delta n_{k'}. \tag{7.47}$$

An exact evaluation of the energy shift would require the knowledge of the quasiparticle occupation numbers in a sector of momentum K. We estimate the cross-over as follows: the summation (7.47) is bounded above by

$$\frac{2(2n-1)|A||B|}{L^2}, \tag{7.48}$$

and we take this bound as an estimate of the width of the fan of levels, which leads to the following estimation for the energy cross-over

$$n(2n-1) \geq \frac{2\pi v_F L}{|A||B|}, \tag{7.49}$$

and assume that this criterium remains valid even in the presence of the energy cut-off E^0 and E_C^0. This criterium is valid only if the number of excitations is given. This is not the case in the thermodynamic limit.

The statistics are computed in the sector $n = 1, 2$, using the regularization procedure described above. The level spacing statistics are found to be poissonian. The statistics also remain poissonian as different number of particle-hole excitations are superposed (figure 7.8 and 7.9).

7.4.2 Thermodynamic limit

In the same way as for the one dimensional case, we analyze the thermodynamic limit by considering an energy cut-off $|\lambda|$ on the momenta, and one calculates the shift of a level containing a number of excitations n proportional to

$$n \sim \frac{2\pi k_F \lambda}{(2\pi/L)^2}. \tag{7.50}$$

The characteristic length L^* associated with the cross-over is obtained by inserting the number n (7.50) of particle-hole excitations into the inequality (7.49), which yields

$$L^* = \left(\frac{4\pi^3}{m k_F \lambda^2 |A||B|}\right)^{1/3}, \tag{7.51}$$

where we have replaced $2n-1$ by $2n$.

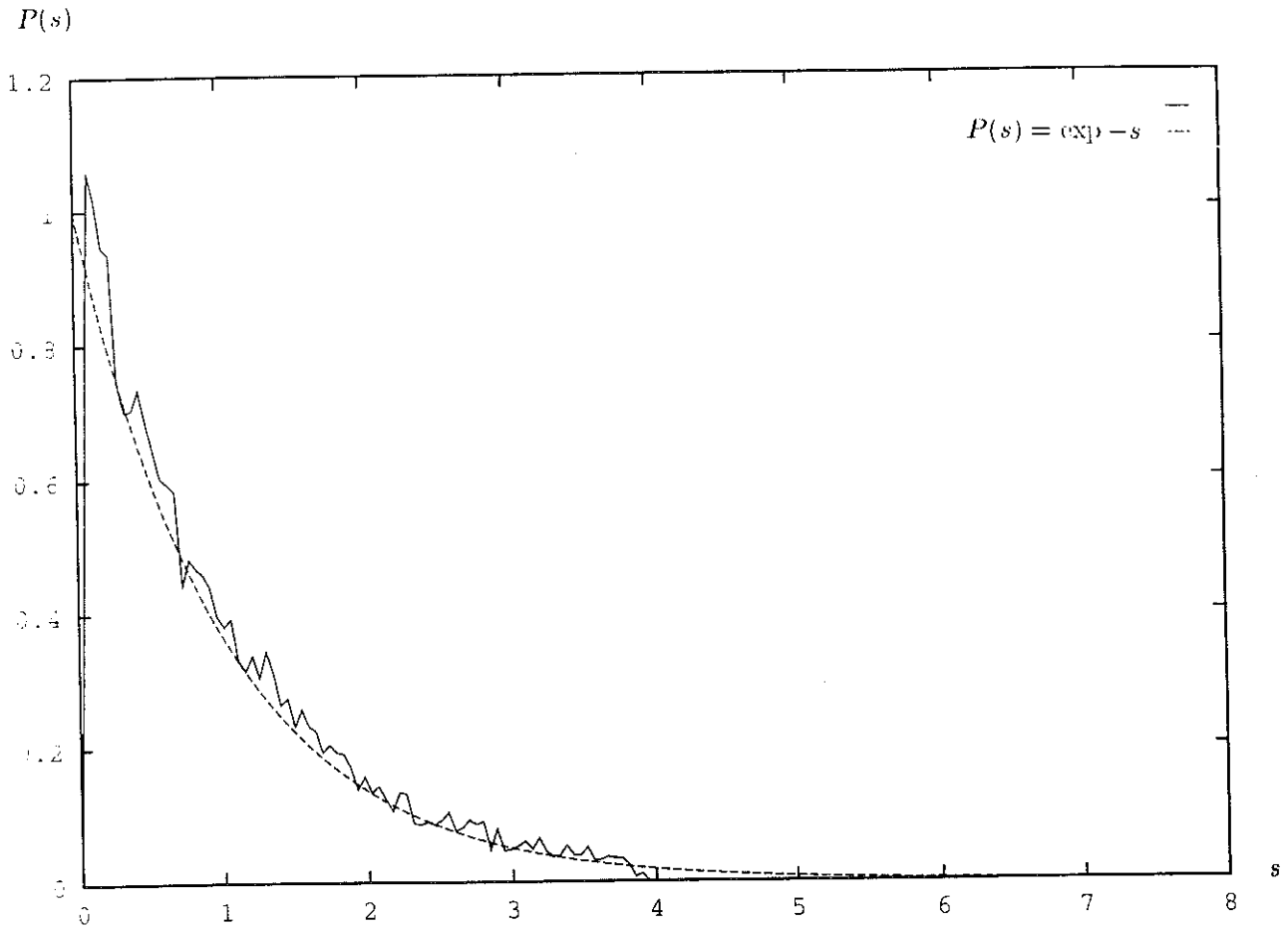

Figure 7.8: Level spacing statistics of the two dimensional Fermi liquid. The parameters of the computation are: $L = 2\pi$, $k_F = 30$, $m = 1/2$, $A = 50$, $B = 50$, $p_x = 5$, $p_y = 4$. Levels belonging to the sectors $n = 1$ and $n = 2$ are superposed. The condition (7.49) is fulfilled since $n(2n-1) = 6$ and $2\pi v_F/|A||B| = 0.95$. The cut-off in the spectrum is chosen equal to $E_{max} = E^0_{max} = 100, 200$. The level statistics are restricted to separations between 0.1 and 4. 163175 levels were generated.

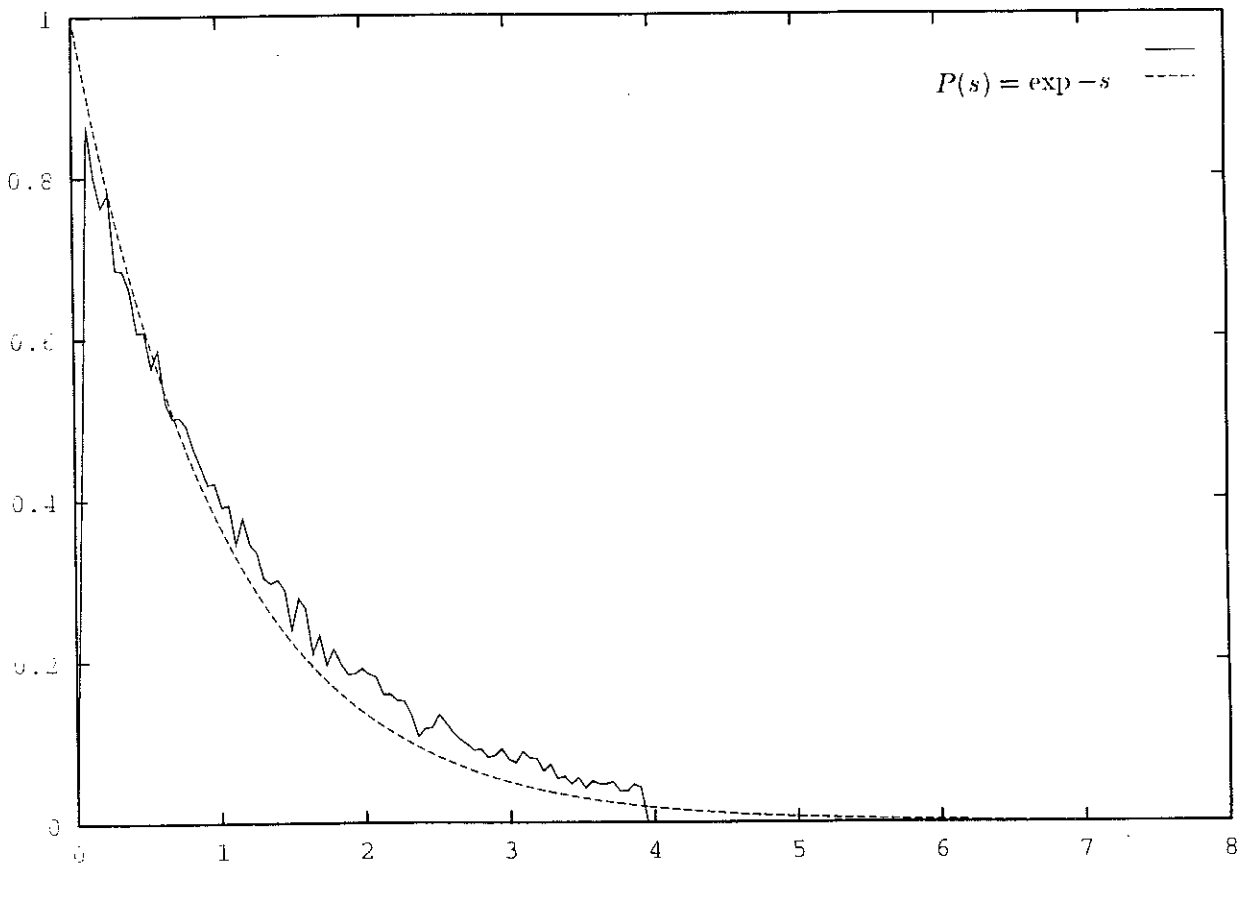

Figure 7.9: Level spacing statistics of the two dimensional Fermi liquid.
The parameters of the computation are: $L = 2\pi$, $k_F = 20$, $m = 1/2$, $A = 50$, $B = 50$, $p_x = 5$, $p_y = 4$. The condition (7.49) is fulfilled: $n(2n-1) = 45$ and $2\pi v_F/|A||B| = 0.63$. The cut-off in the spectrum is chosen equal to $E_{max} = E^0_{max} = 20, 20$. The level statistics are restricted to separations between 0.1 and 4. 44458 levels were generated. Among them, 28679 were eliminated at zero separations.

7.4.3 Conclusion

As expected, the level spacing distribution for this model is poissonian. It seems very likely that this behaviour doesn't depend on the precise form of the interaction function $f_{k,k'}$. However, it should be emphasized that (7.1) is not the exact hamiltonian for a normal Fermi liquid. In a renormalization group approach, which amounts to integrating out states at a distance between Λ and $\Lambda + d\Lambda$ away from the Fermi surface, the hamiltonian in equation (7.1) represents only the contribution of relevant marginal operators [6]. A crucial step would be to study the effect of irrelevant operators on the energy level statistics. For instance, these residual interactions generate a finite life-time for the quasiparticules, which are thus coupled to a continuum of states. It is not clear that the poissonian statistics survive such a coupling. We also did not take into account the contribution of the collective fluctuations of the Fermi surface. We argue that these collective modes do not destroy the poissonian level spacing statistics, since they can be diagonalized in terms of bosonic excitations in the vicinity of the Fermi surface, at least in the thermodynamic limit. However, it is not clear whether integrability survives for finite size systems. More precisely, a complementary study would involve exact diagonalisations of the Hamiltonian [13]

$$H = \sum_{\mathbf{k}} \epsilon^0_{\mathbf{k}} c^+_{\mathbf{k}} c_{\mathbf{k}} + \frac{1}{2V} \sum_{\mathbf{k},\mathbf{k}',\mathbf{q}} f_{\mathbf{k},\mathbf{k}',\mathbf{q}} c^+_{\mathbf{k}+\mathbf{q}/2} c_{\mathbf{k}-\mathbf{q}/2} c^+_{\mathbf{k}'-\mathbf{q}/2} c_{\mathbf{k}'+\mathbf{q}/2}, \tag{7.52}$$

where $\epsilon^0_{\mathbf{k}}$ is the single particule energy term, $f_{\mathbf{k},\mathbf{k}',\mathbf{q}}$ are the Landau parameters and $\mathbf{k}$ and $\mathbf{k}'$ are constrained in the vicinity of the Fermi surface. Moreover, $|\mathbf{q}|$ is inferior as an impulsion cutoff Λ. This study shall be done in a forthcoming article.

7.5 General conclusion

As far as one dimensional integrable models for interacting fermions are concerned, we have studied the Landau liquid and the Luttinger liquid Hamiltonians. In both cases, the level spacing statistics exhibit two regions. If the size of the system L is inferior as a certain length scale L^*, the level spacing statistics are not universal. In this regime, the Luttinger Hamiltonian gas term dominates the interaction term and thus leads to singular level spacing statistics since levels from different degeneracies $E = v_F k$ (where $k = 2\pi n/L$, with n an integer) are not mixed. There exists a second regime, which corresponds to $L \gg L^*$, where the interactions dominate and lead to universal level spacing statistics. In this case, *universality* means the existence of a well-defined thermodynamic limit, but the converged level spacing statistics may not be exactly a Poisson distribution, as it is the case for a one dimensional Landau Hamiltonian with the regularization we have used. One can also formulate the existence of two regimes as follows: for a given length L, there exists a cross-over in the statistics of energy levels as one increases the interaction strength. It appears that the scaling of the cross-over interaction strength as a function of the system size is different in the case of the Luttinger liquid and in the case of the Landau Hamiltonian. It goes as $L^{-1/2}$ for the Luttinger liquid, and as L^{-2} for the Landau liquid. An interesting generalisation of this result would be to know whether level spacing statistics are a good tool to distinguish between different fixed points in two dimensions.

What is the physical content of these two cross-overs? In the case of the Luttinger liquid, the poissonian regime corresponds to a regime of the model in which no electron-like quasiparticule exists [4], whereas quasiparticules obviously exit in the case of the Landau Hamiltonian, since

it describes a collection of interacting quasiparticules. Thus, although it is able to distinghish between a regime of strong interactions and a regime of weak interactions, the level spacing statistics do not contain information about whether the strongly interacting regime of a given integrable liquid is a Fermi liquid or not. This aspect is even more obvious in one dimension, where models which can be solved by the Bethe Ansatz lead to a Landau-like parametrisation of the low-lying levels, although they are not Fermi liquids.

We also studied non universal effects generated by the presence of a curvature in the dispersion relation. For a quadratic dispersion relation, a cross-over exists at high energy, but to a non-universal level spacing statistics. The existence of the non universal regime is attributed to the fact that the spectrum depends only on a few number of independent parameters, which are not numerous enough to disorder it completely, so that the level spacing statistics would be poissonian.

We also studied the case of the dimensionality two for the Landau Fermi liquid. A cross-over similar to the one in one dimension is observed, and the level spacing statistics are poissonian in the regime of strong interactions, or thermodynamic regime. The difference with the one dimensional case is essentialy the presence of aditional symetries, leading to levels separated by zero spacings.

I wish to thank B. Douçot for the discussions which initiated this work, J.C. Anglès d'Auriac and P. Butaud for helpful discussions, and I acknowledge the hospitality of NEC Research Institute at Princeton where part of this job was performed.

References

[1] G. Montambaux, D. Poilblanc, J. Bellissard and C. Sire, Phys. Rev. Lett 70, 497 (1993).

[2] T.C. Hsu and J.C. Anglès d'Auriac, Phys. Rev. B 47, 14291 (1993).

[3] D. Poilblanc, T. Ziman, J. Bellissard, F. Mila and G. Montambaux, preprint (1993).

[4] R. Mélin, B. Douçot and P. Butaud, J. Phys. I France 4, 737 (1994).

[5] F.D.M. Haldane, Phys. Rev. Lett. 66, 1529 (1991).

[6] M.V. Berry and Tabor, Proc. R. Soc. Lond. A 356, 375 (1977).

[7] Martin C. Gutzwiller "Chaos in Classical and Quantum Mechanics" Springer Verlag, 1990.

[8] P.W. Anderson, chapter VI of forthcoming book. Other R.G. approaches to Fermi liquids are: G. Benfatto and G. Gallavotti: Phys. Rev. B 42, 9967 (1990) and R. Shankar in "Strongly correlated electron systems III", World Scientific, Singapore (1992), edited by G. Baskaran, A.E. Ruckenstein, E. Tosatti and Y. Lu.

[9] F.D.M. Haldane, Phys. Rev. Lett. 60, 635 (1988).

[10] B.S. Shastry, Phys. Rev. Lett. 60, 639 (1988).

[11] M. Fabrizio and A. Parola, Phys. Rev. Lett. 70, 226 (1993).

[12] J.M.P. Carmelo, P. Horsch and A.A. Ovchinikov, Phys. Rev. B 45, 7899 (1992).

[13] Q.H. Castro Neto and E. Fradkin, to be published (1993).

Chapitre 8

Article 3

Level spacing statistics of bidimensional Fermi liquids: II. Landau fixed point and quantum chaos[1]

R. Mélin

CRTBT-CNRS, 38042 Grenoble BP 166X cédex France

We investigate the presence of quantum chaos in the spectrum of the bidimensional Fermi liquid by means of analytical and numerical methods. This model is integrable in a certain limit by bosonization of the Fermi surface. We study the effect on the level statisticsof the momentum cutoff Λ present in the bidimensional bosonization procedure. We first analyse the level spacing statistics in the Λ-restricted Hilbert space in one dimension. With g_2 and g_4 interactions, the level statistics are found to be Poissonian at low energies, and G.O.E. at higher energies, for a given cut-off Λ. In order to study this cross-over, a finite temperature is introduced as a way of focussing, for a large inverse temperature β, on the low energy many-body states, and driving the statistics from G.O.E. to Poissonian. As far as two dimensions are concerned, we diagonalize the Fermi liquid Hamiltonian with a small number of orbitals. The level spacing statistics are found to be Poissonian in the Λ-restricted Hilbert space, provided the diagonal elements are of the same order of magnitude as the off-diagonal matrix elements of the Hamiltonian.

[1] J. Phys. I France 5, 787 (1995)

8.1 Introduction

The ideas of quantum chaos have recently been applied to the field of strongly correlated electron theory [1] [2] [3]. These methods allow a non perturbative description of the statistical properties of a Hamiltonian of strongly correlated electrons, and may be a tool to extract some information from finite size systems. The aim of this article is to understand whether the methods of quantum chaos can shed some new light on the problems of strongly correlated bidimensional Fermi systems. The question whether the bidimensional Hubbard model is a Fermi liquid or not is controversial. From a theoretical point of view, Anderson [4] suggests that the ground state of the bidimensional Hubbard model is similar to the one of the one-dimensional Luttinger liquid, with $Z = 0$ in the thermodynamic limit, whereas Engelbrecht and Randeria [5] argue that the Fermi-liquid theory is not violated, so that this question is controversial [6]. Numerical computations lead also to controversial answers. For instance, Dagotto et al [7] [8] observe quasiparticules in the bidimensional t-J model, whereas Sorella [9] emphasizes the Luttinger liquid behaviour. From the point of view of quantum chaos, one has to answer the question: do level spacing statistics contain information about the Fermi liquid behaviour or non Fermi liquid behaviour of the t-J model? Before analysing the level spacing statistics of the t-J model [10], we analyze in this paper models with a well established physical content, that is the Fermi liquid. As we shall see, we can answer only partially the previous question: one can detect integrable modes at low energy, but quantum chaos by itself does not give information as to whether these modes are quasiparticule modes or Luttinger liquid modes. However, there is one case in which one can conclude from quantum chaos: in the absence of integrable degrees of freedom at low energy, one can conclude to the absence of a Fermi liquid at low energy. Notice here the difference between the approach of [1] and our point of view. In [1], all the energy levels of the t-J model are analyzed on an equal footing, whereas we shall focus essentially on the low energy degrees of freedom of the Fermi liquid.

We have established in the first article of this series [11], that the level spacing statistics of the bidimensional Landau Hamiltonian are poissonian. In this model, the quasiparticules are in a one to one correspondence with the non interacting gas of spinless electron excitations, and thus occupy orbitals labelled by the same quantum numbers k as in the case of the gas. The quasiparticules interact among themselves in a diagonal manner

$$H[\{\delta n_{\mathbf{k}}\}] = \sum_{\mathbf{k}} \epsilon_{\mathbf{k}} \delta n_{\mathbf{k}} + \frac{1}{L^D} \sum_{\langle \mathbf{k},\mathbf{k}' \rangle} f_{\mathbf{k}\mathbf{k}'} \delta n_{\mathbf{k}} \delta n_{\mathbf{k}'}. \tag{8.1}$$

A numerical computation proved that the level spacing statistics of the Hamiltonian (8.1) are poissonian in two dimensions, and close to Poisson in one dimension, with our truncation of the Hilbert space. The notion of level spacing statistics seems to be relevant for quantum fluids, and one has to distinguish between one and two dimensions. The link between the breakdown of the Fermi liquid picture in one dimension and the level spacing statistics has already been studied in reference [13]. As far as two dimensions are concerned, we showed in the paper I [11], that the Landau liquid was characterized by its generical integrability, namely by Poisson level spacing statistics in two dimensions. Again, the level spacing statistics are a good tool to see whether the Fermi system is at the Landau fixed point or not. For the liquid to be a Fermi liquid, one should be able to generate quasiparticules of the interacting system by a switching on procedure. In the framework of the Landau theory, the success of the switching-on procedure [14] [15] suggests the conservation of the number of conserved quantities

at low energy during the switching-on procedure, namely that the level spacing statistics of the gas and of the interacting liquid belong to the same universality class. Typically, adding a non diagonal perturbation to (8.1) and obtaining a Gaussian Orthogonal Ensemble (G.O.E.) level spacing statistics would mean a departure from the Landau fixed point. To be at the Landau fixed point, one must exclude strong correlations between levels. The corresponding generic level spacing statistics are poissonian. However, the case of the one dimensional Landau Hamiltonian shows that the statistics may not be exactly poissonian, but close to a Poisson law. Poisson or close to Poisson level spacing statistics are not a sufficient condition for the system to exhibit quasiparticules since one could imagine a situation in which the same mechanism as in one dimension for the breakdown of the Fermi liquid holds, so that the level spacing statistics would remain poissonian even in the non Fermi liquid case. However, the adiabatic procedure, as emphasized by Anderson [14], is performed within a finite characteristic time $1/\epsilon$, and the thermodynamic limit is taken for a finite ϵ which is then much larger than the typical level spacing. So the adiabatic continuation does not generate true eigenstates (for this to be the case, one should take the limit $\epsilon \to 0$ first, before the thermodynamic limit). This is why the notion of adiabatic continuation advocated to introduce Fermi liquid is weaker than a similar requirement for all the eigenstates taken separately. So, this is why we should ask whether a Fermi liquid follows Poisson or G.O.E. statistics.

The aim of the present paper is to study the level spacing statistics of the Hamiltonian of spinless electrons

$$H = H^0 + H^1 \tag{8.2}$$

$$H^0 = \sum_{\mathbf{k}} \epsilon(\mathbf{k}) c^+_{\mathbf{k}} c_{\mathbf{k}} \tag{8.3}$$

$$H^1 = \frac{1}{2V} \sum_{\mathbf{k},\mathbf{k}',\mathbf{q}} f_{\mathbf{k},\mathbf{k}',\mathbf{q}} c^+_{\mathbf{k}+\mathbf{q}} c^+_{\mathbf{k}'-\mathbf{q}} c_{\mathbf{k}'} c_{\mathbf{k}}, \tag{8.4}$$

where V is the volume of the system. The Hamiltonian (8.1) describes a Fermi liquid for times inferior as the decay time of the quasiparticules, and leads to good thermodynamical predictions [15]. However, the phenomenon of decay of the quasiparticules is not described by the Landau form (8.1). Since quasiparticules are true eigenmodes of (8.1), they have an infinite life-time. By contrast, the form (8.2) takes into account the decay of the quasiparticules and it is indeed possible to calculate the decay rate of the quasiparticules from the Hamiltonian (8.2) [16]. Even though the Hamiltonian (8.2) it is not diagonal, it can be brought to diagonal form using some asumptions and by bosonizing the Fermi surface [18]. We shall review the main assumptions and the bosonization of (8.2) in the thermodynamic limit and in the limit of a zero curvature of the Fermi surface. One of the ingredients of the solution via bosonization is the existence of a momentum Λ which determines the single particule states which participate in the formation of bosons in the vicinity of the Fermi surface. Λ is a necessary ingredient, because of the curvature of the Fermi surface, but is also a source of difficulty since the objects with a true bosonic character in the limit $\Lambda \to +\infty$ are no more exactly bosonic in the limit of a finite momentum cutoff Λ.

Of course, numerical computations cannot be performed in the thermodynamic limit since one can only diagonalize matrices of size 2000 by a Jacobi method. This technical limitation imposes to work with small systems and to impose a drastic cutoff Λ, so that the Hamiltonian (8.2) is no more integrable in the framework of the Hilbert space of the numerical diagonalisations. In the case of the presence of a cutoff, and for finite size systems, one may thus expect the

universal Poisson level spacing statistics to be replaced by the universal G.O.E. level spacing statistics of the form

$$P(s) = \frac{\pi}{2} s \exp\left(-\frac{\pi s^2}{4}\right). \tag{8.5}$$

It is necessary to determine the importance of the cutoff Λ on the level spacing statistics and whether the statistics evolve towards G.O.E. level spacing statistics as Λ is reduced. This has not only a numerical interest, but also a physical one. For instance, lattice models have a natural cutoff $\Lambda \sim 1/a$, where a is the lattice spacing. To answer this question, we come back to one dimensional spinless fermionic systems, but with a cutoff Λ and study the level spacing statistics for g_2 and g_4 interactions. As we shall see, the level spacing statistics are drastically affected by the presence of the cutoff since the bosonic superpositions of particule-hole pairs which guarantee the integrability, do not survive in the presence of the cutoff. If the cutoff Λ is fixed and the size L of the system increases, one expects for a crossover from a G.O.E. level spacing statistics in the high energy part of the spectrum to a Poisson level spacing statistics at low energy, which shows that finite size effects are drastic in the presence of the cutoff. In order to determine the crossover scale between the Poisson regime and the G.O.E. regime, we introduce temperature-dependent level spacing statistics. The statistics at finite temperatures are found to pass from a non integrable statistics at high temperatures to Poisson statistics at low temperature.

As far as two dimensionnal systems are concerned, we carry out numerical diagonalisations of a small system of electrons, with a small number of orbitals. In these conditions, the Hamiltonian (8.2) is non integrable. We found Poisson level spacing statistics even for a small system. We attribute this property to the fact that the interactions generate extra diagonal matrix elements in the Hamiltonian which are in competition with diagonal interaction matrix elements, but the interaction connects only a small number of states, leaving a lot of zero matrix elements in the Hamiltonian. Provided the off-diagonal matrix elements are of the same order than the diagonal ones, the statistics are dominated by the diagonal matrix elements. However, by keeping only off-diagonal interaction matrix elements, we were able to exhibit G.O.E. level spacing statistics.

This paper is organized as follows. We first treat the one dimensional case, in the Hilbert space restricted by the momentum cut-off Λ. The results established in one dimension are helpful in two dimensions since the presence of the momentum cut-off is also a source of non integrability. In a second step, we come to the bidimensional Fermi liquids, with the study of the level spacing statistics of the Hamiltonian (8.2).

8.2 Level spacing statistics of 1 D spinless fermion systems in the Λ-restricted Hilbert space

8.2.1 Bosonization and level spacing statistics in the unrestricted Hilbert space (Luttinger liquid)

Using the bosonization procedure of Haldane [22], we can solve the one dimensional spinless Luttinger liquid with a linear dispersion relation and g_2 and g_4 interactions. The Hamiltonian

reads, in term of fermions

$$H = v_F \sum_{k,\alpha} (\alpha k - k_F) : c^+_{k,\alpha} c_{k,\alpha} : + \frac{\pi}{L} \sum_{\alpha,\alpha'} \sum q (g_{4q} \delta_{\alpha\alpha'} + g_{2q} \delta_{\alpha,-\alpha'}) \rho_{q,\alpha} \rho_{-q,\alpha'}, \tag{8.6}$$

where the label α indexes the branch α=R(ight),L(eft)= $+1, -1$. The interaction g_4 describes the diffusion of two fermions on the same right or left branch whereas g_2 describes the diffusion of two fermions belonging to the right and left branch. The density operators are defined as

$$\rho_{q,\alpha} = \sum_k : c^+_{k+q,\alpha} c_{k,\alpha} :, \tag{8.7}$$

and obey bosonic commutation relations

$$[\rho_{q,\alpha}, \rho^+_{q',\alpha'}] = -\delta_{\alpha,\alpha'} \delta_{q,q'} \frac{L\alpha q}{2\pi}, \tag{8.8}$$

which allows the definition of boson operators

$$a^+_q = (\frac{2\pi}{L|q|})^{1/2} \sum_\alpha \theta(\alpha q) \rho_{q,\alpha}, \tag{8.9}$$

and make it possible to diagonalize the Hamiltonian (8.6) via a Bogoliubov transformation:

$$H = E_0 + \sum_q \omega_q b^+_q b_q + \frac{\pi}{2L}(v_N N^2 + v_J J^2), \tag{8.10}$$

where

$$\begin{aligned}
b^+_q &= \cosh \varphi_q a^+_q - \sinh \varphi_q a_{-q} && (8.11)\\
\tanh 2\varphi_q &= -\frac{g_{2q}}{v_F + g_{4q}} && (8.12)\\
\omega_q &= |(v_f + g_{4q})^2 - (g_{2q})^2|^{1/2} |q| && (8.13)\\
v_S &= \left((v_F + g_{40})^2 - (g_{20})^2\right)^{1/2} && (8.14)\\
v_N &= v_S \exp -2\varphi_0 && (8.15)\\
v_J &= v_S \exp 2\varphi_0. && (8.16)
\end{aligned}$$

The interaction functions $g_2(q)$ and $g_4(q)$ are supposed to tend to a constant in the limit $q \to 0$, and to zero in the limit $q \to +\infty$. Their decrease is controlled by the impulsion scale $2\pi/R$, where R is a given length scale. In the thermodynamic limit ($L \gg R$), one can define an effective low energy Hilbert space. To do so, we assume that $\omega_q \simeq \omega_0$ for all the wave vectors q. Of course, this approximation is only valid if the temperature is low enough. In this limit, the Hamiltonian (8.10) depends only on two velocities v_N and v_J:

$$H = E_0 + \sum_{q \neq 0} (v_N v_J)^{1/2} |q| b^+_q b_q + \frac{\pi}{2L}(v_N N^2 + v_J J^2). \tag{8.17}$$

In one dimension, the link between the breakdown of the Fermi liquid picture and the level spacing spacing statistics is well understood. The absence of a Fermi surface in one dimension, in

the presence of long range g_2 and g_4 interactions was known to Dzyaloshinskii and Larkin in the 70's [17]. The breakdown of the Fermi liquid picture is already present at the level of the static correlation functions, and in the Hilbert space of low energy. The usual infrared divergencies are governed by the $q \to 0$ limit of $g_2(q)$ and $g_4(q)$, and are related to the orthogonality catastrophy and the absence of a Fermi surface. The infrared spectrum is described by the Hamiltonian (8.17). If the total charge and current quantum numbers are given, the $q \neq 0$ excitations are bosons with a linear dispersion relation, but with a renormalized velocity. The departure from the gas behaviour is measured by the anomalous exponents which appear in the static Green's functions. The interaction energy scale associated to this *static* breakdown of the Fermi liquid is given by [13]

$$g_2^{stat} \sim v_F \left(\ln \frac{L}{2\pi R} \right)^{-1/2} . \tag{8.18}$$

However, as emphasized in [13], the static part of the Green's function does not contain all the physics of the breakdown of the Fermi liquid theory. From a calculation of the two points Green's function, and from a calculation of the switching-on pocedure, we found in [13] a *dynamical* breakdown of the Fermi liquid picture, controlled by the interaction scale

$$g_2^{dyn} \sim \frac{4\pi v_F}{(kL(kR)^\alpha)^{1/2}}, \tag{8.19}$$

where α is defined by

$$g_{2q} = g_{20}(1 - (qR)^\alpha). \tag{8.20}$$

The static process of breakdown of the Fermi liquid picture does not modifie the level spacing statistics, which remain singular, as in the case of the gas, since the dispersion relation of the bosons remain linear. By contrast, the dynamical breakdown of the Fermi liquid appears to be related to a cross-over in the energy level spacing statistics, namely from singular level spacing statistics to generical Poisson level spacing statistics. As far as symetries are concerned, the gas case and the Luttinger liquid possess the conformal symetry. The static breakdown of the Fermi liquid preserves the conformal invariance. The theory is the antiperiodic-antiperiodic sector of the compactified boson, with an interaction-dependent radius of compactification. The dynamical breakdown of the Luttinger liquid corresponds to a massless loss of conformal invariance [12].

8.2.2 Fourier transform of the gas spectrum and temperature-dependent level spacing statistics

We first wish to characterize the spectrum of the gas in the absence of interactions, a momentum cutoff Λ and a finite size L. The idea is to find a criterium to detect when a boson of given wave vector q is present or not in the system. Since g_2 and g_4 interactions are diagonal on the basis of bosonic excitations, this tool is a good way to characterize the degree of integrability of the model with a momentum cut-off. We consider a one branch model, and the number of quantum states is simply the integer part of $2\Lambda L/2\pi$. The spectrum is made up of levels with an equidistant separation $2\pi v_F/L$. In order to characterize the spectrum, we use its Fourier transform

$$f_L(\tau) = \int_{-\infty}^{+\infty} e^{i\omega\tau} \sum_{\{E_i\}} \delta(\omega - E_i) = \sum_{\{E_i\}} e^{iE_i\tau}. \tag{8.21}$$

In the thermodynamic limit,

$$f_\infty(\tau) = \int_{-\infty}^{+\infty} e^{i\omega\tau} \sum_{\{n_q\}} \delta(\omega - v_f \sum_{n_q=0}^{+\infty} q n_q), \tag{8.22}$$

leading to

$$|f_\infty(\tau)| = \prod_{q>0} \frac{1}{2|\sin v_f \tau q/2|}. \tag{8.23}$$

This function presents poles which are characteristic of the bosonic modes for $\tau_{n,q} = 2\pi n/v_f q$, with n an integer. If we rescale τ by a factor 2π and choose $v_f = 1$, we obtain a pole for $\tau_{n,q} = n/q$, that is for every rational number. We plotted $|f_\infty(\tau)|$ for 5 bosonic modes on figure 8.1. One can easily recognize the different bosons in the sequence of poles. In the presence of interactions, the poles are deplaced. We also studied the Fourier transform of the spectrum in the case of a finite size system. The result is depicted on figure 8.2. We can see that the poles are not so well defined. However, we can recognize the formation of peaks which replace the poles, and attribute well defined boson wave vectors to some peaks. The corresponding truncated density operators are defined by

$$\rho_\Lambda(q) = \sum_k \theta_\Lambda(k)\theta_\Lambda(k+q) c^+_{k+q} c_k, \tag{8.24}$$

where $\theta_\Lambda(k) = \theta(\Lambda - |k - k_f|)$. We can ask under which condition a peak corresponding to a truncated boson $\rho_\Lambda(q)$ appears on the modulus of the Fourier transform of the spectrum $|f_L(\tau)|$. To answer this question, we assume that the number n_q of bosonic excitations of wave vector q appearing in the presence of a cutoff is such as $qn_q \sim 2\Lambda$, so that $f_L(\tau_{1,q}) \sim 2\Lambda/q$ for the peak at $\tau = \tau_{1,q}$. A boson of wave vector q is well defined provided $f_L(\tau_{1,q}) \gg 1$, that is if $\Lambda \gg q/2$. For a given cut-off, the statistics are expected to be Poisson at low energies, and G.O.E. at higher energies. This is due to the fact that truncated bosons are created essentially at low energy. In order to test this idea, we introduce temperature-dependent level spacing statistics, which are defined as follows. If $\{E_i\}$ is the full spectrum and $\{\epsilon_i\}$ are the energy levels after the smoothing procedure [23], the density of level spacing $P(s)$ is

$$P_\beta(s) = \left(\sum_i \exp\left(-\beta \frac{E_{i+1} + E_i}{2}\right)\right)^{-1} \sum_i \exp\left(-\beta \frac{E_{i+1} + E_i}{2}\right) \delta(s - (\epsilon_{i+1} - \epsilon_i)). \tag{8.25}$$

Moreover, for the statistics to be comparable, one needs to scale $P_\beta(s)$ and s such as $\langle P_\beta(s)\rangle = 1$, and $\langle sP_\beta(s)\rangle = 1$. The reason why we have to rescale these quantities is that they were equal to unity after the smoothing procedure, which was carried out in the zero temperature limit. This property is no more valid with the statistical weights of equation (8.25). For an infinite temperature ($\beta = 0$), we recover the usual level spacing statistics. As the inverse temperature β increases, the low energy levels carry more and more statistical weight. As we saw from the description in terms of the truncated bosons (8.24), the spectrum is expected to be integrable at low energies, so that the level spacing statistics should evolve from G.O.E. statistics, or at least intermediate statistics (that is, with $0 < P(0) < 1$), to Poisson level spacing statistics as β increases.

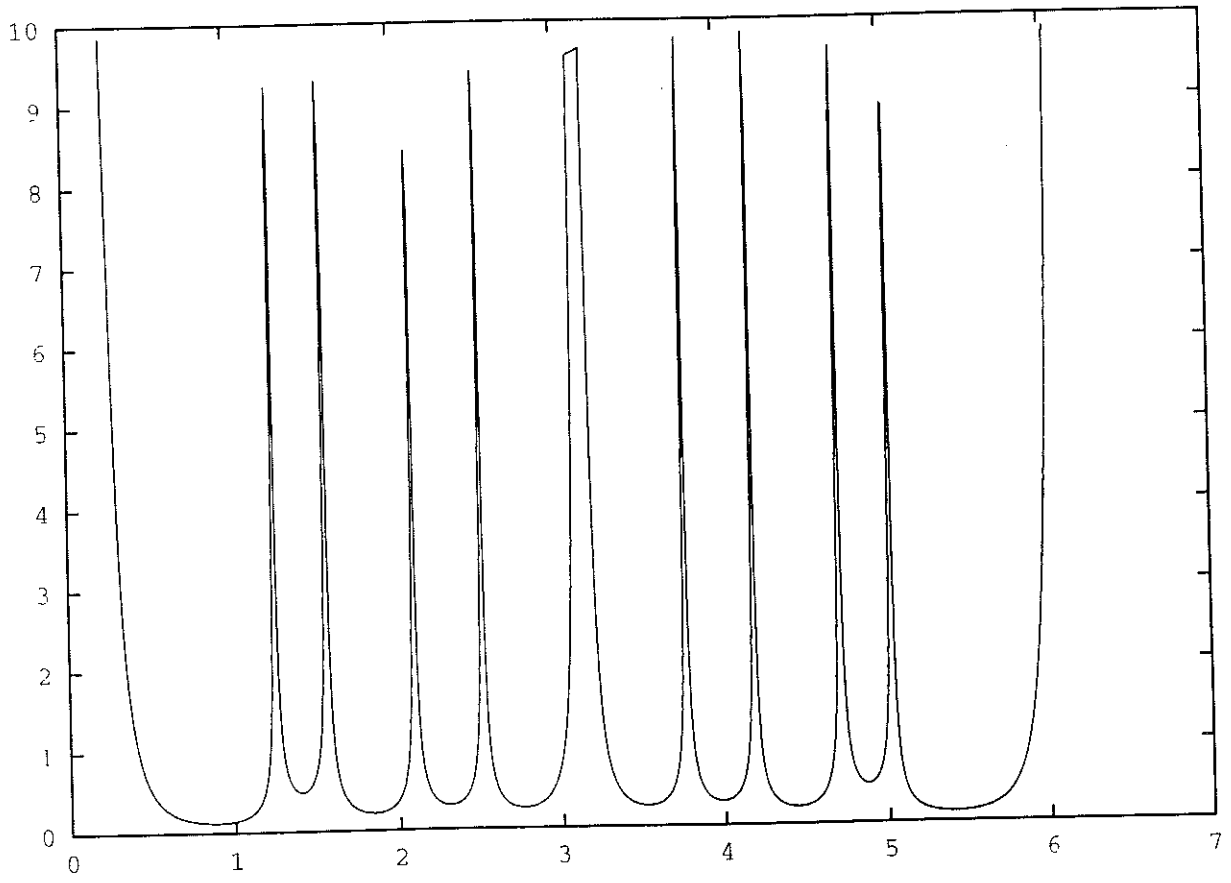

Figure 8.1: Modulus of the Fourier transform of the spectrum in the thermodynamic limit $|f_\infty(\tau)|$ for 5 bosons. Each pole corresponds to one or several definite boson excitations. We have chosen $v_f = 1$ and $L = 2\pi$. A given boson $q > 0$ generates a sequence of poles at $\tau_{n,q} = 2\pi n/q$. The poles are denoted by their corresponding rational number n/q.

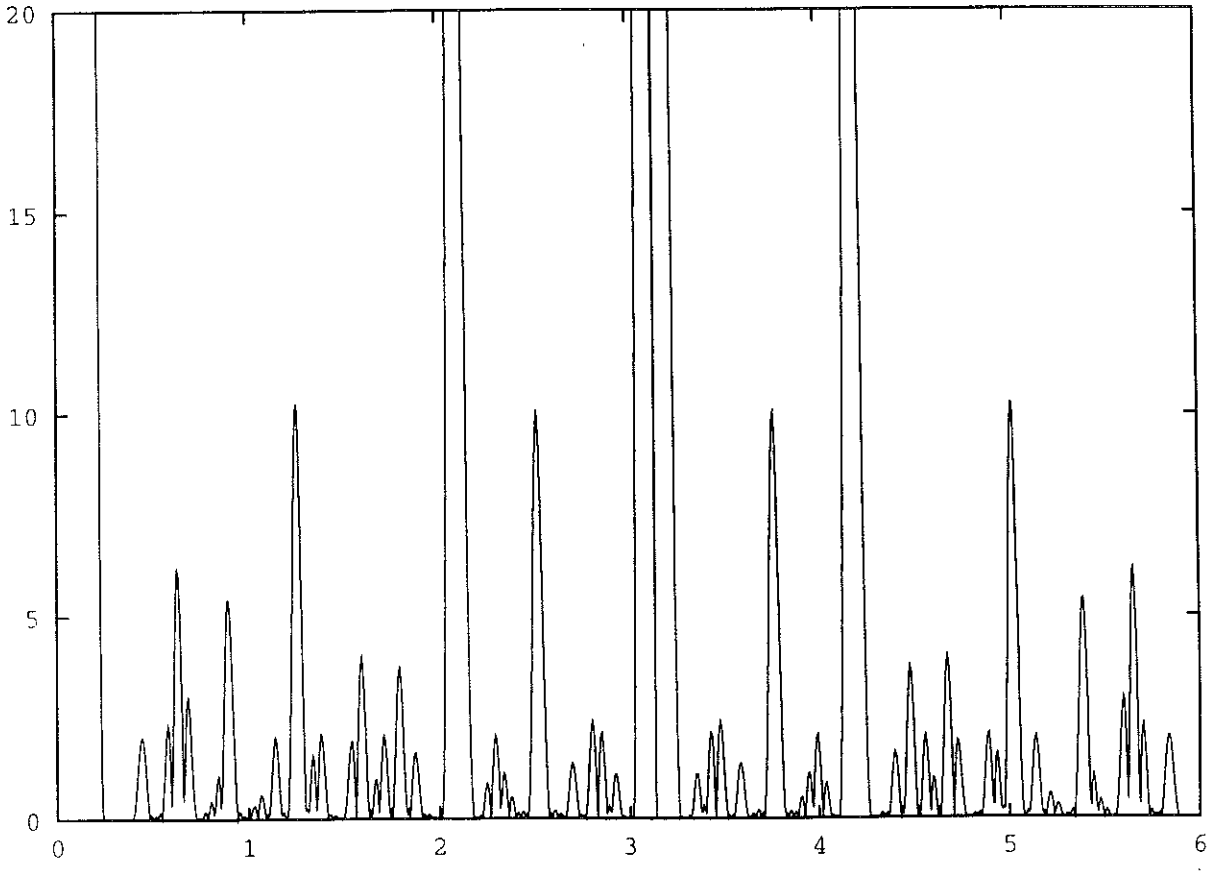

Figure 8.2: Finite size effects of the modulus of the Fourier transform of the spectrum $|f_L(\tau)|$. We have chosen $v_f = 1$ and $L = 2\pi$, $\Lambda = 11$. As shown on the figure, we can attribute boson quantum numbers to some peaks. We recognize the fractions 1/5, 1/4, 1/3,2/5,1/2,3/5,2/3,3/4, 4/5.

8.2.3 Level spacing statistics with g_2 interactions in the Λ-restricted Hilbert space

The numerical method to compute the level spacing statistics of two branch models with a momentum cutoff Λ and g_2 interactions consists in tabulating the states of the Hilbert space by generating all the different fillings of the two branches, the number of particules on each branch being kept constant. The second step consists in computing all the matrix elements of the hamiltonian and diagonalising the Hamiltonian by the use of the Jacobi method. The interactions are of the form

$$g_{2q} = g_{20} \exp - \left(\frac{qL}{2\pi R}\right). \tag{8.26}$$

The scale of the interactions R is chosen equal to Λ, so that all the matrix elements of the interaction are important. The evolution of the spectrum as a function of g_{20} is plotted on figure 8.3. This figure is to be compared with the figure 2 of reference [13], where we have plotted the evolution of the energy levels as a function of g_{20} but in the absence of cutoff. The obvious difference between the two plots is the presence of level repulsion with a cutoff Λ, and the existence of level crossings in the absence of cutoff. The level spacing statistics corresponding to a spectrum analog to the one of figure 8.3 are plotted on figure 8.4. They are in good agreement with G.O.E. level spacing statistics. In our computation, $\Lambda L/2\pi = 3$, so that the criterium $\Lambda \gg 2\pi/L$ is not verified. We could not go to higher values of $\Lambda L/2\pi$ because increasing the ratio $\Lambda L/2\pi$ increases the size of the Hilbert space and numerical diagonalizations are no more possible. We conclude that the statistics depend drastically on the length of the system, if the momentum cutoff is fixed. If we apply the ideas of temperature-dependent statistics of level spacings to the system, we find that the statistics of level spacings are driven from a G.O.E. law at $\beta = 0$ to a Poisson law as β increases, as depicted on figure 8.5.

This evolution reveals the fact that "nearly integrable" degrees of freedom exist at low energy. These bosonic degrees of freedom are exactly integrable in the absence of cut-off. In term of classical trajectories (provided one is able to find a classical phase space for the Fermi liquid !), this situation corresponds to the existence of conserved torii at low energy, which transform into chaotic trajectories as the energy increases. The cross-over temperature scale shall be derived later.

8.2.4 Level spacing statistics with g_4 interactions in the Λ-restricted Hilbert space

We now consider the case of g_4 interactions. The interaction Hamiltonian is

$$H^1 = \sum_{q\neq 0} \sum_{k,k'\neq k+q} g_{4q} c^+_{k+q} c^+_{k'-q} c_{k'} c_k. \tag{8.27}$$

The interest of the g_4 term is that we can use only a one branch model, and we can reach higher values of the ratio $\Lambda L/2\pi$ without increasing the size of the Hilbert space. We could reach $\Lambda L/2\pi = 12$ in a sector of total momentum $P = 24.2\pi/L$. P is the impulsion with respect to the fundamental. As long as $P \leq \Lambda L/\pi$, one has generated the complete Hilbert space in the absence of interactions. This fact motivates the choice $P = \Lambda L/\pi$. The condition $\Lambda L/\pi = 24 \gg 1$ is respected. However, we did not find Poisson statistics, but statistics which are intermediate between a Poisson law and G.O.E. statistics. Namely, the value of the density of normalized zero crossings is not 1 but 0.5. The statistics are plotted on figure 8.6. This

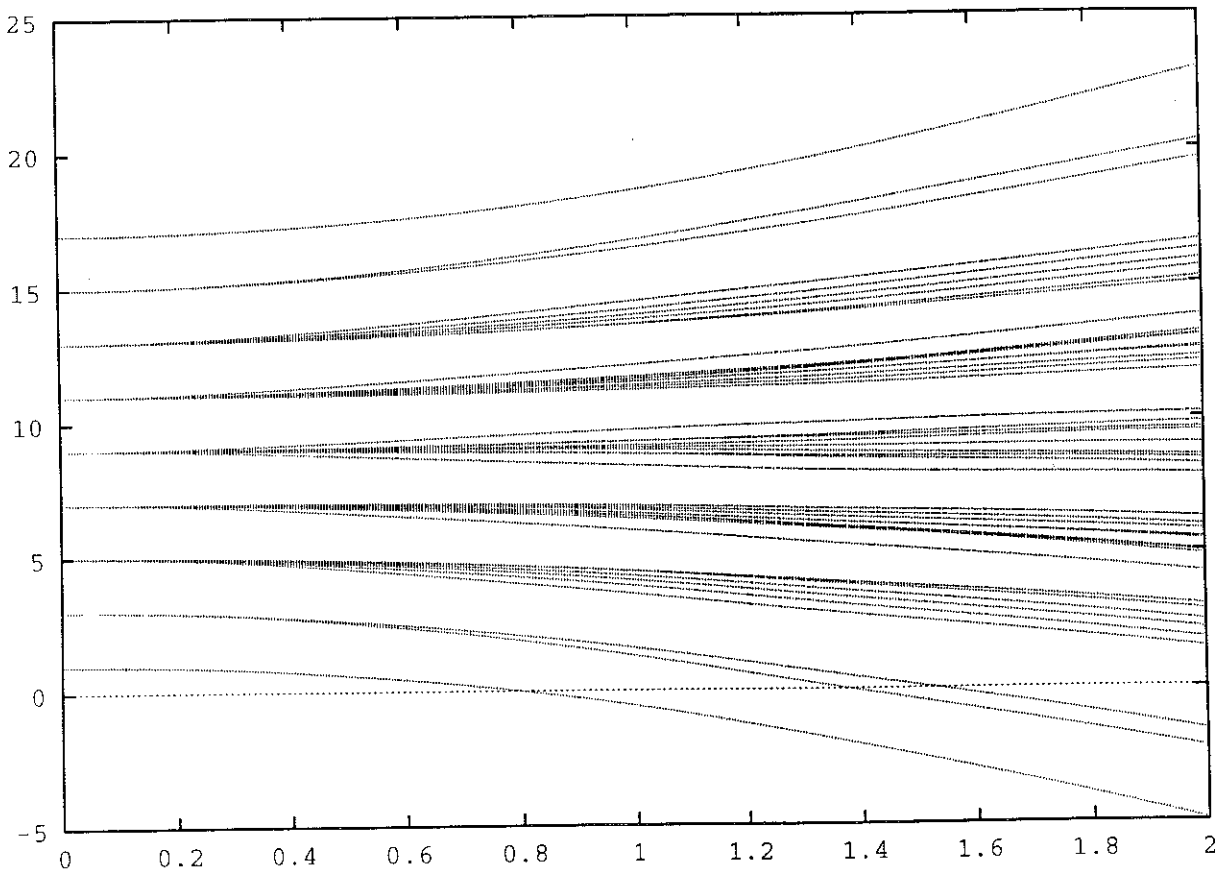

Figure 8.3: Evolution of the energy levels in the presence of g_2 interactions with a momentum cutoff. The parameters of the model are $v_f = 1$ and $L = 2\pi$. The cutoff is chosen equal to 3, so that we have 3 fermions on each branch, for 6 available quantum states. The interactions are of the form $g_{2q} = g_{20} \exp(-q/R)$. with $R = 6$. The momentum sector is 1, leading to 45 states in the Hilbert space. Because of the particule-hole symmetry, the spectrum is symmetric, but with no level crossings.

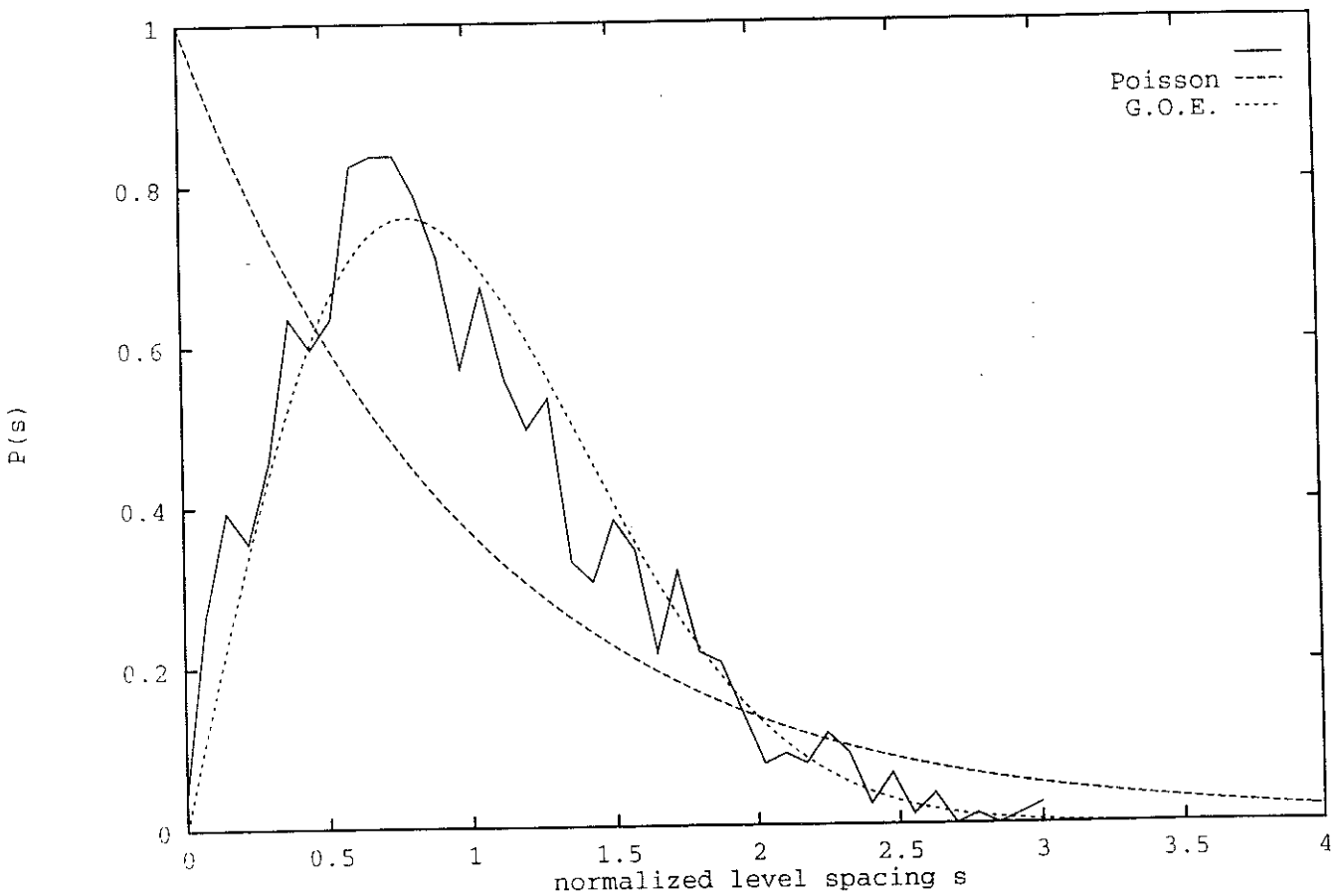

Figure 8.4: Level spacing statistics of 1D spinless fermions with g_2 interactions and a cutoff. The parameters are $v_f = 1$, $L = 2\pi$. In order to eliminate the particule-hole symmetry present on figure 8.3, we chose a non symmetric cutoff for particules and holes: the number of fermions on the right branch is 4, and the number of quantum states is 9. On the left branch, the number of fermions is 5 for 9 quantum states. The Hilbert space contains 1052 states in the sector of momentum 1. The level spacing statistics are found to be well fitted by G.O.E. statistics.

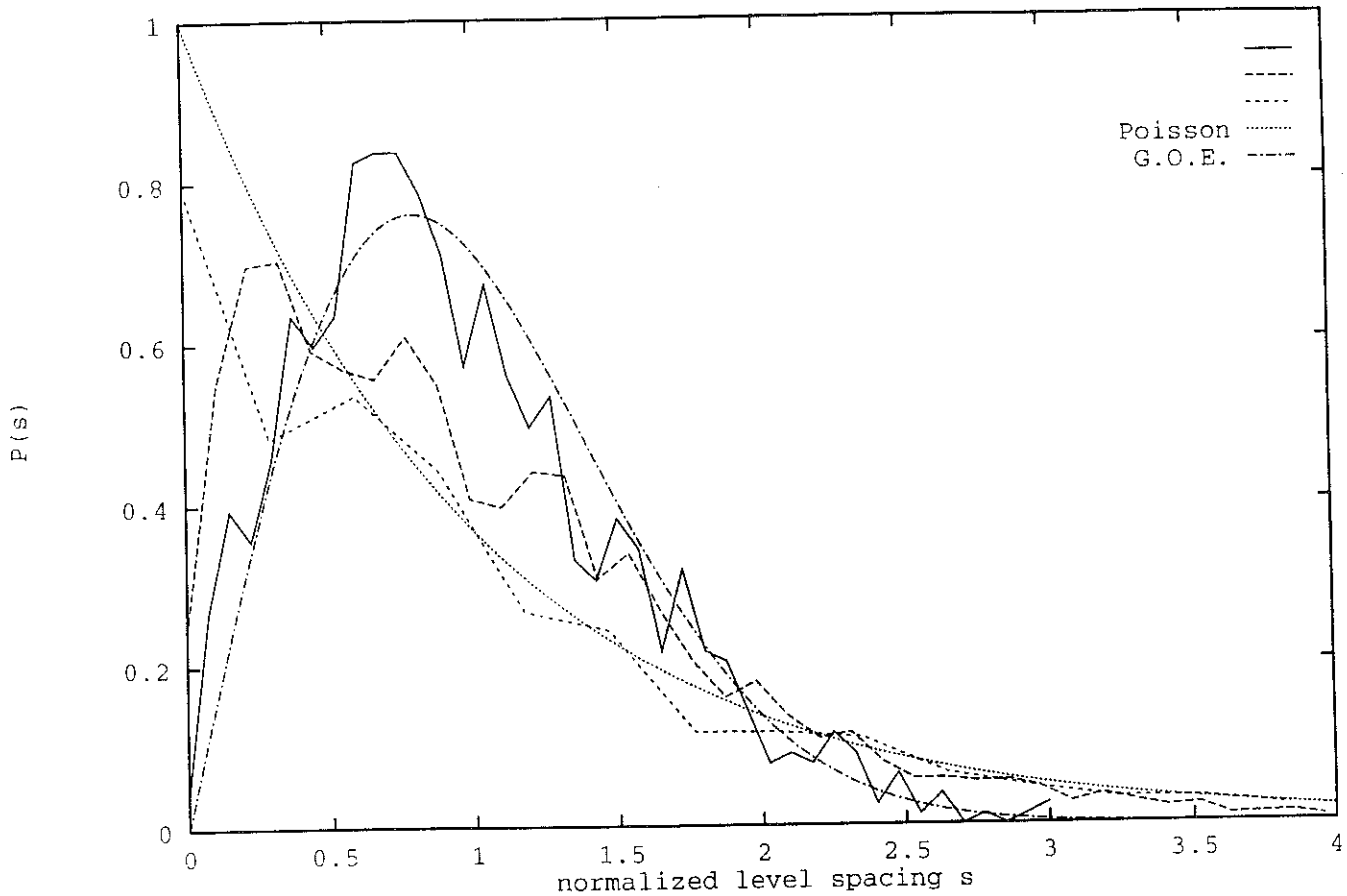

Figure 8.5: Level spacing statistics of 1D spinless fermions with g_2 interactions and a cutoff at finite temperature.
The parameters are $v_f = 1$, $L = 2\pi$. In order to eliminate the symmetry present on figure 8.3, we chose a non symmetric cutoff for particules and holes: the number of fermions on the right branch is 4, and the number of quantum states is 9. On the left branch, the number of fermions is 5 for 9 quantum states. The Hilbert space contains 1052 states in the sector of momentum 1. The level spacing statistics are plotted for inverse temperature equal to $\beta = 0, 0.1, 0.5$ A cross-over is found from G.O.E. statistics as $\beta = 0$ to Poisson statistics as β increases.

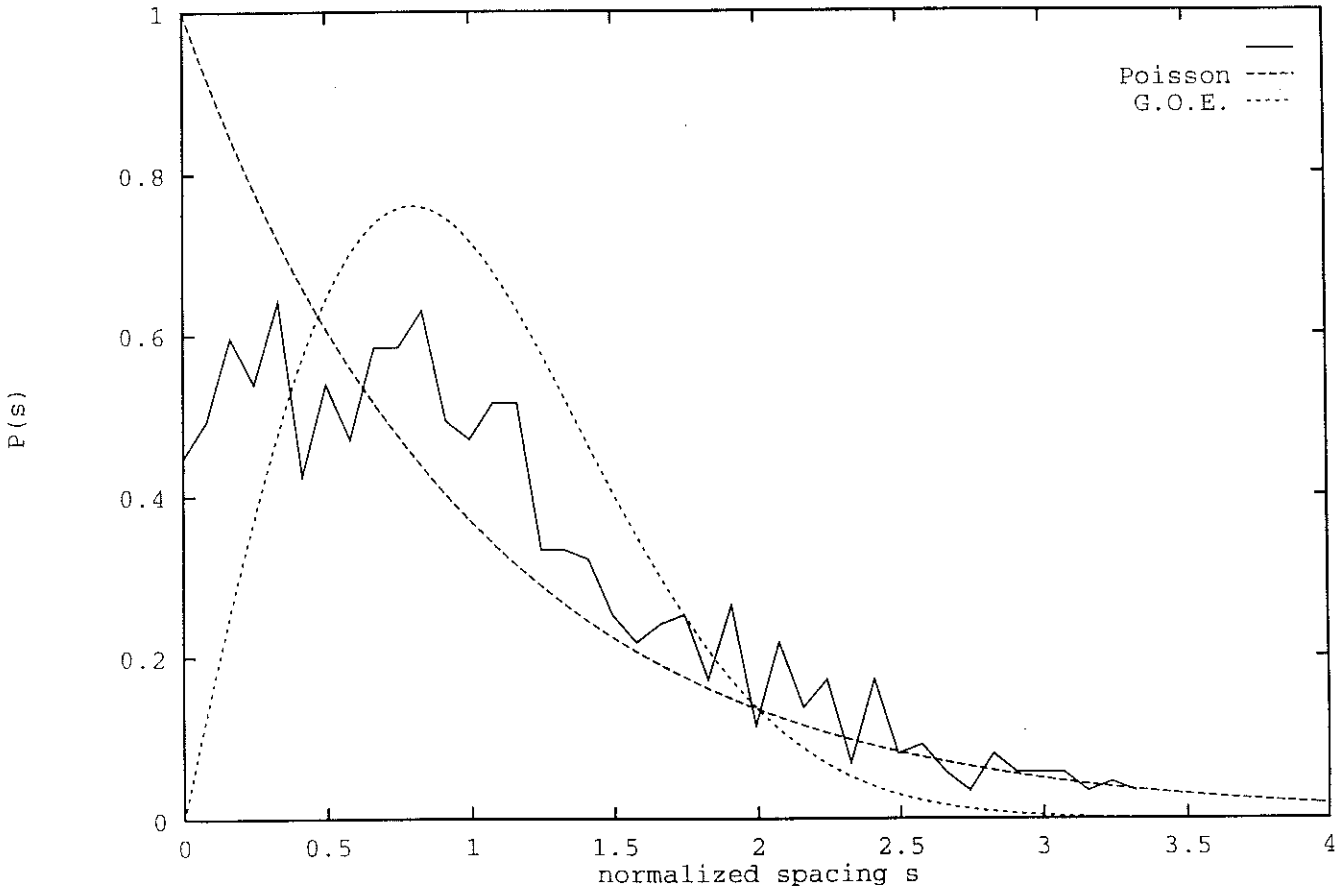

Figure 8.6: Level spacing statistics of 1 D spinless fermions with g_4 interactions and with a momentum cutoff. The parameters are chosen such as $v_F = 1$ and $L = 2\pi$. The value of the momentum cutoff Λ is 12 and the total momentum is 24. The Hilbert space contains 1185 states. The statistics is found to be intermediate between a G.O.E. statistics and a Poisson statistics.

computation gives an idea of the extension of the crossover as a function of $\Lambda L/2\pi$, since we obtain intermediate statistics for $\Lambda L/2\pi = 24$. We computed also the temperature-dependent level spacing statistics. We found a cross-over to Poisson statistics as the inverse temperature increases, as plotted on figure 8.7.

This cross-over is much more rapid than in the case of the g_2 interaction. However, the values of the cutoff in the g_2 case and the g_4 case are not comparable.

8.2.5 Cross-over scales

In order to get an idea of the temperature cross-over between the G.O.E. and Poisson regime, we look for the energy scale $k_B T^*$ below which the energy levels are decorrelated. To do so, we make the approximation that the only effect of interactions is to compress the spectrum by an amount $((1+g_4/v_f)^2 - (g_2/v_f)^2))^{1/2}$, where g_2 and g_4 are typical energy interactions. This compression of the spectrum means that the effective mass increases if g_2 is large compared to g_4. This approximation corresponds to taking local interactions in the real space. Then, we see that the integrable modes under request are such as

$$v_f|q| \leq \left(\left(1 + \frac{g_4}{v_f}\right)^2 - \left(\frac{g_2}{v_f}\right)^2 \right)^{-1/2} k_B T. \tag{8.28}$$

These modes are integrable provided they lead to well-defined bosons. We say that a boson is well-defined provided a sufficient number of particule-hole excitations enter into the summation (8.24), that is if $2\Lambda - |q| \geq 2\pi\alpha/L$, where α is a dimensionalless coefficient, which counts the number of non-zero terms in (8.24), and is thus a measure of integrability. We get that

$$k_B T \simeq (2\Lambda - 2\pi\alpha/L) \left((1+g_4/v_f)^2 - (g_2/v_f)^2\right)^{1/2} \tag{8.29}$$

The energy scale $k_B T^*$ thus increases as the cut-off Λ increases, and decreases if the interaction strength g_2 increases.

8.3 Level spacing statistics of a 2 D spinless fermion system in the Λ-restricted Hilbert space

8.3.1 Bosonization of the bidimensional Fermi surface

The bosonization of the Fermi liquid [19], [20], [21] involves a covering of the Fermi surface by spheres of radius Λ. Each small sphere is labelled by an integer α and one assumes that the Fermi surface is flat at the scale Λ. Assuming that $\Lambda \gg 2\pi/L$, the commutation relations of the operators

$$\rho_{q,\alpha} = \sum_{\mathbf{q}} \theta_\alpha(\mathrm{k}+\mathrm{q}/2)\theta_\alpha(\mathrm{k}-\mathrm{q}/2) n_{\mathbf{q}}(\mathrm{k}), \tag{8.30}$$

with

$$n_{\mathbf{q}}(\mathrm{k}) = c^+_{\mathbf{k}-\mathbf{q}/2} c_{\mathbf{k}+\mathbf{q}/2}, \tag{8.31}$$

must include a Schwinger term, leading to the commutation relation

$$[\rho_{\mathbf{q},\alpha}, \rho^+_{\mathbf{q}',\alpha'}] = \delta_{\alpha,\alpha'}\delta_{\mathbf{q},\mathbf{q}'} \sum_k C_\alpha(\mathrm{k},\mathrm{q})(n^0_{\mathbf{k}+\frac{\mathbf{q}}{2}} - n^0_{\mathbf{k}-\frac{\mathbf{q}}{2}}), \tag{8.32}$$

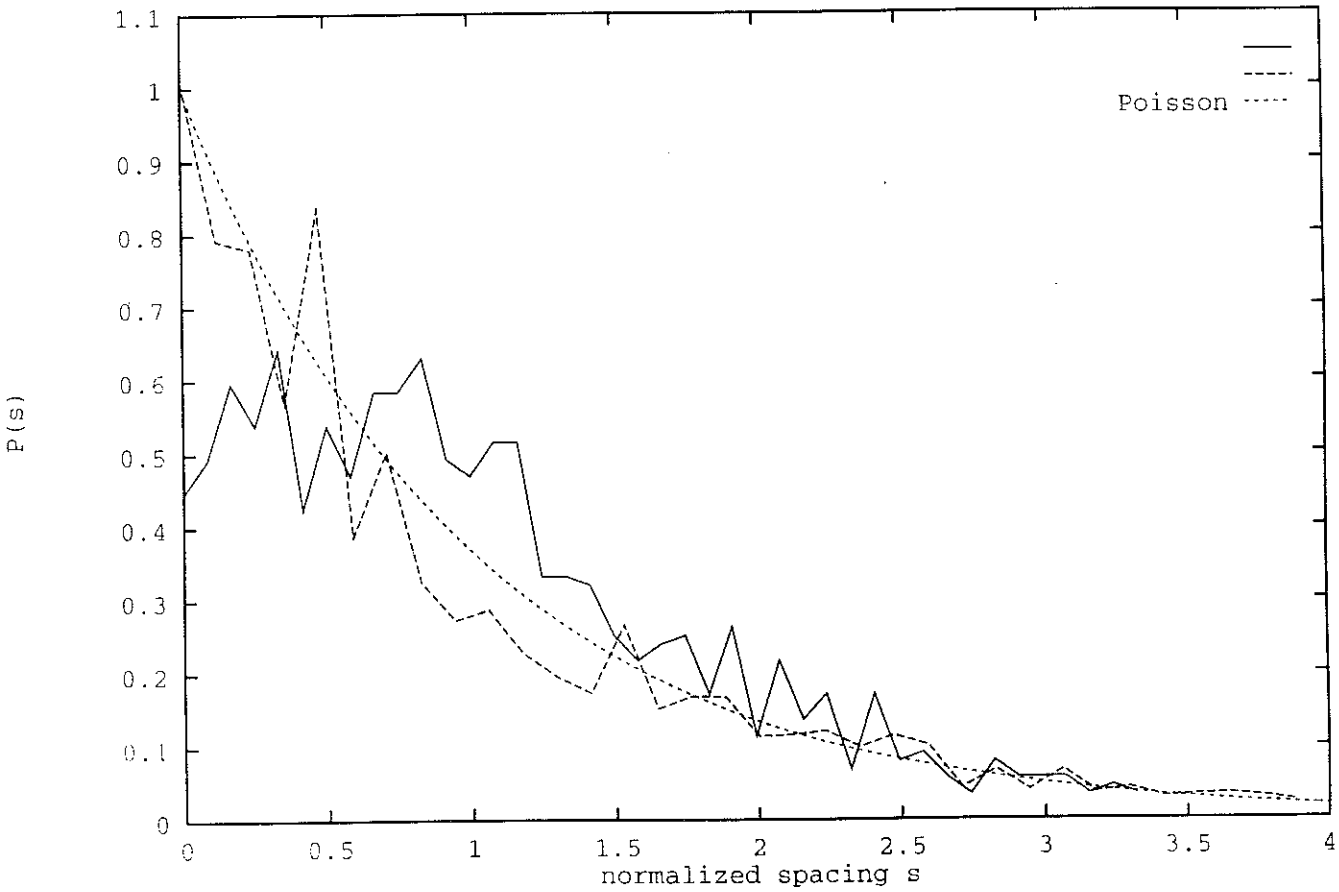

Figure 8.7: Level spacing statistics of 1 D spinless fermions with g_4 interactions and with a momentum cutoff. The parameters are chosen such as $v_F = 1$ and $L = 2\pi$. The value of the momentum cutoff Λ is 12 and the total momentum is 24. The Hilbert space contains 1185 states. The statistics are plotted for the inverse temperature equal to $\beta = 0$ and $\beta = 0.3$. The statistics for $\beta = 0.3$ is close to the Poisson statistics.

where the constraint C_α is

$$C_\alpha(\mathrm{k},\mathrm{q}) = \theta_\alpha(\mathrm{k}+\frac{\mathrm{q}}{2})\theta_\alpha(\mathrm{k}-\frac{\mathrm{q}}{2})\theta_\alpha(\mathrm{k}'+\frac{\mathrm{q}'}{2})\theta_\alpha(\mathrm{k}'-\frac{\mathrm{q}'}{2}). \tag{8.33}$$

To simplify the expression (8.32), one makes the assumption of a flat Fermi surface in each sphere of radius Λ. In order to specify this condition, one imposes that no bosonic excitations with an angle $\theta > \pi/2$ exist, where θ denotes the angle between $\mathbf{k_f}$ and $\mathbf{q}$. The maximal angle theta is such as

$$\tan\left(\theta - \frac{\pi}{2}\right) \leq \frac{2\pi}{L\Lambda}, \tag{8.34}$$

which leads to

$$\Lambda \leq (\frac{4\pi k_f}{L})^{1/2}. \tag{8.35}$$

The equation (8.35) means that the curvature is negligeable in a sphere of radius Λ, and is compatible with the condition

$$\Lambda \gg 2\pi/L \tag{8.36}$$

provided the linear length is large enough: $L \gg \pi/k_f$. If $\Lambda \ll 2\pi/L$ and $|\mathbf{q}| \ll \Lambda$, the leading term in (8.32) is of the form $[\rho_{\mathbf{q},\alpha}, \rho^+_{\mathbf{q}',\alpha'}] = \delta_{\alpha,\alpha'}\delta_{\mathbf{q},\mathbf{q}'}Va(\mathbf{q}.\mathbf{n}_\alpha)$. We evaluate the corrections under the conditions $\Lambda \gg 2\pi/L$ and $|\mathbf{q}| \ll \Lambda$. Under these assumptions, the leading term represents the number of states in the parallelogram of figure 8.8.

To obtain the corrections, one has to substract the number of states contained in the small shaded triangle. The number of states to be removed is approximately equal to

$$\frac{1}{2}\left(\frac{L}{2\pi}\right)^2 |\mathbf{q}|^2 \cos\theta \sin\theta = Va(\mathbf{q}.\mathbf{n}_\alpha).\frac{|\mathbf{q}\wedge\mathbf{n}_\alpha|}{2k_f}. \tag{8.37}$$

The commutation relations are thus of the form

$$[\rho_{\mathbf{q},\alpha}, \rho^+_{\mathbf{q}',\alpha'}] = \delta_{\alpha,\alpha'}\delta_{\mathbf{q},\mathbf{q}'}Va(\mathbf{q}.\mathbf{n}_\alpha)\{1 + O(\frac{|\mathbf{q}\wedge\mathbf{n}_\alpha|}{k_f})\}. \tag{8.38}$$

Following reference [21], we define

$$a_{\mathbf{q}}(\mathbf{k_f}) = \sum_{\mathbf{k}} \phi_\Lambda(|\mathbf{k}-\mathbf{k_f}|)[n_{\mathbf{q}}(\mathbf{k})\theta(\mathbf{q}.\mathbf{v_k}) + n_{-\mathbf{q}}(\mathbf{k})\theta(-\mathbf{q}.\mathbf{v_k})], \tag{8.39}$$

and

$$b_{\mathbf{q}}(\mathbf{k_f}) = (N_\Lambda V|\mathbf{q}.\mathbf{v_k}|)^{-1/2}a_{\mathbf{q}}(\mathbf{k_f}), \tag{8.40}$$

where ϕ_Λ is a smearing function such as $\phi_\Lambda \to \delta_{\mathbf{k},\mathbf{k_f}}$ if $\Lambda \to 0$, and N_Λ is the local density of states:

$$N_\Lambda = \frac{1}{V}\sum_{\mathbf{k}} |\phi_\Lambda(|\mathbf{k}-\mathbf{k_f}|)^2\delta(\mu - \epsilon_{\mathbf{k}}). \tag{8.41}$$

Provided the curvature of the Fermi surface is negligeable, that is provided condition (8.35) is satisfied, one can bosonize the Hamiltonian (8.2) to obtain

$$H = \sum_{\mathbf{k_f}} \sum_{\mathbf{q},\mathbf{q}.\mathbf{v_k}>0} |\mathbf{q}.\mathbf{v_k}| b^+_{\mathbf{q}}(\mathbf{k_f})b_{\mathbf{q}}(\mathbf{k_f}) + \frac{1}{2V}\sum_{\mathbf{k},\mathbf{k}',\mathbf{q}} f_{\mathbf{k},\mathbf{k}',\mathbf{q}}n_{-\mathbf{q}}(\mathbf{k})n_{\mathbf{q}}(\mathbf{k}'). \tag{8.42}$$

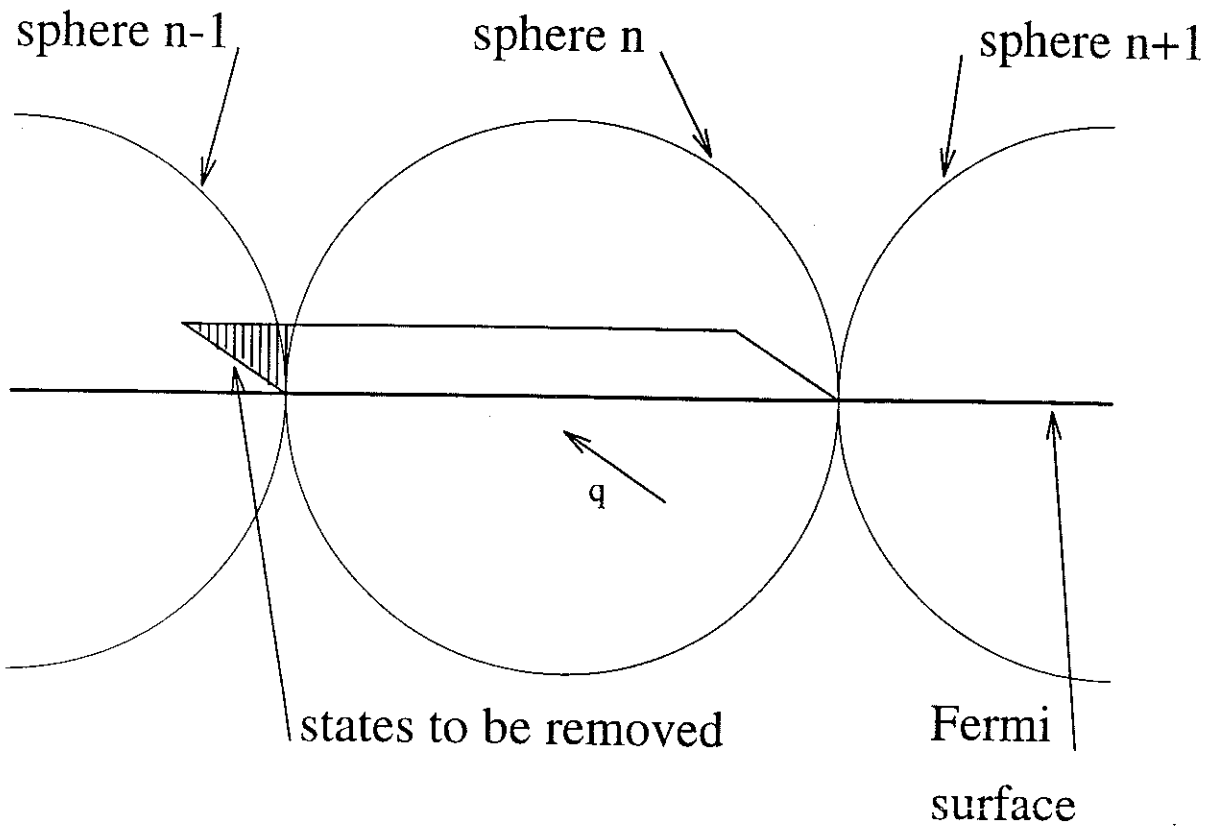

Figure 8.8: Representation of a sphere at the Fermi surface.
The commutation relation (8.32) is proportional to the number of states contained in the intersection of the parallelogram and the sphere n. The leading order term takes into account all the states in the parallelogram.

Since the interactions are quadratic in the boson operators, one can diagonalize them via a generalized Bogoliubov transformation. However, in numerical computations, one can only treat a Hilbert space of size 2000. This means that the cutoff Λ must be reduced drastically, as well as the Fermi wave vector k_f. In particular, the conditions (8.35) and (8.36) are no longer valid and one cannot diagonalize the Hamiltonian as described above. Two scenarios are candidates for the appearance of chaos in the spectrum of the bidimensional Fermi liquid. The first scenario is the effect of curvature. In the limit $L \to +\infty$, and for a cut-off independent of L, the condition (8.35) is no more valid, and one cannot solve the model by bosonization. We shall not study this effect in the present paper. The second scenario comes from the fact that, even with a flat Fermi surface, the condition (8.36) may be violated, so that the system is no more integrable by bosonization. We shall study the last type of effect in the rest of the paper.

8.3.2 Level spacing statistics of a 2 D spinless fermion system in the Λ-restricted Hilbert space

We now turn to the bidimensional case in the presence of a momentum cutoff. The Fermi sea in its fundamental state is pictured on the insert of figure 8.9.

We treated a Fermi sea of 5 electrons for a total of 29 available quantum states. The Hamiltonian is given by the expression (8.2). The interaction term can be split into two terms as follows

$$H^1 = H_0^1 + H_1^1 \tag{8.43}$$

$$H_0^1 = -\frac{1}{V}\sum_{\mathbf{k},\mathbf{q}} f_{\mathbf{k},\mathbf{k}+\mathbf{q},\mathbf{q}} n_{\mathbf{k}+\mathbf{q}} n_{\mathbf{k}} \tag{8.44}$$

$$H_1^1 = \frac{1}{V}\sum_{\mathbf{q}\neq 0}\sum_{\mathbf{k},\mathbf{k}'\neq\mathbf{k}+\mathbf{q}} f_{\mathbf{k},\mathbf{k}',\mathbf{q}} c^+_{\mathbf{k}+\mathbf{q}} c^+_{\mathbf{k}'-\mathbf{q}} c_{\mathbf{k}'} c_{\mathbf{k}} \tag{8.45}$$

$$\tag{8.46}$$

The term H_0^1 is of the same nature as the diagonal Landau interaction between quasiparticules. The only difference is that δn_k represents occupation numbers of renormalized quasiparticules in the Landau theory, whereas n_k is the number operator of bare fermions. The Hamiltonian made up of the kinetic term H^0 (8.3) plus the term H_0^1 (8.44) has already been studied in reference [11] and leads to Poisson statistics in two dimensions. In the limit in which the bidimensional bosonization procedure is applicable, it has been established in [21] that the Hamiltonian $H + H_0^1 + H_1^1$ is integrable, namely that the effect of $H_0^1 + H_1^1$ is to renormalize the free theory without breaking the integrability. We question whether this property is still valid for a system of electrons such as the one drawn on the insert of figure 8.9. To see this, we diagonalize the Hamiltonian $H^0 + H_0^1 + H_1^1$ for the electron system of the insert of figure 8.9, in a sector of fixed total momentum. As expected from bosonization [21] and from R.P.A. theory [24], we obtain a collective bound state which detaches itself from the particule-hole continuum. The energy of the collective mode is greater as the continuum energy for repulsive interactions, and lower for attractive interactions. Because of the small value of the momentum cutoff Λ, the energy width of the continuum is small compared to the energy of the bound state, so that the bound state renormalizes the level spacing statistics of the continuum towards small values, since the mean value of the level spacing distributions is rescaled to unity. If we suppress the bound state from the spectrum, we obtain level spacing statistics in good agreement with Poisson level

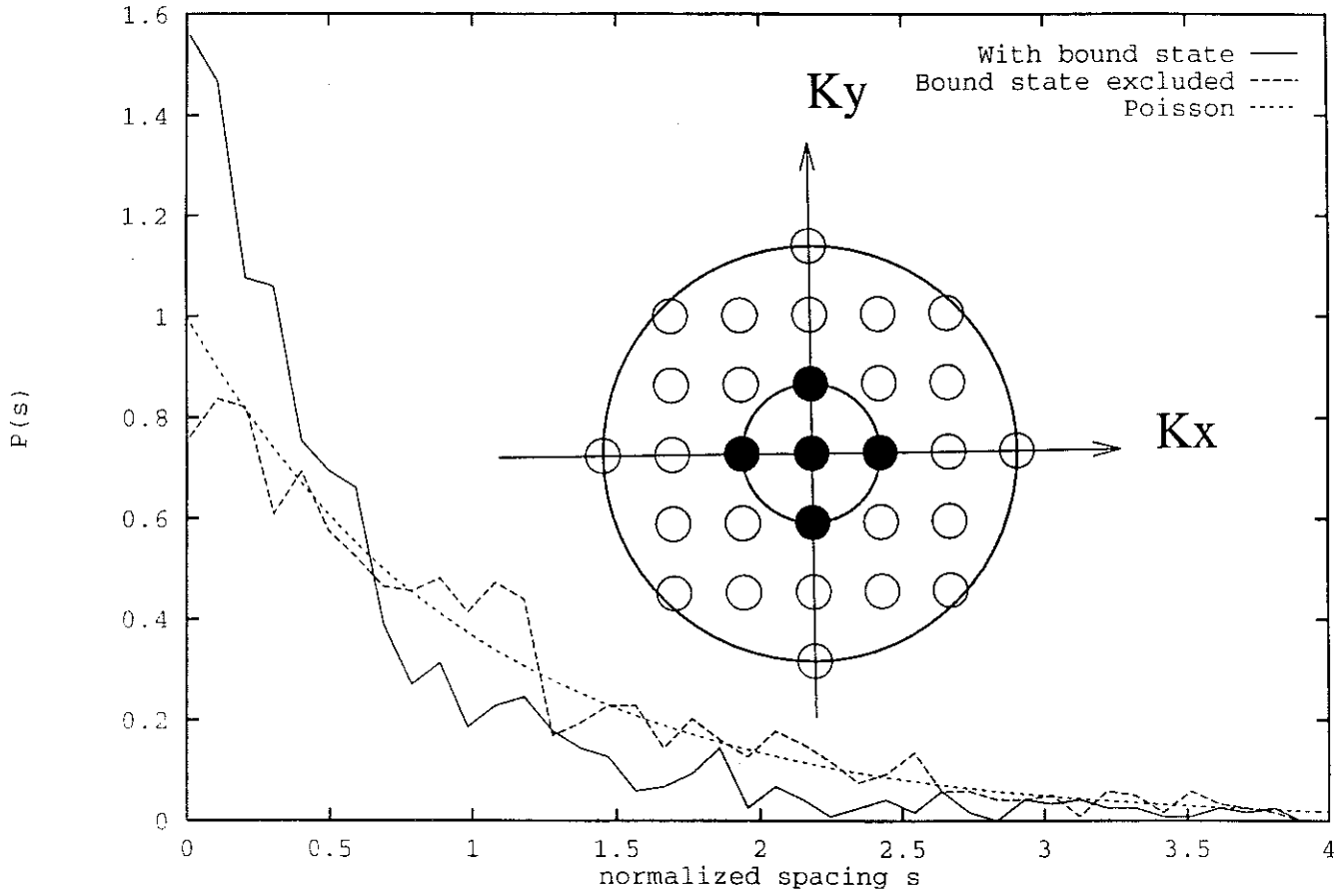

Figure 8.9: Level spacing statistics of the Hamiltonian $H^0+H_0^1+H_1^1$. The level spacing statistics are poissonian if one excludes the bound state, and renormalized towards $s = 0$ in the presence of the bound state. The linear size of the box is 2π. The kinetic term $\epsilon(k)$ is quadratic, with a mass equal to 3. The interactions have the form $f_{k,k',q} = f^0 \exp(-|q|/R)$, with $R = 6$. The insert represents the Fermi sea which was used. The Hilbert space contains 1042 states in the sector of momentum $P = (2\pi/L)(2,1)$.

spacing statistics, as shown on figure 8.9. It shows that whereas the cutoff Λ is very small and the number of electrons small too, the result we obtain is consistent with the result predicted in the limit in which the bosonization procedure is valid, with a large cutoff compared to $2\pi/L$. However, there is no contradiction with what has been done in one dimension. If we assume that in two dimensions the statistics are poissonian provided a sufficient number of truncated bosons (8.30) have a sufficient number of non zero terms in their linear combination, we obtain the same criterium as in one dimension, namely that the statistics are poissonian provided $\Lambda \gg 2\pi/L$. Using the cross-over scale we obtained from the diagonalization of g_4 interactions, we reach the conclusion that the level spacing statistics of the Hamiltonian $H^0 + H_2^1$ should be of the G.O.E. type. This is indeed the case, as shown on figure 8.10. We attribute the fact that the level spacing statistics of $H^0 + H_0^1 + H_1^1$ are poissonian to the presence of only a small number of off-diagonal terms, which are not numerous enough to change significatively the statistics.

8.4 Conclusion

In this paper, we have studied the effect of the momentum cutoff on the level spacing statistics of interacting Fermi systems. We found that the presence of the cutoff could change drastically the level spacing statistics of a finite size system, namely to drive the level spacing statistics from a poissonian shape to G.O.E. statistics. Using temperature-dependant level spacing statistics and one dimensional models, we have shown that the system of electrons in the presence of a cutoff is integrable at low energy. As far as g_2 interactions are concerned, we obtained G.O.E. level spacing statistics, which evolve to a Poisson level spacing statitics as the temperature decreases from $+\infty$. In the g_4 case, we could reach higher values of the cutoff since the two branches of the dispersion relation are decoupled. The infinite temperature level spacing statistics were intermediate between Poisson and G.O.E., and were driven to a Poisson shape as the temperature decreases. The main feature of a system of spinless correlated fermions in the presence of a momentum cutoff in the k-space is that, inspite of the loss of integrability there subsists nearly uncorrelated levels at low energy. This conclusion is analogous to the conclusions of reference [25] for another model. In two dimensions, one has to distinguish between two cases. The first case corresponds to off-diagonal interactions only. In this case, the level spacing statistics are G.O.E. statistics. It is clear that in this case, no switching on procedure can connect the excitations of the gas and the excitations of the interacting system, since the nature of the two spectra is different, which means that the system is not at the Landau fixed point. In the second case, diagonal interactions of the Landau type are taken into account. The Poisson level spacing statistics are restored because the off-diagonal matrix elements are not numerous enough, whereas their amplitude is comparable to the amplitude of the diagonal matrix elements. The Fermi liquid behaviour of the Hamiltonian in the presence of diagonal interactions is thus not destroyed. This result is to be compared with the fact that the Hamiltonian is diagonal in the limit in which the bidimensional bosonization procedure is valid. In spite of the small number of fermions and the small number of orbitals in our numerical computations, we obtain a result in good agreement with the bosonization of the Fermi surface theory. It should be stressed that the limit in which the bosonization theory is valid is not the thermodynamic limit in which Λ is fixed and $L \to +\infty$, because of the constraint (8.35). The problem of the thermodynamic limit, with the condition (8.35) violated remains open.

The finite temperature level spacing statistics seem to be an appealing tool for the study

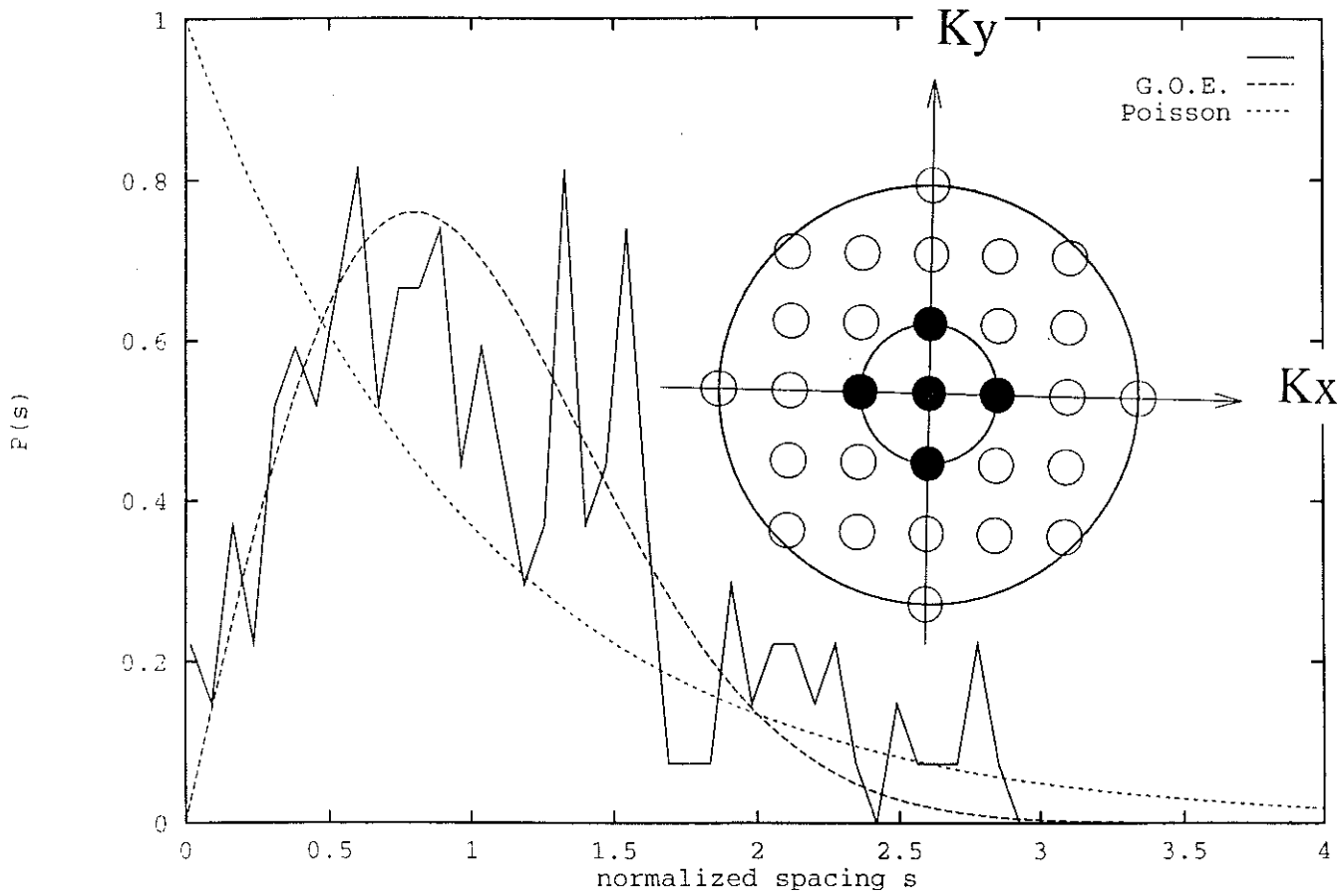

Figure 8.10: Level spacing statistics of the Hamiltonian $H^0 + H_1^1$ with the bound state excluded. The number of zero level spacing is equal to 1114 , leaving only 186 non zero level spacings for the statistics, which explains the important fluctuations of the level spacing statistics which agree with the G.O.E. shape. The insert represents the Fermi sea which was used. The Hilbert space contains 1042 states in the sector of momentum $P = (2\pi/L)(2,1)$.

of the spectrum of strongly correlated electronic systems. From a finite size study, one can characterize the integrability at low energy, and the cross-over temperature measures how far the low energy degrees of freedom are from being integrable. However, it is clear that the level spacing statistics retain only information about the the symetries, and give no information about the decay of the correlation functions, so that, in principle, we cannot solve entirely the problem whether the bidimensional t-J model is a Fermi liquid or not. Nonetheless, we can characterize the degree of integrability of the low energy degrees of freedom. A forthcoming paper shall be devoted to the case of finite size t-J models [10].

The author acknowledges B. Douçot for underlying the role of the momentum cutoff, and J.C. Anglès d'Auriac for help with algorithms.

References

[1] G. Montambaux, D. Poilblanc, J. Bellisard and C. Sire, Phys. Rev. Lett. 70, 497 (1993).

[2] T.C. Hsu and J.C. Anglès d'Auriac, Phys. Rev. B 47, 14291 (1993).

[3] D. Poilblanc, T. Ziman, J. Bellissard, F. Mila and G. Montambaux, Europhys. Lett. 22, 537 (1993).

[4] P.W. Anderson, Phys. Rev. Lett. 65, 2306 (1990).

[5] J.R. Engelbrecht and M. Randeria, Phys. Rev. Lett. 65, 1032 (1990).

[6] P.W. Anderson; J.R. Engelbrecht and M. Randeria, Phys. Rev. Lett. 66, 3225 (1991).

[7] E. Dagotto, A. Nazarenko and M. Boninsegni, Phys. Rev. Lett. 73, 728 (1994).

[8] A. Morea, S. Haas, A. Sandwik and E. Dagotto, preprint (1994).

[9] Sorella, preprint cond-mat/9308001.

[10] R. Mélin, in preparation.

[11] R. Mélin, J. Phys. I France 5, 159(1995).

[12] P. Degiovanni and R. Mélin, unpublished.

[13] R. Mélin, B. Douçot and P. Butaud, J. Phys. I France 4, 737 (1994).

[14] Anderson, Basic Notions of Condensed Matter Physics, Frontiers in Physics, The Benjamin/Cummings Publishing Company (1984).

[15] D. Pines and P. Nozieres, The Theory of Quantum Liquids, vol 1, Addison-Wesley Publishing Company (1966,1989).

[16] A. Houghton, H.J. Kwon and J. B. Marston, preprint (1993).

[17] I. E. Dzyaloshinskii and A.I. Larkin Sov. Phys. JETP 38, 202 (1974)

[18] Castro Neto and E. Fradkin, to be published.

[19] F.D.M. Haldane, unpublished.

[20] A. H. Castro Neto and E. H. Fradkin, Phys. Rev. Lett. 72, 1393 (1994).

[21] A. H. Castro Neto and E. H. Fradkin, to be published.

[22] F. D. M. Haldane, J. Phys. C 14,1285 (1981).

[23] M. C. Gutzwiller, Chaos in Classical and Quantum Mechanics, Springer Verlag (1990).

[24] J.W. Negele and H. Orland, Quantum Many Particule Systems, Frontiers in Physics (Vol. 68), Addison-Wesley Publishing Compagny, Inc (1987).

[25] M. Di Stasio and X. Zotos, to be published.

Chapitre 9

Article 4

Monopoles in the gauge theory of the t-J model[1]

R. Mélin, B. Douçot

CRTBT-CNRS, 38042 Grenoble BP 166X cédex France

We consider a RG approach for the plasma of magnetic monopoles of the Ioffe-Larkin approach to the t-J model. We first derive the interaction parameters of the 2+1 plasma of magnetic monopoles. The total charge along the time axis is constrained to be zero for each lattice plaquette. Under the one-plaquette approximation, the problem is equivalent to a one dimensional neutral plasma interacting via a potential $V(t) \sim t^{\alpha}$, with $\alpha = 1/3$. The plasma is in a dipolar phase if $\alpha \geq 1$ and a possibility of transition towards a Debye screening phase arises if $\alpha < 1$, so that there exists a critical Fermi wave vector k_f^* such as the plasma is Debye screening if $k_f < k_f^*$ and confined if $k_f > k_f^*$. The 2+1 dimensional problem is treated numerically. We show that k_f^* decreases and goes to zero as the number of colors increases. This suggests that the assumption of spin-charge decoupling within the slave-boson scheme is self-consistent at large enough values of N and small enough doping. Elsewhere, a confining force between spinons and antiholons appears, suggesting a transition to a Fermi liquid state.

[1] submitted to Phys. Rev. B

9.1 Introduction

The physics of strongly interacting electron systems has received considerable attention over the recent years, and it still bears many challenges, especially on the theoretical side. Among the various methods and ideas which have been explored in this context, gauge theories seemed to offer a rather attractive approach [1]-[7]. Their essence is to focuss on the presence of a non double occupancy constraint, which leads to a local $U(1)$ symmetry if a slave boson representation is used [1]-[3]. Although it is possible to derive these gauge theories from an expansion around a large N mean field theory of the t-J model [4] [5], they could also be regarded as promising candidates for an effective low-energy theory in order to describe for instance the anomalous normal state properties of high-T_c superconductors. They seem to predict a phase diagram for the single band t-J model which qualitatively ressembles the experimental ones for copper-oxide superconductors [6]. Further more, they reconcile the existence of a large Fermi surface corresponding to Luttinger's theorem, as shown by photoemission experiments, and the anomalous transport properties, which are mostly governed by holes [6] [7]. Thermodynamic properties have also been investigated, and a good agreement with high temperature expansions for the t-J model has been reached [8]. However, this work has also pointed out that fluctuations of the gauge field are large, in the sense that the variance of the local statistical flux around a given plaquette is not small in units of 2π, even down to low temperatures. This feature suggests that the presence of the lattice may not be inessential, since it induces a periodic action as a function of the time and space dependent flux per plaquette. As demonstrated by Poliakov, this periodic nature of the gauge field has dramatic consequences on 2+1 dimensional electrodynamics since it allows for non trivial space time configurations of the gauge field (monopoles), which induce charge confinement [9]. It should be emphasized that in the context of the t-J model, the gauge field Lagrangian density is not the usual $-\frac{1}{4}F_{\mu\nu}F^{\mu\nu}$ term, but it is generated upon integrating out fermionic and bosonic fluctuations [3]. A perturbative estimate of a single monopole action has also been derived in [3], and was found to diverge. However, it is clear that some globally neutral configurations (i.e. with the same number of instantons and anti-instantons) have a finite action, and the main question is whether the corresponding two-component plasma exhibits Debye-screening or not. This viewpoint has been developed by Nagaosa [10] where he assumed a dissipative-type action for the gauge field, which may be relevant for the t-J model at small temperatures, since it requires a finite dc conductivity for the fermions. His main conclusion is that no major instanton effect is present in the t-J model range of parameter since the dissipative nature of the gauge field dynamics strongly inhibits quantum tunneling. In the present paper, we address this question from a slightly different perspective, with emphasis on the possible zero temperature transitions. By contrast to the results of reference [10], we find that assuming a Ioffe-Larkin form for the monopole plasma action leads to a phase transition between a Debye screening phase (which corresponds to a confining force between spinons and antiholons), and a dipole phase (leading to unconfined spinons and antiholons). The control parameters are the band filling of the underlying t-J model, and the number N of fermion colors (the physical case being $N = 2$). In rather good agreement with physical intuition, the dipole phase of the plasma is found at large N and small doping. In this regime, spin-charge separation may then be a self-consistent hypothesis. We note however that this leads either to a renormalized Fermi liquid or an anomalous liquid depending on whether Bose condensation of holons occurs or not. In the other phase, the gauge field cannot be treated perturbatively, and the corresponding mesons (bound states of

spinons and antiholons) are physical electrons. By contrast, a transition to the dipole phase is obtained in reference [10] in the presence of an infinitesimal dissipation. The main difficulty of the problem is the determination of the phase diagram of the monopole plasma which exhibits long range interactions (in space and imaginary time). Furthermore, unlike the case of the standard compact 2+1 electrodynamics, a strong anisotropy exists between space and time directions, reflecting the lack of Lorentz invariance in the model. This reduced symmetry increases the difficulty of real space RG analysis since the functional form of the monopole interaction potential is not stable under a RG transformation. Our approach has attempted to take advantage of the fact that the interaction is much stronger along the time direction, with a $\tau^{1/3}$ dependence. The corresponding one dimensional problem exhibits a phase transition between a Debye-screening phase and a dipole phase. We argue and give some numerical indication that the unbinding of the monopole-antimonopole pairs along the time direction triggers a 2+1 dimensional unbinding, leading to a globally Debye-screening phase. The paper is organized as follows: section 9.2 defines the statistical problem of the monopole plasma. The next section focusses on the 0+1 dimensional problem along a time direction, giving strong arguments in favor of a phase transition. The extension to the 2+1 dimensional situation is then discussed, leading to a phase diagram as a function of N and fermion filling, which is the main result of the paper. The conclusion is dedicated to a comparison with previous work and stresses open questions.

9.2 Statistical mechanics of the monopole plasma

As already stressed in the introduction, we shall assume a Lagrangian of the form

$$\begin{aligned} L &= \sum_i \sum_{\sigma=1}^{N} \left(\bar{c}_{i\sigma}(\tau) \frac{\partial}{\partial \tau} c_{i\sigma}(\tau) + \bar{b}_{i\sigma}(\tau) \frac{\partial}{\partial \tau} b_{i\sigma}(\tau) \right) - t_f \sum_{\langle i,j \rangle} \left(e^{-ia_{ij}} c^+_{i\sigma} c_{j\sigma} + \text{h.c.} \right) \\ &\quad - t_b \sum_{\langle i,j \rangle} \left(e^{-ia_{ij}} b^+_i b_j + \text{h.c.} \right) + i \sum_j \lambda_j \left(c^+_{j\sigma} c_{j\sigma} + b^+_j b_j - \frac{N}{2} \right). \end{aligned} \tag{9.1}$$

The fields $c_{i\sigma}(\tau)$ and $b_i(\tau)$ are respectively fermionic and bosonic, and they are defined on a two dimensional square lattice with continuous imaginary time. The hopping constants t_f and t_b can be derived from a large N saddle point approximation of the one band t-J model [5] [8]. We shall from now on focus on the effective dynamics of the $U(1)$ gauge field (a_{ij}, λ_i), assuming that fermions and bosons have been traced out. As shown in the references [3] [6], the gauge field action to gaussian order is dominated by the fermion contribution at low doping, and with the assumptions that the holons have not condensed. Keeping only the transverse part which is responsible of the non-Fermi liquid behavior gives [3]

$$S_{eff}(a, \lambda) = T \sum_{\omega_n = 2\pi n T} \int_{BZ} \frac{1}{2} \left(\epsilon_1(k, \omega) \omega^2 + \mu(k, \omega) k^2 \right) \left(\delta_{i,j} - \frac{k_i k_j}{k^2} a_i(k, \omega) a_j(-k, -\omega) \right). \tag{9.2}$$

In this equation,

$$\epsilon_1 = \frac{k_f}{2\pi k |\omega|} \tag{9.3}$$

for $|\omega| \ll 2 t_f k_f k$, $k \ll k_f$ and $\mu(k, \omega) = t_f / 12\pi$. The gauge field variables $a_{r,r+n}$, where n is a lattice vector and r a lattice site are denoted in the continuum limit by $a_n(r + n/2)$, in

order to define the two component field $a_i(\rho)$. The time component of a is identified with λ. Most of the time, we shall use the axial gauge $a_0 = 0$. Latin indices such as i and j denote spatial components, whereas Greek indices correspond to arbitrary components. The quantities ϵ_1 and μ are derived with the approximation of a circular Fermi surface, and by taking the long wavelength, small frequency limit of the fermion current-current correlation function. The main drawback of this action is that the fundamental periodicity of the original action (9.1), namely its invariance under $a_{ij} \rightarrow a_{ij} + 2\pi$ is lost. This periodicity allows for non-trivial space-time configurations of the field corresponding to tunneling events where the flux threading a given plaquette may change by integer multiples of 2π. Ioffe and Larkin suggest to express (9.2) in terms of gauge invariant field strength $F_{\mu\nu} = \partial_\mu a_\nu - \partial_\nu a_\mu$, with $\mu = 0, 1, 2$, and to replace the flux par plaquette F_{12} by its value modulo 2π. This algorithm sounds quite natural on physical grounds. However, (9.2) has been derived perturbatively for 'flat' configurations which satisfy Faraday's law: $\partial_\mu b_\mu = 0$, where

$$b_\mu = \frac{1}{2}\epsilon_{\mu\nu\rho}F_{\nu\rho}. \tag{9.4}$$

After the field strength b_μ is taken modulo 2π, it satisfies

$$\partial_\mu b_\mu = \sum_i 2\pi n_i \delta(r - r_i)\delta(\tau - \tau_i), \tag{9.5}$$

where n_i are the integer charges located at r_i,τ_i. An ambiguity arises in extending the result (9.2) to non trivial configurations. We may add to equation (9.2) any quadratic form

$$T\sum_{\omega_n}\int \frac{d^2k}{(2\pi)^2}C(k,\omega)\left(\omega^2 b(k,\omega)b(-k,-\omega) - k^2 e_\perp(k,\omega)e_\perp(-k,-\omega)\right) \tag{9.6}$$

without changing the result on 'flat' configurations, but the action for non trivial configurations will depend on the kernel $C(k,\omega)$. In (9.6), $e_\perp$ and b denote the transverse part of the electric field, and the magnetic field respectively. We also note that the perturbative evaluation of the fermion loop generates only the function $\epsilon_1(k,\omega)\omega^2 + \mu(k,\omega)k^2$. Physical intuition suggests that $\mu(k,\omega)$ is identical to the static diamagnetic susceptibility in the $\omega \rightarrow 0$ limit. This determines the two functions $\epsilon_1(k,\omega)$ and $\mu(k,\omega)$ as given above, and with such a determination, (9.2) becomes

$$S_{eff}(a,\lambda) = T\sum_{\omega_n}\int \frac{d^2k}{(2\pi)^2}\frac{1}{2}\epsilon_1(k,\omega)e_\perp(k,\omega)e_\perp(-k,-\omega) + \frac{1}{2}\mu(k,\omega)b(k,\omega)b(-k,-\omega). \tag{9.7}$$

Equation (9.7) is then extended to non-trivial configurations thus lifting the ambiguity in the choice of the kernel $C(k,\omega)$. But if the procedure seems perfectly sound at low frequencies, the separation between the electric and magnetic parts is less obvious to access at higher frequencies. In the bulk of this paper, we assume that this procedure is valid. The action for a many monopole configuration with a topological charge $q(r,\tau) = \pm 2\pi$ is then given by

$$S_{plasma} = \frac{T}{2}\sum_{\omega_n}\int \frac{d^2k}{(2\pi)^2}q(k,\omega)\frac{\epsilon_1(k,\omega)\mu(k,\omega)}{\epsilon_1(k,\omega)\omega^2 + \mu(k,\omega)k^2}q(-k,-\omega), \tag{9.8}$$

where $q(k,\omega)$ is the Fourier transform of the charge density, namely

$$q(k,\omega) = \int_0^\beta d\tau \sum_r e^{-i(k.r+\omega\tau)}q(r,\tau), \tag{9.9}$$

where r is a lattice site. More specifically, this gives

$$S_{plasma} = \frac{N t_f}{24\pi} T \sum_{\omega_n} \int \frac{d^2k}{(2\pi)^2} \frac{q(k,\omega)q(-k,-\omega)}{|\omega|\left(|\omega| + \frac{t_f}{6k_f}k^3\right)}. \tag{9.10}$$

In this formula, the global factor N has been added. It is simply the number of fermion colors in the large N approaches. Rescaling energies and frequencies by setting $t_f = \pm 1$, the model depends only on two dimensionaless parameters, N and k_f. Assuming a circular Fermi surface, the maximal value of k_f corresponds to $1/2$ electron per site for a given color, which gives $k_f \leq (2\pi)^{1/2}$.

Before going further, we should mention that equation (9.8) is not the only candidate for the monopole plasma action. Developing an analogy with Josephson junction arrays, and emphasizing the dissipative nature of the gauge field, Nagaosa has also considered the following action [10]:

$$S_{diss} = \frac{\gamma}{4\pi} \int_{-\infty}^{+\infty} d\tau \int_0^\beta d\tau' \sum_{r,n} \frac{1}{(\tau - \tau')^2} \left(1 - \cos\left(a_\perp(r,n,\tau) - a_\perp(r,n,\tau')\right)\right). \tag{9.11}$$

for the dissipative part of the gauge field dynamics. As shown in reference [11], it is possible to map it into a statistical model in some regimes, but mostly a bidimensional model is obtained. The key variables are the winding number $m(r,n)$ along the time direction:

$$a_\perp(r,n,\beta) - a_\perp(r,n,0) = 2\pi m(r,n) + \nu(r,n), \tag{9.12}$$

with $\nu(r,n) \in]-\pi,\pi]$ and $m(r,n)$ and integer. It seems that both approaches respect the 2π periodicity and the quadratic expansion of the gauge field around $a = 0$. In the absence of a fully first principle derivation, we shall adopt equation (9.8) as a working hypothesis, and hope to clarify this issue in a future work.

Going back to equation (9.10), it is important to stress that for any k value, the ω integral diverges if $\lim_{\omega\to 0} q(k,\omega)$ is non vanishing. Therefore, we shall impose a constraint on the allowed topological charge configurations, namely that $q(k,\omega = 0) = 0$ for any k. In real space, it means that

$$\int_0^\beta d\tau q(r,\tau) = 0 \tag{9.13}$$

for any plaquette located at r. The partition function of the plasma is then

$$Z = \sum_{n=0}^{+\infty} \frac{1}{(n!)^2} \prod_{i=1}^{2n} \left(\int_0^\beta \frac{d\tau_i}{\tau_0} \sum_{r_i} \right) \chi(r_1,...,r_n) \exp\left(-\frac{1}{2} \sum_{i,j} q_i q_j V(r_i - r_j, \tau_i - \tau_j) \right). \tag{9.14}$$

In this equation, r_i, τ_i denote the space-time coordinates of the monopoles with topological charge q_i. We set $q_i = 2\pi$ if $1 \leq i \leq n$ and $q_i = -2\pi$ if $n+1 \leq i \leq 2n$. $\chi_{2n}(r_1,...,r_{2n})$ expresses the constraint and $\chi = 1$ if for any r we have

$$\sum_{i=1}^{2n} q_i \delta_{r,r_i} = 0. \tag{9.15}$$

The interaction potential $v(r,\tau)$ is obtained by Fourier transform of equation (9.10)

$$v(r,\tau) = \frac{N}{12\pi} T \sum_{\omega_n} \int \frac{d^2k}{(2\pi)^2} \frac{e^{i(k.r+\omega\tau)}}{|\omega|\left(|\omega| + \gamma|k|^3\right)}, \tag{9.16}$$

with $\gamma = 1/6k_f$ (we set $t_f = 1$). An important ingredient in (9.14) is the imaginary time scale τ_0 which is obtained by calculating the ratio of the two gaussian determinants in the presence and in the absence of an instanton. We have carried out this calculation for the broken parabola model of Ioffe and Larkin, which leads to

$$\frac{1}{\tau_0} = \sqrt{2\pi}\mu \left(T \sum_{\omega_n} \int \frac{d^2k}{(2\pi)^2} \frac{k^2}{\epsilon_1(k,\omega)\omega_n^2 + \mu k^2} \right)^{1/2}. \tag{9.17}$$

The interested reader will find a derivation of this result in the appendix. We note that the integral is divergent at large frequencies. This may be another signal that we have not yet found a satisfactory derivation of this monopole plasma action. Since this τ_0 depends on the full non linear action of the gauge field, which is still unknown, we shall assume it equal to unity in the following discussion (since we have used $t_f = 1$ as energy unit). The following sections are now dedicated to an analysis of the classical statistical system given by equation (9.14).

9.3 Monopoles in dimension 0+1

We deduce from the interaction (9.16) that the interaction betwen two monopoles is

$$-V(r,\tau) = \frac{Nt}{12\pi} \int \frac{d\omega}{2\pi} \int \frac{d^2k}{(2\pi)^2} \frac{\cos(k.r) - \cos(k.r + \omega\tau)}{|\omega|\,(|\omega| + \gamma|k|^3)}. \tag{9.18}$$

We have shifted the interaction by an infinite constant so that the pair interaction between two monopoles is finite. The energy of a configuration of monopoles satisfying the neutrality condition $\int q(r,\tau)d\tau = 0$ is finite and does not depend on the regularization of the pair potential.

From now on, we are interested in the quantum problem at zero temperature, so the system is infinite along the imaginary time direction. We shall now use $\beta = Nt/12\pi$ to denote the inverse fictitious temperature of the monopole plasma, which shouldn't introduce confusion. The two parameters associated to (9.18) are $\gamma = 1/6k_F$ and the prefactor β. The interaction (9.18) decreases as the distance $|r|$ between two plaquettes increases. In order to have an idea of the interaction ranges, we calculate the interaction $V(r,\tau)$ as a function of τ for different values of the interplaquette distance. We first rearrange the expression (9.18) using the change of variables $u = \omega\tau$ and $q = (\gamma\tau)^{1/3}k$. We obtain

$$-\frac{1}{\beta}V(r,\tau) = \frac{\tau^{1/3}}{\gamma^{2/3}} F\left(\frac{|r|}{(\gamma\tau)^{1/3}}\right), \tag{9.19}$$

with

$$F(x) = \int_0^{+\infty} \frac{qdq}{2\pi} J_0(qx) \int_{-\infty}^{+\infty} \frac{du}{2\pi} \frac{(1-\cos u)}{|u|(|u| + q^3)}. \tag{9.20}$$

We plotted on figure 9.1 the interaction for different values of the interplaquette distance $|r|$. In a first approximation, we take into account only the one-plaquette interaction along the time direction. In section 9.4, we renormalize the bidimensional problem with a cut-off for the distance between two plaquettes.

The interactions of the one-plaquette problem are simply $V(\tau) = -\tau^{1/3}F(0)/\gamma^{2/3}$. We look for the phase diagram of the potential $V(\tau) \sim -\tau^{\alpha}$ in one dimension as a function of the exponent α. Fortunately, some exact results concerning the phase diagram of one-dimensional

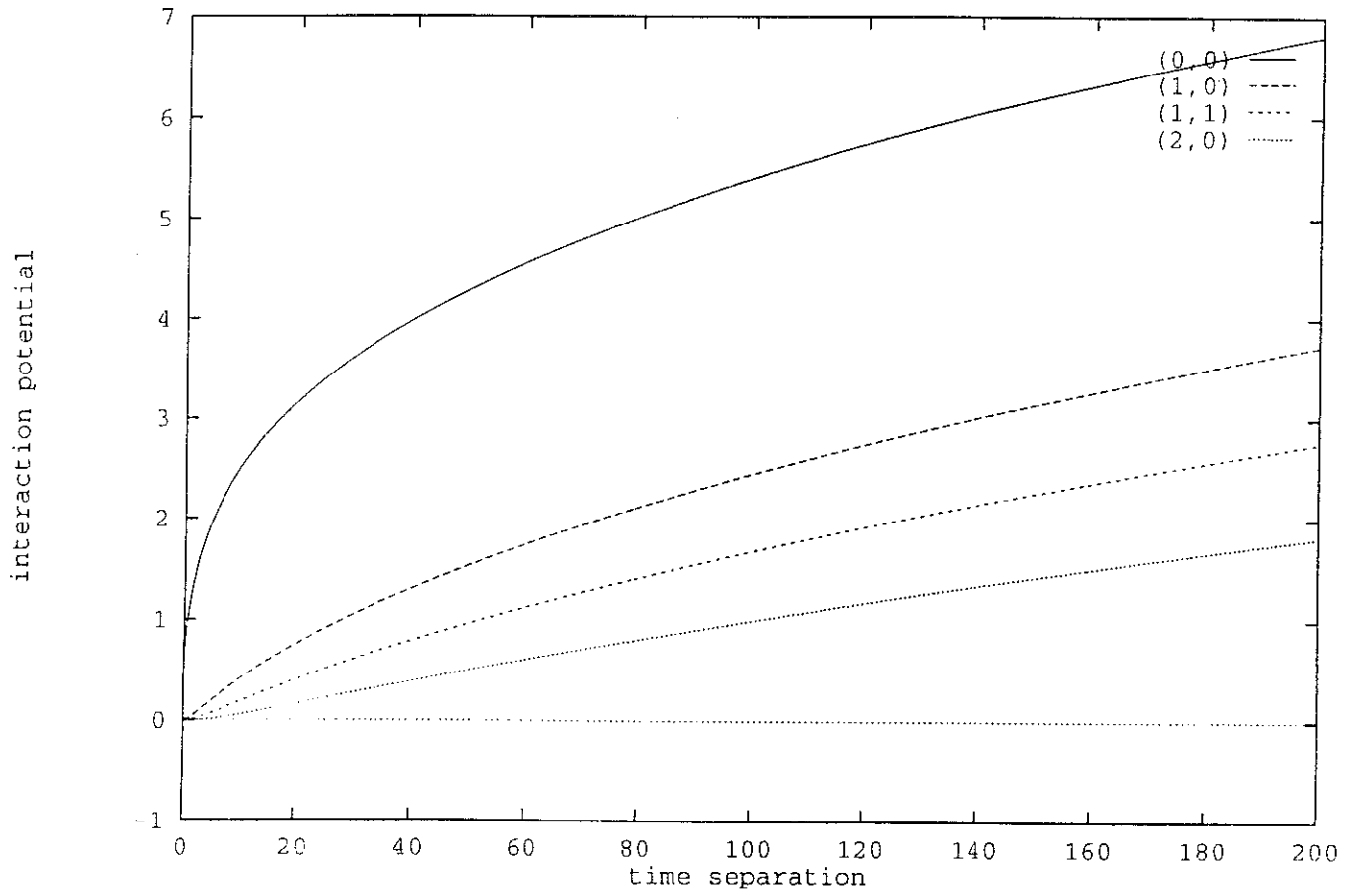

Figure 9.1:
Interaction potential $V(|r|,\tau)$ of equation (9.18) for $k_f = 4$ and for different values of the interplaquette spacing as a function of the time coordinate. The notation (0,0) corresponds to $|\mathbf{r}| = 0$, (1,0) stands for $|\mathbf{r}| = 1$, (1,1) stands for $|\mathbf{r}| = \sqrt{2}$ and (2,0) stands for $|\mathbf{r}| = 2$.

systems with long-range interactions are available [12]. The main result shows rigorously the existence of a finite temperature phase transition for the 1D ferromagnetic Ising model if the coupling $J(n-n') \propto 1/|n-n'|^\gamma$, with $1 < \gamma < 2$ [13]. To some extent, these results can be transposed to generalized Coulomb gas models, by considering a representation of the Ising model in terms of kink and antikink configurations. The potential energy for a single kink-antikink pair is then proportional to $|n-n'|^{2-\gamma}$, n and n' being the locations of the kink and antikink. The Ising and corresponding Coulomb gas problems are however not equivalent since the Ising model generates only rather special configurations where kinks and antikinks alternate. We expect intuitively the unrestricted Coulomb gas to be less ordered than the corresponding Ising model. By ordered state, we mean the dipolar phase. As a result, an unrestricted generalized Coulomb gas with $V(r) \propto r^\alpha$ is expected to have a high temperature Debye-screening phase if $\alpha < 1$. The fact that $\alpha = 1$ (the 1D genuine Coulomb potential) is the borderline is confirmed by several exact investigations [14] [15] showing that this system is always in the dipolar phase at any temperature. Our problem is a special case, with $\alpha = 1/3$. We shall now attempt to estimate the transition temperature to the Debye phase. It is then tempting to use a real space RG analysis along the lines of references [16]-[18]. For instance, the Coulomb potential in any dimension d ($\alpha = 2-d$) has been analyzed in reference [18]. For $d > 2$, the system is always in a Debye screening phase, whereas for $d < 2$, there exists a finite temperature transition. We note that this simple RG analysis still predicts a non trivial fixed point for $d = 1$ and $\alpha = 1$, in discrepancy with the exact results of references [14] and [15]. But as d is decreased from 2 to 1, the unstable fixed point is found for higher values of the plasma fugacity, so that the dilute approximation leading to the RG equations is no longer valid. Hopefully, $\alpha = 1/3$ is not too large, so the usual RG procedure is consistent.

In order to analyse the one plaquette problem, we wish to treat the more general problem of the generalized Coulomb potential V_α in one dimension. We show that if $\alpha < 1$, the plasma has a Debye phase. We call Z_τ the partition function of the plasma with a minimal separation τ betwen the charges, which position is allowed to vary from $x = 0$ to $x = L$. For a neutral system of $2n$ particles, this defines an integration domain denoted $D_{2n}(L, d\tau)$. We wish to perform one renormalization step, that is to express Z_τ as a function of $Z_{\tau+\delta\tau}$. To do so, we write Z_τ under the form

$$Z_\tau = \sum_{m=0}^{+\infty} \frac{K^{2m}}{(m!)^2} \sum_{p=0}^{m} \binom{m}{p}^2 p!(d\tau)^p \int_{D_{2(m-p)}(L,\tau+d\tau)} dr_1 ... dr_{2(m-p)} W_B(r_1, ..., r_{2(m-p)}) \quad (9.21)$$
$$\prod_{i=1}^{p} \int_0^L d\rho_i 2\cosh(\beta q \tau E(\rho_i)).$$

We have introduced a fugacity denoted by $z = K\tau$. In this equation, we have taken into account p dipoles with their center of gravity located at ρ_i ($i = 1, ..., p$) and with a size between τ and $\tau + d\tau$. W_B is the Boltzmann weight of the $2(m-p)$ remaining isolated charges located at $r_1, ..., r_{2(m-p)}$. $E(\rho)$ is the electric field at ρ, created by the $2(m-p)$ isolated charges. More specifically,

$$W_B(r_1, ..., r_{2n}) = \exp\left(-\beta^{-1} \sum_{i<j} q_i q_j V_{\alpha,\tau}(r_i - r_j)\right), \quad (9.22)$$

with

$$V_{\alpha,\tau}(r) = -\frac{1}{\alpha}\left(\left|\frac{r}{\tau}\right|^\alpha - 1\right), \quad (9.23)$$

and

$$E(\rho) = -\sum_i q_i \nabla_\rho V_{\alpha,\tau}(\rho - r_i) = \sum_i \frac{q_i}{\tau} \left| \frac{\rho - r_i}{\tau} \right|^{\alpha-1} . \tag{9.24}$$

The p dipoles are assumed to be independent. The integration over the dipole coordinates ρ_i must take into account the position of the other charges located at $r_1, ..., r_{2(m-p)}$. We expand the cosh in (9.21) up to second order in the electric field, and we write

$$\int_0^L 2\cosh(\beta q \tau E(\rho)) d\rho = 2L + \varphi(r_1, ..., r_{2n}), \tag{9.25}$$

where we have used the notation $n = m-p$ and where the integration domain takes into account the presence of a hard core condition. We first need to determine the function φ. To do so, we write

$$\begin{aligned} \int_0^L 2\cosh(\beta q \tau E(\rho)) d\rho &= \sum_{i=1}^{2n} \theta(x_{i+1} - x_i - 3\tau) \\ &\int_{x_i+2\tau/2}^{x_{i+1}-3\tau/2} d\rho \left(2 + \beta^2 \tau^2 q^2 \sum_{j=1}^{2n} \sum_{k=1}^{2n} q_j q_k V'_\tau(\rho - x_j) V'_\tau(\rho - x_k) \right) . \end{aligned} \tag{9.26}$$

If we take only the two-body interactions, and the thermodynamic limit, the expression of φ takes the form

$$\begin{aligned} \varphi(r_1, ..., r_{2n}) &= -3\tau(2n) + \lim_{L\to+\infty} \beta^2 q^2 \left[\sum_{i\neq j} q_i q_j \int_0^L d\rho \left| \frac{\rho - r_i}{\tau} \right|^{\alpha-1} \left| \frac{\rho - r_j}{\tau} \right|^{\alpha-1} \right. \\ &\text{sign}((\rho - r_i)(\rho - r_j)) \theta\left(\left| \frac{\rho - r_i}{\tau} \right| - \frac{3}{2} \right) \theta\left(\left| \frac{\rho - r_j}{\tau} \right| - \frac{3}{2} \right) \\ &\left. + \sum_i q^2 \int_0^L d\rho \left| \frac{\rho - r_i}{\tau} \right|^{2(\alpha-1)} \theta\left(\left| \frac{\rho - r_i}{\tau} \right| - \frac{3}{2} \right) \right] . \end{aligned} \tag{9.27}$$

The $L \to +\infty$ limit exists provided the system is neutral and $\alpha < 3/2$. Indeed, the $2n$ charges create a dipolar field at large distances which decays as $\rho^{\alpha-2}$ or faster. Taking the square gives the upper bound on α for long distance convergency. This property also enables us to shift variables and recast the previous expression as a sum of pair contributions which all converge separately. We thus obtain

$$\begin{aligned} \varphi(r_1, ..., r_{2n}) &= -3\tau(2n) + \beta^2 q^2 \sum_{i\neq j} q_i q_j \int_{-\infty}^{+\infty} d\rho \left[\left| \frac{\rho - r_i}{\tau} \right|^{\alpha-1} \left| \frac{\rho - r_j}{\tau} \right|^{\alpha-1} \right. \\ &\text{sign}((\rho - r_i)(\rho - r_j)) \theta\left(\left| \frac{\rho - r_i}{\tau} \right| - \frac{3}{2} \right) \theta\left(\left| \frac{\rho - r_j}{\tau} \right| - \frac{3}{2} \right) \\ &\left. - \left| \frac{\rho}{\tau} - \frac{r_i + r_j}{2\tau} \right|^{2(\alpha-1)} \theta\left(\left| \rho - \frac{r_i + r_j}{2} \right| - \frac{3}{2}\tau \right) \right] . \end{aligned} \tag{9.28}$$

After some rather simple calculations, and extracting the dominant behavior, we have

$$\varphi(r_1, ..., r_{2n}) = \beta^2 q^2 \tau \sum_{i\neq j} q_i q_j c(\alpha) \left[\left| \frac{r_i - r_j}{\tau} \right|^{2\alpha-1} - 1 \right] - 2n\tau \left(3 + (c(\alpha) + d(\alpha)) \beta^2 q^2 \right) . \tag{9.29}$$

The coefficients $c(\alpha)$ and $d(\alpha)$ are given in terms of the Euler B function:

$$c(\alpha) = \frac{2(\alpha-1)}{2\alpha-1}B(\alpha,2(1-\alpha)) - B(\alpha,\alpha) \tag{9.30}$$

$$d(\alpha) = \frac{2}{2\alpha-1}\left(\frac{3}{2}\right)^{2\alpha-1}. \tag{9.31}$$

We note that φ has the dimension of a length, so that Z_τ is dimensionless. The scaling equations are now obtained and read

$$\frac{d\ln\beta}{d\ln\tau} = \alpha + 2(2\alpha-1)c(\alpha)K^2\tau^2\beta q^2 \tag{9.32}$$

$$\frac{d\ln K}{d\ln\tau} = -\frac{\beta q^2}{2} - \left(3 + (c(\alpha)+d(\alpha))\beta^2q^4\right)K^2\tau^2. \tag{9.33}$$

And the interaction function is modified by

$$\frac{dV}{d\ln\tau} = 2(2\alpha-1)c(\alpha)K^2\tau^2\beta q^2\left[\frac{1}{2\alpha-1}\left(\left|\frac{\Delta}{\tau}\right|^{2\alpha-1}-1\right) - \frac{1}{\alpha}\left(\left|\frac{\Delta}{\tau}\right|^{\alpha}-1\right)\right], \tag{9.34}$$

where Δ is the particle separation. These equations are obtained by imposing the normalization constraints $V(\tau)=0$ and

$$\frac{dV}{d\Delta}(\Delta=\tau) = -1. \tag{9.35}$$

Since the fundamental form of the interactions is preserved only for the Coulomb potential ($\alpha=1$), these prescriptions are meaningful mostly near $\alpha=1$. In the case $\alpha=1$, we recover Kosterlitz's RG equations as derived in [18]. We note that the second term in the r.h.s. of equation (9.33) is not given in [18], but it doesn't change the critical behavior. Its meaning is a natural reduction of fugacity because of excluded volume effects. The structure of these equations, and in particular, the fact that $\alpha > 0$ and $2(2\alpha-1)c(\alpha)K^2\tau^2\beta q^2 < 0$ shows that the model keeps a finite temperature transition, and that the size of the Debye screening phase increases as α decreases. Coming back to our problem, α is fixed to $1/3$ for the single plaquette problem. The interaction strength is larger if N increases and if γ decreases, so if k_f increases. The dipolar phase is then expected at large N and large electron filling, in agreement with the physical intuition that spin-charge separation is more likely to occur in the vicinity of the Mott insulator and in the large N limit. This defines a critical Fermi wave vector $k_f^*(N)$ such that spin-charge separation occurs for $k_f > k_F^*(N)$. The aim of section 9.4 is to obtain quantitative results for the variation of $k_f^*(N)$ with the number of colors N.

9.4 Monopoles in dimension 2+1

We now consider the 2+1 dimensional problem. The derivation of the RG equations is a straightforward generalization of what has already been done in the 0+1 dimensional case. The potential $V(\tau,\tau)$ is given by equation (9.19) and (9.20). We use periodic boundary conditions in time, with a period L. This regularization will also be used in the numerical calculations. Small dipoles (with a length between τ and $\tau+d\tau$) can only be parallel to the temporal direction since

we require the local neutrality condition $\int q(r,\tau)d\tau = 0$, so that the cut-off τ is only introduced in the temporal direction. The function φ is given by

$$\begin{aligned}\varphi(r_1 t_1, ..., r_{2n} t_{2n}) &= 2\beta^2 q^2 \tau^2 \sum_r \sum_{j\neq k} q_j q_k \int_{3\tau/2}^{L/2} d\tau \partial_0 V(0,\tau)\partial_0 V(r_k - r_j - r, \Delta_{j,k} - \tau) \\ &\quad + 2\beta^2 q^2 \tau^2 \sum_r \sum_j q_j^2 \int_{3\tau/2}^{L/2} (\partial_0 V(r,\tau))^2 \, d\tau. \end{aligned} \tag{9.36}$$

In this expression, the summation over r is a summation over the plaquettes which contain the small dipoles (with a separation in the temporal direction between τ and $\tau + d\tau$). $\Delta_{j,k}$ is the difference between the time coordinates of the monopole j and the monopole k. As in the expression (9.27), the integration over the time coordinate of the small dipole contains a hard core condition. We evaluated numerically the integrals in (9.36), and took into account only the potentials $V(r,\tau)$ such as $|r| < \Lambda$, with Λ a lattice cut-off. The RG trajectories are plotted on figure (9.2) for different values of the Fermi wave vector. Notice that some trajectories are free to cross each other since the potential depends on the initial conditions via γ. We can check the validity of the predictions of the 0+1 dimensional approach: if $k_f < k_f^*$, the plasma is deconfined whereas it is confined if $k_f > k_f^*$. For a one-color model, we find $k_f^* = 0.5 \pm 0.05$. However, the Fermi wave vector is bounded above by $\sqrt{2\pi}$ since there is less than $1/2$ electron of a given color per plaquette. We conclude that there exists a transition even for the one-color model. We now adress the question of the N colors monopole model. The action is simply multiplied by N, inducing a change in the initial conditions of the renormalization procedure. We plotted on figure 9.3 the critical Fermi wave vector k_f^* as a function of the number of colors. We see that for $N = 2$, which is the case of physical interest, that a possibility of a non Fermi liquid arises as the doping increases.

9.5 Conclusion

To conclude, the main result of this investigation is the possibility of tuning the microscopic parameters of the model (here the number of colors and the filling factor) in such a way that confinement between spinons and antiholons arises or not, depending on these parameters. Using a different approach, it had been previously claimed that the Ioffe-Larkin type of plasma relevant to the t-J model is always in the dipolar phase, so that spinons and holons have a chance not to form a Fermi liquid [10]. It is true that our plasma action (equation (9.10)) is obtained from the simplest fermion loop, without dressing the fermion Green's function, and this may be the source of the difference between the results. We were guided here by the very strong anisotropy of the intermonopole potential, making it much stronger along the time direction, and requiring the neutrality constraint for each plaquette along the time direction. Our intuition is that screening may only be more effective if the two spatial dimensions are added to the one plaquette problem, thus weakening the strength of the large distance inter-monopole interaction. We hope that these ideas may lead to a more rigourous approach, and possibly Monte-Carlo studies of this plasma. Moreover, we have also presented arguments showing that a satisfactory microscopic derivation of the plasma action is still missing. One difficulty is connected to the ambiguity present while implementing the necessary periodicity requirement from a perturbative calculation which by essence assumes 'flat' field configurations. A second

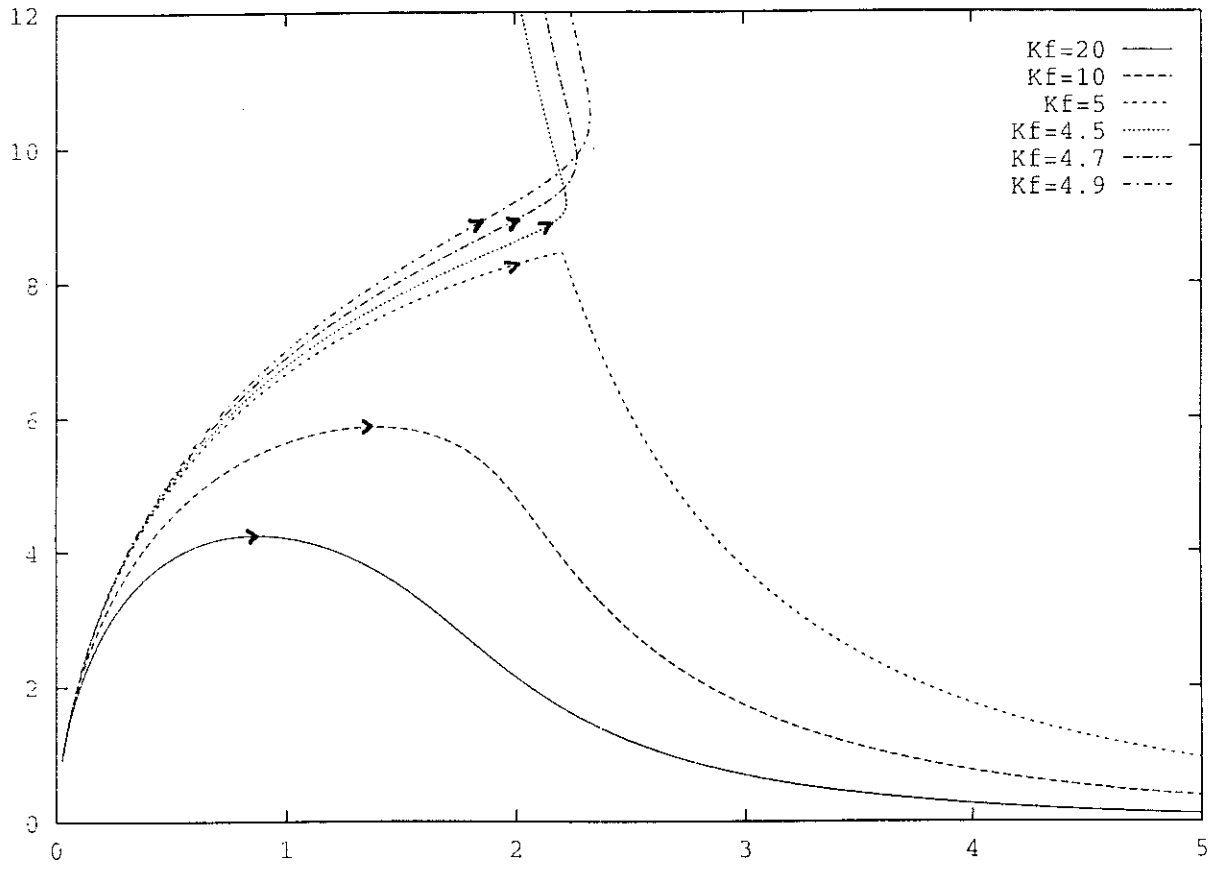

Figure 9.2:
RG trajectories for $N = 1$ and different values of the Fermi wave vector. The time coordinate is compactified on a circle of length 400. We took $\tau = 1$. Some trajectories cross each other. This is due to the fact that the potential (9.19) (9.20) depends explicitely on γ and thus on the initial conditions. We have plotted the square of he fugacity fugacity $z^2 = K^2\tau^2$ as a function of the effective inverse fictitious temperature of the monopole plasma. The dipolar phase corresponds to the fixed point $(\beta, z) = (\infty, 0)$ and the Debye screening phase corresponds to the fixed point $(\beta, z) = (0, \infty)$.

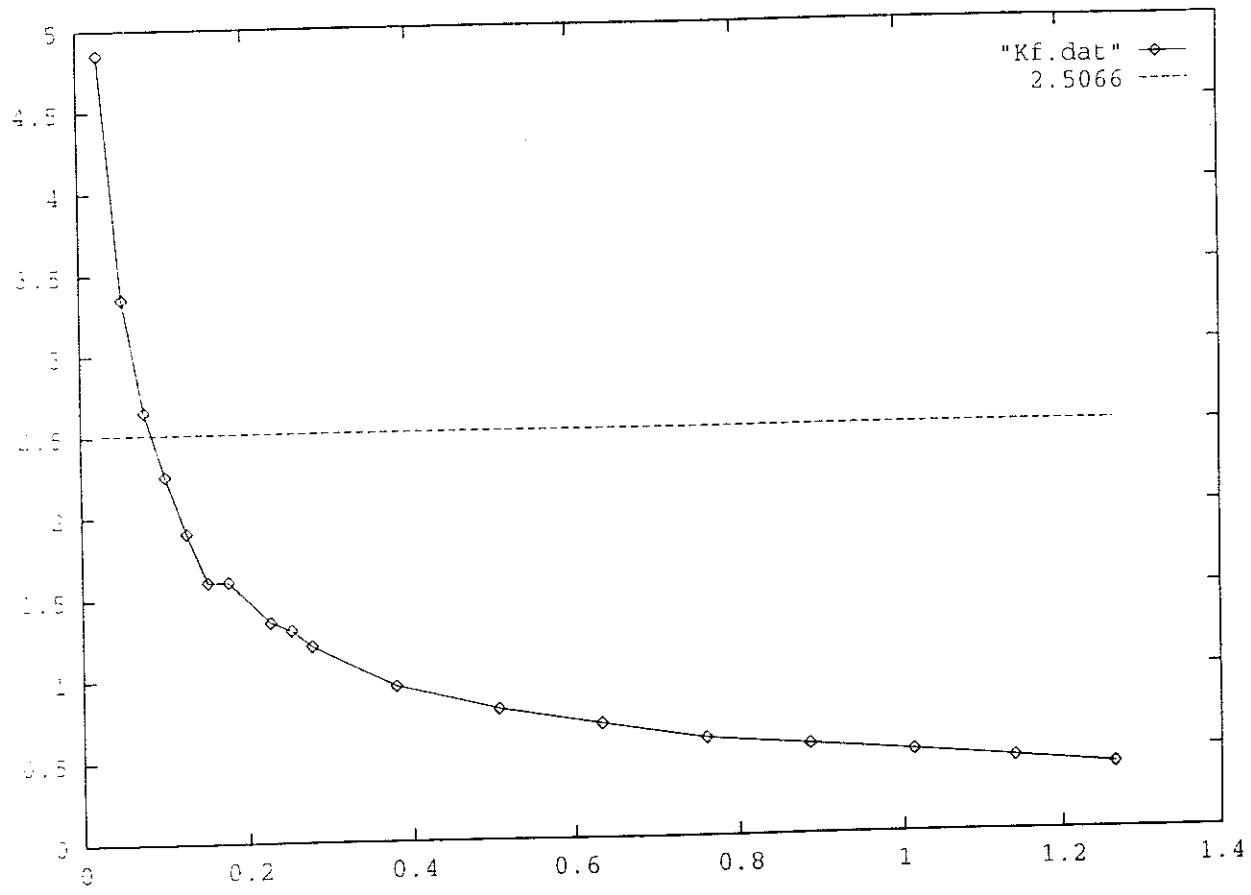

Figure 9.3:
Critical Fermi wave vector as a function of the number of colors. The errorbars indicate the precision in the location of the fixed point. The dashed line indicates the maximal value of the Fermi wave vector ($\sqrt{2\pi}$).

one, and maybe related to the previous remark, is the diverging bare fugacity which results from the Villain-type treatment developed in the Appendix. At least, we hope that the present work may stimulate a new reflection on these issues.

B.D. would like to thank J. Wheatley and D. Khveshchenko for their stimulating participation in earlier attempts to address the question of collective effects in the monopole plasma, and S. Sachdev for an interesting discussion.

9.6 Appendix: derivation of the monopole fugacity in the Ioffe-Larkin approach

We start from the quadratic action in the transverse subspace

$$S = \frac{1}{2}\frac{T}{N_s}\sum_{\omega}\sum_{k}\epsilon_1(k,\omega)e_\perp(k,\omega)e_\perp(-k,-\omega) + \mu b(k,\omega)b(-k,-\omega). \tag{9.37}$$

In this expression, b is a scalar field and $e_\perp$ is related to b by the Faraday equation

$$\omega b(k,\omega) = k \times e_\perp(k,\omega).\hat{z}. \tag{9.38}$$

Suppose we consider an instanton located on a given plaquette r_0 at time τ_0. The idea is to replace $b(r,\tau)$ by $b(r,\tau) - 2\pi\theta(b(r,\tau)-\pi)\delta_{r,r_0}$. Minimizing over transverse configurations of b leads to the instanton profile

$$e_\perp(k,\omega) = -i\frac{\mu\hat{z}\times k}{\epsilon_1(k,\omega)\omega^2+\mu k^2}q(k,\omega) \tag{9.39}$$

$$b(k,\omega) = \left(-\frac{i}{\omega} + i\frac{\epsilon_1(k,\omega)\omega}{\epsilon_1(k,\omega)\omega^2+\mu k^2}\right)q(k,\omega). \tag{9.40}$$

Here, $q(k,\omega) = 2\pi\exp\left(-i(k.r_0+\omega\tau_0)\right)$ is the corresponding topological charge density. The fugacity is obtained from considering quadratic fluctuations around the single-instanton solution and integrating them out. We have to single out the zero mode which corresponds to a global translation along the time direction of this solution. This is a standard procedure, and we just quote the result [19]

$$K = \frac{A}{\sqrt{2\pi}}\left(\frac{\prod\epsilon_i^{(0)}}{\prod_{i\neq 0}\epsilon_i}\right)^{1/2}. \tag{9.41}$$

In this formula, A is the norm of the zero mode function

$$(r,\tau) \mapsto \frac{\partial b(r,\tau)}{\partial\tau}. \tag{9.42}$$

From equation (9.40), we obtain

$$A = 2\pi\mu\left(\frac{T}{N_s}\sum_{k,\omega}\frac{k^4}{(\epsilon_1(k,\omega)\omega^2+\mu k^2)^2}\right)^{1/2}. \tag{9.43}$$

The second term is related to the ratio of the product of eigenvalues of the Hessian matrix in the vacuum and in the presence of the instanton. In the denominator, it is necessary to exclude the

zero eigenvalue coming from translation invariance. The Hessian matrix is found by expanding the action (9.37) with the shift $b(\tau,\tau) \to b(\tau,\tau) - 2\pi\theta(b(\tau,\tau)-\pi)$, up to quadratic order in field deviations $\delta b(\tau,\tau)$ around the instanton solution. Written in Fourier space, the quadratic part of the action is

$$\begin{aligned}\delta^2 S &= \frac{1}{2}\frac{T}{N_s}\sum_{k,\omega}\Delta(k,\omega)\delta b(k,\omega)\delta b(-k,-\omega) \\ &\quad -\frac{\pi\mu}{|b_0'|}\frac{T^2}{N_s^2}\sum_{k,\omega}\sum_{k',\omega'} e^{i((k-k')\tau_0+(\omega-\omega')\tau_0)}\delta b(k,\omega)\delta b(-k',-\omega').\end{aligned} \tag{9.44}$$

We have used the notations $\Delta(k,\omega) = \mu + \epsilon_1(k,\omega)\omega^2/k^2$, and

$$b_0' = \frac{\partial b}{\partial \tau}(\tau_0,\tau_0), \tag{9.45}$$

where b is the instanton profile. The eigenmodes corresponding to equation (9.44) are obtained from a rational secular equation since the scattering potential is separable. This equation reads

$$-\frac{2\pi\mu}{|b_0'|}\frac{T}{N_s}\sum_{k,\omega}\frac{1}{\epsilon-\Delta(k,\omega)} = 1. \tag{9.46}$$

From the structure of this equation, it is possible to derive the determinant ratio as

$$\frac{\prod_{i\neq 0}\epsilon_i}{\prod\epsilon_i^{(0)}} = \frac{2\pi\mu}{|b_0'|}\frac{T}{N_s}\sum_{k,\omega}\frac{k^4}{(\epsilon_1(k,\omega)\omega^2+\mu k^2)^2}. \tag{9.47}$$

Using equation (9.41), and the expression for A leads to $K = (\mu|b_0'|)^{1/2}$. From equation (9.40), we finally get

$$K = \sqrt{2\pi}\mu\left(\frac{T}{N_s}\sum_{k,\omega}\frac{k^2}{\epsilon_1(k,\omega)\omega^2+\mu k^2}\right)^{1/2}. \tag{9.48}$$

References

[1] G. Baskaran and P.W. Anderson, Phys. Rev. B 37, 580 (1988).

[2] Z. Zou and P.W. Anderson, Phys. Rev. B 37, 627 (1988).

[3] L.B. Ioffe and A.I. Larkin, Phys. Rev. B 39, 8988 (1989).

[4] M. Grilli and G. Kotliar, Phys. Rev. Lett. 64, 1170 (1990).

[5] J.P. Rodriguez and B. Douçot, Europhys. Lett. 11, 451 (1990).

[6] N. Nagaosa and P.A. Lee, Phys. Rev. Lett. 64, 2450 (1990).

[7] L.B. Ioffe and P.B. Wiegmann, Phys. Rev. Lett. 65, 653 (1990); L.B. Ioffe and G. Kotliar, Phys. Rev. B 42, 10348 (1990).

[8] R. Hlubina, W.O. Putikka, T.M. Rice, D.V. Khveshchenko, Phys. Rev. B 46, 11224 (1992).

[9] See for instance A.M. Polyakov, *Gauge fields and strings*, Hardwood Academic Publishers, Chur (1987), chapters 4 and 5.

[10] N. Nagaosa, Phys. Rev. Lett. 71, 4210 (1993).

[11] R. Fazio and G. Schön, Phys. Rev. B 43, 5307 (1991).

[12] For a brief review, see for instance E.H. Lieb in *Mathematical problems in theoretical physics*, Lecture notes in Physics, volume 80, Springer-Verlag (1978), edited by G. Dell'Antonio, S. Doplicher and G. Jona-Lasinio; and M. Toda, R. Kubo and N. Saito in *Statistical physics I*, Springer Series in Solid State Science 30, Springer-Verlag (1983), pp 135-137.

[13] F.J. Dyson, Comm. Math. Phys. 12, 212 (1969); J. Fröhlich, R. Israel, E. Lieb and B. Simon, Comm. Math. Phys. 62, 1 (1978).

[14] A. Lenard, Jour. Math. Phys., 2, 682 (1961).

[15] M. Aizenman and J. Fröhlich, Jour. Stat. Phys. 26, 347 (1981).

[16] P.W. Anderson, G. Yuval and D.R. Hamman, Phys. Rev. B 1, 4464 (1970).

[17] J.M. Kosterlitz, J. Phys. C 7, 1046 (1974).

[18] J.M. Kosterlitz, J. Phys. C 10, 3753 (1977).

[19] See for instance J.S. Langer, Ann. Phys. 41, 108 (1967).

Chapitre 10

Effet Hall quantique à demi remplissage

Le but de ce chapitre est de présenter une introduction à l'effet Hall quantique à demi remplissage. Nous nous contenterons de donner quelques idées sur le problème de l'effet Hall quantique fractionnaire en général. Dans le cas d'un remplissage ν appartenant à la hiérarchie, le liquide obtenu est *incompressible*, c'est-à-dire qu'il existe un gap dans le spectre d'excitations, alors que le cas $\nu = 1/2$ correspond à un fluide de Hall *compressible*, avec des excitations sans gap. Une autre différence entre le cas $\nu = 1/2$ et les autres fractions de la hiérarchie est l'absence d'un plateau dans la conductivité de Hall tracée en fonction du champ magnétique. Une des notions importantes dans la théorie de l'effet Hall quantique à demi remplissage est la notion de statistique fractionnaire et de champ de jauge de Chern-Simons. Ces idées seront exposées dans ce chapitre. Nous présenterons ensuite le traitement en champ moyen du champ de jauge statistique, tel que l'ont développé Halperin, Lee et Read[1]. Le chapitre suivant présentera une expérience propre à tester la validité de cette théorie de champ moyen. Mais commençons tout d'abord par calculer le spectre d'un système d'électrons bidimensionnels sans interactions sous champ magnétique.

10.1 Fermions bidimensionnels sans interactions sous champ magnétique

On considère un système de fermions sans spin astreints à se mouvoir dans le plan (O, x, y), et soumis à un champ magnétique uniforme B dirigé le long de l'axe (Oz). Ce problème a été résolu par Landau, dans la jauge dite de Landau. Il est clair que le résultat final, à savoir le spectre, ne dépend pas du choix de la jauge, c'est pouquoi nous travaillons dans une jauge particulière, avec les composantes suivantes du potentiel vecteur:

$$A_x = -By \tag{10.1}$$

$$A_y = 0 \tag{10.2}$$

$$A_z = 0 \tag{10.3}$$

[1] B.J. Halperin, P.A. Lee and N. Read, *Theory of the half-filled Landau level*, Phys. Rev. B 47, 7312-7343 (1993).

En choisissant la charge électrique égale à $-e$, le Hamiltonien d'un seul fermion s'écrit

$$H = \frac{1}{2m}(i\hbar\nabla + e\mathbf{A})^2 \tag{10.4}$$

$$= \frac{\hbar^2}{2m}((-i\frac{\partial}{\partial x} - \frac{eB}{\hbar}y)^2 - \frac{\partial^2}{\partial y^2}). \tag{10.5}$$

On cherche les solutions sous la forme

$$\psi(x,y) = e^{ikx}\phi(y), \tag{10.6}$$

et l'équation de Schrödinger s'écrit

$$\frac{\hbar^2}{2m}\frac{eB}{\hbar}\left((kl - \frac{y}{l})^2 - (l\frac{\partial}{\partial y})^2\right)\phi(y) = E\phi(y), \tag{10.7}$$

où l est la longueur magnétique

$$l = \left(\frac{\hbar}{2B}\right)^{1/2}. \tag{10.8}$$

En posant $u = kl - y/l$, l'équation de Schrödinger se met sous la forme

$$\frac{\hbar\omega_c}{2}\left((i\frac{\partial}{\partial u})^2 + u^2\right)\phi = E\phi, \tag{10.9}$$

où la fréquence cyclotron ω_c est définie par

$$\omega_c = \frac{eB}{m}. \tag{10.10}$$

On reconnaît ici le Hamiltonien d'un oscillateur harmonique, dont le spectre est donné par

$$E_n = (n + \frac{1}{2})\hbar\omega_c, \tag{10.11}$$

et les états propres sont

$$\psi_{k,n}(x,y) = e^{ikx}H_n(\frac{y}{l} - kl)\exp - \left(\frac{(y - kl^2)^2}{2l^2}\right), \tag{10.12}$$

où $H_n(x)$ est le n-ième polynôme d'Hermite. Pour un échantillon de taille finie (L_x, L_y), et si l'on impose des conditions aux limites périodiques le long de l'axe (Ox), la dégénérescence d'un niveau de Landau est finie et se calcule comme suit. Le vecteur d'onde k est quantifié en unités $2\pi/L$: $k = 2\pi n/L$, où n est un entier relatif, et la fonction d'onde est centrée le long de la ligne $y = kl^2$. Le nombre de façons de centrer une fonction d'onde sur le rectangle est simplement

$$N_\phi = \frac{L_y}{\frac{2\pi}{L_x}l^2}, \tag{10.13}$$

d'où la dégénerescence N_ϕ de chaque niveau de Landau qui vaut

$$N_\phi = \frac{L_xL_y}{2\pi l^2} = \frac{\phi}{\phi_0}, \tag{10.14}$$

où $\phi_0 = h/e$ est le quantum de flux. On appelle taux de remplissage ν le rapport du nombre d'électrons N sur le nombre d'états N_ϕ dans un niveau de Landau:

$$\nu = \frac{N}{N_\phi}. \tag{10.15}$$

10.2 Effet Hall quantique

Comment se comporte un liquide d'électrons bidimensionnels sous champ magnétique intense et à basse température? La réponse à cette question fut d'abord donnée par l'expérience. Ensuite suivi la théorie de Laughlin du cas $\nu = 1/3$. Nous décrivons tout d'abord l'expérience de Von Klitzing[2]. Ensuite, nous aborderons brièvement l'approche théorique[3].

10.2.1 Mise en évidence expérimentale de l'effet Hall quantique fractionnaire

Le dispositif physique qui permet de réaliser une couche d'électrons bidimensionnels est une *hétérojonction* ou MOSFET. A l'interface entre une couche d'isolant et une couche de semi-conducteur, les électrons sont confinés dans un puits de potentiel profond localisé sur le plan $(0, x, y)$. Le courant est alors nul le long de la direction (Oz). Un exemple d'hétérojonction est la jonction GaAs-GaAlAs. L'interface est refroidie à quelques Kelvins et placée sous champ magnétique intense perpendiculaire à l'interface. On appelle *résistance de Hall* le rapport

$$R_H = \frac{V_x}{I_y}, \tag{10.16}$$

où l'on applique une différence de potentiel V_x le long de la direction (Ox) et on mesure l'intensité I_y dans la direction (Oy). La quantité R_H est une constante, indépendante de V_x. La théorie classique stipule que la force de Lorentz et la force électrique s'annulent le long de la direction (Oy), ce qui conduit à la valeur suivante pour la résistance de Hall:

$$R_H = \frac{1}{\nu}\frac{h}{e^2}. \tag{10.17}$$

La conductivité de Hall σ_H est définie par

$$\sigma_H = \frac{h}{e^2} R_H^{-1} = \nu. \tag{10.18}$$

La théorie classique prédit donc une variation linéaire de la conductivité de Hall σ_H avec le facteur de remplissage ν.

Les principaux faits concernant les expérience d'effet Hall quantique sont les suivants[4]. Les résultats expérimentaux ont montré que la conductivité de Hall σ_H possédait des plateaux en fonction de ν pour des valeurs entières de ν. Ces plateaux sont corrélés avec une très forte diminution de la résistance longitudinale (dans la direction (Ox)). Il s'avère que la précision avec laquelle se produit l'effet Hall quantique entier est très élevée puisque les plateaux se produisent avec une précision de 10^{-8}. Une mesure d'effet Hall quantique permet de mesurer la constante de structure fine α. Cette constante régit le couplage du champ électromagnétique à la matière en électrodynamique quantique, et s'exprime selon

$$\alpha = \frac{\mu_0 c}{2}\frac{e^2}{h} = \frac{\mu_0 c}{2}\frac{1}{\nu R_H} \tag{10.19}$$

[2]K. von Klitzing, G. Dorda and M. Pepper, *New method for high accuracy determination of the fine structure constant based on quantized Hall resistance*, Phys. Rev. Lett. 45, 494 (1980).

[3]Laughlin, *Anomalous quantum Hall effect: an incompressible quantum fluid with fractionally charged excitations*, Phys. Rev. Lett. 50, 1395 (1983).

[4]J. Fröhlich *Mathematical aspects of the quantum Hall effect* (1992).

pour ν entier. La très grande précision obtenue pour α à partir d'une expérience d'effet Hall quantique entier permet de comparer α avec les calculs les plus précis d'électrodynamique quantique. Une mesure d'effet Hall quantique entier permet donc de tester l'électrodynamique quantique.

En 1982, ont été mis en évidence[5] des plateaux pour des valeurs rationnelles du taux de remplissage ν, ce qui constitue l'effet Hall quantique fractionnaire. Plus récemment[6] on a prouvé expérimentalement que pour un plateau à remplissage fractionnaire, le système présente des excitations de charge fractionnaire.

10.2.2 Théorie de l'effet Hall quantique: quelques idées

L'effet Hall quantique entier s'explique comme un phénomène à une particule dans des échantillons relativement sales. Au contraire, l'effet Hall quantique fractionnaire correspond à des effets de corrélations dans des échantillons propres. Nous allons donner les grandes lignes de la théorie de l'effet Hall quantique fractionnaire, pour passer ensuite à la théorie du cas $\nu = 1/2$. La théorie de l'effet Hall quantique fractionnaire à $\nu = 1/3$ est due à Laughlin. En utilisant la jauge symétrique

$$\mathbf{A} = \frac{B}{2}(y, -x), \tag{10.20}$$

et en supposant le fondamental non dégénéré, Laughlin cherche la fonction d'onde du fondamental sous forme d'un *produit de Jastrow*

$$\psi(z_1, ..., z_N) = \prod_{j<k} f(z_j - z_k) \exp\left(-\frac{1}{4}\sum_{l=1}^{N} |z_l|^2\right), \tag{10.21}$$

où $f(z) \to 0$ lorsque $z \to +\infty$, et $z_i = x_i + iy_i$ dénote la coordonnée complexe de la i-ème particule. En utilisant le fait que tous les états restent sur le premier niveau de Landau, que la fonction d'onde est fermionique, et donc $f(-z) = -f(z)$, que la fonction d'onde est un état propre du moment angulaire, on obtient la *fonction d'onde de Laughlin*

$$\psi(z_1, ..., z_N) = \prod_{j<k} (z_j - z_k)^m \exp\left(-\frac{1}{4}\sum_{l=1}^{N} |z_l|^2\right). \tag{10.22}$$

Cette fonction d'onde d'essai décrit l'état fondamental de l'effet Hall quantique pour un taux de remplissage $\nu = 1/m$. Les excitations de l'état de Laughlin s'obtiennent par passage adiabatique d'un quantum de flux ϕ_0 localisé en un point z_0 du fluide de Hall. On peut montrer que ces excitations portent une charge $1/m$ car une fraction $1/m$ d'un électron a été expulsée du voisinage de z_0. Il existe également un gap Δ entre le fondamental et l'excitation d'énergie la

[5] D.C. Tsui, H.L. Störmer and A.C. Gossard, *Two-dimensional magneto-transport in the extreme quantum limit*, Phys. Rev. Lett. 48, 1559 (1982).

[6] R.G. Clark, J.R. Mallet, S.R. Haynes, J.J. Harris and C.T. Foxon, *Experimental determination of fractional charge e/q for quasiparticule excitations in the fractional quantum Hall effect*, Phys. Rev. Lett. 60, 1747 (1988); A.M. Chang and J.E. Cunningham, *Transmission and reflection probabilities between $\nu = 1$ and $\nu = 2/3$ quantum Hall effects, and between $\nu = 2/3$ and $\nu = 1/3$ effects*, Solid State Comm. 72, 652 (1989); J.A. Simons, H.P. Wei, L.W. Engel, D.C. Tsui and M. Shayegan, *Resistance fluctuations in narrow AlGaAs-GaAs heterostructures: direct evidence of fractional charge in the fractional quantum Hall effect*, Phys. Rev. Lett. 63, 1731 (1989); S.W. Huang and al, Surf. Sc. 263, 72 (1992).

plus basse, et les excitations de l'effet Hall quantique fractionnaire obéissent à des statistiques fractionnaires[7,8] d'angle topologique π/m.

La description des autres fractions de l'effet Hall fractionnaire conduisant à l'existence d'un plateau pour des taux de remplissage différents de $1/m$, avec m impair, se fait à l'aide de *hiérarchies*, dont le point de départ est la théorie de Laughlin. L'idée centrale de la hiérarchie de Halperin[7] et de Haldane[9] consiste à faire condenser les quasiparticules de l'état de Laughlin, de même que dans la théorie de Laughlin, les électrons condensent en quasiparticules. En itérant ce processus, on obtient une hiérarchie de taux de remplissages pour lesquels on prédit l'existence d'un plateau dans la conductivité de Hall.

10.3 Statistiques fractionnaires

La théorie de l'effet Hall quantique fractionnaire fait intervenir des anyons au sens de fermions décorés par un champ topologique de Chern-Simons, mais ces anyons ont la particularité de posséder des statistiques fermioniques, c'est-à dire un angle topologique de 3π. J'oublie provisoirement cette valeur particulière de l'angle topologique pour présenter la notion de statistique fractionnaire sur le cas plus général d'un angle topologique quelconque. Le point de vue dans cette section est également différent de celui adopté dans l'effet Hall quantique à $\nu = 1/2$. Dans ce dernier cas, on part d'un système de fermions, puis on effectue une transformation de jauge qui transforme les fermions initiaux en fermions décorés par des tubes de flux. Dans cette section, on se donne au contraire un système d'anyons et on cherche la transformation de jauge qui transforme ce système d'anyons en bosons décorés par des tubes de flux. Bien que le point de vue soit quelque peu différent, il apparait dans les deux cas un champ de jauge de Chern-Simons associé à un changement de statistique.

Adoptons donc le point de vue formel qui consiste à se donner un système de particules à statistiques fractionnaires[10,11]. Soit donc N particules indiscernables, dans un espace physique de dimension D. On cherche à décrire l'espace des configurations C_N^D du système. La topologie de C_N^D est décrite par son groupe fondamental ou groupe d'homotopie π^1. Si $D = 3$, le groupe d'homotopie est isomorphe au groupe des permutations de N objets S_N. C'est la raison pour laquelle la statistique à trois dimensions est soit bosonique, soit fermionique. C'est-à-dire que si $\psi(\mathrm{x}_1, ..., \mathrm{x}_N)$ désigne la fonction d'onde du système avec la particule 1 en x_1, ..., la particule N en x_N, et si $P \in S_N$, alors,

$$P\psi(\mathrm{x}_1, ..., \mathrm{x}_N) = \epsilon(P)\psi(\mathrm{x}_1, ..., \mathrm{x}_N), \tag{10.23}$$

où $\epsilon(P)$ vaut $+1$ pour des bosons et la signature de la permutation P pour des fermions. A deux dimensions, la situation est différente car le groupe fondamental de C_N^2 est isomorphe au groupe des tresses T_N. Le groupe des tresses est défini par ses générateurs σ_i (avec $\sigma_i^2 \neq 1$) et par les relations

$$\sigma_i\sigma_{i+1}\sigma_i = \sigma_{i+1}\sigma_i\sigma_{i+1} \tag{10.24}$$

$$\sigma_i\sigma_j = \sigma_j\sigma_i, \tag{10.25}$$

[7] B.I. Halperin, Phys. Rev. Lett. 53, 1583 (1984).

[8] D.P. Arovas, J.R. Schrieffer and F. Wilczek, *Fractional statistics and the quantum Hall effect*, Phys. Rev. Lett. 53, 722 (1984).

[9] F.D.M. Haldane, Phys. Rev. Lett. 51, 605 (1983).

[10] D. Carpentier, rapport de stage de Maîtrise sous la direction de B. Douçot (1994).

[11] Lerda, *Anyons, quantum mechanics of particles with fractional statistics*, to be published

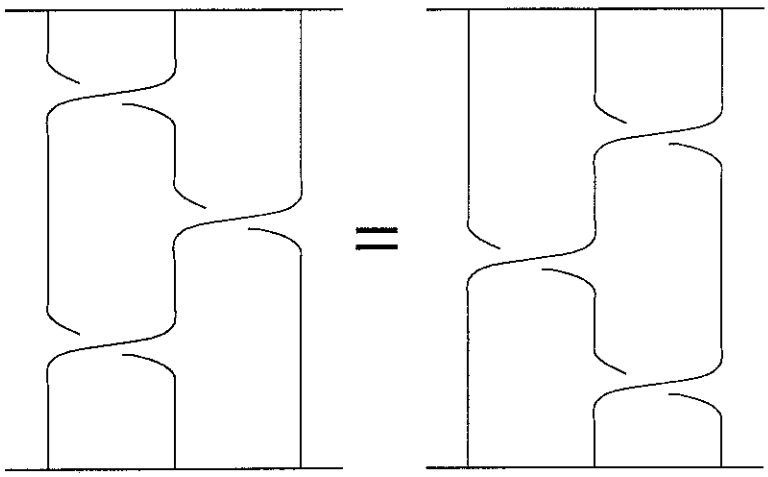

Figure 10.1: Représentation de la relation de Yang-Baxter $\sigma_i\sigma_{i+1}\sigma_i = \sigma_{i+1}\sigma_i\sigma_{i+1}$.

où la dernière relation est valable si $|i-j| \geq 2$. Tout élément du groupe des tresses s'écrit comme le produit des σ_i et de leurs inverses. On peut représenter une tresse de façon picturelle en se donnant un point base et un entrelacement de N fils, en excluant la possibilité d'avoir simultanément deux fils au même point. Par exemple, la relation (10.24) est représentée par la figure 10.1. La mécanique quantique du système d'anyons est donnée par l'intégrale de chemin pour le propagateur[11]

$$K(\mathbf{q},t,\mathbf{q},t') = \sum_{\alpha\in T_N} \chi(\alpha) K_\alpha(\mathbf{q},t,\mathbf{q},t'), \tag{10.26}$$

où $\mathbf{q}$ désigne le vecteur à N composantes $(\mathbf{x}_1,...,\mathbf{x}_N)$, χ est une représentation unitaire du groupe des tresses et K_α est le propagateur dans une classe d'homotopie donnée. On se restreint au cas où le point de départ est identique au point d'arrivée[12]. La relation (10.25) impose que $\chi(\sigma_i) = \chi(\sigma_{i+1})$, et il reste un seul paramètre $\chi(\sigma_1) = \exp(i\pi\theta)$ où θ est l'angle statistique. La mécanique quantique d'un système d'anyons est donc décrite par le Hamiltonien

$$H = \sum_{i=1}^{N} \frac{\mathbf{p}_i^2}{2m} \tag{10.27}$$

et par l'action sur la fonction d'onde des générateurs du groupe des tresses

$$\sigma_i\psi(\mathbf{x}_1,...,\mathbf{x}_N) = e^{i\pi\nu}\psi(\mathbf{x}_1,...,\mathbf{x}_N). \tag{10.28}$$

Nous allons montrer que ce problème est équivalent à un système de bosons en interaction via un champ de jauge de Chern-Simons. On définit la transformation de jauge suivante:

$$\psi'(\mathbf{x}_1,...,\mathbf{x}_N) = e^{-i\nu\sum_{i<j}\theta_{ij}}\psi(\mathbf{x}_1,...,\mathbf{x}_N), \tag{10.29}$$

où θ_{ij} est l'angle entre l'axe (Ox), choisi arbitrairement, et le vecteur $\mathbf{r}_{ij} = \mathbf{x}_i - \mathbf{x}_j$. En écrivant la transformation des angles θ_{ij} sous l'action d'un générateur σ_i du groupe des tresses, il n'est pas difficile de voir que

$$\sigma_i\psi' = \psi', \tag{10.30}$$

[12]Dans le cas contraire, le groupe de tresses est remplacé par la notion de groupoïde fondamental

c'est-à-dire que le système transformé de jauge possède une statistique bosonique. Le prix à payer pour le passage à la statistique bosonique est l'apparition d'une interaction instantanée de type Chern-Simons dans le Hamiltonien. Le gradient de la fonction d'onde ψ' s'écrit

$$\nabla_k \psi' = \left(\nabla_k - i\nu \sum_{i<k} (\nabla_k \theta_{ki}) \right) \psi' = \left(\nabla_k - i\nu \sum_{i \neq j} \frac{\mathbf{z} \wedge \mathbf{r}_{ij}}{|\mathbf{r}_{ij}|^2} \right) \psi'. \tag{10.31}$$

On en déduit l'opérateur impulsion après transformation de jauge

$$\mathbf{p}'_i = \mathbf{p}_i - e\mathbf{a}(\mathbf{x}_i) \tag{10.32}$$

avec le potentiel vecteur topologique

$$\mathbf{a}(\mathbf{x}) = \frac{\hbar\nu}{e} \sum_i \frac{\mathbf{z} \wedge (\mathbf{x} - \mathbf{x}_i)}{|\mathbf{x} - \mathbf{x}_i|^2} \tag{10.33}$$

Si l'on interprète **a** comme un potentiel vecteur électromagnétique, on voit que le champ magnétique correspondant est nul en dehors des singularités de a et vaut

$$\mathbf{B}(\mathbf{x}) = \nabla \wedge \mathbf{a}(\mathbf{x}) \tag{10.34}$$

$$= \frac{h\alpha}{e} \sum_{j \neq i} \delta(\mathbf{x} - \mathbf{x}_i)\mathbf{z}. \tag{10.35}$$

Tout se passe donc comme si l'on avait attaché à chaque boson un solénoïde infiniment fin perpendiculaire au plan et traversé par un flux $\nu\phi_0$. Comme nous le verrons par la suite, cette interprétation est à la base de la théorie de champ moyen de l'effet Hall quantique à demi remplissage. Cependant, il est clair que a ne représente en aucun cas un potentiel vecteur électromagnétique. Par exemple, ce champ ne vérifie pas les équations de propagation issues des équations de Maxwell.

10.4 Effet Hall quantique à $\nu = 1/2$

Nous abordons maintenant la théorie de l'effet Hall quantique à demi remplissage. Le système est constitué d'électrons en interaction Coulombienne et sous champ magnétique tel que $\nu = 1/2$. Le champ magnétique est suffisamment intense pour polariser les spins, et on peut donc oublier que les électrons portent un spin. La théorie de ce système est traitée dans l'article de Halperin, Read et Lee[1]. Le Hamiltonien est égal à un terme cinétique auquel s'ajoute une interaction Coulombienne entre électrons:

$$H = K + V \tag{10.36}$$

En seconde quantification, le terme cinétique s'écrit

$$K = \frac{1}{2m_b} \int d\mathbf{x} \psi^+(\mathbf{x}) \left(-i\hbar\nabla + e\mathbf{A}(\mathbf{x}) \right)^2 \psi(\mathbf{x}), \tag{10.37}$$

et le terme potentiel vaut

$$V = \frac{1}{2} \int d\mathbf{x} d\mathbf{x}' v(\mathbf{x} - \mathbf{x}') : \rho(\mathbf{x})\rho(\mathbf{x}') :, \tag{10.38}$$

où

$$v(\mathrm{r}) = \frac{e^2}{4\pi\epsilon_0\epsilon_r|\mathrm{r}|}. \tag{10.39}$$

L'opérateur de densité est défini par

$$\rho(\mathrm{x}) = \psi^+(\mathrm{x})\psi(\mathrm{x}), \tag{10.40}$$

et l'ordre normal est pris par rapport aux opérateurs de création et d'annihilation. La masse m_b est la masse de bande des électrons, c'est-à-dire la masse renormalisée en présence de phonons. Partant de ce système de fermions, on peut réaliser la transformation de jauge décrite au paragraphe précédent. Le paramètre initial de la statistique est $\nu = 1$, qui correspond à une statistique de fermions. On choisit la transformation de jauge de telle sorte que le paramètre final de la statistique soit $\nu = 3$. L'opérateur de champ après transformation de jauge se déduit aisément de (10.28) selon

$$\psi'^+(\mathrm{x}) = \psi^+(\mathrm{x}) \exp\left(-2i \int d\mathrm{x}'\theta(\mathrm{x},\mathrm{x}')\rho(\mathrm{x}')\right), \tag{10.41}$$

où $\theta(\mathrm{x},\mathrm{x}')$ est l'angle est l'axe (Ox) arbitraire et le vecteur $\mathrm{x}-\mathrm{x}'$. Le Hamiltonien transformé de jauge vaut

$$K = \frac{1}{2m_b} \int d\mathrm{x}\psi'^+(\mathrm{x}) \left(-i\hbar\nabla + e\mathbf{A}(\mathrm{x}) - e\mathbf{a}(\mathrm{x})\right)^2 \psi'(\mathrm{x}), \tag{10.42}$$

où le potentiel vecteur topologique vaut

$$\mathbf{a}(\mathrm{x}) = \frac{2h}{e} \int d\mathrm{x}' \frac{\mathbf{z} \wedge (\mathrm{x}-\mathrm{x}')}{|\mathrm{x}-\mathrm{x}'|^2} \rho(\mathrm{x}'). \tag{10.43}$$

Cette transformation de jauge présente la particularité de préserver la statistique tout en introduisant un champ de Chern-Simons dont le flux moyen est exactement opposé au flux du champ magnétique extérieur, à cause de la condition $\nu = 1/2$. Par ailleurs, l'interaction Coulombienne est covariante sous la transformation de jauge car

$$\rho(\mathrm{x}) = \psi^+(\mathrm{x})\psi(\mathrm{x}) = \psi'^+(\mathrm{x})\psi'(\mathrm{x}) = \rho'(\mathrm{x}). \tag{10.44}$$

Pourquoi avoir apparemment compliqué le problème de départ en introduisant des anyons? La raison est que l'on est maintenant en mesure de formuler une théorie de champ moyen et une théorie R.P.A. pour les fermions composites non locaux $\psi'^+(\mathrm{x})$ sous un flux total nul (flux du champ magnétique extérieur + flux du champ topologique). Le champ moyen correspond à la situation où le champ de jauge est uniforme (c'est-à-dire que la densité de fermions est uniforme) et égal à sa valeur moyenne. Le Hamiltonien de champ moyen vaut simplement

$$H_{C.M.} = \frac{1}{2m_b} \int d\mathrm{x}\psi'^+(\mathrm{x})(-i\hbar\nabla)\psi'(\mathrm{x}). \tag{10.45}$$

Au niveau du champ moyen, et en se plaçant en géométrie torique, l'état fondamental est une mer de Fermi de vecteur d'onde de Fermi

$$k_F = 1/l = (4\pi n)^{1/2}, \tag{10.46}$$

où l est la longueur magnétique donnée par (10.8) et n est la densité moyenne. C'est cette théorie de champ moyen que nous utiliserons dans le chapitre 11 pour décrire le fluide de Hall à $\nu = 1/2$. Il est possible de développer une théorie R.P.A. pour ressommer une partie des fluctuations du champ de jauge. Une telle approche conclut au caractère *liquide de Fermi* compressible de l'état $\nu = 1/2$. Cette conclusion est vérifiée numériquement[13] à partir de diagonalisations numériques. Du point de vue expérimental, Jiang *et al*[14] ont observé que le gaz d'électrons de l'effet Hall quantique à demi remplissage forme un état métallique même à très basse températures. Les expériences suggèrent donc que l'état $\nu = 1/2$ forme donc un état métallique à température nulle. Ces expériences ont motivé une série de travaux théoriques, dont la théorie de Halperin, Lee et Read[1].

[13] E. Rezzayi and N. Read, *Fermi liquid like state in a half-filled Landau level*, Phys. Rev. Lett. 72, 900 (1994).
[14] H. W. Jiang *et al*, Phys. Rev. B 40, 12013(1989).

Chapitre 11

Article 5

$\nu = 1/2$ quantum Hall effect in the Aharonov-Casher geometry[1]

R. Mélin and B. Douçot

CRTBT-CNRS, 38042 Grenoble BP 166X cédex France

We study the effect of an electric charge in the middle of a ring of a electrons in a magnetic field such as $\nu = 1/2$. In the absence of the central charge, a residual current should appear due to an Aharanov-Bohm effect. As the charge varies, periodic currents should appear in the ring. We evaluate the amplitude of these currents, as well as their period as the central charge varies. The presence of these currents should be a direct signature of the existence of a statistical gauge field in the $\nu = 1/2$ quantum Hall effect. Numerical diagonalizations for a small number of electrons on the sphere are also carried out.

[1]Submitted to Phys. Rev. B

11.1 Introduction

Recently, new experimental and theoretical developments have generated alternative viewpoints in the current understanding of the fractional quantum Hall effect. It seems the key idea is the notion of composite fermions, first introduced by Jain [1], which establishes a aorrespondence between the fractional quantum Hall effect at lowest Landau level filling $\nu = p/(2mp \pm 1)$ and the integer quantum Hall effect with p filled Landau levels. The mapping is achieved by attaching $2m$ flux quanta to each electron, which preserves fermionic statistics, and by first treating the statistical fluxes at the mean field level. This description has received considerable attention especially in the vicinity of $\nu = 1/2$. Experimentally, the system is characterized by a vanishing energy gap, and various physical properties strongly suggest the presence of a new Fermi liquid [2] in this problem. On the theoretical side, the composite picture with $m = 1$ has been advocated by Halperin, Lee and Read as a powerfull microscopic basis to understand these Fermi liquid-like properties in the vicinity of $\nu = 1/2$ [3]. The vanishing of the gap for the sequence of states at $\nu = p/(2p \pm 1)$ as p goes to infinity receives for instance a very simple interpretation in this framework in this framework since the composite fermions experience an average flux equal to ϕ_0/p per particle, so the corresponding Landau level spacing goes as $1/p$. If the statistical gauge field fluctuations are taken into account, some complications arise since a logarithmic divergence of the effective mass as $p \to +\infty$ is predicted [3] [5]. There has been some trends in recent observation suggesting an effective mass enhancement [6] but this question is not settled yet. This theory has also been tested by numerical diagonalizations on finite systems [7] [8], and the composite fermion picture has been shown to predict for instance the right quantum numbers for the ground state and low-lying states [7], as well as the scaling of the ground state energy versus particule number [8]. Furthermore, a trial wave function inspired by these considerations provides a very good understanding of ground state correlations. We note however that this wave function is not merely the singular gauge transformation applied to the Slater determinant of composite fermions moving in zero external field, but it has to be improved by the combined effect of a short range Jastrow factor and a global projection on the lowest Landau level.

In this paper, we suggest a different test for the composite fermion approach. The basic idea is connected to the fact that if an external electric field generates a spatially dependent electronic density, the average flux acting on the composite fermions is no longer vanishing everywhere. We wish to detect such a variation of the effective flux. To this purpose, the most sensitive experiment would involve the detection of an Aharonov-Bohm type effective flux, since large fluxes may be obtained from tiny magnetic fields if particules move around large enough loops. In the experiment we propose, local density fluctuations are created in a ring of $\nu = 1/2$ fermions, thanks to the presence of an electric charge localized in the middle of the ring. Due to the presence of this charge, the electrons have a trend to accumulate at the external edge of the ring if the central charge is negative, which creates a non zero effective flux through the ring. A consequence of this non zero flux is the existence of observable persistent currents which vary periodically with the value of the charge in the center of the ring. At first galnce, this phenomenon is reminiscent of the Aharonov-Casher effect, which is expected to take place if a flux tube moves around a fixed charge. [9]. This effect is a direct consequence of the Aharonov-Bohm effect and of Lorentz invariance, since the static electric field generated by the charge induces a non-vanishing magnetic field in the flux-tube co-moving frame. Experimentally, it has been observed with superconducting vortices in Josephson junction arrays [10]. However,

we should emphasize here that the composite fermions do not carry the physical magnetic field which obeys Maxwell's equations, but rather a Chern-Simon flux, so the two situations are physically quite different.

This paper is organized as follows. We first sum up the formalism to deal with the mean field approach of the $\nu = 1/2$ quantum Hall effect. We then describe the geometry of the experiment, and propose a simplified geometry to get rid of the effects of curvature. In the absence of the central charge, one is able to solve exactly the eigenstates of the problem in the geometry of the experiment. In the presence of a central charge, the ring is electrically polarized. We propose a self consistent approach to find the electron density in the ring. Due to the presence of screening, the density fluctuations are localized in the vicinity of the edges of the ring. We finally obtain an order of magnitude for the average magnetic field through the ring. The value of the average flux is rederived using a classical approach. We calculate the current in the ring as a function of the central charge. We then present numerical computations of the effect on the sphere. After briefly writing the mean field theory on the sphere, we give numerical results for $\nu = 1/2$ as well as for $\nu \neq 1/2$. A conclusion discusses the various results and mentions some open questions.

11.2 Mean field theory at $\nu = 1/2$

11.2.1 Gauge transformation at $\nu = 1/2$

We first sum up the mean field theory treatment of the half field Landau level [3]. It is possible to transform the original fermions in the magnetic field into new fermionic composite particules, with two flux quanta attached to them. The reason why attaching two flux quanta leads to fermions is that when one interchanges two particules with a flux ϕ attached to them, one gets a phase factor of $\exp i\theta$ in the wave function, with

$$\theta = \pi(1 + \frac{\phi}{\phi_0}), \tag{11.1}$$

where $\theta = \pi$ refers to fermionic particules. $\phi_0 = h/e$ is the quantum flux. The case $\phi = 2\phi_0$ thus corresponds to fermionic particules since in this case θ is π modulo 2π. The flux tubes are fixed via a non local gauge transformation, implemented in the following way. The second quantized form of the kinetic term in the Hamiltonian reads

$$\hat{K} = \frac{1}{2M} \int d^2\mathrm{x}\psi^+(\mathrm{x})(-i\hbar\nabla + e\mathbf{A}(x))^2\psi(\mathrm{x}), \tag{11.2}$$

where M is the band electronic mass, e the absolute value of the electronic charge and $\psi^+(\mathrm{x})$ the electronic field. The gauge transformation which realizes the passage from the electronic field $\psi^+(\mathrm{x})$ to the composite fermionic field $\psi_C^+(\mathrm{x})$ is given by

$$\psi_C^+(\mathrm{x}) = \psi^+(\mathrm{x}) \exp\{-2i \int d^2\mathrm{x}' arg(\mathrm{x} - \mathrm{x}')\hat{\rho}(\mathrm{x}')\} \tag{11.3}$$

where

$$\hat{\rho}(\mathrm{x}) = \psi^+(\mathrm{x})\psi(\mathrm{x}) = \psi_C^+(\mathrm{x})\psi_C(\mathrm{x}) = \hat{\rho}_C(\mathrm{x}), \tag{11.4}$$

and $arg(\mathbf{x}-\mathbf{x}')$ is the angle between the vector $\mathbf{x}-\mathbf{x}'$ and the x axis. The factor 2 in the exponential of (11.3) stands for two tube fluxes attached to the electrons to form the composite fermions. In terms of the composite fermions, the kinetic energy reads

$$\hat{K} = \frac{\hbar^2}{2M}\int d\mathbf{x}\psi_C^+(\mathbf{x})(-i\nabla + \frac{e}{\hbar}\mathbf{A}(\mathbf{x}) - \mathbf{a}(\mathbf{x}))^2\psi_C(\mathbf{x}), \tag{11.5}$$

where the statistical gauge field is

$$\mathbf{a}(x) = 2\int d\mathbf{x}'\frac{\hat{\mathbf{z}}\wedge(\mathbf{x}-\mathbf{x}')}{|\mathbf{x}-\mathbf{x}'|^2}\hat{\rho}_C(\mathbf{x}'). \tag{11.6}$$

The interaction term is

$$\hat{V} = \frac{1}{2}\int d\mathbf{x}d\mathbf{x}'v(\mathbf{x}-\mathbf{x}') : \hat{\rho}(\mathbf{x})\hat{\rho}(\mathbf{x}') : \tag{11.7}$$

$$= \frac{1}{2}\int d\mathbf{x}d\mathbf{x}'v(\mathbf{x}-\mathbf{x}') : \hat{\rho}_C(\mathbf{x})\hat{\rho}_C(\mathbf{x}') :, \tag{11.8}$$

$v(\mathbf{x})$ being the Coulomb interaction

$$v(\mathbf{x}) = \frac{e^2}{4\pi\epsilon_0\epsilon_r|\mathbf{x}|}, \tag{11.9}$$

where ϵ_r is the relative dielectric constant of the material. For GaAs, $\epsilon_r = 12.6$.

11.2.2 Mean field theory

In the mean field theory approach, the density of fermions $\rho(\mathbf{x})$ is assumed to be constant. Since the average density n_0 is related to the field by the condition of half filling

$$n_0 = \frac{B}{2\phi_0}, \tag{11.10}$$

the mean field value of the statistical field exactly cancels the external magnetic field, and gives a zero residual magnetic field. The Hamiltonian of the system of composite fermions is simply the Hamiltonian of a collection of free fermions, but with a renormalized effective mass M^*

$$\hat{H}_{M.F.} = \frac{1}{2M^*}\int \psi^+(\mathbf{x})(-i\hbar\nabla)^2\psi(\mathbf{x})d\mathbf{x}. \tag{11.11}$$

If $B = 10T$, the value of the effective mass for GaAs is $M^* \simeq 4M \simeq 0.27M_e$, where M_e is the bare electronic mass. M^* increases as the square root of the magnetic field for larger magnetic fields [3]. If the density $n(\mathbf{x})$ deviates from the average density n_0, then a residual effective magnetic field appears, equal to

$$B - 2\phi_0 n(\mathbf{x}) = 2\phi_0(n_0 - n(\mathbf{x})) = -2\phi_0\delta n(\mathbf{x}). \tag{11.12}$$

11.3 Geometry of the experiment

The electrons are confined on a small bidimensionnal ring. The ring is the set of points x, such as $r_0 < |\mathrm{x}| < r_0 + L$. The dimensions of the ring are of the order $r_0 \simeq 1\mu m$ and $L \simeq 0.1\mu m$. We look for the response of the system to an extra charge Q added in the center of the ring. As we shall see in the next section, one is able to solve exactly the Schrödinger equation of the electrons on the ring in the absence of the central charge. The wave functions are given in terms of Bessel functions. In order to simplify the treatment of the problem, we change the geometry. Instead of a ring, we shall use a rectangle of size L and $R = 2\pi r_0$. The x axis is chosen along the R side of the rectangle, and the y axis along the L side of the rectangle.We impose cyclic boundary conditions in the x direction, which means that $\psi(x + R, y) = \psi(x, y)$ for the wave functions. The spectrum and the wave functions are much more simpler for the approximate geometry.

11.4 $\nu = 1/2$ electrons on the ring in the absence of the central charge

One is able to solve exactly the eigenvalue problem in the absence of the central charge, in the ring geometry, as well as in the simplified geometry. The magnetic field is related to the density by the condition of half filling (11.10), so that the total effective magnetic field through the ring is zero, and the magnetic field in the hole inside the ring is uniform and given by

$$B = 2\phi_0 n_0. \tag{11.13}$$

The number of electrons N on the ring is given by

$$N = \frac{\pi B L(L + 2r_0)}{2\phi_0}. \tag{11.14}$$

If we take $B = 20T$, the number of electrons on the ring is $N = 1494$. These N composite fermions feel a zero magnetic field, but feel the vector potential created by the flux tube in the middle of the ring. This is a typical Aharanov-Bohm situation [4] and one expects the presence of electronic currents which are periodic in φ/ϕ_0, where φ denotes the flux in the center of the ring. Its value is simply

$$\frac{\varphi}{\phi_0} = \frac{\pi r_0^2 B}{\phi_0}. \tag{11.15}$$

Similar situations have already been analyzed in different geometries [11] [12]. The gauge is chosen such as $\mathbf{A}(\mathrm{x}) = A(|\mathrm{x}|)\mathrm{e}_\theta$, with

$$A(r) = \frac{\varphi}{2\pi r} \tag{11.16}$$

if $r > r_0$. One is left with a problem of free electrons in the vector potentiel $\mathbf{A}(r)$ with a Hamiltonian

$$\hat{H} = \frac{1}{2M^*}(-i\hbar\nabla + e\mathbf{A})^2. \tag{11.17}$$

Because of the rotational invariance of the problem, the wave functions can be chosen with a definite kinetic orbital momentum $m\hbar$

$$\psi(r, \theta) = e^{im\theta}\chi(r). \tag{11.18}$$

The Schrödinger equation for $\chi(r)$ reads

$$\chi''(r) + \frac{\chi(r)}{r} + (k^2 - \frac{1}{r^2}(m + \frac{\varphi}{\phi_0})^2)\chi(r) = 0, \tag{11.19}$$

which is a Bessel equation where we have set $E = \hbar^2 k^2 / 2M^*$. The general solution of this equation is

$$\chi(r) = AJ_{|m+\frac{\varphi}{\phi_0}|}(kr) + BY_{|m+\frac{\varphi}{\phi_0}|}(kr). \tag{11.20}$$

The coefficients A and B are determined by the normalisation of the wave function and by the fact that the wave function vanishes at the edges of the sample, so that $\chi(r_0) = \chi(r_0 + L) = 0$. The wave vector k is found to be the solution of

$$J_{|m+\frac{\varphi}{\phi_0}|}(kr_0)Y_{|m+\frac{\varphi}{\phi_0}|}(k(r_0 + L)) - Y_{|m+\frac{\varphi}{\phi_0}|}(kr_0)J_{|m+\frac{\varphi}{\phi_0}|}(k(r_0 + L)) = 0. \tag{11.21}$$

In order to obtain simpler equations for the energy levels and the wave functions, we give the form of the solution in the simplified geometry. We first treat the case $\varphi = 0$. In this case, the problem simply corresponds to free electrons on a rectangle. The wave functions are given by

$$\psi_{m,n}(x, y) = \sqrt{\frac{2}{RL}} e^{-im\frac{2\pi}{R}x} \sin n\frac{\pi}{L}y, \tag{11.22}$$

and the energy levels are

$$E(m, n) = \frac{\hbar^2}{2M^*}((\frac{2\pi}{R})^2 m^2 + (\frac{\pi}{L})^2 n^2). \tag{11.23}$$

The electrons belong to a Fermi sea, and the Fermi wave vector k_F is approximately determinated by the relation

$$k_F = \sqrt{\frac{4\pi N}{LR}}, \tag{11.24}$$

where the number of fermions N is given by (11.14). Since $L \ll R$, the wave vector increment $2\pi/R$ in the k_x direction is much smaller than the increment π/L in the k_y direction, so that the Fermi sea can be viewed as a collection of channels labeled by the integer $n > 0$. The fermi sea is drawn on figure 11.1. In the case $B = 20T$, the Fermi sea is made up of six channels. In the absence of a magnetic flux φ through the hole of the ring, or if the magnetic flux is a multiple of the flux quantum ϕ_0, one can compute the electronic density of the state

$$|\psi_0\rangle = \prod_{m,n \in F.S.} \psi^+_{m,n}|0\rangle, \tag{11.25}$$

where the fermionic quantum numbers m and n belong to the Fermi sea of figure 11.1 and $|0\rangle$ is the vacuum. The density profile is plotted on figure 11.2. As expected, the density is zero on the edges and the density profile exhibits Friedel oscillations. The non uniformity of the density induces a non uniform electrostatic field, which modifies the one-particule states. Thus, due to finite size effects, (11.25) is not the true ground state for the mean field approximation, whereas it would be the true ground state on an infinite plane.

What happens if the flux φ in the hole of the ring is non zero? Let us first consider the case where φ/ϕ_0 is an integer. As we see from equation (11.19), we can deduce the physics from the

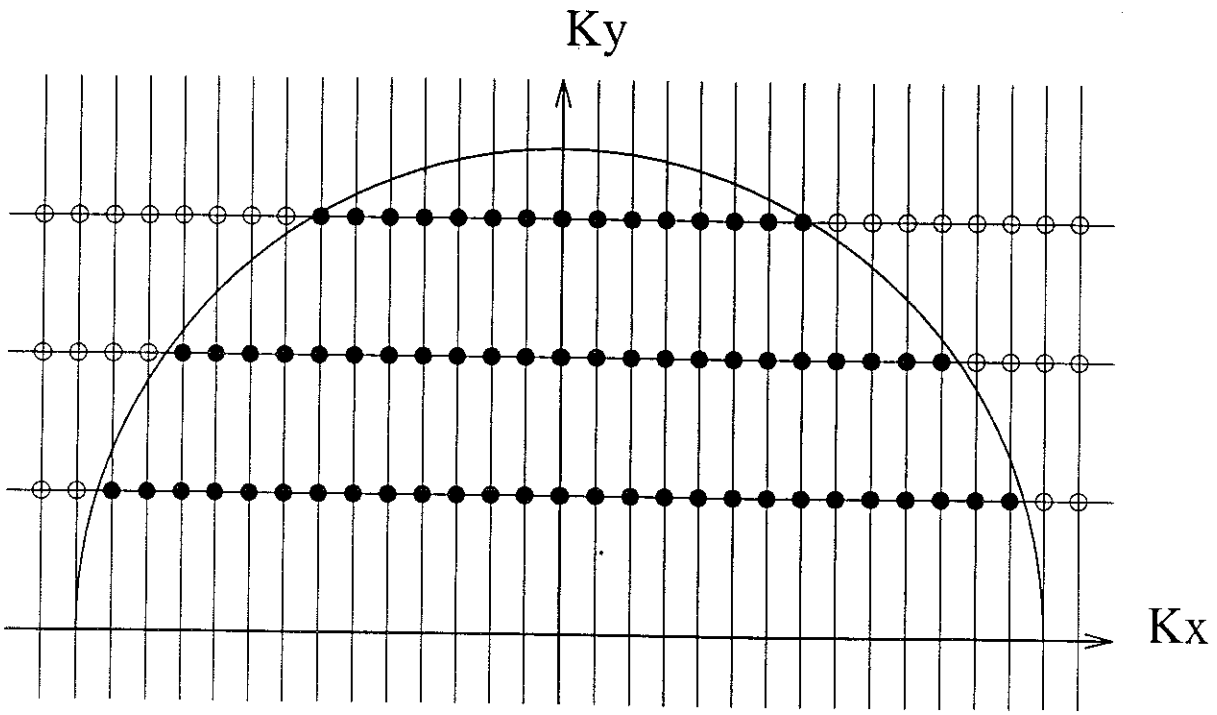

Figure 11.1:
Fermi sea of quasiparticles at the mean field level in the simplified geometry. k_x is a multiple of $2\pi/R$ amd k_y is a multiple of π/L.

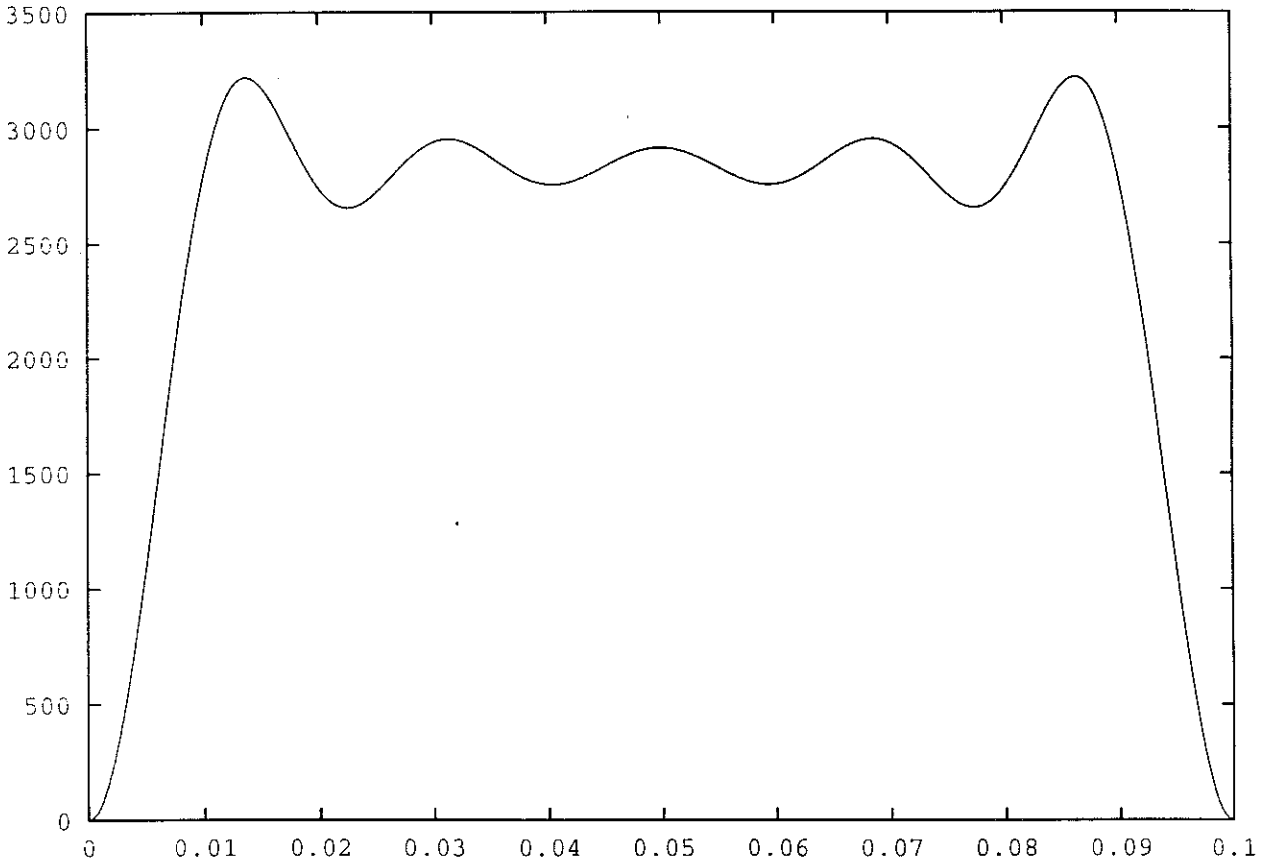

Figure 11.2:
Electronic density of the state (11.25) $\rho(x) = |\langle x|\psi_0\rangle|^2$. The electronic density vanishes at the edges and exhibits Friedel oscillations. The fermi sea contains 6 channels and 1494 electrons. The density is plotted in μm^{-2} and the radial coordinate in μm.

case $\varphi = 0$ by replacing m by $m + \varphi/\phi_0$. The Fermi sea is translated in the reciprocal space by a factor $\Delta k_x = 2\pi\varphi/R\phi_0$ along the k_x direction.

If φ/ϕ_0 is not an integer, the situation is somewhat different. One expects in this case the appearance of a current due to an Aharanov-Bohm effect [13]. We note $\varphi/\phi_0 = \Delta m + \delta m$, with Δm an integer and δm a real number, such as $|\delta m| < 1/2$. The energy $E(m,n)$ reads

$$E(m,n) = \frac{\hbar^2}{2M^*}[(\frac{2\pi}{R})^2(m + \Delta m + \delta m)^2 + (\frac{\pi}{L})^2 n^2]. \tag{11.26}$$

The Fermi sea is translated by the wave vector $\Delta k_x = -2\pi\Delta m/R$, so that the wave functions become

$$\psi_{m,n}(x,y) = \sqrt{\frac{2}{RL}} e^{i(m-\Delta m)\frac{2\pi}{R}x} \sin n\frac{\pi}{L}y \tag{11.27}$$

The Fermi sea becomes unstable as $|m| = 1/2$. To see this, consider $2N_0 + 1$ fermions in a given channel n. If $|\delta m|$ is inferior as $1/2$, the fermions have the possibility to have their orbital quantum numbers in the interval $[-\Delta m - N_0, -\Delta m + N_0]$, or in the interval $[-\Delta m - N_0 \pm 1, -\Delta m + N_0 \pm 1]$. The condition for the latter configuration to be stable is that it has a lower energy than the former, namely

$$\frac{\hbar^2}{2M^*}(\frac{2\pi}{R})^2 \sum_{m=-\Delta m-N_0}^{-\Delta m+N_0} (m + \Delta m + \delta m)^2 < \frac{\hbar^2}{2M^*}(\frac{2\pi}{R})^2 \sum_{m=-\Delta m-N_0\pm1}^{-\Delta m+N_0\pm1} (m + \Delta m + \delta m)^2, \tag{11.28}$$

which is satisfied for $|\delta m| < 1/2$, independently on N_0. The Fermi sea of $2N_0 + 1$ fermions in the channel n is thus in the interval $m \in [\Delta m - N_0, \Delta m + N_0]$ if $-1/2 < \delta m < 1/2$. What is the Aharonov-Bohm current in the ring for a non integer value of φ/ϕ_0 ? The quantum mechanical, jauge invariant current operator reads

$$\mathrm{j(x)} = \frac{-i\hbar}{2M^*}(\overline{\psi}\nabla\psi - \psi\nabla\overline{\psi}) + \frac{e}{M^*}\mathbf{A}|\psi|^2. \tag{11.29}$$

In the simplified geometry, the current has only a component parallel to the x axis. The contribution of the first term in (11.29) is

$$\frac{\hbar}{M^*}\frac{2\pi}{R}(m - \Delta m), \tag{11.30}$$

and the contribution of the term proportionnal to the vector potential reads

$$\frac{\hbar}{M^*}\frac{2\pi}{R}(\Delta m + \delta m). \tag{11.31}$$

The total current is thus

$$j_x(m,n) = \frac{\hbar}{M^*}\frac{2\pi}{R}(m + \delta m)|\psi_{m,n}|^2. \tag{11.32}$$

After a summation over the Fermi sea, we obtain the total current

$$J_x(y) = \sum_{(m,n)\in F.S.} j_x(m,n) = \frac{2\hbar}{M^*}\frac{2\pi}{R}\delta m \sum_{(m,n)\in F.S.} |\psi_{m,n}|^2, \tag{11.33}$$

If $\delta m = 0$, the flux in the hole of the ring is a multiple of the quantum flux, and everything happens as if the fermions would not see the flux. If $\delta m \neq 0$, a current exists. The intensity of the current is given by

$$I = -e \int_0^L J_x(y) dy = -\frac{2\pi e\hbar N}{M^* R^2} \delta m. \tag{11.34}$$

The maximum value of the current is

$$I_{max} = \frac{ehN}{2M^* R^2}. \tag{11.35}$$

The numerical value of I_{max} is $5.8nA$ for $B = 20T$.

11.5 $\nu = 1/2$ electrons on a ring in the presence of the external charge

In the presence of a positive central charge, the electrons are expected to accumulate near the internal edge of the ring and a depletion of electrons is expected at the external edge, leading to a charge transfer from the external to the internal edge. This charge transfer induces a deviation from the $\nu = 1/2$ value and, if ones applies the ideas of the mean field theory, the total effective flux, due to the external magnetic field plus the statistical gauge field is no longer zero, so that an effective flux penetrates through the sample, creating an Aharanov-Bohm current which is periodic as a function of the central charge.

The first step is to evaluate the screening of the central charge by the electron gas on the ring. Many levels of approximation are possible. The most accurate approximation is to take into account that the one particule Slater determinant (11.25) is not the true ground state of the fermions, due to Friedel oscillations induced by the edges. This can be implemented in a recursive way by starting from the state (11.25), computing the electronic density, deducing from it the electrostatic field, and reiterating, that is to compute the corrections to the one-particule states in the presence of the Friedel oscillations, and re-compute the electronic density. The effect of the charge is then treated at the linear order, with the full response function. Within these approximations, one expects the density of electrons to increase near the internal edge of the ring, and to decrease near the external edge. Moreover, this average density profile should be modulated by Friedel oscillations as well as oscillations at the Thomas-Fermi wave vector. In our case, as we shall see, the Thomas-Fermi wave vector is greater than the Fermi wave vector. We shall not use this refined approximation scheme because of its computational complexity. Since we focus only on the charge transfer from one edge of the ring to the other, and not on the details of the variations of the density profile, we do not take into account the existence of Friedel oscillations. We take the state (11.25) as an approximate ground state and we look for the effects of the screening of the central charge. In other words, we hope the density-density response functions are not very different if we replace the true Hatree-Fock state by the approximate one given by (11.25).

At this stage, two approximations are possible. The most refined one consist in taking into account the full response function of the fermions. This shall be done in section 5.4. A more approximate treatment is to treat the screening in the Thomas-Fermi approximation, which is the aim of section 5.3. As we shall see, the two approximations lead to similar results as far as averaged quantities are concerned, namely the average effective flux penetrating through the

ring due to the presence of the central charge. We shall compare these results with the lowest possible degree of approximation for this system, that is the total absence of screening. What we observe under this crude approximation is a transfer of charge from the center of the internal edge of the ring to the external edge. We find that the response of the electrons to the central charge is more important in the absence of screening than in the presence of screening.

11.5.1 Screening in two dimensions

As an introduction to the problem of screening in a finite geometry, we treat the case of the screening of a single charge in an infinite bidimensional gas of electrons. The solution of this problem will lead to the expression of the Thomas-Fermi wave vector q_{TF} in two dimensions. The case of the screening of a charge in three dimensions is treated in reference [14] with the Thomas-Fermi approximation. We do nothing but transpose the argument of [14] to the case of an electron gas constrained on a bidimensional layer, with three dimensional Coulomb interactions. The potential created by the external point charge located at the origin is noted ϕ^{ext}. We note ρ^{ind} the variation of density induced by the presence of the extra charge in the gas of electrons, plus the uniform background of positive charges. ϕ is the total potential created by the extra charge, the electrons and the background of positive charges. Since the bidimensional Fourier transform of $1/|\mathbf{x}|$ is $2\pi/|\mathbf{q}|$, we have

$$\phi(\mathbf{q}) - \phi^{ext}(\mathbf{q}) = \frac{\rho^{ind}(\mathbf{q})}{2\epsilon_0\epsilon_r|\mathbf{q}|}. \tag{11.36}$$

the dielectric constant is defined by

$$\phi^{ext}(\mathbf{q}) = \epsilon(\mathbf{q})\phi(\mathbf{q}), \tag{11.37}$$

and we assume

$$\rho^{ind}(\mathbf{q}) = \chi(\mathbf{q})\phi(\mathbf{q}). \tag{11.38}$$

We thus obtain

$$\epsilon(\mathbf{q}) = 1 - \frac{\chi(\mathbf{q})}{2\epsilon_0\epsilon_r|\mathbf{q}|}. \tag{11.39}$$

If the total potential is a slowly varying function of the position, one can define

$$\epsilon(\mathbf{k}) = \frac{\hbar^2\mathbf{k}^2}{2M^*} - e\phi(\mathbf{x}), \tag{11.40}$$

so that the local distribution function reads

$$n(\mathbf{x}) = \int \frac{\mathbf{dk}}{(2\pi)^2} \frac{\mathbf{1}}{\mathbf{1} + \exp\{\beta(\hbar^2\mathbf{k}^2/2\mathbf{M}^* - \mathbf{e}\phi(\mathbf{x}) - \mu)\}}, \tag{11.41}$$

and the density of the background positive charge is

$$n^0(\mu) = \int \frac{d\mathbf{k}}{(2\pi)^2} \frac{1}{1 + \exp\{\beta(\hbar^2\mathbf{k}^2/2M^* - \mu)\}}. \tag{11.42}$$

Thus, we can write the induced density of electrons as

$$\rho^{ind}(\mathbf{x}) = -e\{n^0(\mu + e\phi(\mathbf{x})) - n^0(\mu)\}. \tag{11.43}$$

If ϕ is small,

$$\rho^{ind}(\mathbf{x}) = -e^2 \frac{\partial n^0}{\partial \mu} \phi(\mathbf{x}), \tag{11.44}$$

so that

$$\chi(\mathbf{q}) = -e^2 \frac{\partial n^0}{\partial \mu} = -\frac{M^* e^2}{2\pi\hbar^2}. \tag{11.45}$$

The dielectric constant reads

$$\epsilon(\mathbf{q}) = 1 + \frac{q_{TF}}{|\mathbf{q}|}, \tag{11.46}$$

where q_{TF} is the Thomas-Fermi wave vector

$$q_{TF} = \frac{M^*}{\hbar^2} \frac{e^2}{4\pi\epsilon_0\epsilon_r}. \tag{11.47}$$

If one adds an extra charge Q at the origin,

$$\phi(\mathbf{q}) = \frac{1}{\epsilon(\mathbf{q})} \phi^{ext}(\mathbf{q}) \tag{11.48}$$

$$= \frac{Q}{2\epsilon_0} \frac{1}{|\mathbf{q}| + q_{TF}}. \tag{11.49}$$

A Fourier transform yields

$$\phi(\mathbf{x}) = \frac{Q}{4\pi\epsilon_0 |\mathbf{x}|} F(q_{TF}|\mathbf{x}|), \tag{11.50}$$

with

$$F(z) = \int_0^{+\infty} J_0(u) \frac{u}{u+z} du. \tag{11.51}$$

The interaction is screened if $x \gg 2\pi/q_{TF}$. The numerical value of the Thomas-Fermi lenght $\lambda_{TF} = 2\pi/q_{TF}$ is $\lambda_{TF} = 15.6$nm.

11.5.2 Linear response approach

The aim of the section is to present the real space linear response formalism. From a numerical point of view, this means that we must discretize the radial coordinate at a scale smaller than the Thomas-Fermi length λ_{TF}. Within the linear response, the density variation is linearly related to the local potential, but in a non local way:

$$\delta\rho(\mathbf{x}) = \int_0^L \chi^{(0)}(x, x') V_{loc}(x') dx', \tag{11.52}$$

where $x \in [0, L]$ is the radial coordinate , with the origin taken at the interior edge of the ring. Notice that the conservation of charge carriers implies that

$$\int_0^L \chi^{(0)}(x, x') dx = 0. \tag{11.53}$$

The local potential is the sum of the potential created by the electrostatic field of the central charge $V_{ext}(x)$, plus the potential $V_{ind}(x)$ induced by the electrons on the ring. Since the distance L between the two edges is small ($L = 0.1\mu m$), we linearize the Coulomb potential

created by the central charge in the vicinity of the ring, which leads to the following expression of $V_{ext}(x)$:

$$V_{ext}(x) = \frac{Qe^2}{4\pi\epsilon_0\epsilon_r(r_0 + L/2)}(x - \frac{L}{2}) \tag{11.54}$$

On the other hand, the induced potential has the expression

$$V_{ind}(x) = \frac{e^2}{4\pi\epsilon_0\epsilon_r}\int_0^L (1 + \frac{x'}{r_0})\delta\rho(x')dx' \tag{11.55}$$

$$\int_{-\pi}^{\pi} \frac{d\theta}{\sqrt{(1+\frac{x}{r_0})^2 + (1+\frac{x'}{r_0})^2 - 2(1+\frac{x}{r_0})(1+\frac{x'}{r_0})\cos\theta}}. \tag{11.56}$$

Using the notations $u = 1 + x/r_0$ and $1 + x'/r_0$, the angular integral takes the form of an elliptic integral

$$\int_{-\pi}^{\pi} \frac{d\theta}{\sqrt{u^2 + v^2 - 2uv\cos\theta}} = 4\int_0^{\pi/2} \frac{d\theta}{\sqrt{((u+v)^2 - 4uv\cos^2\theta}} \tag{11.57}$$

$$= \frac{4}{u+v} K\left(\frac{2\sqrt{uv}}{u+v}\right). \tag{11.58}$$

Since u and v are close to unity, the elliptic integral can be approximated as

$$K\left(\frac{2\sqrt{uv}}{u+v}\right) = \ln\left(\frac{4|u+v|}{|u-v|}\right) + O\left((u-v)^2 \ln|u-v|\right), \tag{11.59}$$

which leads to

$$V_{ind}(x) \simeq \frac{e^2}{2\pi\epsilon_0\epsilon_r}\int_0^L \ln\left(\frac{8r_0}{|x-x'|}\right)\delta\rho(x')dx' \tag{11.60}$$

Notice that the factor $8r_0$ does not come into account since

$$\int_0^L \delta\rho(x)dx = 0. \tag{11.61}$$

The equation (11.52) reads

$$\delta\rho = \chi^{(0)}(V_{ext} + V_{ind}\delta\rho), \tag{11.62}$$

where the quantities are understood as matrices for χ^0 and V_{ind} and vectors for $\delta\rho$ and V_{loc}. A discretization of the radial coordinate has been assumed. In order to perform the linearization, we used a parabolic approximation for the integrals. A special attention has to be paid to the logarithmic divergence of (11.60) which has to be integrated explicitely using a parabolic approximation. Equation (11.62) can be inverted into the form

$$\delta\rho = \frac{1}{1 - \chi^{(0)}V_{ind}}\chi^{(0)}V_{ext}, \tag{11.63}$$

which has the well known form of a R.P.A. resummation. Numerically, we use a Gauss-Jordan method for inverting the linear system (11.60). The size of the matrix to be inverted is about 1000, which corresponds to 1000 points for the discretization of the interval $[0, L]$. Since $L \sim 0.1\mu m$, the condition $L/1000 \ll \lambda_{TF}$ is well respected. We now examine successively two approximations for the response function $\chi^{(0)}(x, x')$.

11.5.3 Thomas-Fermi approach to the response function

In the Thomas-Fermi approach, the response function is purely local:

$$\chi_{TF}^{(0)}(x,x') = -\frac{m}{2\pi\hbar^2}(\delta(x-x') - \frac{1}{a}) \tag{11.64}$$

Using this form of the response function, we inverted the system (11.62). The resulting density profile is given on figure 11.3. In terms of the effective flux through the sample (flux of the magnetic field plus flux of the statistical gauge field), one is interested in

$$\phi(x) = -2\phi_0(r_0 + L/2)\int_0^x \delta\rho(x)dx. \tag{11.65}$$

The function $\phi(x)$ is plotted on figure 11.4.

As we shall see in section 5.5, the total current is given in terms of the mean flux through the ring

$$\overline{\phi} = \frac{1}{L}\int_0^L \phi(x)dx \tag{11.66}$$

We find that $\overline{\phi}$ is such that a charge $Q = 14e^-$ is required to induce one flux quantum on average through the ring, which means that the periodicity of the currents as a function of the central charge is 14 electrons.

11.5.4 Screening of the central charge with the full response function

We calculate the full response function using the first order perturbation theory in the potential induced by the central charge.We also use the simplified geometry. The matrix elements of the local potential V_{loc} on the basis of function (11.22) are

$$V_{n,n'}^{loc} = \frac{2}{L}\int_0^L \sin\left(\frac{\pi}{L}nx\right)V_{loc}(x)\sin\left(\frac{\pi}{L}n'x\right)dx, \tag{11.67}$$

so that

$$\hat{V}_{loc} = \sum_m \sum_{n,n'} V_{n,n'}^{loc}\psi_{m,n}^+\psi_{m,n'}. \tag{11.68}$$

The first order corrections to the state $|\psi_0\rangle$ of equation (11.25) are

$$|\psi\rangle = |\psi_0\rangle + \sum_m \sum_{n,n'} \frac{V_{n,n'}^{loc}}{E(m,n') - E(m,n)}\psi_{m,n}^+\psi_{m,n'}|\psi_0\rangle. \tag{11.69}$$

The second-quantized form of the electron density operator is

$$\hat{\rho}(x,y) = \frac{2}{RL}\sum_{m,m'}\sum_{n,n'} e^{-i(m'-m)\frac{2\pi}{R}x}\sin\left(\frac{\pi}{L}ny\right)\sin\left(\frac{\pi}{L}n'y\right)\psi_{m,n}^+\psi_{m',n'}|\psi_0\rangle. \tag{11.70}$$

One can readily calculate the average of $\hat{\rho}(x,y)$ in the presence of the central charge, which leads to

$$\begin{aligned}\langle\hat{\rho}(x,y)\rangle_Q - \langle\hat{\rho}(x,y)\rangle_{Q=0} &= \frac{4}{RL}\sum_m\sum_{n,n'}\frac{V_{n,n'}}{E(m,n') - E(m,n)}n^0(m,n') \\ &\quad (1-n^0(m,n))\sin\left(\frac{\pi}{L}ny\right)\sin\left(\frac{\pi}{L}n'y\right),\end{aligned} \tag{11.71}$$

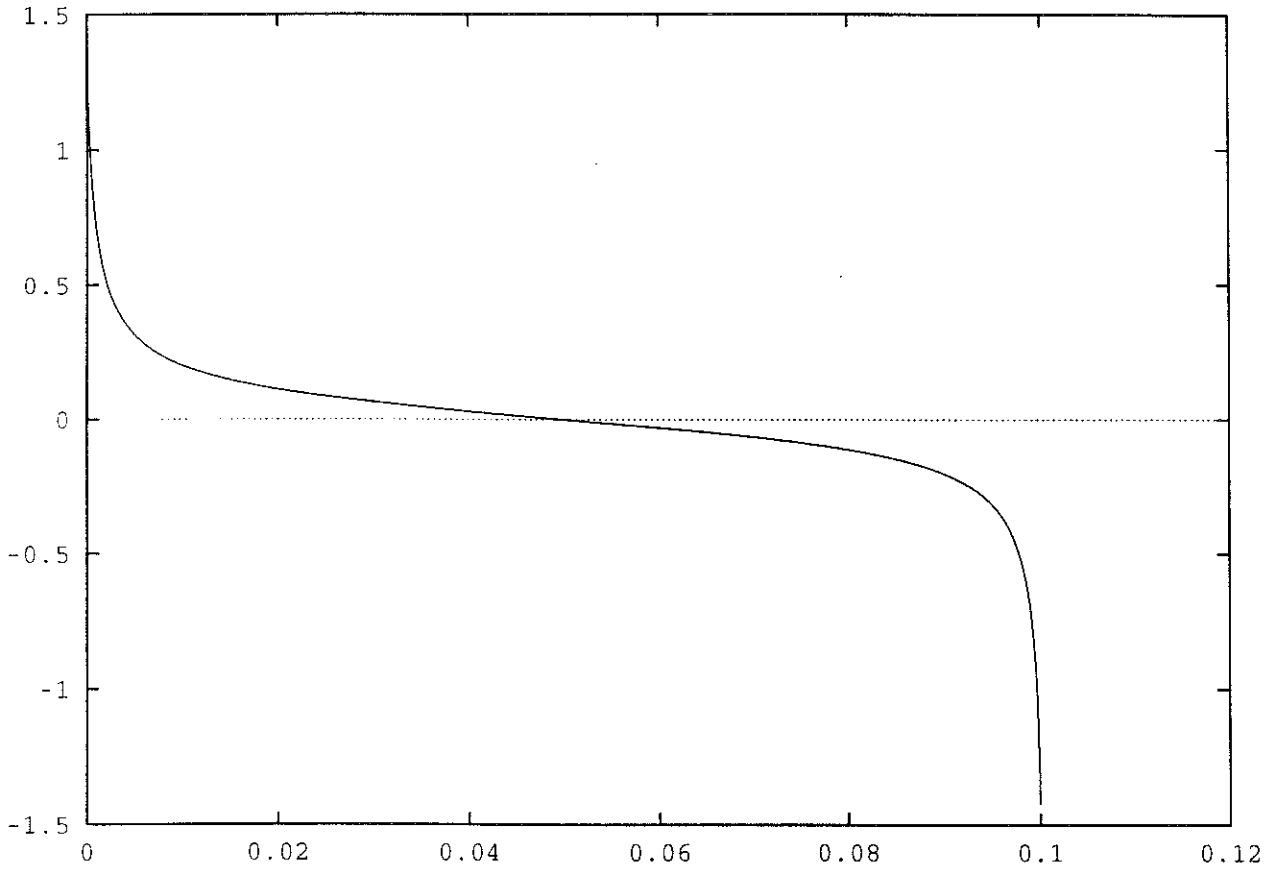

Figure 11.3:
Profile of the electronic density variations induced by the central charge in the Thomas-Fermi approach to the response function. The computation has been made in the simplified geometry. The central charge is $Q = -1e^-$. The density is plotted in μm^{-2} and the radial coordinate in μm.

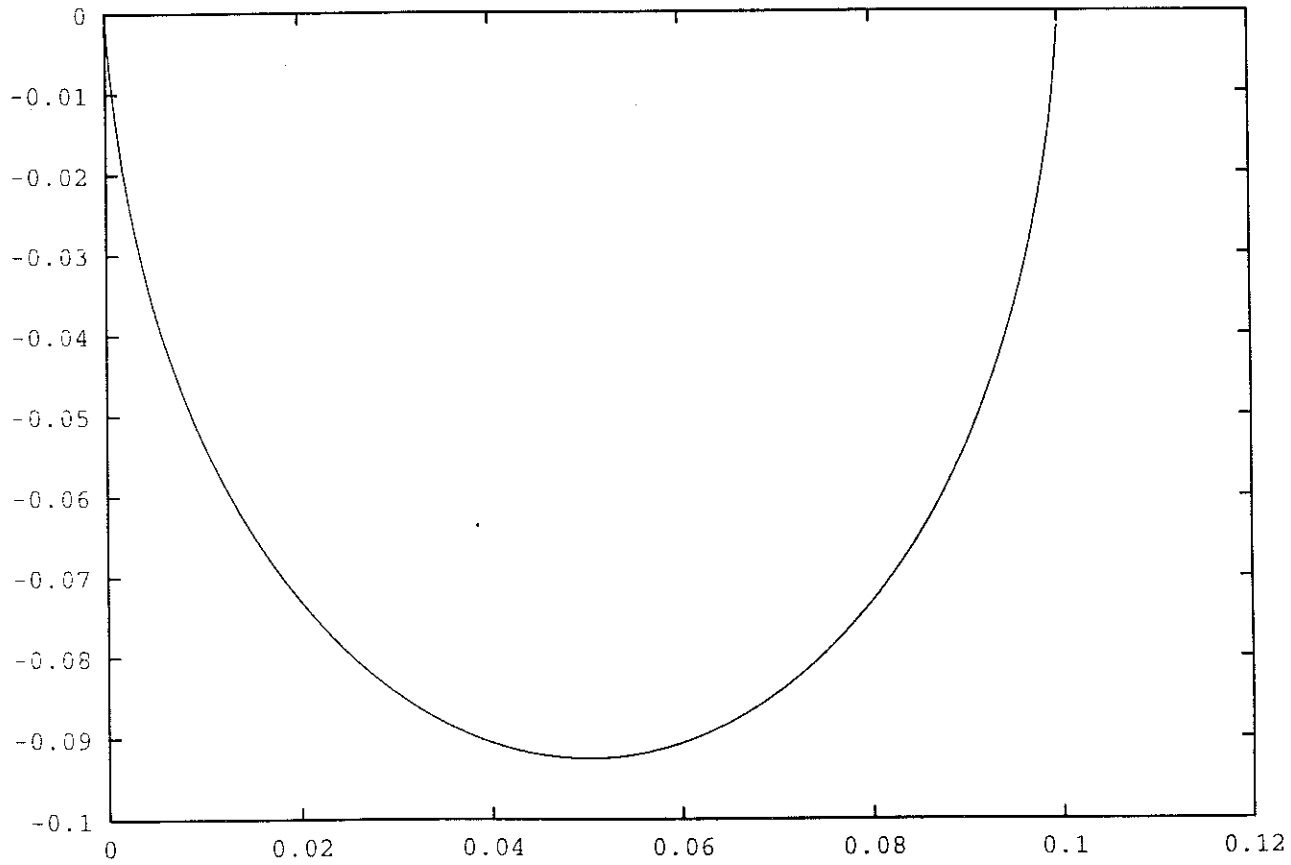

Figure 11.4:
Flux through the ring in the Thomas-Fermi approach to the response function. The central charge is $Q = -1e^-$. The flux is plotted in units of the flux quantum ϕ_0 and the radial coordinate in μm.

where $n^0(n,m)$ is unity if (m,n) belongs to the Fermi sea and zero otherwise. The summation over m can be evaluated by noticing that the Fermi sea is made up of a collection of nested one dimensional Fermi seas (one for each channel), and we obtain

$$\delta\langle\hat{\rho}(x,y)\rangle = \frac{8M^*}{\pi\hbar^2} \left\{ \sum_{n=1}^{N}\sum_{n'=n+1}^{N} \frac{\sqrt{\nu^2-n^2}-\sqrt{\nu^2-n'^2}}{n^2-n'^2} \sin\left(\frac{\pi}{L}ny\right)\sin\left(\frac{\pi}{L}n'y\right)V^{loc}_{n,n'} + \sum_{n=1}^{N}\sum_{n'=N+1}^{+\infty} \frac{\sqrt{\nu^2-n^2}}{n^2-n'^2} \sin\left(\frac{\pi}{L}ny\right)\sin\left(\frac{\pi}{L}n'y\right)V^{loc}_{n,n'}\right\}. \quad (11.72)$$

In this expression, ν is related to the Fermi energy by

$$E_F = \frac{\hbar^2}{2M^*}\frac{\pi^2}{L^2}\nu^2 \quad (11.73)$$

and N is the integer such as $\nu \in [N, N+1[$. We deduce from (11.72) the response function $\chi^{(0)}(y,y')$:

$$\chi^{(0)} = \frac{16}{\pi^2\hbar^2 L} \left\{ \sum_{n=1}^{N}\sum_{n'=n+1}^{N} \frac{\sqrt{\nu^2-n^2}-\sqrt{\nu^2-n'^2}}{n^2-n'^2} \sin\left(\frac{\pi}{L}ny\right)\sin\left(\frac{\pi}{L}n'y\right)\sin\left(\frac{\pi}{L}ny'\right)\sin\left(\frac{\pi}{L}n'y'\right) + \sum_{n=1}^{N}\sum_{n'=N+1}^{+\infty} \frac{\sqrt{\nu^2-n^2}}{n^2-n'^2} \sin\left(\frac{\pi}{L}ny\right)\sin\left(\frac{\pi}{L}n'y\right)\sin\left(\frac{\pi}{L}ny'\right)\sin\left(\frac{\pi}{L}n'y'\right)\right\} \quad (11.74)$$

With the form (11.74) for $\chi^{(0)}$, it is straighforward to compute the density of electrons, using the matrix relation (11.63). The profile of the electron density variations induced by the central charge is plotted on figure 11.5. We notice the existence of oscillations at the Thomas-Fermi wave vector, which were absent in the calculation using the Thomas-Fermi approach to the response function. However, these oscillations do not affect the averaged quantities under interest. The total flux through the sample $\phi(x)$ is plotted on figure 11.6, and has the same shape as the flux computed in the Thomas-Fermi approximation. The mean flux through the ring is such as 16 e^- are required to produce one flux quantum through the ring. This value is in good agreement with the calculations in the Thomas-Fermi approximation.

11.5.5 Currents induced by the charge

The magnetic flux through the ring generates permanents currents, in the same way as a flux through the hole of the ring generates currents. Let us call $\delta\mathbf{A}$ the variation in the vector potential due to the presence of the charge. The variation in the Hamiltonian due to the shift in the vector potential is

$$\delta H = \frac{e^2}{2M^*}(2\mathbf{A}.\delta\mathbf{A} + \delta\mathbf{A}^2) + \frac{ie\hbar}{M}\delta\mathbf{A}.\nabla. \quad (11.75)$$

Applying first order perturbation theory, we obtain the variation of a given energy level

$$\langle\delta H\rangle = \frac{e^2}{M^*}\langle\mathbf{A}.\delta\mathbf{A}\rangle - \frac{e\hbar}{M^*}m\langle\frac{\delta A(r)}{r}\rangle. \quad (11.76)$$

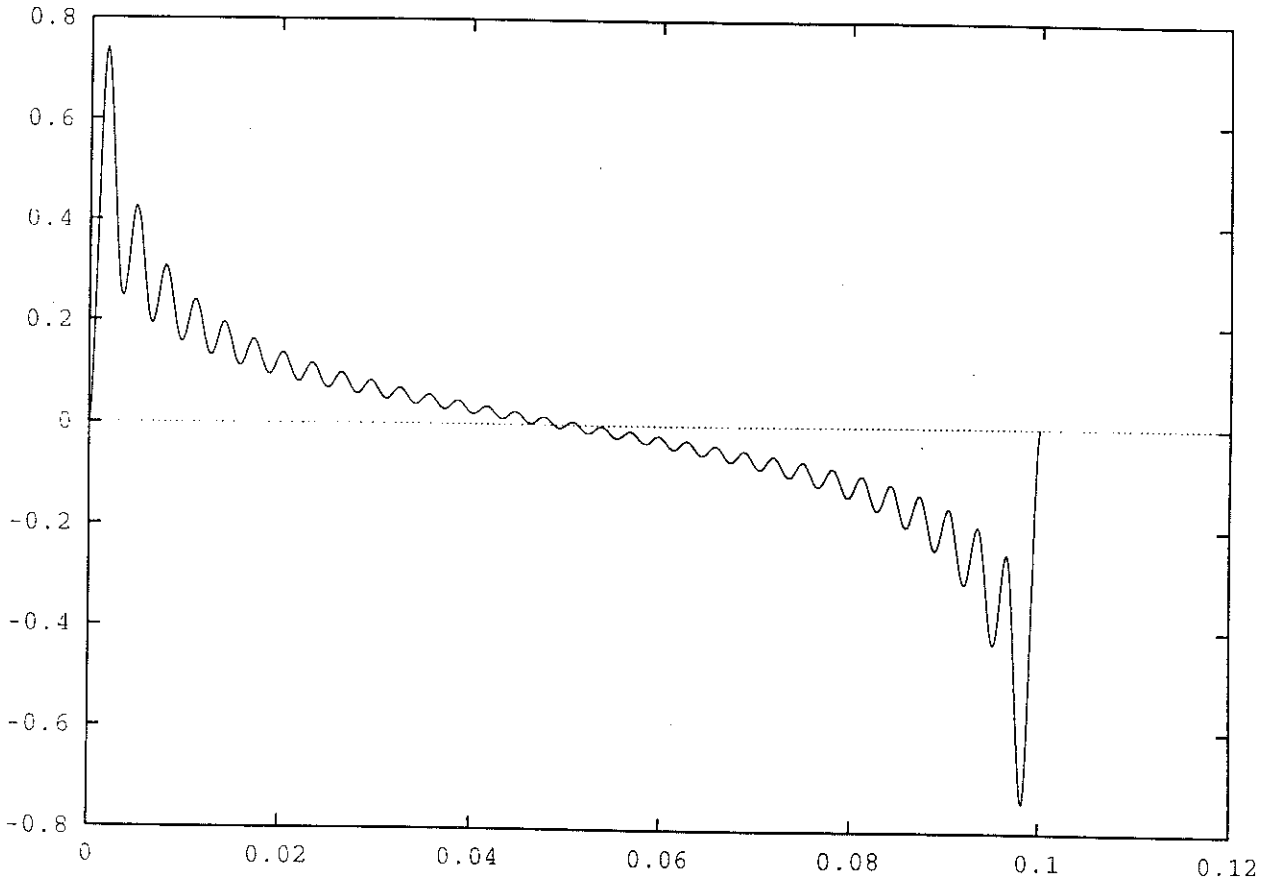

Figure 11.5:
Profile of the electronic density variations induced by the central charge with the full response function.The computation has been made in the simplified geometry. The central charge is $Q = -1e^-$. The density is plotted in μm^{-2} and the radial coordinate in μm.

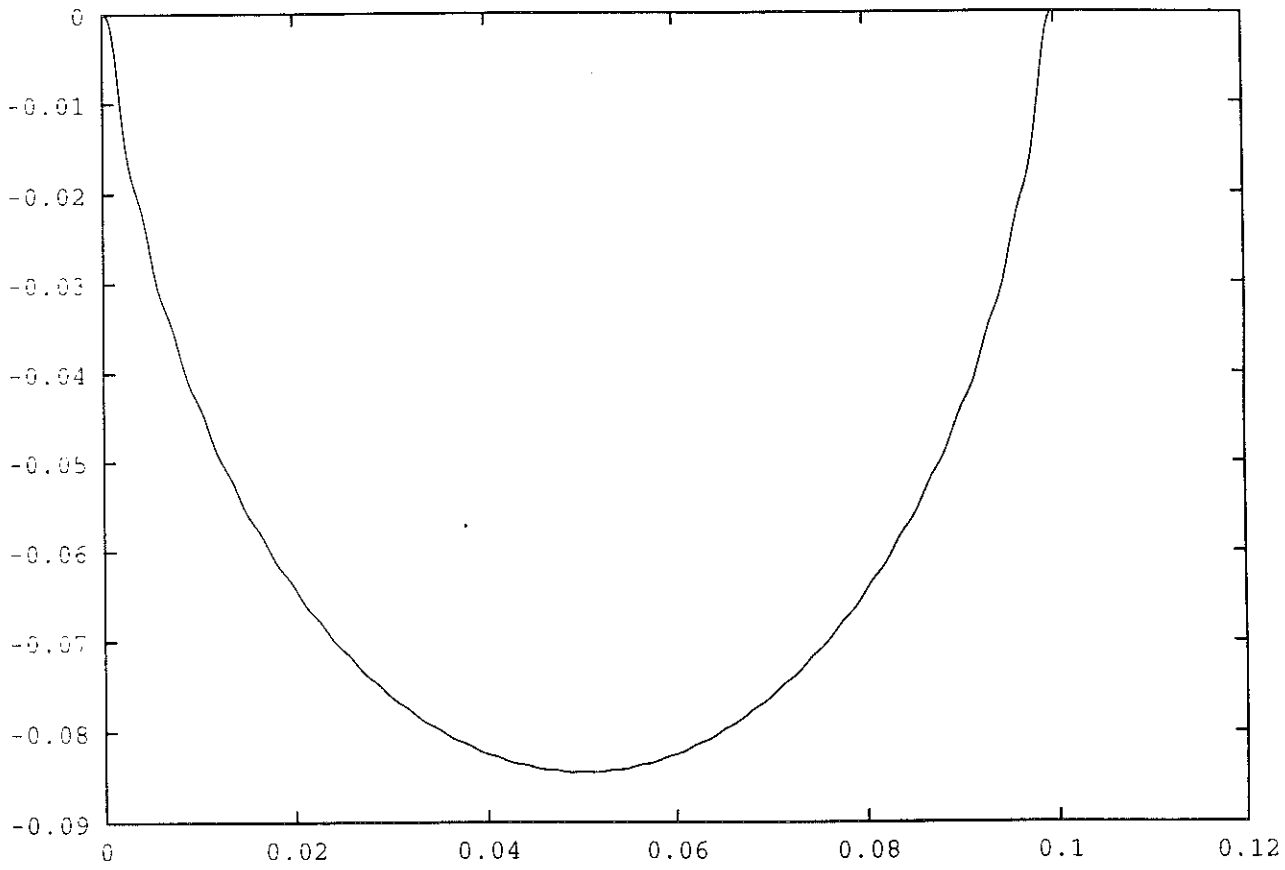

Figure 11.6:
Flux through the ring with the full response function. The central charge is $Q = -1e^-$. The flux is plotted in units of the flux quantum ϕ_0 and the radial coordinate in μm.

We now make the approximation that the spatial dependence of $\delta\mathbf{A}$ and $\delta A(r)/r$ are averaged on the ring, that is to say

$$\frac{\delta A(r)}{r} \simeq \frac{\overline{\phi}}{2\pi r_0^2}, \tag{11.77}$$

where $\overline{\phi}$ is the average magnetic flux induced by the central electric charge. The first term in δH is simply an energy variation independent on n and m. This term is then dropped. Thus we get

$$\langle \delta H \rangle = -\frac{e\hbar}{M^*} m \frac{\overline{\phi}}{2\pi r_0^2} + \frac{\hbar^2}{2M^*} \frac{4\pi^2}{L^2} n^2, \tag{11.78}$$

so that the total energy reads

$$E(m,n) = \frac{\hbar^2}{2M^* r_0^2}(m - \frac{\overline{\phi}}{\phi_0})^2 - \frac{\hbar^2}{2M r_0^2}(\frac{\overline{\phi}}{\phi_0})^2. \tag{11.79}$$

If we apply the result of section 4 about currents, we find that the currents are periodic in $\overline{\phi}$. The maximum value of the current is given by (11.35) and the period is such as $\overline{\phi} = \phi_0$.

11.6 Numerical approach in the spherical geometry

We now make use of the spherical geometry in order to perform numerical computations with a small number of electrons on a sphere of radius R. A magnetic monopole is put at the center of the sphere, creating a total magnetic flux through the sphere equal to $2S\phi_0$. The Dirac's monopole quantization requires $2S$ to be an integer. An electric charge Q is put at the north pole of the sphere. The extra charge is treated as a classical, point charge. We first generalize the mean field theory argument to the spherical geometry case. In a second step, we present numerical computations for a small number of electrons on the sphere for various filling fractions.

11.6.1 Mean field theory at $\nu = 1/2$

We adapt the argument of the mean field theory, previously established in the geometry of the ring, to the spherical geometry. The filling fraction

$$\nu = \frac{N-1}{2S} \tag{11.80}$$

is chosen to be $1/2$ in this section. The non local gauge transformation leads to a statistical field which generates a flux equal to $-2\phi_0(N-1)$ because there is no statistical flux coming from a particle onto itself. The mean field Hamiltonian simply corresponds to fermions on the sphere in the absence of a magnetic field. If one neglects the Coulomb interactions, the Hamiltonian is diagonal on the basis of the spherical harmonics $Y_{l,m}(\theta,\varphi)$ normalized such as

$$\int Y_{l,m}(\theta,\varphi) d\Omega = 1 \tag{11.81}$$

The wave function is simply $\psi_{l,m}(\theta,\varphi) = Y_{l,m}(\theta,\varphi)/R$. The single particle states are labelled by the positive integer l and the integer m such as $-l \leq m \leq l$. The energy of a state labelled by (l,m) reads

$$E(l,m) = \frac{\hbar^2}{2M^* R^2} l(l+1). \tag{11.82}$$

In the presence of a negative (positive) electric charge at the north pole, a depletion (accumulation) of electrons arises at the north pole, and an accumulation (depletion) arises at the south pole. The mean field model in the presence of the charge at the north pole consists of electrons in a zero magnetic field plus a flux tube $\overline{\phi}$ penetrating through the south pole and emerging at the north pole. The problem of quantum motion around a flux tube $\overline{\phi} = \alpha\phi_0$ in the spherical geometry was considered in [16]. We now rederive the solution. This problem is non perturbative in $\overline{\phi}$, since infinite quantities appear in the first order perturbation theory in $\overline{\phi}$. This is why we adopt an algebric approach. The flux tube $\overline{\phi}$ is absorbed in a gauge transformation, leading to multivalued wave functions

$$\psi(r, \theta + 2\pi) = e^{2i\pi\gamma}\psi(r, \theta). \tag{11.83}$$

The eigenvalues of l_z are thus quantized by $l_z = m + 2\pi\gamma$, m being an integer. The eigenstates of the Hamiltonian are also eigenstates of l^2, since

$$H = -\frac{\hbar^2}{2m}\Delta = -\frac{\hbar^2}{2M^*R^2}\mathrm{l}^2. \tag{11.84}$$

A priori, it is not obvious to produce a basis of commun eigenvectors to l^2 and l_z., since the rotational invariance is broken by the presence of the flux tube. Nonetheless, as we shall see, it is possible to diagonalize simultaneously l^2 and l_z. The spherical representation of the kinetic momentum algebra is [17]:

$$l^+ = e^{i\varphi}\left(\frac{\partial}{\partial\theta} + i\cot\theta\frac{\partial}{\partial\varphi}\right) \tag{11.85}$$

$$l^- = e^{-i\varphi}\left(-\frac{\partial}{\partial\theta} + i\cot\theta\frac{\partial}{\partial\varphi}\right) \tag{11.86}$$

$$l_z = \frac{1}{2}[l^+, l^-] = \frac{1}{i}\frac{\partial}{\partial\varphi} \tag{11.87}$$

The operator algebra gives rise to two ladders of states. The $(-)$ ladder corresponds to states descending, by the repeated action of l^-, from the highest weight state $\psi_0^{(-)}$, such as $l^+\psi_0^{(-)} = 0$. The states $\psi_0^{(-)}$ have the form

$$\psi_0^{(-)}(\theta, \varphi) = f^{(-)}(\theta)e^{i(l+\gamma)\varphi}, \tag{11.88}$$

with l an integer, and is such as

$$\left(\frac{\partial}{\partial\theta} + i\cot\theta\frac{\partial}{\partial\varphi}\right)e^{i(l+\gamma)\varphi}f^{(-)}(\theta) = 0, \tag{11.89}$$

so that $f^{(-)}(\theta) \propto (\sin\theta)^{l+\gamma}$, with $l + \gamma > 0$. We take $\gamma \in]0, 1[$, and $l = 0, 1, ...$ For a given l, we can produce $l + 1$ descending states by the repeated action of l^-. For these states, $l_z = \gamma, 1+\gamma, ..., l+\gamma$ and $\mathrm{l}^2 = (l+\gamma)(l+\gamma+1)$. The $(+)$ ladder correspond to states ascending, by the repeated action of l^+, from the highest weight state $\psi_0^{(+)}$ such as $l^-\psi_0^{(+)} = 0$. $\psi_0^{(+)}$ has the form

$$\psi_0^{(+)}(\theta, \varphi) = f^{(+)}(\theta)e^{i(l+\gamma)\varphi}, \tag{11.90}$$

with l and integer, and is such as

$$\left(-\frac{\partial}{\partial\theta}+i\cot\theta\frac{\partial}{\partial\varphi}\right)e^{i(l+\gamma)\varphi}f^{(+)}(\theta)=0, \tag{11.91}$$

so that $f^{(+)}(\theta)\propto(\sin\theta)^{-(l+\gamma)}$, with $l+\gamma<0$, so that $|l|\leq -1$. The repeated action of l^+ produces $|l|$ states with $l_z=l+\gamma,l+\gamma+1,...,-1+\gamma$ and $\mathbf{l}^2=(l+\gamma)(l-1+\gamma)$.

We now enumerate the first states. With $l=0$, $E=\gamma(\gamma+1)$ and the degeneracy g is 1. With $l=-1$, $E=(1-\gamma)(2-\gamma)$ and $g=1$. With $l=1$, $E=(1+\gamma)(2+\gamma)$ and $g=2$. If $l=-2$, $E=(2-\gamma)(3-\gamma)$ and $g=2$. If $l=2$, $E=(2+\gamma)(3+\gamma)$ and $g=3$. If $l=-p$, $E=(p-\gamma)(p+1-\gamma)$ and $g=p$ and if $l=p$, $E=(p+\gamma)(p+1+\gamma)$ and $g=p+1$.

We now turn to the calculation of permanent currents, since this is the quantity we shall compute using numerical diagonalizations for a small number of electrons. We distinguish between two cases: $p(p-1)\leq N\leq p^2$ and $p^2\leq N\leq p(p+1)$. First, if $p(p-1)\leq N\leq p^2$, we note $\rho=N-p(p-1)$. The total energy is given by

$$\begin{aligned}E_{tot} &= \sum_{m=1}^{p-1}\left((m-1+|\gamma|)(m+|\gamma|)+(m-|\gamma|)(m+1-|\gamma|)\right)m+(p-1+|\gamma|)(p+|\gamma|)\rho \qquad (11.92)\\ &= \frac{1}{2}p^2(p-1)^2+p(p-1)\rho+\left((2p-1)\rho-p(p-1)\right)|\gamma|+\left(\rho+p(p-1)\right)\gamma^2 \qquad (11.93)\end{aligned}$$

for $\gamma\in[-1/2,1/2]$. If $p^2\leq N\leq p(p+1)$, we note $\rho'=N-p^2$ and, for $\gamma\in[-1/2,1/2]$, we obtain

$$E_{tot}=\frac{1}{2}p^2(p-1)^2+p^2(p-1)+p(p+1)\rho'+\left(p^2-(2p+1)\rho'\right)|\gamma|+\left(p^2+\rho'\right)\gamma^2. \tag{11.94}$$

The current $dE_{tot}/d\gamma$ is discontinuous for half integer values of γ, as for the ring, but further discontinuities appear for integer values of γ. The jump in the current at $\gamma=0$ is

$$\frac{dE_{tot}}{d\gamma}(0^+)-\frac{dE_{tot}}{d\gamma}(0^-)=2\left((2p-1)\rho-p(p-1)\right), \tag{11.95}$$

or

$$\frac{dE_{tot}}{d\gamma}(0^+)-\frac{dE_{tot}}{d\gamma}(0^-)=2\left(p^2-(2p+1)\rho'\right). \tag{11.96}$$

The first term corresponds to the case $p(p-1)\leq N\leq p^2$, and the second case to $p^2\leq N\leq p(p+1)$. The jump of the current at $\gamma=1/2$ is

$$\frac{dE_{tot}}{d\gamma}(\frac{1}{2}^+)-\frac{dE_{tot}}{d\gamma}(\frac{1}{2}^-)=-4p\rho, \tag{11.97}$$

or

$$\frac{dE_{tot}}{d\gamma}(\frac{1}{2}^+)-\frac{dE_{tot}}{d\gamma}(\frac{1}{2}^-)=-4p(p-\rho'). \tag{11.98}$$

We now specialize to the case $N=6$, since we shall perform exact diagonalizations for 6 electrons. In this case, $\rho=0$ and the current has only discontinuities for integer values of $\gamma=\overline{\phi}/\phi_0$. The shape of the current as a function of the central charge is similar to the case of the ring, which is plotted on figure 11.7, excepted that a discontinuity is present for $Q=0$.

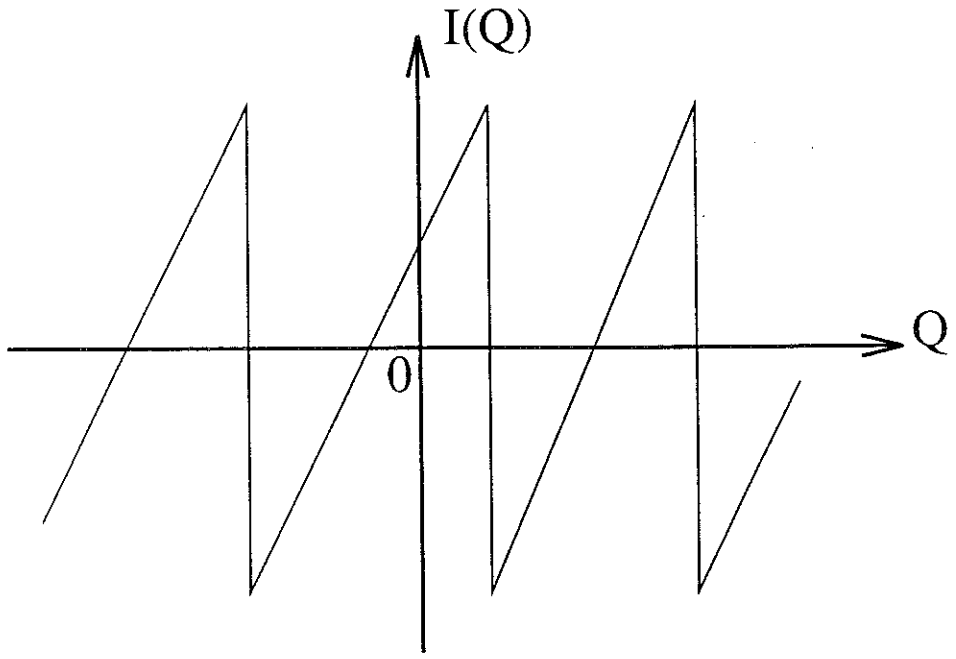

Figure 11.7:
Variations of the electronic current as a function of the central charge in the mean field approach. The period of the variations is of the order of 16 e^-. The residual current at $Q = 0$ originates from the Aharanov-Bohm currents induced by the presence of the flux in the hole of the ring.

11.6.2 Numerical procedure

We assume that the magnetic field is large enough to neglect the excitations from the first Landau level to higher Landau levels. We propose to diagonalize numerically the Coulomb interaction inside the Hilbert space generated by the set of the occupations of the lowest Landau level. The quantum Hall effect on the sphere has been studied by Haldane [15]. He proposes a set of coherent states which span the lowest Landau level Hilbert space. From this set of coherent states, we can extract the following basis of the lowest Landau level Hilbert space

$$\phi_\alpha(\mathrm{x}) = \langle \mathrm{x}|\alpha\rangle = N_\alpha(\sin\frac{\theta}{2})^\alpha(\cos\frac{\theta}{2})^{2S-\alpha}e^{i\varphi(S-\alpha)}, \tag{11.99}$$

where N_α is chosen in such a way that

$$\int |\phi_\alpha(\mathrm{x})|^2 d\mathrm{x} = 1. \tag{11.100}$$

The label α indexes the orbitals of the lowest Landau level and runs from 1 to $2S+1$. One needs to compute the matrix elements of the Coulomb interaction. The interaction V_1 between the electrons on the sphere and the classical charge located at the north pole is a one-body operator and the interactions V_2 between the electrons on the sphere is represented by a two-body operator. Using the second quantization, it is straightforward to derive expressions for the matrix elements of $\hat{V}_1$ and $\hat{V}_2$ on the basis of the states with all the possible occupation numbers of the lowest Landau level. We do not give here the details of the calculations. One is left with a symmetric matrix to be diagonalized using a Jacobi method. The ground state is used to calculate the expectation value of the one-body current operator. The total intensity is obtained after an integration of the current $j(\theta)$ over the angular coordinate.

11.6.3 Results

The intensity as a function of the charge is plotted on figure 11.8 for $\nu = 1/2$ and for 6 electrons. The computed intensity variations are more complex than the one predicted in the mean field theory for $\rho = 0$. Even though some discontinuities are present, which are reminiscent of the mean field behaviour, the intensity variations are not periodic as a function of the charge at the north pole, which is in qualitative disagreement with mean field calculations.

At this stage however, we are not yet ready for a detailed comparison between the composite mean-field theory perdiction and the exact diagonalization result. First and certainly crucial, previous studies have shown that the $\nu = 1/2$ state on the sphere with 6 electrons is degenerate, since the corresponding angular momentum is $L = 3$ [7]. The physics of this degeneracy lifting due to the external charge has not been addressed in our previous approach. It may also be that our assumption of replacing the induced effective Aharonov-Bohm flux by its average value is questionable for such a system. Clearly, further studies are needed, bu chosing non degenerate ground states($N = 4$ and $N = 9$ are the possible candidates), and by performing a detailed analysis of the composite fermion mean-field model on the sphere, taking explicitely into account the possible degeneracies. However, the positive result gained here is that under the influence of the external charge, the ground state undergoes some level crossings as this charge is varied, as signaled by the discontinuities of the persistent current. The existence of these crossings is not obvious a priori , and shows that the composite fermion mean-field model is at least qualitatively correct in predicting their existence. It shows also that this phenomenon goes

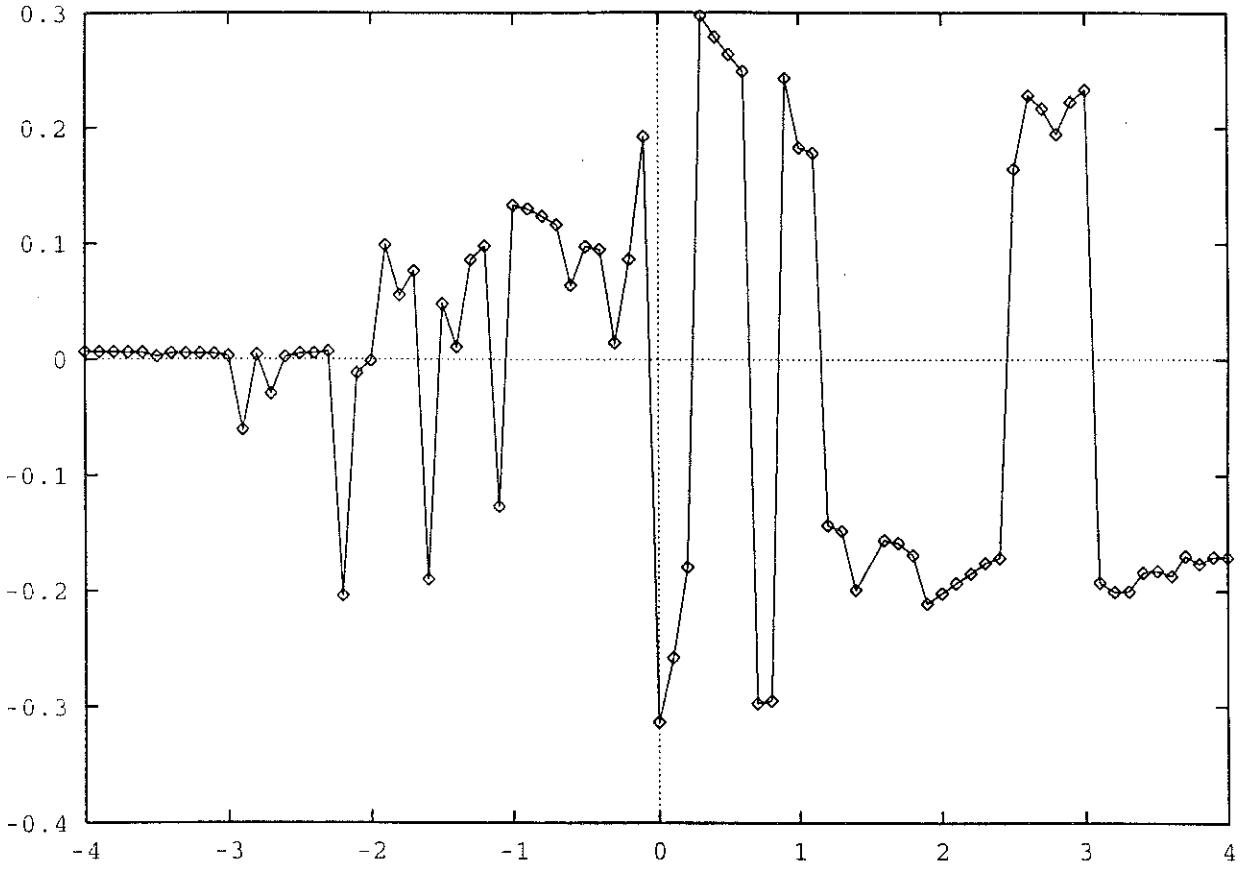

Figure 11.8:
Intensity as a function of the charge for $\nu = 1/2$. The intensity is $I = \int j(\theta) d\theta$. The radius R of the sphere is taken to be 1. The charge $-Q$ is plotted in units of the electronic charge e. The current is plotted in units of $2e\hbar/M^*$. The system contains 6 electrons. The size of the Hilbert space is 462.

beyond ordinary linear response theory, so an experiment in this geometry probes maybe more delicate properties of this system than for instance measurements of the q and ω dependent conductivity.

We also computed the intensity at filling fractions away from $\nu = 1/2$. The variations of the intensity for $\nu = 1/3$ and 4 electrons are plotted on figure 11.9. Even way from $\nu = 1/2$, discontinuities are present in the intensity variations. So far, we have not attempted to provide a simple model for other fillings than 1/2. But, as was done recently for instance in [18] to evaluate response functions, it is still possible to consider $2\phi_0$ flus tubes, and a non-vanishing effective flux which corresponds to p filled Landau levels for the composite fermions to describe the $\nu = p/(2p+1)$ system. On the spherical geometry, the typical problem to solve involves free spinless fermions with a Dirac monopole inside the sphere, superimposed to an Aharonov-Bohm flux. We leave this problem for a future investigation. The qualitative difference from the $\nu = 1/3$ case is that the intensity is negative for $\nu = 1/3$ whereas the sign of the intensity changes in the $\nu = 1/2$ case. Notice that, on figure 11.8, the intensity becomes positive for a charge equal to -4 electronic charge. In this case, the total charge on the sphere is of the same order than the charge at the north pole. This situation does not correspond to the physical regime we investigate.

In the spherical geometry, one can have a simple estimation of the bound charge at the north pole. To do so, we simply compute the weight $\langle 0|c_\alpha^+ c_\alpha|0\rangle$ of the orbital centered around the north pole, that is the orbital $\alpha = 0$ in equation (11.99). In the case $\nu = 1/2$, the variations of the bound charge are plotted on figure 11.10. We find that the bound charge at the north pole is strongly correlated with the total intensity of figure 11.8. We observe that for some values of a negative charge at the north pole, it is possible to bind one electron, in spite of the Coulomb repulsion. Clearly, this situation is not predicted in the mean field theory. In the mean field theory, we expect that a negative charge at the north pole would repel the quasiparticules on the sphere from the north pole. Since the density operator is the same for quasiparticules and real electrons, the density of real electrons should decrease as a decreasing negative charge is present at the north pole.

The variations of the bound state in the case $\nu = 1/3$ are plotted on figure 11.11. These variations are not obviously correlated to the intensity variations of figure 11.9. For negative charges at the north pole, no electron is bound at the north pole. If the charge at the north pole is positive, it is possible to form bound states for certain values of the charge. In particular, we observe that, for a charge $+1/3$ at the north pole, a charge $-1/3$ is bound, which is consistent with 1/3 fractionally charged excitations. However, one open question is to understand why no fractionally charged quasiholes are bound for negative charges at the north pole.

11.7 Conclusion

We have shown that a charge in the middle of ring of $\nu = 1/2$ electrons induces currents which vary periodically as a function of the central charge. The mechanism for the generation of these periodic currents involves a polarization of the electron liquid on the ring. A positive charge variation appears on the interior edge of the ring, and an accumulation of negative charges appears on the external edge of the sample. These charges screen the field of the central charge. A quantum mechanical as well as a classical calculation lead to the same order of magnitude for the polarization charge. The appearance of currents on the ring is mediated by the variation of the Chern-Simons gauge field at mean field level. The presence of polarization charges on

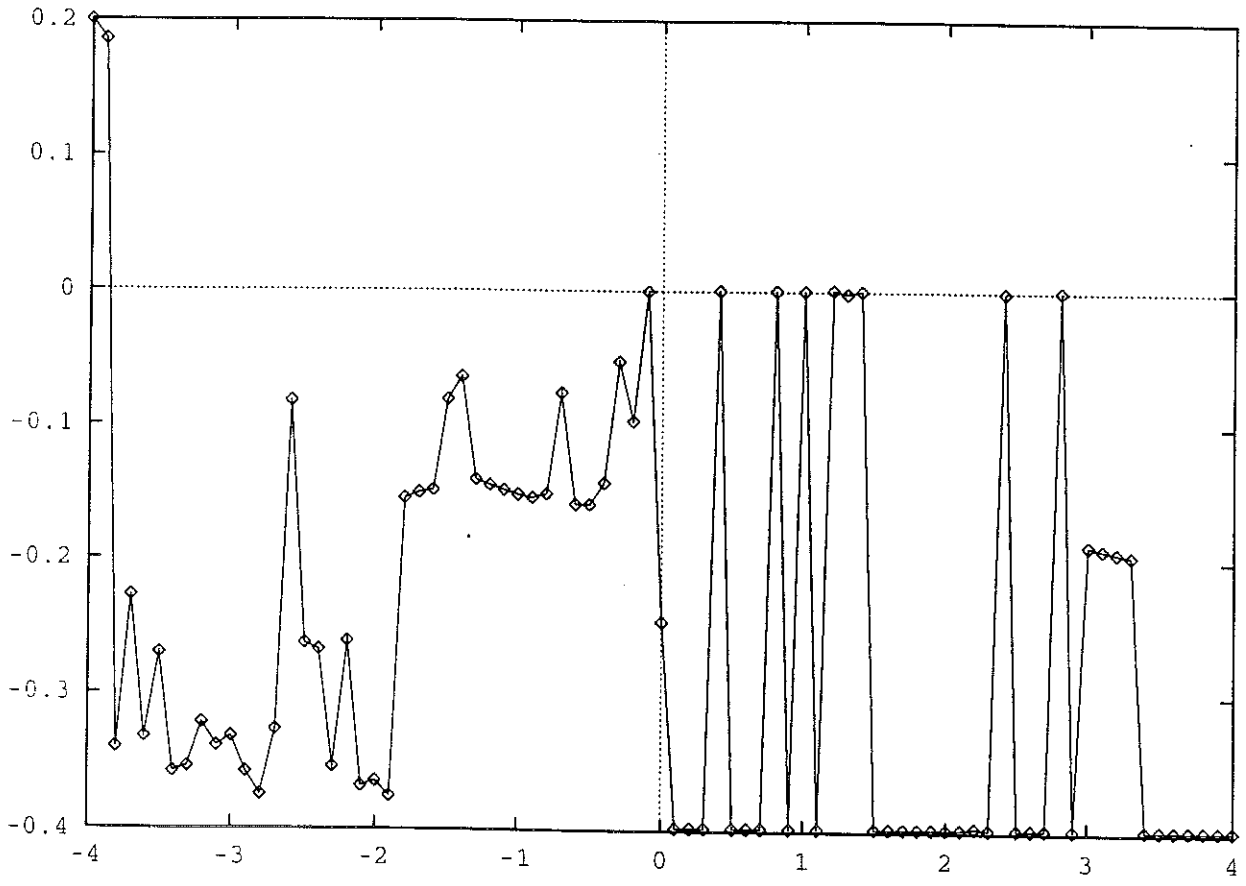

Figure 11.9:
Intensity as a function of the charge for $\nu = 1/3$. The intensity is $I = \int j(\theta) d\theta$. The radius R of the sphere is taken to be 1. The charge $-Q$ is plotted in units of the electronic charge e. The current is plotted in units of $2e\hbar/M^*$. The system contains 4 electrons. The size of the Hilbert space is 210.

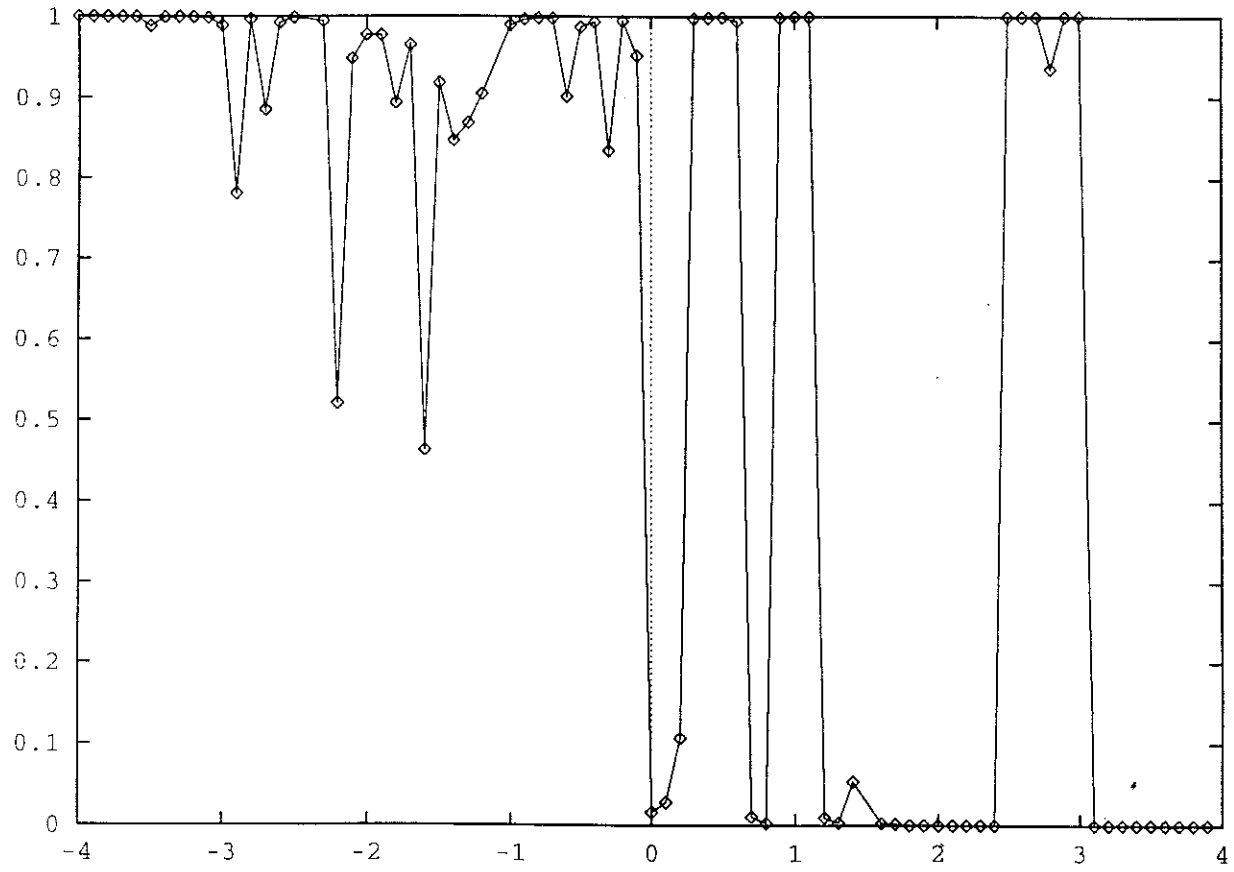

Figure 11.10:
Variations of the bound charge at the north pole as a function of the charge at the north pole in the case $\nu = 1/2$. The charge $-Q$ is taken in units of the electronic charge e.

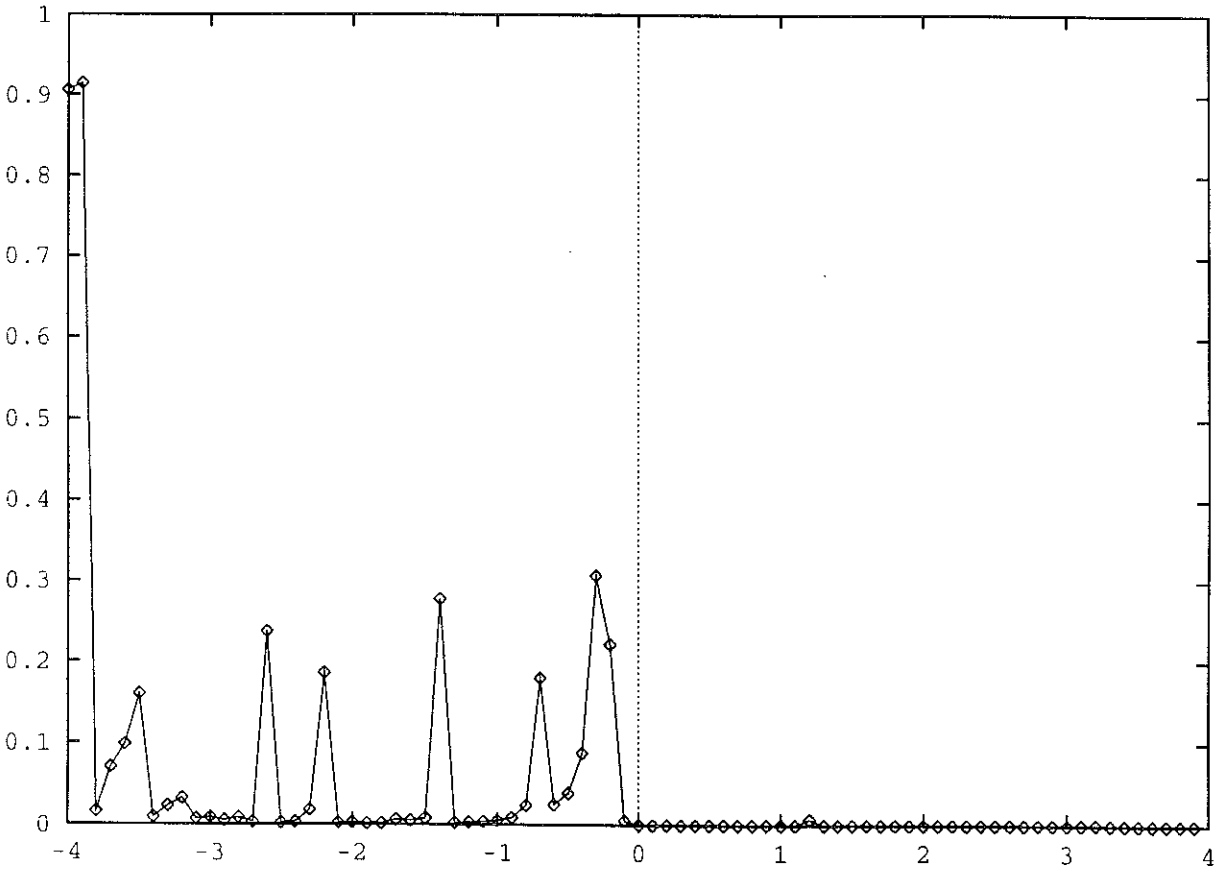

Figure 11.11:
Variations of the bound charge at the north pole as a function of the charge at the north pole in the case $\nu = 1/3$. The charge $-Q$ is taken in units of the electronic charge e.

the edges on the sample induces a non-zero average flux through the ring. By increasing the charge, one should be able to produce periodic currents in the ring. The order of magnitude of these Aharonov-Bohm currents is such that they can be measured [19]. The amplitude of the current fluctuations is typically 2.0 nA for a ring of radius 1 μm and transverse dimension 0.1 μm and a magnetic field of 20 T. If one can produce a continuous charge in the middle of the ring, one should be able to find experimentally the period of the phenomenon, which is of the order of 16 electrons. Residual currents should also appear in the absence of the charge, because of the presence of a magnetic flux through the ring. The experimental observation of such currents should be a direct test of the existence of a statistical gauge field in the $\nu = 1/2$ quantum Hall effect. We also carried out numerical computations in the spherical geometry. The mean field picture at $\nu = 1/2$ predicts discontinuities in the intensity plotted as a function of the extra charge. This qualitative feature of the variations of the intensity is indeed observed from exact diagonalization results, and is the main result of this work. However, the current is not periodic as a function of the charge at the north pole, possibly because we considered a degenerate ground state. Numerical computations at other filling fractions than $1/2$ were also carried out, and discontinuities also appear at $\nu = 1/3$ even though the Fermi liquid picture does not hold at these filling fractions. The analysis of the bound charge at the north pole as a function of the external charge at the same place reveals qualitative differences with the mean field theory at $\nu = 1/2$. In particular, bound states are possible between a negative charge at the north pole and an electron, for certain values of the external charge. The existence of such bound states is not predicted by the mean field theory.

Our analysis shows that the type of experiment we consider would be a good test for the mean field theory of the $\nu = 1/2$ quantum Hall effect since the presence of an extra charge allows to explore excited states properties, and this in a way which goes beyond linear response theory, since it involves level crossings and non-trivial reshuffling of the many body ground state as the external charge is varied.

The authors acknowledge L. Lévy for stimulating discussions which encouraged us to carry on this investigation.

References

[1] J.K. Jain, Phys. Rev. Lett. 63, 199 (1989); Phys. Rev. B 41, 7653 (1990); Adv. Phys. 41, 105 (1992).

[2] R.L. Willet et al, Phys. Rev. Lett. 71, 3846 (1993); W Kang et al, Phys. Rev. Lett. 71, 3850 (1993); R.R. Du et al, Phys. Rev. Lett. 70, 2944 (1993); D.R. Leadley et al, Phys. Rev. Lett. 72, 1906 (1994); R.R. Du et al, Solid State Comm. 90, 71 (1994); V.J. Goldman, B. Su and J.K. Jain, Phys. Rev. Lett. 72, 2065 (1994).

[3] B.I. Halperin, P.A. Lee and N. Read, Phys. Rev. B; see also A. Lopez and E. Fradkin, Phys. Rev. B 44, 5246 (1991); V. Kalmeyer and S.C. Zhang, Phys. Rev. B 46, 9889 (1992).

[4] Y. Aharanov, D. Bohm, Phys. Rev. 115, 125 (1959).

[5] Y.B. Kim, P.A. Lee, X.G. Wen and P.C.E. Stamp, Phys. Rev. B 51, 10779 (1995); A. Stern and B.I. Halperin, Harvard University preprint (1995).

[6] Compare for instance the paper by D.R. Leadly et al and the second paper by R.R. Du et al in Ref. [2].

[7] E. Rezzayi and N. Read, Phys. Rev. Lett. 72, 900 (1994).

[8] R. Morf and N. d'Ambrumenil, Phys. Rev. Lett. 74, 25 (1995).

[9] Y. Aharonov and A. Casher, Phys. Rev. Lett. 53, 319 (1984).

[10] W.J. Elion, J.J. Wachters, L.L. Sohn and J.E. Mooij, Phys. Rev. Lett. 71, 2311 (1993).

[11] E.N. Bogachek, G.A. Gogadze, J.E.T.P. 36, 973 (1973).

[12] M.S. Svirskii, J.E.T.P. Lett. 42, 270 (1985).

[13] See for instance M. Büttiker, Y. Imry and R. Landauer, Phys. Lett. 96 A, 365 (1983).

[14] N.W. Ashcroft and N.D. Mermin *Solid State Physics*, Saunders (1976).

[15] F.D.M. Haldane, Phys. Rev. Lett. 51, 605 (1983).

[16] S. Olariu and I. Popescu, Rev. Mod. Phys. 57, 339 (1985).

[17] R. Shankar *Principles of Quantum Mechanics*, Plenum Press, New York (1980) pp 343-345.

[18] S.H. Simon and B.I. Halperin, Phys. Rev. B 50, 1807 (1994) and S. He, S.H. Simon and B.I. Halperin, Ibid, 50, 1823 (1994).

Chapitre 12

Compléments au chapitre 11

Le but de cette partie est d'introduire quelques points techniques qui sont utilisés dans l'article présenté au chapitre 11. D'une part, lors du calcul de l'écrantage en géométrie finie, il est utile de savoir calculer numériquement des intégrales comportant une divergence logarithmique. Ces intégrales sont calculées par la méthode des paraboles et la divergence logarithmique est traitée explicitement. D'autre part, il faut savoir calculer les éléments de l'opérateur de potentiel Coulombien sur les différents états du premier niveau de Landau. Ces deux points techniques sont traités successivement dans ce qui suit.

12.1 Calcul d'intégrales par la méthode des paraboles

Soit une fonction continue f définie sur le segment $[0, a]$. L'intervalle $[0, a]$ est discrétisé en $2M$ segments de même largeur s. L'approximation des paraboles s'écrit

$$\int_0^a f(x)dx = \sum_{m=0}^{M-1} \int_{2ms}^{2(m+1)s} f(x)dx \tag{12.1}$$

$$\simeq \sum_{m=0}^{M-1} 2s \left(\frac{1}{6} f(2ms) + \frac{2}{3} f((2m+1)s) + \frac{1}{6} f(2(m+1)s) \right). \tag{12.2}$$

Une formule utile est celle de l'intégrale d'une fonction possédant une divergence logarithmique. En utilisant la méthode des paraboles, et en intégrant explicitement la divergence logarithmique, nous obtenons

$$\begin{aligned} \int_0^a \ln \frac{1}{|ns - x|} f(x)dx &\simeq s \sum_{m=0}^{M-1} \left(\frac{A_m}{3}(a_m^3 + 1) + \frac{B_m}{2}(a_m^2 - 1) + C_m(a_m + 1) \right) \ln \frac{1}{s|a_m + 1|} \\ &- \left(\frac{A_m}{3}(a_m^3 - 1) + \frac{B_m}{2}(a_m^2 - 1) + C_m(a_m - 1) \right) \ln \frac{1}{s|a_m - 1|} \\ &+ \frac{2}{3} A_m (a_m^2 + \frac{1}{3}) + B_m a_m + 2C_m, \end{aligned} \tag{12.3}$$

où

$$a_m = n - 2m - 1 \tag{12.4}$$

$$A_m = \frac{1}{2}(f(2(m+1)s) + f(2ms) - 2f((2m+1)s)) \quad (12.5)$$

$$B_m = \frac{1}{2}(f(2(m+1)s) - f(2ms)) \quad (12.6)$$

$$C_m = f((2m+1)s) \quad (12.7)$$

12.2 Eléments de matrice de la perturbation Coulombienne

Haldane[1] propose de considérer l'effet Hall quantique en géométrie sphérique, dans le champ d'un monopôle magnétique. Haldane donne une famille d'états cohérents qui génèrent le premier niveau de Landau. De cette famille d'états cohérents, il est possible d'extraire une base du premier niveau de Landau, donnée par

$$\phi_\alpha(\mathrm{x}) = \langle \mathrm{x}|\alpha\rangle = N_\alpha(\sin\frac{\theta}{2})^\alpha(\cos\frac{\theta}{2})^{2S-\alpha}e^{i\varphi(S-\alpha)}, \quad (12.8)$$

où N_α est choisi de telle sorte que chaque orbitale soit normée:

$$\int |\phi_\alpha(\mathrm{x})|^2 d\mathrm{x} = 1. \quad (12.9)$$

L'index α repère les orbitales du premier niveau de Landau et varie de 1 à $2S+1$. Nous nous proposons de calculer les éléments de matrice de l'interaction Coulombienne entre les états (12.8). L'interaction $\hat{V}_1$ entre les électrons sur la sphère et la charge classique localisée au pôle nord est un opérateur à un corps et l'interaction $\hat{V}_2$ entre les électrons sur la sphère est un opérateur à deux corps. Nous calculons tout d'abord les éléments de matrice de l'opérateur à un corps $\hat{V}_1$. Les éléments de matrice de $\hat{V}_1$ sur la base $\{|\alpha\rangle\}$ s'écrivent

$$\langle\alpha|V_1|\beta\rangle = \int \bar{\phi}_\alpha(\mathrm{x})\frac{Qe}{4\pi\epsilon_0 d(\mathrm{x})}\phi_\beta(\mathrm{x})d\mathrm{x}, \quad (12.10)$$

où $d(\mathrm{x})$ est la distance entre le pôle nord et le point x sur la sphère. L'expression de $\hat{V}_1$ en seconde quantification est

$$V_1 = \sum_{\alpha,\beta} V_{\alpha\beta}c^+_\alpha c_\beta. \quad (12.11)$$

Les nombres d'occupation du niveau de Landau le plus bas sont notés α_i, où $i \in \{1,...,N\}$ indexe l'état

$$|(\alpha)\rangle = c^+_{\alpha_1}...c^+_{\alpha_N}|0\rangle. \quad (12.12)$$

Nous cherchons les éléments de matrice de $\hat{V}_1$ entre deux états donnés $|(\alpha)\rangle$ et $|(\beta)\rangle$. Il est clair que $\hat{V}_1$ ne connecte entre eux que des états ne différant que de zéro ou une excitation particule-trou du type $c^+_\alpha c_\beta$. Les éléments de matrice diagonaux de $\hat{V}_1$ sont

$$\langle(\alpha)|V_1|(\alpha)\rangle = \sum_{i=1}^{N} V_{\alpha_i\alpha_i}. \quad (12.13)$$

Les éléments non diagonaux sont calculés comme suit. Si nous notons

$$|(\alpha)\rangle = \pm c^+_{\alpha_k}c_{\beta_l}|(\beta)\rangle, \quad (12.14)$$

[1] F.D.M. Haldane, Phys. Rev. Lett. 51, 605 (1983).

l'élément de matrice s'écrit

$$\langle(\alpha)|V_1|(\beta)\rangle = (-1)^{k+l}\langle\alpha_k|V_1|\beta_l\rangle. \tag{12.15}$$

En fait, ces éléments de matrice sont nuls: à cause de l'intégration sur l'angle φ, la matrice $(V_1)_{\alpha,\beta}$ est diagonale. En ce qui concerne l'opérateur à deux corps, les éléments de matrice de $\hat{V}_2$ sur la base $\{|\alpha\rangle\}$ sont

$$\langle\alpha\beta|V_2|\gamma\delta\rangle = \int \bar{\phi}_\alpha(\mathrm{x})\bar{\phi}_\beta(\mathrm{x}')\frac{e^2}{4\pi\epsilon_0 d(\mathrm{x}-\mathrm{x}')}\phi_\gamma(\mathrm{x})\phi_\delta(\mathrm{x}')d\mathrm{x}d\mathrm{x}', \tag{12.16}$$

et $\hat{V}_2$ est représenté en seconde quantification par

$$V_2 = \frac{1}{2}\sum_{\alpha\beta\gamma\delta}\langle\alpha\beta|V_2|\gamma\delta\rangle c_\alpha^+ c_\beta^+ c_\delta c_\gamma. \tag{12.17}$$

$\hat{V}_2$ possède des éléments de matrice non nuls seulement entre les états $|(\alpha)\rangle$ et $|(\beta)\rangle$ avec zéro, une ou deux excitations particule-trou. Si nous appelons

$$I[(\alpha),(\beta)] = \frac{1}{2}\sum_{\alpha=1}^{2S+1}|n_\alpha - n_\beta|, \tag{12.18}$$

nous pouvons voir que les différents cas correspondent à $I = 0, 1, 2$. Commençons par les éléments diagonaux ($I = 0$). Après un peu d'algèbre, nous obtenons

$$\langle(\alpha)|V_2|(\alpha)\rangle = \sum_{\langle i,j\rangle}(\langle\alpha_i\alpha_j|V_2|\alpha_i\alpha_j\rangle - \langle\alpha_j\alpha_i|V_2|\alpha_i\alpha_j\rangle). \tag{12.19}$$

La somme porte sur les paires d'indices dans l'ensemble $\{1,...,N\}$. Considérons maintenant le cas $I[(\alpha),(\beta)] = 1$ en utilisant la notation de l'équation (12.14). Nous trouvons alors

$$\langle(\beta)|V_2|(\alpha)\rangle = \sum_{i=1,i\neq k}^{N}(-1)^{k+l+i+j+\theta(i-k)+\theta(j-l)}(\langle\beta_l\alpha_i|V_2|\alpha_k\alpha_i\rangle - \langle\alpha_i\beta_l|V_2|\alpha_k\alpha_i\rangle), \tag{12.20}$$

où l'index de particule j est choisi de telle sorte que $\alpha_i = \beta_j$. Nous traitons maintenant le cas $I[(\alpha),(\beta)] = 2$, et nous notons

$$|(\alpha)\rangle = \pm c_{\alpha_{k_1}}^+ c_{\alpha_{k_2}}^+ c_{\beta_{l_1}} c_{\beta_{l_2}}|(\beta)\rangle \tag{12.21}$$

avec $k_1 < k_2$ et $l_1 < l_2$. Les éléments de matrice sont donnés par

$$\langle(\beta)|V_2|(\alpha)\rangle = (-1)^{k_1+k_2+l_1+l_2}(\langle\beta_{l_1}\beta_{l_2}|V_2|\alpha_{k_1}\alpha_{k_2}\rangle - \langle\beta_{l_2}\beta_{l_1}|V_2|\alpha_{k_1}\alpha_{k_2}\rangle). \tag{12.22}$$

Les relations définissant les éléments de matrice peuvent être utilisées dans un programme pour écrire la matrice de l'interaction Coulombienne. La seconde étape consiste à diagonaliser cette matrice. C'est cette démarche que nous avons suivie au chapitre 11.

Partie II

Dynamique de systèmes vitreux

Chapitre 13

Introduction aux systèmes de spins vitreux

Il existe de nombreux livres et articles de revue sur les verres de spin. Pour écrire ce chapitre, j'ai utilisé le cours de R. Rammal et J. Souletie[1], le livre de Fisher et Hertz[2], l'article de revue de G. Toulouse[3] et la revue de l'école russe[4]. Je développerai certains aspects expérimentaux des systèmes 'verres de spin' ainsi que certains aspects numériques. C'est volontairement que je n'aborderai pas la théorie du modèle SK et la brisure de symétrie de répliques, car je n'ai pas utilisé cette approche dans le chapitres suivants.

13.1 Susceptibilité statique et dynamique

Les expériences sur les composés dits *verres de spin* datent des années 1970[5]. Le problème à une impureté est le problème Kondo. Lorsqu'un ion mangétique est en interaction avec les électrons de conduction, il perd son caractère magnétique en dessous de la température Kondo T_K. Dans un certain nombre de systèmes comme CuMn, AuMn, AgMn, AuFe, AuCr,..., la température Kondo T_K est suffisamment petite pour qu'il existe une interaction entre impuretés sur une large gamme de concentrations. L'interaction entre impuretés magnétiques est de type Ruderman-Kittel-Kasuya-Yosida[6](R.K.K.Y.). A longues distances, l'interaction vaut

$$H_{i,j} = \frac{J}{k_F r_{i,j}^3} \cos(2k_F r_{i,j}) \mathbf{S}_i . \mathbf{S}_j, \tag{13.1}$$

avec

$$J = \frac{9\pi}{8} \frac{Z^2 j^2}{E_F}, \tag{13.2}$$

[1] R. Rammal and J. Souletie, *Spin Glasses* (1981).

[2] K.H. Fisher and J.A. Hertz, *Spin Glasses*, Cambridge study in magnetism, Cambridge University Press (1991).

[3] G. Toulouse *Frustration de désordre: problèmes nouveaux en mécanique statistique. Histoire des verres de spin* dans le compte rendu du Congrès de la Société Française de Physique (1981).

[4] V.S. Dotsenko, M.V. Feigel'man and L.B. Ioffe, *Spin Glasses and Related Problems*, Soviet Scientific Reviews, section A, Vol. 15 (1990).

[5] V. Canella and J.A. Mydosh, *Magnetic ordering in gold-iron alloys*, Phys. Rev. B 6, 4220-4237 (1972).

[6] M.A. Ruderman and C. Kittel, Phys. Rev. 96, 99 (1954); T. Kasuya, Prog. Theoret. Phys. 16, 45 (1956); K. Yosida, Phys. Rev. 106, 893 (1957).

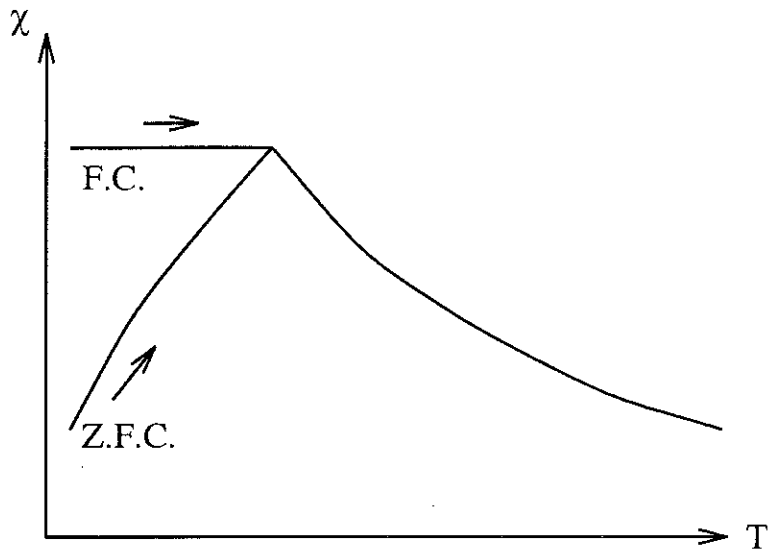

Figure 13.1: Allure des variations de la susceptibilité statique pour un verre de spin. La courbe 'Field Cooled' (F.C.) correspond à une expérience pendant laquelle le champ est resté branché pendant le refroidissement. La courbe 'Zero Field Cooled' (Z.F.C.) correspond à une expérience pendant laquelle l'échantillon a été refroidit en champ nul.

où le Hamiltonien entre les électrons de conduction de spin s et l'impureté de spins S vaut

$$H = -2jSs. \tag{13.3}$$

Z est la différence entre la charge électronique d'un atome du réseau et la charge électronique de l'impureté. Les propriétés des verres de spin sont universelles dans le sens où de nombreux composés présentent la même physique. Par exemple les alliages dilués de métaux de transition (Fe,Mn) dans des métaux nobles (Cu,Ag,Au), ou des isolants concentrés (par exemple $Eu_xSr_{1-x}S$), des solides non cristallins (par exemple $CrSnTe_4$) ou encore des ferroélectriques désordonnés (par exemple $K_{1-x}Li_xTaO_3$). Dans une image simplifiée, on peut dire que les moments magnétiques d'un verre de spin gèlent en dessous d'une température de transition T_g dans une configuration aléatoire déterminée par la réalisation des interactions aléatoires dans un échantillon donné. Nous allons maintenant décrire les expériences de susceptibilité statique et dynamique.

13.1.1 Susceptibilité statique

L'allure des variations de la susceptibilité statique est représentée schématiquement sur la figure 13.1[7]. En dessous d'une température T_g, la susceptibilité dépend de l'histoire de l'échantillon. Dans le cas d'un refroidissement sous champ, la susceptibilité présente un plateau alors que dans l'expérience de refroidissement en champ nul, la susceptibilité présente un maximum. La température correspondant au bord du plateau de l'expérience F.C. est identique à la

[7]La figure 13.1 est tracée d'apès l'article S. Nagata, P.H. Keesom and H.R. Harrison, *Low d.c. field susceptibility of CuMn spin glass*, Phys. Rev. B 19, 1633-1638 (1979). Leur expérience porte sur le composé CuMn avec une concentration en Mn de l'ordre de 2%.

température du maximum de l'expérience Z.F.C. et est identifiée à la température de transition vitreuse T_g.

13.1.2 Susceptibilité dynamique

L'expérience de la susceptibilité dynamique est définie comme suit[8]. On soumet le système à un champ magnétique sinusoïdal oscillant autour d'une moyenne nulle avec une fréquence ω (on peut également envisager l'existence d'une composante continue du champ magnétique, mais nous n'abordons pas cette question ici). L'aimantation de l'échantillon est alors forcée à la fréquence ω et vaut

$$M(\omega, t) = \sum_k \theta'_k \cos(k\omega t) + \theta''_k \sin(k\omega t). \tag{13.4}$$

qui ne contient que des harmoniques impaires au-dessus de T_g et en l'absence de champ magnétique statique. Il s'avère qu'à la température de transition, toutes les susceptibilités d'ordre 3,5,... sont divergentes. Il est donc important de tenir compte de la réaction des processus mesurables d'ordre supérieur sur les processus d'ordre inférieur. Dans la limite statique, les modes de Fourier de l'aimantation sont reliés aux susceptibilités selon

$$\theta'_1 = \chi'_1 h + \frac{3}{4}\chi'_3 h^3 + \frac{35}{64}\chi'_7 h^7 + ... \tag{13.5}$$

$$\theta'_3 = \frac{1}{4}\chi'_3 h^3 + \frac{5}{16}\chi'_5 h^5 + \frac{21}{64}\chi'_7 h^7 + ... \tag{13.6}$$

$$\theta'_5 = \frac{1}{16}\chi'_5 h^5 + \frac{7}{64}\chi'_7 h^7 + ... \tag{13.7}$$

$$\theta'_7 = \frac{1}{64}\chi'_7 h^7 + ... \tag{13.8}$$

Une mesure de θ'_7 permet donc de remonter à χ'_7 en utilisant (13.8). On déduit alors χ'_5 à l'aide de (13.7), puis χ'_3 à l'aide de (13.6) et enfin χ'_1 à l'aide de (13.5). Nous avons également utilisé cette méthode au chapitre 16 dans des simulations numériques de systèmes vitreux. Les variations de χ'_1 sont représentées sur la figure 13.2. Les variations de la susceptibilité alternative en fonction de la température à différentes fréquences présentent trois caractéristiques:

- pour une fréquence donnée, il existe un point anguleux à une certaine température.
- la température du point anguleux se déplace vers les basses températures lorsque la fréquence diminue.
- Le maximum de susceptibilité au point anguleux augmente lorsque la température diminue.

D'autre part, il existe une divergence pour la susceptibilité χ'_3. Dans les expériences et dans les simulations numériques, cette divergence se manifeste par un maximum très prononcé de χ'_3 en fonction de la température.

[8] Pour des données sur les expériences de susceptibilité dynamique, voir L. Lévy, *Critical dynamics of metallic spin glasses*, Phys. Rev. B 38, 4963-4973 (1988).

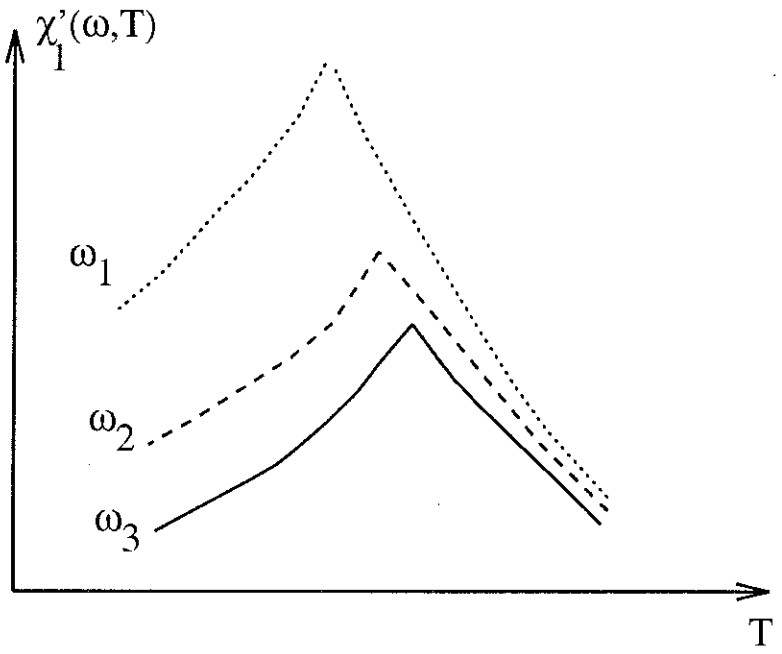

Figure 13.2: Allure des variations de la susceptibilité χ_1' en fonction de la température pour différentes fréquences ω_1, ω_2 et ω_3 telles que $\omega_1 < \omega_2 < \omega_3$.

13.2 Vieillissement

Les résultats différents des expériences de susceptibilité dans l'expérience field cooled et zero field cooled suggèrent que le comportement d'un échantillon dépend fortement du traitement qu'il a subit dans son passé. Nous allons mettre en évidence d'autres effets caractérisés dans les expériences dites de viellissement.

13.2.1 Expérience d'aimantation 'Zero Field Cooled'

Dans cette expérience[9], la température initiale est très supérieure à la température de transition vitreuse T_g. L'échantillon est alors refroidi à une température T inférieure à la température de transition vitreuse T_g. On attend ensuite un certain temps t_w (pouvant atteindre plusieurs heures) avant d'appliquer un champ magnétique et d'enregistrer les variations d'aimantation en fonction du temps. On observe que si $T > T_g$ la courbe d'aimantation ne dépend pas du temps d'attente t_w. Par contre, si $T < T_g$, la courbe d'aimantation dépend explicitement du temps d'attente t_w (voir figure 13.3). Cet effet est appelé *vieillissement*. L'âge de l'échantillon corrrespond au temps d'attente t_w.

13.2.2 Expérience d'aimantation thermorémanente

Cette expérience permet également de mettre en évidence les effets de vieillissement dans les verres de spin. L'échantillon est refroidi sous champ magnétique à une température T inférieure

[9]Nous nous appuyons sur les expériences de L. Lundgren, P. Svedlindh, P. Nordblad and O. Beckman, *Dynamics of the relaxation-time spectrum in a CuMn spin glass*, Phys. Rev. Lett. 10, 911 (1983).

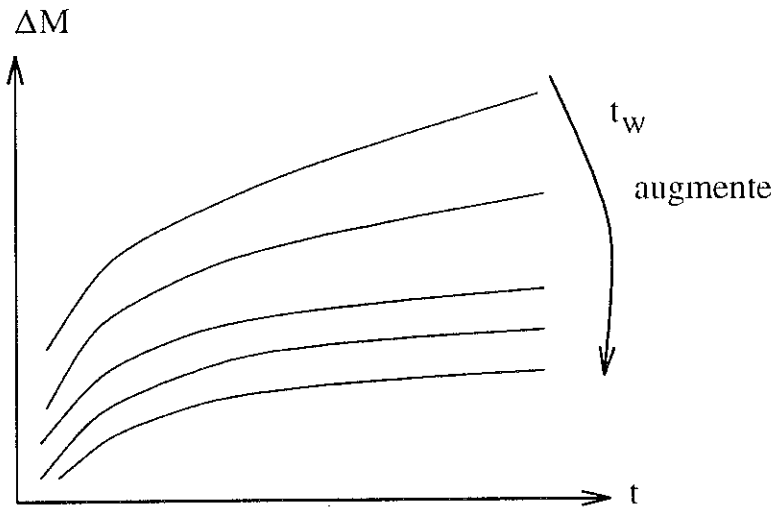

Figure 13.3: Courbe d'aimantation en fonction du temps après avoir attendu un temps t_w. L'origine des temps correspond au branchement du champ magnétique.

à la température de transition T_g. Après un temps d'attente t_w (bien plus grand que le temps nécessaire au refroidissement), on supprime le champ magnétique et on enregistre les variations de l'aimantation en fonction du temps. L'allure des courbes d'aimantation est représentée sur la figure 13.4[10]. En effectuant un changement de variables sur la variable temporelle, il est possible de ramener toutes les courbes de la figure 13.4 sur une courbe universelle. Le changement de variable utilisé est

$$\frac{d\xi}{dt} = \left(\frac{t_0}{t_w + t}\right)^{\mu} dt \tag{13.9}$$

$$\xi = \frac{t_0^{\mu-1}}{1-\mu}\left((t_w + t)^{1-\mu} - t_w^{1-\mu}\right), \tag{13.10}$$

où t_0 est une échelle de temps arbitraire. L'ensemble des courbes d'aimantation thermorémanente s'aligne alors sur une courbe maîtresse lorsqu'elles sont tracées en fonction de ξ. Il n'existe pas actuellement d'explication quantitative de ces expériences de vieillissement.

13.2.3 Expériences numériques

Au niveau numérique, il est possible d'implémenter l'algorithme de Monte Carlo pour mettre en oeuvre la dynamique d'un système de spins. L'unité de temps est alors le 'Monte Carlo step'. Pendant un pas de temps, on tire au hasard un nombre de sites égal au nombre total de sites et pour chaque site tiré au sort, on remet en question l'orientation du spin en utilisant les poids de Boltzmann avec une distribution figée des plus proches voisins. En utilisant cet algorithme, on peut donc mettre en oeuvre toutes les techniques expérimentales décrites précedemment. Nous renvoyons le lecteur au chapitre 16 pour une mesure des susceptibilités dynamiques. Les expériences de type 'aimantation zero field cooled' et 'aimantation thermorémanentes' sont

[10] d'après les expériences de M. Alba, M. Ocio and J. Hammann *Ageing process and response function in spin glasses: an analysis of the thermoremanent magnetization decay in AgMn (2.6%).*, Europhys. Lett. 2, 45-52 (1986).

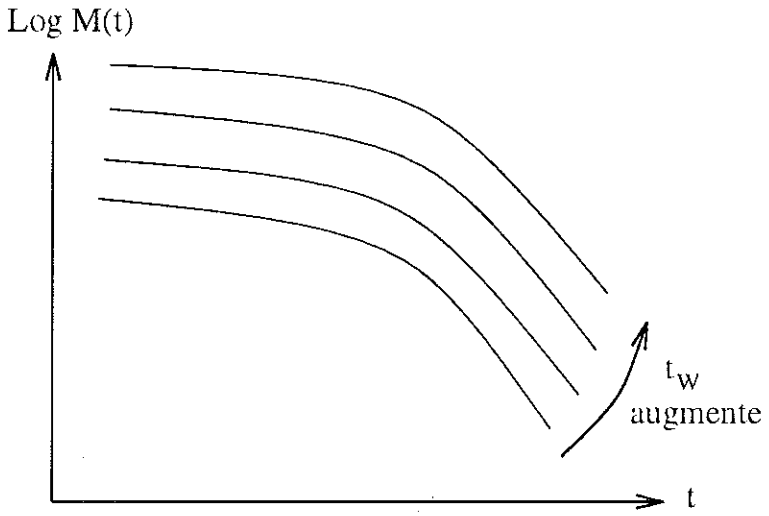

Figure 13.4: Allure des courbes d'aimantation dans l'expérience d'aimantation thermorémanente.

également possibles[11]. Les expériences numériques de type Monte Carlo donnent également accès à des quantités inaccessibles aux expérimentateurs. Une quantité interessante est la fonction d'autocorrélation des spins après un temps d'attente t_w

$$C(t, t_w) = \frac{1}{N} \sum_{i=1}^{N} \overline{\langle \sigma_i(t + t_w) \sigma_i(t_w) \rangle}, \tag{13.11}$$

où $\langle\rangle$ désigne une moyenne thermique sur les différentes réalisations du bruit thermique, mais avec la même configuration initiale, et où la barre désigne une moyenne sur les réalisations du désordre de liens. Si l'on s'intéresse à un modèle sans désordre (ce qui sera le cas dans les chapitres suivants), la moyenne sur le désordre disparaît. L'existence de vieillisement a été mise en évidence dans différents systèmes de type 'verre de spin', par exemple dans le verre d'Ising tridimensionnel[12]. Cependant, le phénomène de vieillissement n'est pas spécifique des systèmes possédant une transition verre de spin. En effet, il existe un certain nombre de phénomènes de physique statistique 'vieillisants' sans désordre ni frustration. C'est par exemple le cas des marches au hasard, des champs gaussiens libres, de la dynamique du modèle XY et de la décomposition spinodale[13]. Nous pouvons également ajouter un certain nombre de modèles de spins sur des réseaux non euclidiens. Par exemple, le modèle d'Ising sur des clusters de percolation devient vitreux pour une température de transition de l'ordre de $J/\ln s$ où s est le nombre de sites dans l'amas[14]. Nous étudions la dynamique du modèle d'Ising sur l'arbre (voir

[11] Voir L.F. Cugliandolo, J. Kurchan and F. Ritort, *Evidence of aging in spin-glass mean field models*, Phys. Rev. B 49, 6331 (1994).

[12] H. Rieger, *Non-equilibrium dynamics and aging in the three-dimensional Ising spin-glass model*, J. Phys. A 26, L615-L621 (1993); J.O. Andersson, J. Matsson and P. Svendlindh, *Monte Carlo studies of Ising spin-glass systems: aging behaviour and crossover between equilibrium and nonequilibrium dynamics*, Phys. Rev. B 46, 8297 (1992).

[13] Ces exemples sont traités en détail dans le preprint de L.F. Cugliando, J. Kurchan and G. Parisi, *Off equilibrium dynamics and aging in unfrustrated systems*, preprint cond-mat/9406053.

[14] Voir R. Rammal, *Spin dynamics and glassy relaxation on fractals and percolation structure*, J. Physique 46, 1837-1842 (1985).

chapitre 16) et nous montrons que la température de transition varie comme $J/\ln n$, où n est le nombre de générations. Nous étudions également le modèle XY sur l'arbre (chapitre 15), qui présente également un relaxation vitreuse à basses températures.

Chapitre 14

Article 6

Diffusion and random walks on the Cayley tree[1]

R. Mélin

CRTBT-CNRS, 38042 Grenoble BP 166X cédex France

We investigate diffusion and random walks on the Cayley tree. These two dynamics are inequivalent on the Cayley tree. A numerical approach reveals that, due to the boundary, the time scales are proportional to the exponential of the length scales, whereas the time scales are proportional to the square of the length scales on Euclidian lattices. To understand this property, we study the Laplacian on the tree. We derive exact equations for the eigenvalues on a Cayley tree. The characteristic polynomial of the Laplacian is splitted into a hierarchy of polynomials (one polynomial per generation on the tree) with a degree inferior or equal to n, the number of generations. The eigenvalues are found to be the root of continuous fraction equations. The behaviour of the largest non zero eigenvalue is related to the anomalous diffusion behaviour. Finally, we compare these results with the Bethe-Peierls approximation via a mapping to a tight-binding problem. The anomalous diffusion properties are not explained in the Bethe-Peierls approximation. Finally, we compare our results with the diffusion problem on the Sierpinsky gasket.

[1]submitted to the Journal of Statistical Physics.

14.1 Introduction

Eventhough it has no physical realisation, it is interesting to develop statistical and quatum physics on the Cayley tree. The infinite limit of a Cayley tree is called a Bethe lattice. In what follows, we consider only the case of coordination 3, but straighforward generalizations to a coordination z are possible. We shall work with full Cayley trees, starting from a center (called the ancestor) with three sons. Each of the ancestor's son has two sons, etc. The ancestor is peculiar, since it has three sons, and the leaves are peculiar too, because they have only one neighbour. We shall also work with *half-space-trees*, for which the ancestor has only two sons. As far as trees are considered, two cases are to be distinguished. First, the Bethe-Peierls approximation consists in considering only the bulk properties, that is the properties of the ancestor. For spin models, this approximation was first implemented in the thirties by Bethe and Peierls [1] [2]. The Bethe-Peierls approximation has been reconsidered recently as an alternative to mean field theories for various problems [3]. For a pedagogical introduction to Bethe lattices and Husimi cactus, we refer the reader to the article by Thorpe [4], where various problems are reviewed, such as the spins 1/2 model, the percolation problem (which is also reviewed in [5]), tight-binding Hamiltonians and phonons.

A second point of view on trees is to consider the properties of Cayley trees, with their boundary included. This approach was developped in the seventies for Ising spin models, where people discovered an unusual transition [6],[7]. At that time, the notion of spin glasses merely emerged and people did not focus on the dynamical properties. The dynamics on the Cayley tree was analyzed only recently [8], and a cross-over towards a glassy phase was found at a temperature $T_g \sim J/\ln n$, with n the number of generations. We underline that a general class of thermodynamic limits was considered in [8], where the properties of m generations are considered, in the limit $m < n$, with $m, n \to +\infty$.

In a previous article [9], we have studied one problem related to the Laplacian on the Cayley tree: the XY model at low temperatures. We showed that below a temperature scale T_g, the Hamiltonian can be replaced by a Gaussian Hamiltonian in terms of differences of angles between two adjacent spins. The Langevin dynamics below T_g is given by

$$\eta \frac{d\theta}{dt} = \Delta\theta + \xi(t), \tag{14.1}$$

where θ denotes the vector of N angles, one per site, and $\xi(t)$ is the vector of N Gaussian white noises. Δ is the Laplacian.

In the present paper, we study two problems on the Cayley tree which are similar to (14.1) but with no noise: the random walk problem on the tree and the diffusion problem on the tree. These two problems are equivalent on Euclidian lattices but become non equivalent on a non Euclidian structure since the coordination is not a constant from one site to the other. On a Cayley tree, the coordination of the leaves is one whereas the coordination of the other sites is 3. On a half-space-tree, the coordination of the ancestor is 2. We shall begin with the diffusion problem, with the evolution equation

$$\tau \frac{\partial \mathbf{P}(t)}{\partial t} = D\Delta\mathbf{P}. \tag{14.2}$$

$\mathbf{P(t)}$ is the vector of the $P(i,t)$ and Δ is the Laplacian, which is a symmetric operator. The diffusion equation (14.2) is identical to (14.1), except that no white noise is present. Within the

dynamics (14.2), we study the evolution of the probability $P(i,t|i_0,t_0)$ such as $P(i,t|i_0,t_0) = \delta_{i,i_0}$. In order to emphasize the boundary effects, we choose i and i_0 among the leaves of the tree. We first treat the problem by means of numerical diagonalizations. This study reveals the existence of an anomalous scaling: if the distance between i and i_0 increases by a constant, the associated time scales for the diffusion are multiplied by a constant. This scaling is to be compared with what happens on an Euclidian structure. The continuous limit of a diffusion process on an Euclidian structure leads to the kernel of the diffusion equation in the continuum [10]

$$p(\mathrm{x},t) = \frac{1}{(4\pi t)^{d/2}} \exp\left(-\frac{|\mathrm{x}|^2}{4t}\right), \tag{14.3}$$

so that the scaling on an Euclidian structure is such as $\mathrm{x} \to \lambda \mathrm{x}$ $t \to \lambda^2 t$, which means that the Hausdorf dimension of random walks is two in Euclidian spaces. To understand the anomalous scaling on the tree, we study the spectrum of the Laplacian by analytical methods. We find that the anomalous diffusion behaviour is related to the behaviour of the largest non zero eigenvalue of the Laplacian, which can be characterized approximately.

As far as the random walk problem is concerned, we investigate the conditional probability $P(i,t|i_0,t_0)$ for the walker to be at site i at time t, knowing that it was localized at site i_0 at time t_0. The site i_0 is chosen among the leaves, as well as the sites i. The local conservation of walkers is given by

$$\tau \frac{\partial \mathbf{P}(t|i_0,t_0)}{\partial t} = \tilde{\mathbf{\Delta}} \mathbf{P}(t|i_0,t_0), \tag{14.4}$$

with τ the time increment. The operator $\tilde{\mathbf{\Delta}}$ shall be defined in what follows. We stress that $\tilde{\mathbf{\Delta}}$ is non symmetric, and distinct from the Laplacian $\mathbf{\Delta}$. These properties are due to the fact the the coordination of the Cayley tree is not a constant, because the leaves have one neighbour whereas the other sites have three neighbours. On lattices with a constant coordination, the operator $\tilde{\mathbf{\Delta}}$ is equal to the Laplacian. In equation (14.4), $\mathbf{P}(t|i_0,t_0)$ is the vector of probabilities $P(i,t|i_0,t_0)$.

We first study (14.4) by means of numerical diagonalizations of the Laplacian. We find that the scaling of the time scales as a function of the distance is anomalous, as in the diffusion case. As for the diffusion case, the scaling of the largest non zero eigenvalue explains the anomalous properties of random walks on the edge of a Cayley tree.

Finally, we analyze the two problems in the Bethe-Peierls limit. In this approximation, the operators $\mathbf{\Delta}$ and $\tilde{\mathbf{\Delta}}$ are identical, and the eigenvalue problem can be mapped onto a tight-binding Hamiltonian problem. The density of eigenvalues for this problem has already been investigated in [4], and we conclude that no anomalous diffusion is present in the Bethe-Peierls approximation.

14.2 Diffusion problem

14.2.1 Numerical simulation

We call $P(i,t|i_0,t_0)$ the conditional probability of the diffusion process, with $P(i,t|i_0,t_0) = \delta_{i,i_0}$. A corresponding physical situation would be a tree at low temperatures with a localized heat

pulse at site i_0. The diffusion equation is

$$P(i,t+\tau|i_0,t_0) - P(i,t|i_0,t_0) = \frac{D}{3} \sum_{i' \in V(i)} \left(P(i',t|i_0,t_0) - P(i,t|i_0,t_0) \right). \tag{14.5}$$

The dynamics is discrete, with an increment in time τ, and $V(i)$ is the set of neighbours of site i. Equation (14.5) is the discrete diffusion equation. One can make the time continuous by taking a first order derivative instead of a finite difference:

$$\tau \frac{\partial P(i,t|i_0,t_0)}{\partial t} = \frac{D}{3} \sum_{i' \in V(i)} \left(P(i',t|i_0,t_0) - P(i,t|i_0,t_0) \right). \tag{14.6}$$

Using the vectorial notation $\mathbf{P}(t|i_0,t_0)$ for the set of probabilities $P(i,t|i_0,t_0)$, we obtain

$$\tau \frac{\partial \mathbf{P}(t|i_0,t_0)}{\partial t} = D\mathbf{\Delta}\mathbf{P}(t|i_0,t_0). \tag{14.7}$$

The operator $\mathbf{\Delta}$ is the Laplacian, and depends only on the underlying lattice. $\mathbf{\Delta}_{i,i}$ is minus the coordination of site i over 3, and $\mathbf{\Delta}_{i,j}$ is $+1/3$ if a link connects the sites i and j, and 0 otherwise. The factor $1/3$ is a convention and is chosen in such a way that $\mathbf{\Delta}$ and $\tilde{\mathbf{\Delta}}$ have the same Bethe-Peierls limit. $\tilde{\mathbf{\Delta}}$ is symmetric whatever the underlying lattice. It is clear that, in order to solve the diffusion equation (14.7), one has to diagonalize the Laplacian. We note $\mathbf{u}_i$ the eigenvectors of $\mathbf{\Delta}$: $\mathbf{\Delta}\mathbf{u}_i = \lambda_i \mathbf{u}_i$, and $\mathbf{Q}$ is the matrix of eigenvectors:

$$\mathbf{u}_i = \sum_j \mathbf{Q}_{i,j} \mathbf{e}_j, \tag{14.8}$$

with $\{\mathbf{e}_j\}$ the canonical basis. The decomposition of $\mathbf{P}(t|i_0,t_0)$ over the eigenvalue basis is

$$\mathbf{P}(t|i_0,t_0) = \sum_i a_i(t) \mathbf{u}_i, \tag{14.9}$$

with

$$\tau \frac{\partial a_i(t)}{\partial t} = \lambda_i a_i(t), \tag{14.10}$$

which is solved easily, with the initial conditions $a_i(t_0) = \mathbf{Q}_{i,i_0}$. We thus obtain

$$\mathbf{P}(t|i_0,t_0) = \sum_i \mathbf{Q}_{i,i_0} \exp\left(\frac{\lambda_i}{\tau}(t-t_0) \right) \mathbf{u}_i, \tag{14.11}$$

so that

$$P(i,t|i_0,t_0) = \sum_j \mathbf{Q}_{j,i_0} \mathbf{Q}_{j,i} \exp\left(\frac{\lambda_j}{\tau}(t-t_0) \right). \tag{14.12}$$

In practise, we study small trees, and diagonalize the Laplacian by means of a Jacobi method. The starting site i_0 is chosen among the leaves, as shown on figure 14.1. The probability is calculated at the other leaves. One can gather equivalent leaves according to the distance from the starting point. The label of the leaves is the half the distance from the starting point. The probability $P(n,t)$ is plotted on figure 14.2 in a log-log plot. The logarithm of the time scale is proportional to the distance from the starting point, so that if one increments the length scale $x \to x + \lambda$, the associated time scale behaves as $\tau \to \mu\tau$. The scaling of the time scales is identical to the scaling of the number of sites as a function of the distance on the tree.

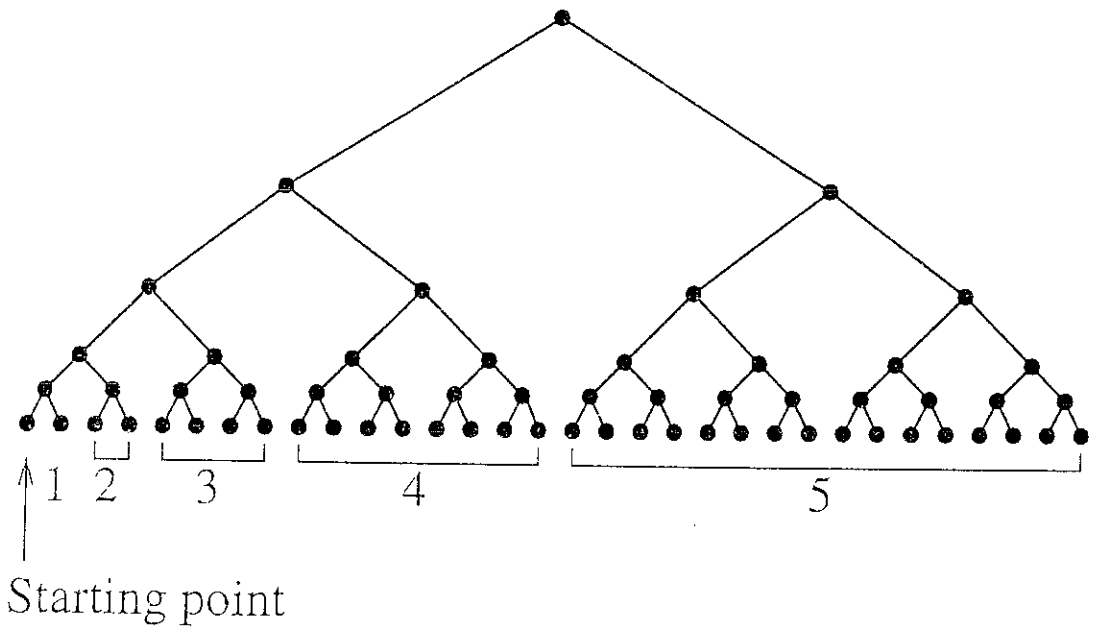

Figure 14.1: The starting point in chosen among the leaves. We study the probility for the walker on the other leaves as a function of time. The equivalent leaves are labeled according to the distance from the starting point. The distance between the leaves i and the starting point is $2i$.

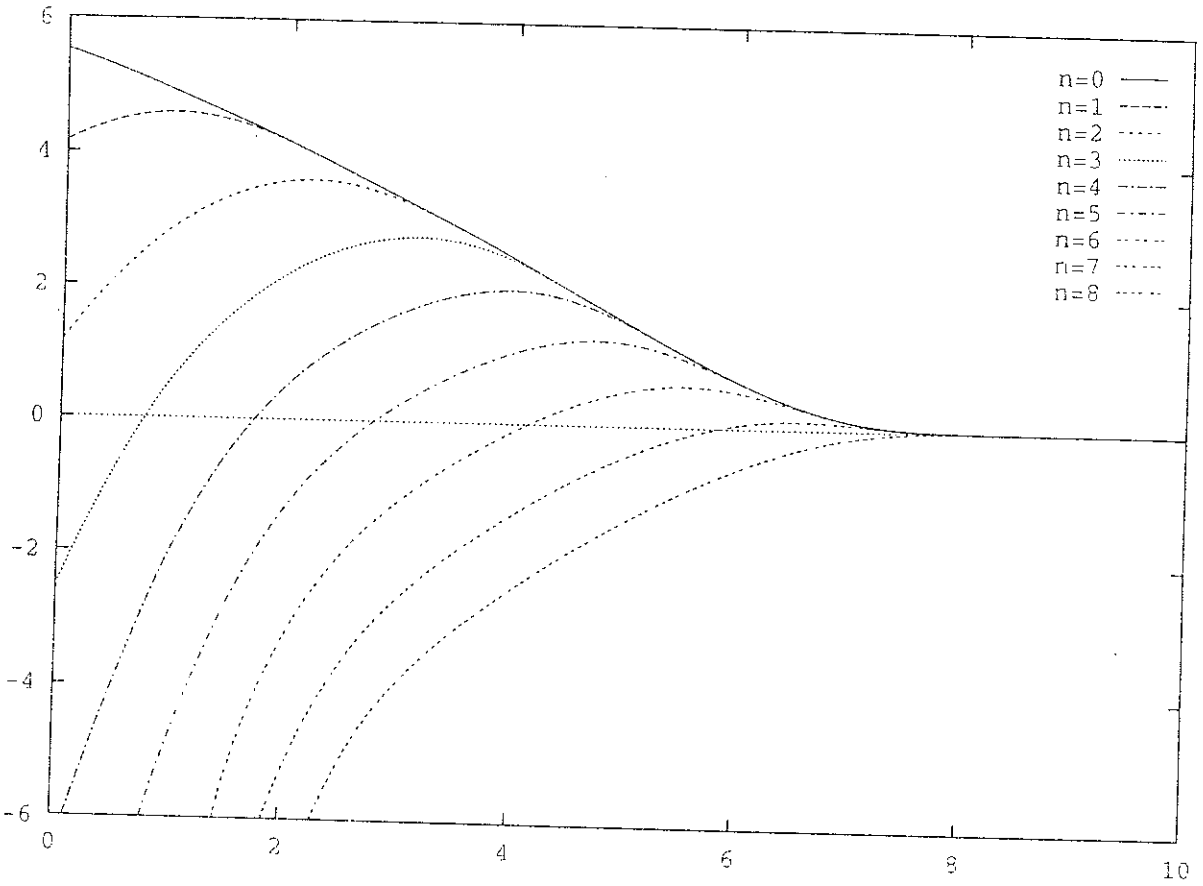

Figure 14.2: Probability $P(n,t)$ of the diffusion process,
with n the label of the leave (see figure 14.1) at time t, for $D/\tau = 3$. We plotted $NP(n,t)$ in logarithmic scale, with N the number of sites, as a function of the logarithm of time, for a half-space tree with 9 generations. Using these scales, the asymptotic probabilities are 0 (the equilibrium distribution is uniform).

14.2.2 Analytical results

We wish to understand analytically the numerical result of the previous section. To do so, we analyze the problem of the diagonalization of the Laplacian on a half-space-tree. We first need to label the sites of a half-space-tree. At the first generation, the labels are 0 and 1. At the second generation, the labels of the sons of 0 are 00 and 01, the labels of the sons of 1 are 10 and 11, etc. The elements of the eigenvectors of the laplacian are noted $\psi_n(\epsilon_1, ..., \epsilon_n)$, where $\epsilon_k = 0$ or 1 and n is the number of the generation of the site. If λ denotes an eigenvalue of the Laplacian, then the corresponding eigenvector must verify

$$\begin{aligned}
(\lambda + \frac{1}{3})\psi_n(\epsilon_1, ..., \epsilon_n) &= \frac{1}{3}\psi_{n-1}(\epsilon_1, ..., \epsilon_{n-1}) \\
(\lambda + 1)\psi_{n-1}(\epsilon_1, ..., \epsilon_{n-1}) &= \frac{1}{3}\left(\psi_{n-2}(\epsilon_1, ..., \epsilon_{n-2}) + \psi_n(\epsilon_1, ..., \epsilon_{n-1}, 0) + \psi_n(\epsilon_1, ..., \epsilon_{n-1}, 1)\right) \\
&\cdots \\
(\lambda + 1)\psi_{n-p}(\epsilon_1, ..., \epsilon_{n-p}) &= \frac{1}{3}\left(\psi_{n-p-1}(\epsilon_1, ..., \epsilon_{n-p-1}) + \psi_{n-p+1}(\epsilon_1, ..., \epsilon_{n-p}, 0) + \psi_{n-p+1}(\epsilon_1, ..., \epsilon_{n-p}, 1\right. \\
&\cdots \\
(\lambda + 1)\psi_1(\epsilon_1) &= \frac{1}{3}\left(\psi_0 + \psi_2(\epsilon_1, 0) + \psi_2(\epsilon_1, 1)\right) \\
(\lambda + \frac{2}{3})\psi_0 &= \frac{1}{3}\left(\psi_1(0) + \psi_1(1)\right).
\end{aligned} \tag{14.1}$$

The first and the last equations are peculiar since the leaves have only one neighbour and the ancestor has only two neighbours, whereas the other sites have 3 neighbours. If $\lambda \neq 0$, there is a suplementary constraint

$$\sum_j \Delta_{i,j} = 0, \tag{14.14}$$

which expresses the fact that the eigenvector is orthogonal to the $\lambda = 0$ uniform mode. We decude that, if $\lambda \neq 0$,

$$\sum_k \sum_{\epsilon_1} ... \sum_{\epsilon_k} \psi_k(\epsilon_1, ..., \epsilon_k) = 0. \tag{14.15}$$

To discuss the eigensystem (14.13), we start from the leaves. The first case is $\lambda = -1/3$. With this value of λ, the eigensystem (14.13) becomes

$$\begin{aligned}
0 &= \psi_{n-1}(\epsilon_1, ..., \epsilon_{n-1}) \\
0 &= \psi_{n-2}(\epsilon_1, ..., \epsilon_{n-2}) + \psi_n(\epsilon_1, ..., \epsilon_{n-1}, 0) + \psi_n(\epsilon_1, ..., \epsilon_{n-1}, 1) \\
2\psi_{n-2}(\epsilon_1, ..., \epsilon_{n-2}) &= \psi_{n-3}(\epsilon_1, ..., \epsilon_{n-3} + \psi_{n-1}(\epsilon_1, ..., \epsilon_{n-2}, 0) + \psi_{n-1}(\epsilon_1, ..., \epsilon_{n-2}, 1) \\
&\cdots \\
2\psi_{n-p}(\epsilon_1, ..., \epsilon_{n-p}) &= \psi_{n-p-1}(\epsilon_1, ..., \epsilon_{n-p-1}) + \psi_{n-p+1}(\epsilon_1, ..., \epsilon_{n-p}, 0) + \psi_{n-p+1}(\epsilon_1, ..., \epsilon_{n-p}, 1) \\
&\cdots \\
2\psi_1(\epsilon_1) &= \psi_0 + \psi_2(\epsilon_1, 0) + \psi_2(\epsilon_1, 1) \\
\psi_0 &= \psi_1(0) + \psi_1(1).
\end{aligned} \tag{14.16}$$

In order to obtain an intuition of the number of states in the subspace $\lambda = -1/3$, we first treat the exemple of figure, 14.3. For comodity, the sites are labelled by letters and integers (see

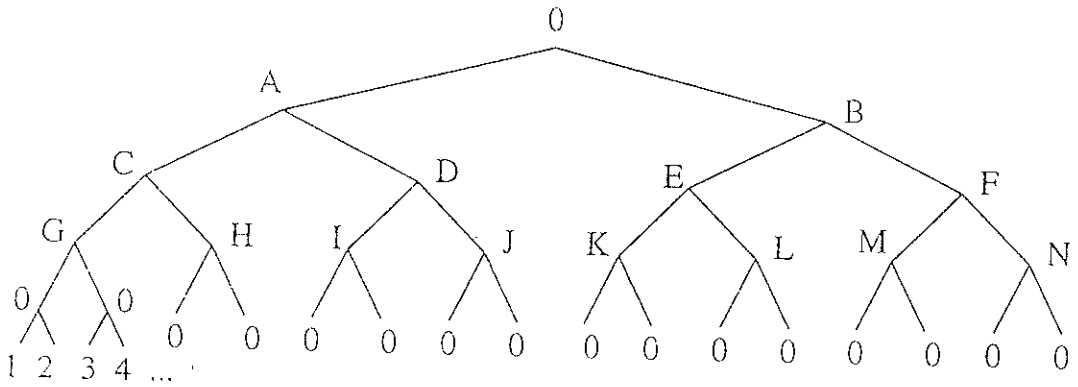

Figure 14.3:

Labelling of the tree that we choose in the exemple of section 14.2.2.

figure 14.3). For this half-space-tree, we have, $\psi_G = \psi_H = \psi_C/2$. From the equation

$$2\psi_C = \psi_A + \psi_G + \psi_H, \tag{14.17}$$

we deduce that $\psi_C = \psi_D = \psi_A$. From $2\psi_A = \psi_C + \psi_D + \psi_0$, we deduce that $\psi_0 = 0$. We note $\psi_A = \psi$, $\psi_B = -\psi$. Then, $\psi_C = \psi_D = \psi$ and $\psi_E = \psi_F = -\psi$. We have also

$$\psi_G = \psi_H = \psi_I = \psi_J = \frac{1}{2}\psi \tag{14.18}$$

$$\psi_K = \psi_L = \psi_M = \psi_N = -\frac{1}{2}\psi. \tag{14.19}$$

This exemple shows that there is one mode for each site belonging to a generation where the eigenfunction is zero. If we note $n-1 = 4p+q$ (with $0 \leq q \leq 3$), the sites corresponding to a cancellation of the eigenfunction are $n-1-4r = 4(p-r)+q = 4s+q$, with $0 \leq s \leq p$, so that the dimension of the $\lambda = -1/3$ subspace is

$$D(n) = \sum_{s=0}^{p} 2^{4s+q} = 2^{n-1} + \frac{1}{15}\left(2^{n-1} - 2^q\right). \tag{14.20}$$

This expression is valid if $q = 0$ (this is the case of figure 14.3). It is also valid if $q = 1$ or $q = 3$. However, if $q = 2$, there exists one supplementary mode compared to (14.20).

We now turn to the case $\lambda \neq -1/3$. Under this condition,

$$\psi_n(\epsilon_1, ..., \epsilon_{n-1}, 0) = \psi_n(\epsilon_1, ..., \epsilon_{n-1}, 1) = \frac{1}{3\lambda+1}\psi_{n-1}(\epsilon_1, ..., \epsilon_{n-1}), \tag{14.21}$$

so that, the eigensystem (14.13) leads to

$$\left(\lambda + 1 - \frac{2/3}{3\lambda+1}\right)\psi_{n-1}(\epsilon_1, ..., \epsilon_{n-1}) = \frac{1}{3}\psi_{n-2}(\epsilon_1, ..., \epsilon_{n-2}). \tag{14.22}$$

Two cases are to be considered: $\lambda + 1 - 2/3(3\lambda+1) = 0$ and $\lambda + 1 - 2/3(3\lambda+1) \neq 0$.

We first consider the case $\lambda+1-2/3(3\lambda+1) = 0$, that is $\lambda = \lambda_\pm = \left(-2 \pm \sqrt{3}\right)/3$. Under this condition, $\psi_{n-2}(\epsilon_1, ..., \epsilon_{n-2}) = 0$, and we impose $\psi_{n-1}(\epsilon_1, ..., \epsilon_{n-2}, 0) + \psi_{n-1}(\epsilon_1, ..., \epsilon_{n-2}, 1) = 0$. This condition is compatible with what follows. We deduce that $\forall k \leq n-2$, $\forall \epsilon_1, ..., \epsilon_k$, $\psi_k(\epsilon_1, ..., \epsilon_k) = 0$. Each eigenvalue $\lambda_\pm$ gives rise to one eigenspace of dimension 2^{n-2}. The eigenvectors are easily calculated. If we note $x = \psi_{n-1}(\epsilon_1, ..., \epsilon_{n-2}, 1) = -\psi_{n-1}(\epsilon_1, ..., \epsilon_{n-2}, 0)$, the amplitudes of the children are

$$\psi_n(\epsilon_1, ..., \epsilon_{n-2}, \epsilon', \epsilon) = \frac{1}{3\lambda+1}\psi_{n-1}(\epsilon_1, ..., \epsilon_{n-2}, \epsilon') = (2\epsilon' - 1)\frac{x}{3\lambda+1}. \tag{14.23}$$

Since ψ is normalized to unity,

$$x_\pm = \frac{1}{\sqrt{2 + \frac{4}{(3\lambda_\pm+1)^2}}}, \tag{14.24}$$

so that the eigenvectors are completely determined.

In the case $\lambda+1-2/3(\lambda+1)\neq 0$, we continue the same procedure. Since the forthcoming step is the first one to be generic, that is which does not depend on the special coordinance of the sites of the border, we outline it explicitly. It is possible to invert the relation (14.22) into

$$\psi_{n-1}(\epsilon_1,...,\epsilon_{n-1}) = \frac{1/3}{\lambda+1-\frac{2/3}{3\lambda+1}}\psi_{n-2}(\epsilon_1,...,\epsilon_{n-2}), \tag{14.25}$$

so that

$$\left(\lambda+1-\frac{2/9}{\lambda+1-\frac{2/3}{3\lambda+1}}\right)\psi_{n-2}(\epsilon_1,...,\epsilon_{n-2}) = \frac{1}{3}\psi_{n-3}(\epsilon_1,...,\epsilon_{n-3}). \tag{14.26}$$

To use general notations, we write

$$f_1(\lambda) = \frac{2/3}{3\lambda+1} \tag{14.27}$$

$$f_{n+1}(\lambda) = \frac{2/9}{\lambda+1-f_n(\lambda)}. \tag{14.28}$$

With these notations, equation (14.26) is of the form

$$(\lambda+1-f_2(\lambda))\,\psi_{n-2}(\epsilon_1,...,\epsilon_{n-2}) = \frac{1}{3}\psi_{n-3}(\epsilon_1,...,\epsilon_{n-3}). \tag{14.29}$$

To proceed with the recurence, we denote by H_p the following hypothesis:

$$H_p \Longleftrightarrow (\lambda+1-f_p(\lambda))\,\psi_{n-p}(\epsilon_1,...,\epsilon_{n-p}) = \frac{1}{3}\psi_{n-p-1}(\epsilon_1,...,\epsilon_{n-p-1}). \tag{14.30}$$

We have shown that H_2 is true. If H_p is true, two cases are to be considered: $\lambda+1-f_p(\lambda)=0$ and $\lambda+1-f_p(\lambda)\neq 0$. We first treat the case $\lambda+1-f_p(\lambda)=0$. This equation can be brought under a polynomial form, and has $p+1$ *real* roots. A graphical representation shows immediately that the roots are indeed real. Each root gives rise to an eigenspace of dimension 2^{n-p-1}. We do not enter into the detail of the construction of the eigenstates, since the principle is the same as in the $p=1$ case $p=1$ which has been previously developed. Now, if $\lambda+1-f_p(\lambda)\neq 0$, the hypothesis H_{p+1} is true. To see this, we use the following equation of the eigensystem (14.13):

$$\begin{aligned}(\lambda+1)\psi_{n-p-1}(\epsilon_1,...,\epsilon_{n-p-1}) &= \frac{1}{3}\left(\psi_{n-p-2}(\epsilon_1,...,\epsilon_{n-p-2})+\psi_{n-p}(\epsilon_1,...,\epsilon_{n-p-1},0)\right.\\ &\left.+\psi_{n-p}(\epsilon_1,...,\epsilon_{n-p-1},1)\right),\end{aligned} \tag{14.31}$$

and combine it to H_p to find

$$\lambda+1-\frac{2/9}{\lambda+1-f_p(\lambda)} = \lambda+1-f_{p+1}(\lambda)=0 \Longleftrightarrow H_{p+1} \tag{14.32}$$

We now treat the last two equations of the eigensystem (14.13). We assume that we reach the step H_{n-2}:

$$(\lambda+1-f_{n-2}(\lambda))\,\psi_2(\epsilon_1,\epsilon_2) = \frac{1}{3}\psi_1(\epsilon_1). \tag{14.33}$$

If $\lambda + 1 - f_{n-2}(\lambda) = 0$, we have $n-1$ eigenspaces of dimension 2. If $\lambda + 1 - f_{n-2}(\lambda) \neq 0$, we obtain

$$(\lambda + 1 - f_{n-1}(\lambda))\,\psi_1(\epsilon) = \frac{1}{3}\psi_0. \tag{14.34}$$

If $\lambda + 1/3 - f_{n-1}(\lambda) = 0$, we get n eigenspaces of dimension 1. If $\lambda + 1/3 - f_{n-1}(\lambda) \neq 0$, we obtain the last equation

$$\lambda + \frac{2}{3} = \frac{1}{3\,(\lambda + 1 - f_{n-1}(\lambda))}, \tag{14.35}$$

which leads to $n+1$ eigenspaces of dimension 1. Among the roots of (14.35), we find automatically $\lambda = 0$, since $\forall p, f_p(\lambda) = 2/3$. The corresponding eigenvector is a constant, corresponding to the equilibrium distribution of walkers. The procedure splits the characteristic polynomial of degree N, with N the number of sites into a product of polynoms with a degree inferior or equal to n, the number of generations.

Finally, we focus on the largest non zero eigenvalue which is obtained at the step p of the recursion precedently described. We note $\lambda_+^{(p)}$ this eigenvalue, and we note

$$\lambda + 1 - f_p(\lambda) = \left(\lambda - \lambda_+^{(p)}\right) F_p(\lambda). \tag{14.36}$$

Since $\lambda_+^{(p)}$ is close to zero, the equation for $\lambda_+^{(p+1)}$ can be approximated as

$$\lambda_+^{(p+1)} + 1 - \frac{2/9}{\left(\lambda_+^{(p+1)} - \lambda_+^{(p)}\right) F_p(0)} = 0. \tag{14.37}$$

this equation is a second order equation for $\lambda_+^{(p+1)}$:

$$\left(\lambda_+^{(p+1)}\right)^2 + \lambda_+^{(p+1)}\left(1 - \lambda_+^{(p)}\right) - \frac{2}{9F_p(0)} - \lambda_+^{(p)} = 0, \tag{14.38}$$

which is solved as

$$\lambda_+^{(p+1)} = \frac{1}{2}\left(\lambda_+^{(p)} - 1 + \sqrt{(1 - \lambda_+^{(p)})^2 + 4(\lambda_+^{(p)} + \frac{2}{9F_p(0)})}\right). \tag{14.39}$$

However, $f_1(0) = f_2(0) = \ldots = f_p(0) = 2/3$, so that $F_p(0) = -1/3\lambda_+^{(p)}$. Reporting this expression into (14.39), we deduce that $\lambda_+^{(p+1)} \simeq \lambda_+^{(p)}/3$. This property explains the anomalous scaling of the diffusion times that was observed numerically in the previous section. In order to check this conclusion, we computed the function $\lambda + 1 - f_n(\lambda)$ for consecutive values of n. The behaviour of the largest root of this equation is in agreement with our analytical conclusion (see figure 14.4).

14.3 Random walk problem

14.3.1 Numerical simulation

We call $P(i,t|i_0,t_0)$ the conditional probability to find the walker at the site i at time t, the walker being at site i_0 at time t_0. The local conservation of walkers reads

$$P(i,t+\tau|i_0,t_0) - P(i,t|i_0,t_0) = \sum_{i' \in V(i)} \left(\frac{1}{z_{i'}} P(i',t|i_0,t_0) - \frac{1}{z_i} P(i,t|i_0,t_0)\right), \tag{14.40}$$

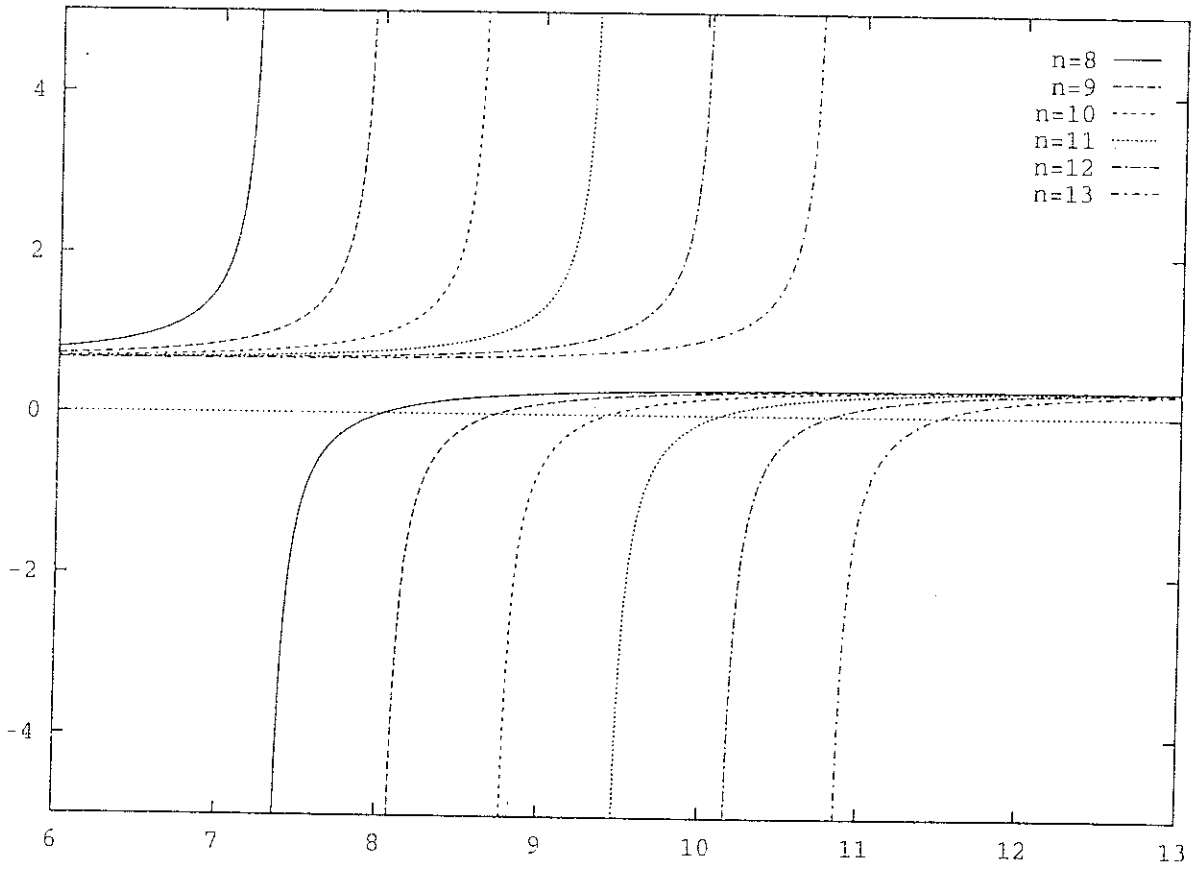

Figure 14.4: $\lambda + 1 - f_n(\lambda)$ as a function of $\ln(-\lambda)$ in the vicinity of the largest root, for different values of λ. In this semi-log plot, the zeros are equidistant, which is consistent with the analytically predicted scaling.

and leads to the following continuous dynamics:

$$\tau \frac{\partial P(i,t|i_0,t_0)}{\partial t} = \sum_{i' \in V(i)} \left(\frac{1}{z_{i'}} P(i',t|i_0,t_0) - \frac{1}{z_i} P(i,t|i_0,t_0) \right). \tag{14.41}$$

Using the vectorial notation $\mathbf{P}(t|i_0,t_0)$ for the set of probabilities $P(i,t|i_0,t_0)$, we obtain

$$\tau \frac{\partial \mathbf{P}(t|i_0,t_0)}{\partial t} = \tilde{\mathbf{\Delta}} \mathbf{P}(t|i_0,t_0). \tag{14.42}$$

$\tilde{\mathbf{\Delta}}_{i,i}$ is $-1/z_i$, and $\tilde{\mathbf{\Delta}}_{i,j}$ is $+1/z_j$ if a link connects the sites i and j, and 0 otherwise. $\tilde{\mathbf{\Delta}}$ is not symmetric on the Cayley tree. However, the operator $\tilde{\mathbf{\Delta}}$ is diagonalizable and its eigenvalues are real. The reason is the same as the reason why the Glauber matrix is diagonalizable and its eigenvalues are real, eventhough it is not symmetric [8]. We call $\mathbf{P^{(0)}}$ the equilibrium distribution of the dynamics (14.42). It is clear that $\mathbf{P}_i^{(0)} \propto z_i$, with z_i the coordinance of the site i. The prefactor is chosen to normalize $\mathbf{P^{(0)}}$. Then, the dynamics verifies the detailed balance

$$\tilde{\mathbf{\Delta}}_{i,j} \mathbf{P}_j^{(0)} = \mathbf{P}_i^{(0)} \tilde{\mathbf{\Delta}}_{j,i}, \tag{14.43}$$

so that the matrix

$$\hat{\mathbf{\Delta}}_{i,j} = \left(\mathbf{P}_i^{(0)} \right)^{-1/2} \tilde{\mathbf{\Delta}}_{i,j} \left(\mathbf{P}_j^{(0)} \right)^{1/2} \tag{14.44}$$

is symmetric. Moreover, if $\mathbf{P}$ is an eigenvector of $\tilde{\mathbf{\Delta}}$, then $\hat{\mathbf{P}}_i = \left(\mathbf{P}_i^{(0)} \right)^{-1/2} \mathbf{P}_i$ is an eigenvector of $\hat{\mathbf{\Delta}}$. We have thus proven that the non symmetric matrix $\tilde{\mathbf{\Delta}}$ is diagonalizable, and that its eigenvalues are real. In practise, we shall use the symmetric representation $\hat{\mathbf{\Delta}}$ of $\tilde{\mathbf{\Delta}}$ since the algorithm to diagonalize and find the eigenvectors works with symmetric matrices. We are now in position to study $P(i,t|i_0,t_0)$ numerically, as we did in section 14.2 for the diffusion problem. The dynamics equation (14.42) is covariant as one goes in the symmmetric representation:

$$\tau \frac{\partial \hat{\mathbf{P}}(t|i_0,t_0)}{\partial t} = \hat{\mathbf{\Delta}} \hat{\mathbf{P}}(t|i_0,t_0). \tag{14.45}$$

However, the initial condition $P(i,t_0|i_0,t_0) = \delta_{i,i_0}$ must be transformed into

$$\hat{P}(i,t_0|i_0,t_0) = \left(\mathbf{P}_{i_0}^{(0)} \right)^{-1/2} \delta_{i,i_0}. \tag{14.46}$$

It is now p-ossible to apply the method of section 14.2 to compute the evolution in the symmetric representation, and come back to the actual probabilities at the end of the calculation. The resulting probabilities are plotted on figure 14.5. As in the case of the diffusion process, the scaling of the time scales is anomalous, in the sense that the time scales are multiplied by a constant as the length scales are incremented by a constant.

14.3.2 Analytical results

As in the case of the diffusion, is possible to derive continuous fraction equations for the eigenvalues of the operator $\tilde{\mathbf{\Delta}}$ on the tree. The generic equation is of the form

$$\lambda + 1 - \frac{2/9}{\lambda + 1 - \frac{2/9}{\lambda + 1 - \ldots}} = 0. \tag{14.47}$$

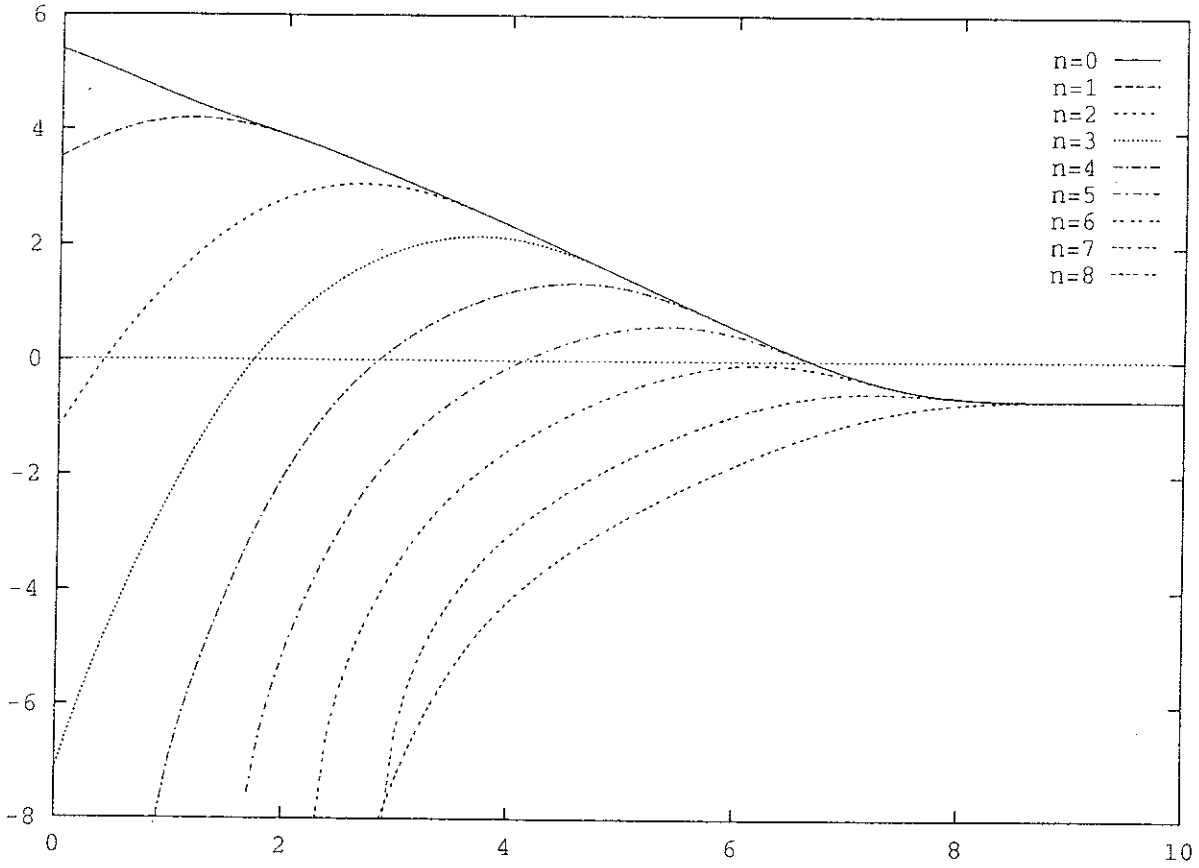

Figure 14.5:
Probability $P(n,t)$ for the walker to be on a leave labeled by n (see figure 14.1) at time t. We plotted $NP(n,t)$ in logarithmic scales, with N the number of sites, as a function of the logarithm of time, for a half-space tree with 8 generations. The assymtotic probability is inferior to unity, due to the fact that the coordinance of the leaves is inferior to the average coordinance (the equilibrium distribution is such as $P_i \propto z_i$).

However, the last nested fraction is different from what we obtain for the diffusion. We do not repeat the construction of the eigenvalues, but we just notice that the scaling of the eigenvalue $\lambda_+^{(p)}$ is the same as for the diffusion process: $\lambda_+^{(p+1)} \simeq \lambda_+^{(p)}/2$, and this scaling explains the scaling of the time and length scales in the random walk process.

14.4 Bethe-Peierls approximation

In the Bethe-Peierls approximation, we can forget the border, so that the operators $\tilde{\mathbf{\Delta}}$ and $\mathbf{\Delta}$ become equivalent and can can be thought of as a tight-binding Hamiltonian:

$$\mathbf{\Delta} = -\mathbf{Id} + \frac{1}{3}\sum_{i,j} |i\rangle\langle j|. \tag{14.48}$$

The tight-binding problem has already been analyzed in [4], so that we shall use the results of [4] without proving them. The tight-binding Hamiltonian reads

$$H = V \sum_{i,j} |i\rangle\langle j|. \tag{14.49}$$

The correspondance between the Laplacian and the tight-binding Hamiltonian if thus $E = \lambda + 1$, with E denoting the energy levels of (14.49), λ the eigenvalues of $\mathbf{\Delta}$, and $V = 1/3$. The density of eigenvalues can be obtained via a Green's function formalism and leads to

$$\rho(\lambda) = -\frac{3}{2\pi\lambda(\lambda+2)}\sqrt{\left(\frac{2\sqrt{2}}{3} - 1 - \lambda\right)\left(\frac{2\sqrt{2}}{3} + 1 + \lambda\right)} \tag{14.50}$$

for $\lambda \in [-1 - 2\sqrt{2}/3, -1 + 2\sqrt{2}/3]$. The density of eigenvalues $\rho(\lambda)$ is plotted on figure 14.6, and compared to the density of eigenvalues of $\mathbf{\Delta}$ for a finite Cayley tree with 30 generations. In the Bethe-Peierls approximation, there exists a gap between the eigenvalue $\lambda = 0$ and the largest non zero eigenvalue $-1-2\sqrt{2}/3$, so that the existence of long time scales is not predicted in the Bethe-Peierls scheme. We plotted on figure 14.7 the density of eigenvalues weighted by the degeneracies. Since the edge states are much more degenerate than the bulk states, the density of states of the bulk states vanishes, and we are left with a collection of delta functions. This is reminiscent of the different thermodynamic limits depending on whether free boundary conditions are used or not.

14.5 Comparaison with the Sierpinsky gasket

The Laplacian problem on the Sierpinsky gasket has been studied in [11]. Similarly to what we have done in the study of the tree, it is possible to derive recursion equations for the eigenvalues of the Laplacian. The iteration is

$$g_{n+1}(\lambda) = g_n(\lambda(\lambda - 5)) \tag{14.51}$$

$$g_1(\lambda) = 1, \tag{14.52}$$

and the eigenvalues of the Laplacian are the zeros of the equation $g_n(\lambda) = 6$, so that the structure of the problem is very similar to what happens on the Cayley tree. It is possible to approximate

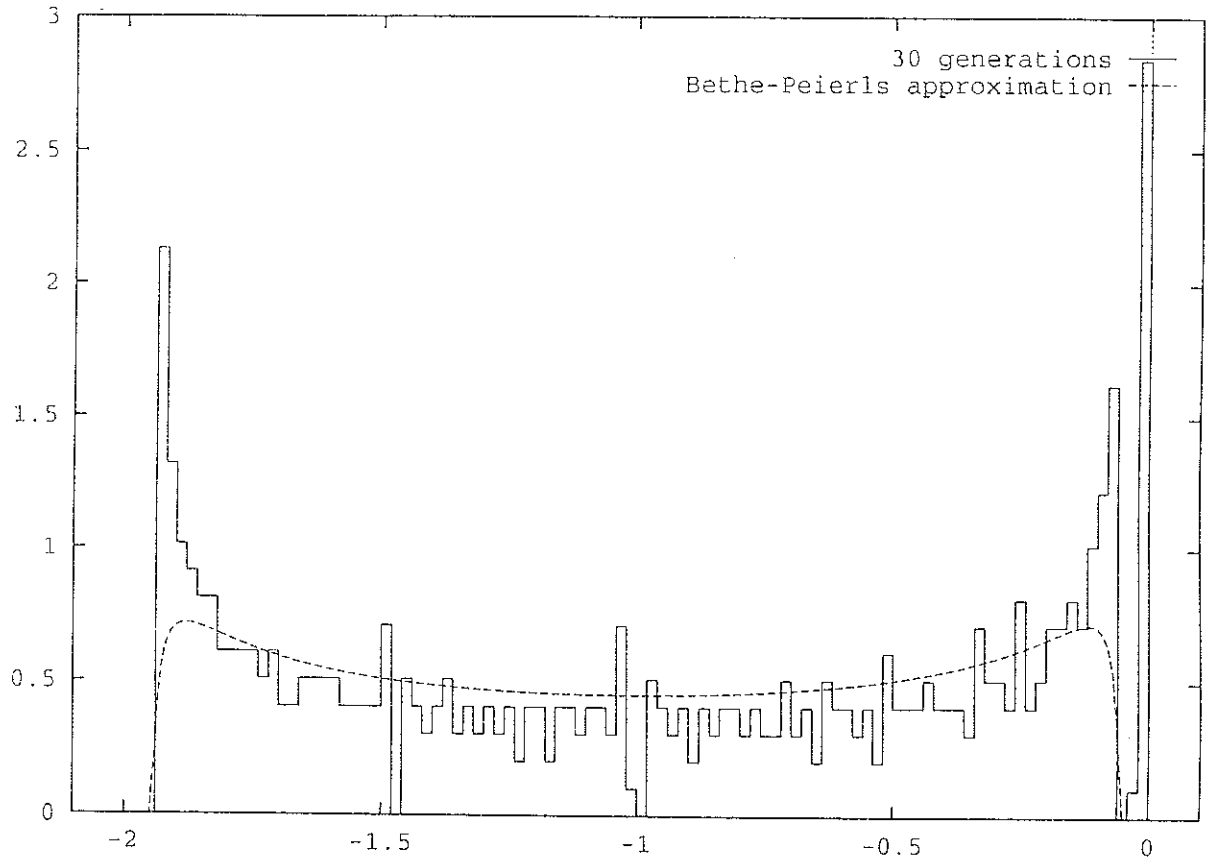

Figure 14.6: Density of eigenvalues of the operator Δ in the Bethe-Peierls approximation and for a finite tree with 30 generations. The degeneracies are not taken into account. It is clear that the small eigenvalues are forgotten in the Bethe-Peierls approximation.

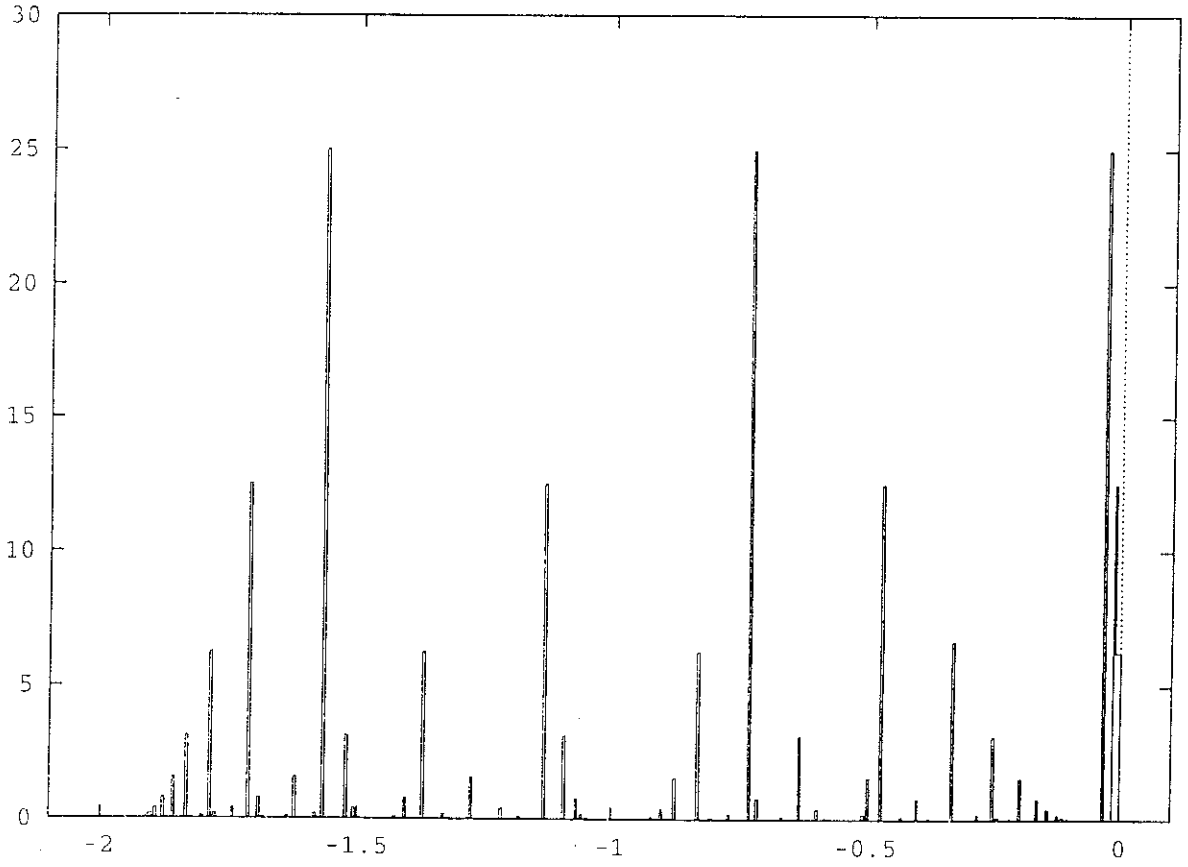

Figure 14.7: Density of eigenvalues of the operator Δ in the Bethe-Peierls approximation and for a finite tree with 30 generations. The weight of a given eigenvalue is proportional to its degenaracy.

scaling of the largest eigenvalue by $n \to n+1$, $\lambda_n^{(+)} \to \lambda_n^{(+)}/5$, so that the associated times scale like $\tau_n \to 5\tau_n$. The extension of the localized states scales like $L_n \to 2L_n$, so that the respective scaling of time scales and length scales is $\mathrm{L} \to \lambda L$, $\tau \to \lambda^{\tilde{d}/\bar{d}}\tau$, with $\tilde{d}$ the spectral dimension [11] [12] and $\bar{d}$ the fractal dimension. In the case we consider, $\tilde{d}/\bar{d} = 2\ln 2/\ln 5$. We see that the scaling in the case of the Sierpinsky gasket is of the same form as the scaling in an Euclidian space, execepted that the spectral and fractal dimensions become non degenerate, whereas the scaling on the tree is different. We notice that the scaling of time scales associated to the eigenmodes is similar in the case of the tree and in the case of the Sierpinsky gasket. However, the extension of localized states is different. On the gasket, the longitudinal extension of the states is multiplicative in n, whereas it is additive in n in the case of the tree.

14.6 Conclusion

We have shown by means of diagonalizations and of analytical methods that the diffusion problem and the random walk problem on the Cayley tree exhibits unusual scalings. Whereas the fractal dimension of random walks is two on an Euclidian structure, this property is no more valid on a Cayley tree. If the length scales are incremented by a certain constant, the time scales are multiplied by a certain constant, which is reminiscent of the scaling of the number of sites as a function of the distance on the tree. This effect is not predicted in the Bethe-Peierls approximation. In the Bethe-Peierls limit, the weight of the eigenvalues which are responsible for the anomalous scaling properties is vanishing. An interesting case is the random walk on a hyperbolic lattice, with a non Euclidian metric. This model shall be treated in a near future [13].

I acknowledge discussions with B. Douçot, and thank J.C. Anglès d'Auriac for lending me his algorithms.

References

[1] H.A. Bethe, Proc. Roy. Soc. A 216, 45 (1935); 150, 552 (1935).

[2] R. Peierls, Proc. Can. Phil. Soc. 32, 477 (1936); Proc. Roy. Soc. 154, 207 (1936).

[3] P.D. Gujrati. Phys. Rev. Lett. 74, 809 (1995).

[4] M.F. Thorpe. *Excitations in Disordered Solids* (NATO Advanced Study Institute Series B 78) Ed M. F., Thorpe (NY: Plenum) pp 85-107 (1982).

[5] Les Houches 1978, Ill Condensed Matter, North-Holland, course1: Percolation and localization by D.J. Thouless.

[6] E. Müller-Hartmann and J. Zittartz, Phys. Rev. Lett. 33, 893 (1974).

[7] J. von Heimburg and H. Thomas, J. Phys. C 7, 3433 (1974).

[8] R. Mélin, J.C. Anglès d'Auriac, B. Douçot and P. Chandra, preprint (1995).

[9] R. Mélin, CRTBT preprint (1995).

[10] C. Itzykson et J.M. Drouffe, *Théorie Statistique des Champs*, volume 1, chapitre 1, InterEditions/Editions du CNRS (1989).

[11] R. Rammal, J. Physique 45, 191 (1984)

[12] R. Rammal and G. Toulouse, J. Physique lettres 44, L13 (1983).

[13] R. Mélin, in preparation.

Chapitre 15

Article 7

XY model on the Cayley tree[1]

R. Mélin

CRTBT-CNRS, 38042 Grenoble BP 166X cédex France

We investigate the dynamical properties of the XY model on the Cayley tree. As for the Ising model, a cross-over towards a glassy phase is found at small temperatures. Below T_g, we can replace the XY Hamiltonian by a Hamiltonian with quadratic interactions. We study the Langevin dynamics of the quadratic model. The dynamics is solved by numerically diagonalizing the Laplacian for small trees. The Edwards-Anderson parameter at small temperatures scales like $q_{EA} \sim T$ for this model. Moreover, the dynamics exhibits aging, and a hierarchy of long relaxation times. Finally, we investigate the Edwards Anderson susceptibility for the XY model and the quadratic model. The XY case is treated numerically, and a Curie law $\chi_{EA} \sim 1/T$ is found above T_g. Below T_g, we calculate analytically the Edwards Anderson susceptibility, which is found to scale like $\chi_{EA} \sim T^2$.

[1]submitted to the Journal of Statistical Physics.

15.1 Introduction

Spin models on the Cayley tree have been essentially studied from the point of view of Ising spins. This problem was first considered in the seventies [1][2] from the thermodynamical point of view. Only recently, [3] the dynamical transition was considered. Below a temperature scale $T_g \sim J/\ln n$, with n the number of generations, the spin system is found to freeze. The glass temperature cross-over tends to zero in the limit $n \to \infty$, but decays very slowly with the system size, so that the glassy domain is still present, even in the macroscopic regime. In this article, we question the existence of such a dynamical cross-over for XY spins. We first study the existence of a glass temperature scale. To do so, we adapt to the case of XY spins the argument which was developped in [3] for Ising spins. The idea in the Ising case is to say that, below a certain temperature T_g, the excitations of the system are local in terms of bond variables, and give rise to large domains with a magnetization which is antiparallel to the average magnetization. To reach this regime, the number of bond excitations must be small enough for the domains to be rarely nested, so that the barriers are essentially the zero temperature barriers. The same criterion is valid for XY spins and leads to a temperature scale T_g. However, the origin of glassiness is different. For Ising spins, the zero temperture barriers scale like $J \ln n$, with n the number of generations. For XY spins, the barriers are zero. However, we show that the typical times scale like $\tau_n \sim \beta J n$, due to the slowing down of the dynamics of the Goldstone mode, which induces a slowing down of the dynamics below T_g.

After these qualitative orders of magnitude, we turn to study an approximate dynamics below T_g, by a Langevin dynamics of a model with quadratic interactions. The Langevin dynamics has the advantage that it is easier to implement than the Monte Carlo dynamics. In fact, the key of the Langevin dynamics lies in the diagonalization of the Laplacian on the tree. Analytical results for this problem will be presented elsewhere [4]. Here, we diagonalize the Laplacian numerically, using a Jacobi method.

Finally, we turn to the analysis of the Edwards Anderson order parameter and susceptibility of the ancestor spin, using a replica trick. Using the recursions of [5], we compute the partition function of two coupled copies of a tree.. We deduce the Edwards Anderson order parameter and susceptibility by differentiation of the partition function with respect to the inter-replica coupling. We find that $\chi_{EA} \sim 1/T$ above T_g. Below T_g, we calculate analytically the Edwards Anderson susceptibility and we find that $\chi_{EA} \sim T^2$.

In what follows, we work with trees with a coordination $z = 3$. We call half-space-trees trees such as the coordination of the ancestor is 2 instead of 3 for a full tree. We call a n-half-space-tree a half-space-tree with n generations.

15.2 Glass temperature scale

The criterion to evaluate the glass cross-over temperature scale T_g in the case of XY spins is adapted from the criterium for Ising spins [3]. In the case of Ising spins, the idea consists in imposing that, below T_g, the number of kinks on one path connecting the center to the leaves is on average smaller than unity. If this criterion is verified, the nesting of spin domains remains rare, and the dynamics is dominated by the presence of barriers which scale like the number of generations on the tree. We generalize this criterion for XY spins. We suppose that the temperature is small enough for the spin angles to be smaller than 2π. Within this approximation, the probability density to find an angle difference $\Delta\theta$ between a spin at a given

generation and its son is

$$P(\Delta\theta) = \frac{e^{-\beta J(\Delta\theta)^2/2}}{\int_{-\infty}^{+\infty} e^{-\beta J(\Delta\theta)^2/2} d(\Delta\theta)}. \tag{15.1}$$

Let us call $\tilde{P}(\varphi)$ the probability to find an angle $|\Delta\theta|$ larger than φ. Then,

$$\tilde{P}(\varphi) = \frac{\int_{\varphi}^{+\infty} e^{-\beta J(\Delta\theta)^2/2} d(\Delta\theta)}{\int_{0}^{+\infty} e^{-\beta J(\Delta\theta)^2/2} d(\Delta\theta)} \simeq 1 - erf\left(\sqrt{\frac{\beta J}{2}}\varphi\right) \sim_{\beta\to+\infty} \sqrt{\frac{2}{\pi\beta J}} \frac{1}{\varphi} e^{-\beta J\varphi^2/2}. \tag{15.2}$$

In the spirit of what has been done with the Ising case, we define the glass temperature scale as $n\tilde{P}(2\pi) \sim 1$, which leads to the following equation for the glass temperature as a function of the number of generations n:

$$\frac{1}{\sqrt{\beta_g J}} e^{-\pi^2 \beta_g J} \sim \frac{2^{1/2}\pi^{3/2}}{n}. \tag{15.3}$$

As in the case of the tree, $T_g(n) \to 0$ in the limit of an infinite tree. However, T_g remains sizable even in the macroscopic regime. An other difference with the case of Ising spins lies in the interpretation of the temperature scale. For Ising spins, the glass temperature scale corresponds to the cross-over temperature in the magnetization probability distribution, from a Gaussian shape above T_g to a non Gaussian shape below T_g. Such an interpretation is absent in the case of XY spins. An other difference lies in the nature of the slow dynamics. The barrier associated to XY spins is zero due to the presence of the Goldstone mode, whereas the barrier to reverse a set of Ising spins is non zero. In the case of Ising spins, below T_g, the excitations are local in terms of bond variables, but non local in terms of spin variables, and relevant barriers can be associated to a bond excitation, leading to a hierarchy of long relaxation times. What happens in the case of XY spins? Let us consider discretized spins with an angular separation ϵ, and let us start from a n-half-space-tree configuration with all the spins pointing in the same direction θ. Then, the magnetization will not decrease with time, if the temperature is sufficiently low. The equilibrium magnetization has been analyzed in [6] in the case of the square lattice. Here, we wish to analyze qualitatively the dynamics of the total magnetization for the Cayley tree. What is the typical time to reverse the spins, that is to reverse the magnetization from θ to $\theta + \pi$? An elementary transformation to reverse the spins is to transit from the configuration where all the spins have an angle θ to the configuration where all the spins have an angle $\theta + \epsilon$. The barrier is proportional to $\frac{1}{2} J\epsilon^2 \ln n$. We deduced this relation from the barrier formula for the Ising spin system on the tree [3]. The time scale associated to a jump of the magnetization from θ to $\theta + \epsilon$ is proportional to

$$n^{\beta J\epsilon^2/2}, \tag{15.4}$$

if we assume an Aharenius law for the jump between θ and $\theta + \epsilon$. Now, we assume that the magnetization diffuses along the Goldstone mode. Then, the typical time for a reversal of the magnetization from θ to $\theta + \pi$ is

$$t \sim \left(\frac{\pi}{\epsilon}\right)^2 n^{\beta J\epsilon^2/2}, \tag{15.5}$$

which diverges in the limit $\epsilon \to 0$. Here, we have assumed a discretization of the angular variable which does not depend on the temperature, and a dynamics where the spins can only jump from θ to $\theta + \epsilon$ or $\theta - \epsilon$. For real XY spins, the spin can jump from θ to θ', not necessarily in

the vicinity of θ. A spin wave argument shows that we must take $\epsilon \sim \sqrt{2/\beta J}$, so that the time scales are related to the temperature according to

$$\tau_n \sim \beta J n. \tag{15.6}$$

The relaxation times diverge in the $n \to +\infty$ limit, so that, like for Ising spins, there exists a hierarchy of relaxation times in the tree model.

15.3 Langevin dynamics below T_g

Below the glass temperature scale T_g, is is legitimate to make the harmonic approximation for the angular variables, and the Hamiltonian becomes

$$H = -\frac{J}{2} \sum_{\langle i,j \rangle} (\theta_i - \theta_j)^2. \tag{15.7}$$

We study the Langevin dynamics of this Hamiltonian

$$\eta \frac{d\theta_i}{dt} = - \sum_{j \in V(i)} (\theta_i - \theta_j) + \xi_i(t), \tag{15.8}$$

with a Gaussian white noise:

$$\langle \xi_i(t) \xi_j(t') \rangle = A \delta_{i,j} \delta(t - t'). \tag{15.9}$$

Using vectorial notations, we note θ the vector of the angular coordinates, and $\mathbf{\Delta}$ the Laplacian, such as the diagonal elements $\mathbf{\Delta}_{i,i}$ are minus the coordinantion of the site i, and the off-diagonal elements $\mathbf{\Delta}_{i,j}$ are $+1$ if a link connects the sites i and j, and 0 otherwise. The diagonalization of the Laplacian on the tree shall be studied analytically in the companion paper [4]. In the present paper, we shall use numerical diagonalizations only. The Langevin equation (15.8) can be integrated for a given noise ξ:

$$\theta(t) = \exp\left(\frac{1}{\eta}\mathbf{\Delta} t\right)\theta(0) + \frac{1}{\eta}\int_0^t \exp\left(\frac{1}{\eta}\mathbf{\Delta}(t-t')\right)\xi(t')dt'. \tag{15.10}$$

Using (15.9), we derive the correlation functions

$$\begin{aligned} \langle \theta_i(t_i)\theta_j(t_j) \rangle &= \sum_{r,s} \left(\exp \frac{1}{\eta}\mathbf{\Delta} t_i\right)_{i,r} \left(\exp \frac{1}{\eta}\mathbf{\Delta} t_j\right)_{j,s} \langle \theta_r(0)\theta_s(0) \rangle \\ &\quad + \frac{A}{\eta^2} \int_0^{\inf(t_i,t_j)} \left(\exp \frac{1}{\eta}\mathbf{\Delta}(t_i + t_j - 2t)\right)_{i,j} dt. \end{aligned} \tag{15.11}$$

As a particular case of (15.12), we are interested in the average $\langle \theta_i(t)^2 \rangle$, which is given by

$$\langle \theta_i^2(t) \rangle = \left(\exp \frac{2}{\eta}\mathbf{\Delta} t\right)_{i,i} \langle \theta^2(0) \rangle + \frac{A}{\eta^2} \int_0^t \left(\exp \frac{2}{\eta}\mathbf{\Delta}(t-t')\right)_{i,i} dt'. \tag{15.12}$$

We restricted ourselves to spatially decorrelated initial conditions: $\langle \theta_r(0)\theta_s(0) \rangle = \delta_{r,s}\langle \theta^2(0) \rangle$. We computed (15.12) for a small tree. We call $\mathbf{u}_i$ the eigenvectors of $\mathbf{\Delta}$: $\mathbf{\Delta}\mathbf{u}_i = \lambda_i \mathbf{u}_i$ and $\mathbf{P}$ the matrix of eigenvectors:

$$\mathbf{u}_i = \sum_j \mathbf{P}_{i,j} \mathbf{e}_j. \tag{15.13}$$

Then,

$$\langle \theta_i(t)^2 \rangle = \langle \theta^2(0) \rangle \sum_j \mathbf{P}_{j,i}^2 \exp\left(\frac{2}{\eta}\lambda_j t\right) + \frac{A}{\eta^2} \sum_j \mathbf{P}_{j,i}^2 \left[t\delta_{\lambda_j,0} - \frac{\eta}{2\lambda_j}\left(1-\delta_{\lambda_j,0}\right)\left(1-\exp\left(\frac{2}{\eta}\lambda_j t\right)\right)\right]. \tag{15.14}$$

We deduce from equation (15.14) the large time behaviour of $\langle \theta_i(t)^2 \rangle$: $\langle \theta_i^2(t) \rangle \simeq at + b_i$ with

$$a = \frac{A}{\eta^2}\mathbf{P}_{0,i}^2 \tag{15.15}$$

$$b_i = -\frac{A}{2\eta}\sum_j \frac{1}{\lambda_j}\mathbf{P}_{j,i}^2\left(1-\delta_{\lambda_j,0}\right) + \langle \theta^2(0) \rangle P_{0,i}^2. \tag{15.16}$$

The coefficients a are independent on the sites i. This is due to the fact that the eigenvector for the zero eigenvalue is a constant so that the asymptotic slope of $\langle \theta_i(t)^2 \rangle$ does not depend on i, and that $a = A/N\eta^2$, with N the number of sites. The diffusion constant of θ_i is thus independent on i, and decreases with the system size. The results are plotted on figure 15.1 for different generations. It is clear that the asymptotic slope of $\langle \theta_i(t)^2 \rangle$ is independent on the generation of the spin. Moreover the intercept which is measured by the coefficient b_i depends on i, and decreases as one goes from the leaves to the center of the tree.

An other quantity of interest is the waiting time correlation functions $C_i(t, t_w) = \langle \theta_i(t_w)\theta_i(t_w + t) \rangle$. This quantity can be expressed as

$$C_i(t,t_w) = \langle \theta(0)^2 \rangle \sum_j \mathbf{P}_{j,i}^2 \exp\left(\frac{1}{\eta}\lambda_j(t+2t_w)\right) + \frac{A}{\eta^2}\sum_j \mathbf{P}_{j,i}^2 \left[t_w\delta_{\lambda_j,0} - \frac{\eta}{2\lambda_j}\left(1-\delta_{\lambda_j,0}\right)\exp\left(\frac{1}{\eta}\lambda_j t\right)\left(1-\exp\left(\frac{2}{\eta}\lambda_j t_w\right)\right)\right]. \tag{15.17}$$

The autocorrelation $C_i(t, t_w)$ is plotted on figure 15.2 for a given waiting time t_w as a function of t. In order to compare the autocorrelation for different waiting times, we have to take into account the diffusion of $\langle \theta_i^2(t) \rangle$, that is we compute the normalized autocorrelation $C(t, t_w)/C(0, t_w) < 1$. For real XY spins, such a diffusion is absent since $\theta_i(t)$ is periodic.

We also studied the asymptotic ratio $C(\infty, t_w)/C(0, t_w)$. This function is plotted on figure 15.3 for a small tree. For $t_w = 0$, this quantity is strictly positive for a finite tree, but is very small. This is due to the fact that $C_i(\infty, 0)$ is equal to $\langle \theta_i(0)^2 \rangle / N$, with N the number of sites, whereas $C_i(0, 0)$ is equal to $\langle \theta_i(0)^2 \rangle$.

In order to illustrate the fact that the system possesses a hierarchy of relaxation times, we focus on the relaxation of the correlation $\langle \theta_i(t)\theta_j(t) \rangle$, where the sites i and j are neighbours. At equilibrium, $\langle (\theta_i - \theta_j)^2 \rangle = 1/\beta J$, as expected from quadratic interactions. We start from $\langle (\theta_i - \theta_j)^2 \rangle = 0$ and we study the dynamics of the relaxation for pairs of neighbouring sites at various generations. The result is plotted on figure 15.4. A hierarchy of relaxation times is visible, which is consistent with the qualitative calculations of equation (15.6).

15.4 Edwards Anderson order parameter

We computed the Edwards Anderson order parameter numerically in the non glassy regime, and analytically in the glassy regime. We first begin with the numerical computation. We use

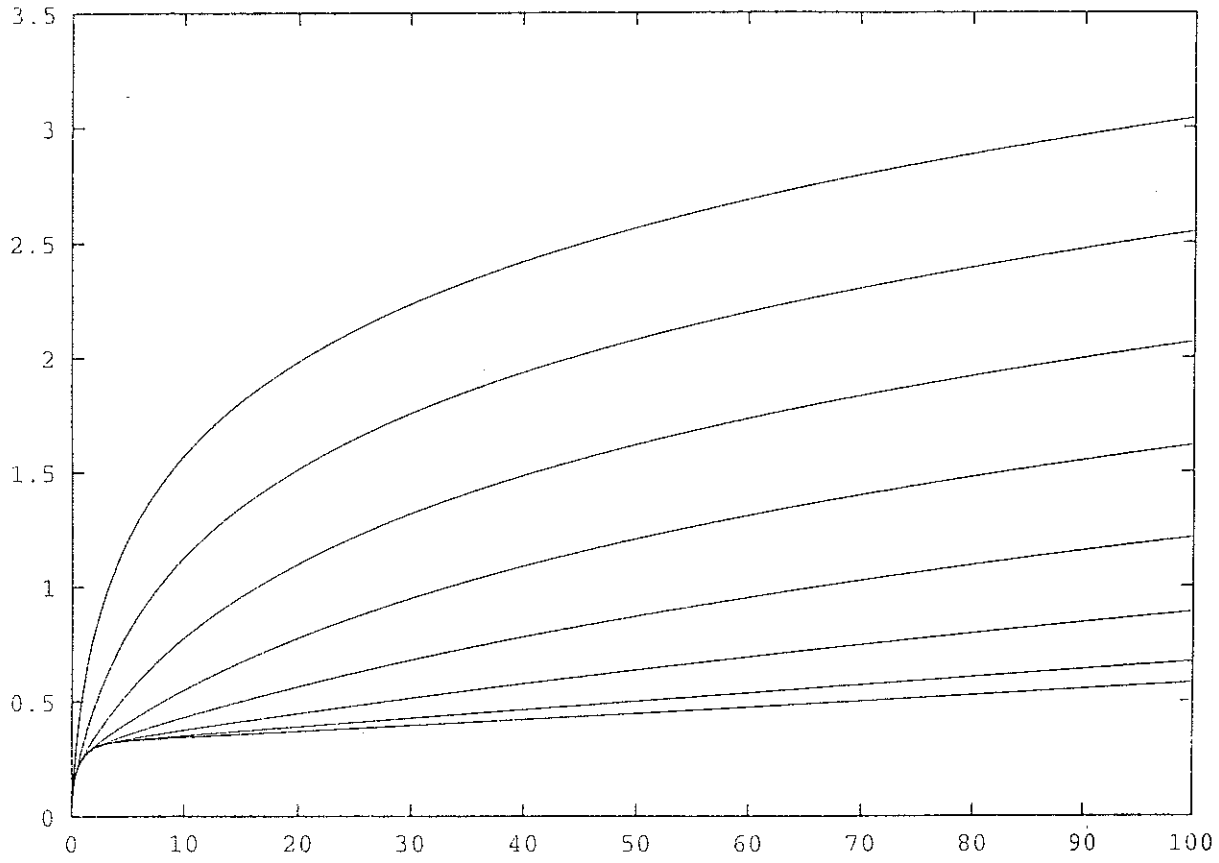

Figure 15.1:
$\langle \theta_i^2(t) \rangle$ as a function of t, for a tree with 7 generations. The coefficients are chosen such as $A = \eta = 1$, and $\langle \theta_i^2(0) \rangle = 0$. The upper curve corresponds to the leaves (7th generation), and the lower curve corresponds to the ancestor (0th generation). The number of spins is $N = 382$. The asymptotic slope is $1/382$. The coefficients b_i are found to increase with i, due to the relaxation of fast processes.

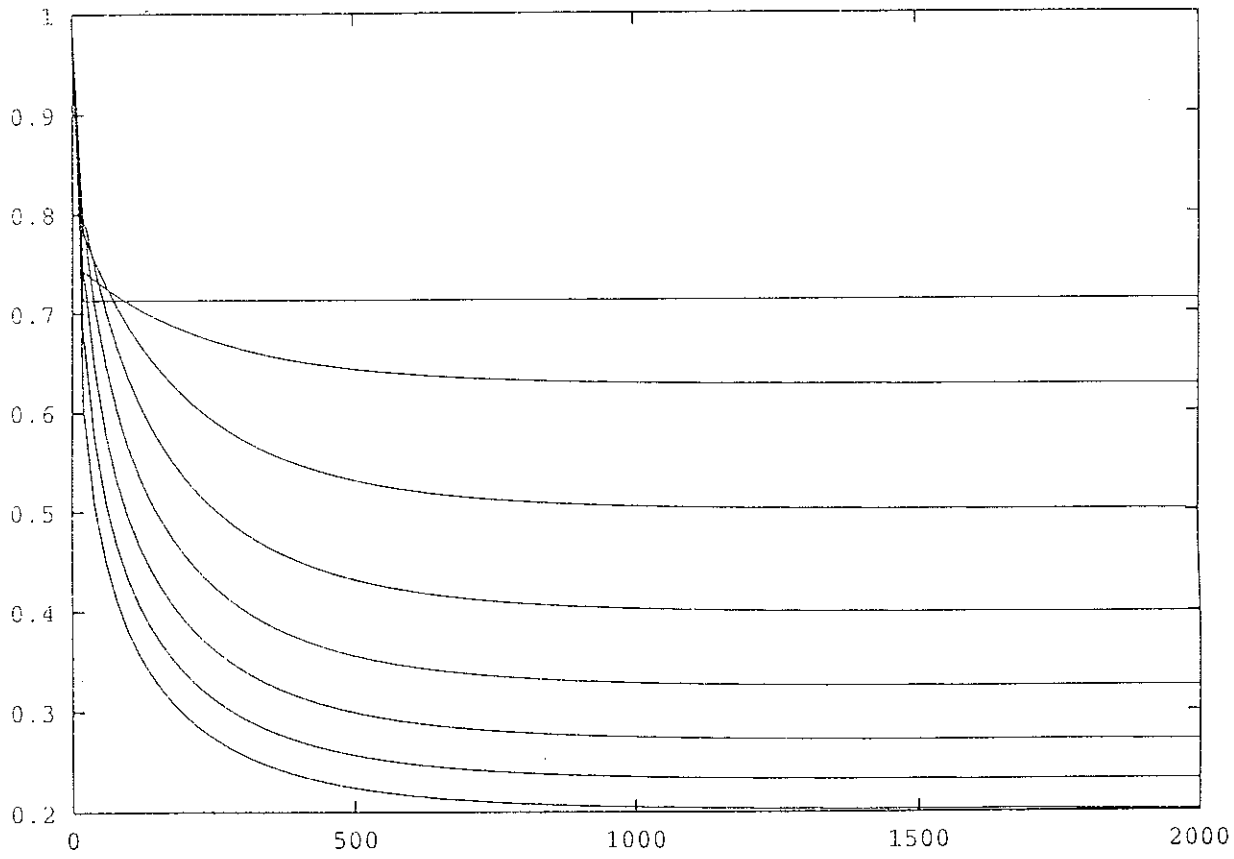

Figure 15.2:
Autocorrelation $C_i(t, t_w)/C_i(0, t_w)$ for a 7 generation tree. We have chosen $A = \eta = \langle \theta^2(0) \rangle = 1$. The autocorrelation is plotted as a function of t for $t_w = 300$. The upper curve corresponds to the ancestor (0th generation) and the lower curve to the leaves (7th generation).

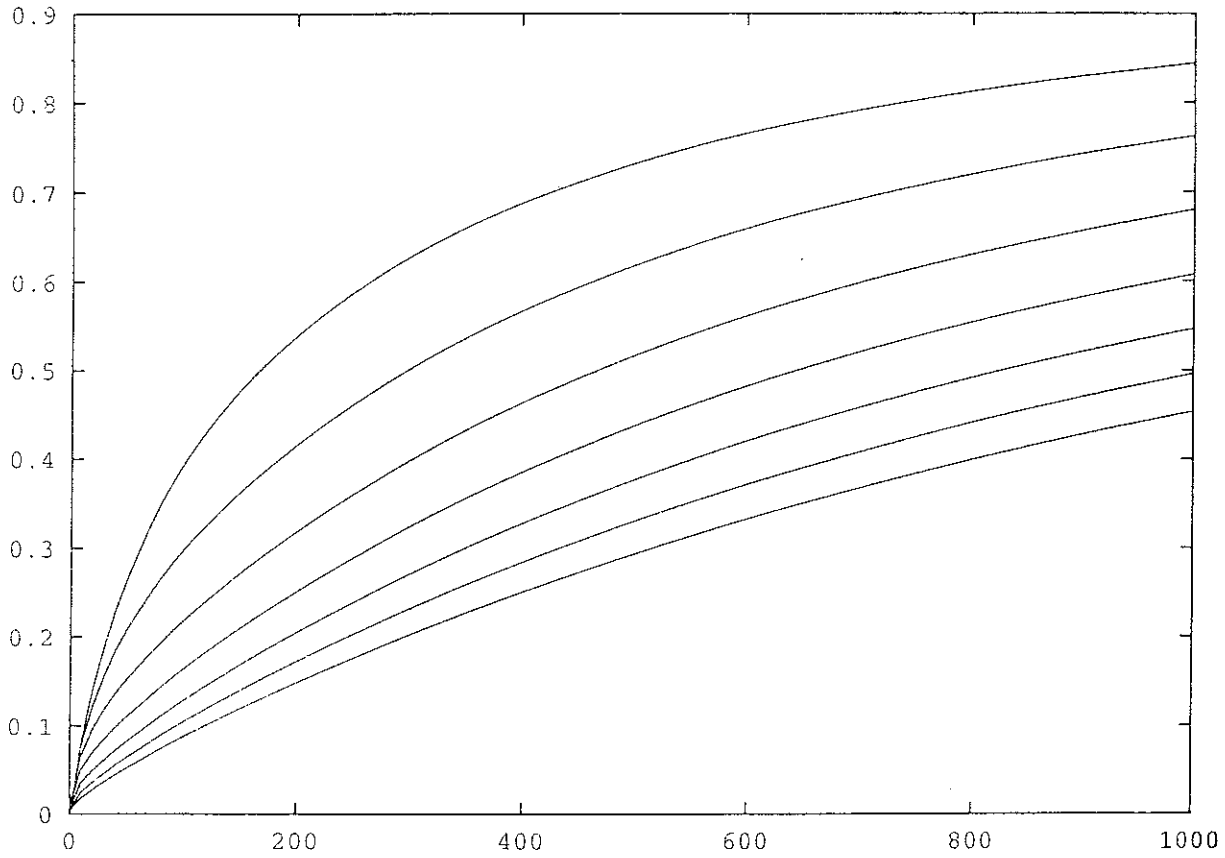

Figure 15.3:
Autocorrelation $C_i(\infty, t_w)/C_i(0, t_w)$ as a function of t_w for a 7 generation tree. We have chosen $A = \eta = \langle \theta^2(0) \rangle = 1$. the upper curve corresponds to the central spin, whereas the lower one corresponds to the leaves.

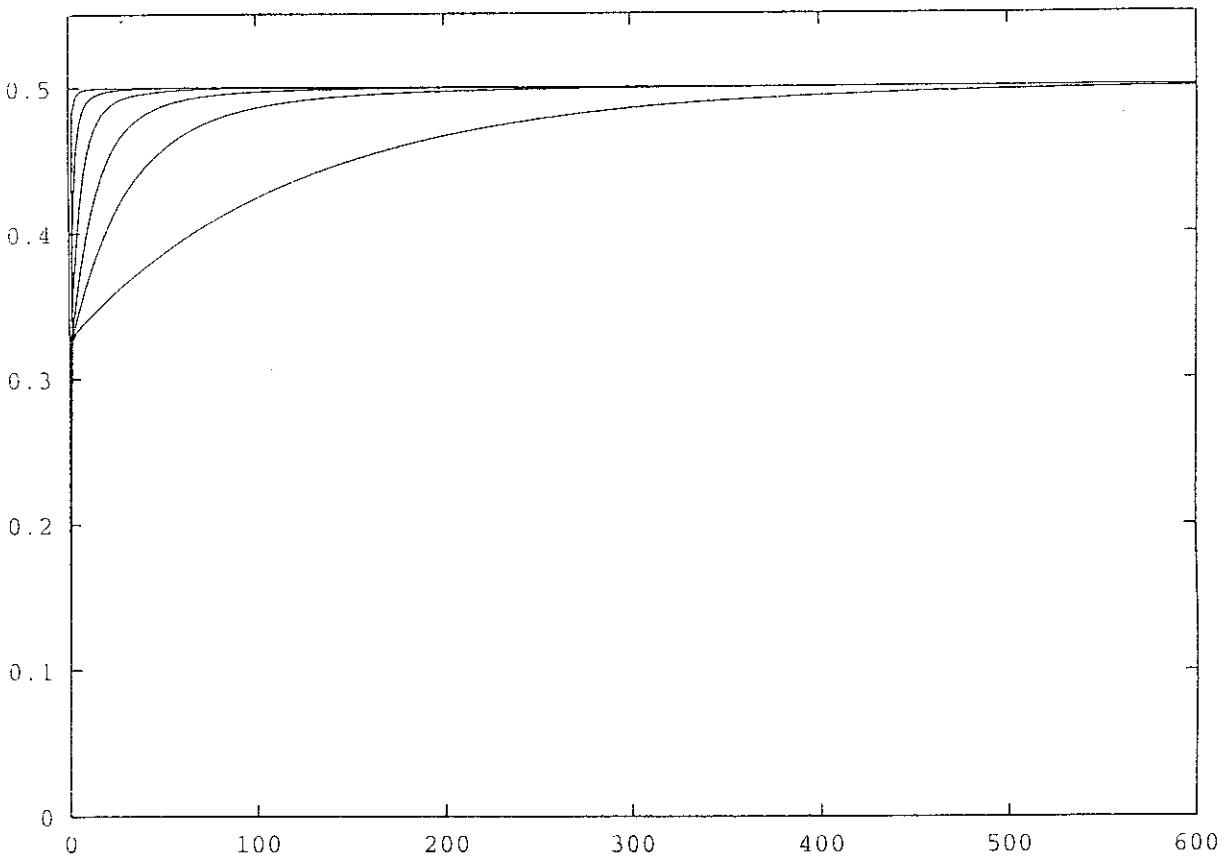

Figure 15.4:
Relaxation of the correlation $\langle(\theta_i - \theta_j)^2\rangle$ for neighbouring sites i and j. The tree has 8 generations. The lower curve corresponds to the correlation between the ancestor and its son, and the lower curve is the correlation between one leaf and its father. Initially, $\langle(\theta_i - \theta_j)^2\rangle = 0$. The parameters of the Langevin dynamics are $A = \eta = 1$.

the replica trick of [5]. Two copies of the XY tree are considered, with an inter-replica coupling R. The total Hamiltonian reads

$$H = -J \sum_{\langle i,j \rangle} \Big(\cos(\theta_i - \theta_j) + \cos(\theta'_i - \theta'_j) \Big) - R \sum_i \cos(\theta_i - \theta'_i). \tag{15.18}$$

The half-space-trees are put together as shown on figure 15.5. If Z_n is the partition function of a half-space-tree with n generations, Z_{n+1} is related to Z_n by

$$Z_{n+1}(\theta - \theta') = e^{\beta R \cos(\theta - \theta')} \left[\int d\theta_1 d\theta'_1 e^{\beta J \left(\cos(\theta - \theta_1) + \cos(\theta' - \theta'_1) \right)} Z_n(\theta'_1 - \theta_1) \right]^2, \tag{15.19}$$

with θ and θ' the angles of the ancestors of each replica. The recurrence is initiated with

$$Z_0(\theta - \theta') = e^{\beta R \cos(\theta - \theta')}. \tag{15.20}$$

The function $Z(\theta)$ can be propagated numerically for different values of the inter-replica coupling R. We note

$$Z = \int Z(\theta) d\theta \tag{15.21}$$

$$Q = \int Z(\theta) \cos\theta d\theta \tag{15.22}$$

The Edwards Anderson order parameter of the ancestor is $q_{EA} = Q(R = 0)$, and the Edwards Anderson susceptibility is

$$\chi_{EA} = \frac{\partial Q}{\partial \beta R}(R = 0). \tag{15.23}$$

Numerically, the Edwards Anderson order parameter is found to be zero, and the Edwards Anderson susceptibility is plotted on figure 15.6. In practise, the angle of the spins is discretized, and the integrals are computed using a five points method. One has to be careful not to handle directly the partition function, which may be large at small temperatures, but its logarithm. However, at low temperatures, even the logarithm of the partition function may become large. In order to compute the susceptibility, one has to estimate differences between large numbers, and make integrals over large numbers, so that the precision is poor at low temperatures, and the results at low temperatures are not reliable. However, it is clear that above T_g, a Curie law $\chi_{EA} \sim 1/T$ is obtained, so that this system may be seen as a zero temperature glass. However, this is not the case since the susceptibility does not diverge in the limit $T \to 0$, but falls down to zero. To see this, we come back to the quadratic model below T_g. Within this approximation, one can evaluate analytically the partition function. We assume that

$$Z_n(\theta - \theta') = A_n \exp\left(-\frac{1}{2} \beta R_n (\theta - \theta')^2 \right). \tag{15.24}$$

The equation relating $Z_{n+1}(\theta - \theta')$ as a function of $Z_n(\theta - \theta')$ is similar to (15.19), but only with Gaussian integrals:

$$Z_{n+1}(\theta, \theta') = A_n e^{\beta R_n (\theta - \theta')^2/2} \left[\int d\theta_1 d\theta'_1 e^{-\frac{1}{2}\beta J \left((\theta - \theta_1)^2 + (\theta' - \theta'_1)^2 \right)} Z_n(\theta_1 - \theta'_1) \right]^2. \tag{15.25}$$

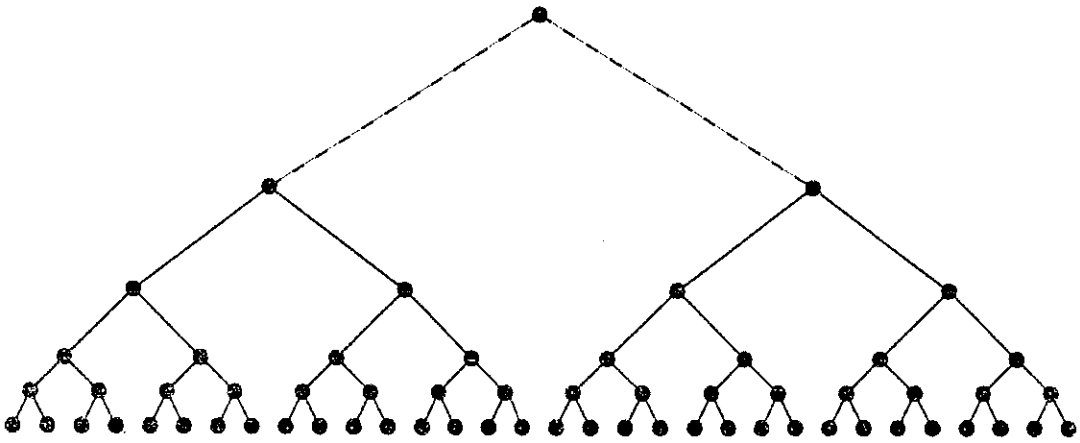

Figure 15.5:
The way two half-space-trees with n generations are put together to obtain a half-space-tree with $n+1$ generations.

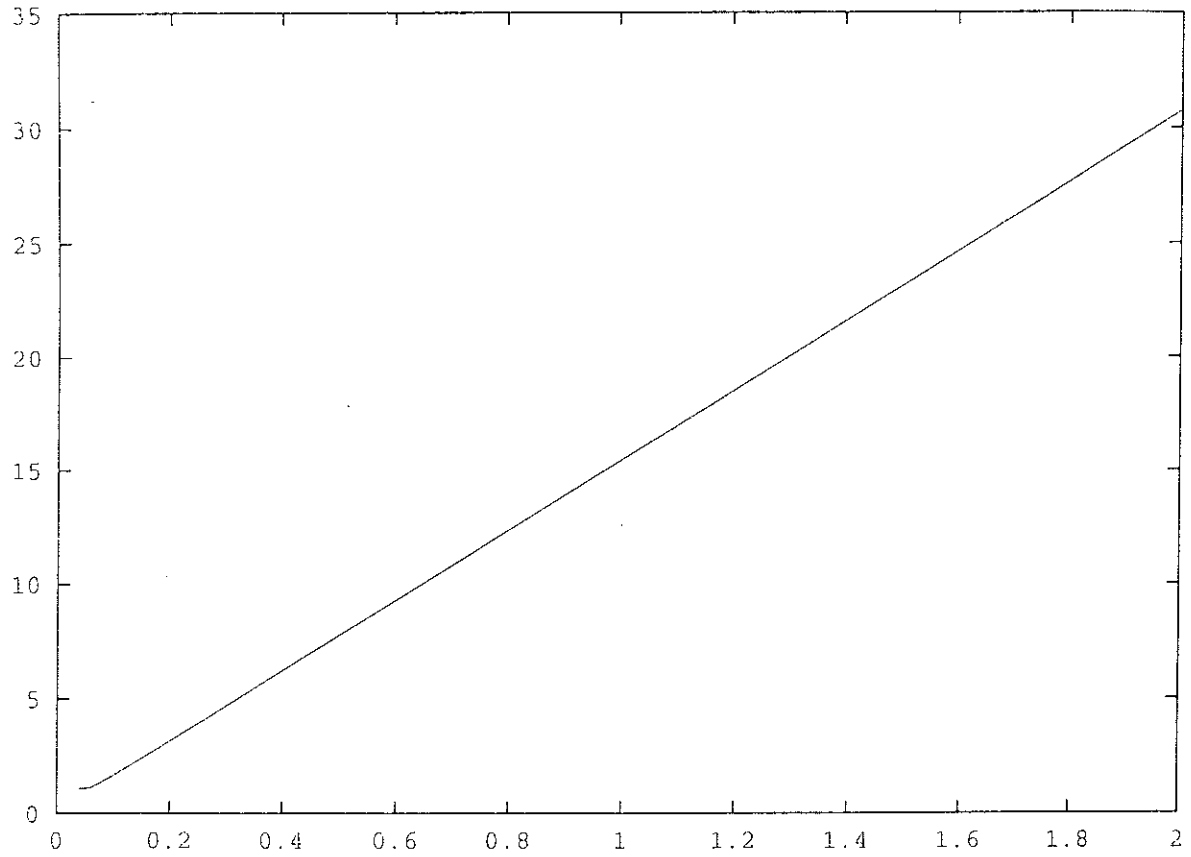

Figure 15.6:
Inverse of the Edwards Anderson susceptibility of the XY model on the Cayley tree as a function of temperature. The number of generations is 16. The number of discretized allowed values of the angle is 15. The values at small temperature are not reliable, since the computer has to form the difference between huge numbers.

The calculation of the Gaussian integrals is straightforward, and leads to the recursion

$$A_{n+1} = A_n \left(\frac{\pi}{\sqrt{J(J+2R_n)}} \right)^2 \tag{15.26}$$

$$R_{n+1} = R + \frac{2JR_n}{J+2R_n}, \tag{15.27}$$

with $R_0 = R$ and $A_0 = 1$. The iteration of R has a fixed point R^*. If we first take the thermodynamic limit, and afterwards the limit $R \to 0$, we have

$$q_{EA} = \langle (\theta - \theta')^2 \rangle = \frac{1}{\beta R^*} = \frac{k_B T}{\alpha J}, \tag{15.28}$$

with $\alpha = 1/2$. In this equation, we have replaced R^* by its limit when $R \to 0$. This result is proportional to the one of relation (15.28). We now turn to the Edwards-Anderson susceptibility

$$\chi_{EA} = \langle (\theta - \theta')^4 \rangle - \langle (\theta - \theta')^2 \rangle^2. \tag{15.29}$$

These averages over Gaussian distributions are readily calculated and we obtain

$$\chi_{EA} = \frac{1}{(\beta R^*)^2} = \frac{(k_B T)^2}{J\alpha^2}. \tag{15.30}$$

Obviously, χ_{EA} does not diverge at small temperatures, but scales as $\chi_{EA} \sim T^2$. In the case of Ising spins, χ_{EA} tends to a constant, independent of n below T_g [3].

15.5 Conclusions

We have shown that below a certain temperature scale T_g, the XY model on the Cayley tree is glassy. The temperature scale T_g is found to tend to zero in the limit of an infinite system. This behaviour is similar to the case of the Ising model. However, the nature of the slow dynamics is different from the Ising case, where barriers are present, which scale like the number of generations. The XY system is characterized by the presence of a Goldstone mode, with a very small barrier. However, the motion of the spins along the Goldstone mode is slow, with time scales proportional to the number of generations. We studied the Langevin dynamics below T_g, where a model with quadratic interactions is valid. A hierarchy of relaxation times is visible on the relaxation of the correlation functions. Finally, we computed the Edwards Anderson susceptibility of the ancestor. Above T_g, $\chi_{EA} \sim 1/T$ and below T_g, $\chi_{EA} \sim T^2$.

I acknowledge discussions with B. Douçot.

References

[1] E. Müller-Hartmann and J. Zittartz, Phys. Rev. Lett. 33, 893 (1974).

[2] J.von Heimburg and H. Thomas, J. Phys. C, 7, 3433 (1974).

[3] R. Mélin, J.C. Anglès d'Auriac, P. Chandra and B. Douçot, preprint.

[4] R. Mélin, CRTBT preprint.

[5] J.M. Carlson, J.T. Chayes, J.P. Sethna and D.J. Thouless, J. Stat. Phys. 61, 1069 (1990).

[6] S.T. Bramwell and P.C.W. Holdsworth, Phys. Rev. B 49, 8811 (1994).

Chapitre 16

Article 8

Glassy Behavior in the Ferromagnetic Ising Model on a Cayley Tree[1]

R. Mélin[(1)], J.C. Anglès d'Auriac[(1)], P. Chandra[(2)] and B. Douçot[(1)]

[(1)]CRTBT-CNRS, 38042 Grenoble BP 166X cédex France
[(2)]NEC Research Institute, 4 Independence Way, 08540 Princeton NJ, USA

We present a detailed study of the nearest neighbor ferromagnetic Ising model on a Cayley tree. In the limit of zero field, the system displays glassy behavior below a crossover temperature, T_g, that scales inversely with the logarithm of the number of generations. Non-Gaussian magnetization distributions are observed for $T < T_g$, reminiscent of that associated with the central spin of the Edwards-Anderson model on the same tree; furthermore a dynamical study indicates metastability, long relaxation times and ageing consistent with the development of glassy behavior for a finite but macroscopic number of sites.

[1]Submitted to J. Phys. A

16.1 Introduction

Recursive structures like the Bethe lattice and the Cayley tree provide a pedagogical enviroment for the study of physical problems; in this setting they can be treated with a direct analytic approach without resorting to approximate methods.[1] The Bethe lattice, an infinite Cayley tree, is a connected dendritic structure with constant coordination, z, and *no* loops, as displayed for $z = 3$ in Figure 16.1. Strictly speaking it is a *pseudo-lattice* since it cannot be embedded in any *real* finite-dimensional lattice; indeed it is often regarded as an infinite-dimensional structure since the number of sites accessible in N steps from a given site ($\sim N^d$ for a d-dimensional lattice) increases exponentially with N. Thus the Bethe lattice provides a setting where mean-field treatments can become exact. This property was first discussed by Domb who showed that the Bethe-Peierls (BP) approximation to the nearest-neighbor (nn) ferromagnetic (FM) Ising problem, with $H = -J \sum_{(ij)} \sigma_i \sigma_j$ where $J > 0$, $\sigma_i = \pm 1$ and (ij) indicates a nn sum, is exact on this structure;[2] its solution is identical to that of the infinite-range FM Ising model.[3] Similarly Thouless, Anderson and Palmer studied the infinite-range Sherrington-Kirkpatrick (SK) model of spin glasses on the Bethe lattice using a mean-field technique;[4] they were able to recover the key results[5] of Sherrington and Kirkpatrick (SK) without using the replica method. More recently there have been several studies of the SK model on the Bethe lattice, particularly in finite fields.[6, 7, 8, 9, 10, 11, 12, 13, 14] In general the study of a variety of problems on this recursive structure has helped to develop our understanding of diverse physical phenomena including self-avoiding polymers,[15] random resistor networks[16] and percolation.[17]

Like the Bethe lattice, a Cayley tree is a connected structure with fixed coordination number and no loops; however it has a *finite* number of generations (cf. Figure 16.1) and hence sites that are dominated by the boundary. More specifically, the total number of sites in a Cayley tree of n generations with coordination z is

$$N = 1 + z + z(z-1) + ...z(z-1)^{n-1} = \frac{(z(z-1)^n - 2)}{(z-2)} \tag{16.1}$$

and the number of surface atoms is

$$N_s = z(z-1)^{n-1} \tag{16.2}$$

so that for large n

$$\frac{N}{N_s} \approx \frac{(z-2)}{(z-1)} \tag{16.3}$$

in contrast to the situation in "real" lattices $\left(\frac{N_s}{N} \sim N^{-\frac{1}{d}}\right)$. Thus the "interior" of a Cayley tree, in the limit of a large number of generations, contains an arbitrarily small fraction of its total number of sites, and the boundary plays a key role in any problem studied on this graph. In particular, the Bethe-Peierls transition for the FM Ising model on a Cayley tree occurs *only* for its central spin; despite its finite moment, the total spontaneous magnetization of *all* the spins remains zero.[18, 19, 20, 21] In a nutshell this occurs because, at zero field and low temperatures, very large domains of flipped spins can nucleate from the boundaries; the resulting finite-size glassiness is the subject of this Paper.

The recursive structure of the Cayley tree permits a detailed analysis of the single-site magnetization distribution as a function of field and generation. In doing so, we find that for fields $h < h_{c0}$, where the crossover field h_{c0} decreases exponentially with the number of

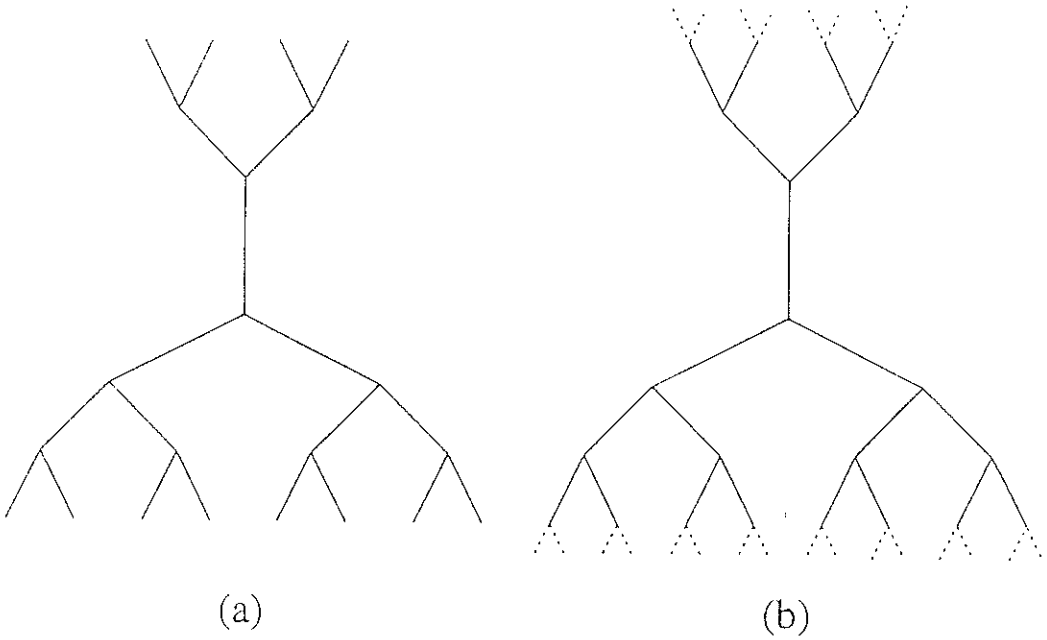

Figure 16.1:
Showing a finite Cayley tree (a) and a piece of a Bethe lattice (b).

generations, there is a temperature-scale T_g below which well-defined, large domains of flipped spins exist. For $T < T_g$ the magnetization distribution becomes non-Gaussian, reminiscent of that associated with the central spin of the magnetized spin glass phase of the $\pm J$ model on the Cayley tree. The cross-over temperature, T_g, scales inversely with the logarithm of the number of generations of the Cayley tree so that the "finite-size" glassiness persists to very large system sizes for a macroscopic number of sites.

We therefore have a short-ranged periodic spin model that has a "glass" cross-over temperature that decreases very slowly with increasing system size; more specifically it is inversely proportional to the logarithm of the logarithm of the number of sites. We characterize it using a combination of analytic and numerical techniques, always retaining open boundary conditions. First we study the magnetization for different thermodynamic limits emphasizing the crucial role of the ratio of surface/bulk sites as $n \to \infty$. We recover the Bethe-Peierls result if this ratio goes to zero; otherwise, for vanishing applied fields, there is a cross-over to a glassy phase characterized by well-defined clusters of flipped spins. We find in that for $h < h_{co}$, the single-site magnetization distribution becomes non-Gaussian for $T < T_g$ similar to that of spin glass models residing on the same structure; however it recovers its Gaussian character with increasing field. For $T < T_g$ the largest barriers associated with developing broken bonds in these domains scale with the number of cluster sites; we thus refer to this low-temperature state as a finite-size glass. A dynamical study of this system, performed numerically, indicates the presence of metastable states and long relaxation times at low temperatures. The autocorrelations for $T < T_g$ are determined after a waiting time, and indicate ageing effects; the variation of χ_1' and χ_3' with temperature also agree with the presence of glassiness. As expected, the Edwards-Anderson susceptibility of the entire tree has a maximum which develops slowly with system-size; no divergence is observed. Finally we find that for this system the density of Lee-Yang zeroes in the presence of a complex field is very high in the vicinity of the real axis below a particular temperature-scale; we identify it as the crossover temperature T_g. We end with a summary of our results and plans for future work.

16.2 The thermodynamic limits

16.2.1 Warming up: Bethe Peierls transition of the central spin

One way to take the thermodynamic limit on a tree with n generations is to look only at the properties of the central spin, and take the limit $n \to +\infty$. As first pointed out in [25], the behavior of the central spin is then characteristic of an infinite dimensional lattice, namely it undergoes a mean-field type transition. In other words, the Bethe-Peierls approximation becomes exact on the Cayley tree, as long as one considers the properties of the central spin. For recent results in this field, see reference [15] We leave for the appendix A the calculation of the recursion relation for the partition function of a tree with a coordinance z, and n generations $Z_n(\beta, H, H_n)$, where β is the inverse temperature, H the magnetic field acting on the spin of generations 0 to $n-1$, and H_n the field on generation n. The result reads

$$Z_n(\beta, h, h_n) = \left(4\cosh^2(\beta J)\cosh^2(\beta h_n)\right)^{\frac{(z-1)^n}{2}} Z_{n-1}(\beta, h, h + T.h_n), \qquad (16.4)$$

where the transformation of the magnetic field reads

$$T.h = \frac{1}{2\beta} \ln \frac{\cosh \beta(J+h)}{\cosh \beta(J-h)}. \tag{16.5}$$

We specialize the recursion (16.5) to the case of a tree with a field ϵ at the border, and ask whether this field is magnified or attenuated under the recursion (16.5). This condition defines the bulk critical temperature β_c as $(z-1)\tanh \beta_c J = 1$. If $\beta < \beta_c$, the magnetization of the central spin is zero, and if $\beta > \beta_c$, there is a broken symmetry for the central spin in the thermodynamic limit. As shown in [3], the critical behavior is the same as the mean field one: $\beta = 1/2$ and $\delta = 3$.

16.2.2 Beyond the Bethe Peierls reigme: the different thermodynamic limits

We now wish to look at the transition, not only of the central spin, but of the entire tree. First, we consider only *half-space-trees*, that is trees such as the coordinance of the ancestor is $z-1$ instead of z. A half-space-tree with n generations shall be called a n-half-space-tree. A half space tree is pictured on figure 16.2. In order to label the generations, the ancestor is at generation n and the leaves at generation 1. We shall keep this convention in the rest of the paper. We look for the properties of the spins of generations $n-m$ to n, and look at the limit $n \to +\infty$. Of course, m is a function of n. We whish to classify the different regimes as a function of $m(n)$, in a given uniform magnetic field h. In order to obtain the magnetization of the generations $n-m$ to n, we have to introduce a source magnetic field λ on these generations, to differentiate the partition function with respect to λ in the limit $\lambda \to 0$:

$$\langle M(n,m,h) \rangle = \frac{\partial}{\partial(\beta\lambda)} \ln Z(n,m,h,\lambda=0). \tag{16.6}$$

The principle of the calculation of the partition function is given in appendix B, and we obtain

$$\langle M(n,m,h) \rangle = \sum_{i=n-m}^{n-1} (z-1)^{n-i} \frac{\sinh \beta h_i \cosh \beta h_i}{\cosh^2 \beta J + \sinh^2 \beta h_i} \frac{dh_i}{d\lambda}(\lambda=0) + \tanh \beta h_n \frac{dh_n}{d\lambda}(\lambda=0). \tag{16.7}$$

The last term is the contribution of the ancestor to the average magnetization, and h_i is the total field at generation i, that is the external uniform field h, plus the source λ between generations $n-m$ and n, plus the recursive field h^{ind} of equation (16.5).

We do not treat exactly the iteration of h^{ind}, but approximate it as follows. We deduce from the iteration (16.5) the shape of h_{i+1}^{ind} as a function of h_i, which is plotted on figure 16.3. If $\beta < \beta_c$, the slope at the origin is less than unity, whereas is is larger than unity for $\beta > \beta_c$. Moreover, for $\beta > \beta_c$, there is one non trivial fixed point, for which $h_{i+1}^{ind} = h_i = h^*$, which depends only on the temperature. This behaviour suggests that the iteration can be approximated by linearizing $h_{i+1}(h_i)$ in the vicinity of the $h_i = 0$ and of $h_i = h^*$. More precisely, we deduce from (16.5) that

$$\frac{dh_{i+1}^{ind}}{dh_n} = (z-1) \frac{\sinh \beta J \cosh \beta J}{\cosh^2 \beta J + \sinh^2 \beta h_i}. \tag{16.8}$$

We use the following notations for the derivatives of h_{i+1}^{ind} with respect to h_i in the vicinity of $h_i = 0$ and $h_i = h^*$:

$$\frac{dh_{i+1}^{ind}}{dh_i}(h_i = 0) \quad = \quad (z-1)\tanh \beta J \equiv 1 + \eta_1 \tag{16.9}$$

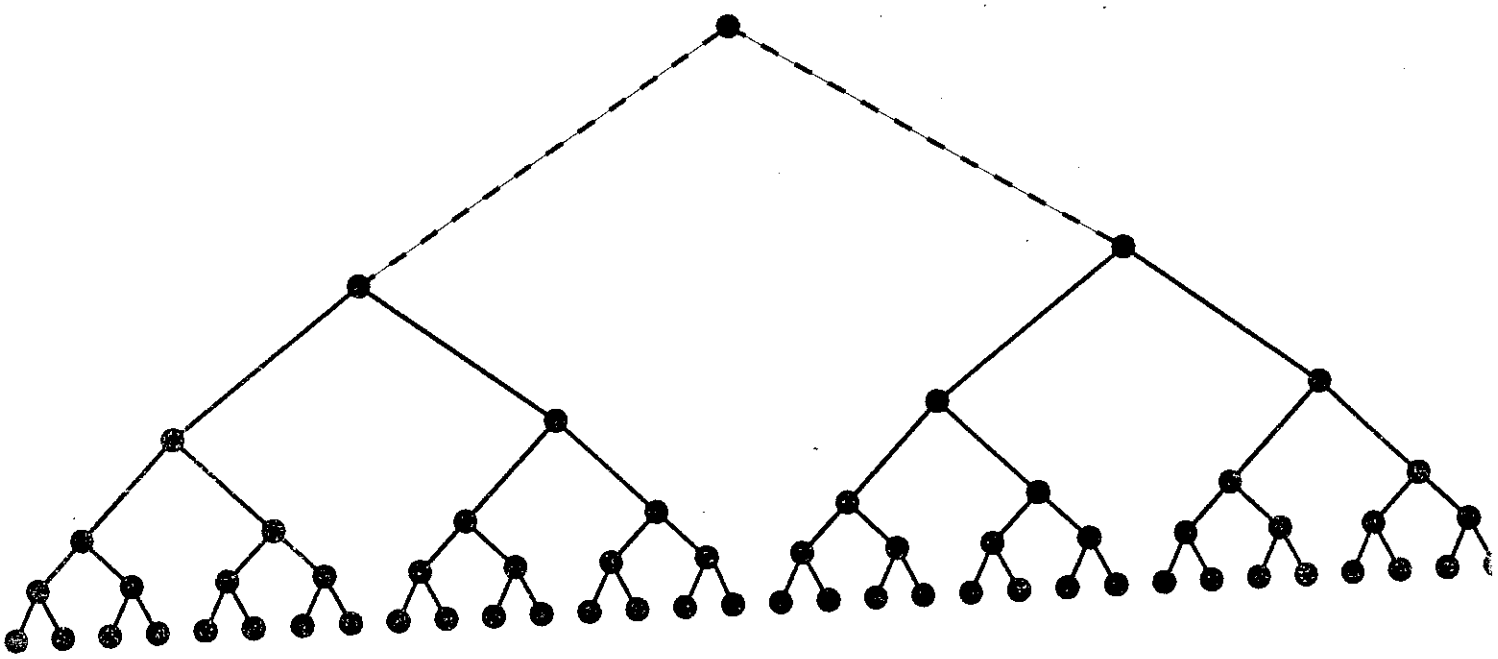

Figure 16.2:
Recursive construction of half-space trees.

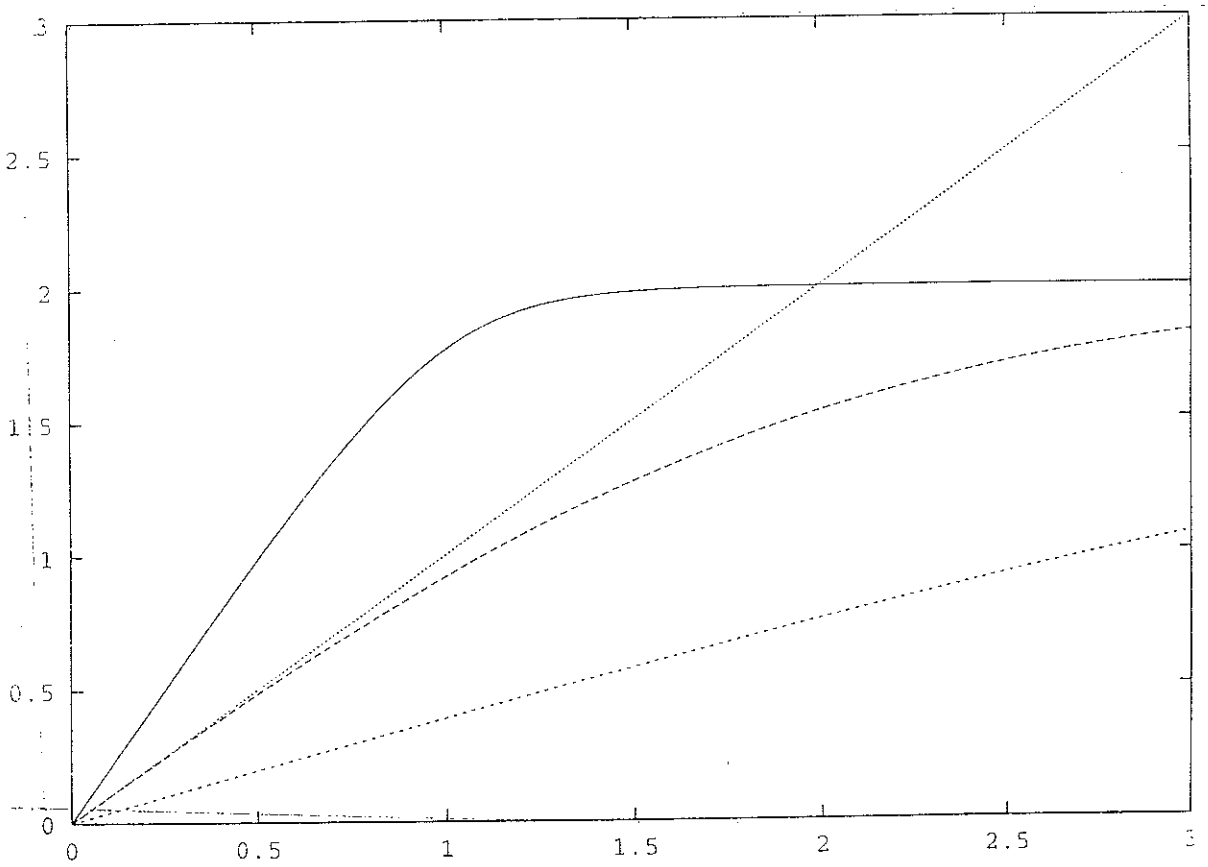

Figure 16.3:
h_{i+1}^{ind} as a function of h_i. h_i is the total magnetic field at generation i, and h_{i+1}^{ind} is the iterated field of equation (16.5). The three curves correspond to the three cases $\beta < \beta_c$. In this case, the only intersection of the curve with the first bissectrice is at the origin. For $\beta = \beta_c$, the curve is tangent to the first bissectrice at the origin. For $\beta > \beta_c$, the curve intersects twice the first bissectrice.

$$\frac{dh_{i+1}^{ind}}{dh_i}(h_i = h^*) \equiv 1 - \eta_2, \tag{16.10}$$

where $\eta_1 \in]0, z-2[$ and $\eta_2 \in]0, 1[$. η_1 and η_2 depend only on the temperature. We then replace the complete recursion by

$$h_{i+1}^{ind} = (1+\eta_1)h_i, \tag{16.11}$$

or

$$h_{i+1}^{ind} = \eta_2 h^* + (1-\eta_2)h_i. \tag{16.12}$$

The first linearization corresponds to $h_i \in [0, h_c]$ and the second one to $h_i \in [h_c, h^*]$, where

$$h_c = \frac{\eta_2}{\eta_1 + \eta_2} h^*. \tag{16.13}$$

If $\lambda = 0$, the iteration of the total magnetic field h_n gives, with this approximation:

$$h_i = \frac{h}{\eta_1}\left((1+\eta_1)^{i+1} - 1\right) \tag{16.14}$$

if $i \leq n_c(h)$ and

$$h_i = h^* + \frac{h}{\eta_2} + \left(h_{n_c} - h^* - \frac{h}{\eta_2}\right)(1-\eta_2)^{i-n_c} \tag{16.15}$$

if $i \geq n_c(h)$. The two regimes are separated by

$$n_c(h) = \left[\frac{1}{\ln(1+\eta_1)} \ln\left(\frac{\eta_1\eta_2}{\eta_1+\eta_2}\frac{h^*}{h} + 1\right)\right], \tag{16.16}$$

where [] denotes the integer part. We distinguish three regimes, which shall be analyzed successively: regime I: $0 \leq n_c \leq n-m$, regime II: $n-m+1 \leq n_c \leq n$ and regime III: $n_c \geq n$.

Regime I: $0 \leq n_c \leq n-m$, rather large fields

Using the approximation exposed in the previous section, we are in position to approximate the average magnetization, given by equation (16.7). We make the following approximations.

$$\frac{dh_i}{d\lambda}(\lambda = 0) = \frac{1}{\eta_2}(1 - (1-\eta_2)^{i-n+m+1}). \tag{16.17}$$

If $0 \leq h_i \leq h_c$ or $i < n_c$, we can approximate

$$\frac{\sinh \beta h_i \cosh \beta h_i}{\cosh^2 \beta J + \sinh^2 \beta h_i} \simeq a_1 h_i, \tag{16.18}$$

where

$$a_1 = \frac{\beta}{\cosh^2 \beta J} \tag{16.19}$$

And if $h_i \geq h_c$ or $n \geq n_c$,

$$\frac{\sinh \beta h_i \cosh \beta h_i}{\cosh^2 \beta J + \sinh^2 \beta h_i} \simeq a_2(h_i - h^*) + b_2, \tag{16.20}$$

where

$$a_2 = \frac{\cosh^2\beta J\cosh^2\beta h^* + \sinh^2\beta J\sinh^2\beta h^*}{(\cosh^2\beta J+\sinh^2\beta h^*)^2} \tag{16.21}$$

$$b_2 = \beta\frac{\sinh\beta h^*\cosh\beta h^*}{\cosh^2\beta J+\sinh^2\beta h^*}. \tag{16.22}$$

It is now tedious but straightforward to replace these approximation into the expression (16.7) for the average magnetization. Since we normalize by the number of sites

$$N_m = 1+(z-1)+...+(z-1)^m = \frac{(z-1)^{m+1}-1}{z-2}, \tag{16.23}$$

we can legitimaly forget the contribution of the ancestor. We obtain

$$\begin{aligned}\langle M(n,m,h)\rangle = \frac{1}{\eta_2}\Bigg[&(b_2+a_2\frac{h}{\eta_2})N_m \\ +\ &(z-1)^m\frac{1-((1-\eta_2)/(z-1))^m}{1-((1-\eta_2)/(z-1))}\left(-(b_2+a_2\frac{h}{\eta_2})(1-\eta_2)+a_2(h_{n_c}-h_\infty)(1-\eta_2)^{n-m-n_c}\right) \\ -\ &a_2(h_{n_c}-h_\infty)(z-1)^m(1-\eta_2)^{n-m-n_c+1}\frac{1-((1-\eta_2)^2/(z-1))^m}{1-((1-\eta_2)^2/(z-1))}\Bigg],\end{aligned} \tag{16.24}$$

where $h_\infty = h^* + h/\eta_2$. We are now in position to discuss the different thermodynamic limits. First, if $n\to\infty$, $m\to\infty$ and $n-m\to\infty$, the thermodynamic limit of the normalized magnetization reads

$$\lim\frac{\langle M(n,m,h)\rangle}{N_m} = \left(b_2+a_2\frac{h}{\eta_2}\right)\frac{z-1}{z-2+\eta_2}. \tag{16.25}$$

If we take a different thermodynamic limit, with $n-m\to b$, where b is a constant thickness boundary, we obtain

$$\lim\frac{\langle M(n,m,h)\rangle}{N_m} = \left(b_2+a_2\frac{h}{\eta_2}\right)\frac{z-1}{z-2+\eta_2} - a_2(h_\infty-h_{n_c})\frac{(z-1)(z-2)(1-\eta_2)^{b-n_c}}{(z-2+\eta_2)(z-1-(1-\eta_2)^2)} \tag{16.26}$$

The absolute value of the corrective term decreases as the thickness of the boundary increases, since $|1-\eta_2|<1$.

Regime II: $n-m\le n_c\le n$, intermediate fields

We want to use again the relation (16.7) in the regime $n-m+1\le n_c\le n$. We shall use the relations (16.18) and (16.20). Moreover, we need approximants to $dh_i/d\lambda$ for $\lambda=0$. If $n-m\le i\le n_c$, we have

$$\frac{dh_i}{d\lambda}(\lambda=0) = \frac{1}{\eta_1}\left((1+\eta_1)^{i-n+m+1}-1\right), \tag{16.27}$$

and if $i\ge n_c$,

$$\frac{dh_i}{d\lambda}(\lambda=0) = \frac{1}{\eta_2}+a(1-\eta_2)^{i-n_c}, \tag{16.28}$$

where

$$a = \frac{1}{\eta_1}(1+\eta_1)^{n_c-n+m+1} - \frac{1}{\eta_1} - \frac{1}{\eta_2}. \tag{16.29}$$

We have used

$$h_i = h^* + \frac{h+\lambda}{\eta_2} + (1-\eta_2)^{i-n_c}\left(h_{n_c}(\lambda) - h^* - \frac{h+\lambda}{\eta_2}\right), \tag{16.30}$$

with

$$h_{n_c}(\lambda) = h_{n_c}(0) + \frac{\lambda}{\eta_1}\left((1+\eta_1)^{n_c-n+m+1} - 1\right). \tag{16.31}$$

We inject these approximations into (16.7) and calculate all the geometric series. The thermodynamic limit can only be taken with $n - m \to b$, where b is some constant. We find that the dominant behaviour at small magnetic field h depends on the temperature. Let T' be the temperature such as $\tanh\beta' = 1/\sqrt{z-1}$. Then if $T' < T < T_c$, the dominant term of the normalized magnetization is linear in h, with corrections in h^α, where $\alpha = \ln(z-1)/\ln(1+\eta_1) - 1$, whereas if $T < T'$, the leading term is of order h^α. We do not write explicitely the corresponding expressions since they are tedious and would not bring anything more to the present discussion.

Regime III: $n_c \geq n$ and finite size effects

In this regime, the average magnetization is approximated by replacing (16.18) and (16.27) into (16.7), which yields

$$\langle M(n,m,h)\rangle = \sum_{i=n-m}^{n-1} (z-1)^{n-i} a_1 h \frac{(1+\eta_1)^{i+1}-1}{\eta_1}\frac{(1+\eta_1)^{i-n+m+1}-1}{\eta_1}. \tag{16.32}$$

After carrying out the geometrical series, we obtain

$$\begin{aligned}\frac{\langle M(n,m,h)\rangle}{N(m)} &= \frac{a_1 h}{\eta_1^2}\frac{z-2}{1-(z-1)^{-m-1}}\left[\frac{1-(z-1)^{-m}}{z-2} - \frac{(1+\eta_1)((1+\eta_1)^b+1)}{z-2-\eta_1}\left(1-\left(\frac{1+\eta_1}{z-1}\right)^m\right)\right.\\ &\left. + \frac{(1+\eta_1)^{b+2}}{z-1-(1+\eta_1)^2}\left(1-\left(\frac{(1+\eta_1)^2}{z-1}\right)^m\right)\right]\end{aligned} \tag{16.33}$$

We can now discuss the cross-over field and temperature. We define the cross-over field h_{co} such as $h_{n-1} = h_c$, that is

$$h_{co} = h^* \frac{\eta_1\eta_2}{(\eta_1+\eta_2)((1+\eta_1)^n - 1)}, \tag{16.34}$$

which is exponentially small in n. If we take the limit of large n and m, but finite $n-m$, we can write

$$\begin{aligned}\frac{\langle M(n,m,h_{co})\rangle}{N(m)} &= h^* \frac{a_1\eta_2}{\eta_1(\eta_1+\eta_2)}(z-2)(1+\eta_1)^{-n}\left[\frac{1}{z-2} - \frac{(1+\eta_1)((1+\eta_1)^b+1)}{z-2-\eta_1}\left(1-\left(\frac{1+\eta_1}{z-1}\right)^m\right)\right.\\ &\left. + \frac{(1+\eta_1)^{b+2}}{z-1-(1+\eta_1)^2}\left(1-\left(\frac{(1+\eta_1)^2}{z-1}\right)^m\right)\right]\end{aligned} \tag{16.35}$$

In the limit $T \to 0$, $(1+\eta_1)/(z-1) = \tanh\beta \to 1$, so that the only term which has a chance not to be small is

$$\frac{(1+\eta_1)^{-n}(1+\eta_1)^{2m}}{(z-1)^m} = (1+\eta_1)^{-b}\left(\frac{1+\eta_1}{z-1}\right)^m. \tag{16.36}$$

Since

$$\ln\left(\frac{1+\eta_1}{z-1}\right)^m \simeq -2me^{-2\beta} \tag{16.37}$$

at small temperature, we obtain the cross-over temperature scale as $T_g = 2/\ln m$. In the next sections, we shall re-derive this cross-over temperature with other methods, and give its significance.

16.3 Magnetization distribution and finite size effects

The aim of this section is to analyze the distribution of magnetization. The analysis of the distribution of magnetization in zero field, shall show that finite size effects are crucial, and we shall recover the temperature T_g. We shall also compute the magnetization distribution in the presence of a magnetic field.

16.3.1 Magnetization distribution in zero field

We begin with the case of a zero magnetic field. Given $z-1$ n-half-space trees with coordinance z, it is straighforward to get a $(n+1)$-half space tree with coordinanace z. One just has to add a commun ancestor and to link this ancestor to the $z-1$ ancestors of each n-tree (see figure 16.2). In order to get a full tree, one has to glue z half-space-trees instead of $z-1$ at the last step. Let $P_n^\sigma(M)$ be the conditional probability for a n-half-space-tree to have a magnetization M, given the spin of the ancestor is σ. Of course,

$$\sum_M P_n^\sigma(M) = 1 \tag{16.38}$$

The recursion relation for $P_n^\sigma(M)$ is

$$\begin{aligned} P_n^\sigma(M) &= \sum_{M_1,\ldots,M_{z-1}} \delta(M-(M_1+\ldots+M_{z-1}+\sigma)) \\ &\sum_{k=0}^{z-1}\binom{z-1}{k}x^k(1-x)^{z-k-1}\prod_{i=1}^{k}P_{n-1}^{-\sigma}(M_i)\prod_{i=k+1}^{z-1}P_{n-1}^{\sigma}(M_i), \end{aligned} \tag{16.39}$$

where x is the probability for breaking one bond:

$$x = \frac{e^{-\beta J}}{e^{\beta J}+e^{-\beta J}}. \tag{16.40}$$

The initialization of the recursion is given by $P_1^\sigma(\sigma') = \delta_{\sigma,\sigma'}$. This recursion can be performed numerically, at least for a small number of generations. The result is plotted on figure 16.4 for $z = 3$ and 10 generations at various temperatures. For a finite size tree and at low temperature, the magnetization distribution presents a non gaussian structure, reminiscent of the magnetization distribution of the central spin in Bethe lattice spin glasses [9] [13]. Notice that the temperature which controls the departure from the Gaussian distribution is lower than the bulk transition temperature.

In order to determine precisely this temperature, we compute the recursion relations for the average magnetization. Using the recursion relations (16.39), we find

$$\langle M\rangle_{n+1}^+ = 1+\sum_{k=0}^{z-1}\binom{z-1}{k}x^k(1-x)^{z-k-1}\left(k\langle N\rangle_n^- + (z-k-1)\langle M\rangle_n^+\right) \tag{16.41}$$

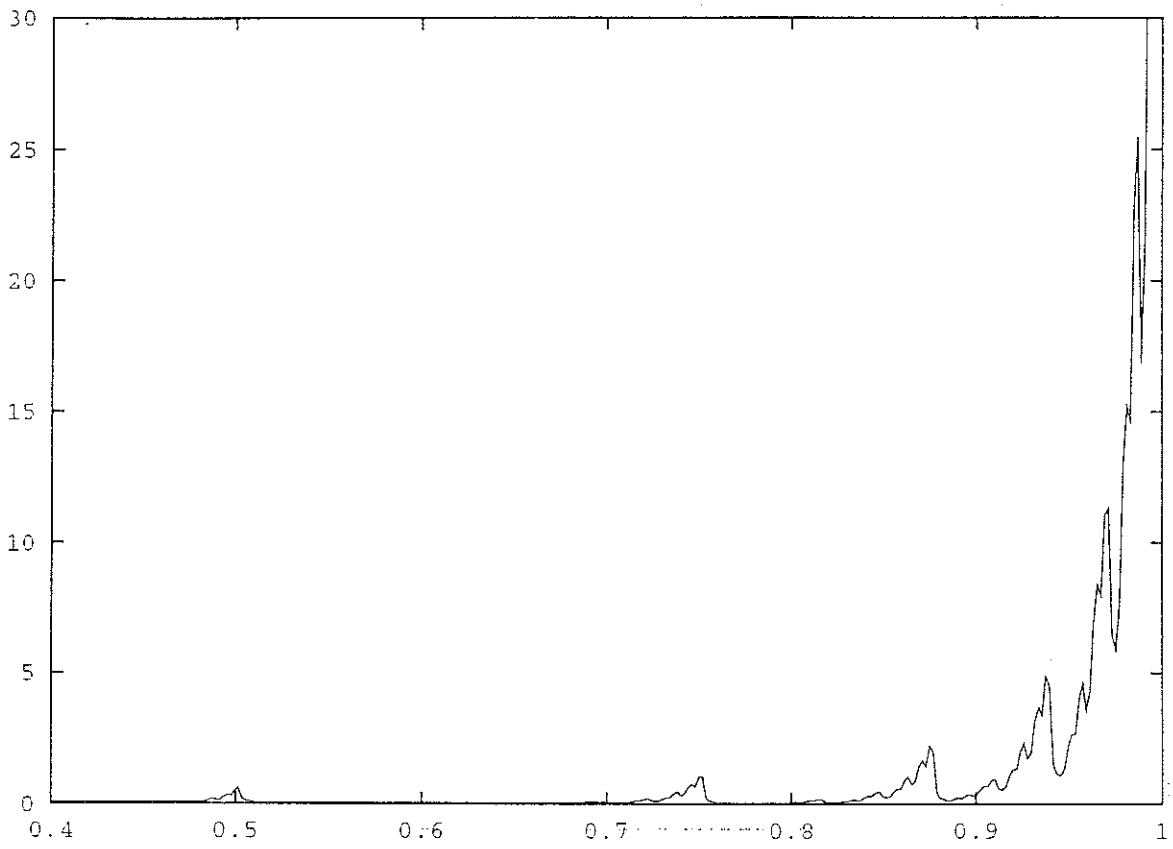

Figure 16.4:
Density probability of the magnetization on a half-space tree. The number of generation is 10, the coordinance is equal to 3. The ancestor spin is fixed to 1. The inverse temperature is $\beta = 3$.

It is clear that, since $P_1^+(\sigma) = P_1^-(-\sigma)$, then, for all n, $P_n^+(M) = P_n^-(-M)$, so that $\langle M\rangle_n^+ + \langle M\rangle_n^- = 0$. Putting this equation into (16.41) and using the well-known relations for the sum of binomial series, we obtain $\langle M\rangle_{n+1}^+ = p\langle M\rangle_n^+ + 1$ and $\langle M\rangle_0^+ = 1$ where p is defined as $p = (z-1)\tanh\beta J$. This recursion can be easily solved, and one gets

$$\frac{\langle M\rangle_n^+}{N_n} = \frac{z-2}{p-1}\frac{p^{n+1}-1}{(z-1)^{n+1}-1}, \tag{16.42}$$

where N_n is the number of sites of a n-half-space-tree, given by (16.23). The structure of the distribution of magnetization is non gaussian provided $2xn \ll 1$, that is

$$T < T_g = \frac{J}{\ln n} = \frac{J}{\ln(\ln N_n/\ln(z-1))}. \tag{16.43}$$

It is clear that the temperature T_g (which will reveal to be the glass temperature) decreases very slowly with the system size. For instance, at the *thermodynamic* limit, if $N \simeq 6.02.10^{23}$, and $z = 3$, $T_g = J/4.4$. We conclude from this analysis that the finite size effects persist in the thermodynamic limit. For T_g to be drastically reduced, one should consider systems of size $\exp 6.02.10^{23}$, that is to be at the *cosmological* limit (!) We also stress the fact that, since the appearance of glasssiness is a finite size effect, T_g is not a *transition* temperature as in the Sherrington-Kirkpatrick model for instance, but a *cross-over* temperature scale, even for macroscopic systems.

16.3.2 Structure of the magnetization distribution for $T < T_g$

We want to understand qualitatively the structure of the maxima of the magnetization probability distribution below T_g, that is we aim to localize the maxima and calculate their weight. To do so, we use the normalized continuous magnetization variable $m = M/N_n \in [-1,1]$, and use the normalized associated density $\rho_n(m) = N_n P_n^+(M)$. The recursion relations for $\rho_n(m)$ are straightforwardly derived from the ones for $P_n^+(M)$, equation (16.39). Since this relation is a convolution, we write the recursion in terms of the Fourier transform $\tilde\rho_n(k)$ of $\rho_n(m)$:

$$\tilde\rho_n(k) = \int_{-\infty}^{+\infty} e^{ikm}\rho_n(m)dm \tag{16.44}$$

We obtain the recursion of the $\tilde\rho$'s:

$$\tilde\rho_{n+1}(k) = \left(x\tilde\rho_n(-\frac{k}{z-1}) + (1-x)\tilde\rho(\frac{k}{z-1})\right)^{z-1} \tag{16.45}$$

$$\tilde\rho_0(k) = e^{ik} \tag{16.46}$$

We now specialize to the case $z = 3$, since the formula are simpler. It is easy to check by recurrence that

$$\tilde\rho_n(k) = (1-2x(2^n-1))e^{ik} + 2x\sum_{\alpha=0}^{n-1} 2^\alpha \exp\left(i(1-\frac{1}{2^\alpha})k\right) + O(x^2). \tag{16.47}$$

As we shall see later, this low temperature expansion is meaningful below T_g, even in the presence of a finite density of kinks. The expansion (16.47) tells us that $\rho_n(m)$ has peaks for

$m_\alpha = 1 - 1/2^\alpha$, where $\alpha \in \langle 0, ..., n-1 \rangle$. Moreover, we get that the weight of the peak $\alpha + 1$ is twice the weight of the peak α. An inspection of figure 16.4 shows that this predictions are correct, at least in the region where the overlap between the peaks is small.

These results can also be interpreted as follows. The expansion (16.47) at order x means that the magnetization density is calculated at the order of one kink. It is clear that a single kink at generation $n - \alpha$ leads to a magnetization $1 - 1/2^\alpha$ and that the number of choices to put a kink at generation $n - \alpha - 1$ is twice the number of choices to put a kink at generation $n - \alpha$, which is the content of equation (16.47). What is striking is that below T_g, this one kink picture is valid, even though we deal with a finite density of kinks x. This means that T_g is the temperature below which the kinks are rarely nested. In order to check this assertion, we calculate the criterium for the kinks to give rise to well-defined domains of flipped spins, which will answer the question of the validity of the expansion (16.47). The overlap between he domains induced by the kinks is small provided $xN_n\langle S\rangle_n < N_n$. In this expression, $\langle S\rangle_n$ is the average size of a domain of flipped spins induced by a single kink. The number of descendants of a kink at level $n - p$ for a n-half-space-tree is $S_{p,n} = 1 + 2 + ... + 2^{n-p} = 2^{n-p+1} - 1$. The average over p of $S_{p,n}$ is

$$\langle S_{p,n}\rangle_n = \frac{\sum_{p=1}^n 2^p S_{p,n}}{\sum_{p=1}^n 2^p} = n\frac{2^n}{2^n - 1} - 1 \simeq n - 1. \tag{16.48}$$

The non overlap condition reads $xn < 1$, that is $T < T_g$. We conclude that below T_g, the number of kinks is low enough for the system to develop well-defined domains of flipped spins. Below T_g, the excitations of the spin system are kinks, which are local in terms of bounds, but highly non-local in terms of spins.

16.3.3 Magnetization distribution in a magnetic field

The magnetization distribution in a magnetic field are computed using

$$P^\sigma_{n,h}(m) = \frac{P^\sigma_{n,0}(m)e^{\beta mh}}{\sum_{m'} P^\sigma_{n,0}(m')e^{\beta hm'}}. \tag{16.49}$$

The conditional magnetization distribution (the central spin being parallel to the field) is found to converge rapidly to a gaussian as the field increases. Since large domains of flipped spins do not survive in a magnetic field, the cross-over field is expected to decrease drastically with the system size. Indeed, we have shown previously that the cross-over field h_{co} of equation (16.34) decreases exponentially with the number of generations. The distribution of magnetizations is plotted on figure 16.5, the central spin being paralell to the field.

16.4 Barrier structure

We have shown that the excitations below T_g are broken bonds. In order to characterize the dynamics, we aim to calculate the barriers associated to these excitations. The energy barriers at zero temperature of a half-space-tree are defined as follows: one starts with a configuration where all the spins are up, and one considers single-spin-flip paths from the initial configuration to a configuration where all the spins are reversed. To such a path, we associate the maximal energy reached during the path, the energy of the initial state being zero. Then, the barrier

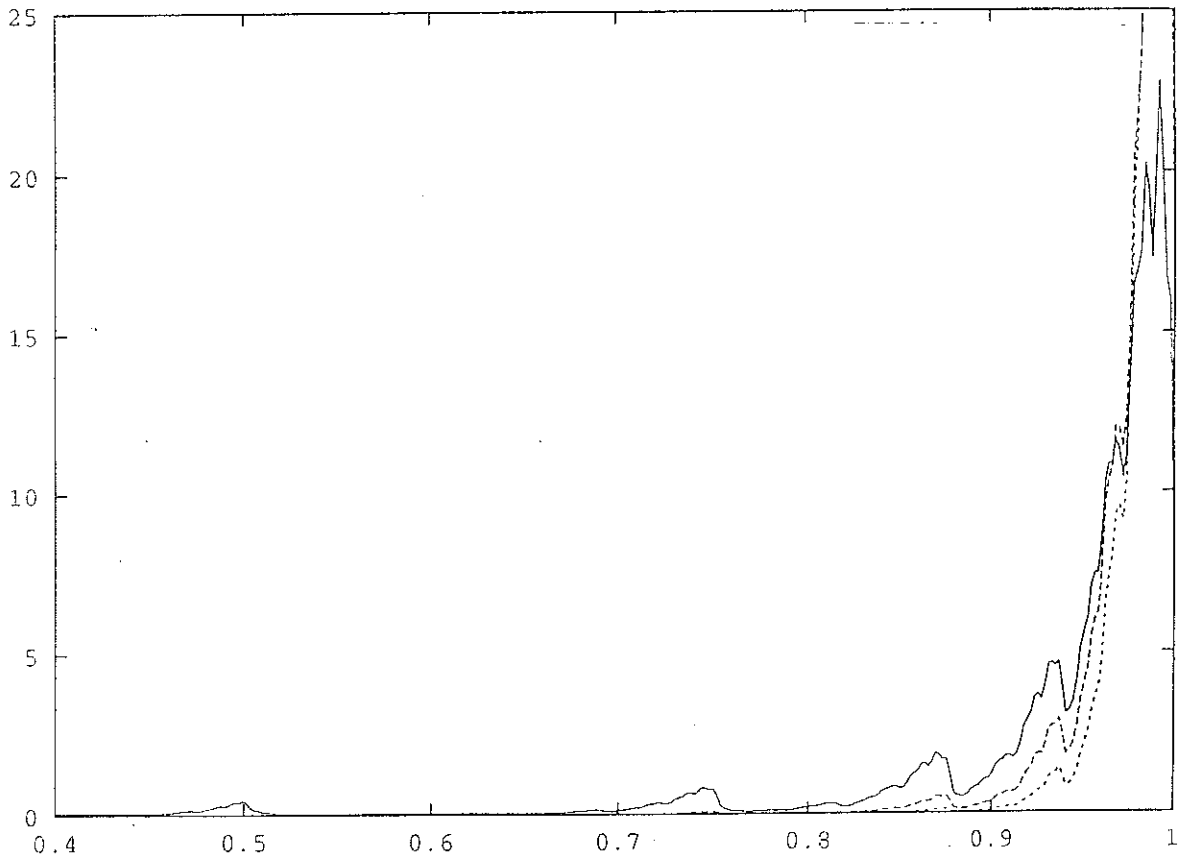

Figure 16.5:
Conditional magnetization distribution in the presence of a magnetic field, the field being parallel to the central spin. The magnetization distribution is plotted for a $z = 3$ tree, $n = 10$ generations, and for magnetic fields $H = 0, 0.001, 0.002$. The magnetization distribution evolves towards a gaussian shape as the magnetic field increases.

is defined as the minimum over all the paths of the maximum energy of one path. Typically, the Monte Carlo algorithm samples all the paths in an ergodic way, by contrast to the Swenson algorithm which does not generate paths with respect to the single spin flip. We leave for the appendix B the calculation of the barriers associated to the n-half-space-tree, and for appendix C the proof that the complexity of the algorithm to find the optimal path is polynomial. We use the asymptotic approximate expression for the zero temperature energy barrier of a α-half-space-tree:

$$E_\alpha^b = \frac{z-1}{2}(\alpha-1)J. \tag{16.50}$$

We aim to calculate the number of states with a given barrier at a given temperature below T_g, for a full n-tree. By convention, the leaves are at the first generation, and the center at the n-th generation.We note n^* the number of kinks at a given temperature: $n^* = Nx$. The barrier for a configuration of n^* kinks is assumed to be only a function of the generation α of the kink which is the closest to the origin. In order to calculate the number of states with an energy barrier E_α^b, we have to enumerate all the configurations with no kink between generation $\alpha+1$ and n, n_α kinks at generation α and $n^* - n_\alpha$ kinks between generations $\alpha-1$ and 1. Let's call $g(\alpha)$ the number of such configurations of kinks. We make the approximation that the energy barrier of all these configurations is E_α^b, that is its life-time is, according the the Arrhenius law

$$\tau_\alpha = \tau_0 \exp\left(\lambda\beta E_\alpha^b\right), \tag{16.51}$$

where λ is a constant. Such a configuration of kinks is pictured on figure 16.6. Clearly, we have

$$g(\alpha) = \sum_{n_\alpha=1}^{n^*} g_\alpha(n_\alpha), \tag{16.52}$$

with

$$g_\alpha(n_\alpha) = \binom{z(z-1)^{n-\alpha-1}}{n_\alpha}\binom{\frac{z}{z-2}\left((z-1)^{n-1}-(z-1)^{n-\alpha}\right)}{n^*-n_\alpha}. \tag{16.53}$$

We can calculate the sum and get

$$g(\alpha) = \binom{\frac{z}{z-2}\left((z-1)^{n-1}-(z-1)^{n-\alpha-1}\right)}{n^*} - \binom{\frac{z}{z-2}\left((z-1)^{n-1}-(z-1)^{n-\alpha}\right)}{n^*}, \tag{16.54}$$

and we get the probability $P(\alpha)$ for the system to be in a valley with a barrier E_α:

$$P(\alpha) = \binom{N}{Nx}^{-1}\left[\binom{N(1-(z-1)^{-\alpha})}{Nx} - \binom{N(1-(z-1)^{-\alpha+1})}{Nx}\right], \tag{16.55}$$

where we have normalized by the total number of accessible states at a given temperature on a $n-$tree. We have also approximated the number of sites as follows:

$$N = \frac{z(z-1)^{n-1}-2}{z-2} \simeq \frac{z(z-1)^{n-1}}{z-2}. \tag{16.56}$$

Assuming both that $x \ll 1$, and that $(z-1)^{-\alpha} \ll 1$, and using Stirling's formula, we get

$$P(\alpha) \simeq \exp\left(-\frac{Nx}{(z-1)^\alpha}\right) - \exp\left(-\frac{Nx}{(z-1)^{\alpha-1}}\right). \tag{16.57}$$

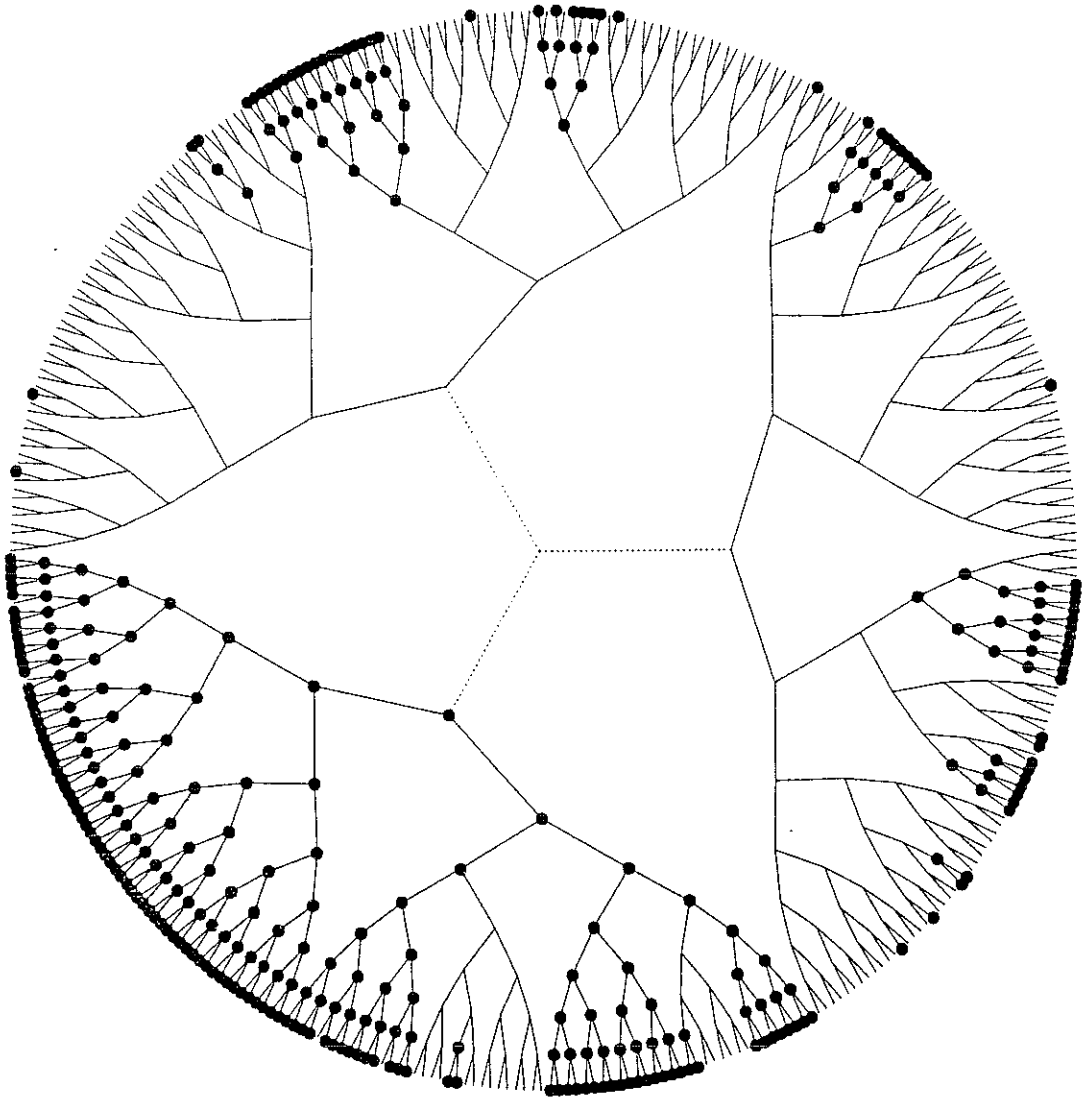

Figure 16.6:
A typical configuration of the tree with 8 generations and $\beta = 1.5$. The vertices with no dot represent up spins and the dots represent flipped spins. Each kink gives rise to a well-defined domain of flipped spins.

If $Nz/(z-1)^\alpha \ll 1$, we get

$$P(\alpha) \simeq Nx\frac{z-2}{(z-1)^\alpha} \tag{16.58}$$

As expected, $P(\alpha)$ decreases as a function of α, which means that the long lived states are less numerous than the short lived states.

16.5 Glauber dynamics

We now examine the Glauber dynamics of the spin system on the Cayley tree.

16.5.1 Glauber matrix

We begin with generalities about the Glauber dynamics. Let $p(\{\sigma\},t)$ be the probability for the system to be in the state $\{\sigma\}$ at time t. Following Glauber [22], we define $w_i(\{\sigma\})$ as the probability per unit time that the spin i flips from σ_i to $-\sigma_i$, while the others remain fixed. The master equation reads

$$\frac{d}{dt}p(\{\sigma\},t) = -\left(\sum_{i=1}^{N} w_i(\{\sigma\})\right)p(\{\sigma\},t) + \sum_{i=1}^{N} w_i(\{\sigma_1,...,-\sigma_i,...,\sigma_N\})p(\{\sigma_1,...,-\sigma_i,...,\sigma_N\},t). \tag{16.59}$$

Since we require the Boltzman distribution to be a fixed point, the coefficients $w_i(\{\sigma\})$ are of the form

$$w_i(\{\sigma\}) = \frac{1}{2}(1-\sigma_i \tanh(\beta J \sum_{j\in V(i)} \sigma_j)), \tag{16.60}$$

where $V(i)$ is the set of neighbors of the site i. If one denotes by $\mathbf{p}(t)$ the 2^N vector of the $p(\{\sigma\},t)$, equation (16.59) can be written as

$$\frac{d}{dt}\mathbf{p}(t) = \mathbf{G}.\mathbf{p}(t), \tag{16.61}$$

where $\mathbf{G}$ is the Glauber matrix. We first show some properties of the matrix $\mathbf{G}$. Since the Boltzman distribution is a steady state of the dynamics, its corresponding eigenvalue is zero whatever the temperature. Eventhough it is non symetric, the matrix $\mathbf{G}$ is diagonalisable and its eigenvalues are real. The proof is as follows. The Glauber matrix verifies detailed balance, that is $\mathbf{G}_{\alpha,\beta}\mathbf{p}^{(0)}_\beta = \mathbf{G}_{\beta,\alpha}\mathbf{p}^{(0)}_\alpha$, where $\mathbf{p}^{(0)}$ is the Boltzman distribution. As a consequence,

$$\left(\mathbf{p}^{(0)}_\alpha\right)^{1/2}\mathbf{G}_{\alpha\beta}\left(\mathbf{p}^{(0)}_\beta\right)^{1/2} = \left(\mathbf{p}^{(0)}_\beta\right)^{1/2}\mathbf{G}_{\beta\alpha}\left(\mathbf{p}^{(0)}_\alpha\right)^{1/2}. \tag{16.62}$$

We call $\mathbf{M}$ the matrix defined by

$$\mathbf{M}_{\alpha\beta} = \left(\mathbf{p}^{(0)}_\alpha\right)^{1/2}\mathbf{G}_{\alpha\beta}\left(\mathbf{p}^{(0)}_\beta\right)^{1/2}. \tag{16.63}$$

Then, $\mathbf{M}$ is symetric. Let $\mathbf{p}$ be an right eigenvector of the Glauber matrix. Then

$$\sum_\beta \mathbf{G}_{\alpha\beta}\mathbf{p}_\beta = \lambda \mathbf{p}_\beta \tag{16.64}$$

is equivalent to

$$\sum_{\beta} \mathbf{M}_{\alpha\beta} \left(\mathbf{p}_{\beta}^{(0)}\right)^{-1/2} \mathbf{p}_{\beta} = \lambda \left(\mathbf{p}_{\alpha}^{(0)}\right)^{-1/2} \mathbf{p}_{\alpha}, \tag{16.65}$$

so that $\left(\mathbf{p}_{\alpha}^{(0)}\right)^{-1/2} \mathbf{p}_{\alpha}$ is an eigenvector of $\mathbf{M}$. We conclude that $\mathbf{G}$ is diagonalizable, and that all its eigenvalues are real.

The spectrum in the infinite temperature limit can be understood as follows. If we call

$$|\psi\rangle = \sum_{\{\sigma\}} f((\{\sigma\})|\sigma_1\rangle \otimes ... \otimes |\sigma_N\rangle, \tag{16.66}$$

then the dynamics reads

$$\frac{d}{dt}|\psi\rangle = -\frac{N}{2}|\psi\rangle + \frac{1}{2}\sum_{i=1}^{N} \sigma_i^x |\psi\rangle, \tag{16.67}$$

so that the eigenvalues of the Glauber matrix at infinite temperature are of the form

$$\lambda = -\frac{N}{2} + \frac{1}{2}\sum_{i=1}^{N} \mu_i, \tag{16.68}$$

where $\mu_i = \pm 1$. The spectrum in the inifinite temperature limit is thus made of levels at integer values between $-N$ and 0, with a degeneracy given by the binomial coefficients.

Another property of $\mathbf{G}$ id that, for bipartite lattices, such as the square lattice of the Caley tree, the spectrum of $\mathbf{G}$ is symetric: if λ belongs to the spectrum, then $-N-\lambda$ is an eigenvalue too. The proof is as follows. Let $\mathbf{X}\{\sigma\}$ be an eigenvector of $\mathbf{M}$, with an eigenvalue λ:

$$\lambda \mathbf{X}\{\sigma\} = -\sum_{i=1}^{N} \frac{1}{2}(1 - \sigma_i \tanh(\beta J h_i)\mathbf{X}\{\sigma\} + \sum_{i=1}^{N} \frac{1}{2\cosh \beta J h_i} \mathbf{X}\{\sigma_1, ..., -\sigma_i, ..., \sigma_N\}, \tag{16.69}$$

where h_i is defined by

$$h_i = \sum_{j \in V(i)} \sigma_j. \tag{16.70}$$

Let $\mathbf{Y}\{\sigma\}$ be defined as

$$\mathbf{Y}\{\sigma\} = (-1)^{\nu\{\sigma\}} \mathbf{X}\{\tilde{\sigma}\}, \tag{16.71}$$

where $\nu\{\sigma\}$ is the number of up spins in the configuration $\{\sigma\}$. $\{\tilde{\sigma}\}$ is deduced from $\{\sigma\}$ by flipping the spins of one of the two sublattices. Then,

$$\begin{aligned}
(\mathbf{MY})\{\sigma\} &= -\sum_{i=1}^{N} \frac{1}{2}(1 - \sigma_i \tanh(\beta H h_i))(-1)^{\nu\{\sigma\}} \mathbf{X}\{\tilde{\sigma}\} + \sum_{i=1}^{N} \frac{(-1)^{\nu\{\sigma_1,...,-\sigma_i,...,\sigma_N\}}}{2\cosh(\beta J h_i)} \mathbf{X}\{\tilde{\sigma}_1, ..., -\tilde{\sigma}_i, ...; \\
&= (-1)^{\nu\{\sigma\}} \left[-\sum_{i=1}^{N} \frac{1}{2}(1 + \tilde{\sigma}_i \tanh(\beta J h_i)) \mathbf{X}\{\tilde{\sigma}\} - \sum_{i=1}^{N} \frac{1}{2\cosh(\beta J h_i)} \mathbf{X}\{\tilde{\sigma}_1, ..., -\tilde{\sigma}_i, ..., \tilde{\sigma}_N\} \right] \\
&= -(N+\lambda)(-1)^{\nu\{\sigma\}} \mathbf{X}\{\tilde{\sigma}\} = -(N+\lambda)\mathbf{Y}\{\sigma\}.
\end{aligned} \tag{1}$$

Given an eigenvector $\mathbf{X}$ for the eigenvalue λ, we have buided an eigenvector $\mathbf{Y}$ for the eigenvalue $-N-\lambda$.

The difference between (16.61) and the Schrödinger equation is that quantum mechanics preserves the scalar product, leading to hermitian Hamiltonians. More over, the space of physical states is a Hilbert space, and each state of the Hilbert state is physical. In the case of the Glauber matrix, no vectorial space is present, in the sense that the sum of two probability distributions is not a probability distribution. However, some quantities are conserved by the dynamics. It is easy to show that the eigenvectors of $\mathbf{G}$ for the non zero eigenvalues have the property that

$$\sum_{\{\sigma\}} \mathbf{p}\{\sigma\} = 0. \tag{16.74}$$

This is a simple consequence of the fact that the Glauber matrix preserves the quantity

$$\sum_{\{\sigma\}} \mathbf{p}\{\sigma\}. \tag{16.75}$$

16.5.2 Spectrum of the Glauber matrix

In this section, we examine the spectrum of the Glauber dynamics as a function of temperature. We make numerical diagonalizations of small clusters, and conjecture the behavior for larger systems, in terms of statistics of eigenvalues. Since this aspect of the Glauber dynamics has not been much studied, we first analyse other models than the tree. We now examine the relaxation spectrum of different models as a function of temperature, and try to conjecture the behavior of the spectrum in the thermodynamic limit. We examine successively the case of the one dimensional Ising model, the bidimensional Ising model, and finally the case of the tree.

Let's begin with the Ising chain. We computed the spectrum as a function of temperature for a 6-sites open chain. The result is pictured on figure 16.7. We also treated the case of a 10 sites ring. Of course, we did not follow the 1024 levels as a function of temperature, but computed the eigenvalues for a given temperature. The spectrum is plotted on figure 16.8. From these results, we conjecture the following behavior for large systems. The spectrum is *completly integrable* in the sense that no level repulsion occurs in the evolution of the eigenvalues as a function of the temperature. It is clear from figure 16.7 that the evolution of $1/\tau_i$ is monotonous as a function of β and that no repulsion is seen. However, the distribution of eigenvalues is non uniform, since a curvature can be seen on figure 16.8. It is not surprising that the spectrum reveals an underlying integrable dynamics since the dynamics was indeed integrated by Glauber in [22]. An other point to be mentionned is the existence of a gap at non zero temperature, which goes to zero in the zero temperature limit. At zero temperature, the zero eigenvalue is doubly degenerate, corresponding to the existence of a symmetry-breaking phase at zero temperature.

As far as the two dimensional Ising model is concerned, we studied small clusters of size 3x3. The spectrum in the low temperature phase is plotted on figure 16.9. The obvious difference with the one dimensional chain is the presence of clusters of relaxation times in the low temperature spectrum. The evolution of the eigenvalues as a function of the inverse temperature is plotted for a small 3x2 cluster on figure 16.10. Level repulsion is visible in the vicinity of the transition temperature. For an infinite size system, one expects the presence of a gap between 0 and the first negative eigenvalue in the spectrum above the transition temperature, which vanishes at the transition temperature and leads to a doubly degenerate zero eigenvalue in the interval $[0, Tc]$, corresponding to the existence of a symmetry-breaking stable phase. If one thinks of the spectrum as a function of β, one expects the spectrum to present chaos in the vicinity

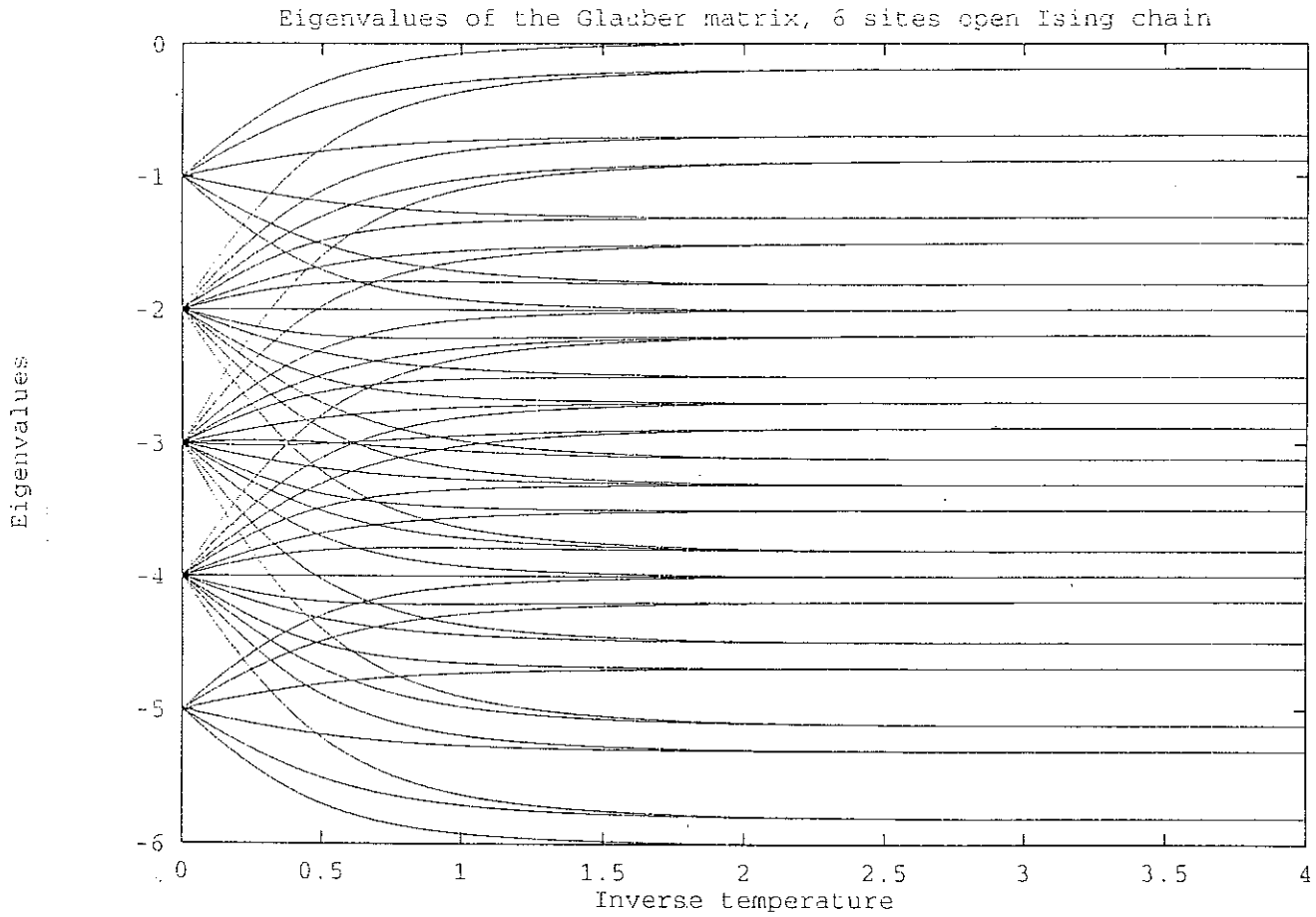

Figure 16.7:
Eigenvalues of the Glauber matrix as a function of the inverse temperature for an open Ising chain. The number of sites is 6, leading to 64 states. The evolution of the energy levels as a function of β is monotonous, and the eigenvalues are free to cross each other.

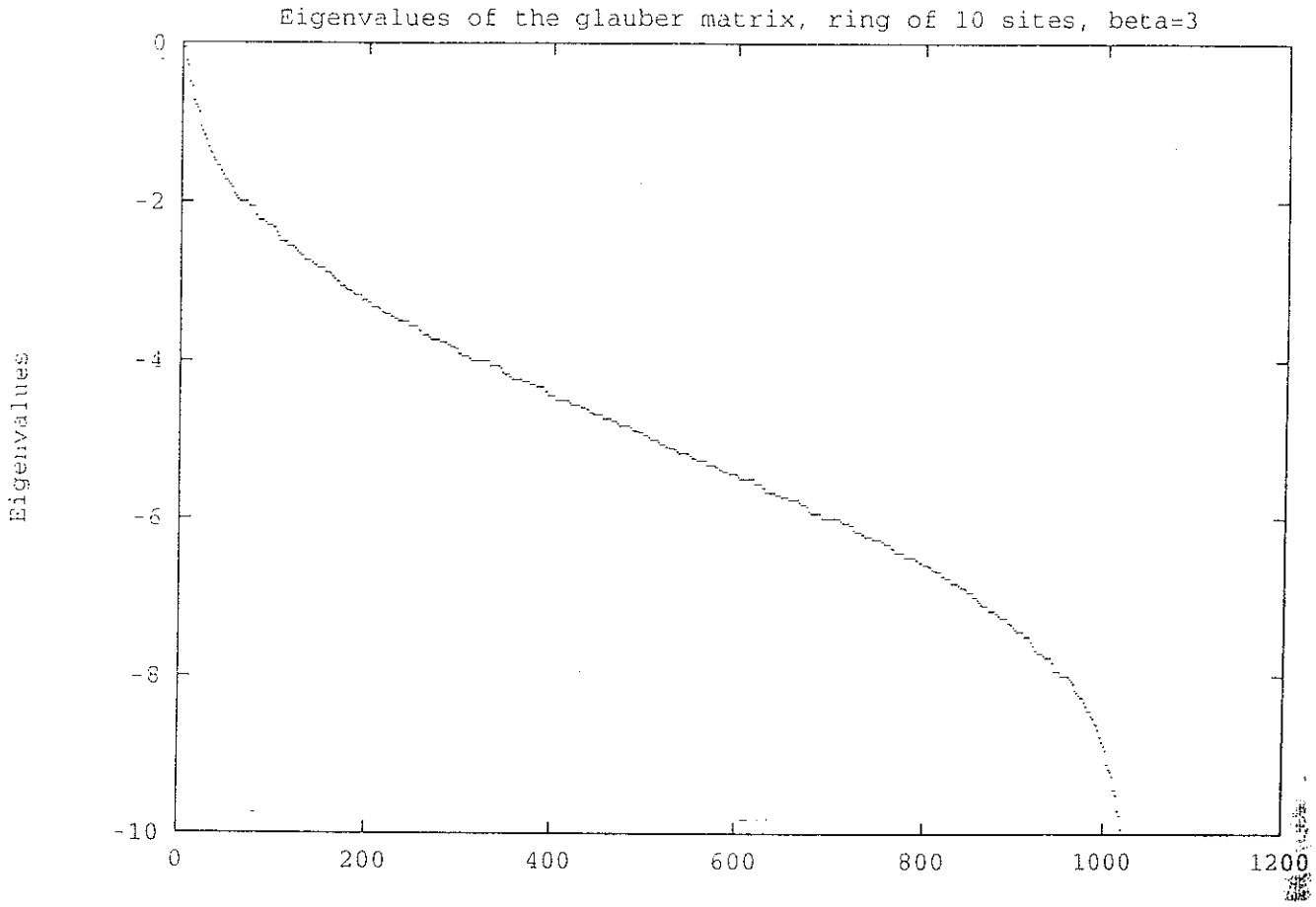

Figure 16.8:
Spectrum of the Glauber matrix at a given temperature for a ring of 10 sites. The inverse temperature is $\beta = 3$. No gap is present.

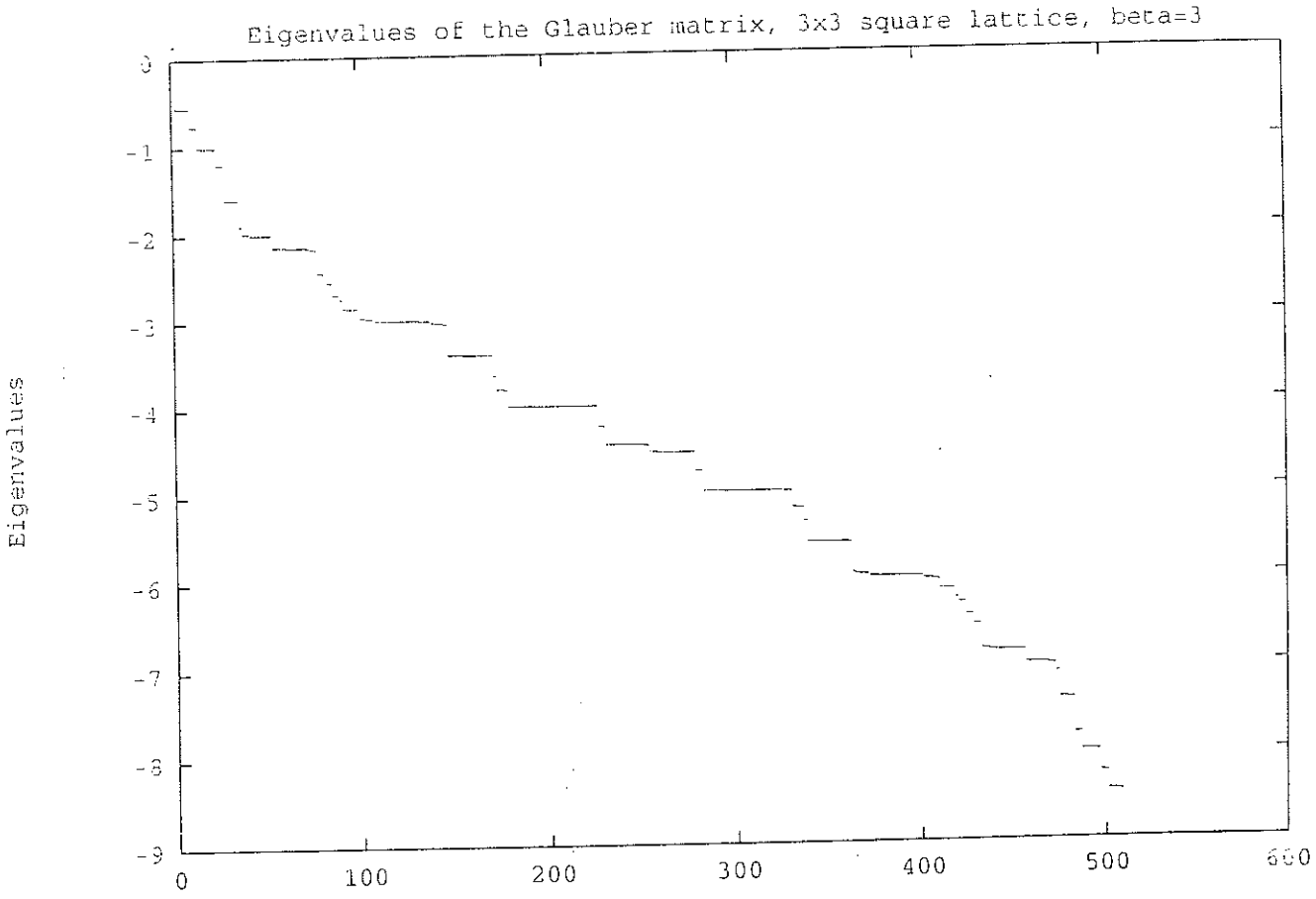

Figure 16.9:
Spectrum of the Glauber matrix at a given temperature for a 3x3 Ising model with open boundary conditions. The inverse temperature is $\beta = 3$. Some degeneracies appear in the spectrum, and the spectrum is symmetric with respect to the $\lambda = -N/2$ line.

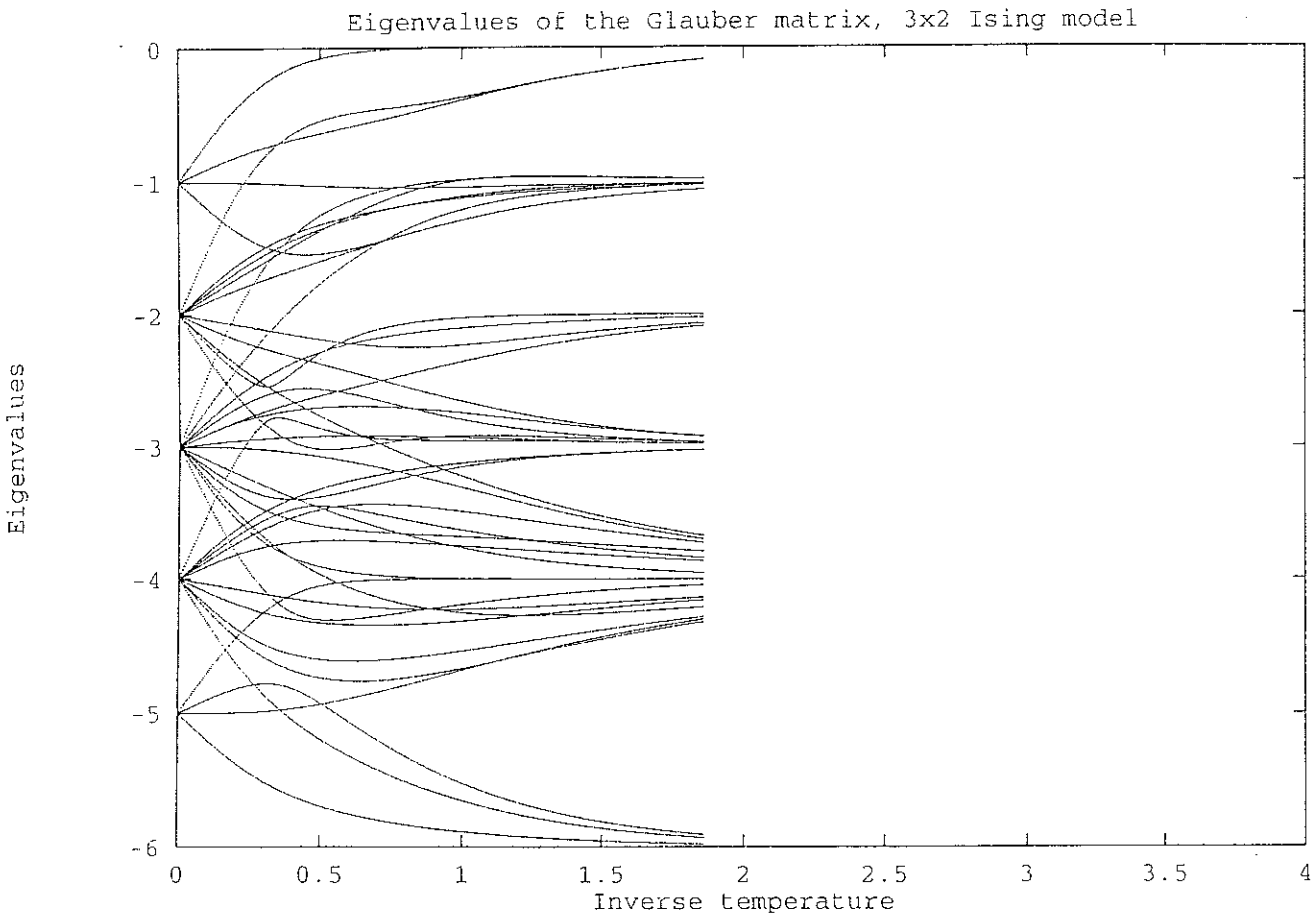

Figure 16.10:
Eigenvalues of the Glauber matrix as a function of the inverse temperature for a 3x2 Ising cluster. The number of sites is 6, leading to 64 states. The evolution of the eigenvalues as a function of β is non monotonous, and avoided crossings are visible.

of the transition temperature, leading to a rearrangement of the inverse relaxation times at low temperature and the presence of clusters of relaxation times in the zero temperature limit. However, it is not clear whether the level spacing statistics should be G.O.E. in an appropriate sector, but one could be left with a mixture of G.O.E. and Poisson statistics. The complete understanding of these level spacing statistics would involve the search of the symetry sectors using group theory, which shall be done in a near future.

In the case of the Cayley tree, we computed the spectrum of eigenvalues as a function of temperature in the case $z = 3$ for one generation, which corresponds to 4 sites. The spagheties are plotted on figure 16.11. Eventhough the size is very small, one can still see repulsion of eigenvalues in the vicinity of the bulk transition temperature. We computed the spectrum of the Glauber matrix at low temperatures with two generations, leading to 1024 eigenmodes. The eigenvalues are plotted on figure 16.12. The spectrum presents clusters, but, unlike the case of the bidimensional Ising model, these clusters are equidistant and happen at integer values. Moreover, the $\lambda = 0$ cluster contains 8 eigenvalues wheras it contains 2 eigenvalues for the bidimensional Ising model. For $N = 10$ and $\beta = 2$, as it is the case on figure 16.12, we find $n^* \simeq 0.18 < 1$. We conclude from relation (16.58) that $P(\alpha)$ is independent on the temperature. This is indeed the case since the $\lambda = 0$ cluster is separated by a gap from the $\lambda = -1$ cluster.

16.5.3 Realisation of the Glauber dynamics

In order to calculate explicitely the dynamics, we diagonalize the Glauber matrix. Let $\mathbf{u}_\alpha$ be the eigenvectors of $\mathbf{G}$: $\mathbf{G}.\mathbf{u}_\alpha = \lambda_\alpha \mathbf{u}_\alpha$, and let $\mathbf{P}$ be the passage matrix from the natural basis of pure states $\mathbf{e}_\alpha$ to the basis $\mathbf{u}_\alpha$:

$$\mathbf{u}_\alpha = \sum_\beta \mathbf{P}_{\alpha\beta}\mathbf{e}_\beta. \tag{16.76}$$

We look for the temporal evolution of the states $\mathbf{e}_\alpha$. At the inital time,

$$\mathbf{p}_\alpha(0) = \mathbf{e}_\alpha = \sum_\beta \mathbf{P}^{-1}_{\alpha\beta}\mathbf{u}_\beta. \tag{16.77}$$

Then, at time $t > 0$, the state is a mixture of pure states and is given by

$$\mathbf{p}_\alpha(t) = \sum_\beta \mathbf{P}^{-1}_{\alpha\beta} e^{\lambda_\beta t} \sum_\gamma \mathbf{P}_{\beta\gamma}\mathbf{e}_\gamma. \tag{16.78}$$

We can easily compute the magnetization of $\mathbf{p}_\alpha(t)$. We applied this procedure to the case of a tree with one generation. The evolution of the magnetization of the 16 pure states is plotted on figure 16.13 at low temperature. Of course, on very long time scales, the magnetization of all the states relaxes to zero, due to the fact that the eigenvalues associated to the symmetry breaking state are not strictly zero. The evolution of the pure states indicate the existence of metastable states, which are the precursors of the metastable states present for larger values of the number of generations.

16.5.4 Factorisation approximation

We recover the bulk critical temperature by considering the asymptotics of a simplified Glauber dynamics. Glauber shows in [22] that one can replace the 2^N variables of the linear dynamics by a hierarchy of N, non linear, coupled equations for the correlations functions. This procedure

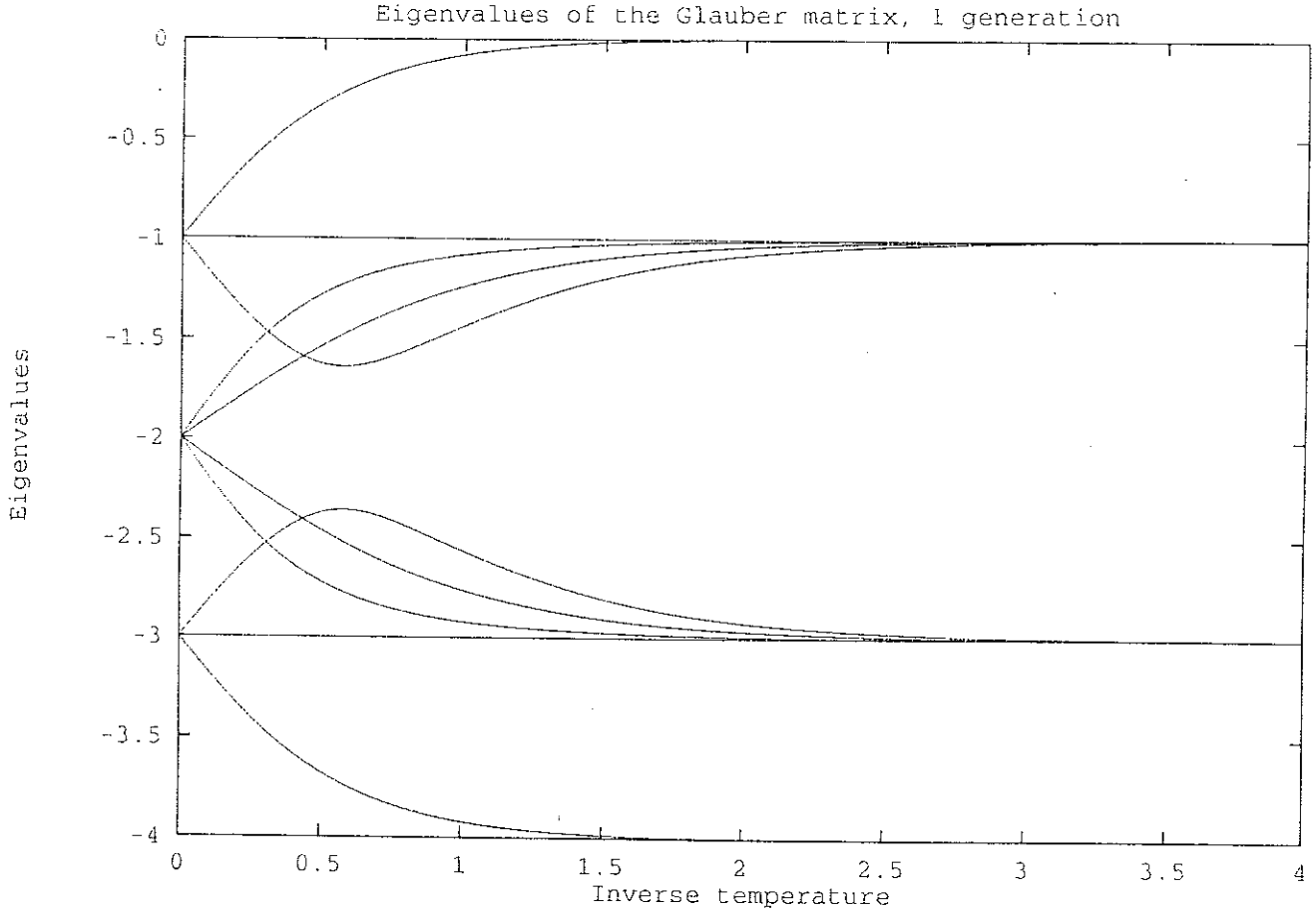

Figure 16.11:
Eigenvalues of the Glauber matrix as a function of the inverse temperature for a one generation, $z = 3$ Cayley tree. The number of sites is 4, leading to 16 states. The evolution of the energy levels as a function of β is non monotonous for certain levels, which is the signature of level repulsion.

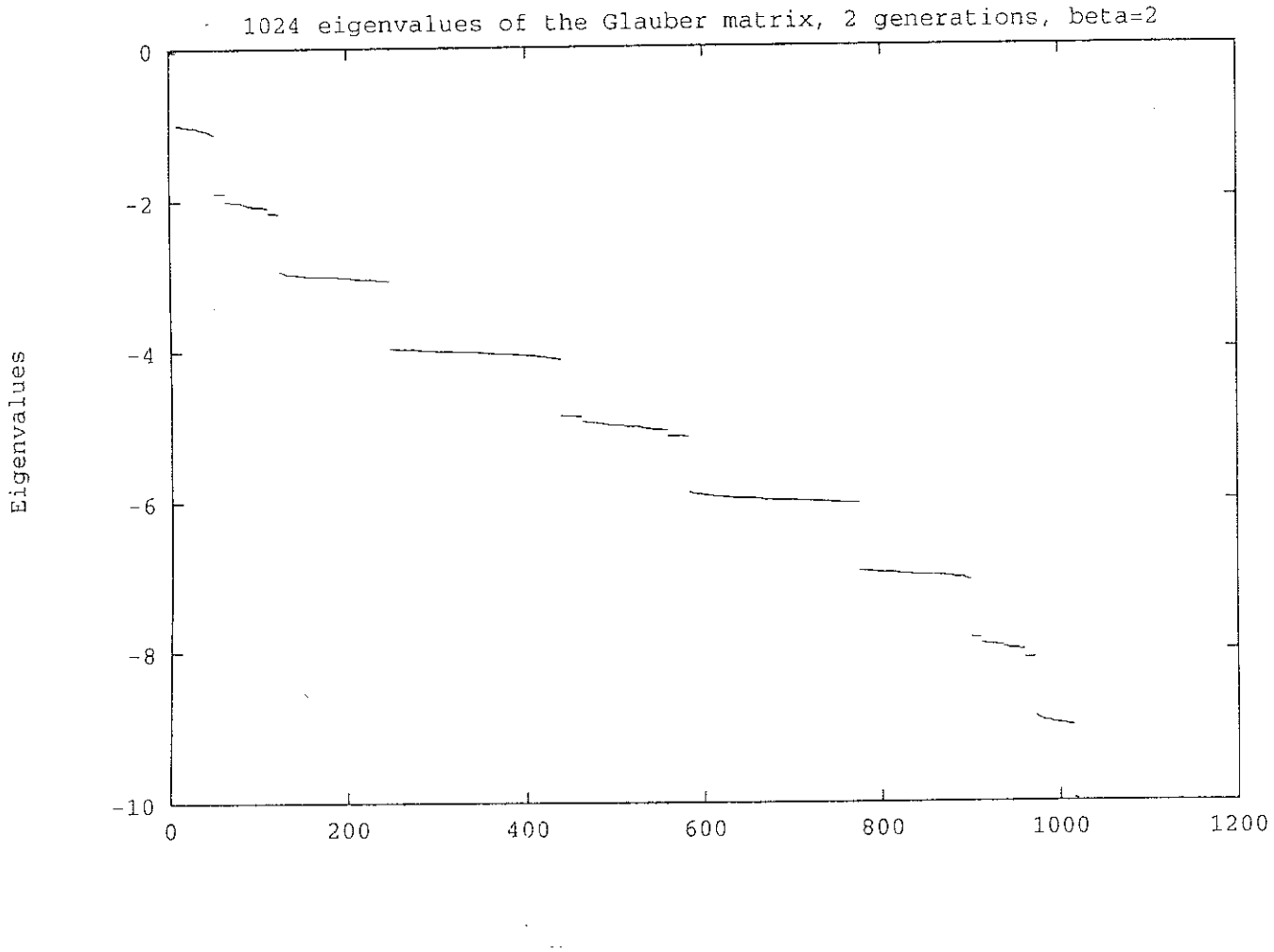

Figure 16.12:
Spectrum of the Glauber matrix at a given temperature for $z = 3$ Cayley tree with 2 generations. The inverse temperature is $\beta = 2$. The spectrum is symmetric with respect to the $\lambda = -N/2$ line. The clusters collapse at integer values.

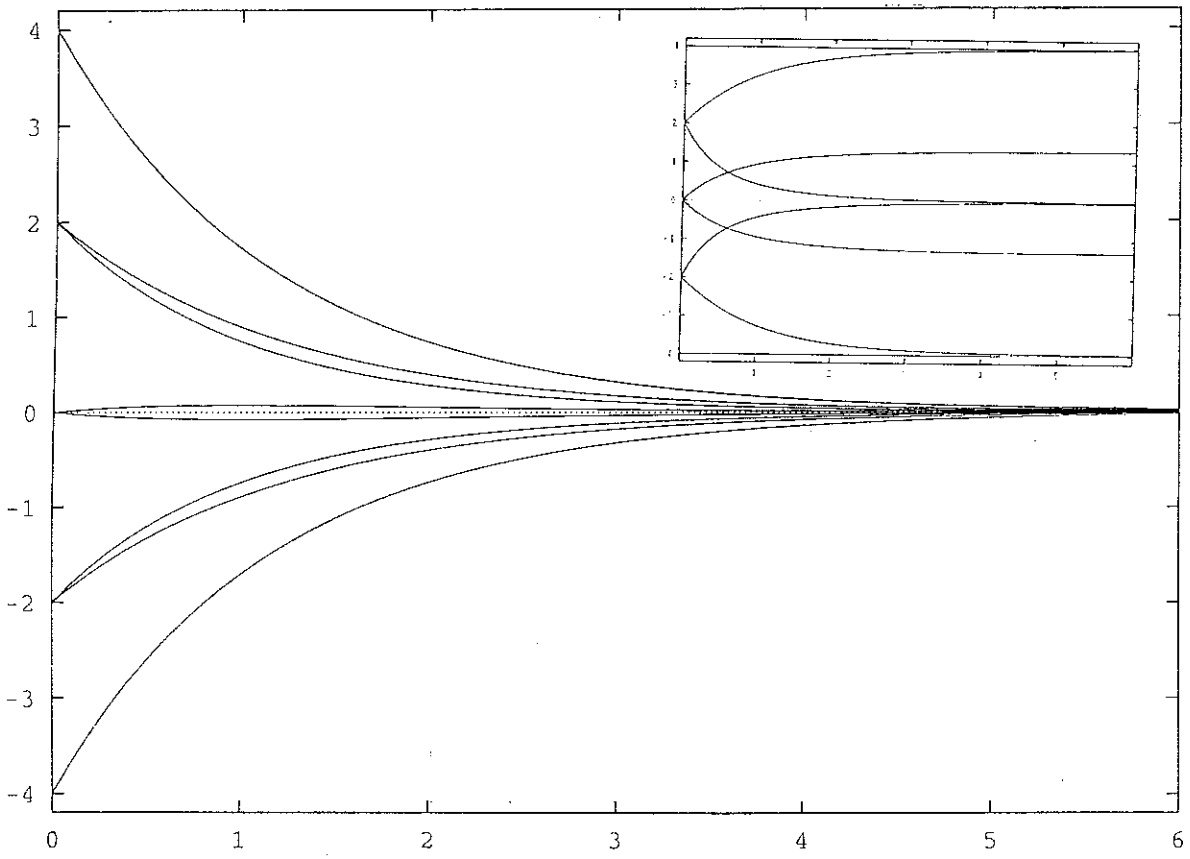

Figure 16.13:
Evolution of the magnetization of the 16 pure states of the tree with one generation. The inverse temperature is $\beta = 3$. Metastable states appear to be present even for such a small size. The insert represents the same curve at short time scales, which shows the transient regime from the natural basis of pure states to the metastable states.

is very similar to the transformation of the Liouville equation into the B.B.G.K.Y. hierarchy in the kinetic theory. The first equation of the hierarchy reads

$$\frac{d}{dt}q_i(t) = -q_i(t) + \langle \tanh(\beta J \sum_{j\in V(i)} \sigma_j)\rangle. \tag{16.79}$$

In this expression, $q = \langle\sigma\rangle$ and $V(i)$ is the set of neighbors of site i. In the case of a one dimensional chain, one can use the fact that

$$\langle \tanh \beta J(\sigma_{i-1} + \sigma_{i+1})\rangle = \frac{1}{2}\tanh(\beta J)(q_{i-1} + q_{i+1}), \tag{16.80}$$

and one gets a close equation for the 1-point correlation functions. It is also clear that the whole hierarchy decouples, and that one can use this decoupling to integrate the dynamics. In the case of a $z = 3$ tree, one has to take into account the fact that the sites inside the tree have three neighbours, whereas the leaves have one neighbour. For this coordination,

$$\tanh \beta J(\sigma_1 + \sigma_2 + \sigma_3) = \alpha(\sigma_1 + \sigma_2 + \sigma_3) + \gamma(\sigma_1 + \sigma_2 + \sigma_3)^3, \tag{16.81}$$

where the coefficients α and γ are determined by

$$\alpha = \frac{1}{24}(27\tanh\beta J - \tanh 3\beta J) \tag{16.82}$$

$$\gamma = \frac{1}{24}(\tanh 3\beta J - 3\tanh\beta J). \tag{16.83}$$

We can thus obtain the first equation of the hierarchy in the case of the $z = 3$ tree. For the sites with three neighbours,

$$\frac{d}{dt}q_i = -q_i + (\alpha + 7\gamma)\sum_{j\in V(i)} q_j + 6\gamma\langle \prod_{j\in V(i)} \sigma_j\rangle \tag{16.84}$$

For the leaves of the tree

$$\frac{d}{dt}q_i = -q_i + q_j \tanh\beta J, \tag{16.85}$$

where j is the neighbour of i. The factorisation approximation consists in decoupling the third order correlations into

$$\langle \prod_{j\in V(i)} \sigma_j\rangle = \prod_{j\in V(i)} q_j. \tag{16.86}$$

This approximation leads to the bulk behaviour in the high temperature phase and in the vicinity of the transition. We start from a configuration of spins such as $q_i(0) = q_j(0)$ if the sites i and j belong to the same generation. Then, for $t > 0$, $q_i(t) = q_j(t)$ if we work with the factorized dynamics. The factorized dynamics depends only on n variables, one per generation, and reads:

$$\begin{aligned}
\frac{dq_n}{dt} &= -q_n + 3(\alpha + 7\gamma)q_{n-1} + 6\gamma q_{n-1}^3 \\
\frac{dq_i}{dt} &= -q_i + (\alpha + 7\gamma)(2q_{i-1} + q_{i+1}) + 6\gamma q_{i-1}^2 q_{i+1} \\
\frac{dq_1}{dt} &= -q_1 + q_2\tanh\beta J,
\end{aligned} \tag{16.87}$$

where i runs from 2 to $n-1$. The equilibrium properties are calculated from the asymptotic values of the dynamics. Notice that the factorized dynamics possesses a non trivial fixed point for a finite size system, whereas the complete dynamics possesses only the Boltzman distribution as a fixed point. The asymptotics of the factorized dynamics is found to reproduce quite well the bulk properties of the tree. On figure 16.14, $q_n(+\infty)$ is plotted as a function of the inverse temperature. This curve is in agreement with the fact that the central spin exhibits a mean field like transition at $\beta_c \simeq 0.54$. We also plotted the asymptotic magnetization of the m generations which are the closest to the central spin. It is clear that the predictions of the factorized dynamics are qualitatively wrong as soon as one goes out from the center. For instance, it is clear that the entire tree does not develop a transition at $\beta = \beta_c$. Notice that, in equations (16.87), the transition temperature is determined entirely by the stability of the 0 fixed point of the linear problem. Below T_c, the largest eigenvalue of the linear problem is positive, and negative above T_c. In the same way as in the Ginzburg-Landau theory, the non linear terms are responsible for the dynamical variables to be bounded above in the low temperature phase.

16.6 Monte Carlo dynamics

16.6.1 Relaxation of a single kink

Instead of treating the case of a finite density of kinks, we first consider the case of a single kink and look for the relaxation of this excitation at low temperatures. Let's call K the set of descendants of the kink. At time $t = 0$, the configuration of kinks is such as $\sigma_i = -1$ is $i \in K$ and $\sigma_i = 1$ if $i \notin K$. We follow the magnetization of the spins of K as a function of time, for various size of K. The result is plotted on figure 16.15. The rapid relaxation at small times is attribuated to the fact that the inital state is not thermalized. The thermalisation occurs at small time scales compared to the collective processes of crossing the barrier. We define the typical relaxation time τ as the time for which the magnetization cancels. We plotted on figure 16.16 $\ln \tau$ as a function of the number of generations of K. The points are approximately aligned, which shows that the Arrhenius law

$$\tau \sim \tau_0 \exp\left(\beta\lambda \frac{z-1}{2} n\right) \tag{16.88}$$

is well satisfied. The case $\lambda = 1$ corresponds to the relaxation of a n-half-space tree, the ancestor being free. However, in our case, the ancestor is not free since the domain K is connected to the remaining up spins. The barrier height is essentially the same as in the case $\lambda = 1$, but the number of paths to reverse the magnetization is changed.

16.6.2 Alternative susceptibility

One experimental procedure to test the presence of glassiness is to measure of the alternative nonlinear susceptibility. We proceed in this section as experimentalists do: the spin system is submitted to a small, uniform, alternative external field $H(t) = h \sin \omega t$, and we measure the magnetization response, expanded into its Fourier components

$$M(\omega, t) = \sum_{k \geq 0} \theta'_k \sin k\omega t + \theta''_k \cos k\omega t, \tag{16.89}$$

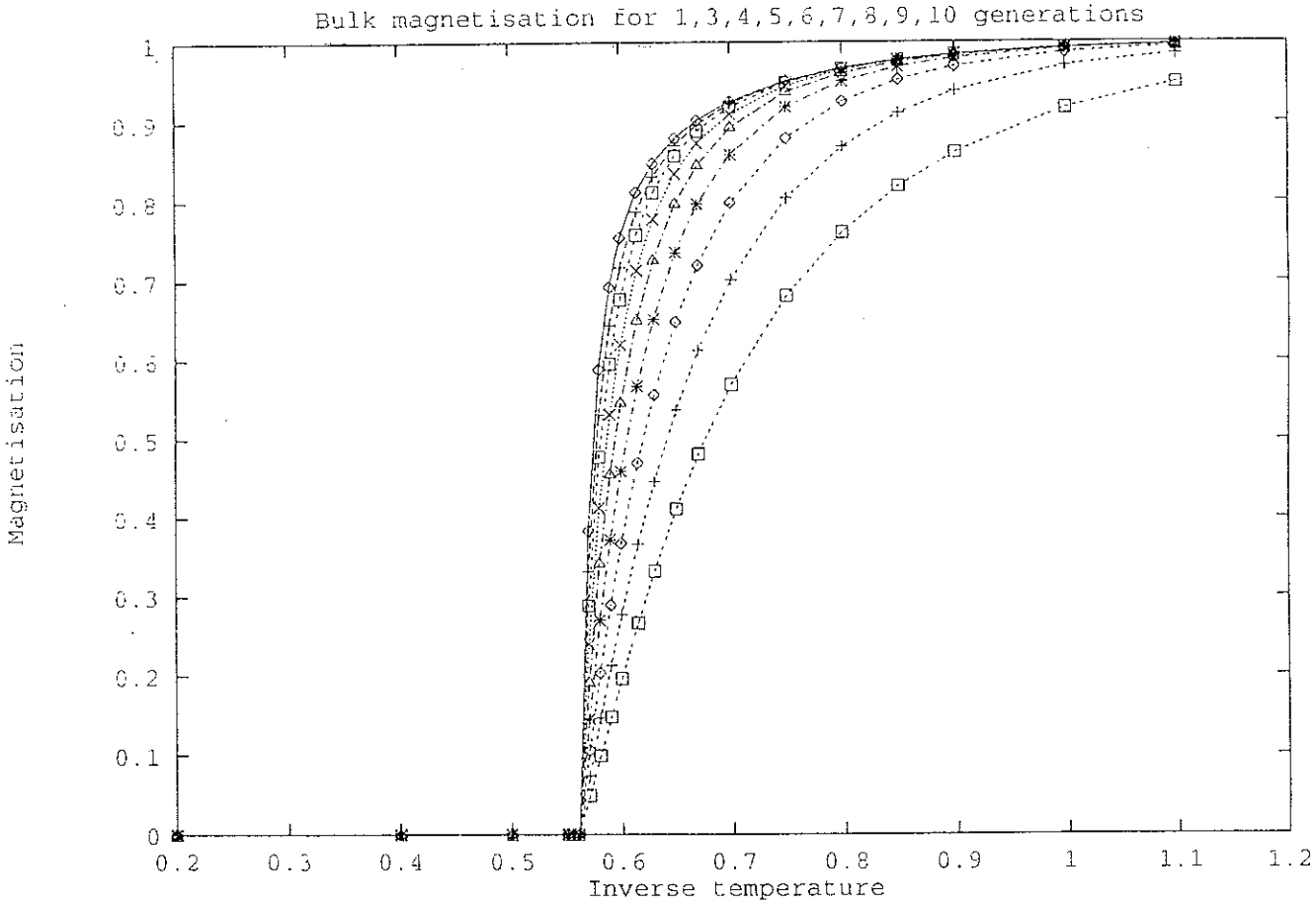

Figure 16.14:
Expectation value of the central spin in the simplified dynamics, as a function of the inverse temperature. The transition temperature is in agreement with the value $\beta_C \simeq 0.54$. The shape of the curve near the transition is in agreement with the existence of a mean field like transition for the central spin. We also plotted the expectation value of the magnetization of the m closest to the origin slices of spins, in the factorisation approximation, for $m = 3, 4, 5, 6, 7, 8, 9, 10$.

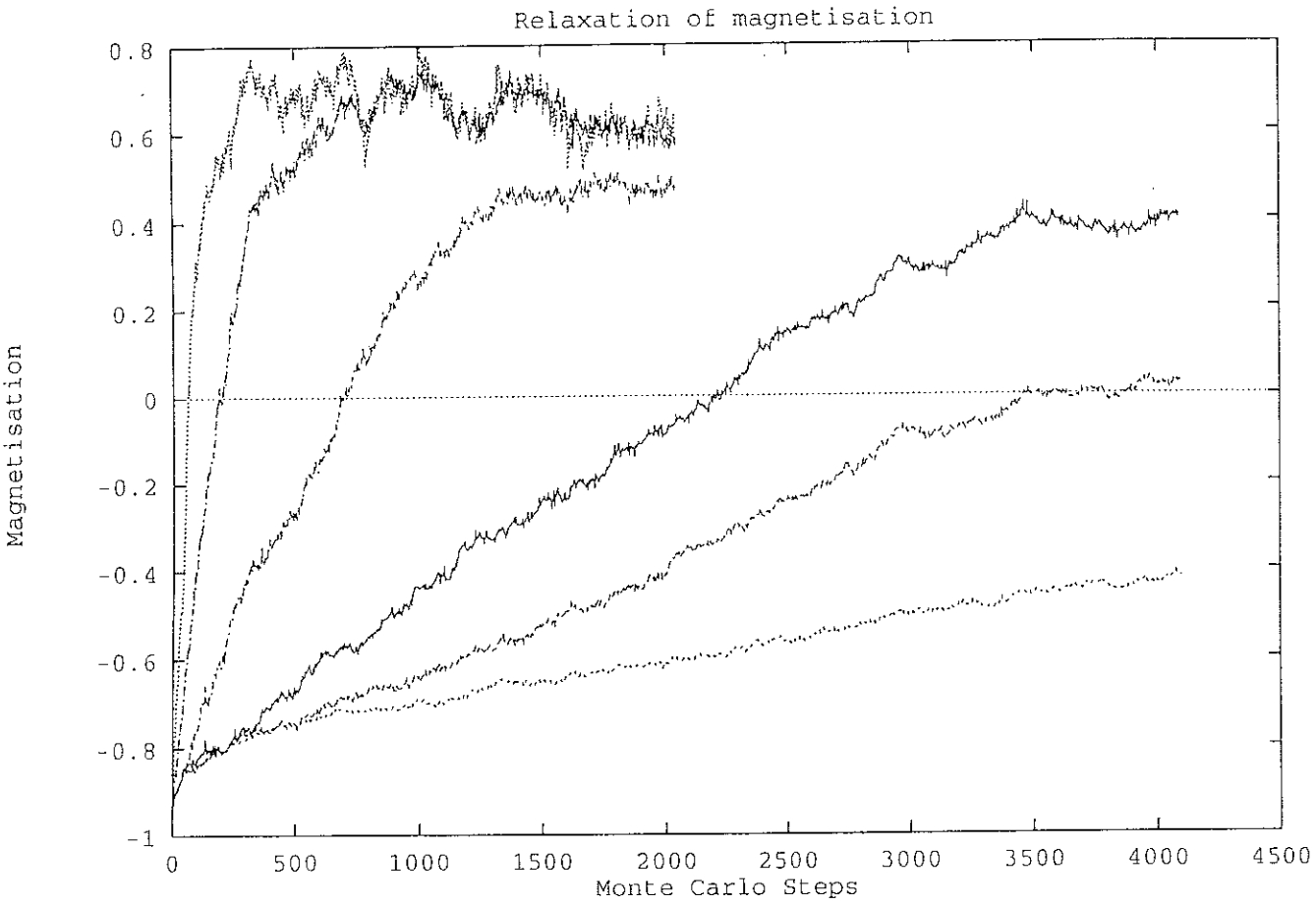

Figure 16.15:
Magnetization relaxation of a single kink. Initially, all the spins of a $z = 3$, $n = 10$ tree are up, and one creates a kink. We call n_0 the number of generations involved in the kink. If $n_0 = 1$, the kink has only one spin, if $n_0 = 2$, the kink has 7 spins, etc. We follow the magnetization of this domain as a function of time. The unit time is one Monte Carlo Step (M.C.S.). One M.C.S. corresponds to repeating N times the process which consists in choosing one spin at random among the N sites, and changing or not its direction, according to the Boltzman distribution. The curves are averaged over 50 different Monte Carlo runs of the dynamics.

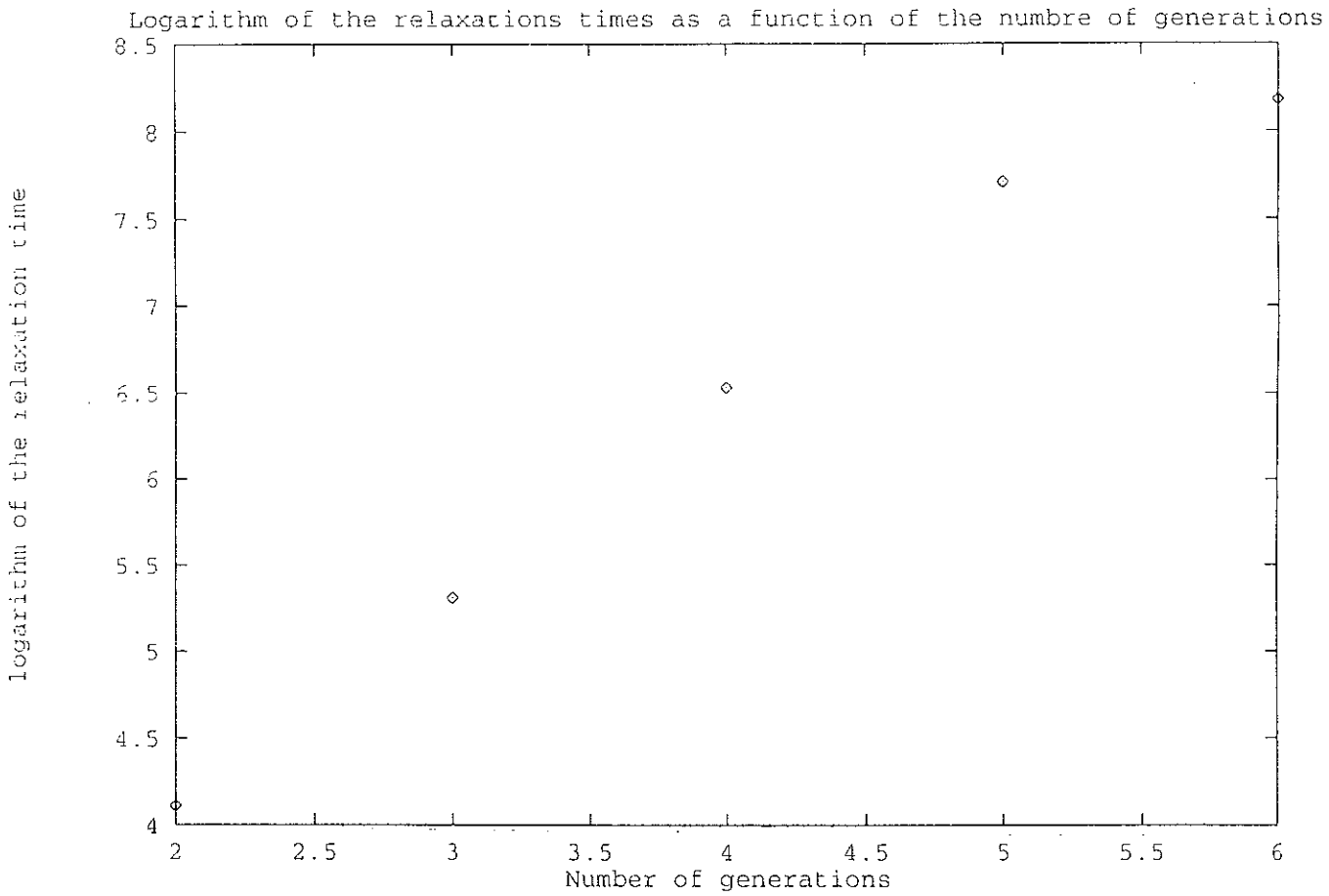

Figure 16.16:
Logarithm of the relaxation time as a function of the number of generations in the kink. The relaxation time is defined from the cancelation of magnetization on figure 16.15. The points are approximately aligned, which is in agreement with the Arrhenius law of equation (16.88).

which has only odd harmonics. In practise, we let the system relax during 4 periods and we take into account only the 5-th period. The in-phase susceptibilities are related to the in-phase Fourier coefficients as [23]

$$\theta_1' = \chi_1' h + \frac{3}{4}\chi_3' h^3 + \frac{5}{8}\chi_5' h^5 + \frac{35}{64}\chi_7' h^7 + ... \quad (16.90)$$

$$\theta_3' = \frac{1}{4}\chi_3' h^3 + \frac{5}{16}\chi_5' h^5 + \frac{21}{64}\chi_7' h^7 + ... \quad (16.91)$$

$$\theta_5' = \frac{1}{16}\chi_5' h^5 + \frac{7}{64}\chi_7' h^7 + ... \quad (16.92)$$

$$\theta_7' = \frac{1}{64}\chi_7' h^7 + ... \quad (16.93)$$

The reason why one has to take into account a large number of harmonics is that, for a spin glass, at the spin glass temperature, all the non-linear susceptibilities are divergent, and one has to take into account the influence of all the measurable higher order processes on the lower ones [23].

The linear susceptibility χ_1' is plotted on figure 16.17 as a function of temperature, for various frequencies. The non-linear susceptibility χ_3' is plotted on figure 16.18 as a function of temperature for various frequencies. It appears that χ_1' presents a maximum, whereas χ_3' has a very pronounced maximum. In real spin glasses and at the thermodynamic limit, one would expect χ_1' to have a maximum, and χ_3' to diverge. However, finite size studies to not lead to a real divergence of χ_3', but to a sharp maximum. χ_3' is negative near its maximum, which agrees with experiments on glasses [23]. The frequency dependence of the position of the maximum in χ_1' and χ_3' also agrees with experiments, since the temperature for which χ_1' and χ_3' are maximum increases with frequency. We conclude from this study that the Cayley tree spin system has a glassy-like behaviour at low temperatures. This notion will be precised in the analysis of the Edwards-Anderson susceptibility.

16.6.3 Autocorrelation functions and aging

One of the usual tests to determine whether a model is glassy is to compute the autocorrelation functions [24] and see whether they exhibit aging. The autocorrelation functions are

$$C(t, t_w) = \frac{1}{N}\sum_{i=1}^{N} \langle \sigma_i(t + t_w)\sigma_i(t_w)\rangle - \langle \sigma_i(t + t_w)\rangle\langle \sigma_i(t_w)\rangle, \quad (16.94)$$

where the sample is quenched below the glass temperature, from a disordered high temperature state. The Monte Carlo dynamics runs from time 0 to time t_w. At t_w, one begins to measure the autocorrelations. The average runs over the initial configurations.

The autocorrelations in the high-temperature phase are plotted on figure 16.19. They decrease rapidly with the time t and are independent of the waiting time. Figure 16.20 represents the autocorrelation functions below T_g. The aucorrrelations *increase* as the waiting time t_w increases. This indicates the presence of aging. Such a behavior has been observed in a wide class of glassy models, for instance recently in the fully frustated hypercubic model [24].

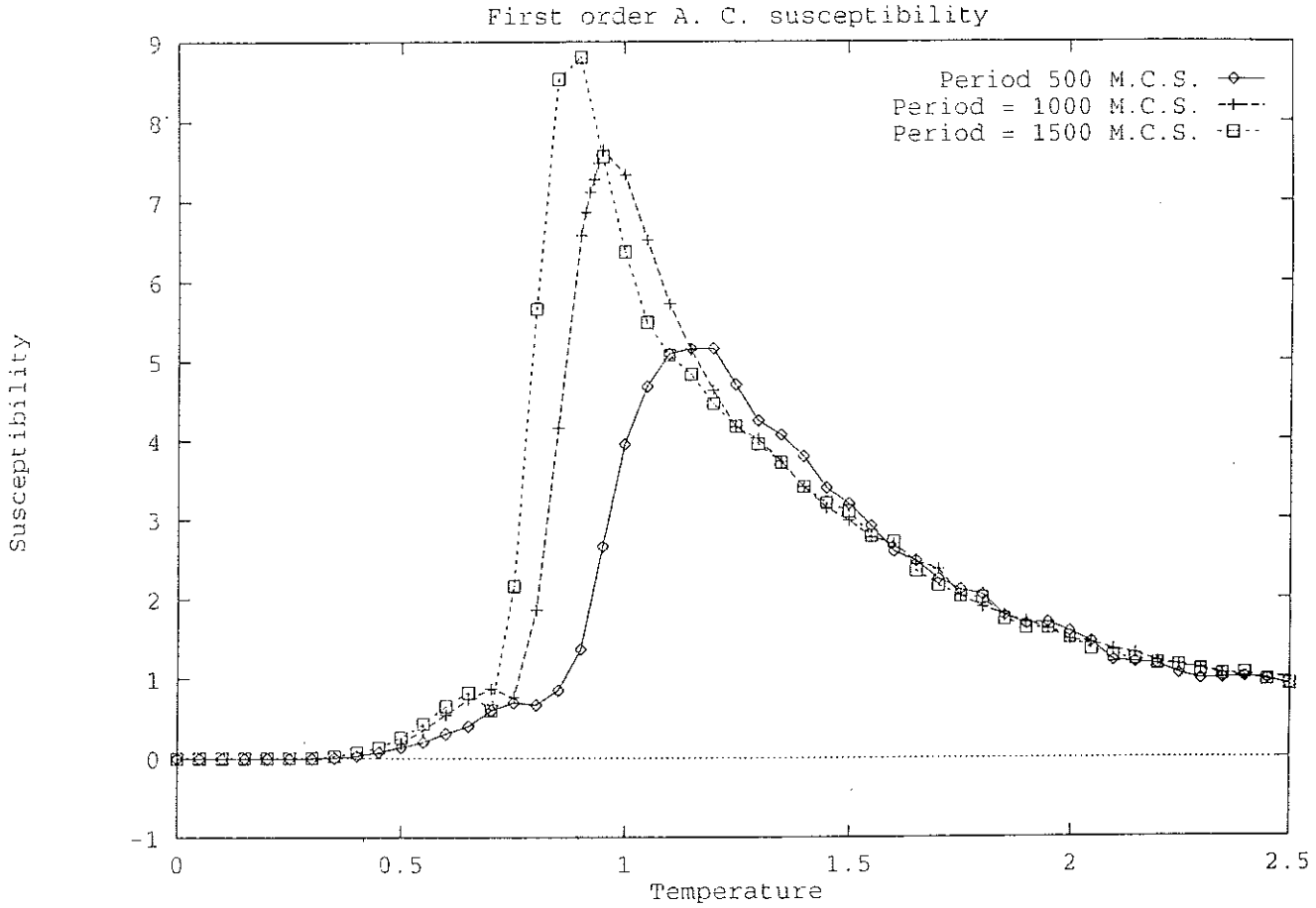

Figure 16.17:
χ_1' susceptibility on the Cayley tree. The tree has 10 generations. The amplitude of the magnetic field is 0.1. The curves are averaged over 50 initial configurations of spins, generated at equilibrium. One has to find a compromise between the amplitude of the magnetic field and the number of configurations to be averaged over, to have a good signal/noise ratio. The curves correspond to a period of the magnetic field equal to 500 M.C.S., 1000 M.C.S. and 1500 M.C.S..

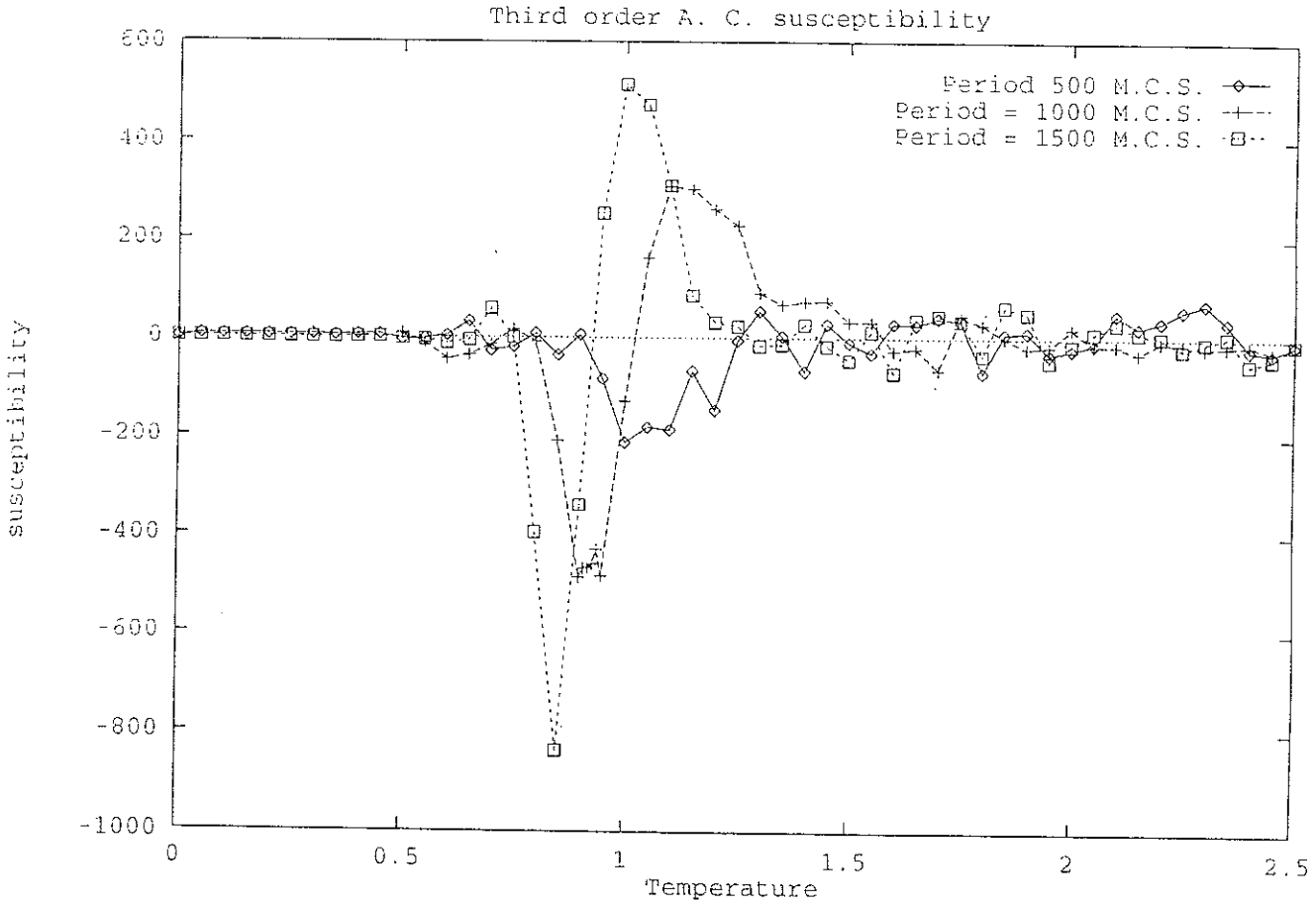

Figure 16.18:
χ_3' susceptibility on the Cayley tree. The tree has 10 generations. The amplitude of the magnetic field is 0.1. The curves are averaged over 50 initial configurations of spins, generated at equilibrium. The curves correspond to a period of the magnetic field equal to 500 M.C.S., 1000 M.C.S. and 1500 M.C.S..

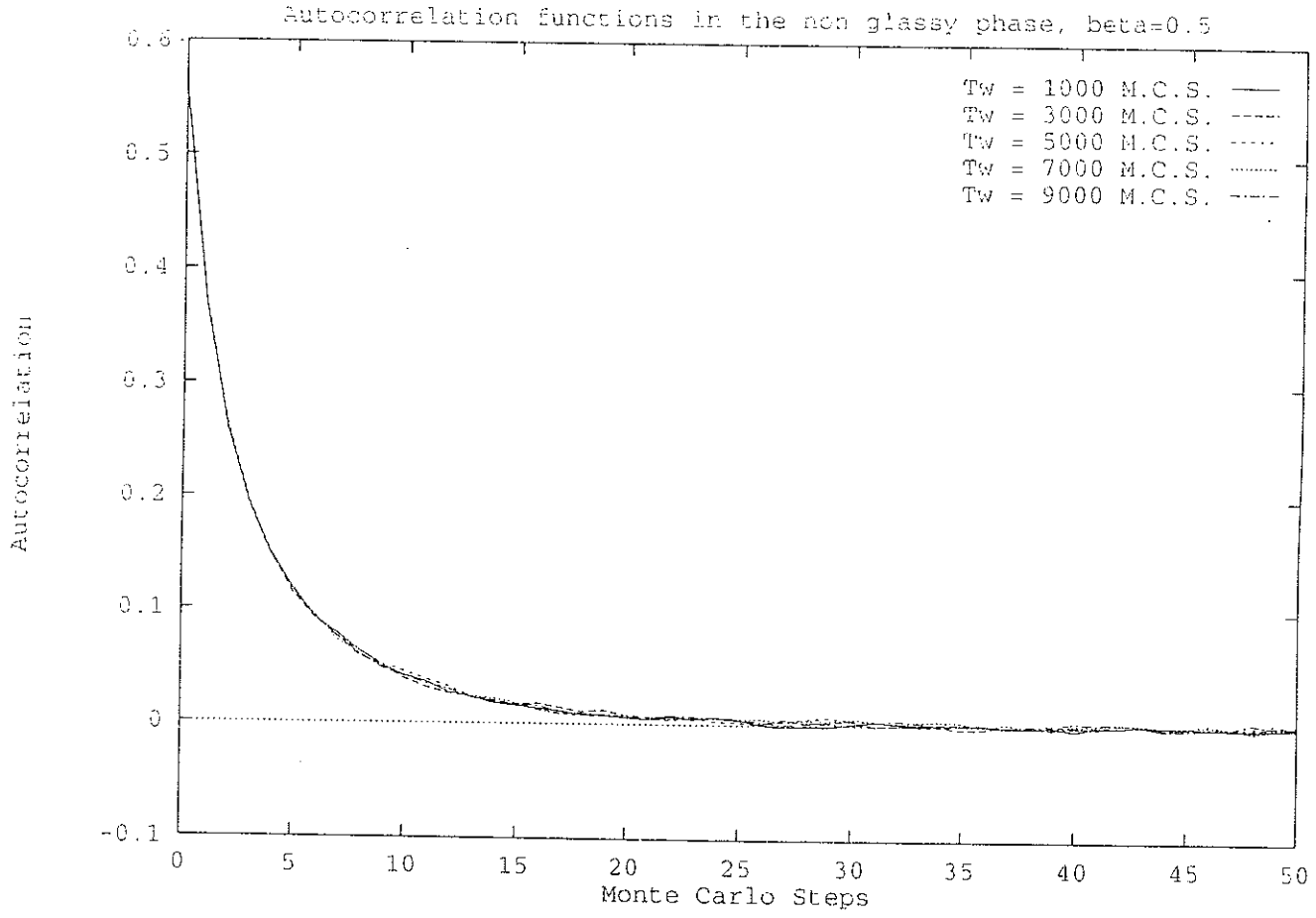

Figure 16.19: --

Spin autocorrelation functions of the $z = 3$ Cayley tree above T_g. The unit time is one M.C.S., the inverse temperature is $\beta = 0.5$, and the averages are taken over 100 random initial configurations. The autocorrelation functions decrease rapidly with t and are independant on t_w.

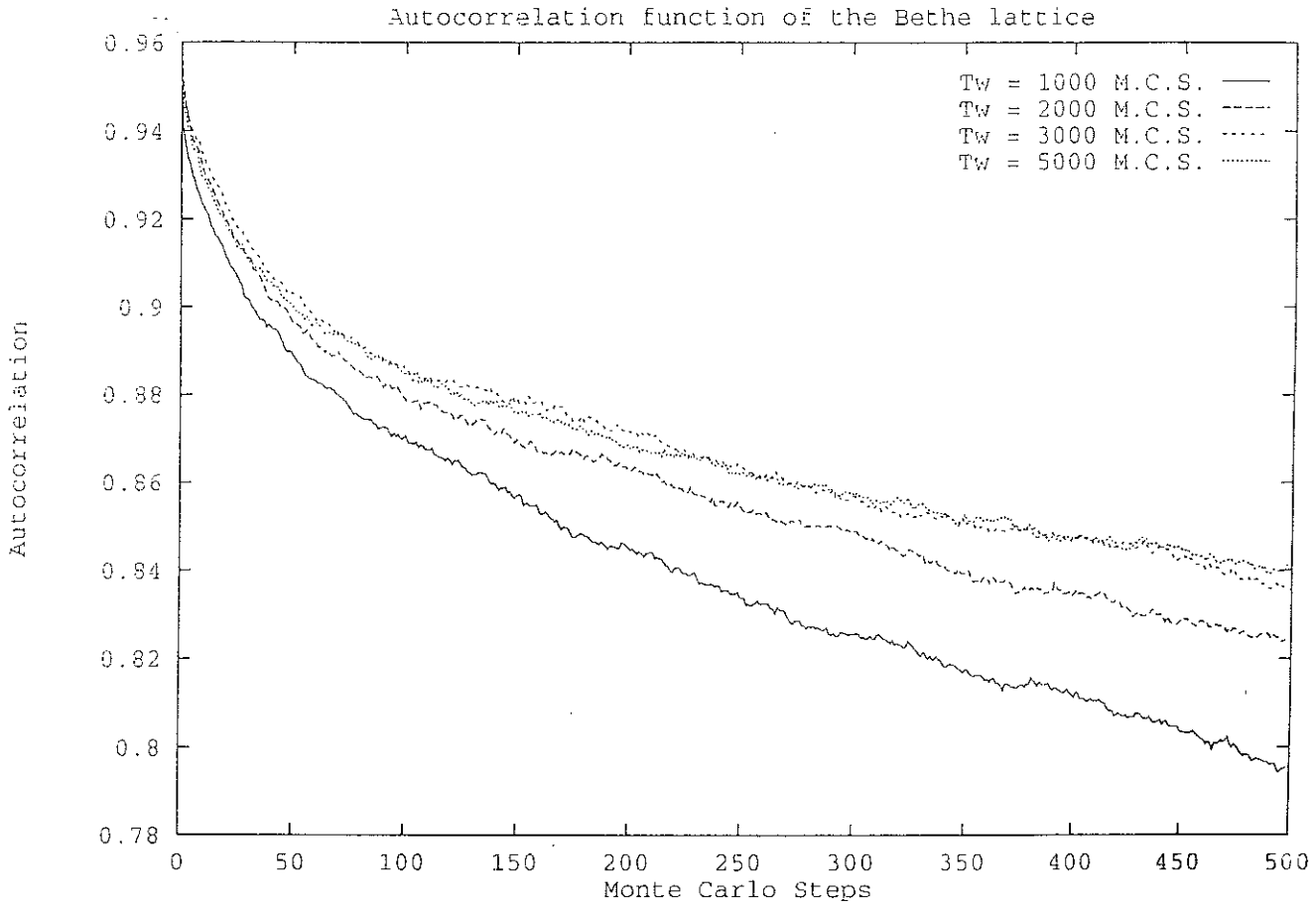

Figure 16.20:
Spin autocorrelation functions of the $z = 3$ Cayley tree below T_g. The unit time is one M.C.S., the inverse temperature is $\beta = 2.$, and the averages are taken over 100 random initial configurations. The autocorrelation functions depend on the waiting time, and *increase* with the waiting time, which is the signature of glassiness.

16.7 Edwards Anderson order parameter and susceptibility

The tree geometry allows us to compute the Edwards Anderson order parameter and susceptibility at all temperatures. This calculation has already been done for the $\pm J$ model with uncorrelated boundary conditions in [9] [13]. These authors come to the conclusion of the existence of an Almeida Thouless line for their spin glass model. We wish to use the same technique to analyse our ferromagnetic model. To compute the Edwards Anderson order parameter and susceptibility, we consider one tree plus one replica, with an intereplica coupling R. If $\{\sigma\}$ and $\{\sigma'\}$ are the spin configurations of the two replicas, the Hamiltonian reads

$$H = -J\sum_{\langle i,j\rangle}(\sigma_i\sigma_j + \tilde{\sigma}_i\tilde{\sigma}_j) - R\sum_{i=1}^{N}\sigma_i\tilde{\sigma}_i + H\sum_{i=1}^{N}(\sigma_i + \tilde{\sigma}_i). \tag{16.95}$$

As usual with free boundary trees, we have to distinguish between the central spin and the whole tree properties. We analyse sucessively both cases.

16.7.1 The whole tree

The partition function can be calculated by the construction of figure 16.2, even in the presence of the intereplica coupling. Derivating the partition function with respect to R yields the Edwards Anderson order parameter:

$$q_{EA} = \frac{1}{N}\langle\sum_{i=1}^{N}\sigma_i\tilde{\sigma}_i\rangle = \frac{1}{N}\frac{\partial}{(\partial\beta R)}\ln Z(R=0). \tag{16.96}$$

Derivating twice the partition function with respect to R yield the Edwards Anderson susceptibility:

$$\chi_{E.A.} = \frac{1}{N}\left(\langle(\sum_{i=1}^{N}\sigma_i\tilde{\sigma}_i)^2\rangle - \langle\sum_{i=1}^{N}\sigma_i\tilde{\sigma}_i\rangle^2\right) = \frac{1}{N}\frac{\partial}{\partial(\beta R)^2}\ln Z(R=0). \tag{16.97}$$

The relations (16.96) and (16.97) show that the Edwards Anderson order parameter and susceptibility are simply related to the first and second derivatives of the function partition with repect to R. Let $Z^{(n)}_{\sigma\sigma'}$ be the conditional partition function of a n-half space tree with respect to the ancestor's spins σ and σ'. It is clear that

$$Z^{(n+1)}_{++} = e^{\beta R}e^{2\beta H}\left(e^{2\beta J}Z^{(n)}_{++} + Z^{(n)}_{+-} + Z^{(n)}_{-+} + e^{-2\beta J}Z^{(n)}_{--}\right)^{z-1} \tag{16.98}$$

$$Z^{(n+1)}_{+-} = e^{-\beta R}\left(Z^{(n)}_{++} + e^{2\beta J}Z^{(n)}_{+-} + e^{-2\beta J}Z^{(n)}_{-+} + Z^{(n)}_{--}\right)^{z-1} \tag{16.99}$$

$$Z^{(n+1)}_{-+} = e^{-\beta R}\left(Z^{(n)}_{++} + e^{-2\beta J}Z^{(n)}_{+-} + e^{2\beta J}Z^{(n)}_{-+} + Z^{(n)}_{--}\right)^{z-1} \tag{16.100}$$

$$Z^{(n+1)}_{--} = e^{\beta R}e^{2\beta H}\left(e^{-2\beta J}Z^{(n)}_{++} + Z^{(n)}_{+-} + Z^{(n)}_{-+} + e^{2\beta J}Z^{(n)}_{--}\right)^{z-1}. \tag{16.101}$$

The initial condition of the recurrence are $Z^0_{++} = e^{\beta R}e^{2\beta H}$, $Z^0_{+-} = Z^0_{-+} = e^{-\beta R}$ and $Z^0_{--} = e^{\beta R}e^{-2\beta H}$. We show easily that, for all n, $Z^{(n)}_{+-} = Z^{(n)}_{-+}$, so that we use the following notations: $Z^{(n)}_1 = Z^{(n)}_{++}$, $Z^{(n)}_0 = Z^{(n)}_{+-} = Z^{(n)}_{-+}$, and $Z^n_{-1} = Z^{(n)}_{--}$. The recurrence becomes

$$Z^{(n+1)}_1 = e^{\beta(R+2H)}\left(e^{2\beta J}Z^{(n)}_1 + 2Z^{(n)}_0 + e^{-2\beta J}Z^{(n)}_{-1}\right)^{z-1} \tag{16.102}$$

$$Z_0^{(n+1)} = e^{-\beta R}\left(Z_1^{(n)} + 2\cosh\beta J Z_0^{(n)} + Z_{-1}^{(n)}\right)^{z-1} \tag{16.103}$$

$$Z_{-1}^{(n+1)} = e^{\beta(R-2H)}\left(e^{-2\beta J} Z_1^{(n)} + 2Z_0^{(n)} + e^{2\beta J} Z_{-1}^{(n)}\right)^{z-1}. \tag{16.104}$$

It is easy to compute the recurence and to obtain q_{EA} and χ_{EA}. $\chi_{E.A.}$ is plotted on figure 16.21 for 10 and 80 generations. The curves corresponding to $n = 10$ and $n = 80$ are similar, even though the number of sites is small for $n = 10$ (2047 sites) and macroscopic for $n = 80$ (4.02 moles of sites). This behaviour is to be related to the very slow variation of the glass temperature T_g with the system size. Figure 16.21 shows clearly that $\chi_{E.A.}$ does not diverge at the thermodynamic limit, but presents a maximum. characteristic of a finite size effect, even in the macroscopic regime.

16.7.2 The central spin

Following the authors of [9] [13], we note

$$Z^{(n)} = Z_1^{(n)} + 2Z_0^{(n)} + Z_{-1}^{(n)} \tag{16.105}$$

$$Q^{(n)} = \frac{1}{Z^{(n)}}(Z_1^{(n)} - 2Z_0^{(n)} + Z_{-1}^{(n)}) \tag{16.106}$$

The Edwards Anderson order parameter of the central spin is $\tilde{q}_{E.A.} = Q^{(n)}$, and the Edwards Anderson susceptibility is

$$\tilde{\chi}_{E.A.}^{(n)} = \frac{\partial \tilde{q}_{E.A.}}{(\partial \beta R)}(R = 0) \tag{16.107}$$

The tilde symbol denotes quantities with respect to the central spin. The central spin Edwards Anderson susceptibility $\tilde{\chi}_{E.A.}$ is plotted on figure 16.22 for various system sizes. Whereas finite size effects were negligeable for the whole system, they become crucial for the central spin. As a function of the coordinance z, the maximum values of the Edwards Anderson susceptibility of the central spin does not increase (see figure 16.23). As the system size becomes macroscopic, the glass temperature T_g does not depend strongly on the number of sites, but depend more strongly on the coordinance, and increases with the coordinance, as shown on relation (16.43).

16.7.3 Central spin in a magnetic field

In usual spin glasses, the glassy behaviour persists even in the presence of a magnetic field, that is the Edwards Anderson susceptibility diverges with an exponent $\gamma = 1$ through the Almeida-Thouless line. In this section, we investigate the behaviour of the Cayley tree ferromagnetic model with free boundary conditions under a magnetic field. We studied the variations of the Edwards Anderson susceptibility in a magnetic field, for different sizes. As pictured on figure 16.24, the maximum of the Edwards Anderson susceptibility as a function of temperature depends on the size. On figure 16.25, we plotted the locus of the maxima of $\tilde{\chi}_{E.A.}$ for different magnetic fields as a function of temperature. The Edwards Anderson susceptibility decreases strongly with the magnetic field, so that the glassy behaviour is expected to vanish in a magnetic field.

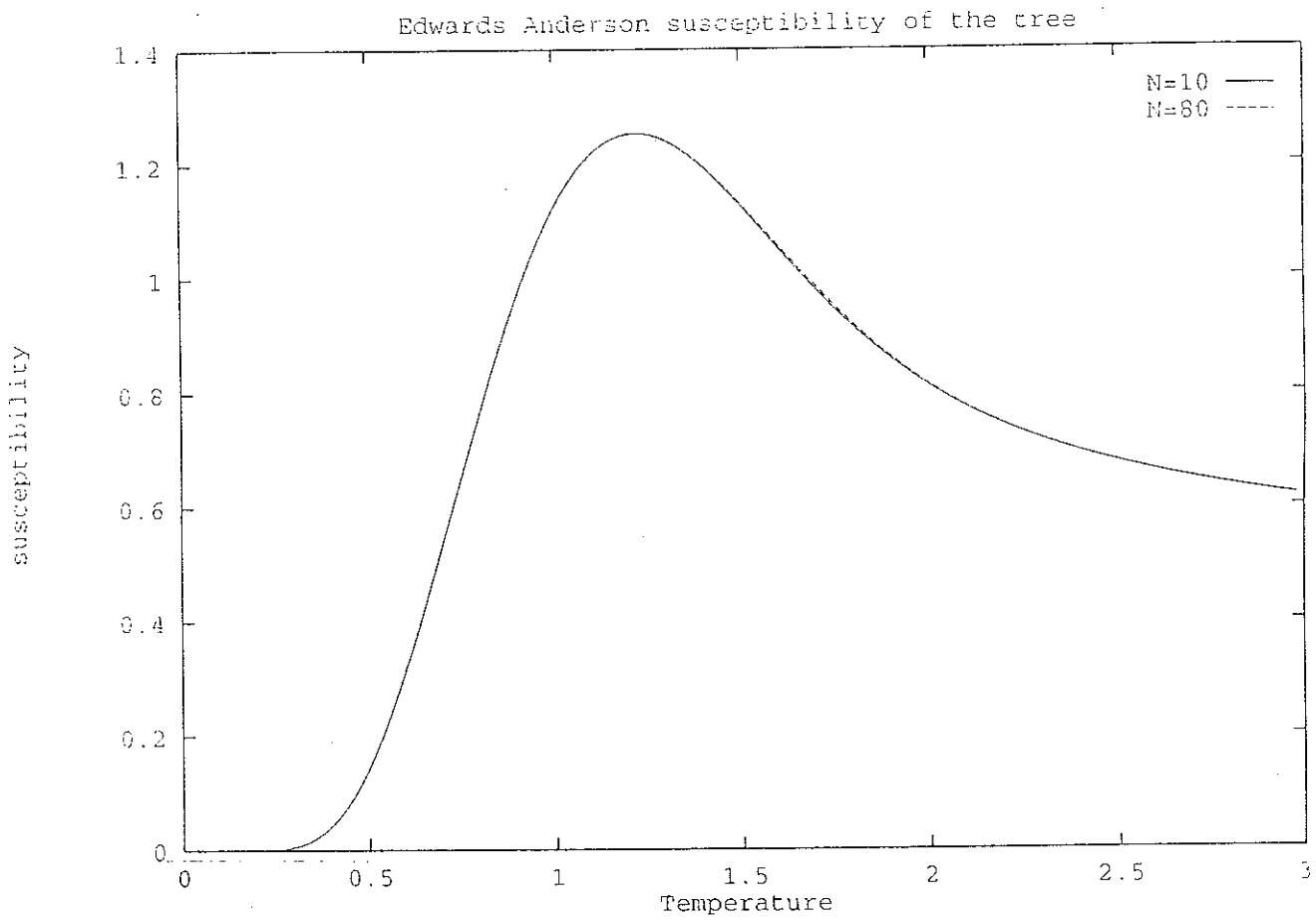

Figure 16.21:
Edwards Anderson susceptibility for the whole spin system. The coordinance is $z = 3$. The Edwards Anderson susceptibility is plotted as a function of temperature for $n = 10$ (2047 spins) and $n = 80$ (4.02 moles of spins). The two curves nearly coincide.

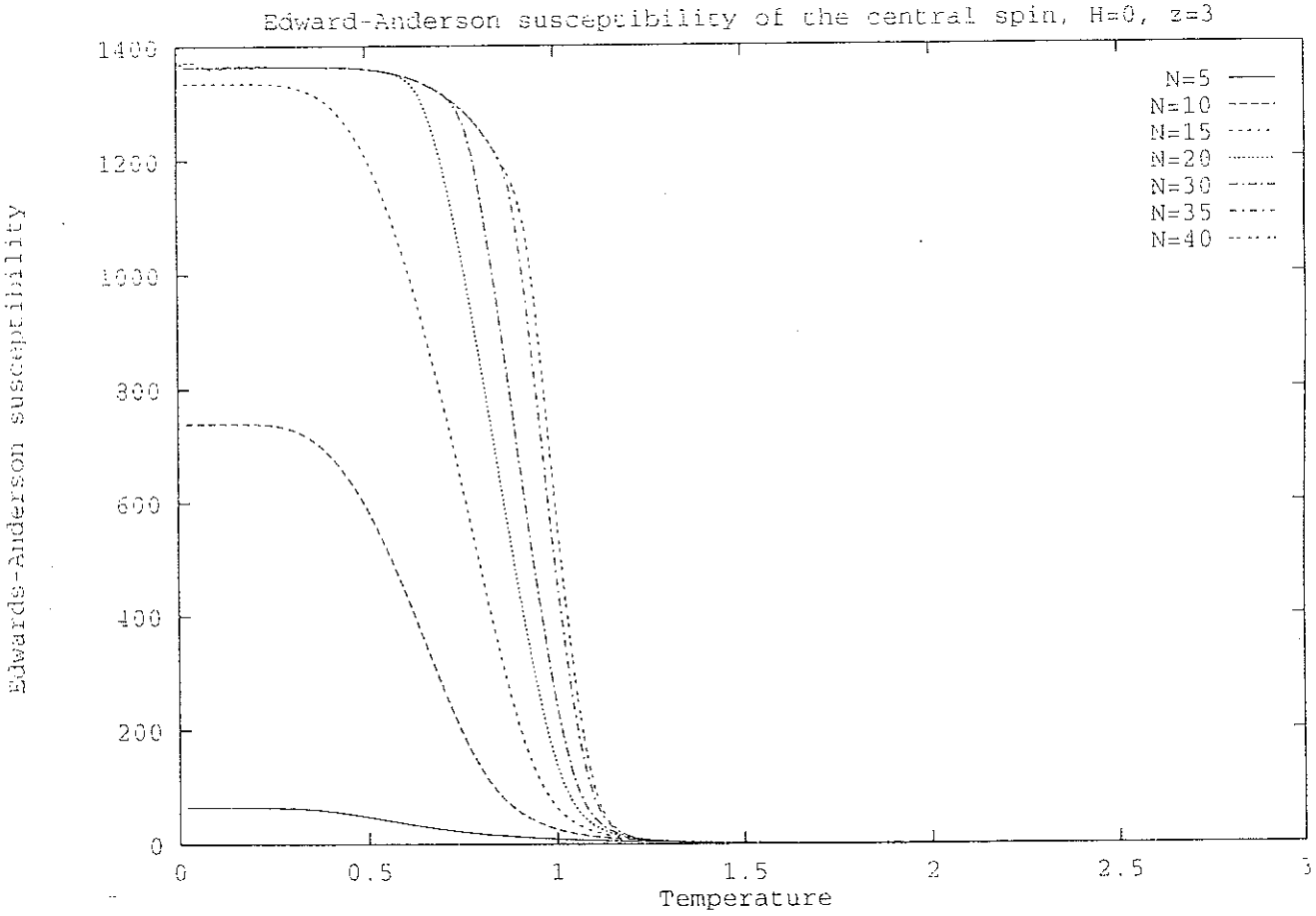

Figure 16.22:
Edwards Anderson susceptibility for the central spin as a function of temperature for $n = 5, 10, 15, 20, 25, 30, 35, 40$ generations. The coordinance is $z = 3$.

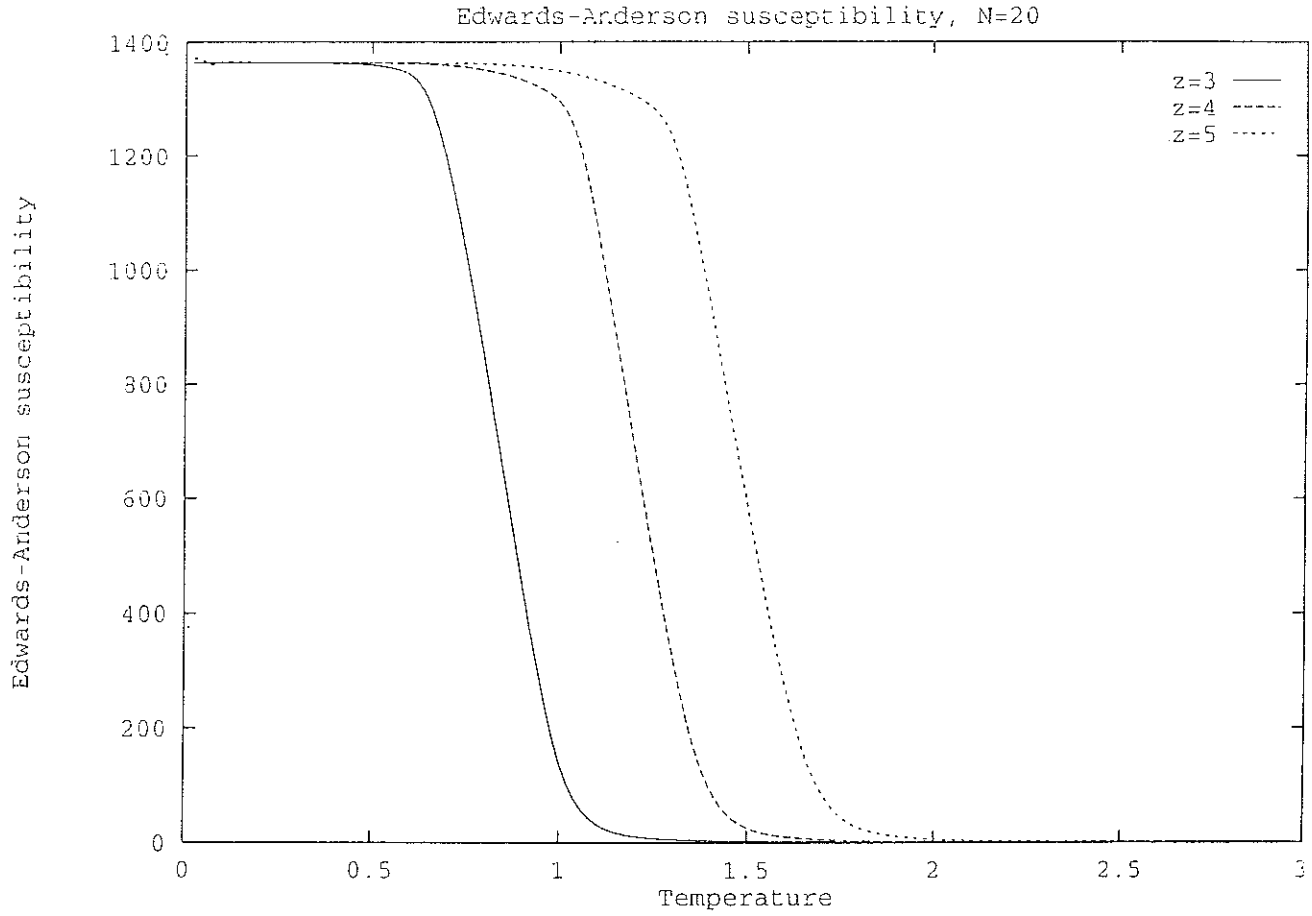

Figure 16.23:
Edwards Anderson susceptibility for the central spin as a function of temperature for $z = 3, 4, 5$. The number of generations is $n = 20$.

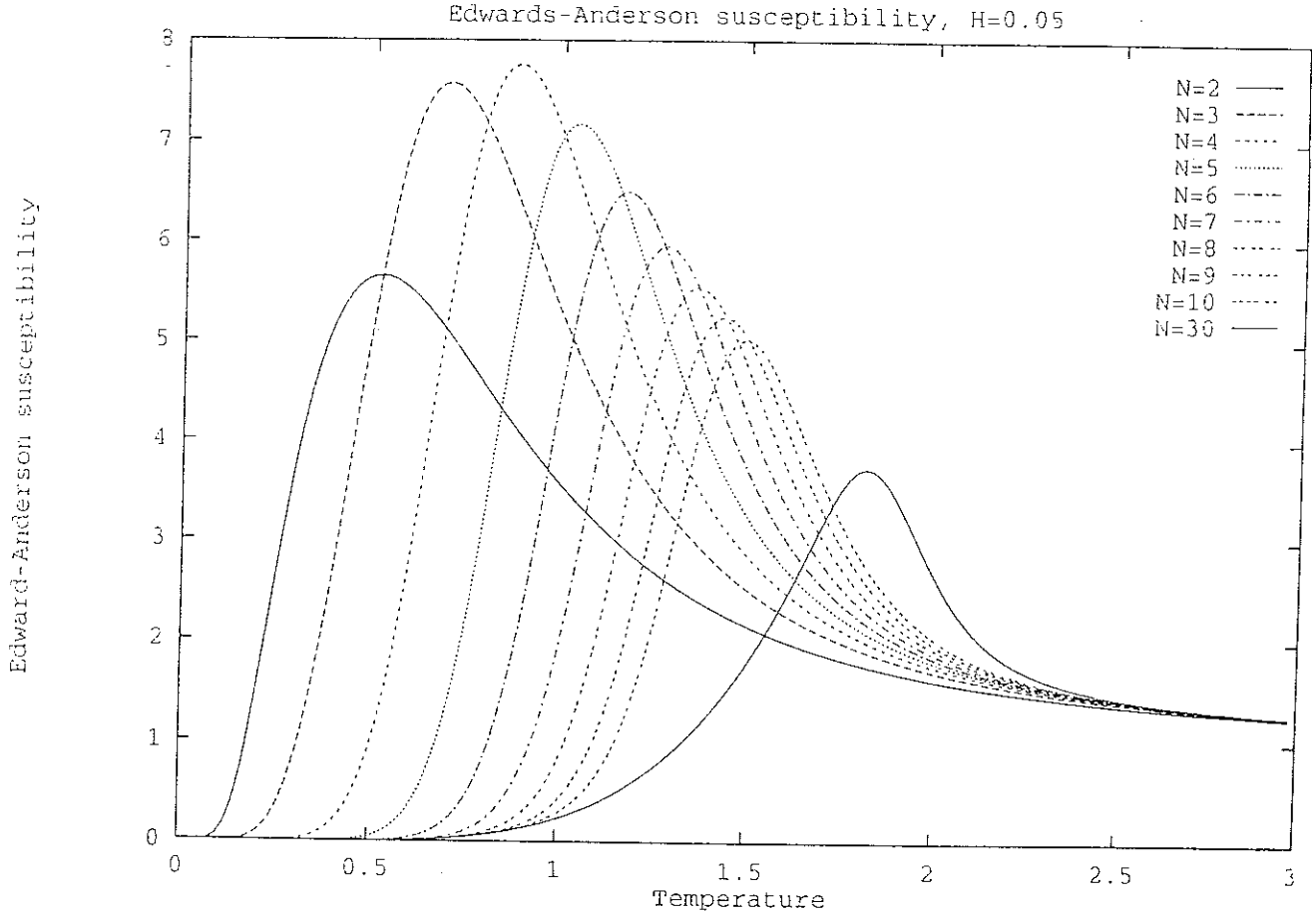

Figure 16.24:
Edwards Anderson susceptibility of the central spin in a magnetic field as a function of temperature, for different sizes. The number of generations is n=2, 3, 4, 5, 6, 7, 8, 9, 10, 30. The magnetic field is $H = 0.05$.

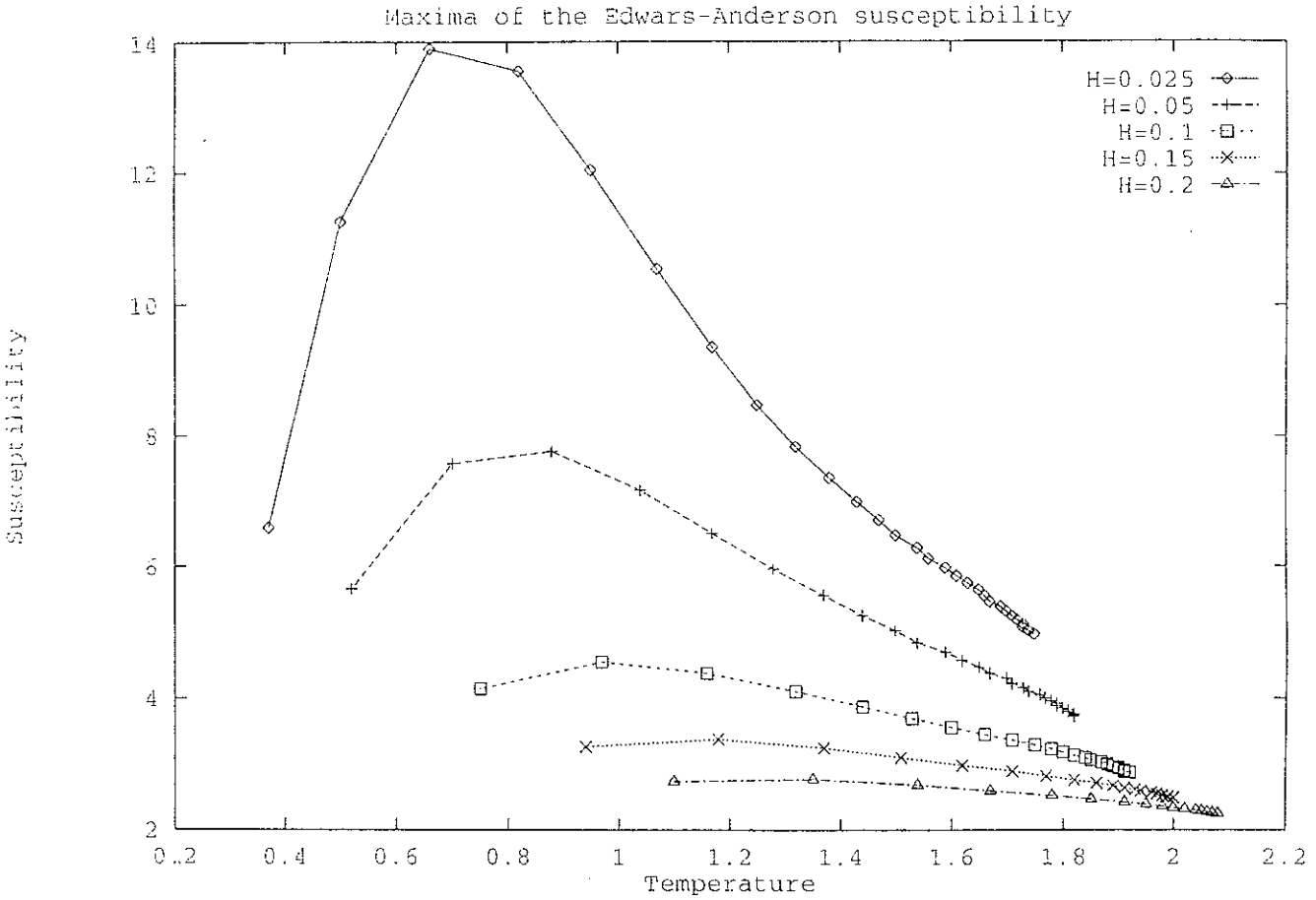

Figure 16.25:
Maxima of χ_{EA} as a function of temperature for different values of the magnetic field. The system size is $n = 10$ generations. The magnetic fields are $H = 0.025, H = 0.05, H = 0.1, H = 0.15, H = 0.2$.

16.8 Lee and Yang zeros

The partition function of the tree in the absence of a magnetic field is equal to the partition function of the linear chain, so that the Lee and Yang zeros in the plane of $\exp 2\beta$ with a zero magnetic field have the same structure as in the case of the linear chain. However, this result does not anymore hold if a magnetic field is introduced. It is interesting to complexify the magnetic field and look for the zeros of the partition function in the complex plane of $\exp 2\beta h$. We do not impose a uniform magnetic field, but only a magnetic field on the leaves of the tree, so that the zeros are very easy to compute, using the recursion (16.5), since one has only to solve second order equations. Since the magnetic field is non uniform, the hypothesis of the circle theorem [26] are not fulfilled. The zero are not exactly on the unit circle, but in the vicinity of the unit circle. More precisely, numerical computations show that the zeros get closer to the unit circle as the number of generations increases. The zeros are plotted on figure 16.26 in the cases $\beta < \beta_c$, $\beta = \beta_c$ and $\beta > \beta_c$.

A quantity of interest is the density of zeros in the vicinity of the point $\exp 2\beta h = 1$. On figure 16.27, we have plotted the ratio of the density of zeros in the vicinity of $\exp 2\beta h = 1$ over the averaged density on the circle. The ratio is zero for temperatures larger than the bulk transition temperature, increases from zero below the bulk transition temperature, and finally gets larger than unity below a certain temperature. By comparison, the same ratio in the case of a Weiss model in a uniform magnetic field is always inferior to unity. In the case of a Weiss model, the density of zeros $g(\theta)$ is given by [27]

$$g(\theta) = \frac{1}{2\pi}(1 - 2r\cos\varphi), \tag{16.108}$$

where

$$r = \sqrt{4 + r^2 - 4r\cos\varphi}\exp\left(-2\frac{T_c}{T}(1 - r\cos\varphi)\right) \tag{16.109}$$

$$\theta = -2\frac{T_c}{T}r\sin\varphi + \varphi + \arctan\left(\frac{r\sin\varphi}{2 - r\sin\varphi}\right). \tag{16.110}$$

It is easy to solve this system numerically. The ratio of the density of zeros at the point $\exp 2\beta h = 1$ over the average density of zeros is plotted on the inset of figure (16.27), and is always less than unity. On the tree, the density of zeros in the vicinity of the real axis is thus anormally high below a certain temperature, which we identify with the temperature scale T_g.

16.9 Discussion

In summary, we have studied the static and the dynamical properties of the nearest-neighbor Ising model on a Cayley tree. At zero field, we find that this system displays glassy behavior below a size-dependent temperature that scales inversely with the logarithm of the number of generations; thus its glassy behavior persists for a finite but macroscopic number of sites. Because the ratio of the number of surface to bulk sites, $\frac{N_s}{N}$, and the strength of the external field, h, play a key role in the physical behavior of the resident spin system, the different thermodynamic limits associated with the values of $\frac{N_s}{N}$ and h are characterized; the cross-over temperature, T_g, is associated with fixed $\frac{N_s}{N}$ in the limit of vanishing applied field. Physically well-defined large domains of flipped spins develop at T_g; at this temperature the probability

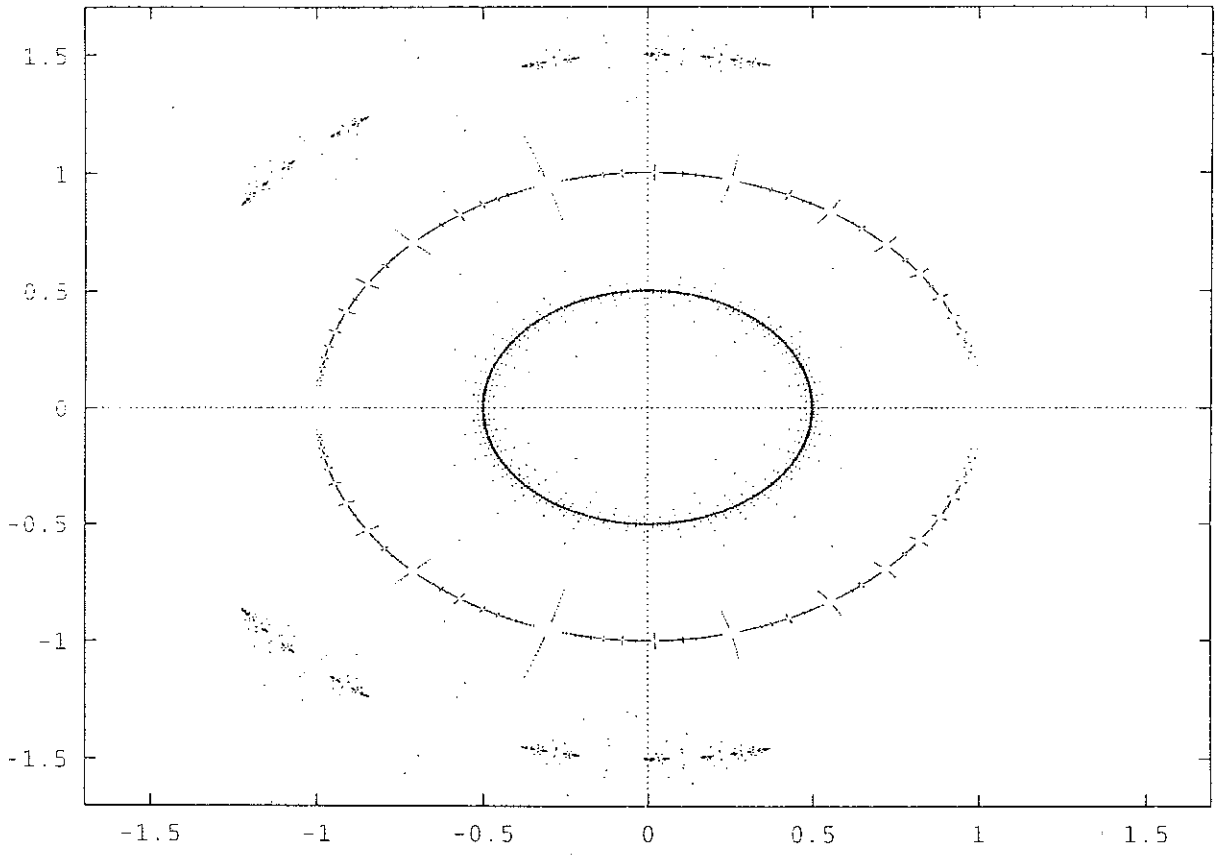

Figure 16.26:
Zeros of Lee and Yang at different temperatures. The radial coordinate is rescaled in order to allow the superposition of different maps of zeros. The external map represents the zeros for 12 generations, $z = 3$ and $\beta = 0.3$. In this case, the zeros are localized on well defined areas of the complex plane, far from the real axis. The intermediate map represents the case $\beta = \beta_c \simeq 0.54$. The zeros begin to fill the circle, with areas of zero density, especially at the intersection of the real axis with the unit circle. The inner map represent the zeros at low temperature, $\beta = 2$. In this case, the circle is filled with zeros. An analysis of the density of zeros reveals an annormally high density in the vicinity of the point $h = 0$.

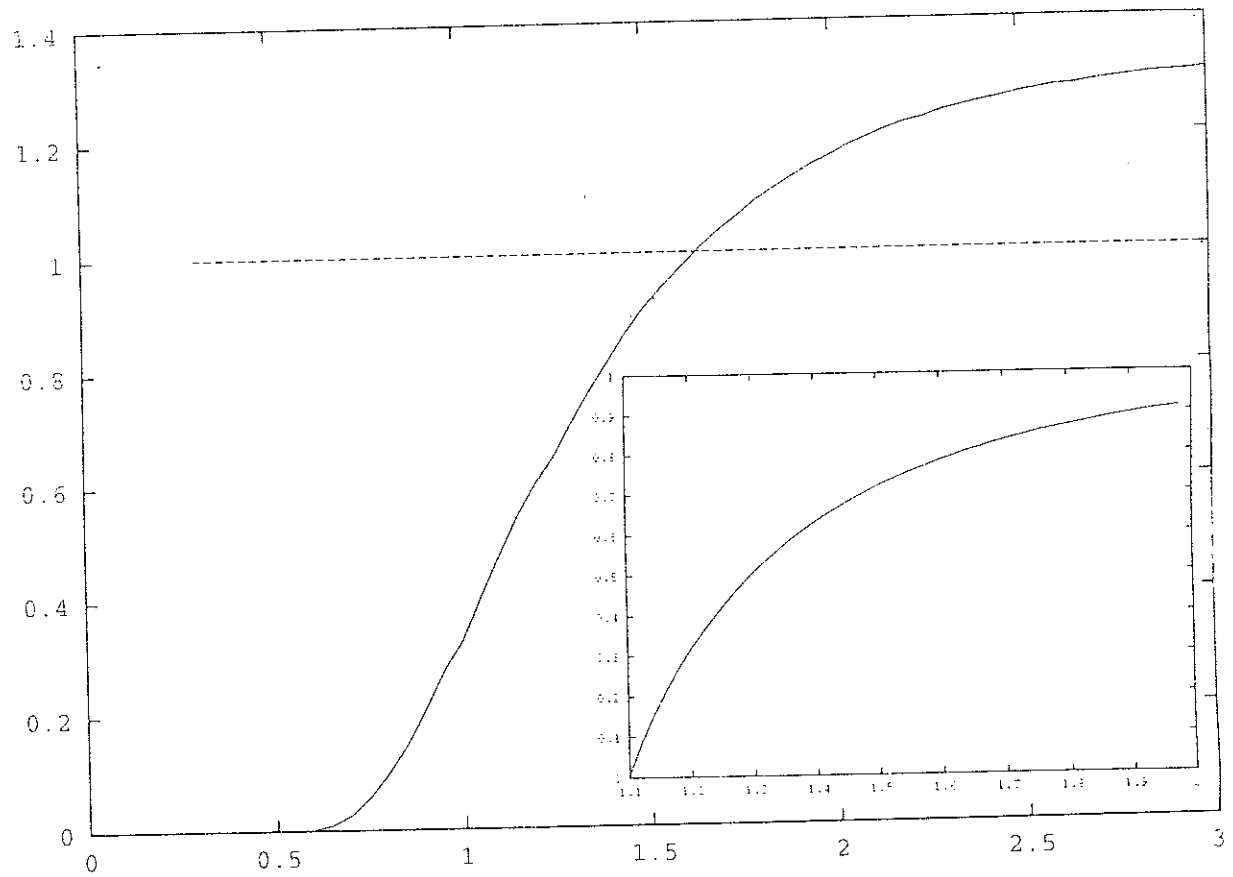

Figure 16.27:
Ratio of the density of zeros in the vicinity of the point $\exp 2\beta h = 0$ over the average density of zeros in the case of the $z = 3$ tree with 17 generations. The inset represents the same quantity for a Weiss model with $T_c = 1$. In the case of the tree, the ration is greater than one below a certain temperature, whereas it is always less than unity for the Weiss model.

of nested spin clusters is small. The largest energy barriers associated with overturning these domains is determined to scale logarithmically with the number of sites at zero temperature, a result that should be valid at finite, low temperatures if overlap between spin clusters does not occur. A dynamical study indicates the appearance of metastable states and long relaxation times at low temperatures. The autocorrelations are computed after a waiting time using Monte Carlo dynamics; they exhibit ageing for $T < T_g$. The temperature variations of the coefficients of χ_1' and χ_3' are also determined and they agree with the existence of finite-size glassiness. Finally the Edwards-Anderson susceptibility of the entire tree displays a maximum (but no divergence) that evolves slowly with increasing system size; that of the central spin has much more marked size-dependence.

We have thus performed a detailed characterization of the low-temperature phase of a short-range periodic spin model resident on a Cayley tree. In this particular case, we have found that it displays finite-size glassy behavior that remains for a macroscopic number of sites; perhaps it is best to characterize this low-temperature phase as a very viscous spin liquid. We note that neither intrinsic disorder nor frustration exist due to the initial Ising Hamiltonian; the possibility of many low-temperature "cluster" states separated by very high energy barriers is a direct consequence of the unusual topology of the Cayley tree. In many ways we hope that this is a warm-up exercise towards the study of spin models on more complicated non-Euclidean lattices, e.g. on a constant triangulation associated with a surface of negative curvature, where the intrinsic geometry of the host may lead to the possibility of glassiness in the absence of both disorder and frustration.

16.10 Appendix A

We propose another derivation of the magnetization distribution for the tree. We note $Z(\beta, h)$ the partition function of the spin system in the presence of an external field. Then,

$$P(M) = \frac{1}{Z(\beta,h)} \sum_{\{\sigma\}} \delta\left(M - \sum_{i=1}^{N} \sigma_i\right) \exp\left(\beta(J \sum_{\langle i,j \rangle} \sigma_i \sigma_j + h \sum_{i=1}^{N} \sigma_i)\right). \tag{16.111}$$

Using the Fourier representation of the delta function

$$\delta\left(M - \sum_{i=1}^{N} \sigma_i\right) = \frac{1}{2\pi} \int_0^{2\pi} d\lambda e^{i\lambda M} e^{-i\lambda \sum_{i=1}^{N} \sigma_i}, \tag{16.112}$$

we obtain

$$P(M) = \frac{1}{2\pi} \int_0^{2\pi} d\lambda e^{i\lambda M} \frac{Z(\beta, h - i\lambda/\beta)}{Z(\beta,h)}, \tag{16.113}$$

where we have used the analytic continuation of the partition function for complex magnetic fields. This method is usefull provided one knows how to calculte the partition function, which is feasable on a tree, but not only on a tree. We proceed by decimation, starting from the border of the n-half-space-tree. For future purpose, we note $Z_n(\beta, h, h_n)$ the partition function of a n-half-space-tree with a magnetic field h acting on the spins of the generations 0 to $n-1$, and h_n on the spins of the generation n. Then,

$$Z_n(\beta, h, h_n) = \left(4(\cosh^2(\beta J) + \sinh^2(\beta h_n)\right)^{\frac{(z-1)^{n-1}}{2}} Z_{n-1}(\beta, h, h + T.h_n), \tag{16.114}$$

where the transformation of the magnetic field reads

$$T.h = \frac{z-1}{2\beta} \ln \frac{\cosh \beta(J+h)}{\cosh \beta(J-h)}. \tag{16.115}$$

The last term of the recurence corresponds to the partition function of the ancestor, which is simply

$$Z_1(\beta, h) = 2 \cosh (\beta T^n.h). \tag{16.116}$$

It is straighforward to compute the partition function using this recurence, to perform the Fourier transform (16.113) in order to obtain the probability distribution of magnetization.

16.11 Appendix B

In this appendix we give the value of the energy barrier $E(T_{n,z})$ for a half–space–tree $T_{n,z}$ with n generations and a coordination number of z for all sites except the root (coordination $z-1$) and the leaves (coordination 1). We also give the energy barrier $E(T^*_{n,z})$ for a complete tree $T^*_{n,z}$ with n generations and a coordination number of z for all sites except the leaves. The derivation of the formula is due to A. Sebő and M. Preissmann, and is published in extenso in [28]. Note that the same problem arises in the VLSI circuit conception! Generically the problem of finding the lowest energy barrier is *NP-complete*, but the sub–problem of finding the lowest energy barrier of a tree is polynomial, and an explicit algorithm is given hereafter. The value of the energy barriers are given by :

$$c(T_{n,z}) = \lceil \frac{n(z-2)}{2} \rceil + 1 \quad (n, z \geq 3) \tag{16.117}$$

$$c(T^*_{n,z}) = \lceil \frac{(n-1)(z-2)}{2} \rceil + \lceil \frac{z-2}{2} \rceil + 1 \quad (n, z \geq 3)$$

In the above formula $\lceil x \rceil$ denotes the closest integer of x. The demonstration of these formula is constructive. Firstly a lower bound for E is given. Then an algorithm is described which produces a labeling of the sites. Flipping the spins in the order of this labeling gives an energy barrier exactly equal to the lower bound. The algorithm is recursive. It tries to produce an optimal labeling of the sites where the root is labeled *before* the configuration of highest energy is reached. We call *strong* labeling such a labeling. This extra constraint is useful when one applies z times the algorithm on a $T_{n,z}$ to compute $E(T_{n+1,z})$, or when one applies the algorithm to $T_{n,z}$ and to $T_{n-1,z}$ to compute $E(T^*_{n+1,z})$. A strong labeling does not exist when z and n are both odd as shown in [28]. Let us now consider on the case of $T_{n,z}$. Formula 16.117 means that

- when z is even the increment in energy when one goes from $T_{n,z}$ to $T_{n+1,z}$ is *constant* and equal to $\frac{z}{2} - 1$
- when z is odd the increment in energy when one goes from $T_{n,z}$ to $T_{n+1,z}$ is *alternatively* $\frac{z-1}{2} - 1$ and $\frac{z-1}{2}$

We give now the algorithm in the case of even z. The case of odd z is a slightly more complicated, but in the same spirit. Consider $T_{n,z}$ as being made of $z-1$ copies of $T_{n-1,z}$ all of them connected to the site 0. Each spin is identified by two numbers k, i with $0 \leq k < z-1$ and $0 \leq i < N_{n-1}$ (N_n is the number of sites of $T_{n,z}$). Let us note π a strong labeling of $T_{n-1,z}$, and n_0 the root of the $(\frac{z-2}{2} - 1)$th copy of $T_{n-1,z}$. The following labeling is a strong labeling of $T_{n,z}$:

1. $(0,\pi(0)),\ (0,\pi(1)),\ldots,\ (0,\pi(N_{n-1}))$
2. $\ldots$
3. $(\frac{z-2}{2}-1,\pi(N_n)),\ (\frac{z-2}{2}-1,\pi(N_n-1)),\ldots,\ (\frac{z-2}{2}-1,\pi(n_0))$
4. 0
5. $(\frac{z-2}{2}-1,\pi(n_0-1)),\ (\frac{z-2}{2}-1,\pi(n_0-2)),\ldots,\ (\frac{z-2}{2}-1,\pi(0))$
6. $(\frac{z-2}{2},\pi(0)),\ (\frac{z-2}{2},\pi(1)),\ldots,\ (\frac{z-2}{2},\pi(N_{n-1}))$
7. $\ldots$
8. $(z-2,\pi(0)),\ (z-2,\pi(1)),\cdots,\ (z-2,\pi(N_{n-1}))$

Note that in step 1, 2, 7, and 8 any admissible permutation can be used instead of the strong labeling π. It is shown in [28] that the above labeling is indeed an optimal labeling and it can be used to implement a recursive algorithm to find a path between the two ferromagnetic states.

References

[1] For a pedagogical review of recursive structures see M.F. Thorpe in *Excitations in Disordered Solids (NATO Advanced Study Institute Series B*, ed. M.F. Thorpe (New York: Plenum, 1982), pp 85-107.

[2] C. Domb, *Adv. Phys.*, **9**, 145 (1960).

[3] e.g. R.J. Baxter, *Exactly Solved Models in Statistical Mechanics*, (Academic Press, London, 1982), Chapter 4.

[4] D.J. Thouless, P.W. Anderson and R.G. Palmer, *Phil.Mag.*, **35**, 593 (1977).

[5] D. Sherrington and S. Kirkpatrick, *Phys. Rev. Lett.*, **35**, 1792 (1975).

[6] D. Bowman and K. Levin, *Phys. Rev. B*, **25**, 3438 (1982).

[7] D.J. Thouless, *Phys. Rev. Lett.*, **56**, 1082, (1986).

[8] S. Katsura, *Prog. Theo. Phys.*, **87**, 139 (1986).

[9] J.T. Chayes, L. Chayes, J.P. Sethna and D.J. Thouless, *Comm. Math. Phys.*, **106**, 41 (1986).

[10] P. Mottishaw, *Europhys. Lett.*, 4, 333 (1987).

[11] Pik-Uin Lai and Y.Y. Goldschmidt, *J. Phys. A*, **22**, 399 (1989).

[12] J.M. Carlson, J.T. Chayes, L. Chayes, J.P. Sethna and D.J. Thouless, *Europhys. Lett.*, **5**, 355 (1988); *J. Stat. Phys.*, **61**, 987 (1990).

[13] J.M. Carlson, J.T. Chayes, J.P. Sethna and D.J. Thouless, *J. Stat. Phys.*, **61**, 1069 (1990).

[14] Y.Y. Goldschmidt, *Phys. Rev. B*, **43**. 8148 (1991).

[15] P.J. Gujrati, *Phys. Rev. Lett.*, **53**, 2453 (1984); *J. Chem. Phys.*, **98**, 1613 (1993).

[16] R.B. Stinchcombe, *J. Phys. C*, **6**, L1 (1973).

[17] R. Rammal, *J. Physique*, **46**, 1837 (1985); R. Rammal and A. Benoit, *J. Physique Lett.*, **46**, L-667 (1985); *Phys. Rev. Lett.*, **55**, 649 (1985).

[18] T.P. Eggarter, *Phys. Rev. B*, **9**, 2989 (1974).

[19] M. Matsuda, *Prog. Theor. Phys.*, **51**, 1053 (1974).

[20] J. von Heimburg and H. Thomas, *J. Phys. C*, **7**, 3433 (1974).

[21] E. Muller-Hartmann and J. Zittartz, *Phys. Rev. Lett.*, **33**, 893 (1974).

[22] R.J. Glauber, Jour. Math. Phys. 4, 294 (1963).

[23] L.P. Lévy, Phys. Rev. B 38, 4963 (1988).

[24] E. Marinari, G. Parisi and F. Ritort, preprint cond-mat/9410089.

[25] M. Kurata, R. Kikuchi and T. Watari, J. Chem Phys, 21, 434 (1953).

[26] C.N. Yang, T.D. Lee, Phys. Rev. 87, 404 (1952), T.D. Lee, C.N. Yang, Phys. Rev. 87, 410 (1952). See also K. Huang, *Statistical Mechanics*, Wiley, N.Y. (1963).

[27] R. Rammal, thèse d'état (1981).

[28] J. C. Anglès d'Auriac, M. Preissmann and A. Sebő submitted to Journal of Mathematics and Combinatorics (1995).

Chapitre 17

Article9

Magnetic field relaxation in ferromagnetic Ising systems[1]

R. Mélin

CRTBT-CNRS, 38042 Grenoble BP 166X cédex France

We study the magnetic field relaxation of various ferromagnetic Ising systems. Four models are considered: the square lattice with periodic boundary conditions, the square lattice on a disk with open boundary conditions, the Cayley tree and the hyperbolic lattice. We carry out the so-called *switching time experiments* and *switching field experiments* for these four models. We reach the conclusion that each of these models has a distinct behaviour with respect to magnetic field relaxation. Finally, we discuss possible links with recent experiments on magnetic grains. The hyperbolic lattice Ising model and the square lattice Ising model are candidates for an effective model for the boundary of magnetic grains.

[1]submitted to the Journal of Magnetism and Magnetic Materials.

17.1 Introduction

It has been shown recently in [1] that the ferromagnetic Ising model on a Cayley tree in a zero magnetic field exhibits glassiness below a temperature scale $T_g \sim J/\ln n$, where n is the number of generations. Since the number of generations is proportional to the logarithm of the number of sites, the glassy domain does not vanish in the macroscopic regime. Similar properties exist on hyperbolic lattices, with some deviations to the glass behaviour [2]. In the present paper, we wish to analyze the magnetic field relaxation for these models, as well as for euclidian models, for comparison. The physical quantities which we measure in our numerical experiments are inspired from the quantities experimentalists measure on magnetic monodomain grains at low temperature [3]. The typical size of the grains is $0.1\mu m$ x $0.05\mu m$, so that, due to dipolar interactions, anisotropy aligns the spins along the largest direction of the grain. The spins are essentially XY spins since the sample is essentially bidimensional. One possible experiment [3], which is called *switching time experiment*, consists in applying from time $t = 0$ a magnetic field opposite to the direction of the magnetization, and to measure the time τ_i for which the magnetization reverses in the experiment number i. Then, τ_i is considered as a statistical variable, and the histogram $P(\tau)$ is built. One possible analysis of the data [3] consists in integrating the histogram and fitting the integrated histogram by the stretched exponential

$$\int_0^\tau P(\tau')d\tau' \simeq 1 - \exp\left(-\left(\frac{\tau}{\tau_0}\right)^{\beta'}\right). \tag{17.1}$$

The stretched exponent is noted β' instead of β in order to avoid confusion with an other exponent that will be introduced later and will be denoted β. An other possible experiment is the *switching field experiment* in which a magnetic field opposite to the averaged magnetization is switched on at a given rate. The magnetic field $\langle H_{sw}(T,\nu)\rangle$ for which the magnetization cancels is measured for various temperatures T and switching rates ν. A possible fit exists [4] that predicts the existence of a master curve for $\langle H_{sw}(T,\nu)\rangle$. The phenomenological arguments of [4] were originally developed in the context of domain wall junctions, but are also applicable to magnetic systems. One of the aim of the present article is to determine to which model the phenomenological model of [4] is applicable.

Eventhough magnetic grains are a candidate for macroscopic quantum tunneling [5], it would be first interesting to understand the effects related to thermally activated processes. Eventhough the models that we study are far from a realistic modeling of magnetic grains, even without quantum aspects, it is interesting to clarify their behaviour as far as the magnetic field induced magnetization relaxation is considered. We want to submit different ferromagnetic Ising spin systems with different lattices and boundary conditions to the two types of magnetic field relaxation experiments that experimentalists carry out on magnetic grains [3]. We shall consider successively square lattices with various boundary conditions, trees and hyperbolic lattices. As mentionned earlier, the zero field behaviour of trees and hyperbolic lattices was only studied recently. It is clear that, in the switching time/field experiments, the phase which is antiparallel to the field at time $t > 0$ is metastable, and that switching time/field experiments are devoted to explore the barrier structure between the initial phase where the spins are aligned antiparallel to the field and the final state, where the spins are parallel to the field. As far as euclidian lattices are concerned, we evaluate the bariers in the case of a free boundary, and in the case of an Ising model with periodic boundary conditions. The barriers are found to be smaller in the case of a free boundary than in the case of periodic boundary conditions, since,

in the first case, droplets of spins parallel to the field can nucleate from the boundary. In the presence of corners, we exhibit a regime where the droplets nucleate from the corners. We study in more details the switching field experiment in the case of the square lattice with periodic boundary conditions, as an exemple of what is going on in euclidian spaces with no boundary. The relaxation is found to agree with some predictions from slow relaxation theories [6], even though these theories are dedicated to the zero field case, namely $P(\ln \tau)$ is gaussian and the variance $\langle (\ln \tau_i - \langle \ln \tau_i \rangle)^2 \rangle$ is linear as a function of the mean value $\langle \ln \tau_i \rangle$. The exponent β' of the stretched exponential (17.1) is found to increase with temperature. The fit of reference [4] does not work in this case, that is it is not possible to find a master curve for $\langle H_{sw}(T, \nu) \rangle$.

We also studied the case of a square lattice with a circular boundary. By constrast to the case of the periodic lattice with periodic boundary conditions, we find the existence of a master curve following the fit of reference [4].

As far as Cayley trees are considered, we first study the relaxation of the autocorrelation $q(t)$ above the glass cross-over temperature in the absence of a magnetic field. The shape of $q(t)$ can be fitted by stretched exponential. The stretched exponent β is less than unity and increases with temperature, as in the case of the three dimensional Ising glass [7]. We also study the magnetic field relaxation at low temperatures. Contrary to the case of the square lattice, no loops are present, so that it is difficult for a droplet of spins parallel to the field to propagate through the structure. The exponent β' is found to be of the order of 19, and does not vary significantly in the range of temperature we consider. As in the case of the tree, we find good agreement with the predictions from slow relaxation theories [6] without magnetic field: $P(\ln \tau)$ is gaussian and the variance $\langle (\ln \tau_i - \langle \ln \tau_i \rangle)^2 \rangle$ is linear as a function of the mean value $\langle \ln \tau_i \rangle$.

In the hyperbolic lattice case, the exponent β' is found to increase with temperature, as in the case of euclidian lattices. However, our results show that the hyperbolic lattice Ising model is not properly described by the zero magnetic field slow relaxation theories [6]. Eventhough the shape of $P(\ln \tau)$ is gaussian, the mean value $\langle \ln \tau_i \rangle$ is non linear as a function of the variance $\langle (\ln \tau_i - \langle \ln \tau_i \rangle)^2 \rangle$.

17.2 Euclidian lattices

17.2.1 Square lattice with periodic boundary conditions

We study the relaxation of the magnetization, under an external applied field, with a direction opposite to the initial magnetization. This model was already considered in [8], where it is shown that many regimes are possible, according to the strength of the magnetic field and the system size. If the field is larger than a certain field scale, we are in the *strong field regime*, where the magnetization reverses rapidly, at time scales of the order of one Monte Carlo Step per Spin. If the field decreases, three regimes are distinguished, according to the system size. For the smallest sizes, the system is in the *coexistence region*, where the up and down phases coexist. For intermediate sizes, one droplet is nucleated and finally invades the entire system. This is the *single droplet regime*. For large sizes, the system is in the *multi droplet regime*. Several droplet coexist and grow. The time scales in Monte Carlo Step per Spin for the magnetization reversal in the multi droplet regime are smaller than in the single droplet regime.

In order to have an idea of the barriers, we calculate the barrier $E_1(R)$ associated to the nucleation of a circular domain of spins parallel to the field. This calculation is only an approxima-

tion, since the droplets are not exactly circular. The barrier is given by $E_1(R) = 2\pi R(2J - hR)$. The first term $4\pi RJ$ is the energy term associated to the antiparallel links at the boundary and $-2\pi hR^2$ is the magnetic energy. $E_1(R)$ is maximum for $R_1^* = J/h$, which corresponds to the critical size of the domain. If $R < R_1^*$, the domain has a trend to regress whereas it naturally grows if $R > R_1^*$. The barrier height is $E_1(R_1^*) = 2\pi J^2/h$. We shall compare these results to the case of a square lattice with free boundary conditions.

In order to describe the distribution of relaxation times, we call τ_i the time for which the magnetization cancels in a given numerical experiment. Of course, τ_i varies from one experiment to the other, since the escape process is stochastic. The theory of slow relaxation processes in zero external field [6] predicts a gaussian distribution of $\ln \tau_i$. The histogram of $\ln \tau_i$ is represented on figure 17.1 for two different temperatures, and the shape of $P(\ln \tau)$ is indeed gaussian. Moreover, according to slow relaxation theories in a zero magnetic field [6], the average $\langle \ln \tau_i \rangle$ is proportional to the variance $\langle (\ln \tau_i - \langle \ln \tau_i \rangle)^2 \rangle$. As shown on figure 17.2, this is indeed the case. However, we underline the fact that the model [6] has been established in a zero magnetic field, and it is not obvious that it should work in the presence of a magnetic field. Nonetheless, it is interesting to study $\langle \ln \tau_i \rangle$ as a function of $\langle (\ln \tau_i - \langle \ln \tau_i \rangle)^2 \rangle$ in the presence of a magnetic field, eventhough the correspondence with the zero field case has not been established to our knowledge.

An other way to characterize the distribution of relaxation times is to integrate the histogram $P(\tau)$ and to fit the integrated histogram by a stretched exponential $1 - \exp\left(-(\tau/\tau_0)^{\beta'}\right)$. This method is used in the analysis of experimental data of the reversal of magnetic grains [3]. In the case of a square lattice with periodic boundary conditions, the exponent β' is found to increase with temperature, as plotted on figure 17.3.

An other possible numerical experiment is the so-called *switching field experiment*. The idea is to start form a low temperature phase, and to switch a field oppposite to the global magnetization. The field increases linearly with a rate $\nu = -dH/dt$. In the presence of the external field, the magnetization reverses and one measures the magnetic field H_{sw} for which the magnetization cancels. The switching field H_{sw} is averaged over a large number of runs, and computed for various temperatures. In order to analyze the data, we use the phenomenological model of reference [4]. In this model, the average switching field is given by

$$\langle H_{sw} \rangle = H_{sw}^0 \left(1 - f_\alpha(T, \nu)\right), \tag{17.2}$$

with

$$f_\alpha(T, \nu) = \left(\frac{k_B T}{E_0} \ln\left(\frac{cT}{\nu \epsilon^{\alpha - 1}}\right)\right)^{1/\alpha} \tag{17.3}$$

H_{sw}^0, E_0 and c are some constants, $\alpha = 2$ for an ideal single domain model and

$$\epsilon = (1 - H_{sw}/H_{sw}^0)^{1/\alpha}. \tag{17.4}$$

The experimental data consist of $\langle H_{sw} \rangle (T, \nu)$ as a function of the temperature T and the switching rate ν. The relation (17.2) predicts the existence of a master curve for $\langle H_{sw} \rangle (T, \nu)$. We carried out numerical simulations for the square lattice with periodic boundary conditions and tried to fit our data with equation (17.2). We come to the conclusion that the master curve does not exist for the square lattice with periodic boundary conditions, so that the fit (17.2) is not valid in the case of the periodic square lattice.

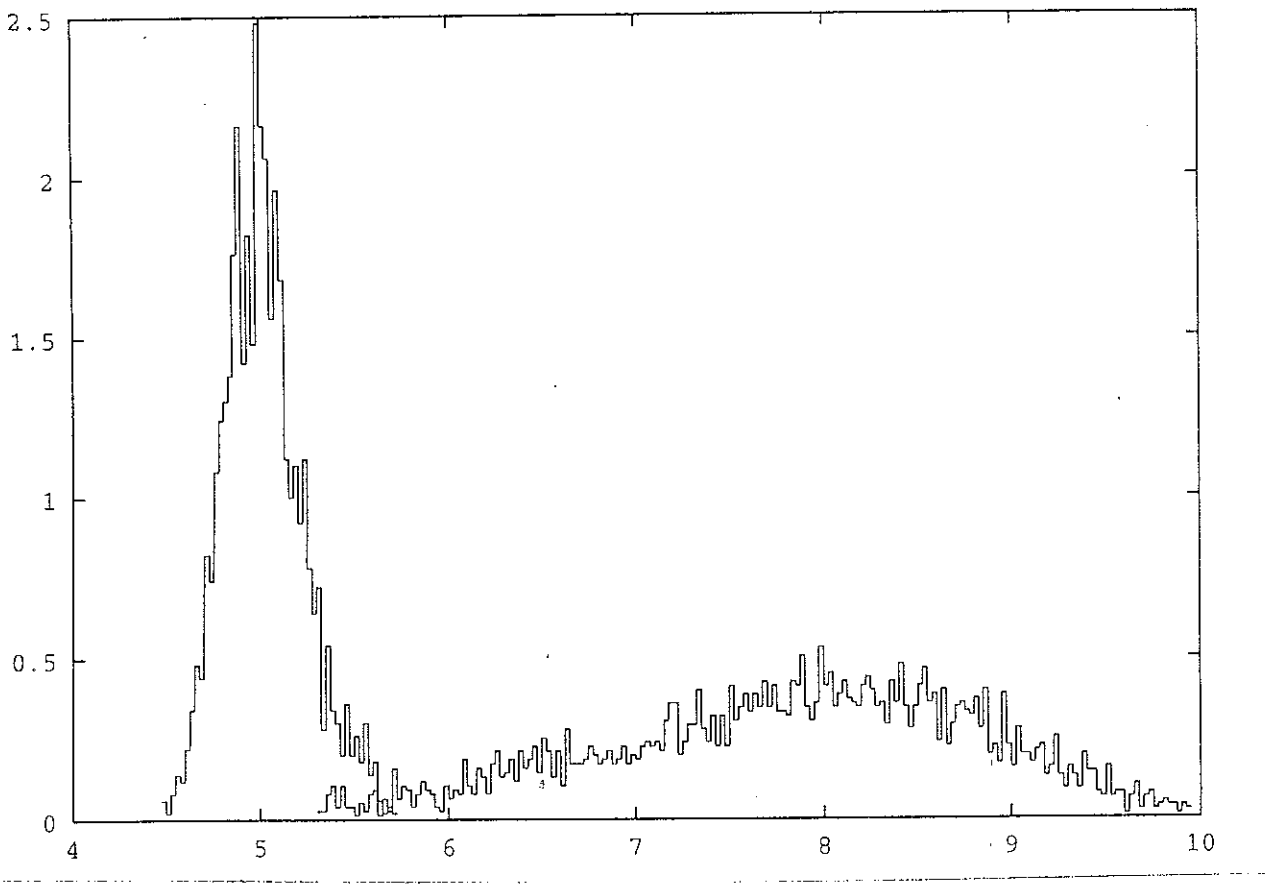

Figure 17.1:
Histogram of the logarithm of the times for which the magnetization cancels, for a periodic square lattice of size 90x90. The exchange constant J is taken equal to unity. The inverse temperature is $\beta = 1.3$ and $\beta = 1.6$. A magnetic field $h = -1$ is applied from time $t = 0$.

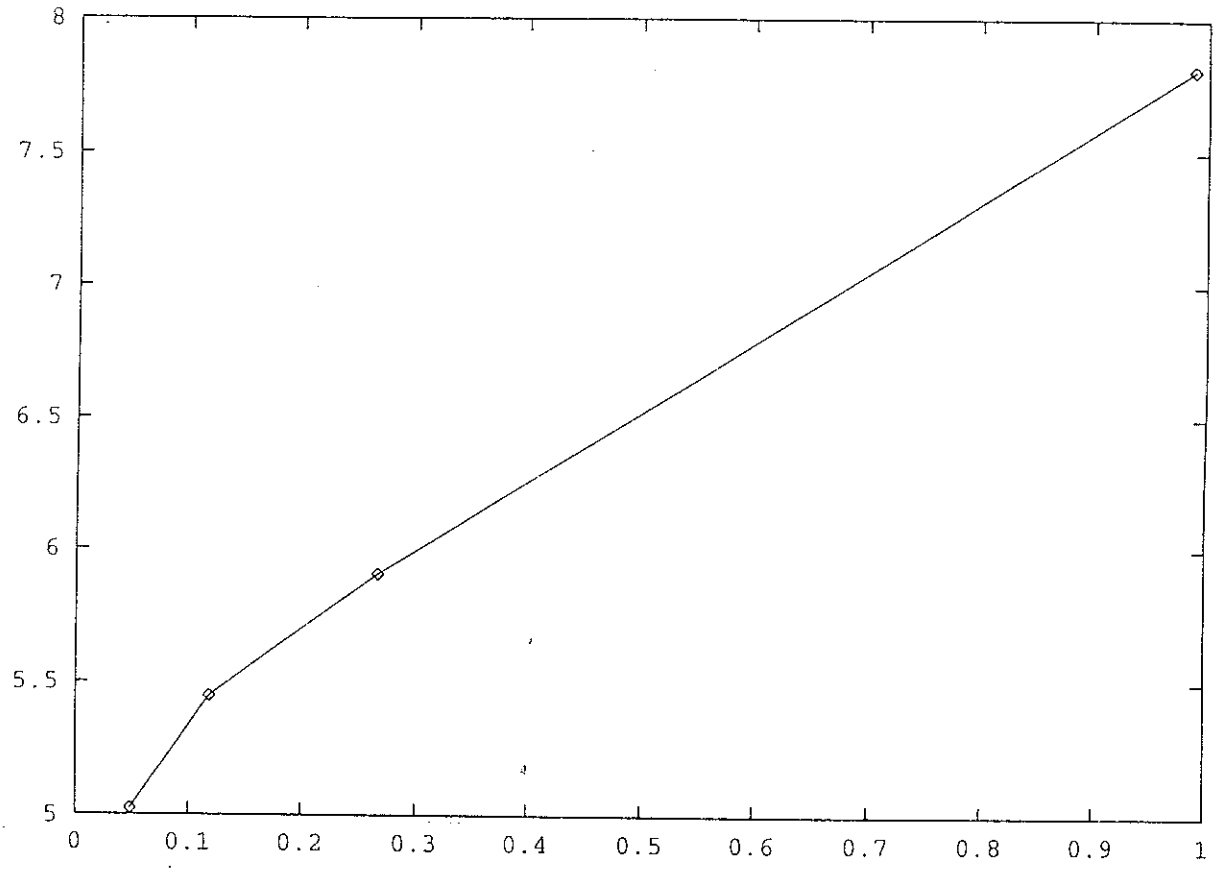

Figure 17.2:
Average logarithm of the relaxation times $\langle \ln \tau_i \rangle$ as a function of the variance $\langle (\ln \tau_i - \langle \ln \tau_i \rangle)^2 \rangle$ for the square lattice with periodic boundary conditions. The size of the lattice is 90x90. A magnetic field $h = -1$ is applied from time $t = 0$, with $J = 1$. The variations are compatible with a linear dependence.

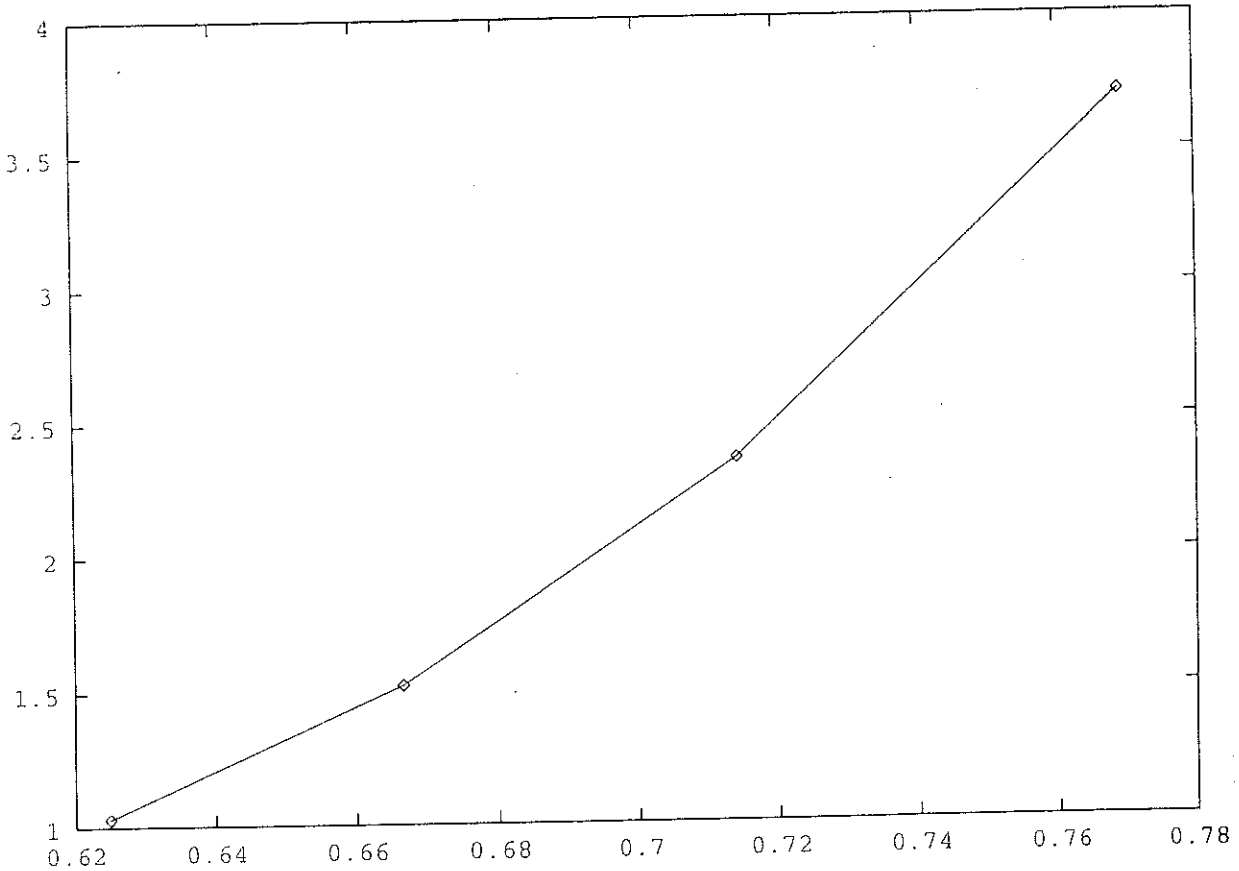

Figure 17.3:
Variations of the exponent β' as a function of temperature in the case of the square lattice with periodic boundary conditions. The size of the lattice is 90x90. A magnetic field $h = -1$ is applied from time $t = 0$, with $J = 1$.

17.2.2 Square lattice with free boundary conditions

In order to emphasize the importance of the boundary conditions, we study the relaxation of the magnetization in an external field. If we compare the relaxation in the periodic and the open case, we find that the reversal of magnetization is easier in the open case for comparable temperatures. The reason is that domains of reversed spins can nucleate from the boundary, whereas in the case of periodic boundary conditions, one has first to nucleate sufficiently large domains, and then, if the size of the nucleated domain is large enough, the propagation is very fast. In order to understand the reason why the relaxation is easier in the case of free boundary conditions than in the case of periodic boundary conditions, we calculate the energy cost $E_2(R)$ to nucleate a half circular domain of $N = \pi R^2/2$ spins parallel to the field. We find that $E_2(R) = \pi R(2J - Rh)$. $E_2(R)$ is maximum for $R_2^* = J/h$, and the barrier is $E_2(R_2^*) = J^2/h$. The barrier $E_2(R_2^*)$ is twice the barrier $E_1(R_1^*)$. In the presence of an edge, the barrier reads $E_3(R) = \pi R(J - hR/2)$, which leads to $E_3(R_3^*) = \pi J^2/2h$, smaller than $E_2(R_2^*)$. We conclude that the spin system is very sensitive to the presence of edges and will first flip from the edges, at least if the magnetic field is not too strong. To see this, we took a snapshot of the system during a given run. The result is pictured on figure 17.4. It is clear that the edges play an important role in the magnetization reversal, since the droplets are pinned at the edges, where the energy barrier is smaller than in the bulk. The pinning of the droplets is here purely geometric. One could also imagine that the droplets are pinned due to the presence of impurities.

In order to eliminate the effect of edges, we studied the case of a square lattice on a disk, so that no edges are present. We carried out the same simulations than in the periodic boundary case, namely the switching time and switching field experiments. We begin with the switching time experiment. The average $\langle \ln \tau_i \rangle$ is plotted on figure (17.5) as a function of the variance $\langle (\ln \tau_i - \langle \ln \tau_i \rangle)^2 \rangle$. The variations are approximately linear. The exponent β' of the fit (17.1) is found to increase with temperature, as pictured on figure 17.6.

Contrary to the case of the square lattice with periodic boundary conditions the fit of equation (17.2) is found to work, that is there exists a master curve for $\langle H_{sw}(T, \nu) \rangle$. The master curve is plotted on figure 17.7.

17.2.3 Square lattice with fixed boundary conditions

We consider the situation where the spins of the boundary are frozen. Initially, the bulk spins have the same direction as the boundary and one applies an opposite field from time $t = 0$. For a finite size system, there is a competition between the boundary which tends to align the spins antiparallel to the field, and the magnetic field, so that for sufficiently small fields, the boundary imposes its magnetization whereas in the strong field regime, the spins are parallel to the field. We tested this idea for an anisotropic sample (in order to approach the shape of some magnetic grains), and computed the mean time for which the magnetization cancels, as a function of the magnetic field. The result is plotted on figure 17.8. If the magnitude of the external field is large enough, the magnetization reverses whithin a finite time.

17.3 Cayley Tree

The tree we consider in this section is built from a center at generation 0. This center gives rise to three sons at generation 1. The sons have two children, etc. The process is stopped

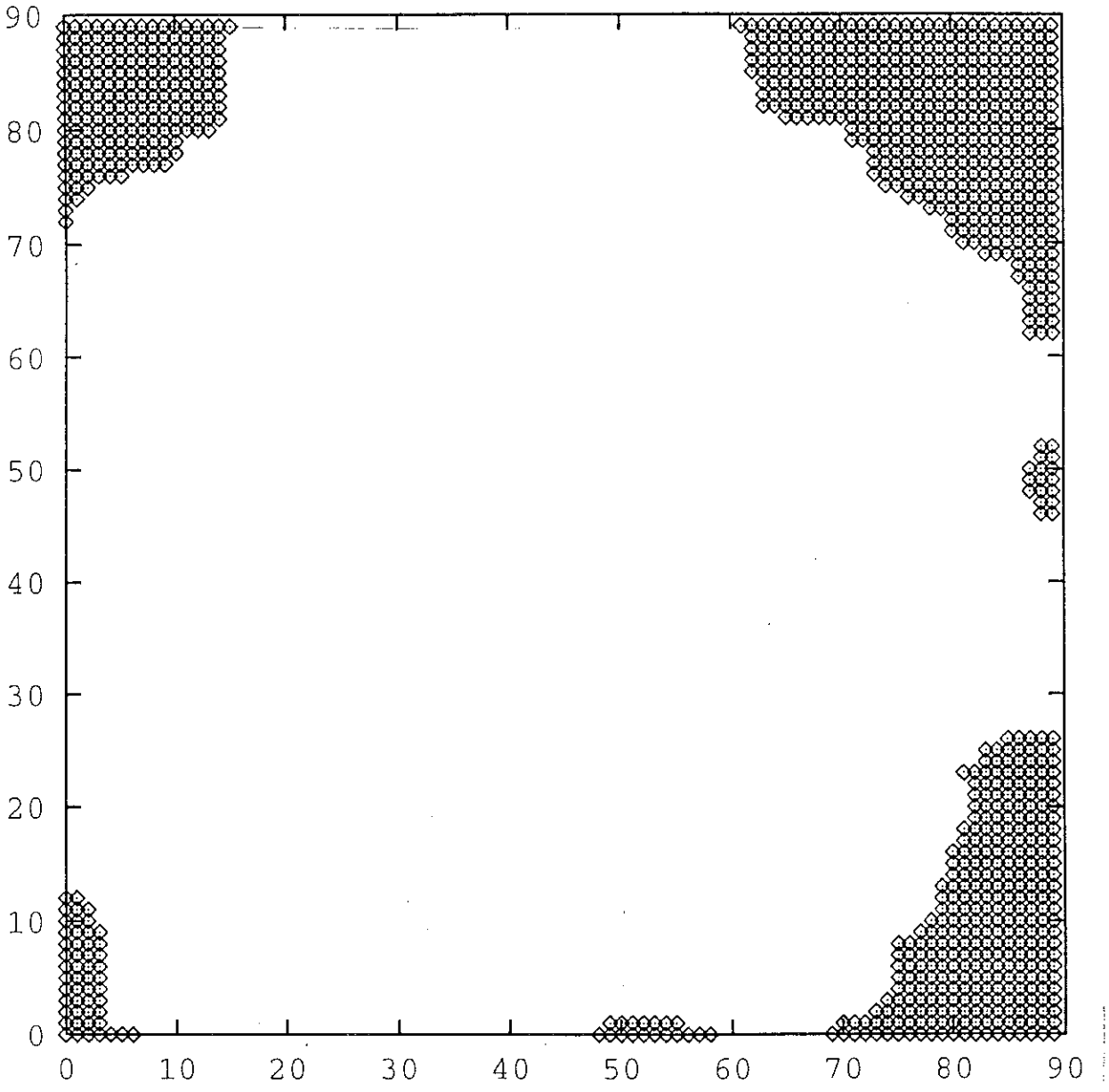

Figure 17.4:
Snapshot of the spin configuration in a given numerical experiment, in the case of a 90x90 square lattice. The magnetization is equal to 3/4. The inverse temperature is $\beta = 1.6$, and the applied magnetic field is $h = -1$, with $J = 1$. A symbol denotes a down spin (parallel to the field) and the spin is up in the absence of symbol. The droplets are pinned at the corners.

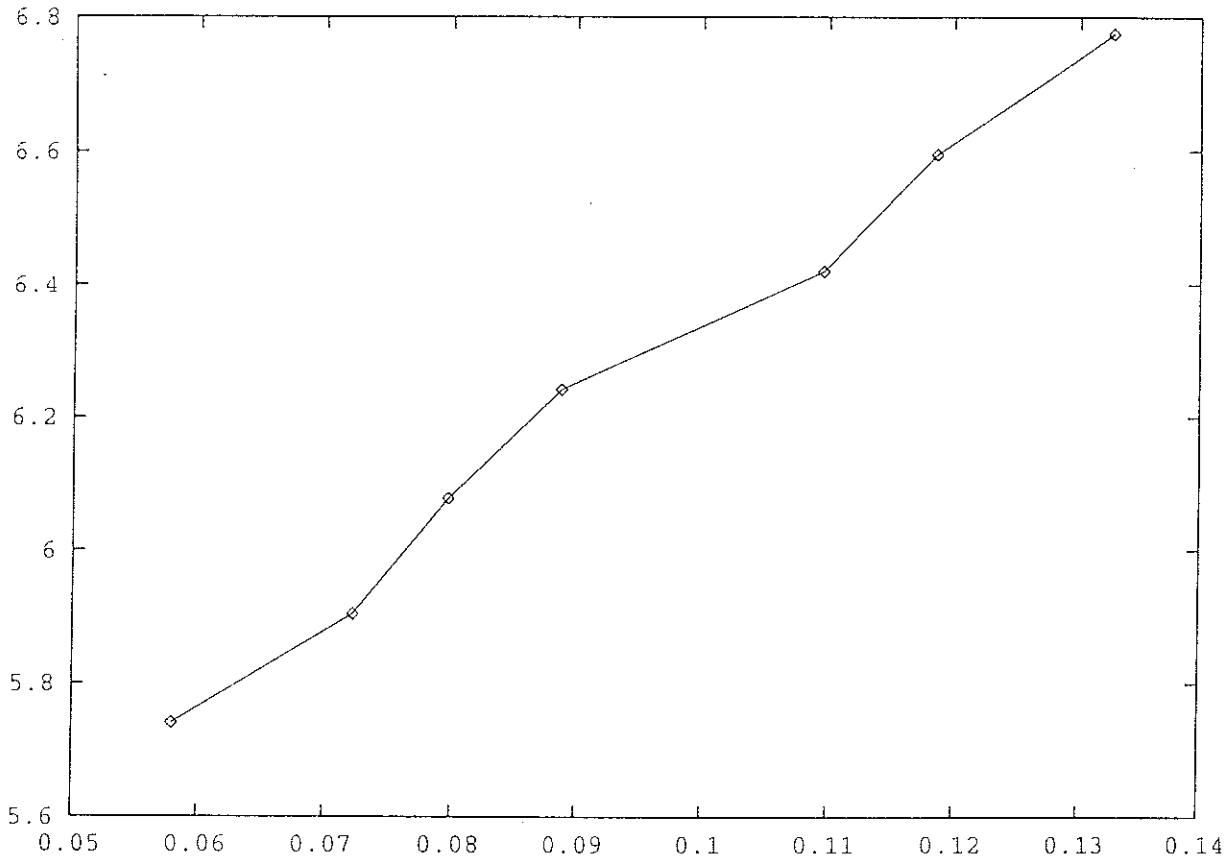

Figure 17.5:
Average logarithm of the relaxation times $\langle \ln \tau_i \rangle$ as a function of the variance $\langle (\ln \tau_i - \langle \ln \tau_i \rangle)^2 \rangle$ for the square lattice on a disk. The number of sites is 2821. A magnetic field $h = -1$ is applied from time $t = 0$, with $J = 1$. The variations are compatible with a linear dependence.

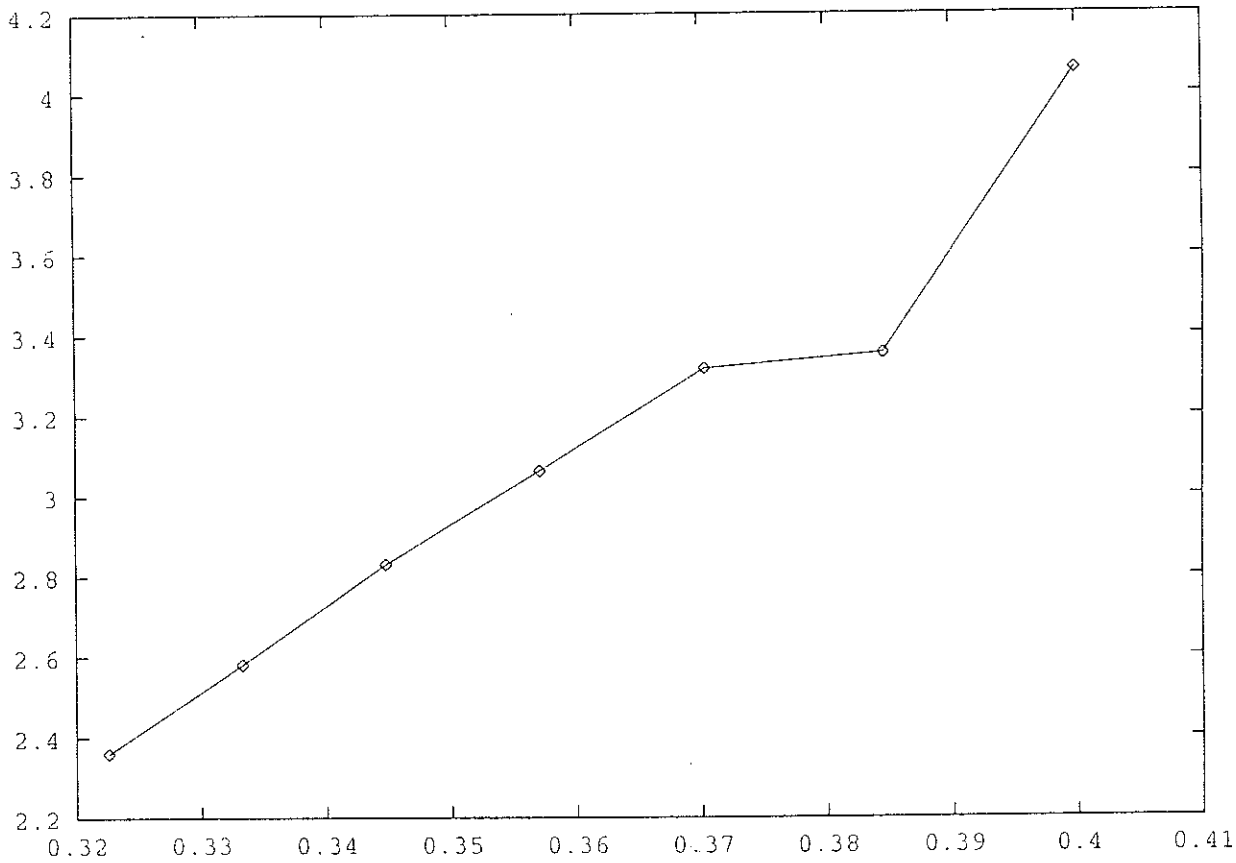

Figure 17.6:
Variations of the exponent β' as a function of temperature in the case of the square lattice on a disk. The number of sites is 2821. A magnetic field $h = -1$ is applied from time $t = 0$, with $J = 1$.

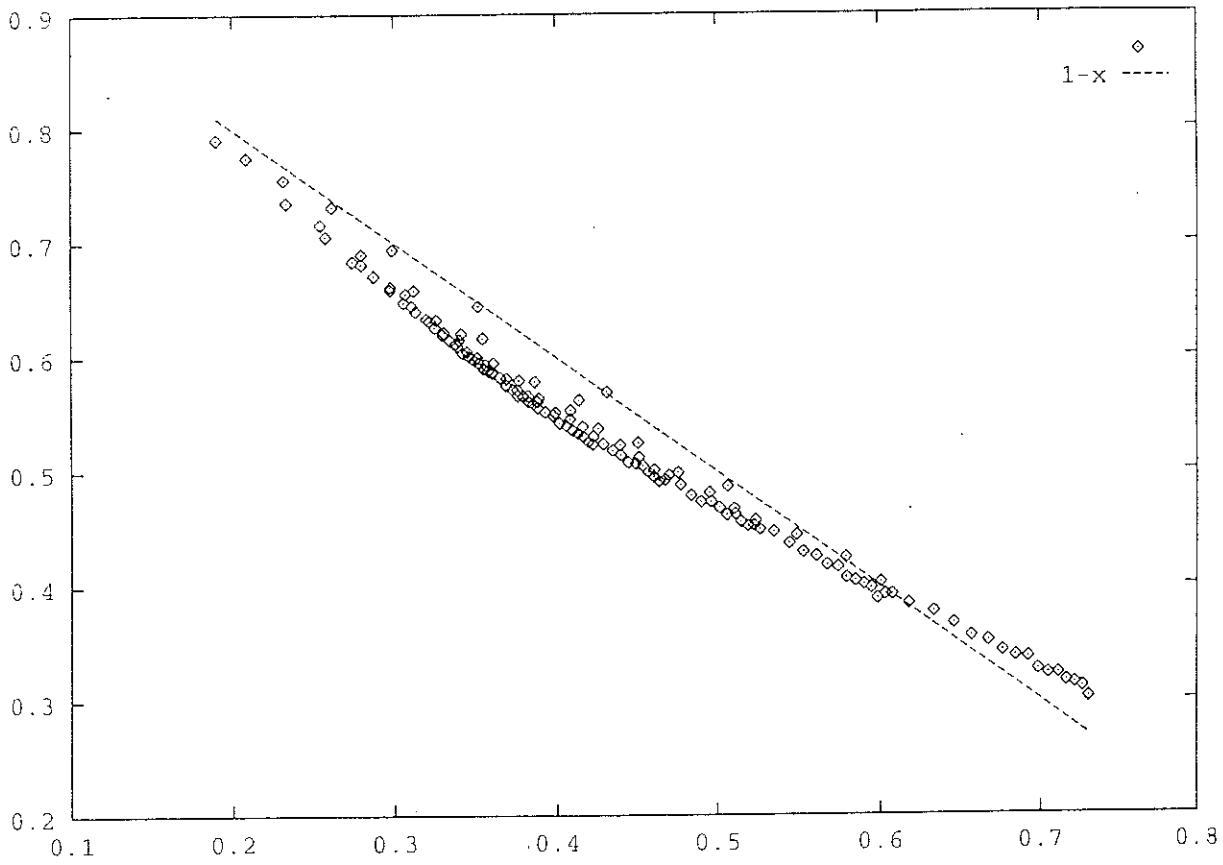

Figure 17.7:
Master curve of the switching field experiment for the square lattice on the disk. We plotted $\langle H_{sw}\rangle / H^0_{sw}$ as a function of $f_\alpha(T,\nu)$. The Boltzmann constant is equal to unity, $\alpha = 1.8$, $H^0_{sw} = 2.4$,$E_0 = 5$ and $c = 1/25$. On this curve, 7 series of measures at 7 different temperatures are superposed. The linear behaviour corresponds to $\langle H_{sw}\rangle / H^0_{sw} = 1 - f_\alpha(T,\nu)$.

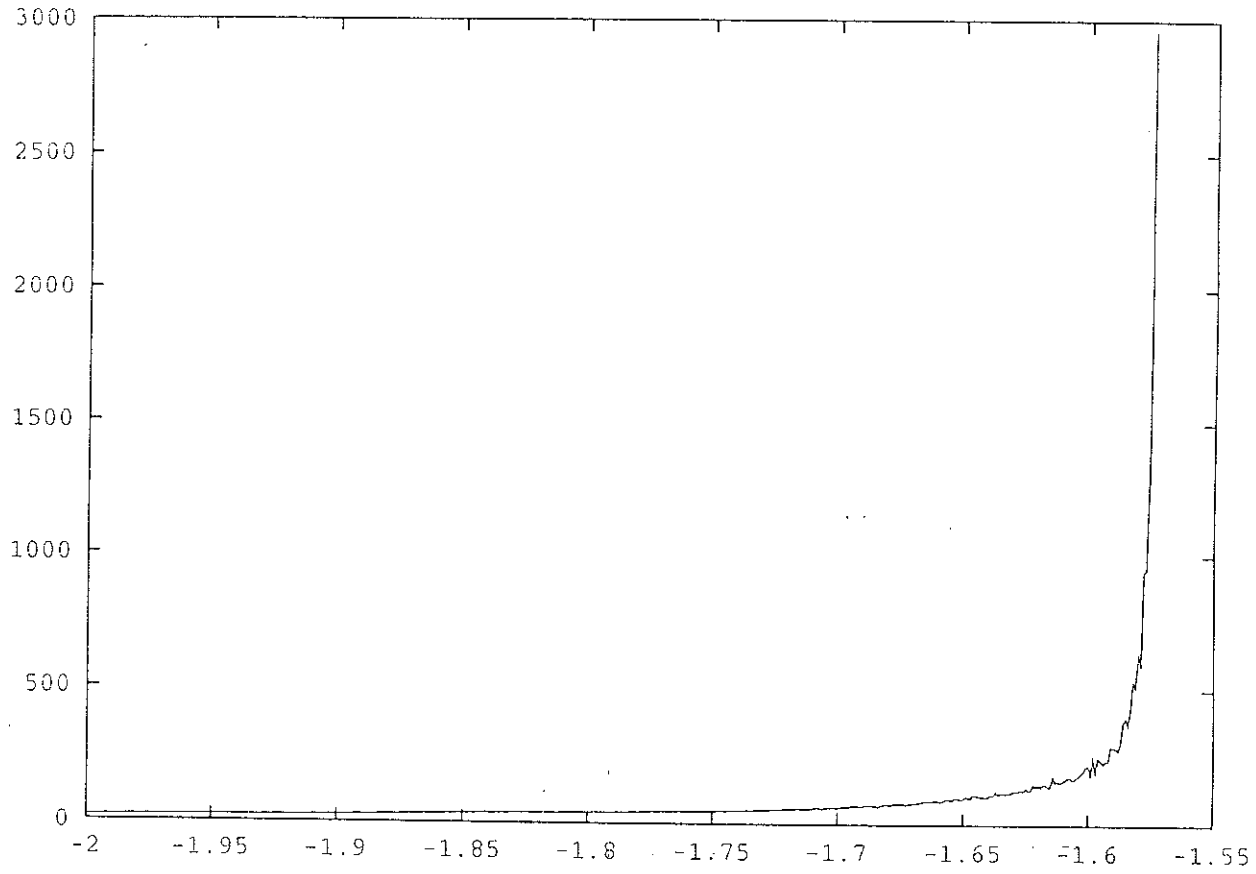

Figure 17.8:
$\langle \tau_i \rangle$ as a function of the magnetic field, in the presence of fixed boundary conditions. τ_i is the time for which the magnetization cancels. At time $t = 0$, the bulk spins are parallel to the boundary spins, and a magnetic field h is switched on from time $t = 0$. The inverse temperature is $\beta = 2$. The averages are taken over 50 runs. The sample has a size 40x200.

at the n-th generation, so that one obtains a finite tree called a Cayley tree. Eventhough the bulk properties of the tree were studied as soon as the 30's as a way to implement mean field calculations [11] [12], the thermodynamics of the tree with its boundary was only studied in the 70's, and people discovered an unusual continuous transition [13] [14]. However, the notion of glassy dynamics merely emerged, and the dynamical problem was only considered recently for Ising spins [1] and XY spins [16]. The Ising model on a tree is glassy below a certain temperature $T_g \sim J/\ln n$, where n is the number of generations [1]. This glassy behaviour can be seen on various thermodynamical properties [1], such as the shape of the magnetization distribution, the density of Lee and Yang zeros in the vicinity of $\exp 2\beta h = 1$. The zero temperature barriers scale like $J \ln n$, where n is the number of generations. Glassiness is also visible from the structure of the eigenvalues of the Glauber matrix, from the waiting time dependence of the autocorrelation functions, and from the behaviour of the dynamical susceptibility χ_1' and χ_3', which behave like in spin glasses. It is thus interesting to study the slow relaxation processes in this model, and to compare with the predictions of the general models for slow relaxation processes. We study the relaxation of two quantities. First, we consider the relaxation of the autocorrelation functions in the absence of a magnetic field. The autocorrelations are fitted by a stretched exponential with an exponent β which is a function of temperature. Second, we consider the relaxation of the magnetization in the presence of a magnetic field. The histogram of relaxation times is also fitted by a stretched exponential, with a temperature dependent stretched exponent β'. We underline the fact that β and β' are distinct quantities. In particular β is less than unity, whereas β' can be larger than unity.

17.3.1 Relaxation of the autocorrelation in a zero field

The autocorrelation function $q(t)$ is defined as

$$q(t) = \frac{1}{N} \sum_{i=1}^{N} \left(\langle \sigma_i(0)\sigma_i(t) \rangle - \langle \sigma_i(0) \rangle \langle \sigma_i(t) \rangle \right). \tag{17.5}$$

The Edwards-Anderson parameter is $q_{EA} = q(\infty)$. The autocorrelation functions are plotted on figure 17.9 for various temperatures. In reference [7], these autocorrelations are fitted by

$$q(t) \sim \frac{1}{t^x} \exp\left(-(\frac{t}{\tau})^\beta \right) \tag{17.6}$$

in the non glassy phase (then $q_{EA} = 0$). We tried this fit in our case, using an optimisation algorithm, with one linear adjustable parameter, and three non linear adjustable parameters. Unfortunately, the optimisation procedure converges only at low temperatures. This lack of convergence is attributed to the fact that the precision of our data is not good enough. It is clear that the data of [7] are more acurate that ours, but our goal here is more qualitative. To get an order of magnitude for the exponent β, we fit the autocorrelation $q(t)$ by

$$q(t) \sim \exp\left(-(\frac{t}{\tau})^\beta \right). \tag{17.7}$$

The variations of the approximate exponent β as a function of temperature are plotted on figure 17.10. It is clear that β increases with temperature and is less than unity. These properties are in agreement with numerical experiments on Ising spin glasses [7]. In the case of the Ising

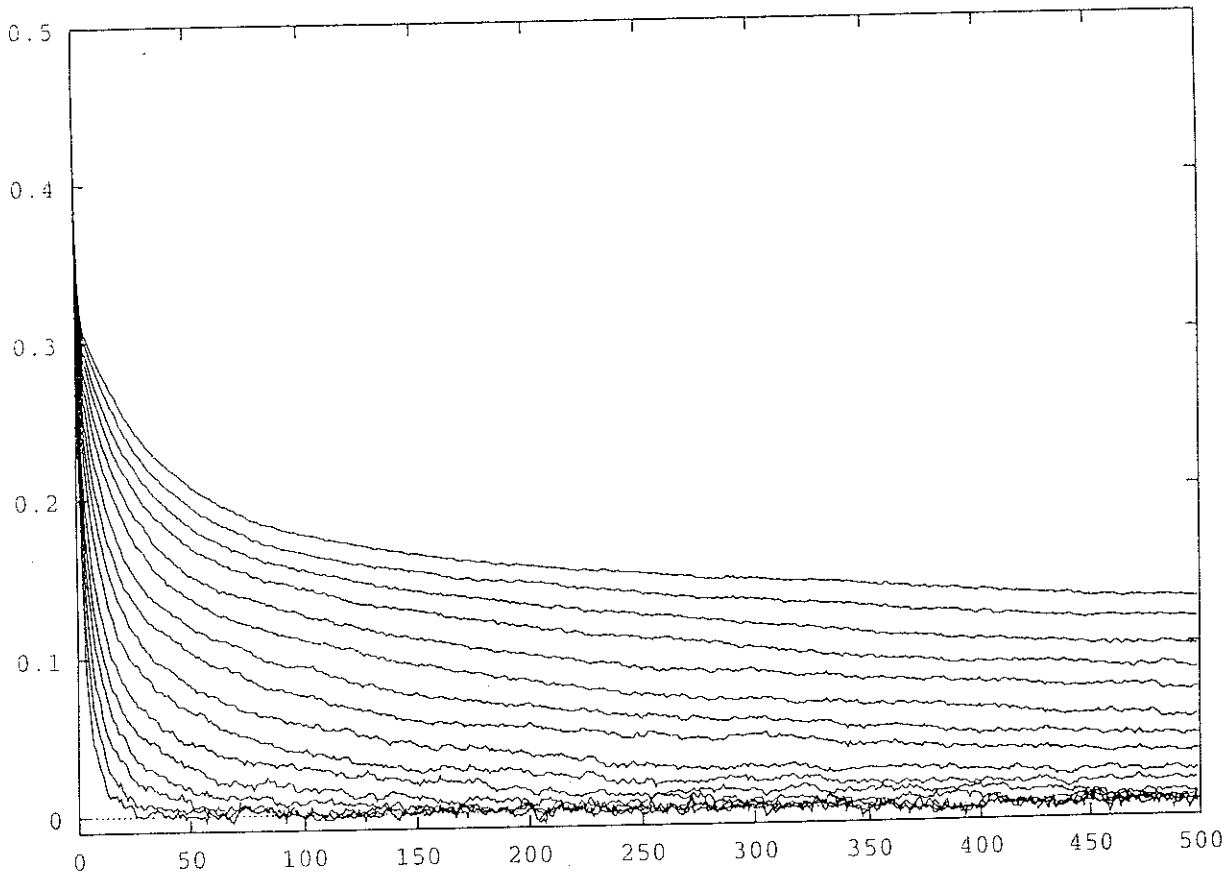

Figure 17.9:
Autocorrelation function $q(t)$ for various temperatures. The inverse temperatures are $\beta = 0.6, 0.7, ..., 2$ from the lower plot to the upper one.

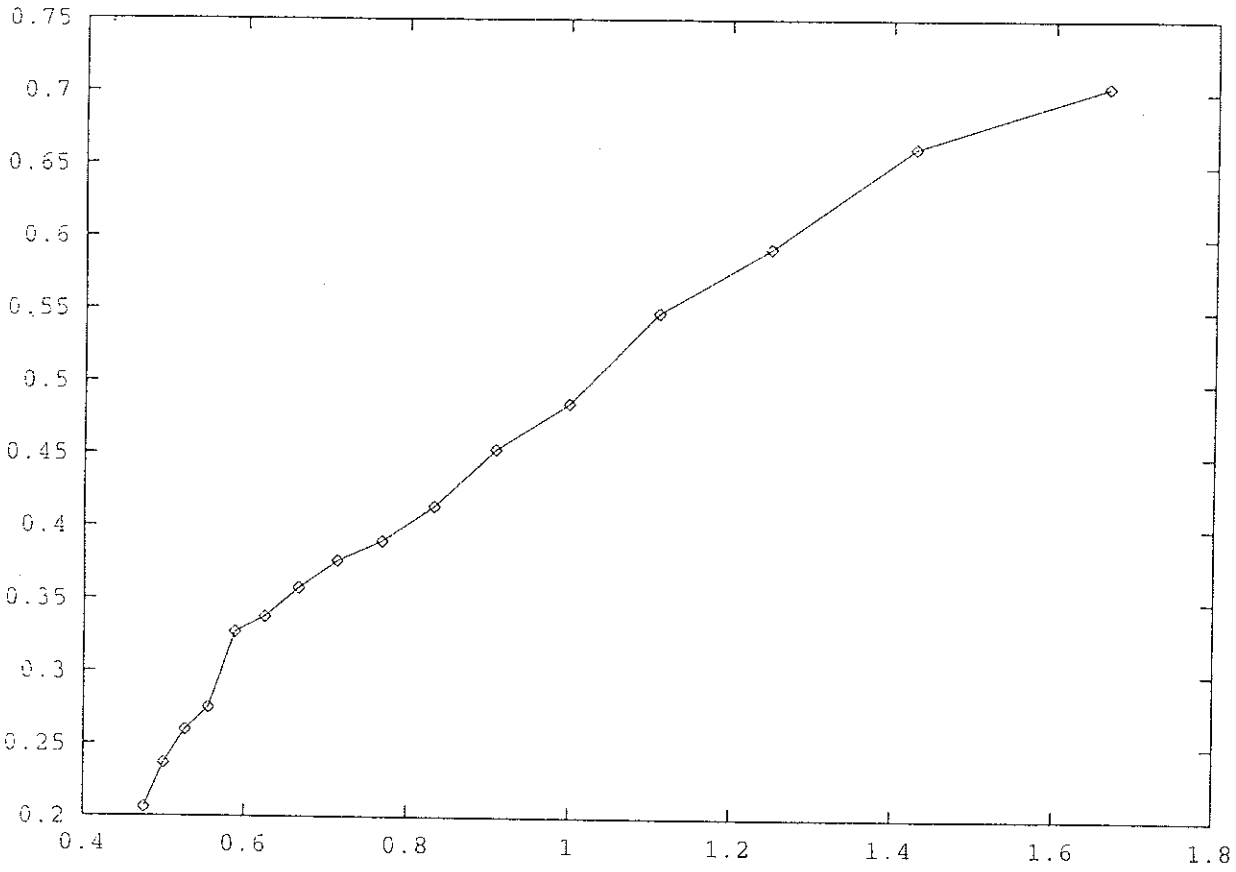

Figure 17.10:
Variations of the exponent β of the stretched exponential (17.7) as a function if temperature for a tree with 10 generations.

spin glass, the temperature T_c which corresponds to $\beta(T_c) = 1$ is the Curie point of the non random Ising model. In the case of the Ising Cayley tree model, one expects that $\beta(T_c) = 1$, where T_c is the bulk transition temperature, that is, above the bulk transition temperature, the relaxation is purely exponential. By extrapolation, we find that $\beta(2.3) = 1$ whereas the bulk transition temperature is $T_c = 1.82$. The temperature 2.3 for which $\beta = 1$ is clearly too large. But it is not surprising because we neglected the power law prefactor in (17.6). At high temperatures, the exponent x increases, so that our estimation of β is underevaluated, leading to an overevaluation of the temperature above which $\beta = 1$. This behaviour is to be compared with the results of Ogielsky [7] who finds that, in the three dimensional Ising spin glass with short range interations, the relaxation is exponential above the Curie point of the non random Ising model.

17.3.2 Magnetization relaxation in a magnetic field

In the same way as for the square lattices with periodic and open boundary conditions, we study the statistics of the time τ_i which correspond to the change of sign in the magnetization. Like the case of the square lattice with periodic or open boundary conditions, the shape of $P(\ln \tau)$ is gaussian, as plotted on figure 17.11. The variance $\langle (\ln \tau_i - \langle \ln \tau_i \rangle)^2 \rangle$ plotted as a function of the mean value $\langle \ln \tau_i \rangle$ has approximately a linear dependence, as shown on figure 17.12.

The streched exponent β' is of order of 19 and does not vary significantly with temperature.

An other way to analyze the distribution of relaxation times is to study the time dependence of the magnetization with respect to the variable $\ln t$. If one assumes a distribution of relaxation times $P(\ln \tau)$, then the magnetization reads [6]

$$M(t) \sim \int e^{-t/\tau} P(\ln \tau) d \ln \tau. \tag{17.8}$$

The exponential can be taken as a cutoff in log scales, and one obtains [15]

$$M(t) \sim \int_{\ln t}^{+\infty} P(\ln \tau) d \ln \tau, \tag{17.9}$$

so that

$$P(\ln \tau) \sim -\frac{dM(t)}{d \ln t}. \tag{17.10}$$

The derivative of $M(t)$ with respect to $\ln t$ thus yields the distribution of relaxation times. For the tree, the result for $P(\ln \tau)$ is plotted on figure 17.13. Compared to a gaussian shape, the distribution of relaxation times is too large for small relaxation times. Compared to the direct computation of the probability of relaxation times of figure 17.11, we find that the direct computation does not lead to an overestimation of the probability of relaxation times for small values of the relaxation times. We deduce that this overestimation for small relaxation times is not a property of the model, but is inherent to the method which consists in deducing the distribution of relaxation times from $-dM(t)/d \ln t$. We have carried out this test on the case of the Cayley tree, but we could have chosen any of the other models as well.

We also carried out switching field experiments. Contrary to the case of the square lattice with periodic boundary conditions, we find that the phenomenological model (17.2) is valid in this case. The master curve is plotted on figure 17.14.

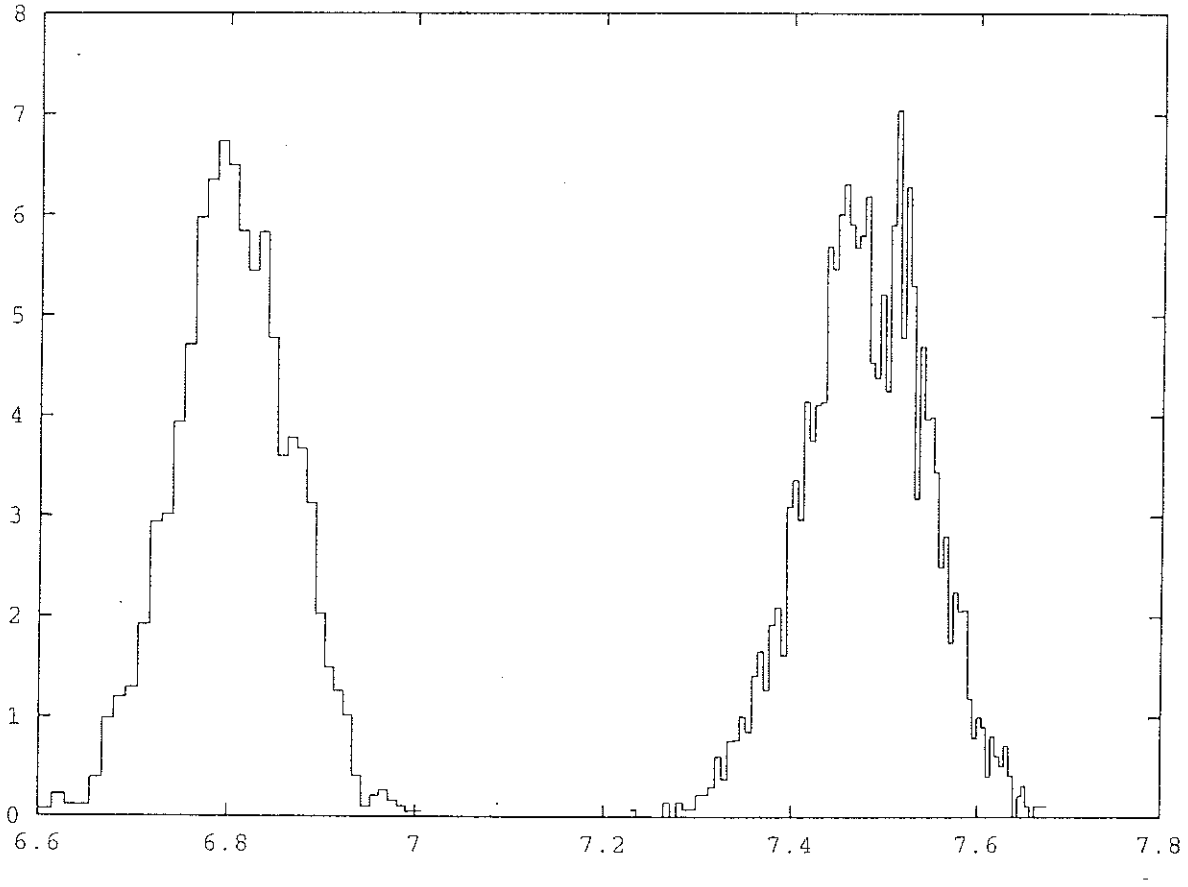

Figure 17.11:
Histogram of the times for which the magnetization cancels $P(\ln \tau)$, for a tree with 10 generations. The exchange constant J is taken equal to unity. The inverse temperature is $\beta = 2.75$ and $\beta = 3$. A magnetic field $h = -0.3$ is applied from time $t = 0$.

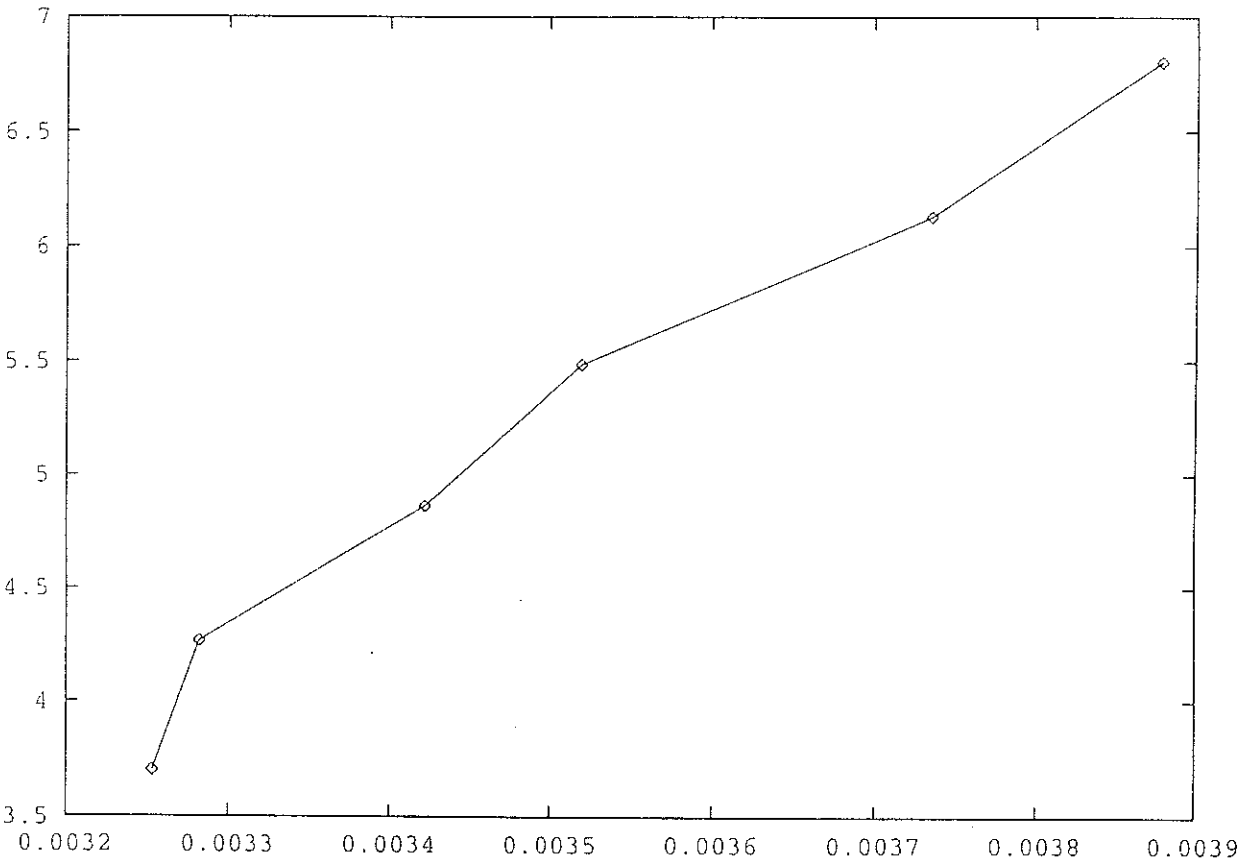

Figure 17.12:
Average logarithm of the relaxation times $\langle \tau_i \rangle$ as a function of the variance $\langle (\ln \tau_i - \langle \ln \tau_i \rangle)^2 \rangle$ for the tree. The tree has 10 generations. A magnetic field $h = -0.3$ is applied from time $t = 0$, with $J = 1$. The variations are compatible with a linear dependence.

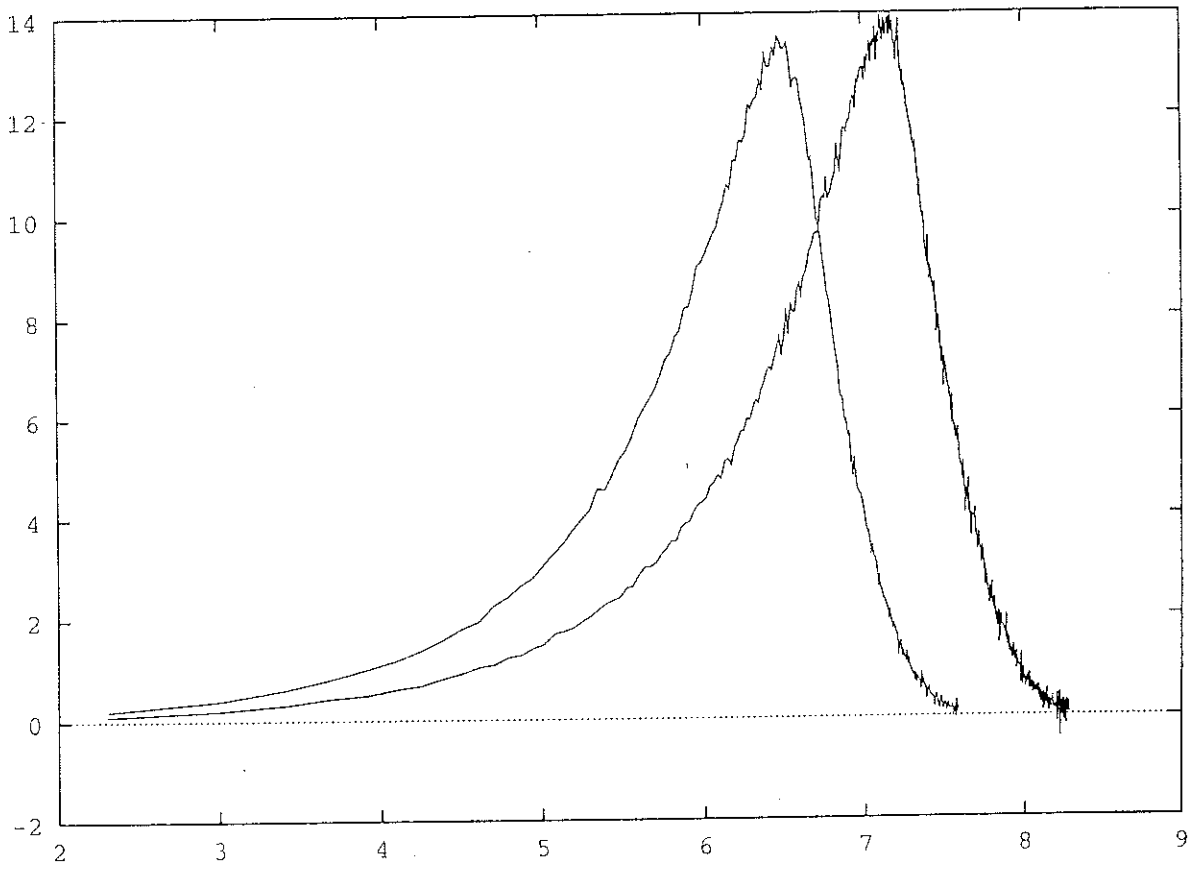

Figure 17.13:
$dM(t)/d\ln t$ as a function of $\ln t$ for the tree with 10 generations. The inverse temperature is $\beta = 2.5$ and $\beta = 2.75$. The shape is approximately gaussian. However, the probability is increased for small relaxation times, compared to a purely gaussian shape.

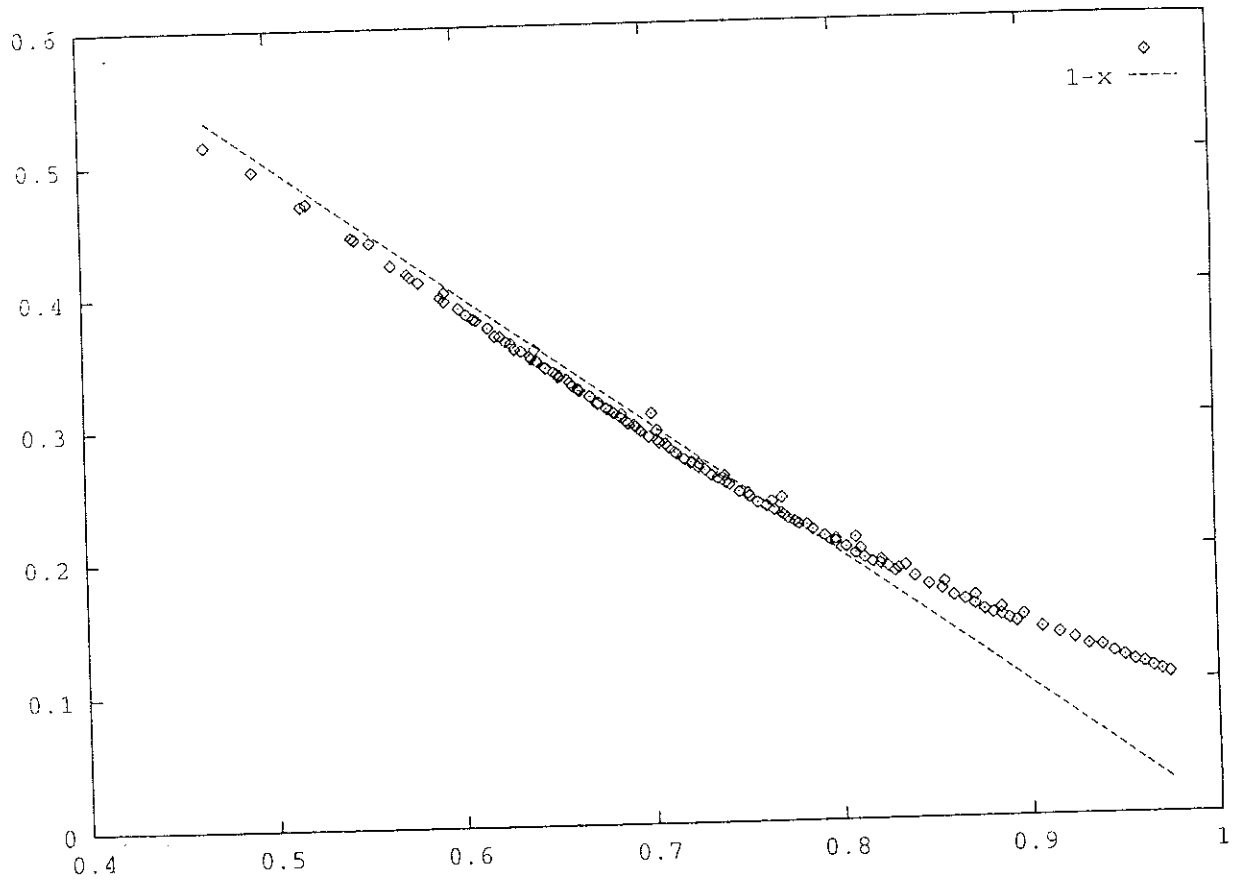

Figure 17.14:
Master curve of the switching field experiment for the Cayley tree with 10 generations. We plotted $\langle H_{sw}\rangle / H^0_{sw}$ as a function of $f_\alpha(T,\nu)$. The Boltzmann constant is equal to unity, $\alpha = 2$, $H_0 = 1.5$,$E_0 = 4$ and $c = 1/5$. On this curve, 7 series of measures at 7 different temperatures are superposed. Notice the deviations with respect to the linear behaviour $\langle H_{sw}\rangle / H^0_{sw} = 1 - f_\alpha(T,\nu)$. The straight line represents $1 - f_\alpha(T,\nu)$.

17.4 Hyperbolic lattices

The lattice is pictured on figure 17.15. The graph is a triangulation and each site (excepted the sites at the border) has 7 neighbours. We refer the reader to reference [2] for a study of the dynamical properties of the ferromagnetic Ising model on a hyperbolic lattice, and we sum up the main results. The magnetization distribution exhibits a non gaussian structure at small temperatures. The dynamical correlation functions exhibit aging. The dynamical susceptibility χ_1' has a maximum, and χ_3' has a sharp maximum which is compatible with a divergence. As the frequency decreases, the maximum of χ_1' decreases in temperature. However, the amplitude of the maximum *decreases* as the frequency decreases, whereas it *increases* as the frequency decreases in real glasses. This is a first difference between the case of the hyperbolic lattice and the case of the tree. We shall exhibit an other difference in what follows. In this section, we study the relaxation of the hyperbolic lattice Ising model in an external magnetic field. The equilibrium configurations are generated by a cluster algorithm [9], and the dynamical properties are studied with the help of a usual single spin flip Monte Carlo algorithm. The two tasks are parallelized: one processor implements the cluster algorithm, sends the spin configuration via an asynchronous transmission to the second processor which runs the Monte Carlo algorithm. In the same way as for the square lattice with periodic boundary conditions, we find gaussian shapes of $P(\ln \tau)$, where τ_i is the time at which the sign of the magnetization changed. The histograms are plotted on figure 17.16 for various temperatures. However, the variance $\langle (\ln \tau_i - \langle \ln \tau_i \rangle)^2 \rangle$ plotted as a function of the mean value $\langle \ln \tau_i \rangle$ is clearly non linear, as plotted on figure 17.17.

When one goes to lower temperatures, the mean value $\langle \ln \tau_i \rangle$ increases and we checked that it follows indeed and Arhenius law. However, the variance $\langle (\ln \tau_i - \langle \ln \tau_i \rangle)^2 \rangle$ increases also, but much faster than in standard theories. This shows that the dynamics of the hyperbolic lattice does not belong to the same class of dynamics as the square lattice or the Cayley tree. In the fit (17.1), the exponent β' increases with the temperature, as is plotted on figure 17.18.

As far as the switching field experiment is concerned, we come to the conclusion that the phenomenological model (17.2) can be applied in the case of the hyperbolic lattice since the points $H_{sw}(T, \nu)$ can be aligned on a master curve, as shown on figure 17.19.

17.5 Summary and discussion

We have considered successively slow relaxation processes under an applied magnetic field in four different cases: the square lattice with periodic boundary conditions, the square lattice on a disk, the Cayley tree and the hyperbolic lattice. Eventhough magnetic field relaxation in the first three cases are consistent with slow relaxation theories [6] in a zero magnetic field, our results show that the Ising model on a hyperbolic lattice does not belong to the classes of models described by [6].

The second set of results is related to the temperature variations of the exponent β' introduced in the fit (17.1). In the case of the tree, β' is found to be of the order of 19 and does not vary much with temperature. In the four cases that we investigated, the exponent β' is found to increase with temperature.

The third set of results is related to the switching field experiment. We find that the square lattice with periodic boundary conditions is not described by the model of [4], but the square lattice on a disk with open boundary conditions, the Cayley tree and the hyperbolic latttice

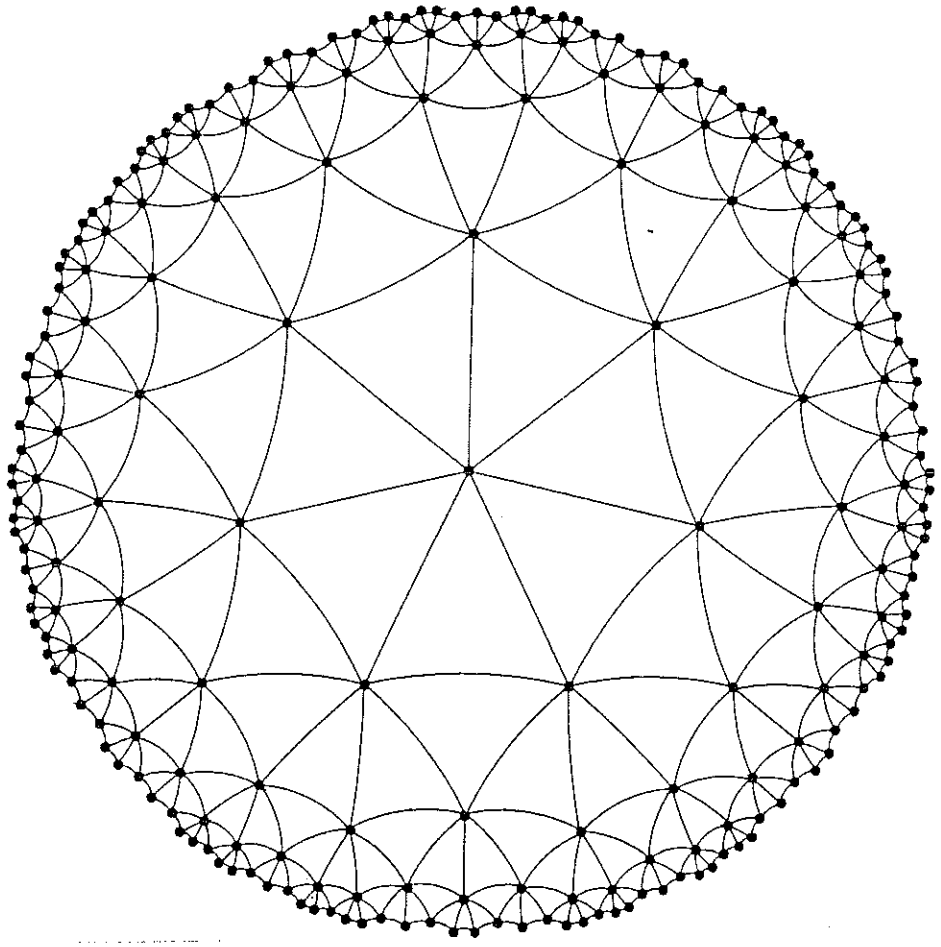

Figure 17.15:
The hyperbolic lattice. Each site of the bulk has seven neighbours.

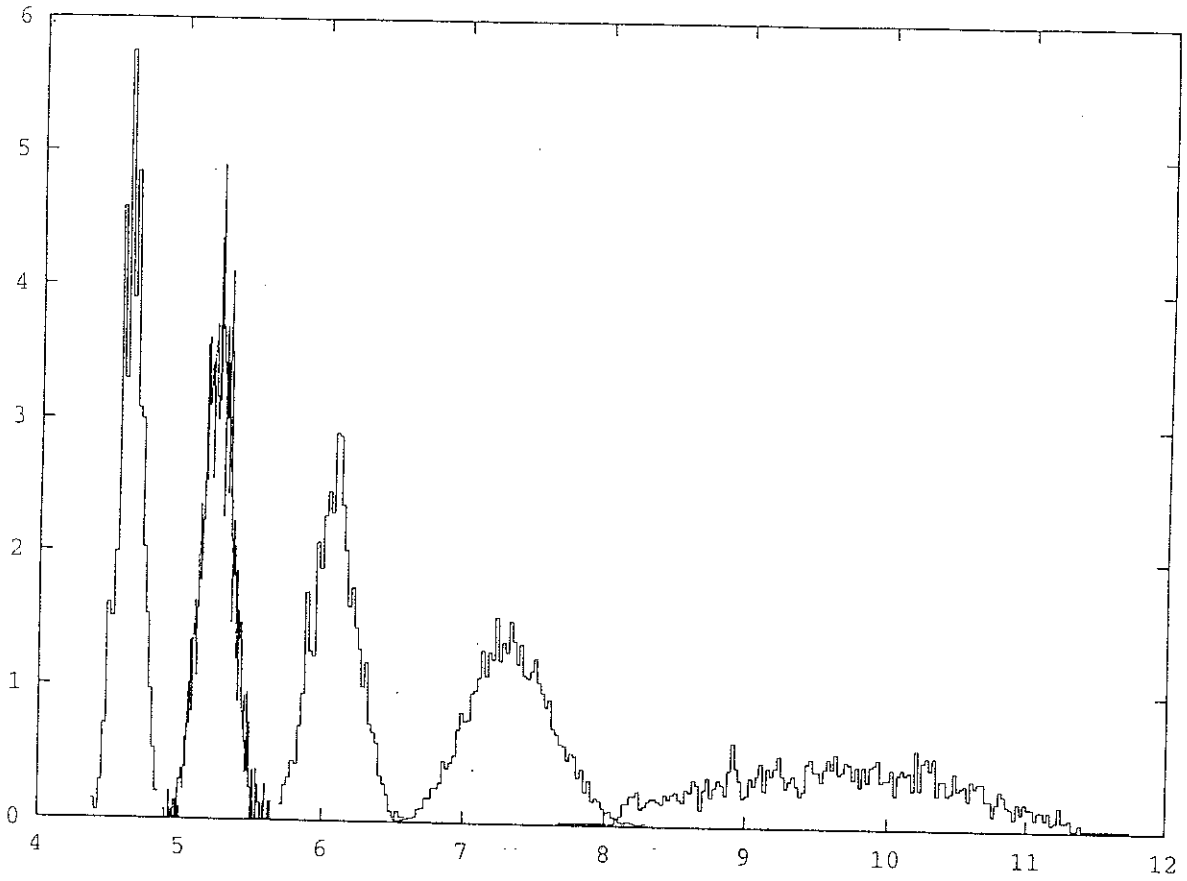

Figure 17.16:
Histogram of the times for which the magnetization cancels $P(\ln \tau)$, for a hyperbolic triangulation, with a coordinance 7 and 8 generations. The exchange constant J is taken equal to unity. The temperatures are $T = 0.3$, $T = 0.4$, $T = 0.5$, $T = 0.6$, $T = 0.7$. A magnetic field $h = -0.6$ is applied from time $t = 0$.

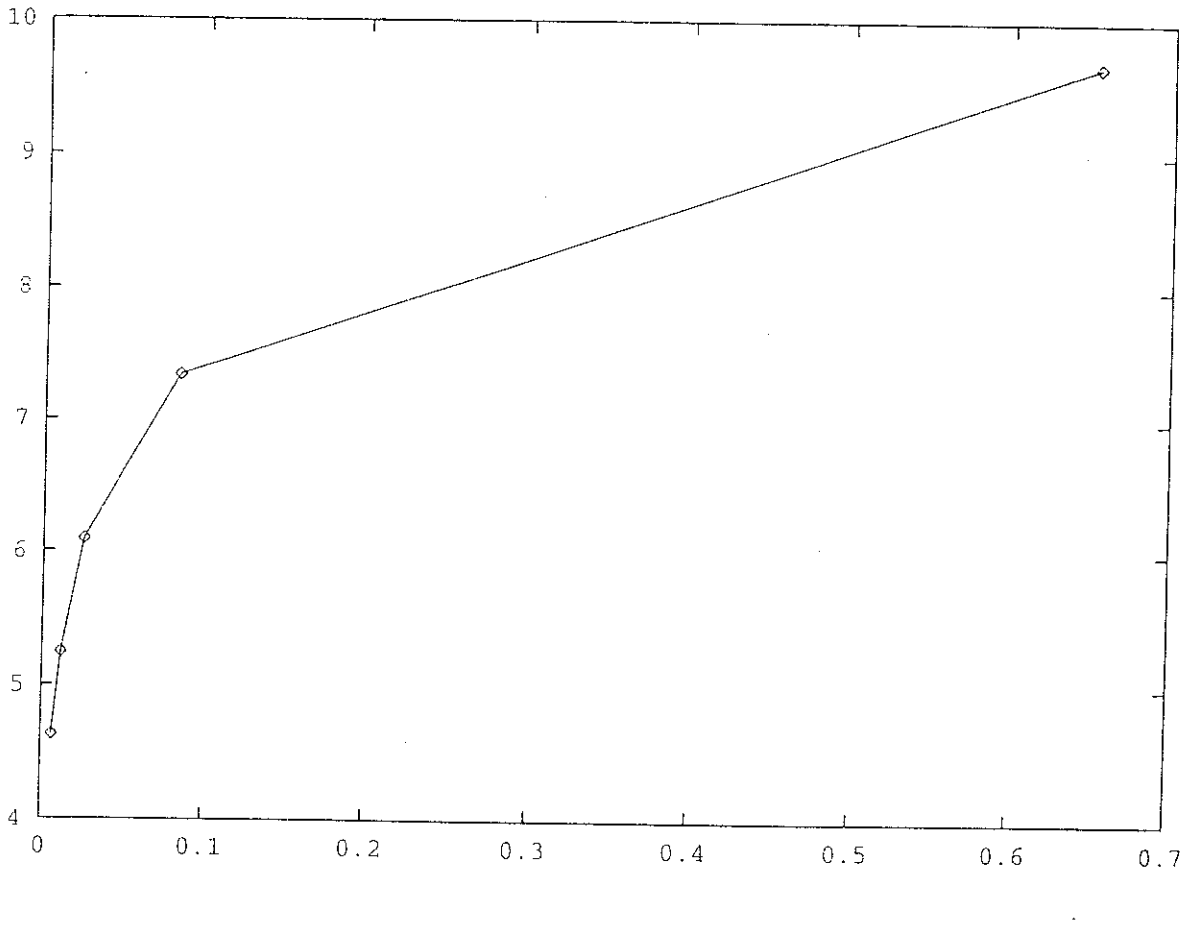

Figure 17.17:
Average logarithm of the relaxation times $\langle \ln \tau_i \rangle$ as a function of the variance $\langle (\ln \tau_i - \langle \ln \tau_i \rangle)^2 \rangle$ for a hyperbolic triangulation, with a coordination 7 and 8 generations. A magnetic field $h = -0.6$ is applied from time $t = 0$, with $J = 1$. The variations are clearly non linear.

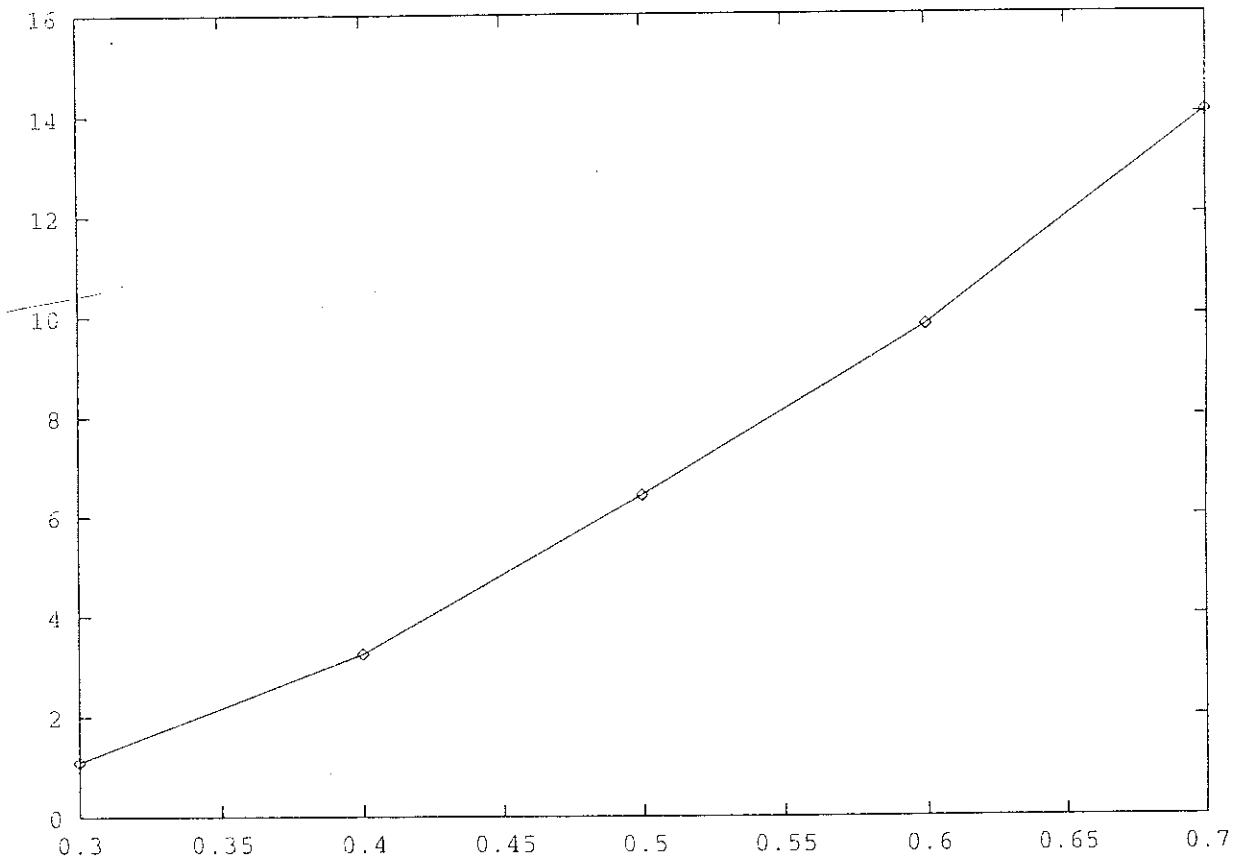

Figure 17.18:
Variations of the exponent β' as a function of temperature in the case of the hyperbolic triangulation with 7 nearest neibours and 8 generations. A magnetic field $h = -0.6$ is applied from time $t = 0$, with $J = 1$.

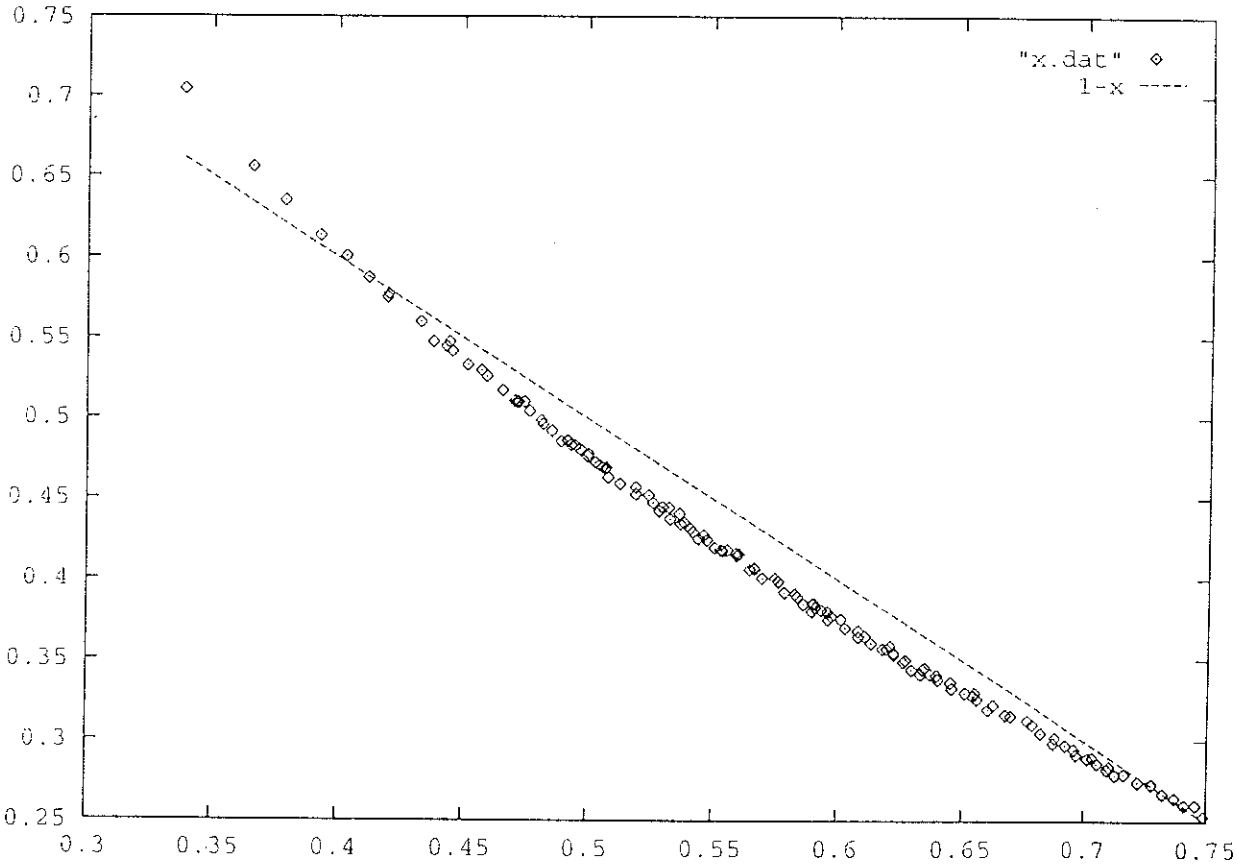

Figure 17.19:
Master curve of the switching field experiment for the hyperbolic lattice with 8 generations and a coordination 7. We plotted $\langle H_{sw} \rangle / H^0_{sw}$ as a function of $f_\alpha(T, \nu)$. The Boltzmann constant is equal to unity, $\alpha = 2$, $H_0 = 2.3J$, $E_0 = 5$ and $c = 1/15$.

enter the class of models for which the approach of reference [4] is valid.

We conclude that the four models that we have considered have four different behaviour with respect to the magnetic field relaxation.

What conclusions can be drawn from the point of view of comparisons with experiments on magnetic grains? Of course, our models are far from a proper modeling of the magnetic grains. However, some of the models that we consider can be considered as effective models for magnetic grains. A probable mechanism for the reversal of magnetization in magnetic grains is that the magnetization flips from the boundary (in the same way the magnetization reverses from the corners for an open boundary Ising model), but there exists a barrier for the reversal of spins at the boundary. The bulk is supposed to reverse its magnetization rapidly. This argument is supported by the shape of the hysteresis cycle of a monodomain magnetic grain [3]. Some of our models may be seen as effective models for the boundary of magnetic grains. An effective model for the boundary of magnetic grains may be analogous to a hyperbolic lattice with open boundary conditions, or to the square lattice on a disk. The barriers are introduced by hand, with no reference to the real physics of magnetic grains. If one assumes such an effective model for the boundary, one can reproduce three qualitative features of magnetic grains. First, the hysteresis cycle possesses a reversible part, and an irreversible part [5]. The reversible part can be thought of as slow relaxation phenomena at the boundary, and the irreversible one as a rapid propagation in the euclidian bulk, which is not present in our simulations. Second, we reproduce the fact that the stretched exponent β' increases with temperature. Third, experimental data [3] show that the phenomenological model of [4] is well realized in experiments, whereas some deviations occur at lower temperatures. We conclude that, among the three models that we have studied, the square lattice on the disk and the hyperbolic lattice are candidates for an effective model for the boundary of magnetic grains. In the case of the hyperbolic lattice, we showed that $\langle \ln \tau_i \rangle$ is non linear as a function of $\langle (\ln \tau_i - \langle \ln \tau_i \rangle)^2 \rangle$, whereas it is approximately linear for the square lattice on a disk. However, to our knowledge, experimental data do not exist which would differentiate between the two behaviours.

The author acknowledges discussion with J.C. Anglès d'Auriac, B. Barbara, B. Douçot, K. Hasselbach, J. Souletie and W. Wernsdorffer.

References

[1] R. Mélin, J.C. Anglès d'Auriac, P. Chandra and B. Douçot, to be published in Phys. Rev. B.

[2] J.C. Anglès d'Auriac, P. Chandra, B. Douçot and R. Mélin, in preparation.

[3] W. Wernsdorfer, K. Hasselbach, A. Benoit, D. Mailly, B. Barbara and L. Thomas, submitted to Phys. Rev. Lett (1995).

[4] L. Gunther and B. Barbara, Phys. Rev. B 49 (1994)

[5] P.C.E. Stamp, E.M. Chudnovsky and B. Barbara, Int. J. of Mod. Phys. B, 6, 1355 (1992).

[6] B. Castaing and J. Souletie, J. Phys. I, 403 (1991); J. Souletie, Physica A, 201, 30 (1993).

[7] A.T. Ogielski, Phys. Rev. B 32, 7384 (1985). J. Phys (France) 45, 1809 (1984).

[8] H. L. Richards, S. W. Sides, M. A. Novotny and P. A. Rikvold, submitted to Jour. of Magnetism and Magnetic Materials (1995).

[9] R.H. Swendsen and J.S. Wang, Phys. Rev. Lett 57, 2606 (1986); Phys. Rev.Lett. 58, 86 (1987). See also R.H. Swendsen, J.S. Wang and A.M. Ferrenberg in *The Monte Carlo Method in Condensed Matter Physics*, K. Binder (Ed.), Topics in Applied Physics 71, Springer-Verlag, Berlin-Heidelberg-New York (1992)

[10] L.P. Lévy, Phys. Rev. B 38, 4963 (1988).

[11] H. A. Bethe, Proc. Roy. Soc. A 216, 45 (1935); 150, 552 (1935).

[12] R. Peierls, Proc. Can. Phil. Soc. 32, 477 (1936); Proc. Roy. Soc. 154, 207 (1936).

[13] E. Müller Hartmann and Z. Zittartz, Phys. Rev. Lett. 33, 893 (1974).

[14] J. von Heimburg and H. Thomas, J. Phys. C 7, 3433 (1974).

[15] R. Omari, J.J. Préjean and J. Souletie,

[16] R. Mélin, CRTBT preprint(1995).

Chapitre 18

Article 10

Glauber dynamics and eigenvalue spacing statistics[1]

R. Mélin

CRTBT-CNRS, 38042 Grenoble BP 166X cédex France

We discuss the eigenvalue spacing statistics of the Glauber matrix for various models of statistical mechanics. The dynamics of the one dimensional Ising model is integrable, and the eigenvalue spacing statistics is non universal. In two dimensions, we investigate the case of an Ising Cluster. The transition seems to be correlated with the fact that the minimal eigenvalue spacing is non zero for temperatures above the transition, and zero for temperatures below the transition. The statistics suggests the presence of 'hidden' conserved quantities. At low temperatures, there exists a peak for $s = 0$ which decreases as the temperature decreases. We investigate a simple frustrated Ising model, with a finite zero entropy per site at zero temperatures. Eventhough no thermodynamic transition is present, the minimal eigenvalue spacing varies in a non trivial way. In the case of the Sherrington-Kirkpatrick model, the eigenvalue spacing statistics are close to G.O.E. at high temperature, and the presence of eigenvalue attraction is found at low temperatures. The attraction between eigenvalues increases as the temperature decreases. In the case of the Cayley tree, the same attraction of eigenvalues is observed. In both cases, the eigenvalues have a trend to condense near integer values.

[1] submitted to the Jour. Phys. (France)

18.1 Introduction

The ideas of level spacing statistics emerged for the first time in the context of nuclear physics [1] [2] [3], where Wigner proposed to consider statistical quantities computed from deterministic spectra. Later, these ideas were applied to quantum systems whose classical analogs are chaotic [4] [5]. The idea of level spacing statistics is to calculate the difference between two consecutive levels, and to study the probability of occurrence $P(s)$ of a level spacing s. The different generic behaviours of $P(s)$ are classified according to the random matrix theory [4] [6]. A generic case is the integrable spectrum. Each level is labelled by a set of quantum numbers, the energy levels are decorrelated and the statistics is Poissonian: $P(s) = \exp(-s)$. If the number of conserved quantities is too small, it is not possible to find a set of quantum numbers for each level, and the levels are correlated, that is, there exists level repulsion. The repulsion is linear and the level spacing statistics has the Gaussian Orthogonal Ensemble (G.O.E.) shape:

$$P(s) = \frac{\pi}{2} s e^{-\frac{\pi}{4}s^2}. \tag{18.1}$$

If time reversal invariance is broken, and if the system is chaotic, the level spacing statistics has a Gaussian Unitary Ensemble (G.U.E.) shape:

$$P(s) = \frac{32}{\pi^2} s^2 e^{-\frac{4}{\pi}s^2}, \tag{18.2}$$

where the repulsion is quadratic. The ideas of quantum chaos have been applied to various fields of condensed matter physics, such as disordered systems [7]. An other field of application is the strongly correlated electron systems [8] [9], with a hope to extract more information from finite size systems. In the present paper, we wish to analyze the dynamics of classical spin systems under the light of eigenvalue spacing statistics. We use here the term 'eigenvalue' rather than 'level' since there are no energy levels as in quantum mechanics. We consider the 2^Nx2^N Glauber matrix, with N the number of Ising spins, and diagonalize it for small clusters. Contrary to the case of quantum mechanics, we do not have any conservation law (such as the total momentum, the total projection of the spins, ...), so that the only symmetries are the lattice symmetries that we treat with group theory. We can thus only study the dynamics for a small number of sites, typically of the order of 10 sites (we studied a 13 site cluster in the case of the tree). The eigenstates are not physical, excepted for the Boltzmann distribution which corresponds to the upper eigenvalue $\lambda = 0$. The other eigenvectors are not probability distributions, since the sum of their components is zero, so that their interpretation is not obvious. However, one may think of the eigenvalues as the typical relaxation times of the system. For instance, in a broken symmetry phase, the eigenvalue $\lambda = 0$ of the Boltzmann distribution is degenerate (in the thermodynamic limit) with the broken symmetry state.

In our study of small clusters, two quantities are of interest. The first quantity is the minimal eigenvalue spacing s_{min}. An other quantity of interest is the full eigenvalue spacing statistics. We study the qualitative variation of these two quantities for various models. We first consider the case of the unidimensional Ising model. In this case, the dynamics is shown to be integrable. The corresponding eigenvalue spacing statistics are found to be non universal, with a peak for $s = 0$ which decreases as the temperature decreases. The minimal eigenvalue spacing s_{min} is always zero. We attribute this behaviour to the presence of degenerate eigenvalues, whatever the temperature. In the case of the bidimensional Ising model with nearest neighbour interactions, it seems that the presence of a transition is correlated with the fact that $s_{min} = 0$ in the broken

symmetry phase, whereas $s_{min} \neq 0$ in the paramagnetic phase. In the ferromagnetic region, the level spacing statistics have a peak for $s = 0$ and this peak decreases as the tempearature is lowered. The $s > 0$ part of the eigenvalue statistics is intermediate between a Poissonian and a G.O.E. behaviour, which seems to suggest the presence of conserved quantities. We next study a frustrated model, with a finite entropy at zero temperature. Although there exists no phase transition, the behaviour of the minimal spacing s_{min} is non trivial, which shows that the variations of s_{min} are not in a one to one correspondence with the existence of a thermodynamic transition. Finally, we adress the question of glassy models. We first begin with the Sherrington-Kirkpatrick (SK) model. The minimal intereigenvalue spacing s_{min} is non zero at high temperatures and, below a given temperature, takes vanishing values. The level spacing statistics are close to G.O.E. at high temperatures and become *overpoissonian* at low temperatures, with an attraction of eigenvalues. An analysis of the density of eigenvalues reveals that the eigenvalues condense for integer values. As far as the Cayley tree is considered, this model exhibits glassiness at small temperatures [10], and, as in the case of the SK model, the eigenvalues condense in the vicinity of integers.

18.2 The Glauber matrix

The Glauber dynamics [11] is a single spin flip dynamics with a continous time. If $p(\{\sigma\}, t)$ is the probability to find the spin sytem in the configuration $\{\sigma\}$ at time t, the Master equation for the single spin flip dynamics is

$$\frac{d}{dt}p(\{\sigma\},t) = -\left(\sum_{i=1}^{N} w_i(\{\sigma\})\right) p(\{\sigma\},t) + \sum_{i=1}^{N} w_i(\{\sigma_1,...,-\sigma_i,...,\sigma_N\})p(\{\sigma_1,...,-\sigma_i,...,\sigma_N\},t). \tag{18.3}$$

The single spin flip transition probabilities are defined as the probabilities that the spin σ_i flips from σ_i to $-\sigma_i$ while the other spins remain fixed. Since the Boltzmann distribution is a fixed point of the dynamics (18.3), the transition probabilities have the form

$$w_i(\{\sigma\}) = \frac{1}{2}(1 - \sigma_i \tanh(\beta J \sum_{j \in V(i)} \sigma_j)), \tag{18.4}$$

where $V(i)$ is the set of neighbours of the site i. We note $\mathrm{p}(t)$ the 2^N vector of the $p(\{\sigma\}, t)$. Then, equation (18.3) can be brought under the form

$$\frac{d}{dt}\mathrm{p}(t) = \mathrm{G}\mathrm{p}(t), \tag{18.5}$$

where the matrix G is the Glauber matrix. Since the Boltzmann distribution is a steady state of the dynamics, its corresponding eigenvalue is zero whatever the temperature. The matrix $\mathbf{G}$ is non symmetric. However, it can be brought under the form of a symmetric matrix $\mathbf{M}$. To do so, we notice that the Glauber matrix verifies the detailed balance, that is $\mathbf{G}_{\alpha,\beta}\mathbf{p}^{(0)}_{\beta} = \mathbf{G}_{\beta,\alpha}\mathbf{p}^{(0)}_{\alpha}$, where $\mathbf{p}^{(0)}$ is the Boltzmann distribution. As a consequence,

$$\left(\mathbf{p}^{(0)}_{\alpha}\right)^{-1/2} \mathbf{G}_{\alpha\beta} \left(\mathbf{p}^{(0)}_{\beta}\right)^{1/2} = \left(\mathbf{p}^{(0)}_{\beta}\right)^{-1/2} \mathbf{G}_{\beta\alpha} \left(\mathbf{p}^{(0)}_{\alpha}\right)^{1/2}. \tag{18.6}$$

We call $\mathbf{M}$ the matrix defined by

$$\mathbf{M}_{\alpha\beta} = \left(\mathrm{p}_\alpha^{(0)}\right)^{-1/2} \mathbf{G}_{\alpha\beta} \left(\mathrm{p}_\beta^{(0)}\right)^{1/2}. \tag{18.7}$$

Then, $\mathbf{M}$ is symmetric. If $\mathbf{p}$ is a right eigenvector of the Glauber matrix, then

$$\sum_\beta \mathbf{G}_{\alpha\beta}\mathrm{p}_\beta = \lambda \mathrm{p}_\beta \tag{18.8}$$

is equivalent to

$$\sum_\beta \mathbf{M}_{\alpha\beta} \left(\mathrm{p}_\beta^{(0)}\right)^{-1/2} \mathrm{p}_\beta = \lambda \left(\mathrm{p}_\alpha^{(0)}\right)^{-1/2} \mathrm{p}_\alpha, \tag{18.9}$$

so that $\left(\mathrm{p}_\alpha^{(0)}\right)^{-1/2} \mathrm{p}_\alpha$ is an eigenvector of $\mathbf{M}$. We conclude that $\mathbf{G}$ is diagonalizable, and that all its eigenvalues are real.

The spectrum in the infinite temperature limit can be understood as follows. If we call

$$|\psi\rangle = \sum_{\{\sigma\}} f(\{\sigma\})|\sigma_1\rangle \otimes ... \otimes |\sigma_N\rangle, \tag{18.10}$$

then the dynamics reads

$$\frac{d}{dt}|\psi\rangle = -\frac{N}{2}|\psi\rangle + \frac{1}{2}\sum_{i=1}^N \sigma_i^x|\psi\rangle, \tag{18.11}$$

so that the eigenvalues of the Glauber matrix at infinite temperature are of the form

$$\lambda = -\frac{N}{2} + \frac{1}{2}\sum_{i=1}^N \mu_i, \tag{18.12}$$

where $\mu_i = \pm 1$. The spectrum in the infinite temperature limit is thus made of eigenvalues at integer values between $-N$ and 0, with a degeneracy given by the binomial coefficients.

Another property of $\mathbf{G}$ is that, for bipartite lattices, such as the square lattice or the Cayley tree, the spectrum of $\mathbf{G}$ is symmetric: if λ belongs to the spectrum, then $-N-\lambda$ is an eigenvalue too. The proof is as follows. Let $\mathbf{X}\{\sigma\}$ be an eigenvector of $\mathbf{M}$, with an eigenvalue λ:

$$\lambda \mathbf{X}\{\sigma\} = -\sum_{i=1}^N \frac{1}{2}(1 - \sigma_i \tanh(\beta J h_i))\mathbf{X}\{\sigma\} + \sum_{i=1}^N \frac{1}{2\cosh \beta J h_i}\mathbf{X}\{\sigma_1, ..., -\sigma_i, ..., \sigma_N\}, \tag{18.13}$$

where h_i is defined by

$$h_i = \sum_{j \in V(i)} \sigma_j. \tag{18.14}$$

Let $\mathbf{Y}\{\sigma\}$ be defined as

$$\mathbf{Y}\{\sigma\} = (-1)^{\nu\{\sigma\}}\mathbf{X}\{\tilde{\sigma}\}, \tag{18.15}$$

where $\nu\{\sigma\}$ is the number of up spins in the configuration $\{\sigma\}$. $\{\tilde{\sigma}\}$ is deduced from $\{\sigma\}$ by flipping the spins of one of the two sublattices. Then,

$$(\mathbf{MY})\{\sigma\} = -\sum_{i=1}^N \frac{1}{2}(1 - \sigma_i \tanh(\beta H h_i))(-1)^{\nu\{\sigma\}}\mathbf{X}\{\tilde{\sigma}\} \tag{18.16}$$

$$+\sum_{i=1}^{N}(-1)^{\nu\{\sigma_1,\ldots,-\sigma_i,\ldots,\sigma_N\}}\frac{1}{2\cosh(\beta J h_i)}\mathbf{X}\{\tilde{\sigma}_1,\ldots,-\tilde{\sigma}_i,\ldots,\tilde{\sigma}_M\}$$

$$= (-1)^{\nu\{\sigma\}}\left[-\sum_{i=1}^{N}\frac{1}{2}(1+\tilde{\sigma}_i\tanh(\beta J h_i))\,\mathbf{X}\{\tilde{\sigma}\}\right. \tag{18.17}$$

$$\left.-\sum_{i=1}^{N}\frac{1}{2\cosh(\beta J h_i)}\mathbf{X}\{\tilde{\sigma}_1,\ldots,-\tilde{\sigma}_i,\ldots,\tilde{\sigma}_N\}\right]$$

$$= -(N+\lambda)(-1)^{\nu\{\sigma\}}\mathbf{X}\{\tilde{\sigma}\} = -(N+\lambda)\mathbf{Y}\{\sigma\}. \tag{18.18}$$

Given an eigenvector $\mathbf{X}$ for the eigenvalue λ, we have built an eigenvector $\mathbf{Y}$ for the eigenvalue $-N-\lambda$.

The difference between (18.5) and the Schrödinger equation is that quantum mechanics preserves the scalar product, leading to hermitian Hamiltonians. More over, the space of physical states is a Hilbert space, and each state of the Hilbert state is physical. In the case of the Glauber matrix, no vector space is present, in the sense that the sum of two probability distributions is not a probability distribution. However, some quantities are conserved by the dynamics. It is easy to show that the eigenvectors of $\mathbf{G}$ for the non zero eigenvalues have the property that

$$\sum_{\{\sigma\}}\mathbf{p}\{\sigma\} = 0. \tag{18.19}$$

This is a simple consequence of the fact that the Glauber matrix preserves the quantity

$$\sum_{\{\sigma\}}\mathbf{p}\{\sigma\}. \tag{18.20}$$

18.3 One dimensional Ising model

18.3.1 Integrability of the dynamics

In the case of the one dimensional model, the Glauber dynamics is integrable. To show this, we follow Glauber and write evolution equations for the correlation functions. We call $R^{(n)}_{i_1,\ldots,i_n}(t)$ the n points correlation function, with $i_\alpha \neq i_\beta$ if $\alpha \neq \beta$, that is

$$R^{(n)}_{i_1,\ldots,i_n}(t) = \langle\prod_{\alpha}\sigma_{i_\alpha}(t)\rangle. \tag{18.21}$$

Then, following Glauber, we write the evolution equation of $R^{(n)}_{i_1,\ldots,i_n}(t)$ under the form

$$\frac{d}{dt}R^{(n)}_{i_1,\ldots,i_n}(t) = -2\langle\sigma_{i_1}(t)\ldots\sigma_{i_n}(t)\,(w_{i_1}(\{\sigma\})+\ldots+w_{i_n}(\{\sigma\}))\rangle, \tag{18.22}$$

where the transition probabilities are given by (18.4). We notice that, in the one dimensional case, each spin has two neighbours, so that $w_i(\{\sigma\})$ can be written as

$$w_i(\{\sigma\}) = \frac{1}{2}\left(1-\frac{\gamma}{2}\sigma_i(\sigma_{i+1}+\sigma_{i-1})\right), \tag{18.23}$$

with $\gamma = \tanh 2\beta J$. Here, we take periodic boundary conditions, but the case of open boundary conditions is similar. Inserting (18.23) into (18.22), we get

$$\frac{d}{dt}R^{(n)}_{i_1,\ldots,i_n}(t) = -nR^{(n)}_{i_1,\ldots,i_n}(t) + \frac{\gamma}{2}\sum_{\epsilon=\pm 1}\sum_{\alpha=1}^{n}\langle\sigma_{i_\alpha+\epsilon}\prod_{\beta\neq\alpha}\sigma_{i_\beta}\rangle. \tag{18.24}$$

The terms with $\epsilon = 1$ collect the right neighbours, and $\epsilon = -1$ corresponds to the left neighbours. The correlation function in (18.24) can lead to a (n-2) points correlator if $\exists\beta, i_{\alpha+\epsilon} = i_\beta$ or to a n points correlator if not. The expression (18.24) can be brought under the form

$$\begin{aligned}\frac{d}{dt}R^{(n)}_{i_1,\ldots,i_n}(t) &= -nR^{(n)}_{i_1,\ldots,i_n}(t) + \frac{\gamma}{2}\sum_{\epsilon=\pm 1}\sum_{\alpha=1}^{n}\left(\sum_{\beta=1}^{n}\delta_{i_\beta,i_\alpha+\epsilon}R^{(n-2)}_{i_1,\ldots,i_{\alpha-1},i_{\alpha+1},\ldots,i_{\beta-1},i_{\beta+1},\ldots,i_n}(t)\right. \\ &\left. + \left(1-\sum_{\beta=1}^{n}\delta_{i_\beta,i_\alpha+\epsilon}\right)R^{(n)}_{i_1,\ldots,i_{\alpha-1},i_\alpha+\epsilon,i_{\alpha+1},\ldots,i_n}(t)\right).\end{aligned} \tag{18.25}$$

If none of the sites $i_1, \ldots, i_n$ are neighbours, the term containing $R^{(n-2)}$ vanishes. However, if at leasrt two sites are neighbours in the set $i_1, \ldots, i_n$, we have to take into account a term containing $R^{(n-2)}$ in the evolution of $R^{(n)}$. It is clear that (18.25) is nothing but a rewritting of (18.3) in the case where all the sites have only two neighbours. The number of distinct correlation functions is

$$\sum_{n=0}^{N}\binom{N}{n} = 2^N, \tag{18.26}$$

which is equal to the number of spin configurations. The system (18.25) is integrable. Glauber gives the explicit solution for $R^{(1)}_i(t)$. The equation giving $dR^{(2)}(t)/dt$ contains only linear combinations of $R^{(2)}$. In order to solve the three points correlation functions, we inject Glauber's solution into the evolution equation for $R^{(3)}$, diagonalize the associated matrix and get a first order differential equation with a second member, which is explicitely integrable and yields the second order correlation functions. The entire hierarchy can be solved by this method since $dR^{(k)}/dt$ does not contain $R^{(p)}$ with $p > k$.

18.3.2 Eigenvalue spacing statistics

In order to calculate the eigenvalue spacing statistics, we need to take all the symmetries of the lattice into account. Here, the symmetries are so obvious that we do not require a group theory treatment. We work with an open Ising chain. This graph is invariant under the reflection and the identity. We note $|\{\sigma\}\rangle$ the basis of our 'Hilbert' space. We use quotes since there is no vector space structure on the probability distributions. However, to diagonalize the Glauber matrix, we can do as if we were in quantum mechanics. If R is the inversion, we form the combinations

$$|\{\sigma\}\rangle_\epsilon = \frac{1}{\sqrt{2}}\left(|\{\sigma\}\rangle + \epsilon R|\{\sigma\}\rangle\right). \tag{18.27}$$

This operation leads to states with a well defined behaviour under the reflection. The resulting state is either symmetric ($\epsilon = 1$) or antisymmetric ($\epsilon = -1$). The antisymmetric state may be zero if $|\{\sigma\}\rangle$ is invariant under the inversion. The dimension of the antisymmetric sector is

$$\frac{1}{2}\left(2^N - 2^{[\frac{N+1}{2}]}\right), \tag{18.28}$$

and the dimension of the symmetric sector is

$$\frac{1}{2}\left(2^N + 2^{\left[\frac{N+1}{2}\right]}\right), \tag{18.29}$$

where [] denotes the integer part. Using this method, we diagonalize the Glauber matrix in the symmetric and the antisymmetric sectors. The evolution of the eigenvalues of one sector as a function of the inverse temperature is plotted on figure 18.1. No avoided crossings are present, which is what is expected for an integrable system. A quantity of interest is the minimal eigenvalue spacing s_{min}. We find that it is zero at all temperatures, eventhough the system does not undergo any transition. We attribute this behaviour to the fact that the one dimensional dynamics with nearest-neighbour coupling possesses a lot of symmetries, so that there exists degenerate eigenvalues whatever the temperature. The eigenvalue spacing statistics are found to be non universal. At low temperatures, the eigenvalue spacing statistics has a peak for $s = 0$ and a part for $s > 0$ which has nothing to do with the Poisson statistics. The eigenvalue spacing statistics are plotted on figure 18.2 for $\beta = 5$. The height of the peak at $s = 0$ decreases as the temperature decreases.

18.4 Bidimensional Ising model

18.4.1 Dynamics

In this case, the dynamics is no more integrable. The evolution of the correlation function is not a linear equation, as it was in the case of the Ising chain. This is essentially due to the fact that, with four neighbours, one has to introduce a cubic term in $w_i(\{\sigma\})$ given by equation (18.23):

$$\tanh\left(\beta J(\sigma_1 + \sigma_2 + \sigma_3 + \sigma_4)\right) = \alpha(\sigma_1 + \sigma_2 + \sigma_3 + \sigma_4) + \alpha'(\sigma_1 + \sigma_2 + \sigma_3 + \sigma_4)^3, \tag{18.30}$$

with

$$\alpha = \frac{1}{12}\left(8\tanh 2\beta J - \tanh 4\beta J\right) \tag{18.31}$$

$$\alpha' = \frac{1}{48}\left(\tanh 4\beta J - 2\tanh 2\beta J\right). \tag{18.32}$$

In the one dimensional case, we could integrate the dynamics because $dR^{(n)}/dt$ was only a function of $R^{(k)}$ with $k \leq n$. In the bidimensional case, $dR^{(n)}/dt$ is also a function of $R^{(k)}$ with $k > n$, so that the hierarchy is no more integrable by this method. It is not because one does not know how to solve a dynamics that this dynamics is not integrable. What we shall see below from the eigenvalue spacing statistics that the dynamics is not integrable, but there exists some 'hidden' conserved quantities.

18.4.2 Use of group theory

We use group theory to find the symmetries of the clusters for which we shall diagonalize the Glauber matrix. Notice that we are restricted to small sizes since the size of the 'Hilbert' space is equal to 2^N. In practise, and to have sensible execution times, we are restricted to $N \leq 13$. The first step is to determine the symmetry group of the lattice, that is to enumerate

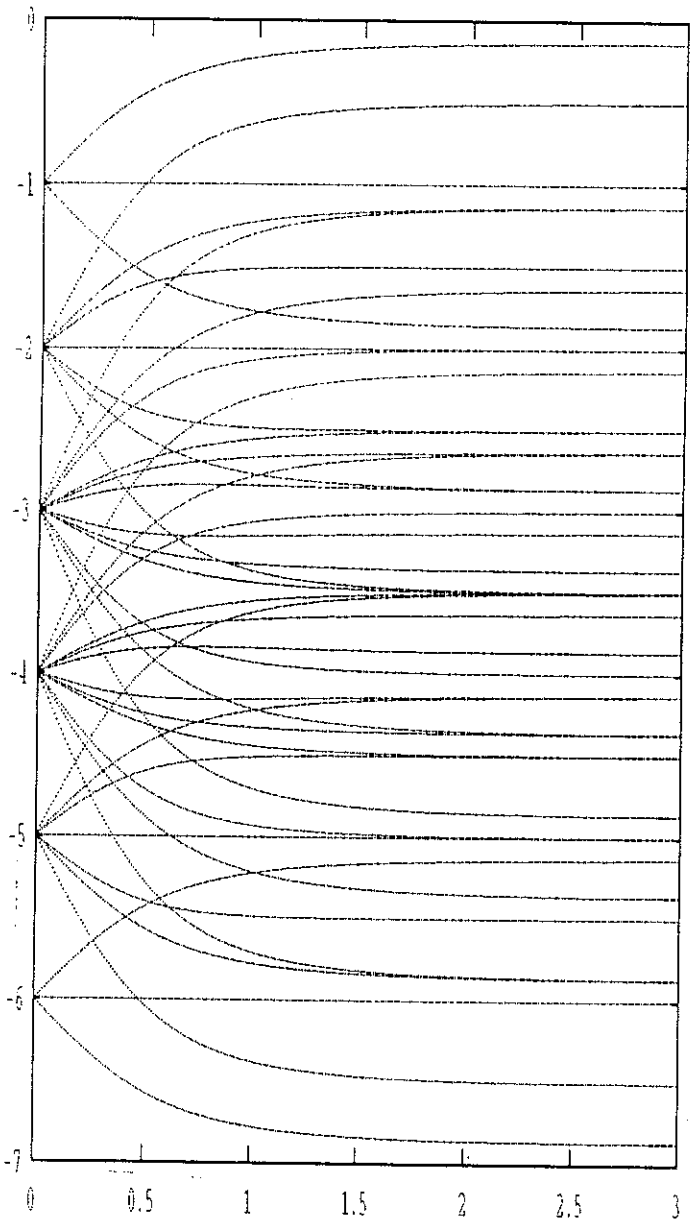

Figure 18.1:
Evolution of the eigenvalues of the Glauber matrix as a function of the inverse temperature, for a 7 site Ising chain in the antiperiodic sector. No avoided crossings are visible.

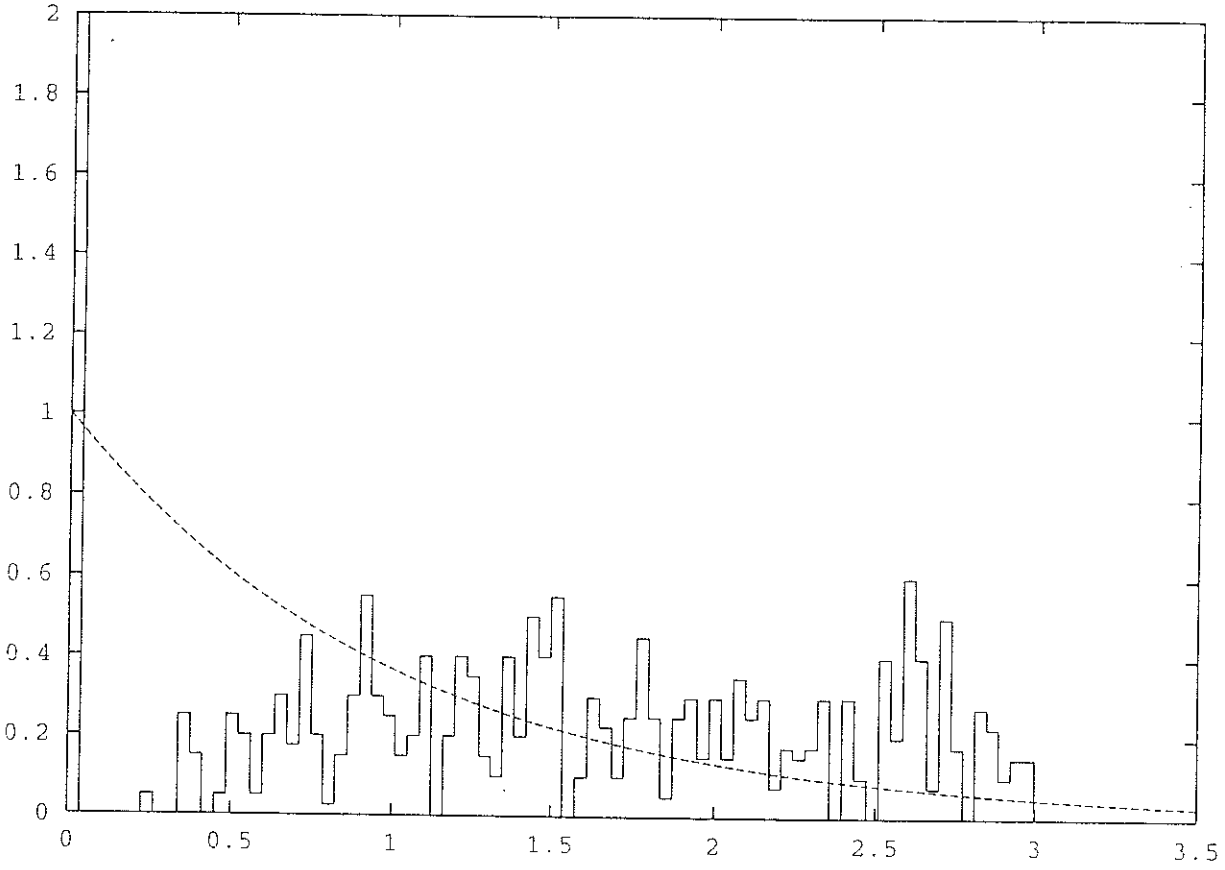

Figure 18.2:
Eigenvalue spacing statistics of the one dimensional Ising model with nearest neighbours couplings. The inverse temperature is $\beta = 5$. The peak at $s = 0$ has been truncated for visibility. Its height is 10.5, which depends on the step of the histrogram. The weight of the peak at $s = 0$ represents 39% of the number of eigenvalue spacings.

all the permutations that leave the lattice invariant. To do so, we do not test all the $N!$ possible permutations since the computation time may be huge. Instead, we use the following procedure. We first label the lattice sites and give the list of bonds. We determine all the possible images $\sigma(1)$ of the site 1, that is all the $N-1$ sites. Then, for each of the possible images of the site 1, we determine the images $\sigma(2)$ of site 2 which respect the lattice symmetry: if there is a bond between 1 and 2, there must be a bond between $\sigma(1)$ and $\sigma(2)$. If there is no bond between 1 and 2, there must be no bond between $\sigma(1)$ and $\sigma(2)$. At this point, we have a list of potential permutations beginning with $\sigma(1)$ and $\sigma(2)$. Then, we determine all the possible images of site 3 which leave the lattice invariant. We thus get a tree structure, but, during the construction, some branches shall stop. At the end of the process, that is when $\sigma(N)$ has been determined, we get all the permutations which leave the graph invariant. The second step is to determine the classes and the table of characters of the group. We use the progam [12], which determines automatically the classes and the table of characters. In a third step, we have to determine the size of the blocs corresponding to the irreducible representations, and how many times a given irreducible representation appears. The dimension of the blocs corresponding to the irreducible representation (j) is equal to

$$Dim^{(j)} = \frac{1}{h} \sum_{g \in G} \chi(\tilde{g}) \chi^{(j)}(\tilde{g}). \tag{18.33}$$

$\tilde{g}$ is the representation of the group element g in the 'Hilbert' space, h is the cardinal of the group G, $\chi(\tilde{g})$ is the trace of $\tilde{g}$ and $\chi^{(j)}(g)$ is read from the table of characters at the intersection of the line corresponding to the representation (j) and the column of the class of $\tilde{g}$. The fourth step is to implement a Gram-Schmidt procedure to determine the basis of one block corresponding to the representation (j). We first use the projector

$$P^{(j)} = \sum_{g \in G} \chi^{(j)}(\tilde{g}) \tilde{g}. \tag{18.34}$$

A basis element of the Hilbert space is coded as a binary number of size N. Zero corresponds to a down spin, and 1 codes an up spin. In order to label the basis vectors, we use the decimal representation of the binary number of size N. We note $|\psi_k\rangle$ the corresponding vector. The procedure consists in scanning all the states $|\psi_k\rangle$ and to determine k_0 such as $P^{(j)}|\psi_k\rangle = 0$ if $k < k_0$ and $P^{(j)}|\psi_{k_0}\rangle \neq 0$. The state $P^{(j)}|\psi_{k_0}\rangle$ is the first vector of the basis that we look for. Once we have found the first vector of the basis, we continue ot scan the all the states $|\psi_k\rangle$, but we project them with

$$P_0^{(j)} = \sum_{g \in G} \langle \psi_{k_0} | \tilde{g} | \psi_{k_0} \rangle \tilde{g}. \tag{18.35}$$

If $P_0^{(j)}|\psi_k\rangle = 0$, we forget about $|\psi_k\rangle$ and project $|\psi_{k+1}\rangle$. If $P_0^{(j)}|\psi_k\rangle \neq 0$, we try to incorporate $P_0^{(j)}|\psi_k\rangle$ into the basis using a modified Gram-Schmidt procedure [13]. If $P_0^{(j)}|\psi_k\rangle$ is a linear combination of the basis vector, then we forget about it and project $|\psi_{k+1}\rangle$. If it is not, we incorporate it into the basis, after having orthogonalized it, and we make the projection test for $|\psi_{k+1}\rangle$. At the end of the procedure, the dimension of the basis must be equal to (18.33). We note that it is not possible to store all the components of the orthonormal basis, because of the limited storage capacities. In order to spare memory, we store only the non zero components. The fifth and last step is o diagonalize the Glauber matrix on the basis that has been determined at the fourth step. The size of the matrices to be diagonalized are small enough, so that we can use the Jacobi method.

18.4.3 Results

We work with a 3x4 lattice. The number of representations is equal to 15, and the maximal block dimension is 335. The spectrum in a given sector of symmetry of the 3x4 square lattice is pictured on figure 18.3 as a function of the inverse temperature. In the limit $\beta \to 0$, we recover degeneracies for integer eigenvalues, which is the expected behaviour for a bipartite lattice (see relation (18.12)). For inverse temperatures $\beta \simeq 0.4$, eigenvalue repulsion is visible, as well as eigenvalue crossings.

A first quantity of interest is the variation of the smallest eigenvalue spacing s_{min} as a function of temperature. In the thermodynamics limit, it is clear that if a system undergoes a ferromagnetic transition, $s_{min}(T) = 0$ it $T < T_c$ since the eigenvalue $\lambda = 0$ is degenerate in the broken symmetry phase. If $T > T_c$, the eigenvalue $\lambda = 0$ is no more degenerate. However, we cannot deduce that $s_{min}(T) > 0$ if $T > T_c$. Nonetheless, it seems that s_{min} takes non zero values in the paramagnetic phase whereas it is zero in the ferromagnetic phase, excepted for very large temperatures. S_{min} is plotted as a function of temperature on figure 18.4. We took only a small number of points on figure 18.4, so that we cannot see the cancelations of s_{min} for the values of the temperature for which there exists eigenvalue crossings. We now discuss the shape of the eigenvalue spacing statistics $P(s)$. In the paramagnetic phase, $P(s)$ is characterized by an intermediate statistics. For instance, for $\beta = 0.4$, that is in the region of figure 18.3 where eigenvalue repulsion is visible, $P(0)$ is close to $1/2$, and the shape of $P(s)$ is well fitted by the G.O.E. distribution for $s > 1$ (see figure 18.5). This non universal eigenvalue spacing statistics can be explained by the fact that the system is not integrable, but possesses non trivial conserved quantities, so that the eigenvalue spacing statistics corresponds to a situation where one mixes different sectors correponding to different conserved quantities. By comparison, in the case of the Sherrington-Kirkpatrick model, we shall find a G.O.E. law at high temperatures. In the region of very high temperatures, and for the 3x4 Ising model, we computed $P(s)$ for an inverse temperature $\beta = 0.02$ (see figure 18.6). The eigenvalue spacing statistics seems to evolve towards a poissonian shape for large separations ($s > 1$), rather than a G.O.E. shape for lower temperatures. For small separations, eigenvalue repulsion is present. We argue that this shape of eigenvalue spacing statistics does not evolve much in the region of small inverse temperatures β since, in this region, the eigenvalues are linear as a function of the inverse temperature β and the dominant contribution to $P(s)$ comes from separation between eigenvalues which are degenerate in the limit $\beta = 0$. In the ferromagnetic region, the eigenvalue spacing statistics presents a peak for $s = 0$, which decreases with the temperature, as well as a non universal part for $s > 0$. The non universal part seems to be intermediate between G.O.E. and Poisson, and does not evolve as a function of temperature. The eigenvalue spacing statistics are plotted on figure 18.7 for $\beta = 2$.

18.5 Frustated one dimensional model

18.5.1 The model

We condider the one dimensional antiferromagnetic Ising model with antiferromagnetic next-nearest-neighbour interactions. This model can be seen as a sucession of triangles, as pictured on figure 18.8 and can be solved via a transfert matrix formalism, with the sites gathered as shown on figure 18.8. The transfert matrix has the form

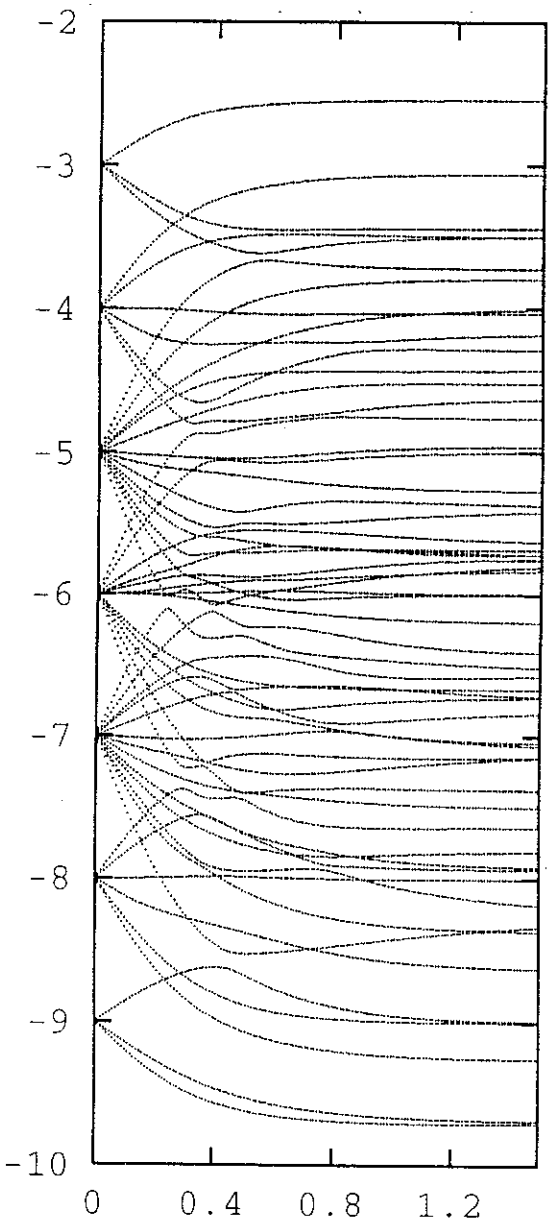

Figure 18.3:
Evolution of the eigenvalues of the Glauber matrix as a function of the inverse temperature for the 3x4 Ising model on a square lattice, in the representation number 3. The number of eigenvalues is 57.

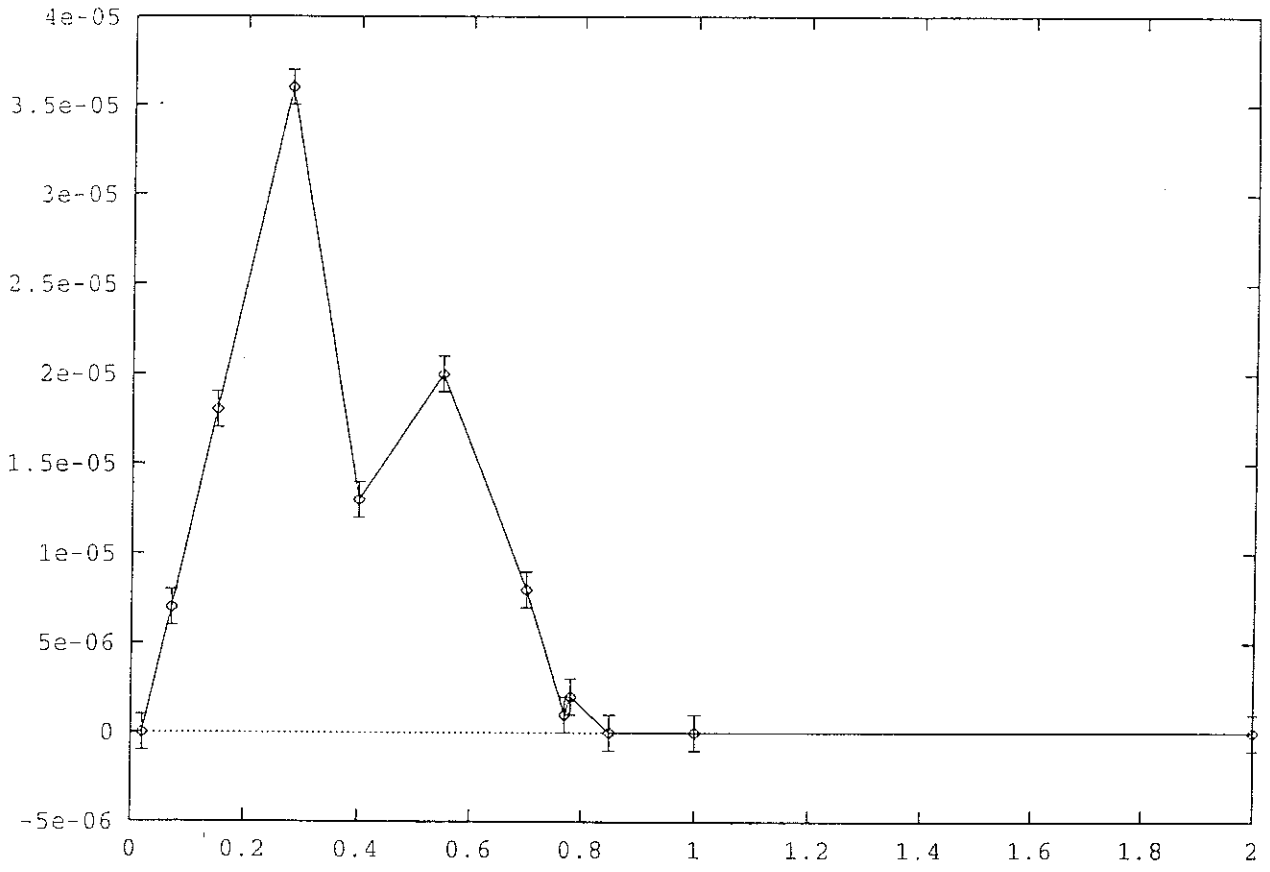

Figure 18.4:
Minimal eigenvalue spacing s_{min} for the 3x4 Ising model as a function of the inverse temperature β. s_{min} is the minimum over all the representations of the spacing between two consecutive eigenvalues. s_{min} tends to zero in the limit $\beta \to 0$, as expected from the organisation of the eigenvalues in the limit $\beta \to 0$ for a bipartite lattice (see figure 18.3). What is not visible on this figure is the fact that s_{min} cancels for some some temperature values, due to the existence of eigenvalue crossings visible on figure 18.3.

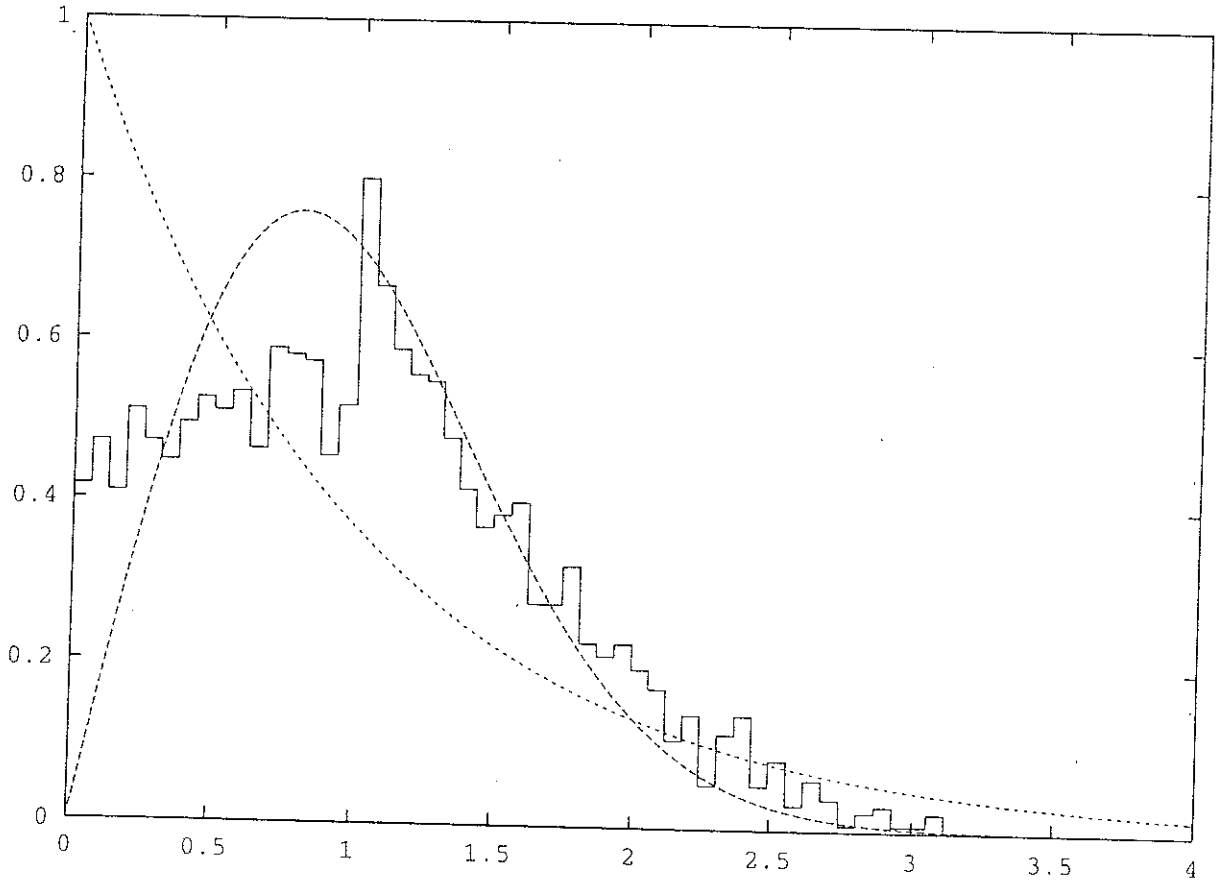

Figure 18.5:
Eigenvalue spacing statistics of the 3x4 square lattice for $\beta = 0.4$. The Poisson and G.O.E. distribution are plotted in dashed lines. For $s > 1$, $P(s)$ is close to the G.O.E. curve.

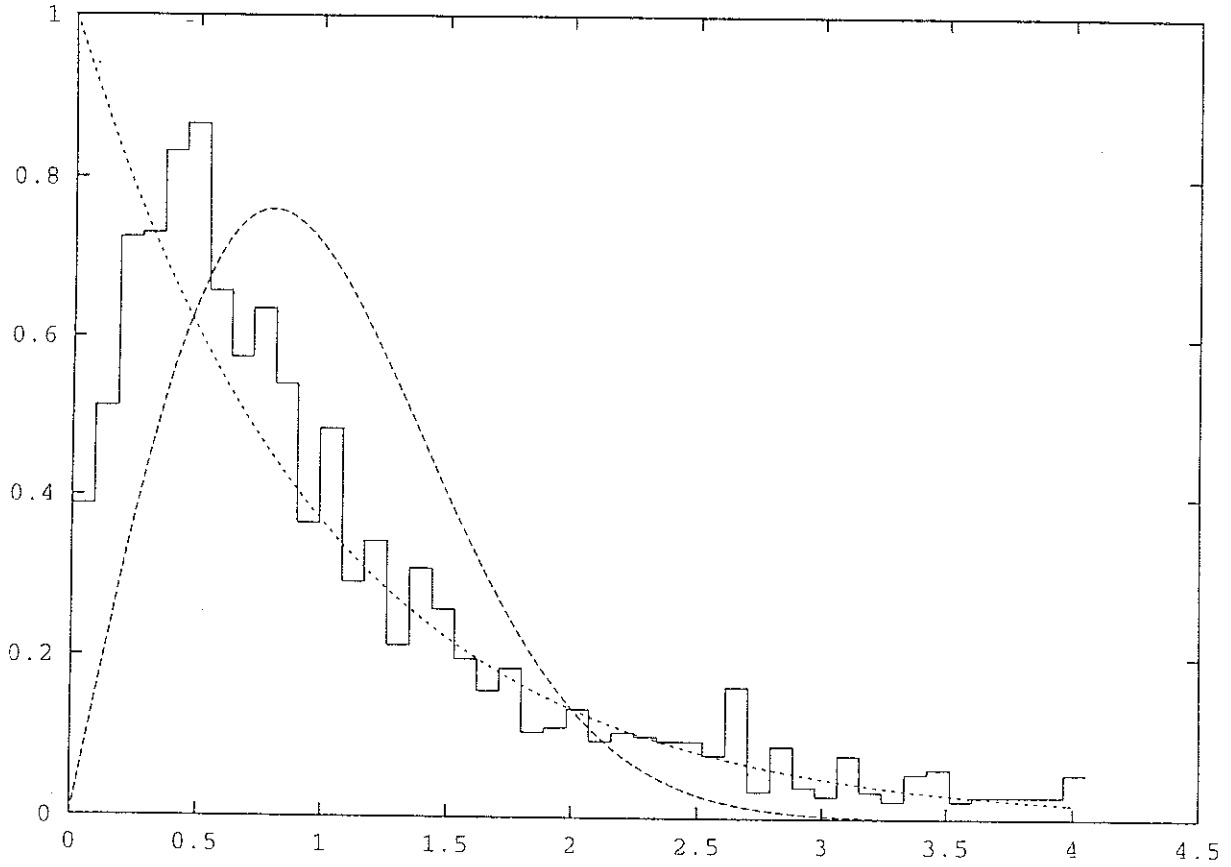

Figure 18.6:
Eigenvalue spacing statistics of the 3x4 square lattice for $\beta = 0.02$. The Poisson and G.O.E. distribution are plotted in dashed lines. For $s > 1$, $P(s)$ is close to the Poisson curve.

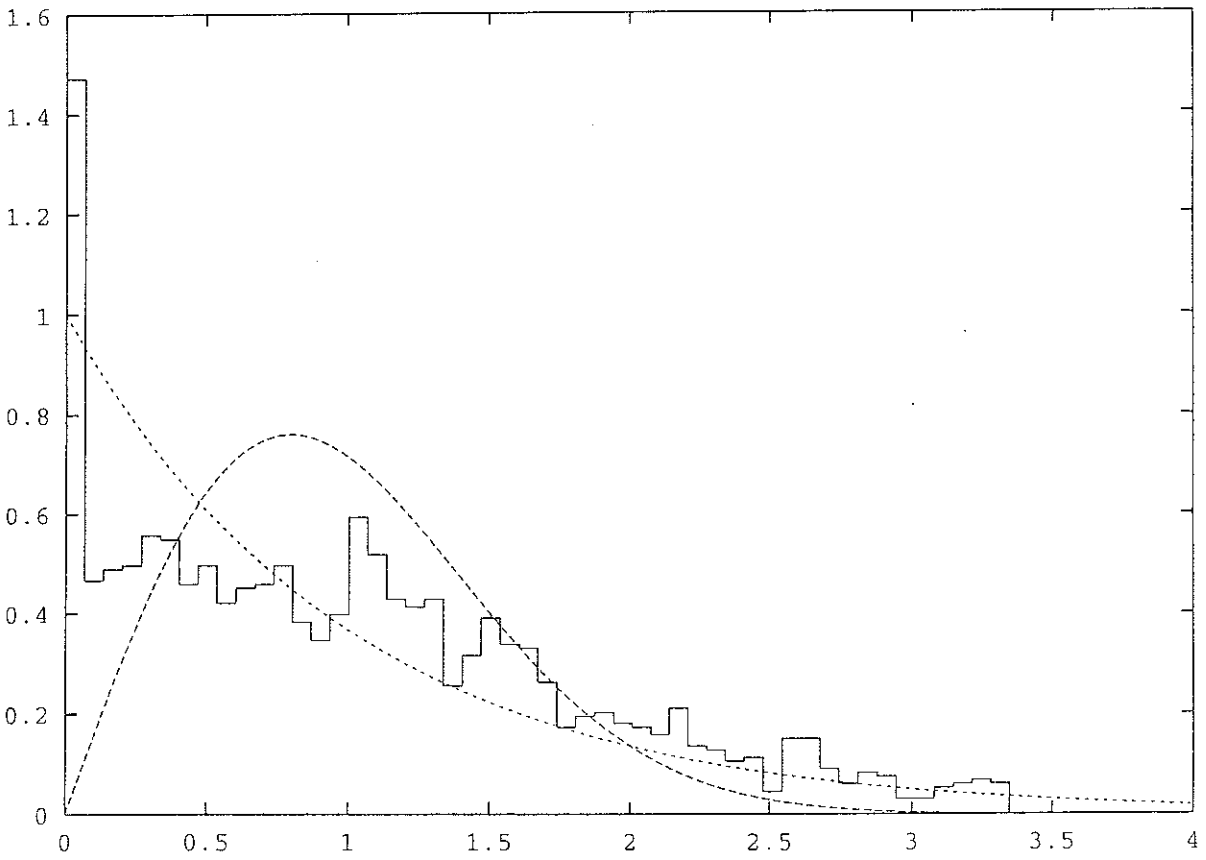

Figure 18.7:
Eigenvalue spacing statistics of the 3x4 square lattice for $\beta = 2$. The Poisson and G.O.E. distribution are plotted in dashed lines. The statistics presents a peak for $s = 0$, which decrease as the inverse temperature increases. The non universal part of the eigenvalue statistics for $s > 0$ is intermediate between Poisson and G.O.E.

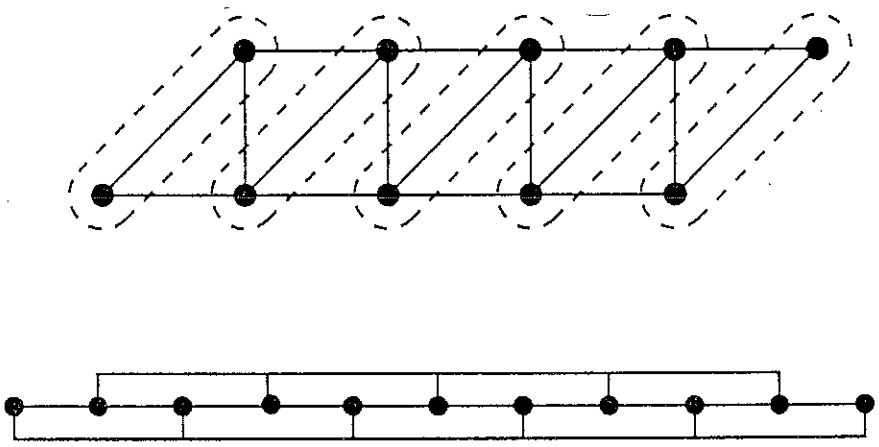

Figure 18.8:
The one dimensional Ising model with next-nearest-neighbour coupling, and its representation as a sucession of triangles. The dashed lines represent how the sites are gathered in the transfert matrix formalism.

$$T = \begin{pmatrix} A & B \\ B & A \end{pmatrix}, \tag{18.36}$$

with

$$A = \begin{pmatrix} e^{-4\beta J} & e^{-2\beta J} \\ e^{2\beta J} & 1 \end{pmatrix}, B = \begin{pmatrix} e^{2\beta J} & 1 \\ 1 & e^{2\beta J} \end{pmatrix}. \tag{18.37}$$

In (18.36), the states are ordered in the form $|\uparrow,\uparrow\rangle$, $|\uparrow,\downarrow\rangle$, $|\downarrow,\downarrow\rangle$, $|\downarrow,\uparrow\rangle$. Because of the form (18.36) of the transfert matrix, if (ψ,φ) is and eigenvector of T, then $(\psi+\varphi,\psi+\varphi)$ and $(\psi-\varphi,\psi-\varphi)$ are eigenvectors of T for the same eigenvalue, so that the eigenvalues of T are the eigenvalues of $A+B$ and $A-B$, and the initial 4x4 problem is reduced to two 2x2 problems, due to the time reversal invariance. The partition function is simply $Z_N = TrT^{N/2}$ for a N sites chain (N is supposed to be even). The zero temperature entropy is found to be extensive, of the form $S(0)/N = \ln 2/2$, whereas in the corresponding ferromagnetic problem, the entropy is finite at zero temperatures. This one dimensional antiferromagnetic model has thus the same properties as the triangular antiferromagnet [14], namely the number of zero temperature ground states is proportionnal to $\exp \alpha N$, with α a constant.

18.5.2 Results

We work with an open chain version, so that the only symmetry is the inversion. We have already explained how to treat this symmetry. The variations of the minimum spacing between two consecutive eigenvalues is plotted on figure 18.9. s_{min} tends to zero in the limit $\beta \to 0$, as well as in the limit $\beta \to +\infty$. In between, there exists a region with non zero values of s_{min}. The limit $\beta \to 0$ is interpreted as the existence of a particular form of the spectrum in this limit (which corresponds to (18.12)). In the limit $\beta \to +\infty$, it seems sensible to assert that $s_{min} = 0$ whatever the model since in this limit, the thermodynamic correlation length is much smaller than the lattice spacing, so degeneracies are expected to occur in the spectrum of relaxation times. This model is interesting since no thermodynamic transition occurs at any temperature though s_{min} is non monotonous. As far as the eigenvalue spacing statistics are considered, the situation is similar to the bidimensional Ising model. The level spacing statistics are plotted on figure 18.10 for $\beta = 0.2$. The statistics is non universal, and intermediate between Poisson and GOE, which suggest the presence of conserved quantities. For small temperatures, a peak at $s = 0$ appears in the eigenvalue statistics and the tail is non universal. In particular, the weight for large intereigenvalue spacing is large, as plotted on figure 18.11.

18.6 SK model

18.6.1 The model

This model was proposed in 1975 as an 'exactly solvable' spin glass model [15]. For general reviews on the problems of spin glasses, we refer the reader to references [16] [17] [18]. The SK model is defined by the disordered, infinite range interaction Hamiltonian

$$H = \sum_{\langle i,j \rangle} J_{ij}\sigma_i\sigma_j, \tag{18.38}$$

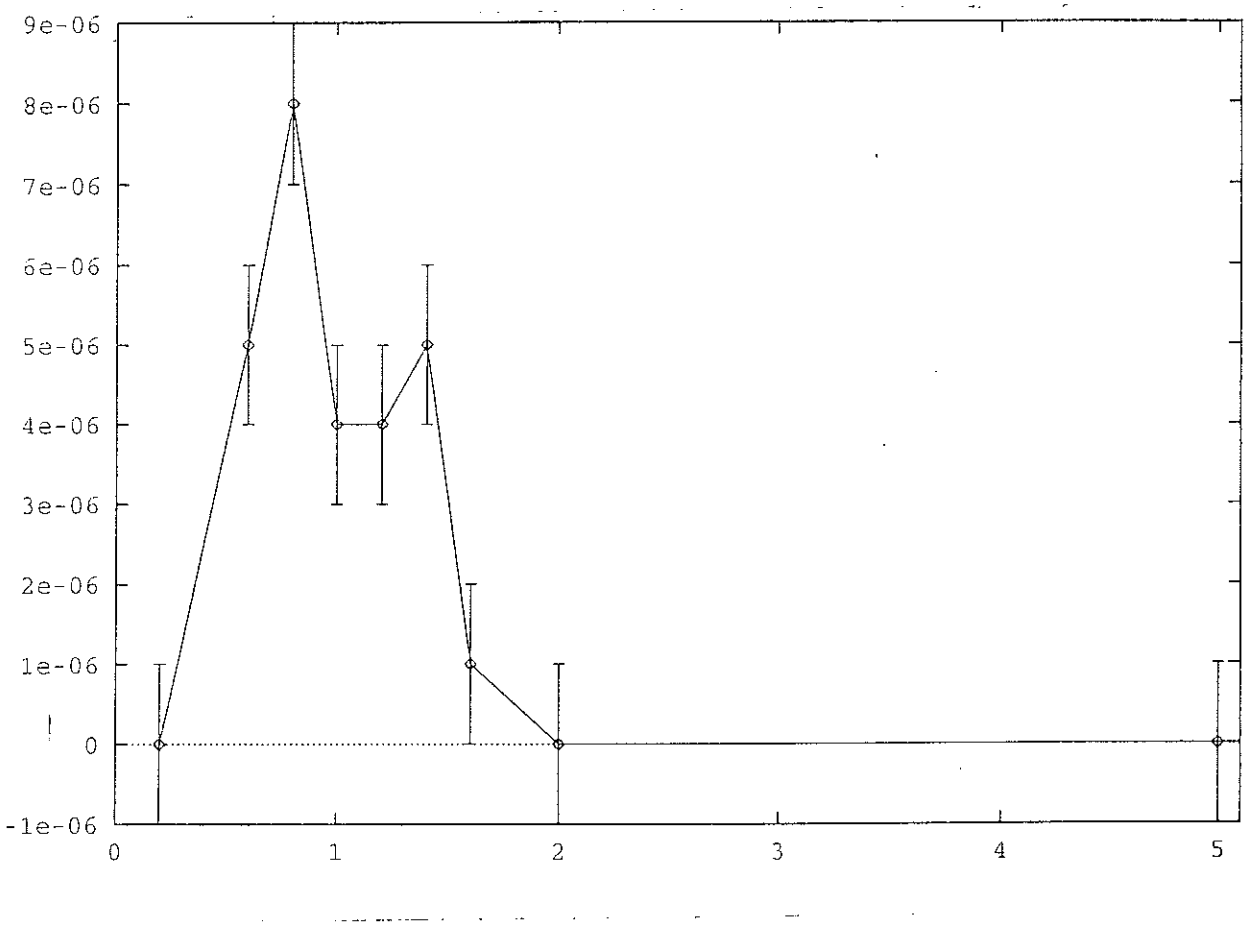

Figure 18.9:
Minimal eigenvalue spacing s_{min} for the one dimensional Ising model with next nearest neighbour interactions as a function of the inverse temperature β. s_{min} tends to zero in the limit $\beta \to 0$, as well as in the limit $\beta \to +\infty$.

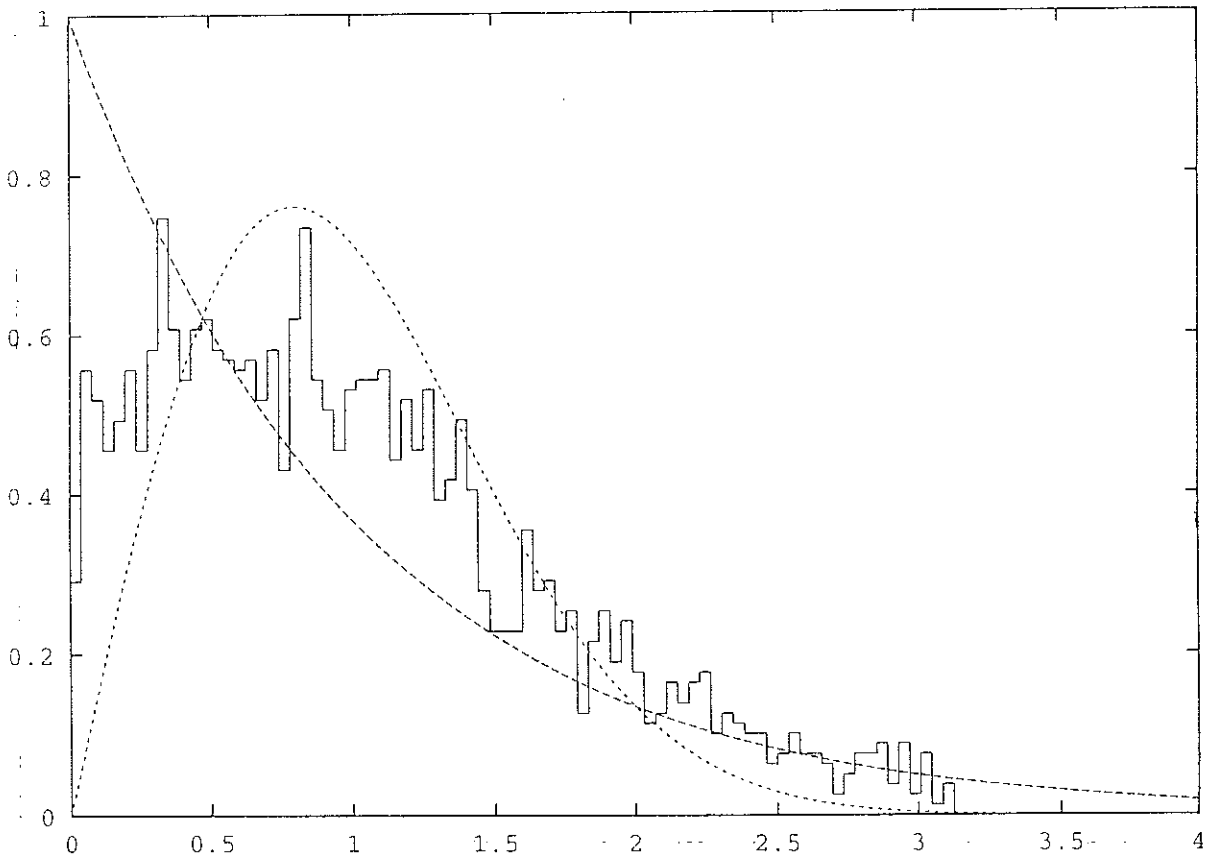

Figure 18.10:
Eigenvalue spacing statistics of the frustrated one dimensional model with nearest neighbour interactions, for an inverse temperature $\beta = 0.2$. The statistics is intermediate between Poisson and G.O.E.

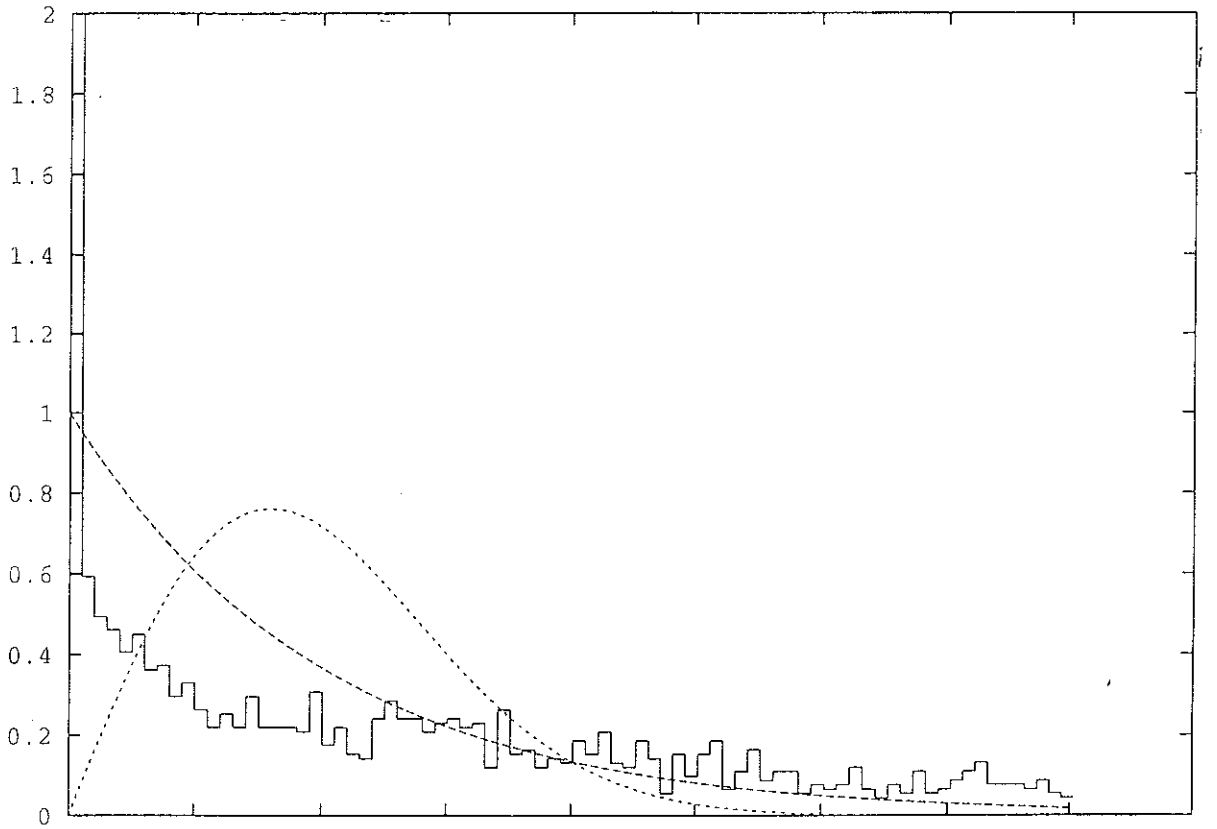

Figure 18.11:
Eigenvalue spacing statistics of the frustrated one dimensional model with nearest neighbour interactions for an inverse temperature $\beta = 5$. The peak at $s = 0$ has been truncated. The total weight of this peak is 29% of the total number of spacings.

with quenched random interactions J_{ij} with a gaussian distribution

$$P(J_{ij}) = \left(\frac{N}{2\pi J^2}\right)^{1/2} \exp\left(-\frac{N J_{ij}^2}{2J^2}\right). \tag{18.39}$$

We refer the reader to the reviews precedently quoted for the solution of this model. For $T < J$, the model is a spin glass, and a paramagnet for $T > J$. In the glass phase, the model presents a large number of thermodynamic phases, with no symmetry connecting ground states. The different ground states are separated by large barriers which scale with the system size. An other feature of glassiness is the presence of aging, associated with slow relaxation processess.

18.6.2 Eigenvalue spacing statistics

We computed the eigenvalue spacing statistics for a 9 sites cluster. In this case, we do not need to look for the lattice symmetries since, excepted for some special cases of zero probability, the random infinite range interactions break all the lattice symmetries. The minimal intereigenvalue spacing s_{min} is plotted on figure 18.12 as a function of the inverse temperature. In the paramagnetic phase, s_{min} is non zero, as in the case of the paramagnetic phase of the bidimensional Ising model. The level spacing statistics in the high temperature limit are found to be in good agreement with the G.O.E. law, as pictured on figure 18.13, eventhough small deviations are visible. These deviations occur in the shape of the eigenvalue statistics. However, the linear eigenvalue repulsion is clearly visible. In the low temperature regime, the level spacing statistics are overpoissonian, as plotted on figure 18.14. We call this statistics *overpoisson* because not only there is a peak for $s = 0$ but also the $s > 0$ statistics is overpoissonian. If we supress the spacings smaller than Δs, ($\Delta s = 0.01, 0.05$ on figure 18.14), the overpoissonian character remains. This indicates a trend to *level attraction*. To our knowledge, this is the first time that such a behaviour is observed. If we decrease the temperature, this level attraction increases. An analysis of the density of eigenvalues (see the insert of figure 18.14) reveals that this attraction favours integer eigenvalues.

18.7 Cayley tree

18.7.1 The model

Trees were introduced in statistical physics as soon as the 30's in order to implement mean field theories [19] [20]. In this case, only the central spin was considered and the border of the tree (which represents a finite fraction of the spins) was sent to infinity. This limit is the Bethe-Peierls limit. However, it is possible to develop statistical physics on a Cayley tree, with the border included. This was done in the seventies, and a continuous transition was discovered [21] [22]. The dynamics was studied only recently [10]. A cross-over to a glassy regime was then found below the temperature scale $T_g \sim J/\ln n$, with n the number of generations. The temperature scale T_g decreases in the limit $n \to +\infty$, but very slowly, so that the glassy regime exists even in the macroscopic regime. The zero temperature barriers scale like $J \ln n$, with n the number of generations. We study the eigenvalue spacing statistics of a small half-space-tree with 2 generations and a coordinance 4. The ancestor has three sons, and each of its sons is connected to 3 grand children. The number of sites is 13.

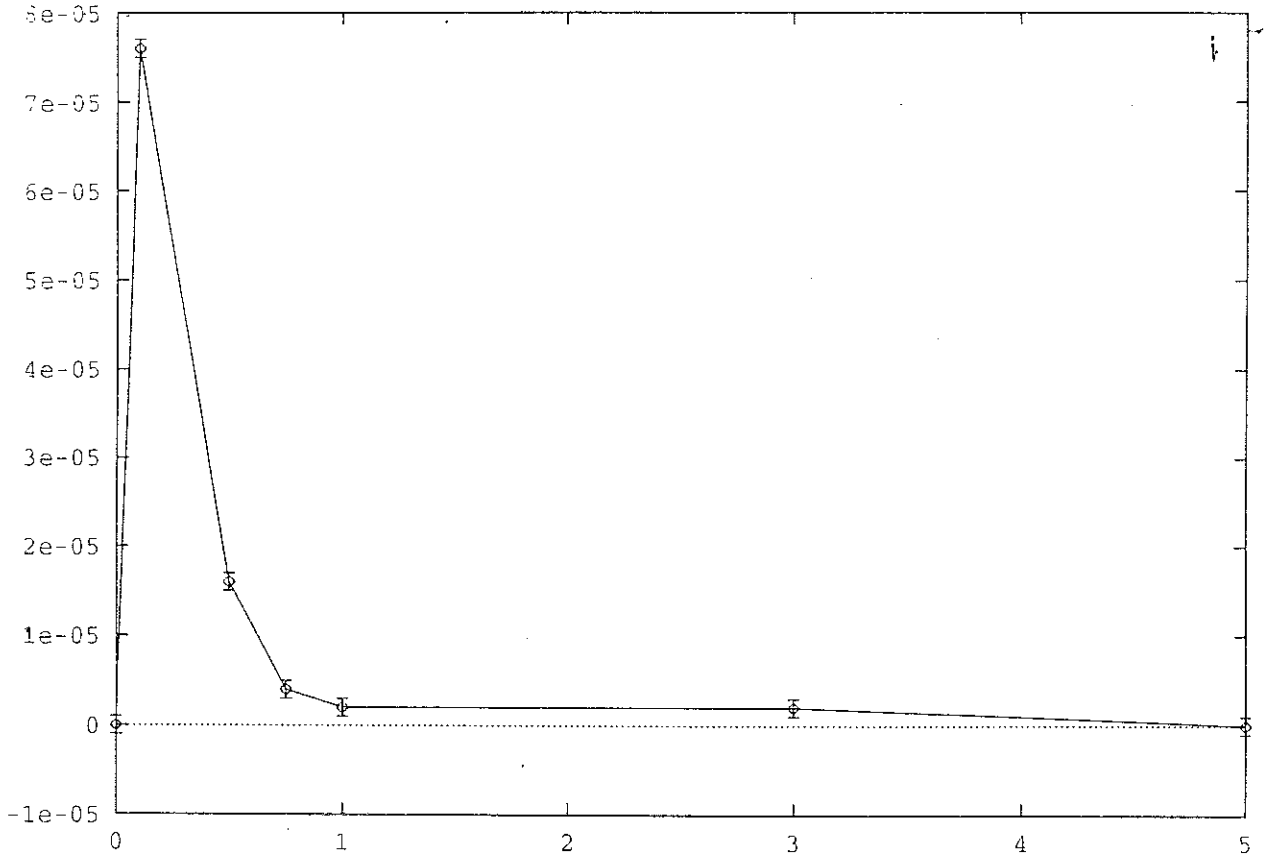

Figure 18.12:
Minimal eigenvalue spacing s_{min} for the SK model as a function of the inverse temperature β. The error bars indicate the precision of the diagonalization procedure. The minimal spacing is computed for 10 realizations of the disorder, so that s_{min} is overevaluated.

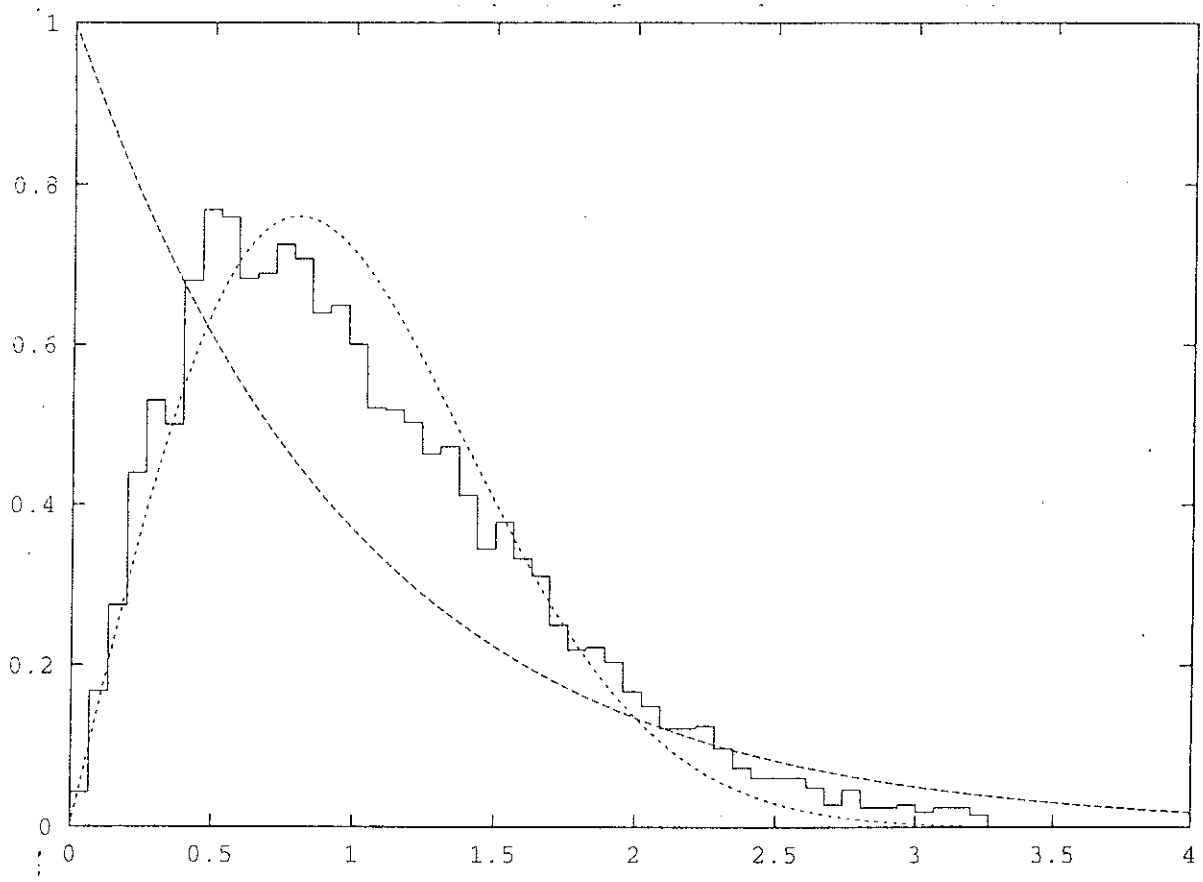

Figure 18.13:
Eigenvalue spacing statistics of the SK model for an inverse temperature $\beta = .1$. The G.O.E. shape and the Poisson shape are plotted in dotted lines. The statistics are in good agreement with the G.O.E. shape, eventhough small deviations are visible.

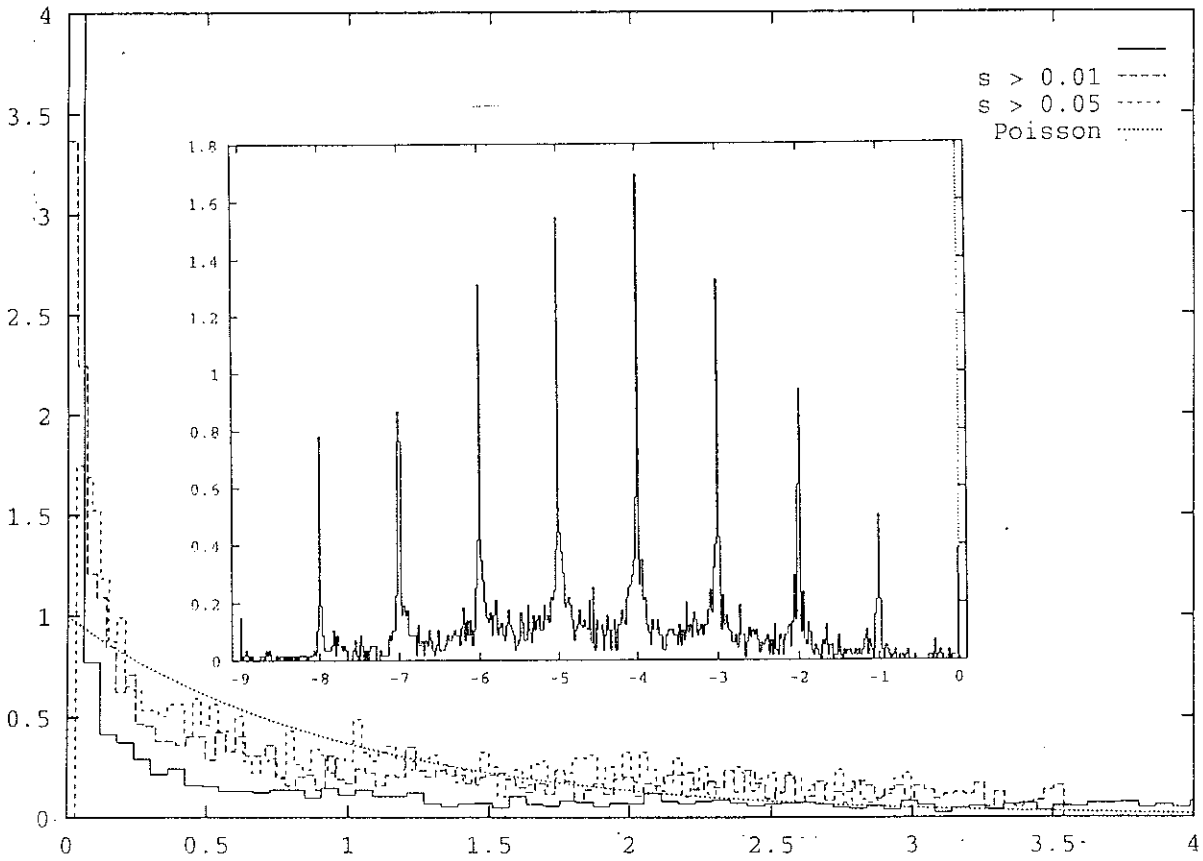

Figure 18.14:
Eigenvalue spacing statistics of the SK model for an inverse temperature $\beta = 10$, averaged over 10 realizations of the disorder. The full line represents the complete statistics for which the value at $s = 0$ is truncated. The dashed lines represent the same statistics, but without the small spacings.We see that the *overpoisson* syndrom does not affect the $s = 0$ part of the statistics but the statistics remain overpoissonian if we eliminate the small spacings. The insert represents the density of eigenvalues for the same temperature, averaged over 10 realizations of the disorder.

18.7.2 Level spacing statistics

We used group theory to determine the subspaces in which the Glauber matrix is to be diagonalized. The generators of the symmetry group of the tree are very simple. At each vertex which is not a leaf, the sons and their descendents ar4e permuted. These permutations generate the symmetry group of the tree. The generators do not commute, so that one has to use group theory. It is clear that the symmetry group is very large. For the small cluster that we studied, we found 10 different blocks of maximal size 336. We diagonalized the Glauber matrix in all these different sectors at low temperatures. The spectrum of the Glauber matrix is pictured on figure 18.15 for the block of size 336. It is clear that there is an obvious trend to clustering. The level spacing statistics for this temperature reveal the existence of a peak for $s = 0$ and some peaks for $s > 0$, but with a very small weight. We conclude that level attraction is also present in the spectrum of the Glauber matrix of the Cayley tree. The set of eigenvalues in a given block is plotted on figure 18.15. As in the case of the SK model, the biggest clusters corresponds to integers.

18.8 Conclusion

Since the content of this paper was already summarized in the introduction, we end up with some final remarks. The one dimensional case is very special due to the existence of an underlying integrable dynamics. In the other cases, it seems that the presence of a paramagnetic phase is signaled by the presence of a non zero minimal intereigenvalue spacing s_{min}. It seems that, in all cases, s_{min} cancels in the zero temperature limit as well as in the infinite temperature limit. It seems also that, in the presence of a second order transition, s_{min} is zero in the ferromagnetic phase. This property is not surprising since we know that in the ferromagnetic phase, the eigenvalue $\lambda = 0$ is degenerate with an the eigenvalue of the broken symmetry state in the thermodynamic limit. In the case of the glass transition, s_{min} is also zero in the glassy phase. An other aspect of this work is the nature of the eigenvalue spacing statistics of paramagnetic phases. In the SK model, the eigenvalue spacing statistics are close to G.O.E., whereas, in the bidimensional Ising model, the statistics is intermediate between G.O.E. and Poisson, which suggests that there exists some conserved quantities in the dynamics of the bidimensional Ising model. The origin of these 'hidden' conserved quantities is not clear at the moment. Finally, it seems that, in glassy systems, the eigenvalues have a trend to condense near integers. This is true for the SK model as well as for the tree. However, this is just a numerical fact. It has not yet been proven that, in a spin glass, the eigenvalues of the Glauber matrix condense in the vicinity of integers.

I thank B. Douçot for a critical reading of the manuscript, and I am indebted to J.C. Anglès d'Auriac and H. Bruus for help with group theory.

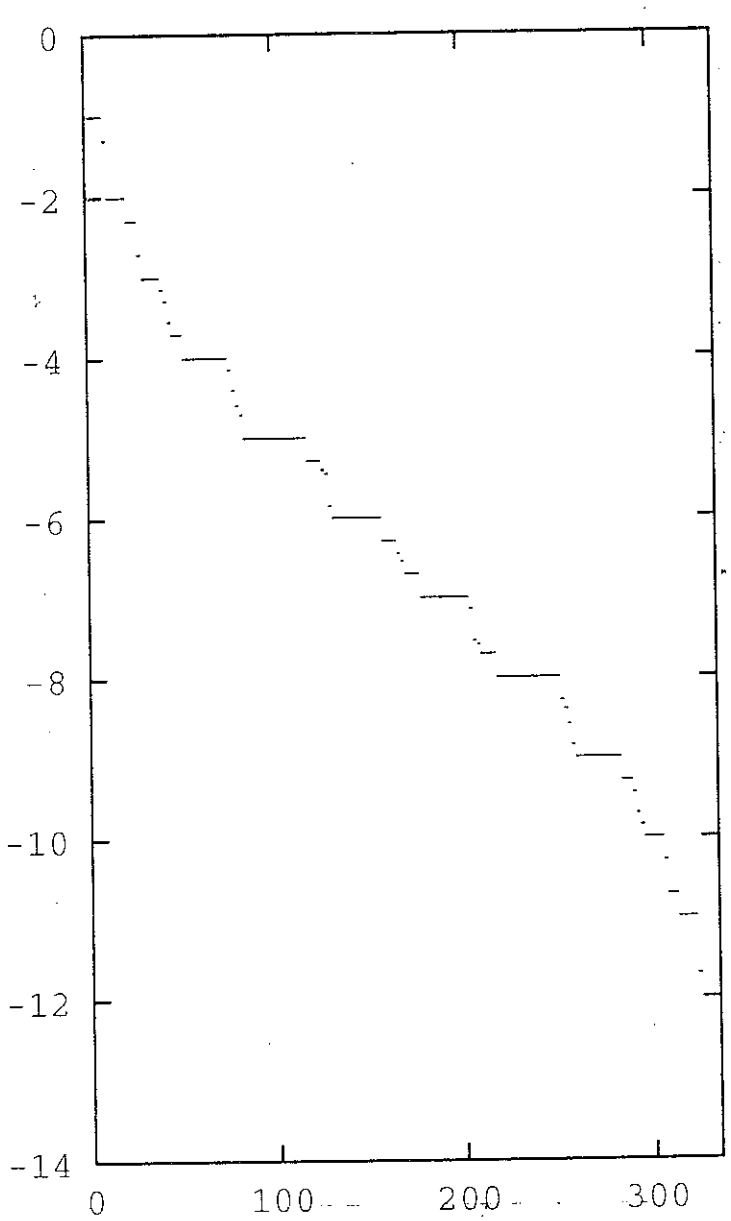

Figure 18.15:
Spectrum of the Glauber matrix for a tree cluster at low temperatures ($\beta = 10$). The x axis represents the eigenvalues label (between 0 and 336), and the y axis represents the eigenvalues. The spectrum exhibits clustering.

References

[1] E.P. Wigner, Ann. Math. 53, 36 (1951); Ann. Math. 62, 548 (1955); SIAM Rev. 9, 1 (1967).

[2] F.J. Dyson, J. Math. Phys. 3, 140 (1962).

[3] C.E. Porter, *Statistics Theory of Spectra: Fluctuations*, Academic Press, New York (1965).

[4] O. Bohigas, *Random matrix theories and chaotic dynamics* in Les Houches, *Chaos and quantum physics*, North Holland.

[5] O. Bohigas, M.J. Giannoni and C. Schmit, Phys. Rev. Lett. 52, 1(1984).

[6] M.C. Gutzwiller, *Chaos in Classical and Quantum Mechanics*, Springer Verlag (1990).

[7] R.A. Jalabert, J.L. Pichard, J. Phys. I (France) 5, 287 (1995).

[8] G. Montambaux, D. Poilblanc, J. Bellissard and C. Sire, Phys. Rev. Lett 70, 497 (1993); T.C. Hsu and J.C. Anglès d'Auriac, Phys. Rev. B 47, 14291 (1993); D. Poilblanc, T. Ziman, J. Bellissard, F. Mila and G. Montambaux, Europhys. Lett. 22, 537 (1993).

[9] R. Mélin, B. Douçot and P. Butaud, J. Phys. I (France) 4, 737 (1994); R. Mélin, J. Phys. I (France) 5, 159 (1995), R. Mélin, to be published in J. Phys. I (France) (1995).

[10] R. Mélin, J.C. Anglès d'Auriac, P. Chandra and B. Douçot, preprint (1995).

[11] R.J. Glauber, Jour. Math. Phys. 4, 294 (1963).

[12] We used the program GAP to determine the classes and to construct the table of characters.

[13] J.K. Cullum and R.A. Willoughby *Lanczos Algorithms for Large Symmetric Eigenvalue Computations*, Birkhäuser (1985).

[14] G.H. Wannier, Phys. Rev. 79, 357 (1950).

[15] D. Sherrington and S. Kirkpatrick, Phys. Rev. Lett. 35, 1792 (1975); S. Kirkpatrick and D. Sherrington, Phys. Rev. B 17, 4384 (1978).

[16] M. Mézard, G. Parisi and M. Virasoro, *Spin glass theory and beyond*, World Scientific Ed (1993).

[17] K.H. Fisher and J.A. Hertz, *Spin glasses*, Cambridge Studies in Magnetism (1991)

[18] V.S. Dotsenko, M.V. Feigelman and L.B. Ioffe, *Spin Glasses and Related Problems*, Physics reviews, hardwood academic publishers (1990).

[19] H.A. Bethe, Proc. Roy. Soc. A 216, 45 (1935); 150, 552 (1935).

[20] R. Peierls, Proc. Can. Phil. Soc. 32, 477 (1936); Proc. Roy. Soc. 154, 207 (1936).

[21] E. Müller-Hartmann and J. Zittartz, Phys. Rev. Lett. 33, 893 (1974).

[22] J. von Heimburg and H. Thomas, J. Phys. C 7, 3433 (1974).